



MOBILE ENERGY RESOURCES IN GRIDS OF ELECTRICITY

ACRONYM: MERGE

GRANT AGREEMENT: 241399

**WP 2
DELIVERABLE D2.2
TASK 2.2, 2.4 & 2.5**

**FUNCTIONAL SPECIFICATION FOR TOOLS TO ASSESS
STEADY STATE AND DYNAMIC BEHAVIOUR IMPACTS,
IMPACT ON ELECTRICITY MARKETS AND IMPACT OF
HIGH PENETRATION OF EV ON THE RESERVE LEVELS**

15 FEBRUARY 2011



CONTENTS

- I Task 2.2 - ADAPTATION AND ENHANCEMENT OF EXISTING SIMULATION PLATFORMS**
- II Task 2.4 - MARKET ISSUES**
- III Task 2.5 - RESERVE ADEQUACY**





MOBILE ENERGY RESOURCES IN GRIDS OF ELECTRICITY

ACRONYM: MERGE

GRANT AGREEMENT: 241399

WP 2

TASK 2.2

DELIVERABLE D2.2

**ADAPTATION AND ENHANCEMENT OF EXISTING
SIMULATION PLATFORMS**

15 FEBRUARY 2011



REVISION HISTORY

VER.	DATE	NOTES (including revision author)
01	31/01/2011	First draft completed
02	07/02/2011	Second draft completed, and submission for approval
03	07/02/2011	Second draft approved by the WP leader and Technical Coordinator, and submission for approval by Prof. Hatziargyriou
04	15/02/2011	Final version approved
05		
06		
07		
08		
09		
10		





AUTHORS

INESC Porto	Mauro Rosa	marosa@inescporto.pt
	Diego Issicaba	diego.issicaba@inescporto.pt
	Nuno Gil	nuno.gil@ipleiria.pt
	Felipe Joel	fsoares@inescporto.pt
	Pedro Almeida	pedro.r.almeida@inescporto.pt
	Carlos Moreira	cmoreira@inescporto.pt
	Paulo Ribeiro	pjsr@inescporto.pt
	Miguel Heleno	mdheleno@inescporto.pt
	Ricardo Ferreira	rjcf@inescporto.pt
	Jean Sumaili	jsa@inescporto.pt
	José Meirinhos	jimm@inescporto.pt
	Luís Seca	luis.seca@inescporto.pt
	João Peças Lopes	jpl@fe.up.pt
	Manuel Matos	mmatos@inescporto.pt
NTUA	Nikos Soultanis	nsoultan@power.ece.ntua.gr
	Anastasiadis Anestis	aanestis@power.ece.ntua.gr
	Evangelos Karfopoulos	ekarfopoulos@gmail.com
Cardiff (task leader)	Yunfei Mu	muy1@cardiff.ac.uk
	Jianzhong Wu	wuj5@cardiff.ac.uk
	Janaka Ekanayake	ekanayakej@cardiff.ac.uk
	Mahinsasa Narayana	mahinsasa@yahoo.com





CONTRIBUTORS

INESC Porto	J. A. Peças Lopes	jpl@fe.up.pt
NTUA	Stavros Papathanasiou	st@power.ece.ntua.gr
	Nikos Hatzigiargyriou	nh@power.ece.ntua.gr
Cardiff	Nick Jenkins	Jenkinsn6@cardiff.ac.uk

APPROVAL

DATE

Project Coordinator	PPC	N. Hatzigiargyriou	15/02/2011
Technical Coordinator	INESC Porto	J. A. Peças Lopes	07/02/2011
Work Package Leader	INESC Porto	J. A. Peças Lopes	07/02/2011

Access:

☒

Project Consortium

☒

European Commission

☐

Public

Status:

☐

Draft Version

☐

Submission for Approval (deliverable)

☒

Final Version (deliverable, approved)



EXECUTIVE SUMMARY

This report is part of the deliverables for the MERGE project Work Package 2: “Developing Evaluation Capability” whose goal is to implement an evaluation suite composed of several simulation tools that will incorporate specific models capable to deal with the integration of electric vehicles (EV) either in “charging-only” mode or under the V2G concept.

This report covers the deliverables for Task 2.2 which looks at “Adaption and enhancement of existing simulation platforms”. It comprises of five main sections that represent the five main sub-tasks from the MERGE project Description of Work (DoW), as shown in Table 1.

SUB-TASK IN DoW	DESCRIPTION	SECTION IN THIS REPORT
2.2.1	“A simulation platform that works over IPSA+ based on its UDM tool and the scripted extension library for Python will be updated considering the specific characteristics brought by the large penetration of EV, e.g. controllability, mobility.”	2
2.2.2	“The simulation platforms based on the MATLAB Simulink software developed within the EU Microgrids projects will be adapted to incorporate EV models for smart charging and V2G operation in both normal and islanded modes.”	3
2.2.3	“A simulation platform that works over Eurostag and MATLAB software will be adapted to incorporate EV models for smart charging and V2G operation in both normal and islanded modes in MV distribution networks.”	4
2.2.4	“A simulation platform that works over PSS/E software will be adapted to incorporate aggregated models of EV, to be seen from the transmission grid side, in order to assess impacts in steady state operation and dynamic behavior for large interconnected transmission systems having conventional generation and the large scale integration of renewable power sources (namely wind power).”	5
2.2.5	“The fuzzy power flow tool will be adapted and enhanced to cope with EV nodal loads in a way that the important dependencies among EV load uncertainties in the nodes are taken into consideration. Besides propagating the uncertainties from the data to the results, providing fuzzy descriptions of the branch flows, node voltages and losses, the tool will identify the risk of congestion in branches and the degree of repression in node injections and in the system. The probabilistic load flow tools will be also adapted to provide probabilistic density functions of flows, voltages and losses.”	6

Table 1: WP2 Task 2.2 sub-tasks

Electric power systems still follow planning rules and procedures defined for the traditional operational paradigm. It is necessary to identify and prepare solutions for the operational problems caused by the large penetration of EVs. There are a number of software models and tools available to carry out steady state and dynamic studies of the electric power system, but without or with very limited capability to consider the impact from EVs. Therefore the main objective of Task2.2 is to adapt and enhance the existing simulation platforms to deal with the integration of EV into the power system. This task has taken into account the possibility of operating networks in two modes: normal interconnected mode and islanding mode (especially for distribution grids having dispersed generation sources). The models and tools to assess the steady state and the dynamic behaviour of LV Microgrids, MV distribution grids, and large interconnected systems having a large scale integration of EV have been adapted and developed. Figure 1 gives an overview of the models and tools which have been adapted/developed and their domains of applicability under the framework of this project. The models and tools in red boxes are covered by this report.

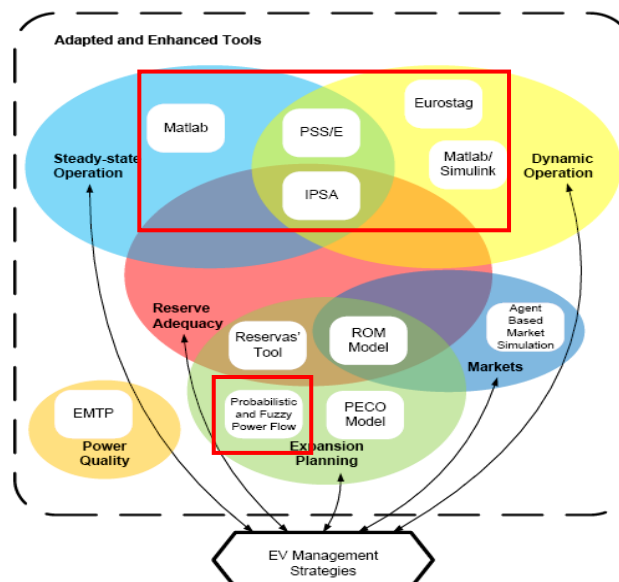


Figure 1: Models and tools which have been adapted/developed

IPSA+ software was adapted/enhanced to accommodate EVs by using its UDM (User Defined Model) tool and the scripted extension library for Python. Various EV-related models have been developed considering two types of interfacing structures, fast charging and shower charging, and different voltage levels, which are capable of incorporating specific control procedures; Reserve and frequency response models were adapted and enhanced to evaluate the performance of a network with different levels of EV penetration for providing the ancillary service; A spatial-temporal analysis tool was developed and integrated into the existing IPSA+ tool to address the correlation of the mobility with population movement in an urban area.

The simulation platforms based on the MATLAB Simulink software developed in the EU Microgrids projects were adapted to incorporate EV models for smart charging and V2G

operation in both normal and islanded modes. This development focuses on assessing impacts of EVs in Microgrids. These simulation platforms are now capable of assessing the steady state and dynamic behaviour of Microgrids in three-phase balanced mode and unbalanced modes. The dynamic stability of inverter dominated Microgrids was investigated.

The simulation platform that works over Eurostag and MATLAB software was adapted to incorporate EV models for smart charging and V2G operating in both normal and islanded modes in MV distribution networks. MATLAB was used as a user interface and logic controller. Specific scripts (describing external procedures that invoke the basic simulation tools) were developed to simulate the step by step response of the system in quasi-steady state and in dynamic behaviour when following the load diagram in critical periods and adopting different charging strategies (dumb, tariff based approaches, smart charging strategies). The capability to perform load following in these networks with large EV presence was addressed with these tools.

A simulation platform that works over PSS/E software was adapted to incorporate aggregated models of EV. This model provides a platform to assess the impacts of EVs in steady state operation and dynamic behavior for large interconnected transmission systems having conventional generation and large penetration of renewable power sources (namely wind power). The aggregated EV response to frequency changes or other control signals was embedded in dynamic load models that represent clusters of aggregated EV. Specific scripts were developed to simulate the step by step response of the system in quasi-steady state and in dynamic behavior when following the load diagram in critical periods and adopting different charging strategies (dumb, tariff based approaches, smart charging strategies). The Models of intermittent renewable generation (in particular wind power) were developed.

Apart from the deterministic simulations used to address steady impacts resulting from the presence of EV on the network for extreme conditions, fuzzy and probabilistic tools were developed to evaluate the ranges of power flows, voltages levels and losses in the transmission network when large variations of EV penetration and the use of different charging strategies takes place leading to significant uncertainty in node injections. The fuzzy power flow tool was adapted and enhanced to cope with EV nodal loads in a way that the important dependencies among EV load uncertainties in the nodes is taken into consideration. Besides propagating the uncertainties from the data to the results, providing fuzzy descriptions of the branch flow, node voltages and losses, the tool is able to identify the risk of congestion in branches and the degree of repression in the node injections and in the system. The probabilistic load flow tools were also adapted and enhanced to provide probabilistic density functions of flows, voltages and losses.

With these adapted and enhanced platforms, comprehensive analysis of the EV impact on the electric power system and the provision of decision-making capability are possible. All the Sub-Tasks detailed in the Description of Work were completed successfully.

TABLE OF CONTENTS

EXECUTIVE SUMMARY	5
1 INTRODUCTION	9
2 IPSA+ SIMULATION PLATFORM.....	13
2.1 Introduction to IPSA+	13
2.2 Method for Adaptation and Enhancement.....	14
2.3 Enhanced IPSA+ Platform	15
2.4 Conclusion	49
2.5 References.....	50
2.6 Appendix.....	51
3 MATLAB SIMULINK SIMULATION PLATFORM.....	52
3.1 The Simulation Platform Developed in INESC Porto.....	52
3.2 The Simulation Platform Developed in NTUA.....	86
3.3 References.....	110
4 EUROSTAG AND MATLAB SIMULATION PLATFORM.....	112
4.1 Description of the Simulation Platform.....	112
4.2 Adaptations and Enhancements	120
4.3 Results	126
4.4 References.....	136
5 PSS/E SIMULATION PLATFORM	138
5.1 Steady-State Simulation	138
5.2 Dynamic Simulation	185
5.3 References.....	215
6 PROBABLISTIC AND FUZZY POWER FLOW PLATFORM.....	217
6.1 Probabilistic Power Flow Platform.....	217
6.2 Fuzzy Power Flow Platform.....	234
6.3 References.....	255
6.4 Appendix.....	258
7 CONCLUSIONS	261

1 INTRODUCTION

Electric power systems are facing a number of challenges, for example, aging infrastructure, decarbonisation of power generation, supply reliability and security, and energy efficiency. There is a major new challenge (but also opportunity) which must be considered seriously: future massive integration of electric plug-in vehicles (EV) in the electric grid. At present electric power systems still follow planning rules and procedures defined for the traditional operational paradigm. It is necessary to identify and prepare solutions for the operational problems caused by the large penetration of EVs. Even though there are a number of software models and tools available for power system analysis, they do not facilitate analysis with EV connections. Therefore the main objective of this report is to adapt and enhance the existing steady and dynamic simulation platforms to deal with the integration of EV into the system. This work has taken into account the possibility of operating networks in two modes: normal interconnected mode and islanding mode (especially for distribution grids having dispersed generation sources). The models and tools to assess the steady state and the dynamic behaviour of LV Microgrids, MV distribution grids, and large interconnected systems having large scale integration of EV have been adapted and developed. Figure 1-1 gives an overview of the models and tools which have been adapted/developed and their domains of applicability under the framework of the whole MERGE project. The models and tools in red boxes are covered by this report.

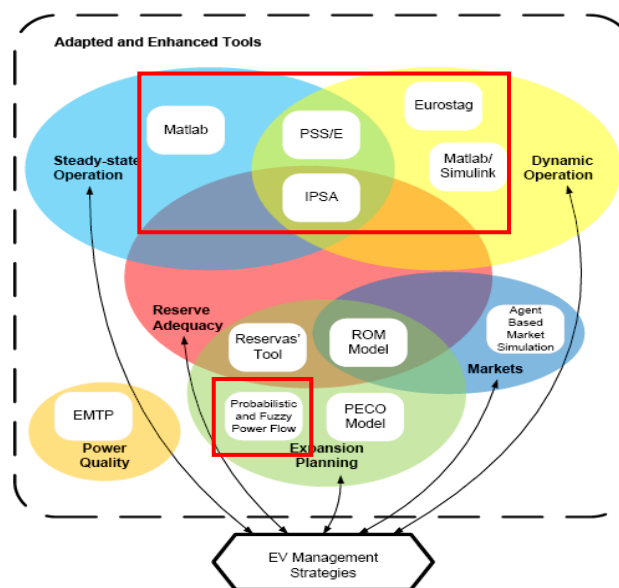


Figure 1-1: Models and tools which have been adapted/developed

The following software were used in this task:

(a) IPSA+

IPSA+ is a power system modelling software. The modelling tools used by IPSA+ have been developed over a period of nearly 30 years, and today continues the philosophy of a software tool which is easy to use without compromising analysis capability. IPSA+ has a full graphical user interface and provides a comprehensive range of analysis functions including load flow analysis, fault level calculation, transient and dynamic stability analysis, harmonics analysis, protection, and grading. Other extended features such as DC network modelling are also available in IPSA+. Various interfaces have been provided to extend the existing functionalities, and they include User Defined Models (UDM), Plug-in Models, and scripting based on Python.

IPSA+ software was adapted/enhanced based on its UDM (User Defined Model) tool and the scripted extension library for Python. Various EV-related models have been developed considering two types of interfacing structures, fast charging and shower charging, and different voltage levels, which are capable of incorporating specific control procedures; Reserve and frequency response models were adapted and enhanced to evaluate the performance of a network with different levels of EV penetration for providing the ancillary service; A spatial-temporal analysis tool was developed and integrated into the exiting IPSA+ tool to address the correlation of the mobility with population movement in an urban area.

(b) MATLAB

MATLAB is a numerical computing environment and fourth-generation programming language developed by MathWorks. MATLAB supports matrix manipulations, plotting of functions and data, implementation of algorithms, creation of user interfaces, and interfacing with programs written in other languages, including C, C++, and Fortran. Simulink was also developed by MathWorks, which is a commercial tool for modeling, simulating and analyzing multi-domain dynamic systems. Its primary interface is a graphical block diagramming tool and a customizable set of block libraries. It offers tight integration with the rest of the MATLAB environment and can either drive MATLAB or be scripted from it. An existing Microgrid simulation platform developed within the EU Microgrids project based on the Matlab/Simulink software was adapted/enhanced for this study.

The simulation platforms based on the MATLAB Simulink software developed in the EU Microgrids projects were adapted to incorporate EV models for smart charging and V2G operation in both normal and islanded modes. This development focuses on assessing impacts in Microgrids. After adaptation, these simulation platforms are capable of assessing the steady state and dynamic behaviour of Microgrids in three phase balanced mode and unbalanced mode. The dynamic stability of inverter dominated Microgrids was investigated.

(c) EUROSTAG

The EUROSTAG software allows fast simulation of power systems static and dynamic behaviors, and it also provides a suitable environment for the implementation of tailor-made models through embedded elementary blocks. However the EUROSTAG has limitations regarding the implementation of control algorithms, especially to establish logic/decision rules. Moreover, the software does not provide support for performing matrix operations and optimization procedures. Such limitations made the simulations with EV impossible if only the EUROSTAG development environment is used. Hence, MATLAB scripts were developed to invoke EUROSTAG functionalities which set up a complementary joint platform.

The simulation platform that works over Eurostag and MATLAB software was adapted to incorporated EV models for smart charging and V2G operating in both normal and islanded modes in MV distribution networks. MATLAB is used as an user interface and logic controller. Specific scripts (describing external procedures that invoke the basic simulation tools) were developed to simulate the step by step response of the system in quasi-steady state and in dynamic behaviour when following the load diagram in critical periods and adopting different charging strategies (dumb, tariff based approaches, smart charging strategies). The capability to perform load following in these networks with large EV presence was addressed with these tools.

(d) PSS/E

Power System Simulator for Engineering (PSS/E) is a software tool used for electric power systems. It is an integrated, interactive program for simulating, analyzing, and optimizing power system performance and provides probabilistic and dynamic modeling features. Since its introduction in 1976 it has become the most widely used commercial program of its type.

A simulation platform that works over PSS/E software was adapted to incorporate aggregated models of EV for steady state and dynamic studies of large interconnected transmission systems having conventional generation and a large penetration of renewable power sources (namely wind power). The aggregated EV response to frequency changes or other control signals was embedded in dynamic load models that represent clusters of aggregated EV. Specific scripts were developed to simulate the step by step response of the system in quasi-steady state and in dynamic behavior when following the load diagram in critical periods and adopting different charging strategies (dumb, tariff based approaches, smart charging strategies). For these studies, the Models of intermittent renewable generation (in particular wind power) were also developed.

(e) Fuzzy and Probabilistic Power Flow Tools

Apart from the deterministic simulations used to address steady impacts resulting from the presence of EV on the network for extreme conditions, the fuzzy and probabilistic tools were developed to evaluate the ranges of power flows, voltages levels and losses in the transmission network when large variations of EV penetration and the use of different charging strategies takes place leading to



significant uncertainty in node injections. The fuzzy power flow tool was adapted and enhanced to cope with EV nodal loads in a way that the important dependencies among EV load uncertainties in the nodes is taken into consideration. Besides propagating the uncertainties from the data to the results, providing fuzzy descriptions of the branch flow, node voltages and losses, the tool is able to identify the risk of congestion in branches and the degree of repression in the node injections and in the system. The probabilistic load flow tools were also adapted and enhanced to provide probabilistic density functions of flows, voltages and losses.

With these adapted and enhanced platforms, the comprehensive analysis of the EV impact on the electric power system and the provision of decision-making capability are possible.



2 IPSA+ SIMULATION PLATFORM

2.1 Introduction to IPSA+ [1]

IPSA+ is a power system modelling software. The modelling tools used by IPSA have been developed over a period of nearly 30 years, and today continues the philosophy of a software tool which is easy to use without compromising analysis capability. IPSA+ has a full graphical user interface and provides a comprehensive range of analysis functions including load flow analysis, fault level calculation, transient and dynamic stability analysis, harmonics analysis, protection, and grading. Other extended features such as DC network modelling are also available in standard IPSA. Various interfaces have been provided to extend the existing functionalities, and they include User Defined Models (UDM), Plug-in Models, and scripting based on Python.

User Defined Models: In general the UDM tools are used for detailed modeling of machine controllers, such as Automatic Voltage Regulators and Governors. The UDM models can be incorporated with a universal machine which acts as the interface between the UDM environment (that allows creating control blocks and user defined blocks) and IPSA environment (that allows creating power system components for steady state and transient analysis). Through a universal machine directly control of the real and reactive current or power injections onto a busbar based on network conditions can be achieved. The UDM application uses a graphical control block diagram to model controllers, so no coding ability or third-party compilers are required for users.

Plugin models: IPSA+ 1.4.5 introduced a new concept to IPSA+: the use of plugin models. This feature allows the creation of external IPSA+ models that are loaded at run time. They have no direct dependencies on IPSA+ so the user does not need to link against IPSA+ or require access to any IPSA+ source code. Originally developed as a parallel modeling technology to User Defined Models to model Wind Turbines, the plugin libraries use a simple customizable set of source code templates to provide the wrappers required to dynamically link to IPSA. Plug-ins are both faster and more flexible than UDM models, and allow developers to restrict access to their controller design. Model parameters can be hard coded within the plug-in, or set via component dialogs. At present plugins provide transient stability models only.

Scripting: IPSA+ has a scripted extension library for Python. This enables IPSA+ to be run without a user interface from within a Python shell. As the real power system becomes large and complex, it is very difficult to model the power system in the drawing canvas of IPSA+. Besides, in order to keep stability and safety, the power system should be monitored in real time, especially when the EVs are integrated to the grid causing more uncertainties. As a result, automatic analysis should be established. Python and Scripting provides a powerful tool to perform these functions. Python is an easy to learn, powerful programming language. It has efficient high-level data structures and a simple but effective approach to object-oriented programming. Python can run on Windows, Linux/Unix, Mac OS X, and has

been ported to the Java and .NET virtual machines. The Python extension dynamic-link libraries (dll) contains quite a lot of IPSA+ components (about 70%), which include the data model; the IIF file reading library; licensing; database, UDM and Protection data model; load flow; fault level; and Harmonics analysis. Based on this scripting interface, it is possible to read and write IPSA+ 'iif' network files; full access to view and/or modify all the network data including the analysis parameters; add, edit and view extension data; perform load flow, fault level and harmonics studies and get all the results; and compare two IPSA+ networks.

Figure 2-1 gives a brief example on how to use python and scripting to conduct the function of load flow in IPSA+.

```
ipsasys = IscInterface()
net = ipsasys.ReadFile("C:\\refinery.iif")
bok = net.DoLoadFlow();
if bok:
    busbars = net.GetBusbars()
    print "Load Flow results:"
    print ""
    print "BusName      Vmag(kV) "
    print "===== "
    for bus in busbars.itervalues():
        name = bus.GetName()
        vm = bus.GetVoltageMagnitudekV()
        res = "%-8s  %10.5f" % (name, vm)
        print res
else:
    print "Load Flow failed!"
```

Figure 2-1 Example of using python and scripting to conduct load flow [1]

2.2 Method for Adaptation and Enhancement

A simulation platform that works over IPSA+ based on its UDM tool and the scripted extension library for Python was developed and updated considering the specific characteristics brought by the large penetration of EV, e.g. controllability, mobility. The updated IPSA+ simulation platform includes

- Various EV-related models considering two types of interfacing structures, fast charging and slower charging, and different voltage levels, which are capable of incorporating specific control procedures;
- Reserve and frequency response models for evaluating the performance of a network with different levels of EV penetration for providing the ancillary services;
- A spatial-temporal model for addressing the correlation of the mobility with population movement in an urban area, which will facilitate the evaluation on the impacts of the large scale deployment of EV on urban electric power system. (There is a common characteristic of highly mobile nature of the population in an urban area, with mass swarming into the city centre typical of the early

morning and back out in the evening. This creates a shift not only of population density, but also a corresponding shift in energy generation and demand from the centre to the periphery along with the move of EV).

The method used for the adaptation and enhancement of IPSA+ simulation platform is shown in Figure 2-2. EV battery models and the EV frequency response model were built based upon UDM interface, the spatial-temporal model was build based upon the IPSA+ scripting interface and a commercial software from the transport area was used to provide analysis supporting functions.

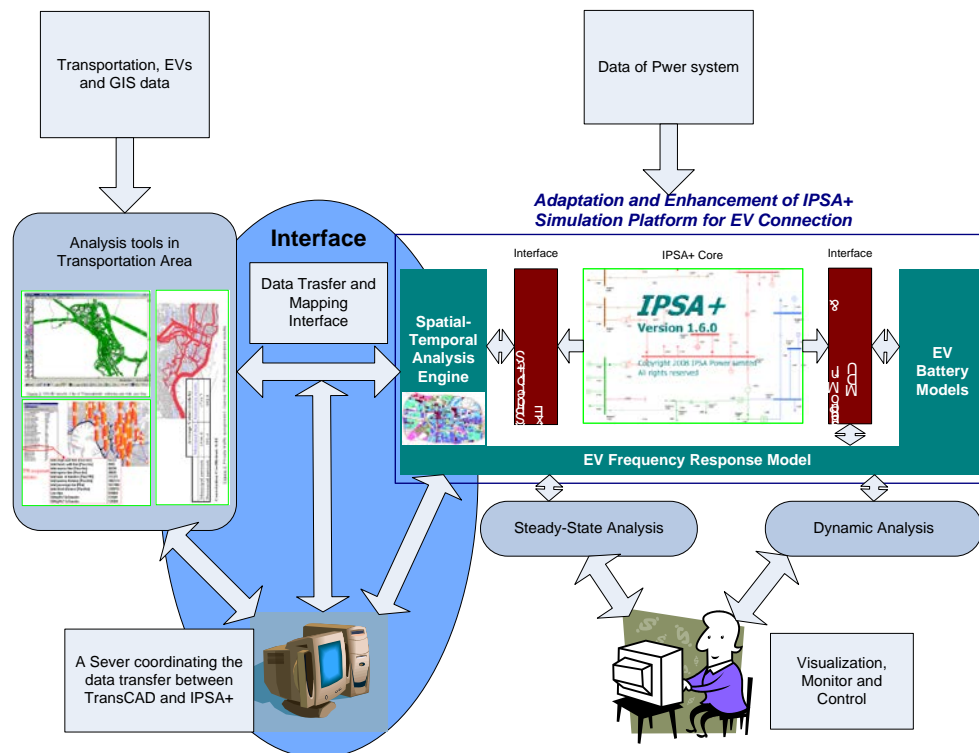


Figure 2-2 Method used for the adaptation and enhancement of IPSA+ simulation platform

2.3 Enhanced IPSA+ Platform

2.3.1 UDM based EV Battery Models

The Universal Machine object in IPSA+ was used to model the battery and converter of the EV. The Universal Machine object in IPSA+ provides a greater degree of flexibility for modelling complex devices such as converters and other power electronic equipment.

In transient studies, a Universal Machine can be represented as a current injection. Alternatively a Universal Machine can be represented as an active and reactive power injection. The injection type is user-defined for UDM models or Plug-in models. The amount of current or power injection is determined by the UDM or Plug-in model, which can represent the mathematical model of a battery or a converter. In

the load-flow, a Universal Machine is a power injection using generator convention for power flow. The Universal Machine has no effect in the fault level or harmonics.

Battery Model

Mathematical model of a battery is described as follows [2][3]:

$$V = E - Ri \quad (2-1)$$

$$E = E_0 - K \frac{Q}{Q-a} + A.e^{(-B.a)} \quad (2-2)$$

$$a = \frac{1}{3600} \int_{ip}^t idt \quad (2-3)$$

$$\text{Initial point (ip)} = (1 - SOC/100)Q \times 3600 \quad (2-4)$$

State of charge (SOC) %

$$SOC = 100 \left(1 - \frac{Q \times 1.05}{\int idt} \right) \quad (2-5)$$

where:

- A - Exponential voltage (V)
- B - Exponential capacity (Ah)
- E - No load Voltage (V)
- E_0 - Constant Voltage (V)
- i - Current (charging (-), discharging (+))
- K - Polarization voltage (V)
- Q - Battery capacity (Ah)
- R - Internal resistance
- SOC - State of charge
- t - Time
- V - Terminal Voltage

The typical battery discharge characteristics are shown in Figure 2-3.

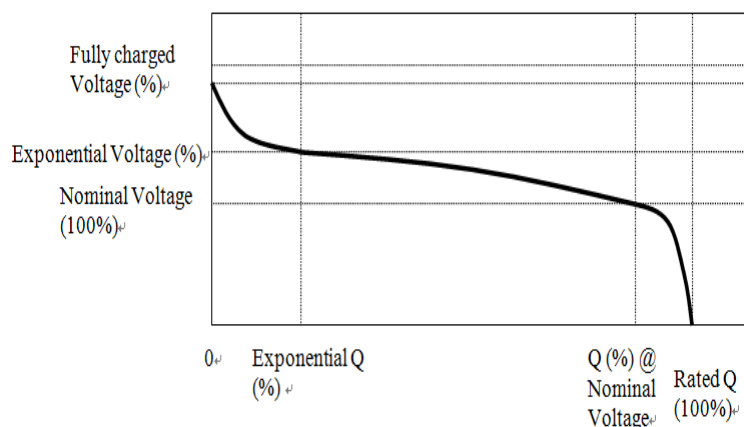


Figure 2-3: Battery discharge characteristics

Note that all the parameters of the model are deduced from discharge characteristics and assumed to be the same for charging for simplification (independent charging characteristics can be obtained using the same method). Various type of battery banks are used for the electrical vehicles. Parameters of different battery types used in the model development are shown in Table 2-1.

Table 2-1: Parameters of different battery types [3]

	Lead acid	Ni-cd	Ni-M-Hy	Lithium-iron
E_0	1.2645	1.2658	1.2848	1.2449
R (at $V_n=1.2V$ and $Q=1.5$)	0.02	0.02	0.02	0.02
K	0.033	0.00038017	0.001875	0.0029221
A	$V_{nominal} * 102.5\%$	$V_{nominal} * 103\%$	$V_{nominal} * 105\%$	$V_{nominal} * 103\%$
B	$Q_{rated} * 0.08\%$	$Q_{rated} * 40\%$	$Q_{rated} * 20\%$	$Q_{rated} * 85\%$
Fully charged V	$V_{nominal} * 108\%$	$V_{nominal} * 115\%$	$V_{nominal} * 117\%$	$V_{nominal} * 116\%$

UDM Module of the Battery Bank

In this study, the specifications of RAVi EV battery bank were selected to develop the UDM module [3]. The specifications of the RAVi EV battery bank are presented in Table 2-2, which were calculated according to the parameters of the battery type, capacity and terminal voltage of the battery bank.

Table 2-2: Specifications of RAVi Battery bank [3]

E	48 V
R	0.00597 Ω
E_0	50.5832 V
K	0.033 V
Q	201Ah
A	49.2V
B	0.1608Ah
SOC	30%
Initial point	506520A.s



RAVi Battery: 48V, 201Ah, Lead acid

The Universal Machine object in IPSA+ was represented as a real current injections device that represents the battery bank. The UDM module for a battery bank was constructed by the operational blocks, which is represented each mathematical operation of the model. No load voltage calculation is presented by equation 2-2 and relevant UDM model blocks are given in Figure 2-4. The battery bank specifications (A , B , K , Q , E_0) are the constant for the UDM module and these are given as constant inputs to the module. The constants parameters represent by nodes of the UDM block diagram (see nodes 2, 7, 8, 9, 17 and 14 in Figure. 2-4).

The operator blocks of the UDM model are given in s-functions. The block No. 18 in Figure 2-4 represents operation of integration. The initial point of the UDM integral operator block was defined according to the state of charge of the battery bank (see equation 2-3). The user defined UDM function block was customized to operate as exponential function ($ax_1e^{bx_2}$; where a , b are constants, x_1 and x_2 are variables) and power operations (ay^{bx} ; where a , b are constant, x is a variable). The block 5 represents the exponential function ($e^{-B.a}$) and the blocks 11, 15 represent the power function (y^{-1}). The functions of equation 2-2 and 2-3 are represented by the Figure 2-4. The current is the variable input to the no-load voltage calculation model.

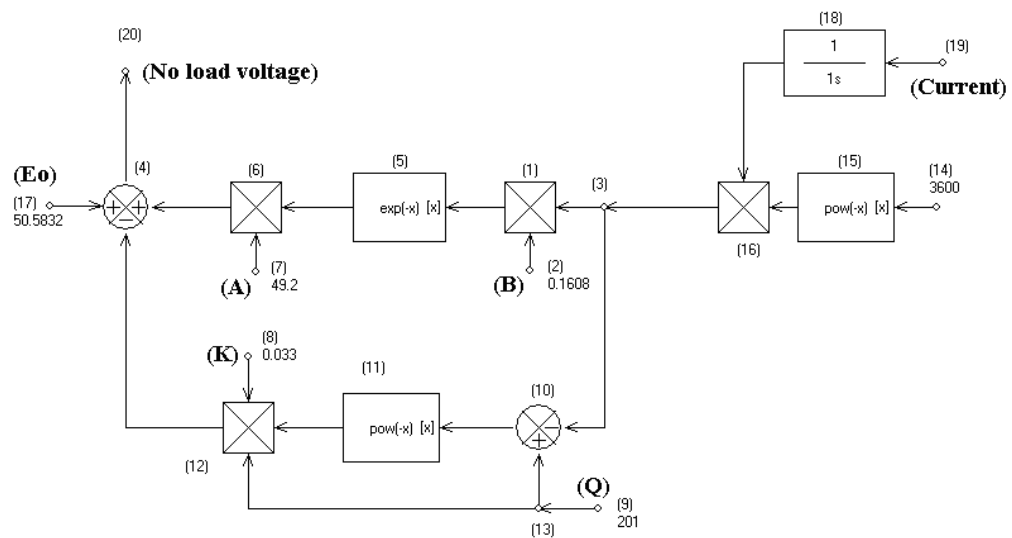


Figure 2-4: UDM model blocks for battery no-load voltage calculation

The UDM model blocks for battery current calculation are given in Figure 2-5. The function of equation 2-1 is represented by Figure 2-5. The internal resistance is a constant input and battery terminal voltage (V) and no load voltage (E) are variables for the model. The battery terminal voltage is input to the model as a p.u. value with reference to the busbar voltage. The block 7 was used to convert this p.u. value to real voltage value. For no load voltage calculations, calculated current value was used as a feedback loop (see Figure 2-4).

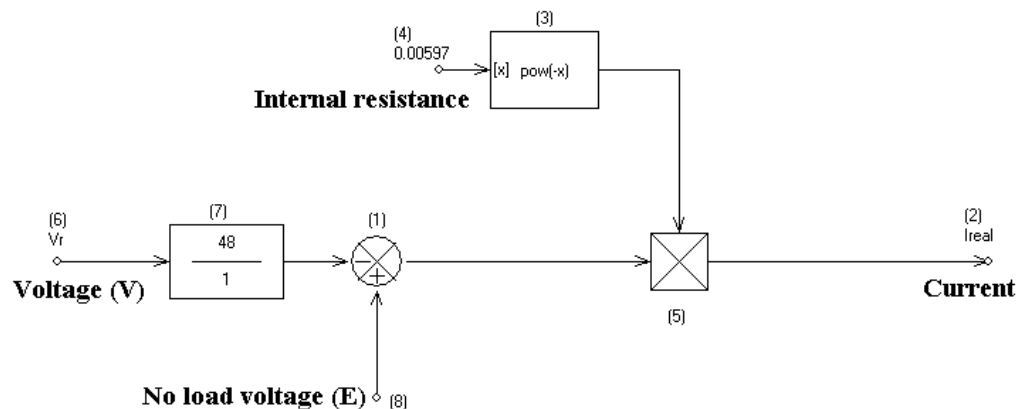


Figure 2-5: UDM model blocks for battery current calculation

The battery bank power output or input is determined by multiplying the calculated current and terminal voltage. Active power input or output of the Universal Machine object is controlled by varying real current, which is determined by the UDM module. The active power of the Universal Machine object was used as the feedback value

for the controlling unit. The UDM blocks for active power controlling are presented in Figure 2-6. Generally a reference value is required to operate the UDM module. In the Universal Machine object in IPISA+, the initial value of real power was assumed as 3kW (0.003MW) since the normal battery charging rate of an EV is 3kW. The blocks 4 and 8 in Figure 2-6 were used for smoothing the signals. The blocks 5 and 9 in Figure 2-6 represent control transfer functions, which were used to control the active power accordance with calculated battery output or input power.

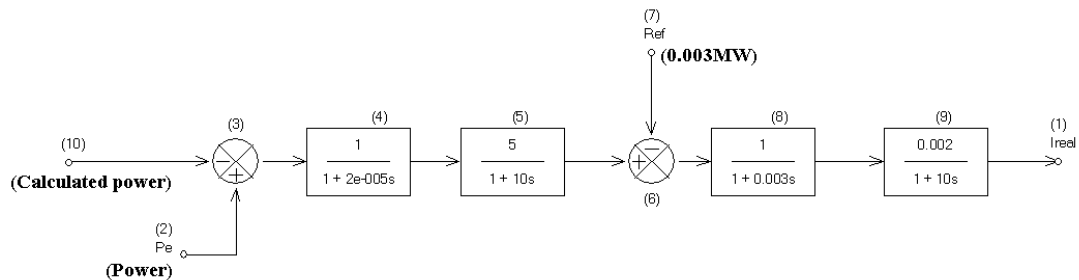


Figure 2-6: UDM blocks for active power controlling

Overall UDM module for a battery bank is given in Figure 2-7. This model was developed with the reference of the power flow. According to the variation of the power flow at the transient condition, the battery input or output power is determined by the battery terminal voltage (V). Active power of the Universal Machine object is adjusted by the control transfer functions (blocks 32 and 38 in Figure 2-7).

The Universal Machine object, which represents a battery bank, is connected to a busbar. Charging rate depends on busbar voltages and state of charge of the battery bank. Higher charging rates are occurred at higher busbar voltage and lower state of charge of the battery. Higher discharging rates are occurred at lower busbar voltage and higher state of charge.

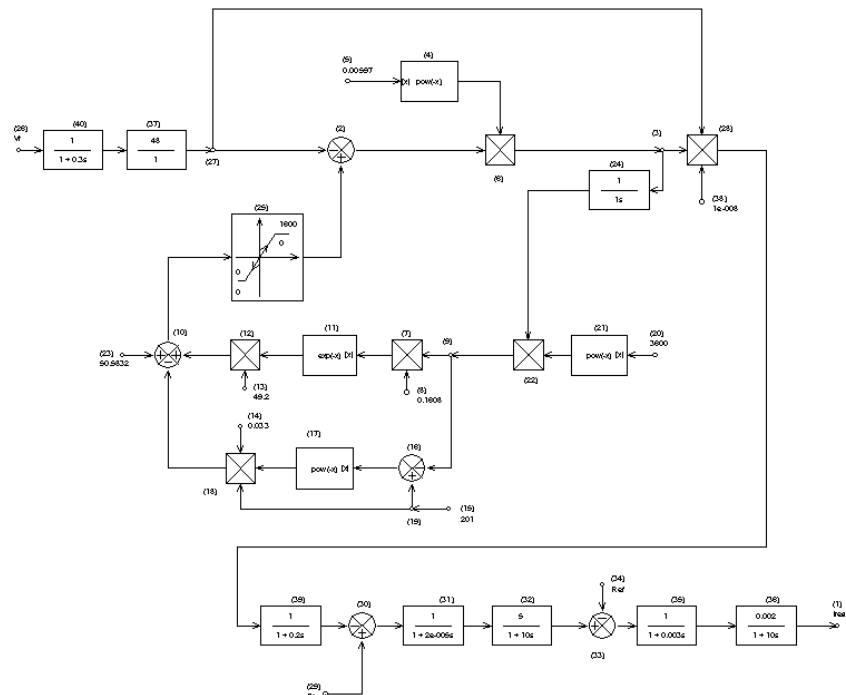


Figure 2-7: UDM Module for a battery bank of an EV

Test Results

A simulation was carried out for a constant battery terminal voltage. The battery charging test results for each battery types are given in Figure 2-8. For this simple test, the state of charge was taken as 70% and terminal voltage as 50V. Figure 2-9 shows that for a constant terminal voltage, the discharging current is decreasing with the time.

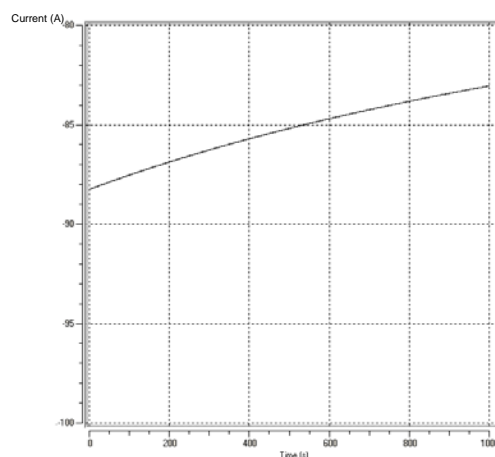
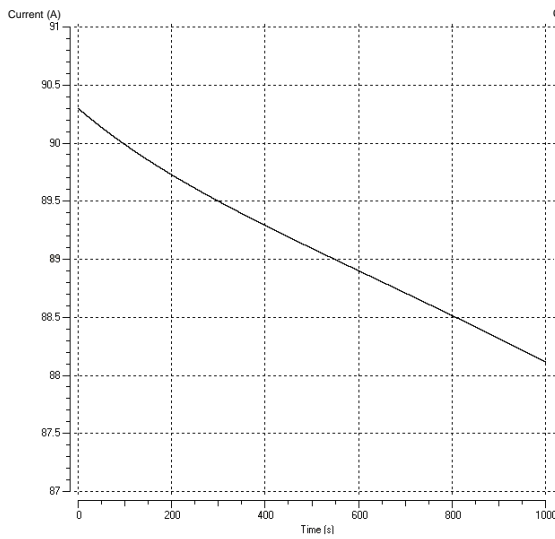
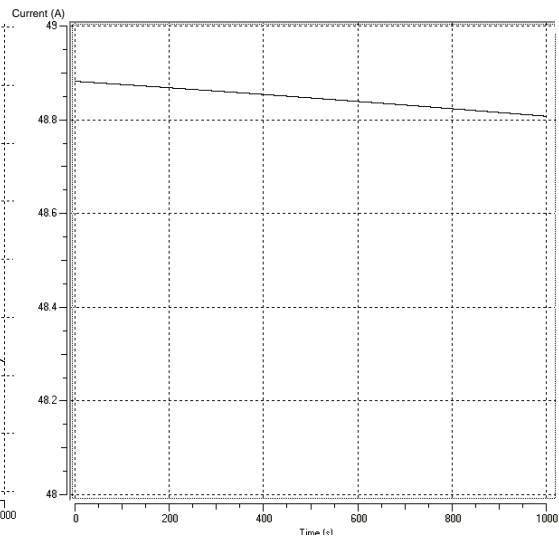


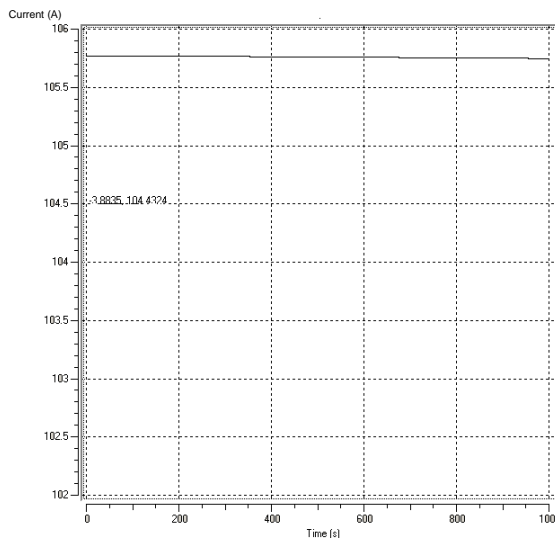
Figure 2-8: Lead-Acid Battery charging



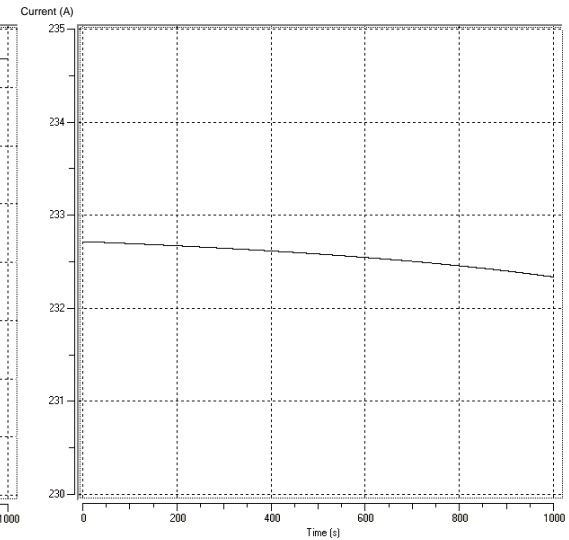
(a) Lead-Acid discharging



(b) Li-Ir discharging



(c) Ni-cd discharging



(d) Ni-m_hy discharging

Figure 2-9: Battery Discharging

2.3.2 Reserve and Frequency Model

Frequency Control in the GB System

Frequency is determined and controlled by balancing system demand and total generation. The nominal frequency of the GB system is 50Hz. If the demand is greater than the generation, the frequency falls below 50Hz. Conversely, if the generation is greater than the demand, the frequency rises above 50Hz. In practice, the frequency varies around 50Hz by a small amount as the system demand continuously changes. When there is a significant power imbalance of the system, the frequency will show a large deviation.

The Electricity Supply Regulations require the system frequency to be maintained at 50Hz $\pm 1\%$ [4]. The Transmission Licence places an obligation on the National Grid Company (NGC) to plan and operate the system to ensure compliance with the Electricity Supply Regulations [5]. To meet these obligations the system is designed to accept the largest credible loss of 1320MW of generation (two of the largest generators, 2 \times 660MW, on the system) and is operated to the following frequency containment policies:

- System frequency under normal operating conditions will be maintained within the operational limits of 50 \pm 0.2 Hz (NGC's current practice),
- For a sudden loss of generation or demand up to 300MW, the maximum frequency change will be limited to \pm 0.2Hz,
- For a sudden loss of generation or demand greater than 300MW and less than or equal to 1000MW, the maximum frequency change will be limited to \pm 0.5Hz,
- For a sudden loss of generation greater than 1000MW and less than or equal to 1320MW, the frequency change will be limited to -0.8 Hz with frequency restored to 49.5Hz within 1 minute.

Any loss of generation greater than 1320MW will be treated as an emergency condition as it may cause the system frequency to fall below 49Hz. Automatic low frequency load shedding arrangements usually commence at 48.8Hz. In the event that the frequency is above 52Hz or below 47Hz, the independent protective actions are permitted to protect generators against danger to plant and/or for personnel safety.

A typical frequency transient for a generation loss of 1320MW is shown in Figure 2-10 [5][6].

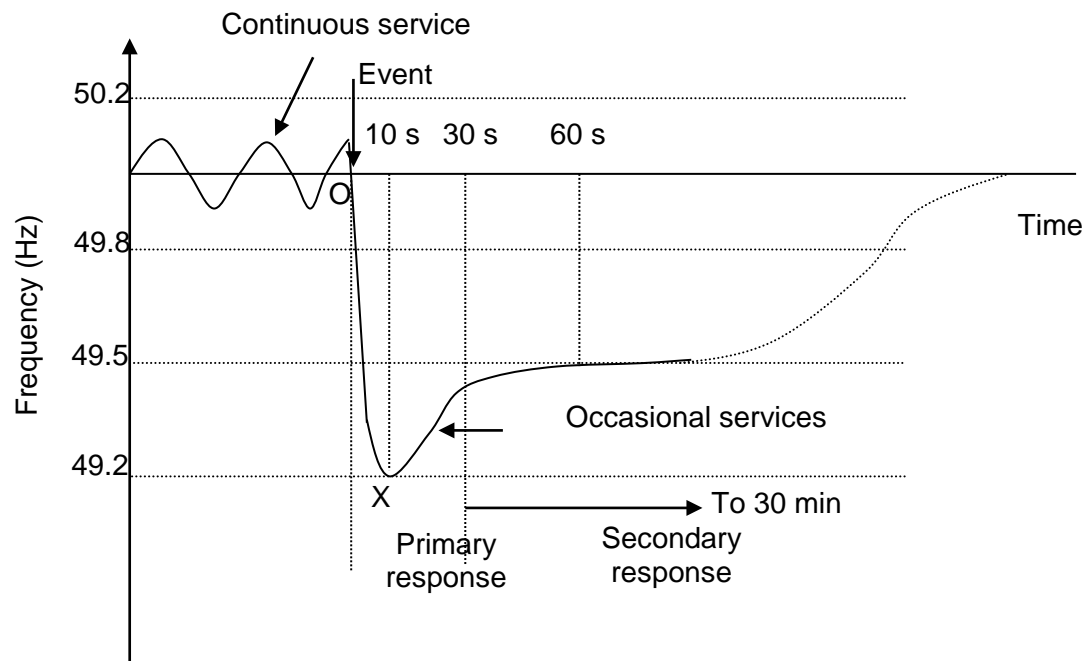


Figure 2-10 Typical frequency deviation following a loss of 1320MW generation [5]

Figure 2-10 shows two frequency control services used by NGC, continuous service and occasional service. Continuous service is primarily provided by the central generators, which are equipped with appropriate governing systems. This service is automatically delivered by synchronised generators, which are agreed to operate in frequency sensitive mode and primarily provided by pump storage and part-loaded steam plants.

Occasional services are called upon during a frequency event so as to maintain the system frequency within the frequency control requirements. These services are provided by both generating plant and loads (mainly some industrial customers who could shed their loads). For the purpose of procuring automatic frequency response services, the following service definition are used [4][5]:

- (1) **Primary response:** Following a loss of generation, the initial short-term, automatic power output increase in response to the negative frequency change is termed primary response. This response is essential to minimise the initial frequency dip shown in Figure 2-10. Power is released increasingly with time, through generator automatic governor action, in the period 0 to 10 seconds from the time of the frequency fall and sustained for a further 20 seconds. In the NGC system frequency containment is normally achieved within 7 to 15 seconds of the initial disturbance, depending on the system demand level, system inertia and size of generation loss.
- (2) **Secondary response:** The automatic positive power response in the subsequent frequency stabilisation phase, beyond 30 seconds to 30 minutes after the incident, is termed secondary response. The purpose of secondary response is to contain and partially recover the frequency after the fall has been

arrested. Full delivery is required within 30 seconds to replace primary response as it is exhausted.

- (3) **High frequency response:** If there is a sudden loss of the system load causing the frequency to rise above its target level, the automatic reduction in power output is termed high frequency response. Generation output is reduced increasingly with time over 10 seconds. This is the characteristic time that is taken for the frequency to rise by 0.5Hz on the NGC system for a demand loss of 1000MW.

Once the system frequency returns to its standby level, NGC calls upon reserve to restore the system frequency to operational limits and to re-establish the level of responsiveness in the system following a short-term loss.

The plug-in electric vehicles will increase the mean system load and the variance. The uncertainty brought by EV loads will demand considerable increase in frequency response and reserve that NGC should maintain to ensure frequency performance within the control limits. Another issue of EV is as they are connected to the grid through a power electronic interface, they will not contribute to the system inertia. This reduction in the overall system inertia and the increase of demand will lead to rapid change in frequency during phase OX (see Figure 2-10).

In this section, the main emphasis will be on the enhancement of existing IPSA+ platform to provide EV frequency response analysis capability.

The GB System Model for Frequency Control

▪ Power System Representation

Assuming a coherent response of all generators in the system to changes in the load, the power system can be represented by an equivalent generator [7]. The equivalent generator has an inertia constant H_{eq} and calculated using the following equation:

$$H_{eq} = \sum_{i=coal, gas, \dots} H_i * \frac{S_i}{S_{sys}} \quad (2-6)$$

where H_i and S_i are the inertia constant and MVA rating of the individual power plant.

A simple model representing the inertia and damping of the GB system without the contribution due to governor action of synchronous generation is shown in Figure 2-11. In the model ΔP_m refers to change in mechanical power of all the generators on the GB system and ΔP_L is any change in total load. The damping providing by rotating loads is lumped into a single damping constant D .

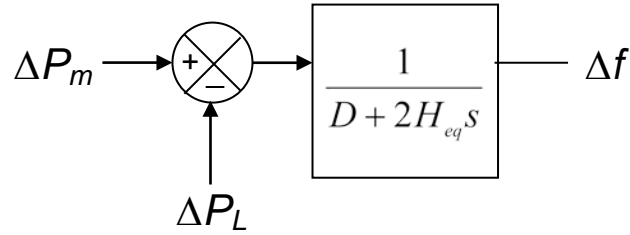


Figure 2-11 The system equivalent for frequency control analysis

▪ Turbine-Governor Model

The composite power/frequency characteristic of the power system depends on the combined effect of the droops (R_1, R_2, \dots, R_n) of all generator speed governors. It also depends on the frequency characteristics of all the loads in the system. For a system with the n generators and a composite load-damping constant of D , the steady-state frequency deviation Δf_{ss} following a load change ΔP_L is given by equation (2-7).

$$\Delta f_{ss} = \frac{-\Delta P_L}{(1/R_1 + 1/R_2 + \dots + 1/R_n) + D} = \frac{-\Delta P_L}{1/R_{eq} + D} \quad (2-7)$$

Where, the composite governor speed droop can be written as equation (2-8):

$$R_{eq} = \frac{1}{1/R_1 + 1/R_2 + \dots + 1/R_n} \quad (2-8)$$

The typical speed droop setting for both thermal and hydro generator governors is around 5% in per unit value. Thus, a system (as above) with a number of machines, each with a droop of 5%, will have a total system speed droop R_{eq} of 5%. However, the actual speed droop may range from 2% to 12%, depending on the different types of unit [7].

Taking account of the characteristics of steam and hydro turbines in the system, a system turbine-governor model shown in Figure 2-12 can be derived. The speed control of the turbine is provided by a droop governor with an equivalent gain value, R_{eq} . It operates on an input of the speed deviation formed between the reference speed and the actual speed. This changes the governor valve (steam turbine) or gate (hydro turbine) position. The typical governor actuator time constant, T_G , is 0.2 second. For a stable performance of the speed control, a transient-droop-compensation, which is a lead-lag transfer function with time constants T_1 and T_2 , is introduced between governor and turbine. The turbine relates the response of mechanical power output following the governor action and is characterised by a time constant T_T which varies between 0.3 and 0.5 second.

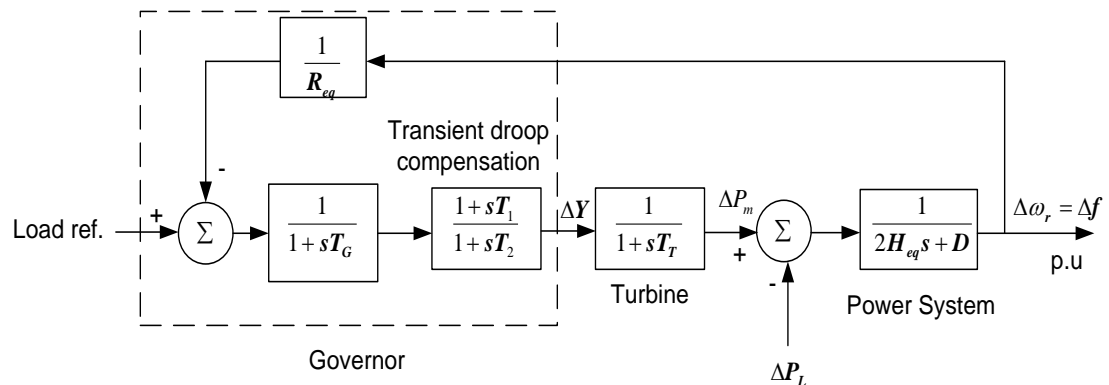


Figure 2-12 Block diagram of a system turbine-governor model

The parameter values of the single generator model shown in Figure 2-12, were obtained through parameter identification and model validation. A severe frequency event shown in Figure 2-13 which occurred in the UK on 27th May 2008 was used for validation.

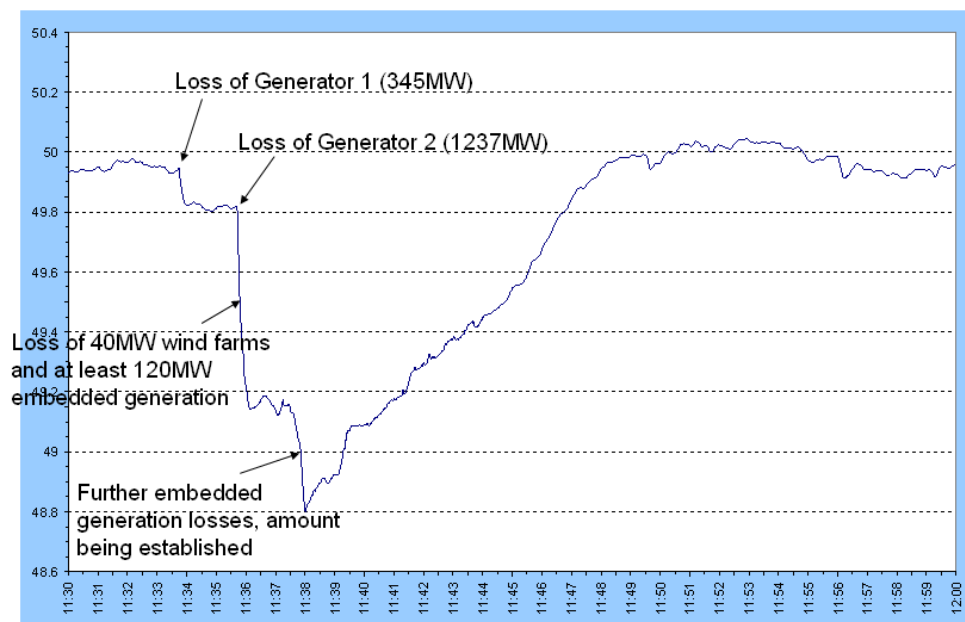


Figure 2-13 Frequency response on 27th May 2008

(<http://www.nationalgrid.com/NR/rdonlyres/D680C70A-F73D-4484-BA54-95656534B52D/26917/PublicReportIssue1.pdf>)

▪ The GB System Model

As the first step towards assessing frequency response from EVs, the GB system model was implemented in Simulink. Initially the model parameters were tuned to meet the 27th May 2008 event. Then H_{eq}^{wa} s calculated for 2020 s_{ys} tem as shown in the following table.

Table 2-3 Parameters used in the model

Generator type	Assumed Capacity	H_i	H
New Coal	2.41	6.0	0.23
Coal	9.30	6.0	0.88
Gas	15.02	9.0	2.13
Nuclear	6.00	4.5	0.43
Interconnector	3.30	0.0	0.00
Other	4.76	6.0	0.45
Onshore wind	5.72	0.0	0.00
Offshore wind	13.68	0.0	0.00
Other renewables	3.36	6.0	0.32
Total	63.54		4.44

Figure 2-14 shows the model used to investigate the EV frequency response for the 2020 GB system. It was assumed that immediately after a frequency event is detected, EVs which are charging on the power system are disconnected using a frequency sensitive switch. In this case it was assumed that the total system speed droop is -9%, thus giving $1/R_{eq}$ of -11.

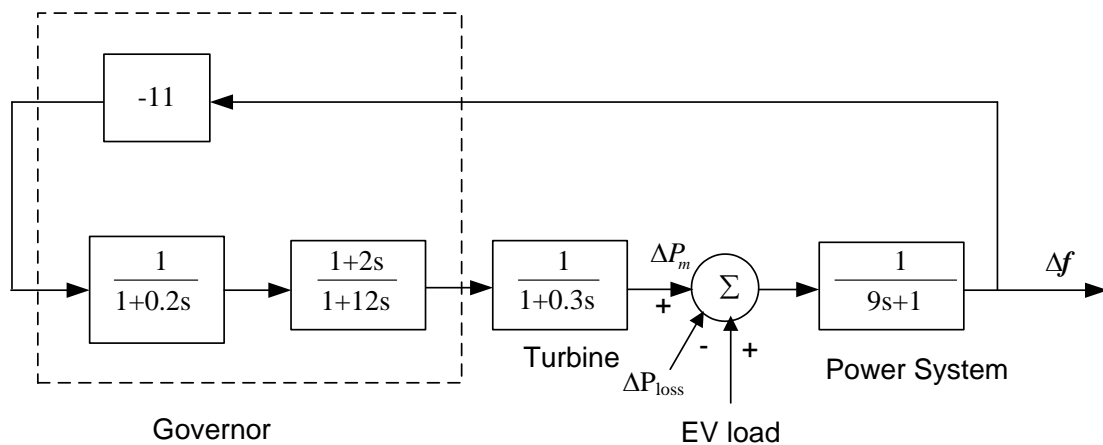


Figure 2-14 GB system model to investigate EV frequency response

A two-stage method was proposed to analysis the frequency response from EVs:

Stage 1: Estimate the grid-connected EV load.

Stage 2: Combine the EV load information with the simplified GB system model and carry out analysis.

This two-stage method is shown in the flow chart shown in Figure 2-15.

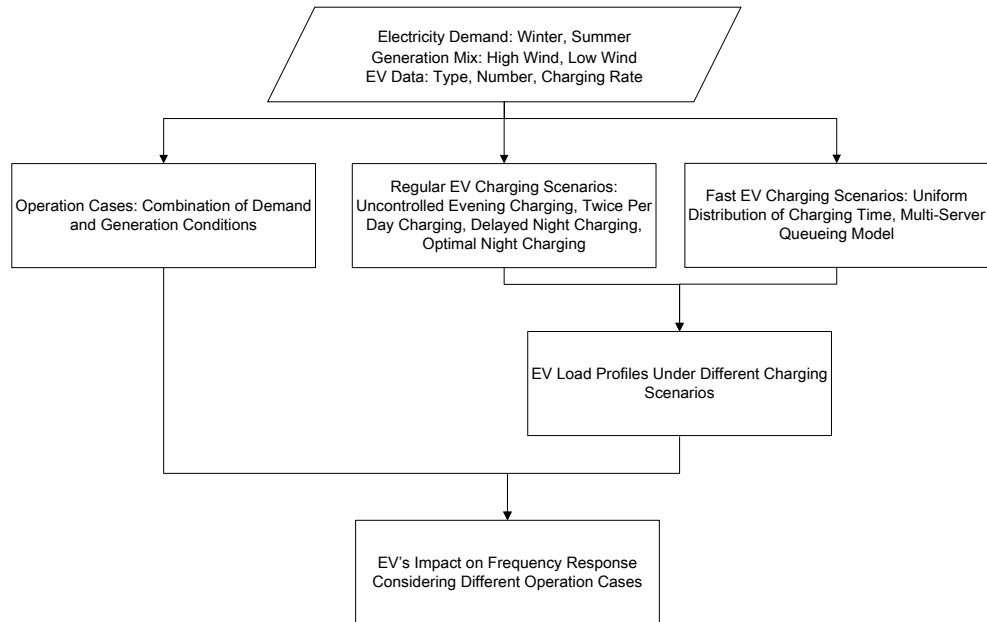


Figure 2-15 Estimation of the grid-connected EV load

Test Systems

The reserve and frequency models were tested to evaluate the performance.

- Estimating the grid-connected EV load

To investigate the impact of the EV participation, the realistic 24-hour EV load profiles were obtained based on reasonable predictions and assumptions of EV market penetration, technical specifications, and use patterns (especially charging patterns), which is different from conventional load forecasting because there is no historical EV use data available for reference..

To determine regular EV charging scenarios shown in Figure 2-15, a probabilistic approach was used. The effective period an EV should be charged depends on the state of charge (SOC) at the beginning of the charging cycle. The SOC level at the starting of charging, SOC_0 , is calculated using equation (2-9) assuming that at the beginning of the day the battery is fully charged and SOC is equal to 1.

$$SOC_0 = 1 - \frac{\text{Daily Mileage}}{\text{EV Range}} \quad (2-9)$$

Figure 2-16 shows a typical charging curve of an EV. Once SOC_0 is established using equation (2-9) (daily mileages and EV range for different EVs considered in this study are given in Appendix 2-I), it is possible to obtain the minimum charging

duration, T_{ECD} , for a given EV. The charging curve given in Figure 2-16 is for an EV having a total charging duration of 8 hrs. Appendix 2-I also gives charging time of different EVs.

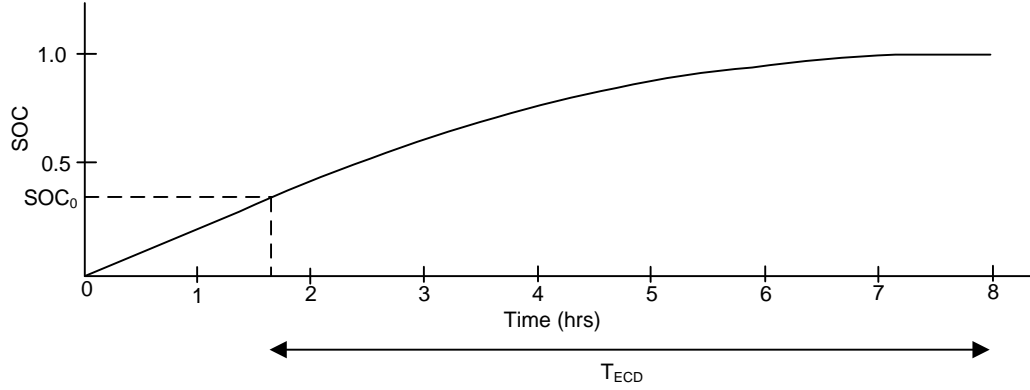


Figure 2-16 Typical charging curve of an EV battery

Once SOC_0 and T_{ECD} are established for each EV, the power demand is calculated using the following equation:

$$E[P_i(t)] = \int_0^t p_i(t, x) f_i(x) dx \quad (2-10)$$

where

x : time instant when charging start;

$f_i(x)$: probability density function of x ;

$p_i(t, x)$: power drawn at time t when charging start at x ;

$E[P_i(t)]$: expectation value of power demand (cumulative) at t .

The above equation is rearranged as

$$\begin{aligned} E[P_i(t)] &= \int_0^t p_i(t, x) f_i(x) dx \\ &= \int_0^{t-T_{ECD}} p_i(t, x) f_i(x) dx + \int_{t-T_{ECD}}^t p_i(t, x) f_i(x) dx. \end{aligned} \quad (2-11)$$

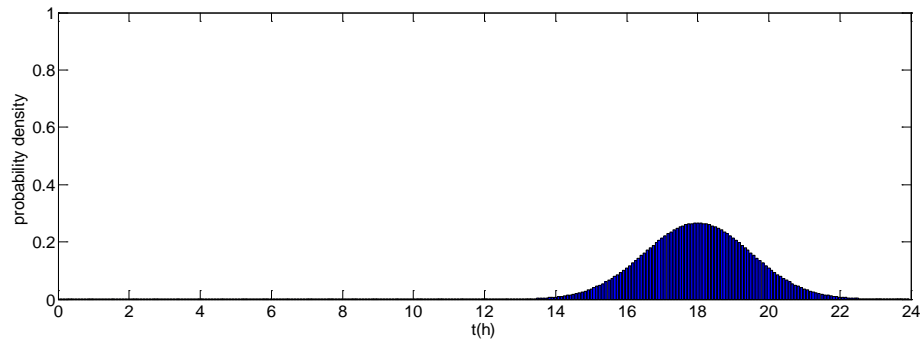
when $x \leq t - T_{ECD}$, i.e., $t \geq x + T_{ECD}$, $p_i(t, x) = 0$ (the battery is full and stops charge), so

$$\begin{aligned} E[P_i(t)] &= \int_0^t p_i(t, x) f_i(x) dx \\ &= \int_{t-T_{EDC}}^t p_i(t, x) f_i(x) dx. \end{aligned} \quad (2-12)$$

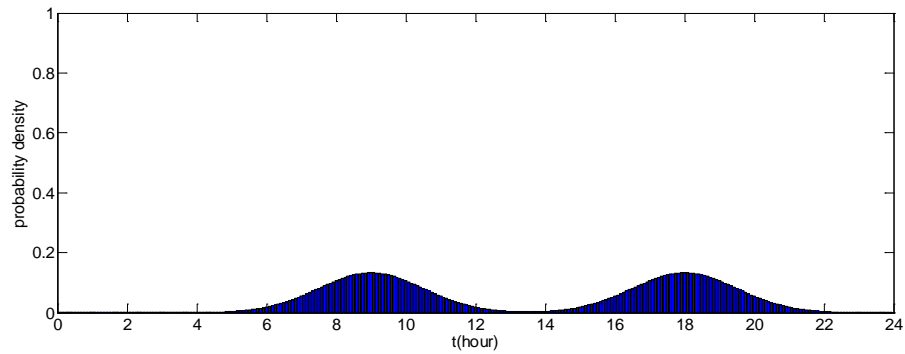
For a fleet with N EVs, the total power demand (expectation value) at any time instant t is computed as

$$E\left[\sum_{i=1}^N P_i(t)\right] = \sum_{i=1}^N E[P_i(t)] \quad (2-13)$$

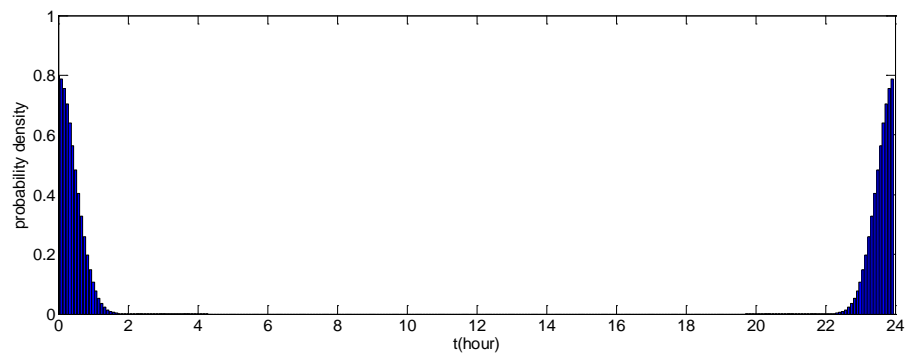
The function $f_i(x)$ is determined by charge mode and in this study three time dependent charging modes namely after-work charging, on-work and after-work charging and delayed night charging were considered. In each case normal distributions shown in Figure 2-17 were assumed.



(a) After-work charging
Mean value $\mu = 18$ and standard deviation $\sigma = 1.5$



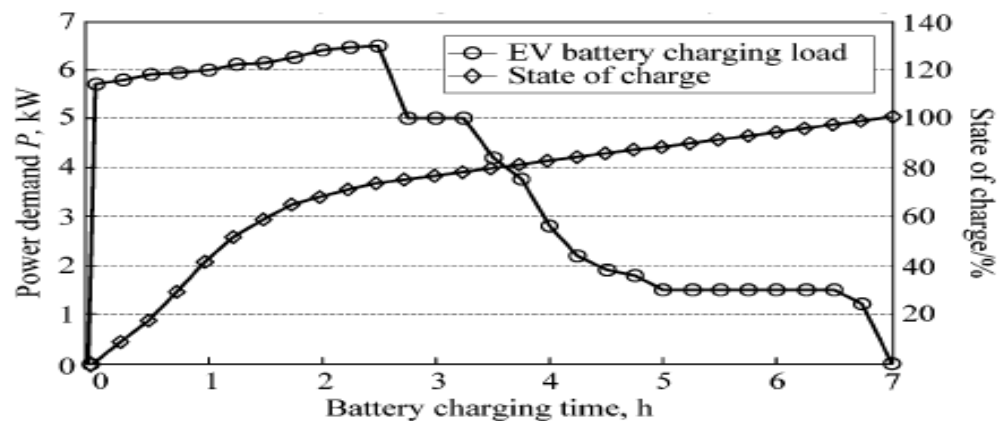
(b) On-work and after-work charging
Mean values $\mu_1 = 9$, $\mu_2 = 18$ and standard deviation $\sigma_1 = \sigma_2 = 1.5$



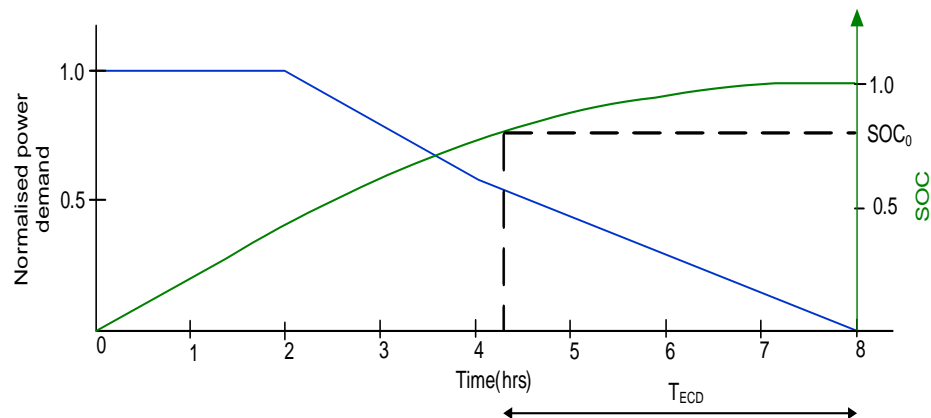
(c) Delayed night charging
Mean value $\mu = 24$ and standard deviation $\sigma = 0.5$

Figure 2-17 Charging modes considered in this study

The value of $p(t, x)$ depends on the battery charge profile. The power being drawn from the power system is not constant during a charge cycle and is generally nonlinear. Figure 2-18(a) shows a typical charging profile of a Lead-Acid battery used in an EV. In order to derive similar curves for different EV types described in Appendix 2-I, the power demand curve given in Figure 2-18(a) was normalized and then it was approximately linearised as shown in Figure 2-18(b).



(a) Typical power demand curve of a EV lead-acid battery [8]



(b) Normalised power demand

Figure 2-18 Typical charging curve of an EV battery

Duration of a fast charge cycle (from 0 to 0.8 SOC) is typically from 10 minutes to 30 minutes. Since the duration is short, it is reasonable not to consider the time-variant characteristics, i.e., power drawn during the cycle is regarded as a constant. Temporal distribution of fast charge activities is much more dispersed than that of slow charging. An assumption was used that the number of fast charging vehicles is proportional to the temporal distribution of vehicle traffic on roads.

▪ Numerical Results (UK)

The information used in this study was mainly from reference [9]. For the mode of slow charging once per day, the average SOC_0 and T_{ECD} for each class of EV was calculated using equation (2-9) and Figure 2-18 and given Table 2-4.

Table 2-4 Parameters used in the study

EV classification and types		SOC_0	T_{ECD} (hour)
I7e	BEV	0.7765	3.576
M1	BEV	0.7811	3.502
	PHEV	0.3617	6.264
	REV	0.4108	5.903
	BEV	0.5333	5.754
N1	PHEV	0.0667	7.680
	REV	0.1765	7.153
N2	BEV	0.0933	7.552

Based on the information obtained above, the EV power demand profiles for 2020 were obtained for three charging modes and shown in Figure 2-19.

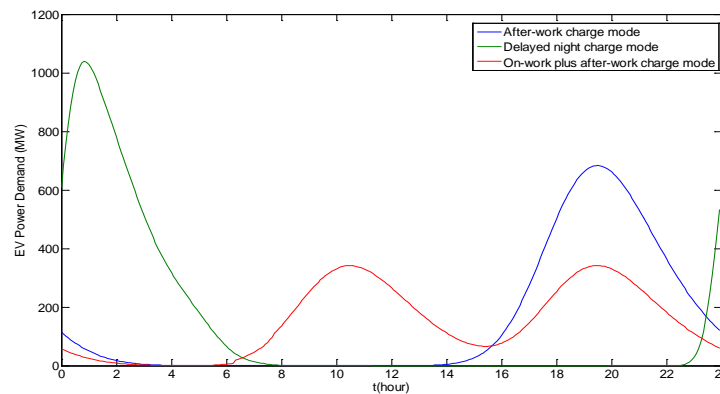


Figure 2-19 EV power demand profile for three charging modes considered

Assuming different proportion of slow charging and fast charging EVs, the daily EV power demand profiles shown in Figure 2-20 were obtained. In this case it was assumed that the fast charge rate is 45 kW and the charge cycle duration is 30 minute.

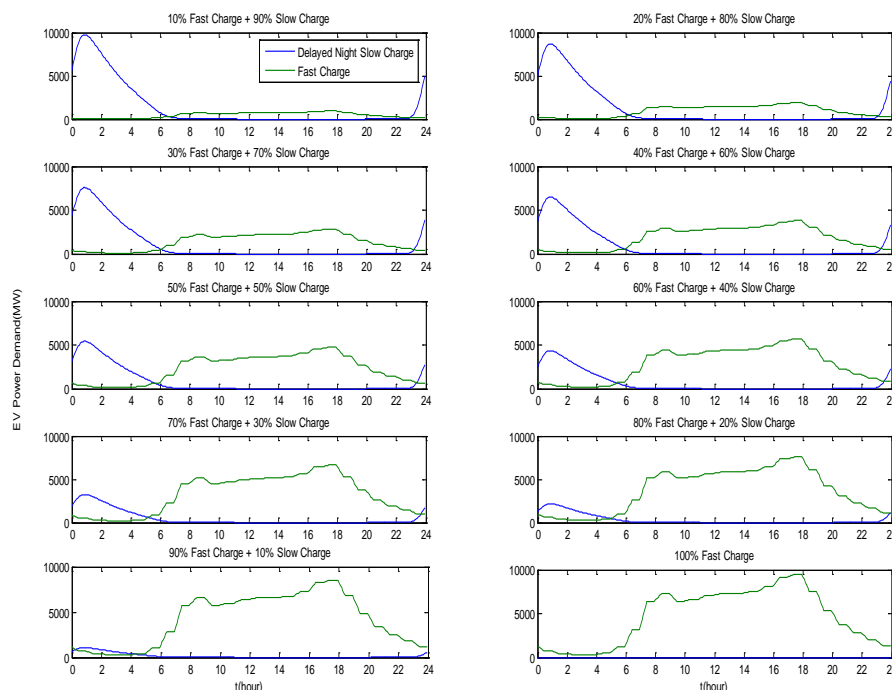
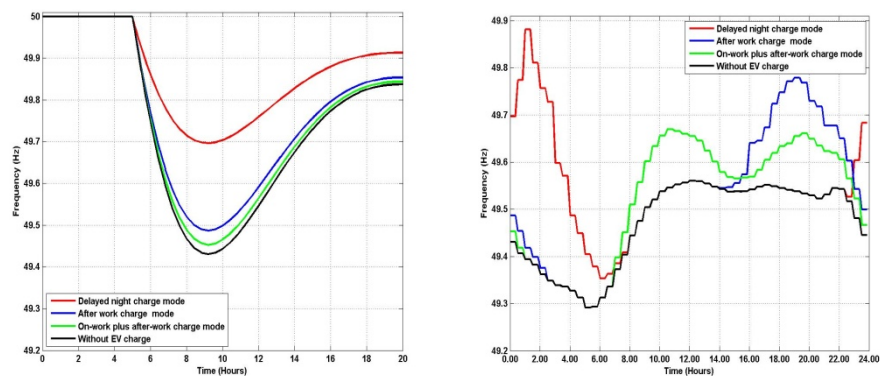


Figure 2-20 Daily EV power demand profile for mixed charging mode

Based on the obtained EV power demand profiles and the developed GB system model, shown in Figure 2-14, the contribution from EVs for frequency response was studied. Figure 2-21 shows the EV contribution to the primary frequency response under three modes considered and with a low GB demand. It was assumed that

demand in 2020 is as same as in 2008 due to electricity network efficiency improvement activities in GB. The demand used in the simulations is the minimum summer GB demand in 2008 plus the three EV load profiles shown in Figure 2-19. It is assumed that the EV loads will be disconnected as soon as frequency starts to drop. The disturbance was assumed to be 1320 MW. Figure 2-21(a) shows the frequency change with time at an arbitrarily selected time (at 12 mid night). Figure 2-21(b) shows the maximum frequency excursion that will experience, without the support of EVs and with their support (by shedding the charging load) under three charging modes considered.



(a) Frequency drops at 00.00 hrs

(b) Maximum frequency drops at every 10 min during a day

Fig 2-21. Change in frequency when 1320 MW generation is lost in 2020 GB system (with minimum demand).

2.3.3 Spatial-Temporal Model Based on IPSA+ and TransCAD

Electrical Vehicles can be considered as a kind of mobile energy resource. The large penetration of plug-in EVs could potentially produce significant impact on the urban electric power distribution infrastructure. The features of EVs are showed as follows:

- Plug-in EVs represent a new type of non-linear load that cannot be characterized by examining any previous comparable loads on the power system.
- EVs are mobile rather than stationary source of demand.
- Because EVs are charged for relatively long time periods and closely related to human behavior, EVs could place significant coincident demand on the system.
- EV load is unpredictable. It can appear on the system without advance notice and in multiple locations. Without proper planning and load management, substation and circuit rebuild costs could be substantial.
- Because of the uncertainty, knowledge of load behavior (EV purchasing, charging behavior, and routine trip in particular) is required in order to determine the location and consequences of load impacts.

Comprehensive analysis on EV transportation patterns is able to reduce uncertainties. For example, a common characteristic of the population in an urban area is early morning mass swarming into the city centre and back out in the evening. This creates a shift in EV energy demand (or generation). Detailed information on such transportation pattern will facilitate the assessment of the EV impact on the power system. The spatial-temporal model was developed as a new tool to address the aforementioned EV features and provide detailed insight into system impact. TransCAD [10][11] is used along with IPSA+ to implement the spatial-temporal model.

Introduction to the TransCAD platform

The TransCAD developed by Caliper Corporation is a Geographical Information System (GIS) designed specifically for use by transportation professionals to store, display, manage, and analyze transportation data. TransCAD combines GIS and transportation modelling capabilities in a single integrated platform [10].

TransCAD is mainly composed of five parts, as shown in Figure 2-22.

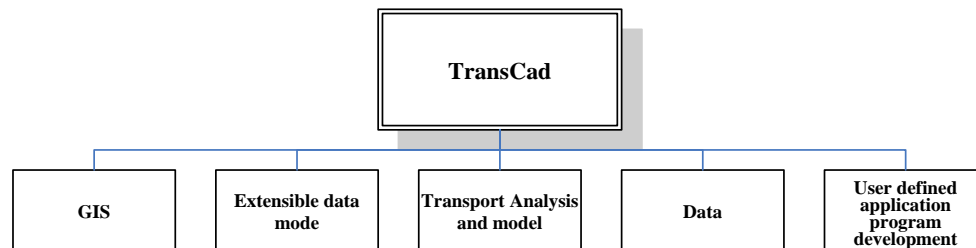


Figure 2-22 Structure of TransCAD

- **GIS:** TransCAD provides completely integrated GIS and transportation analysis to create and customize maps, build and maintain geographical data sets, and perform many different types of spatial analysis.
- **Extensible data mode:** In order to meet the demand of GIS, TransCAD contains several extensible data modes. These new data modes and the conventional GIS data mode can be processed together, which is convenient and powerful to conduct analysis.
- **Transport Analysis and model:** Application modules in TransCAD are fully integrated with GIS functions for improved performance and ease of use, such as the vehicle routing and dispatching. The program and model in TransCAD can also be updated to meet the development of transportation and logistics.
- **Data:** TransCAD has a comprehensive database of geographic, demographic and traffic information. A comprehensive tool is integrated in TransCAD to create, edit, import and export the GIS data.
- **User defined application program's development:** TransCAD has the GIS developer's kit (GISDK) and the programming language of Caliper Script. GISDK is a comprehensive development environment in which the TransCAD can be conducted secondary development in three ways: 1) Create embedded application and macro language program in order to add new functions or repeat the same operation; 2) Establish an application program with completely different user interface and custom program to conduct secondary development. 3) Take the TransCAD as a COM server, in which the macro program and other functions can be called by VB, VC or some other programs in order to create map server and network application program. GISDK allows the users to launch other application program to communicate with itself or the program written by third party, which makes TransCAD become a powerful platform to develop and test new analysis program. This function was used to develop the interface to the IPSA+ platform.

Architecture of the integrated IPSA+ and TransCAD platform

It can be seen from Figure 2-2 that TransCAD is integrated to IPSA+ by a Data Transfer and Mapping Interface, which was developed under MERGE. This interface has the following functions:

- **Data Transfer and Mapping:** TransCAD is used to obtain the transportation, EVs and GIS data, and map them to IPSA+ by dedicated algorithms resided in this interface. The GISDK in TransCAD was used for implementation.
- **Data Flow Management:** The data flow is managed by a master program which can coordinate the data (EV loads data) between TransCAD and IPSA+.

When the EV load data from TransCAD are available, further analysis and simulation can be done by IPSA+. The spatial-temporal model was implemented in a Spatial-Temporal Analysis Engine as shown in Figure 2-2.

Load flow analysis based on the spatial-temporal model

Load flow is an important tool involving numerical analysis applied to a power system. Load flow studies are widely used in the operation and planning of electric power systems. It has been recognised that large-scale adoption of EVs would have a significant impact on nationwide electric power generation and on distribution system. A study in [12] shows that a substantial rise in the number of EVs would have a much lower impact on the national power grid than that of previously thought due to the fact that the UK has sufficient power generation capacity to absorb the EVs charging load. However, EVs are usually connected to the local residential areas which are often heavily loaded during peak time. Hence detailed analysis at the distribution level is required to assess the impact from EVs.

Several studies were carried out on load demand model of the EVs outside the MERGE consortium. The model proposed in [13] was applied to determine the optimum charging time as a function of the exiting load, ambient temperature, and time of day. However, several simplifications were made: all chargers were assumed to start at the same time, and batteries were charged from fully discharged state. In fact, the power demand of EV battery charging loads depend on the number of EVs, the time of switch-on and off of the EVs battery charging, and the initial state-of-charge at the beginning of the charging process. It is obvious that the EV load has a degree of uncertainty. A method was developed in [8] to model numerically EV battery charging load, allowing for considerations of statistical distribution of the states of charge of the batteries at the beginning of the charge cycle, and the stochastic distribution of the instants when EV chargers are switched on and off within a distribution system. EV is a kind of mobile energy resources, therefore the transport patterns of EVs influence when and where to charge. Analysis of the transportation patterns can reduce the uncertainties of power demand caused by EVs thus benefits the power system operation and planning. A new load flow analysis method based on the spatial-temporal model was developed, which employs O-D (Origin-Destination) Analysis from the transportation area.

O-D Analysis:

The O-D survey was used to find out the source and flow of traffic. By using the O-D survey, the EVs original points, destination points and moving routes are available to obtain the O-D matrix. O-D matrix of EVs is a table which can be used to evaluate the traffic volume between different areas, as shown in Figure 2-23. t_{ij} is the traffic volume from area i to area j .

$i \backslash j$	1	2	3	...	n	$P_i = \sum_j t_{ij}$
1	t_{11}	t_{12}	t_{13}	...	t_{1n}	P_1
2	t_{21}	t_{22}	t_{23}	...	t_{2n}	P_2
3	t_{31}	t_{32}	t_{33}	...	t_{3n}	P_3
\vdots	\vdots	\vdots	\vdots	\vdots	\vdots	\vdots
n	t_{n1}	t_{n2}	t_{n3}	...	t_{nn}	P_n
$A_j = \sum_i t_{ij}$	A_1	A_2	A_3	...	A_n	$T = \sum_i P_i = \sum_j A_j$

Figure 2-23 Structure of OD matrix

Usually, the O-D survey can get the OD matrix for a consecutive 24 hours. TransCAD provides a procedure to decompose the overall OD matrix into a series of one hour OD matrix based on different travel mode. Based on this analysis, the space-time distribution of EVs is available. And then follow the method presented in [8], the data of space-time distribution was mapped to EV loads. The load data used in IPSA+ was updated taking into account the EV loads. The calculation procedure is shown in Figure 2-24.

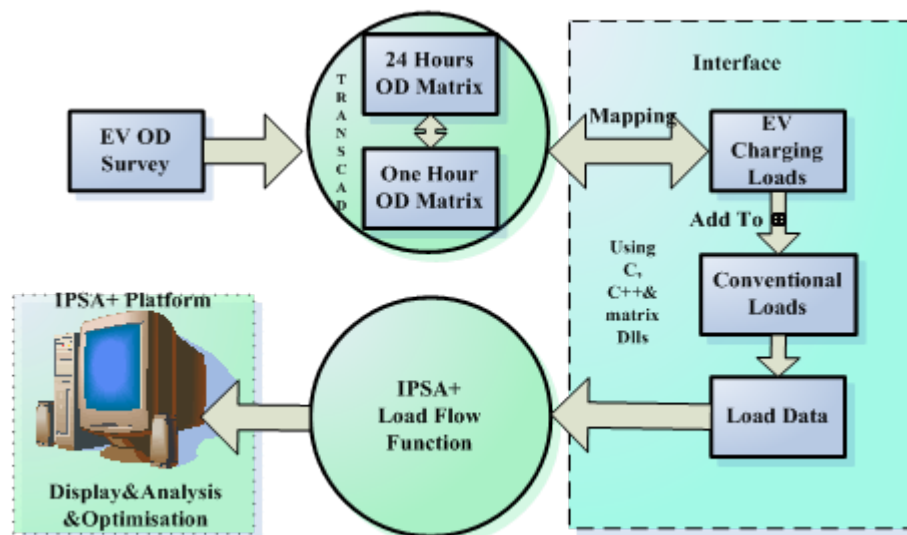


Figure 2-24 Calculation procedure

Several assumptions were made to simplify the test study, which are discussed in the following section. More comprehensive studies can be done through updating the parameters used without any change on the spatial-temporal model.

EV charging mode:

In this section, the fixed electricity rate was used for simplification where energy charge per kWh remains constant regardless the time of use. Based on this, the uncontrolled domestic charging was considered where all EVs start charging when they need, regardless of the peak load time. For this study, 61% of EVs were set as privately owned primarily for commuting, 9% were company owned and used primarily for business purpose, and 30% were owned by people who do not commute (generally characterized by those retired from work or who are unemployed). TransCAD has functions to analyse the different types of EVs based on their usage. These include Home Based Work (HBW), Home Based Other (HBO), and Non Home Based (NHB).

Types of EV batteries:

In this section, two types of EV batteries were considered, which are lead-acid (40%) and lithium-ion (60%) batteries for they have the most mature technology in recent years. Here the capacity of the EVs using lead acid is 27.19 kWh, while the lithium-ion ones are 29.07 kWh when fully charged from a discharged state. The power demand and related battery state-of-charge profiles of lead-acid battery is already given in Figure 2-18 (a). Similar curves for lithium-ion battery is given in Figure 2-25 [8].

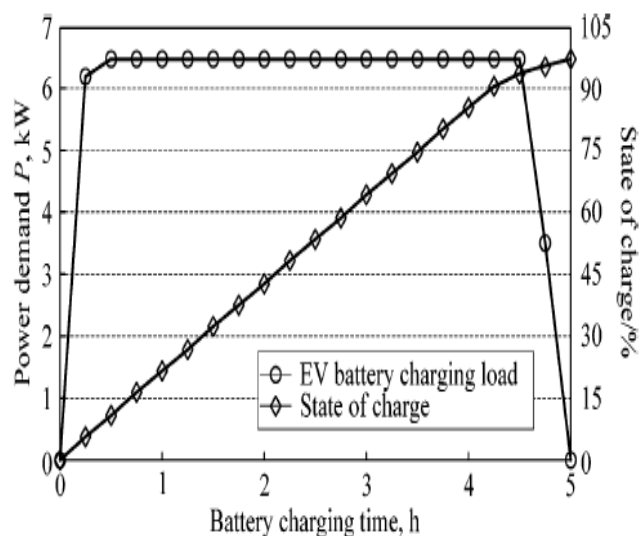


Figure 2-25 Charging profile of lithium-ion [8]

- **Modeling of stochastic nature of EV Load:**

The time of switching on an individual charger is a random variable, with a probability density function $f(t)$, which was determined by the tariff structure and the pattern of vehicle usage. The initial state-of-charge (SOC) of the EV battery was also assumed to be a random function of the total distance it travels since it was last charged. The distribution of initial SOC E_i was assumed therefore to have a probability density function $h(E)$, where E is the SOC, and its value varies from zero to the full capability of the battery. A statistical distribution of the state-of-charge of vehicles is required to determine the EV battery charging load during a recharge cycle. A probability distribution of daily distance driven was developed in [8]. The probability density function for vehicle travel with respect to distance is expressed as:

$$g(d; \mu, \sigma) = \frac{1}{d\sqrt{2\pi\sigma^2}} e^{-\frac{(\ln d - \mu)^2}{2\sigma^2}}, d > 0 \quad (2-14)$$

where d is the daily distance driven by a vehicle, μ is the mean, and σ is the standard deviation of the probability function. Based on the data extracted from [14], for private vehicles, the mean of the distance is 22.3 miles and the standard deviation is 12.2 miles, while for company vehicles the mean daily mileage is 54.1 miles and the standard deviation is 15.2 miles. Then assuming the SOC of an EV drops linearly with the distance of travel, the SOC at the beginning of a recharge cycle was estimated using (2-15):

$$E_i = (1 - \frac{\alpha d}{d_R}) \times 100\% \quad (2-15)$$

where E_i represents the initial SOC of an EV battery, d is the daily distance travelled by a vehicle, which is a random variable subjected to a lognormal distribution, α is the number of days the EV has travelled since last charge, d_R is the maximum range of the EV. A typical value for d_R is 80 miles. Then the probability density function h for the initial battery SOC is given by (2-16):

$$h(E; \mu, \sigma) = \frac{1}{\frac{d_R}{\alpha}(1-E)\sqrt{2\pi\sigma^2}} \times e^{-\frac{[\ln(1-E) - (\mu - \ln(\frac{d_R}{\alpha}))]^2}{2\sigma^2}}, 0 < E < 1. \quad (2-16)$$

According to [8], the initial SOC has a mean of 72% for private vehicles after one day's travel, and 44% after two day's travel, while a mean of 32% for company-owned vehicles after one day's travel. TransCAD provides a series of procedures to determine the d based on the statistics, which made a convenient way to finish the above process. In addition, TransCAD can also provide the EV geographical distribution.

It is important to evaluate the charging demand by an individual EV at any instant of time t . In order to facilitate numerical calculations, the power demand P during the

battery charging process was discretized with its discrete values P_j taken in half-hourly intervals from the curves shown in Figure 2-18 (a) and Figure 2-25. The corresponding power levels of charging load is therefore expressed as:

$$P_j = \frac{P((j-1)\Delta t) + P(j\Delta t)}{2}, j = 1, 2, \dots, n_c \quad (2-17)$$

where n_c is the number of half-hourly intervals in the battery charging profile. n_c is 14 half-hour intervals for the lead-acid battery, as it takes 7 h for this type of battery to be fully charged from a fully discharged state, and $n_c=10$ for the lithium-ion type. The probability of a battery charging load operating at power level P_j at time instant t is represented as $\Phi(P_j, t)$, where Φ is the probability density function, $1 \leq t \leq 24$. If the EV battery starts recharging at time instant k ($k \leq t$), then the charging load at time instant k is $P_{j-(t-k)}$, assuming an initial battery SOC $E_{j-(t-k)}$. Assuming that the charging start time and battery initial SOC are two independent variables, the probability of a battery starting charging at time instant k ($k \leq t$, $1 \leq k \leq 24$) and operating at power level P_j at time instant t is mathematically expressed as:

$$\Phi(P_j, t) = \sum_{k=1}^t f(k)h(E_{j-(t-k)}) \quad (2-18)$$

where $f(k)$ is the probability of charging started at time instant k ($k \leq t$), while $h(E_{j-(t-k)})$ is the probability of an initial battery SOC being at power level $P_{j-(t-k)}$. From equation (2-18), the expected value (mean) $\mu(P)$ and standard deviation $\sigma(P)$ at any time instant t was calculated. The mathematical expectation of the charging load at time instant t for an individual battery is shown in equation (2-19):

$$\mu(P) = \sum_{j=1}^{n_c} P_j \Phi(P_j, t) \quad (2-19)$$

Then the expression of multiple batteries charging loads is shown as follows:

$$P_n = \sum_{i=1}^n \sum_{j=1}^{n_c} P_j \cdot \Phi(P_j, t) \quad (2-20)$$

where P_n is the overall power demand for the n EV battery chargers.

By using the O-D analysis and other functions from TransCAD, the EV load was obtained through aforementioned procedure, which was used to conduct load flow analysis in IPSA+. A simple test example is shown the next section.

Test Results

In this section, a simple test system was developed to evaluate the spatial-temporal model developed. More comprehensive analysis based on this model is being

carried out in WP 3 of the MERGE project. An urban area named FLINTBURY was used for the study. The map of FLINTBURY is shown in Figure 2-26.

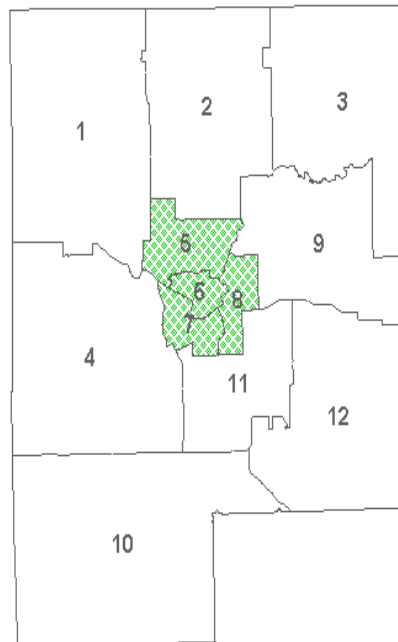


Figure 2-26 Map of FLINTBURY Zones

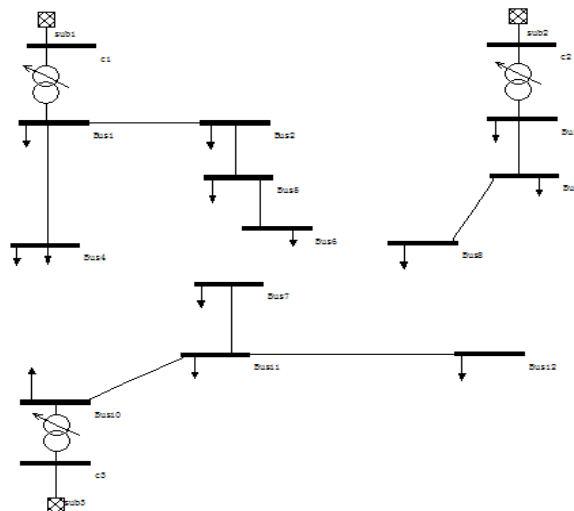
The district area is divided into 12 zones. The zones 5, 6, 7, 8 are the central commercial zones while the areas 9, 11 are the industry areas, and the zones 1, 2, 3, 4, 10, 12 are residential areas.

The electric power is supplied by three substations. The service areas are listed in Table 2-5:

Table 2-5 Service of Substations

Substation	Service Areas
Sub1	1, 2, 4, 5, 6
Sub2	3, 8, 9
Sub3	7, 10, 11, 12

The one line diagram of power system is shown in Figure 2-27, the bus number equals to the number of district. For example, the power of district 1 is supplied by bus 1.



- **Modeling of EV Load Demand under uncontrolled domestic charging:**

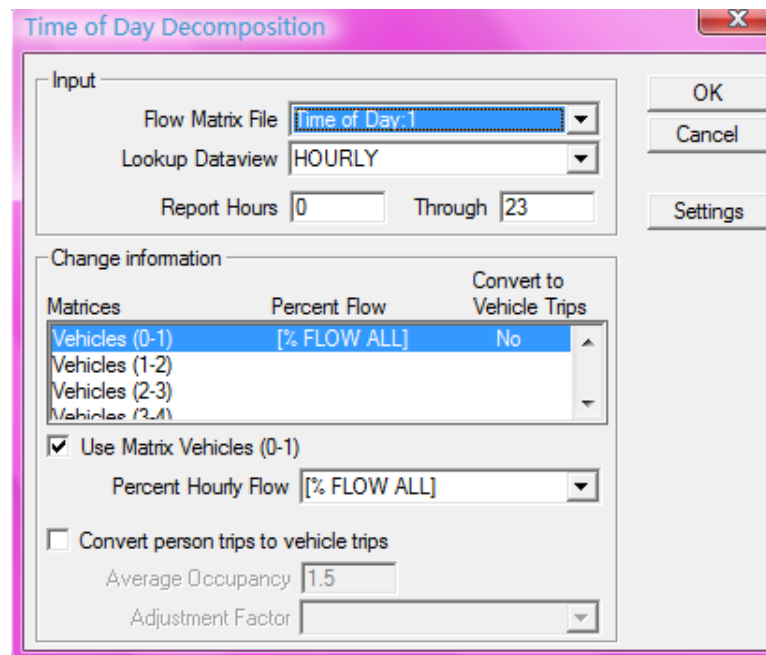
Regarding the EV battery population, 50% lithium-ion and 50% lead acid was used. In this case study, it was assumed that there is no incentive for EV owners to avoid peak load charging, i.e., flat (fixed) electricity rate was employed. HB and NHB EVs were considered in this example. According to the EVs traffic data analysis result in TransCAD, three important charging periods were used. The first charging period is during the evening and night. Most of the HB and NHB vehicles are at home or working place from 21h00 until 06h00 in the morning. Some HB EVs are immediately plugged in on the return from work in order to be ready to use throughout the evening. Thus the second charging period takes place between 18h00 and 21h00. This charging period coincides with the peak load during the evening. The third charging period is between 11h00 and 16h00 during the day. The charging occurs in the urban areas. A group of daily load profiles from the UK Generic Distribution System (UKGDS) was selected as the base data. The load profiles cover 24 hours and the load flow was analyzed every hour. 4000 EVs were considered in the sample system, which is composed of 60% HB cars and 40% NHB cars. And the power factor is set to 1.0, when the EVs are charging from the grid.

- **OD data & Analysis in TransCAD:**

An O-D analysis case from TransCAD was used to represent the EV movement. The EV transportation data then was mapped to EV load data. The key steps are listed as follows:

- The 24-hour OD matrix and Percent Hourly Flow Data were obtained from the OD survey in FLINTBURY;
- The 24-hour OD matrix was then decomposed to several hourly OD matrixes.

- Open the Workspace of FLINTBURY;
- Select Planning-Time of Day Analysis to open the dialog of Time of Day Decomposition and set up the parameters which is shown as Figure 2-28;
- Click OK to finish this analysis and save the hourly OD matrix in a separate file;
- The decomposition result can be viewed in a data view window. And the decomposition result of the HB between 7~8 am is shown in Figure 2-29 as an example.



Time of Day Decomposition

Input

Flow Matrix File: **Time of Day:1**

Lookup Dataview: **HOURLY**

Report Hours: **0** Through **23**

Change information

Matrices	Percent Flow	Convert to Vehicle Trips
Vehicles (0-1)	[% FLOW ALL]	No
Vehicles (1-2)		
Vehicles (2-3)		
Vehicles (3-4)		

☒ Use Matrix Vehicles (0-1)

Percent Hourly Flow: **[% FLOW ALL]**

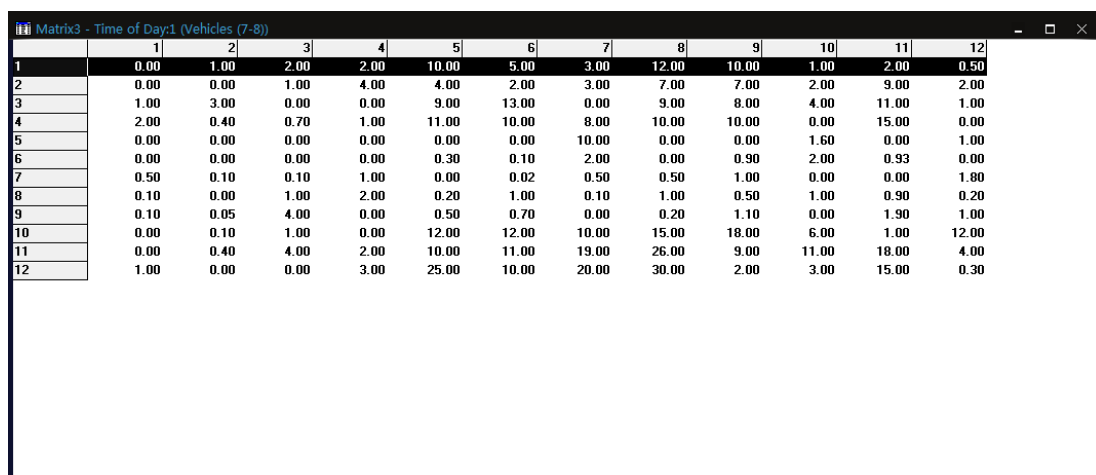
☐ Convert person trips to vehicle trips

Average Occupancy: **1.5**

Adjustment Factor:

Buttons: OK, Cancel, Settings

Figure 2-28 Time of Day Decomposition

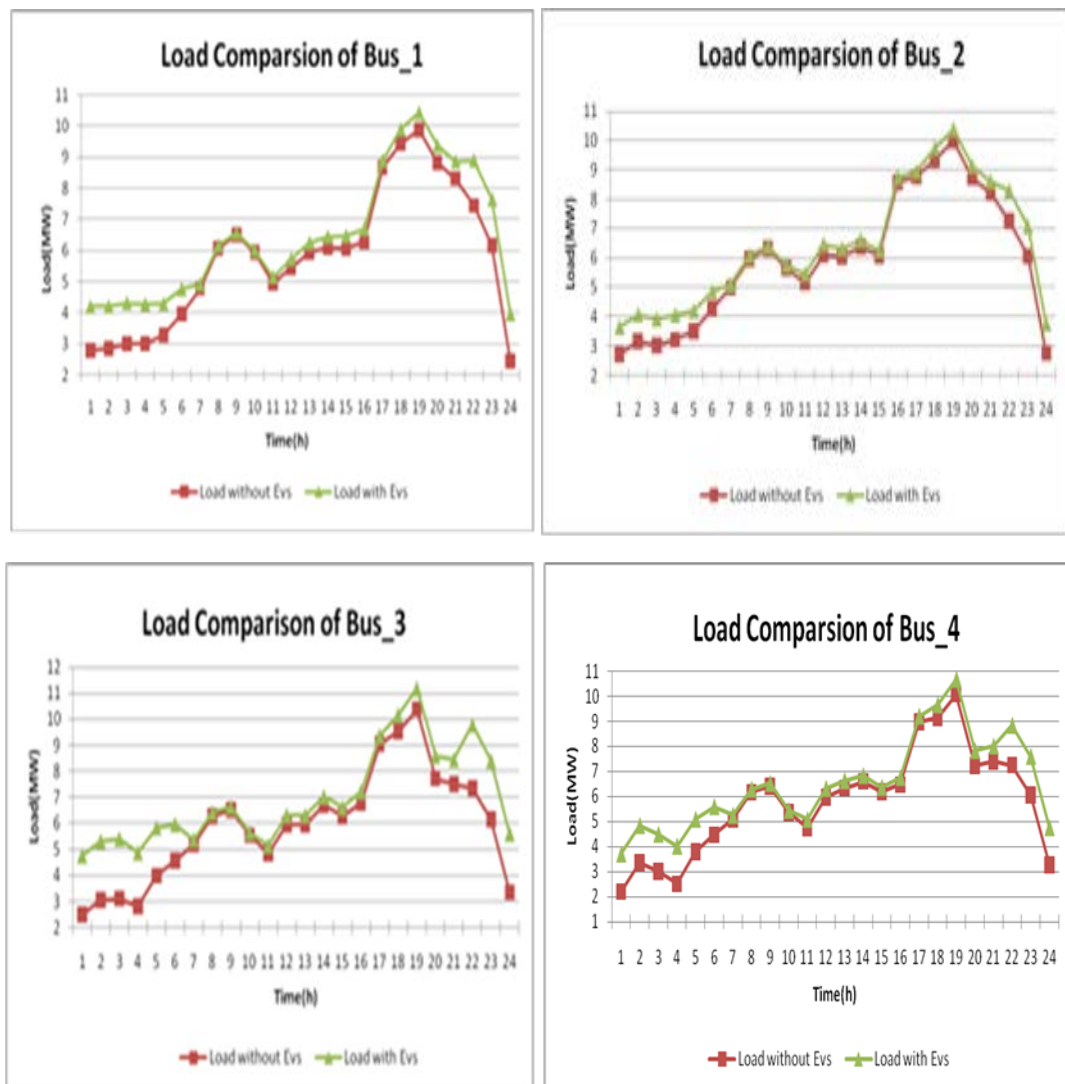


	1	2	3	4	5	6	7	8	9	10	11	12
1	0.00	1.00	2.00	2.00	10.00	5.00	3.00	12.00	10.00	1.00	2.00	0.50
2	0.00	0.00	1.00	4.00	4.00	2.00	3.00	7.00	7.00	2.00	9.00	2.00
3	1.00	3.00	0.00	0.00	9.00	13.00	0.00	9.00	8.00	4.00	11.00	1.00
4	2.00	0.40	0.70	1.00	11.00	10.00	8.00	10.00	10.00	0.00	15.00	0.00
5	0.00	0.00	0.00	0.00	0.00	0.00	10.00	0.00	0.00	1.60	0.00	1.00
6	0.00	0.00	0.00	0.00	0.30	0.10	2.00	0.00	0.90	2.00	0.93	0.00
7	0.50	0.10	0.10	1.00	0.00	0.02	0.50	0.50	1.00	0.00	0.00	1.80
8	0.10	0.00	1.00	2.00	0.20	1.00	0.10	1.00	0.50	1.00	0.90	0.20
9	0.10	0.05	4.00	0.00	0.50	0.70	0.00	0.20	1.10	0.00	1.90	1.00
10	0.00	0.10	1.00	0.00	12.00	12.00	10.00	15.00	18.00	6.00	1.00	12.00
11	0.00	0.40	4.00	2.00	10.00	11.00	19.00	26.00	9.00	11.00	18.00	4.00
12	1.00	0.00	0.00	3.00	25.00	10.00	20.00	30.00	2.00	3.00	15.00	0.30

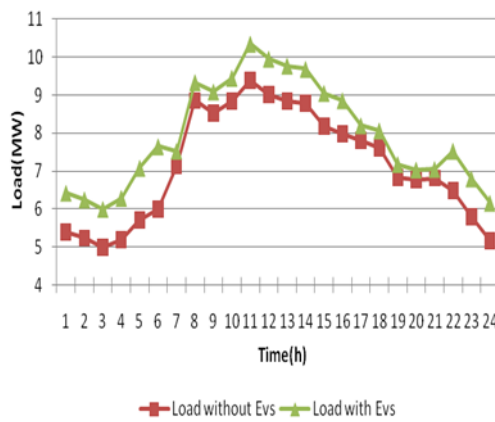
Figure 2-29 Decomposition result of HB at 7~8 am

- **Base case and EVs connection case:**

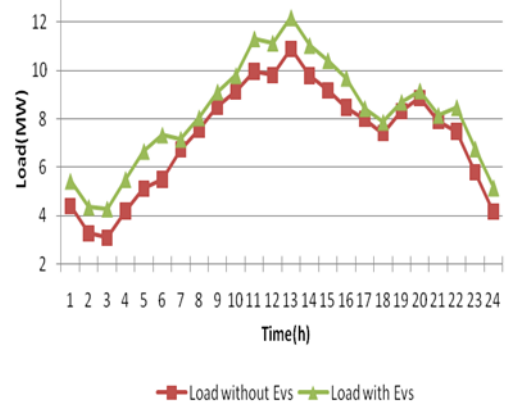
A network without EV connection was used as the base case. When EVs are connected to the grid, the load will suffer an increase based on the characteristics of EVs flow. The load profile comparison of each bus is shown in Figure 2-30.



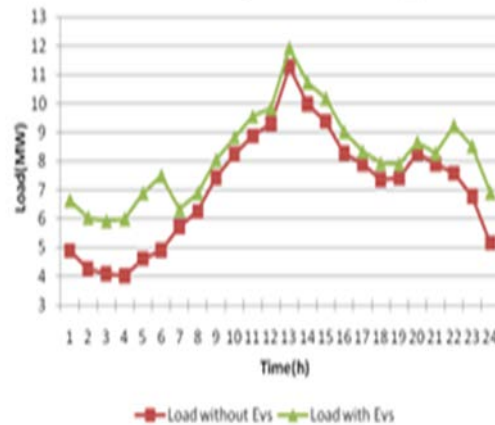
Load Comparison of Bus_5



Load Comparison of Bus_6



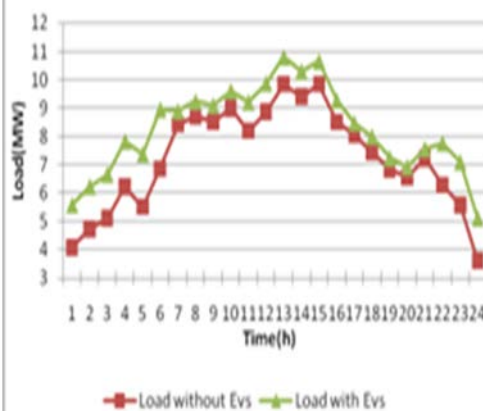
Load Comparison of Bus_7



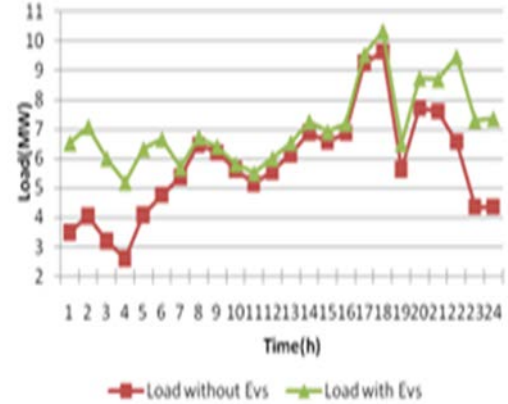
Load Comparison of Bus_8



Load Comparison of Bus_9



Load Comparison of Bus_10



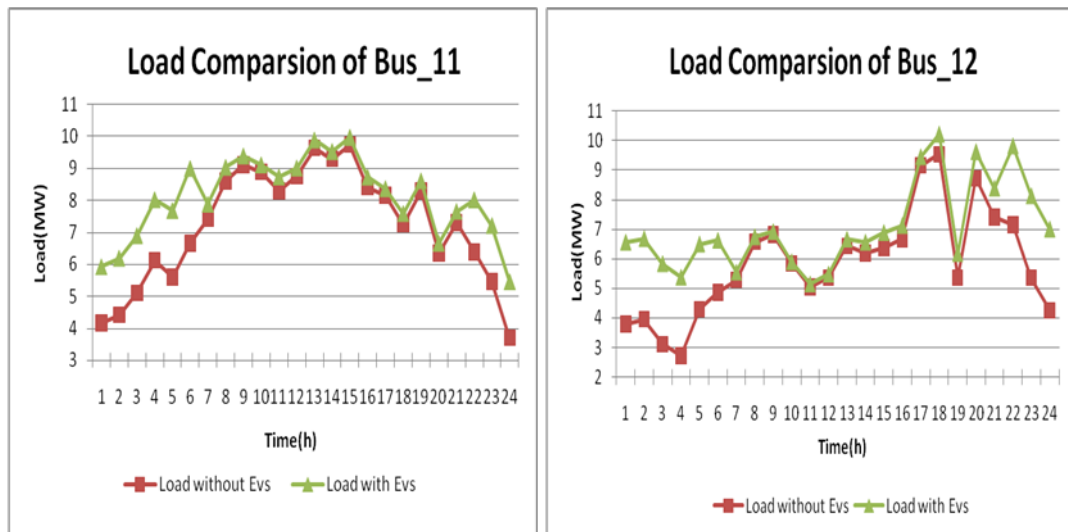


Figure 2-30 Load profile of each bus

Load flow results: By using the EVs load data, the load flow was calculated when EVs were integrated to the grid. Figure 2-31 shows the comparisons of the voltage profiles. And Figure 2-32 shows the loading condition of the substation.

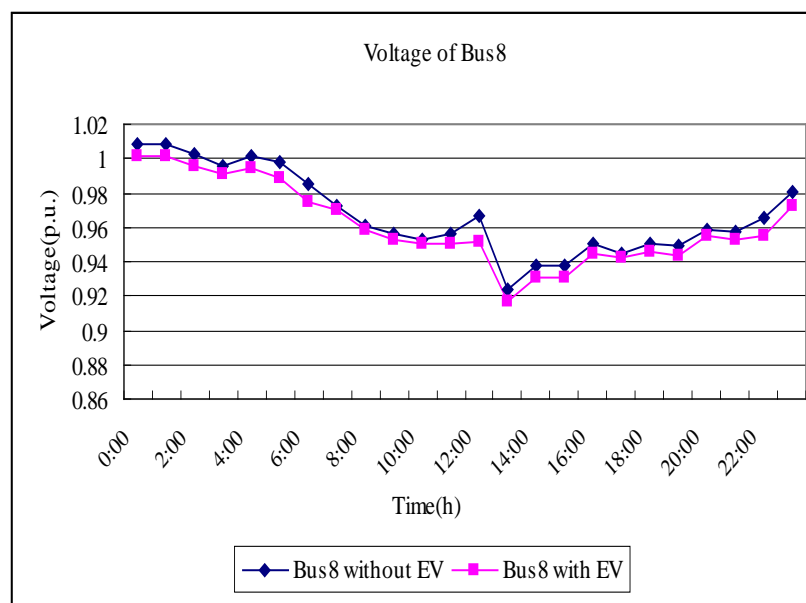


Figure 2-31 Comparison of voltage profiles



Figure 2-32 Loading condition of substation

2.4 Conclusion

IPSA+ software was adapted/enhanced based on its UDM (User Defined Model) tool and the scripted extension library for Python. Various EV-related models have been developed; Reserve and frequency response models were adapted and enhanced to evaluate the performance of a network with different levels of EV penetration for providing the ancillary service; A spatial-temporal analysis tool was developed and integrated into the existing IPSA+ and TransCAD tools to address the correlation of the mobility with population movement in an urban area.

2.5 References

- [1] The introduction to IPSA+, Available: <http://www.ipsa-power.com/software/ipsa-1>.
- [2] O. Tremblay, L.-A. Dessaint, and A.-I. Dekkiche, "A Generic Battery Model for the Dynamic Simulation of Hybrid Electric Vehicles," in Vehicle Power and Propulsion Conference, 2007. VPPC 2007. IEEE, 2007.
- [3] MathWorks, "SimPowerSystems™ Reference," Hydro-Québec and the MathWorks, Natick2010.
- [4] Johnson P. "Technical Requirement and Despatch of Frequency Response Power Reserve Services", IEE Colloquium on Economic Provision of a Frequency Responsive Power Reserve Service, 5th February 1998.
- [5] Erinmez, I.A., Bickers, D.O., Wood, G.F., Hung, W.W., "NGC Experience with Frequency Control in England and Wales- Provision of Frequency Response by Generators", IEEE PES Winter Meeting, 31 January – 4 February, 1999, New York, USA.
- [6] NGC, "Technical and Operational Characteristics of the Transmission System", April 2000
- [7] Kundur P., "Power System Stability and Control, McGraw-Hill, Inc., 1994
- [8] Kejun Qian, Chengke Zhou, Malcolm Allan, and Yue Yuan, "Modeling of Load Demand Due to EV Battery Charging in Distribution Systems", IEEE Transaction on Power Systems, Future Issue, Digital Object Identifier: 10.1109/TPWRS.2010.2057456
- [9] Ricardo, "Tasks 2.1 report: EV penetration scenarios and battery modelling", 2010
- [10] TransCAD Manual, Caliper Company, 2006, Available: <http://www.caliper.com/TransCAD/>.
- [11] Intro to TransCAD GIS, Model Research and Development Unit Transportation Planning Branch, 2008, Available: <http://www.caliper.com/TransCAD/>.
- [12] J.T.Salihi, "Energy requirements for electric cars and their impact on electric generation and distribution systems," *IEEE Trans. Ind. Appl.*, vol. 1A-9, no.5, pp.516-531, Sep./Oct. 1973.
- [13] K. C. Nyns, E. Haesen, "The impact of Charging Plug-in hybrid electric vehicles on a residential distribution grid," *IEEE Trans. Power Del.*, vol. 25, no.1, pp.371-380, Feb.2010.
- [14] National Statistics, Department for Transport, Transport Statistics Bulletin- National Travel Survey: 2008, Apr.9, 2009.

2.6 Appendix 2-I [9]

EV Classification and market penetration estimates in the UK

EV	I7e	M1			N1			N2
Year	BEV	BEV	PHEV	REV	BEV	PHEV	REV	BEV
2020	8,281	266,132	205,343	14,867	30,412	23,466	1,699	5,558
2030	49,97	1,306,35	2,384,27	707,21	148,44	270,94	80,36	49,97

Daily mileage

EV classification	Annual mileage (km)	Daily mileage (km)
I7e	-	19.0
M1	13,985	38.3
N1	20,457	56.0
N2	49,647	136.0

The estimation value considering I7e vehicles feature short-distance trips

Battery specification: Capacity, charge rate and EV range

Vehicle classification and		Capacity (kWh)	Slow charge rate	EV range (km)
I7e	BEV	8.7	3	85
M1	BEV	28.5	3	175
	PHEV	8.2	3	60
	REV	16.9	3	68
	REV	16.9	3	68
N1	BEV	23.0	3	120
	PHEV	8.2	3	60
	REV	16.9	3	68
N2	BEV	85.3	10	150

3 MATLAB SIMULINK SIMULATION PLATFORM

The simulation platforms based on the MatLab Simulink software developed within the EU Microgrids projects were adapted to incorporate EV models for smart charging and V2G operation in both normal and islanded modes. These developments were oriented to assess impacts in Microgrids. These simulation platforms are capable of assessing the steady state and dynamic behaviour of these networks in three phase balanced mode and unbalanced mode for the case of Microgrids. In particular, the dynamic stability analysis of inverter dominated Microgrid is of particular interest. Its unique feature is that it allows the dynamic simulation of isolated networks without rotating masses directly coupled to the network (only interfaced via power electronics). The definition of frequency is particularly challenging in this case. MatLab/Simulink was used to simulate the behaviour of a Microgrid for steady state operation and the dynamic behaviour for islanded modes in voltage unbalanced conditions.

3.1 The Simulation Platform Developed in INESC Porto

The electric power systems industry is about to face a major new challenge: future massive integration in the electric grid of plug-in electric vehicles (EV) [1-2]. Thus, it requires additional studies regarding the identification and quantification of the resulting impact of such challenge. More specifically, this change of paradigm requires a deep understanding on how EV can be integrated in grid control and management structures previously developed and investigated, such as the MicroGrid (MG) concept.

The MICROGRIDS project, *MicroGrids: Large scale integration of Micro Generation to Low Voltage Grids*, Contract no. ENK5-CT-2002-00610 [3], can be considered as a reference point for the development of the first generation of new architectures for electricity grids at EU level. This project developed in depth the MG concept, which can be defined as Low Voltage (LV) distribution system with small modular generation technologies (the MicroSources - MS), storage devices and controllable loads, being operated connected to the main power network or islanded, in a controlled coordinated way [4].

The successful design and operation of a MG, especially when the possibility of exploiting islanding operation is envisaged, required the identification and development of specific control functionalities. The presence of power electronic interfaces in different types of MS such as fuel cells, photovoltaic panels, microturbines or storage devices characterize a new type of power system when compared with conventional systems using synchronous generators. The dynamic behaviour of a system with very low global inertia, comprising some MS with slow responses to control signals, is also quite different from traditional power systems. Aiming to demonstrate the feasibility of the MG concept, namely in terms of islanding operation, a MG dynamic simulation platform was developed under the Matlab/Simulink simulation environment, which required [4-5]:

- Development and selection of adequate models for simulating the operation of different types of MS and storage devices, including the corresponding power electronic interfaces. The understanding of the dynamic behavior of MS and

storage devices was crucial in order to identify the most appropriated decentralized control strategies to be installed in the system in order to assure a seamless transition to islanding operation.

- Development of MG emergency control functionalities for islanding operation: during MG islanding operation, load-tracking problems arise since some micro generators have slow response to control signals and are inertia-less. A system with clusters of MS designed to operate in an island mode requires some form of storage to ensure initial energy balance. The control strategy to be developed has to combine the fast response of storage devices, load shedding mechanisms and secondary frequency control functionalities to be installed in controllable MS.

Taking into consideration the existing MG concepts and models, this section aims at describing the adaptations and enhancements that were made to the existing MG simulation platform in order to deal with the integration of EV into the system. The existing MG simulation platform based on the Matlab/Simulink software developed within the EU Microgrids project, which is briefly described in the next sub-section, was adapted in order to incorporate EV models for smart charging and Vehicle-to-Grid (V2G) operation in both MG normal and islanded operating modes. Additionally, platform adaption and enhancement was oriented in order to allow studies under three-phase balanced and unbalanced operating conditions, including voltage balancing and control for mitigating negative and zero sequence voltage components. This was performed in order to allow incorporating single phase EV battery interfaces. Additionally new models for micro-wind generators were derived and implemented. The unique feature of the simulation platform is that it allows the dynamic simulation of isolated networks without rotating masses directly coupled to the network (only interfaced via power electronics). The definition of frequency is particularly challenging in this case. Matlab/Simulink will be used to simulate the behavior of a MG for steady state operation and the dynamic behavior for islanded modes in unbalanced operating conditions.

3.1.1 Description of the Simulation Platform

A review of MicroGrid Operation and Control

A typical MG architecture is presented in Figure 3-1. The MG operation philosophy is based on an hierarchical type control approach headed by the MicroGrid Central Controller (MGCC). A network of controllers with local intelligence – Load Controllers (LC) and Microsource Controllers (MC) – defines a secondary layer in the hierarchical control structure [3-5].

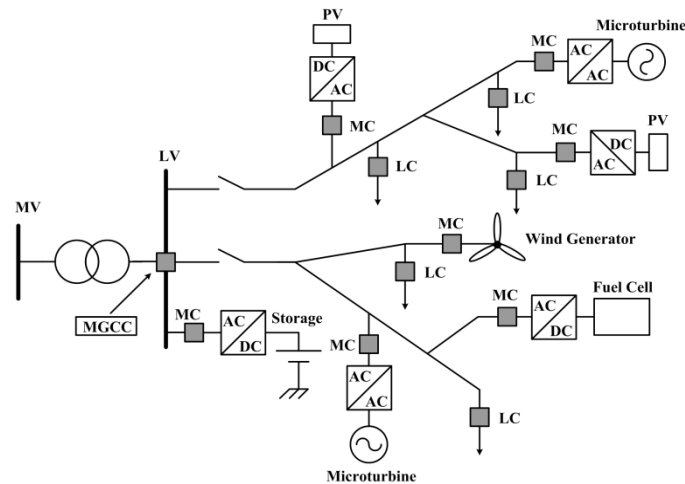


Figure 3-1: MicroGrid architecture

The results presented in [4-5] highlight that under abnormal operating conditions only a network of local controllers can deal effectively with the resulting transient phenomena. However, frequency control problems arise during islanding operation due to the slow response of MS to control signals and due the inexistence of rotating masses directly connected to the grid (inertialess system). Sudden islanding of the MG due to faults occurring in the upstream Medium Voltage (MV) network may cause high unbalances between local load and generation which must be compensated by local MS and through a very efficient use of storage devices and load shedding mechanisms.

The successful design and operation of a MG requires solving a number of demanding technical issues, in particular related to system functions and controls. The presence of power electronic interfaces in fuel cells, photovoltaic panels, microturbines and storage devices are the distinguishing characteristics of a MG when compared with conventional systems using synchronous generators. A system with clusters of MS designed to operate in islanded mode requires some form of energy buffering in order to ensure initial energy balance. The necessary energy storage can be provided by flywheels or supercapacitors connected through appropriated power electronic interfaces to the LV grid. The active power shortage caused in a MG when moving to islanding operation or resulting from load or power variations during islanding operation mode must be compensated by energy storage devices. Additionally, the slow response of controllable MS to the control signals is a specific issue contributing to the need of providing some form of energy storage with fast response in terms of power injection capabilities in order to enable MG operation under islanded conditions [4].

A possible solution for providing fast power balance between load and generation during any islanding operating conditions consists on using at least one Voltage Source Inverter (VSI) coupled to an energy storage device and reacting to grid operating conditions according to droop functions for voltage and frequency, according to the modelling approach described in [4-5]:

$$\begin{aligned}\omega &= \omega_0 - k_p \times P \\ V &= V_0 - k_Q \times Q\end{aligned}\tag{3-1}$$

where P and Q are the inverter active and reactive power outputs, k_p and k_Q are the droop slopes (positive quantities) and ω_0 and V_0 are the idle values of the angular frequency and voltage (values of the inverter angular frequency and terminal voltage at no load conditions).

If a cluster of VSI operates in a standalone AC system, frequency variation leads automatically to power sharing, such that for a system with n VSI the following equality stands:

$$\Delta P = \sum_{i=1}^n \Delta P_i\tag{3-2}$$

where ΔP is the total power variation and ΔP_i the power variation in the i -th VSI. The frequency variation can be computed as:

$$\Delta \omega = \omega_{0i} - k_{p_i} \times P_i - [\omega_{0i} - k_{p_i} \times (P_i + \Delta P_i)] = k_{p_i} \times \Delta P_i\tag{3-3}$$

Equation (3-3) clearly shows that during MG islanding operation, the frequency drifts from the nominal value following power or load variations. During this transient condition, power balance is assured by energy storage devices. However, if the MG frequency stabilizes in a value different from the nominal one, (due to the use of only proportional droop controls) storage devices would keep on injecting or absorbing active power whenever the frequency deviation differs from zero. This should be only admissible during transient situations, where storage devices are responsible for ensuring the energy balance between load and generation within the MG. However, storage devices (flywheels or supercapacitors, with high capabilities for injecting power during small time intervals) have a finite storage capacity and can be loaded mainly by absorbing power from the LV grid. Therefore, they should inject power into the MG only during transient situations in order to not run out of energy. Consequently, the use of a control procedure to correct permanent frequency deviations during any islanded operating conditions should then be considered. In order to perform such control procedure, controllable MS such as fuel cells or microturbines are used to promote adequate secondary control aiming to restore frequency to the nominal value after a disturbance by using a Proportional-Integral controller at each controllable MS level [4-5].

The controllable loads concept plays also an important role under some MG operating conditions, namely those concerning the imbalance between load and generation (load larger than generation). In order to deal with this problem, a load shedding mechanism was proposed to be implemented in a MG as an emergency functionality to aid frequency restoration to its nominal value after MG islanding [4-5]. Load shedding is used as a remedy against large frequency excursions.

Basically, the dynamic behaviour of the system is improved if some percentage of the load is temporarily lost, allowing the generators with frequency regulation functions to react to the frequency deviation. It is important to note that, in addition to frequency deviation, storage devices have a finite storage capability which also determines the amount of load that must be shed following MG islanding.

MicroGrid Simulation platform implementation

This sub-section aims to illustrate the MG dynamic simulation platform that was developed under the Matlab/Simulink environment through the use of the SymPowerSystems toolbox. In this simulation platform it is possible to analyse the dynamic behaviour of several MS and storage devices connected to a LV network, together with specific control strategies for MG islanding operation that were briefly described in the previous section. A detailed description of the control strategies required for MG islanding operation can be found in [5].

The implementation of a low voltage MG test system under the Matlab/Simulink environment is shown in Figure 3-2. According to the developments of the “MicroGrids” project [4-5], several models are available in the simulation platform, namely:

- Storage devices and the corresponding power electronic converter – the VSI;
- Controllable MS such as Solid Oxide Fuel Cells (SOFC) and Single Shaft Microturbines (SSMT), together with the corresponding grid-tied inverters;
- Uncontrollable/partially controllable MS such as micro-wind generator and photovoltaic (PV) panels, also connected to the grid through grid tied inverters;
- Load-shedding mechanisms.

The simulation platform was developed in a modular way, where the control parameters and models can be easily included and modified using the “mask” functionalities provided by Matlab/Simulink. In order to illustrate this feature, Figure 3-3 shows the connection of a SSMT, generally represented by a block, to an external three-phase source. As can be observed, in addition to the electrical connections corresponding to the terminals A, B and C in the SSMT box, it is possible to have access to a set of internal variables of the SSMT, namely its active and reactive output power (P/Q), the voltage in the DC-link (V_{dc}), the rotation speed, etc. This simple system was built in the Matlab/Simulink environment, using what is called the “mask” concept. The mask allows the aggregation of the model representing a specific system in a single block, therefore allowing building user-friendly models from the graphical point of view.

In order to illustrate the Matlab/Simulink “mask” functionality, Figure 3-4 shows the dialog box that is opened when the SSMT box of Figure 3-3 is double clicked. As can be observed in Figure 3-4, this dialog box allows the input of all the SSMT parameters, according to the model described in [5].

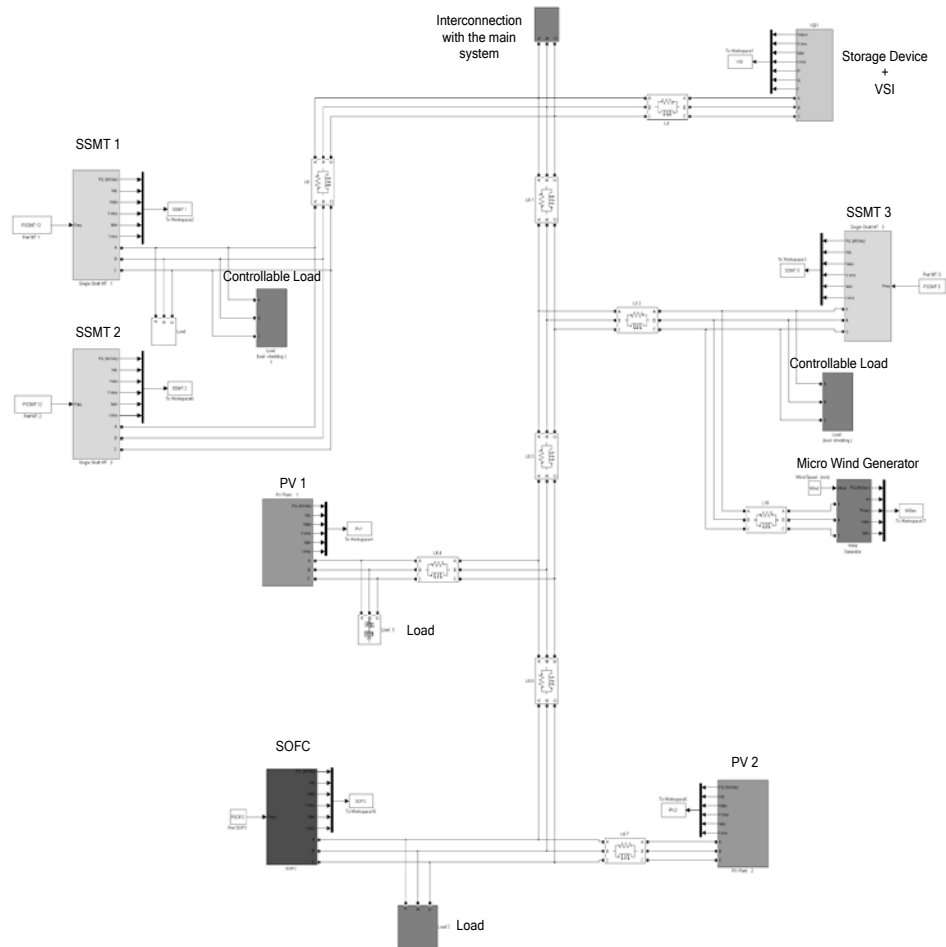


Figure 3-2: General overview of the existing Matlab/Simulink simulation platform

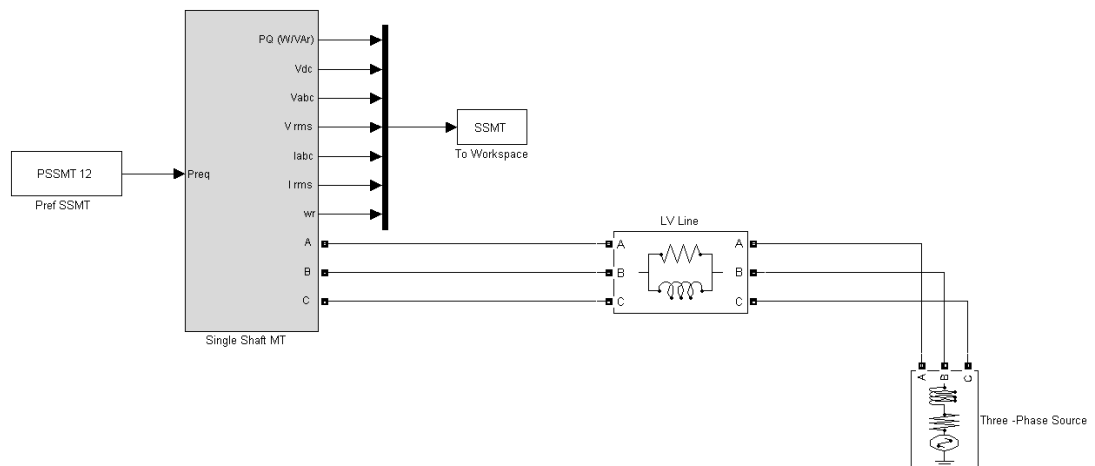
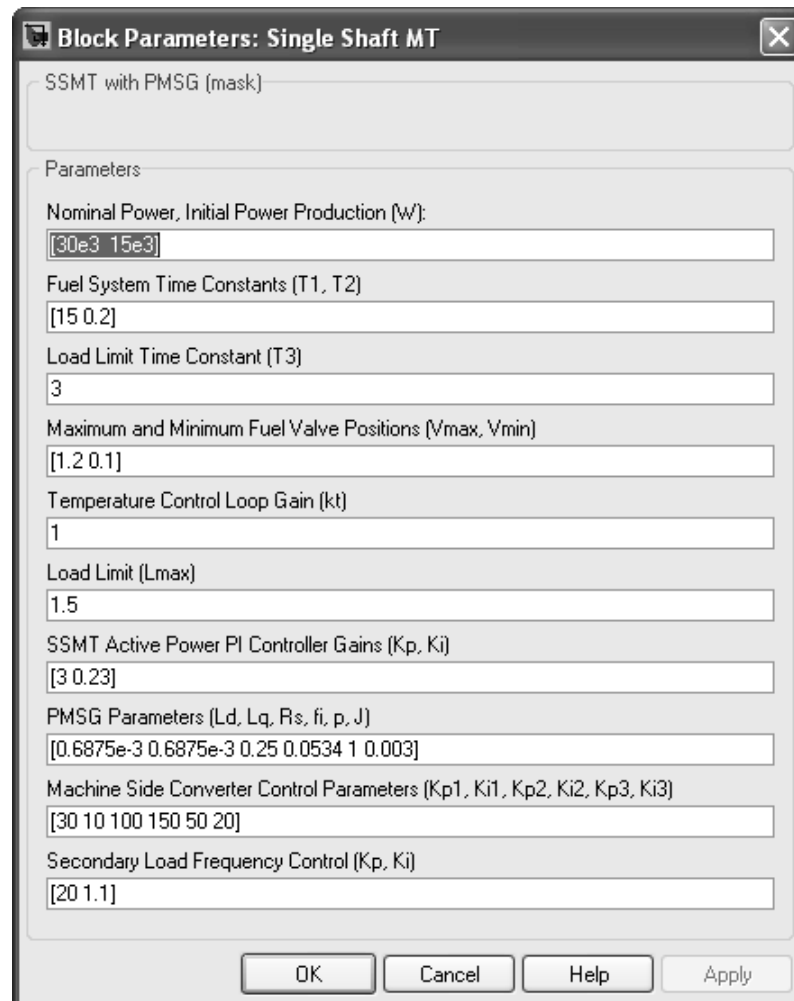


Figure 3-3: SSMT connected to a three-phase source



Block Parameters: Single Shaft MT

SSMT with PMSG (mask)

Parameters

Nominal Power, Initial Power Production (W):

Fuel System Time Constants (T1, T2)

Load Limit Time Constant (T3)

Maximum and Minimum Fuel Valve Positions (Vmax, Vmin)

Temperature Control Loop Gain (kt)

Load Limit (Lmax)

SSMT Active Power PI Controller Gains (Kp, Ki)

PMSG Parameters (Ld, Lq, Rs, fi, p, J)

Machine Side Converter Control Parameters (Kp1, Ki1, Kp2, Ki2, Kp3, Ki3)

Secondary Load Frequency Control (Kp, Ki)

OK Cancel Help Apply

Figure 3-4: Dialog box for the SSMT model input parameters

By looking under the mask of the SSMT block shown in Figure 3-3, it is possible to see additional blocks which contain the detailed dynamic model of the SSMT, the model of the grid-tied inverter and the secondary load frequency control referred in the previous section (Figure 3-5). Continuing to explore the main blocks (masks), it is possible, for example, to observe the implementation of the SSMT model (SSMT mechanical part, the Permanent Magnet Synchronous Generator (PMSG) and the machine side converter).

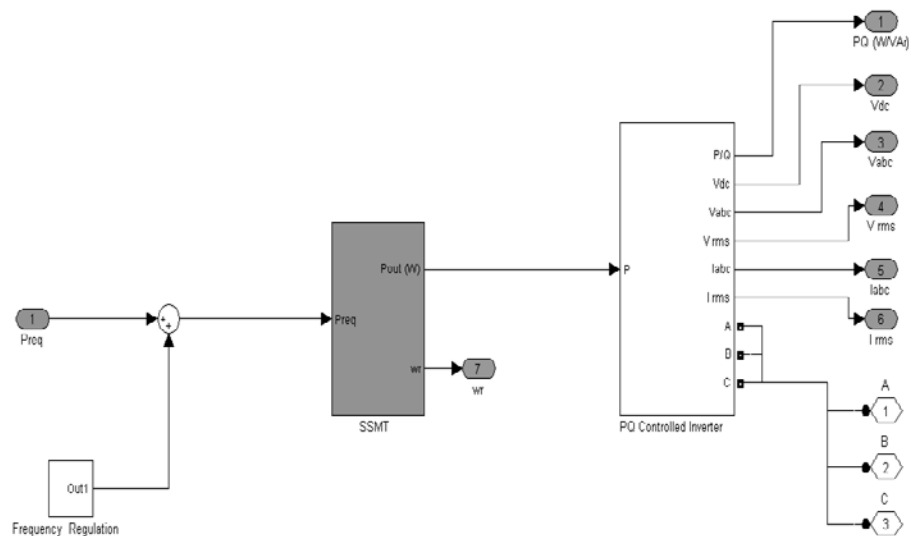


Figure 3-5: A detail of the SSMT mask

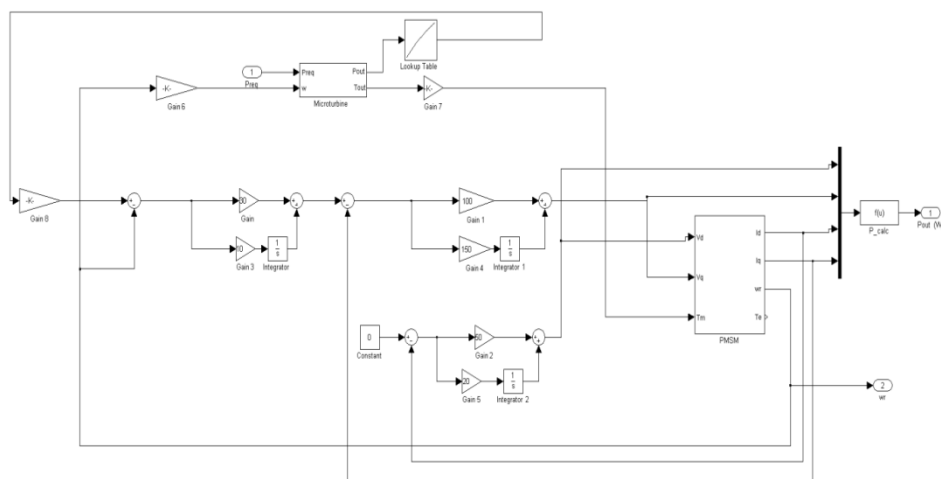
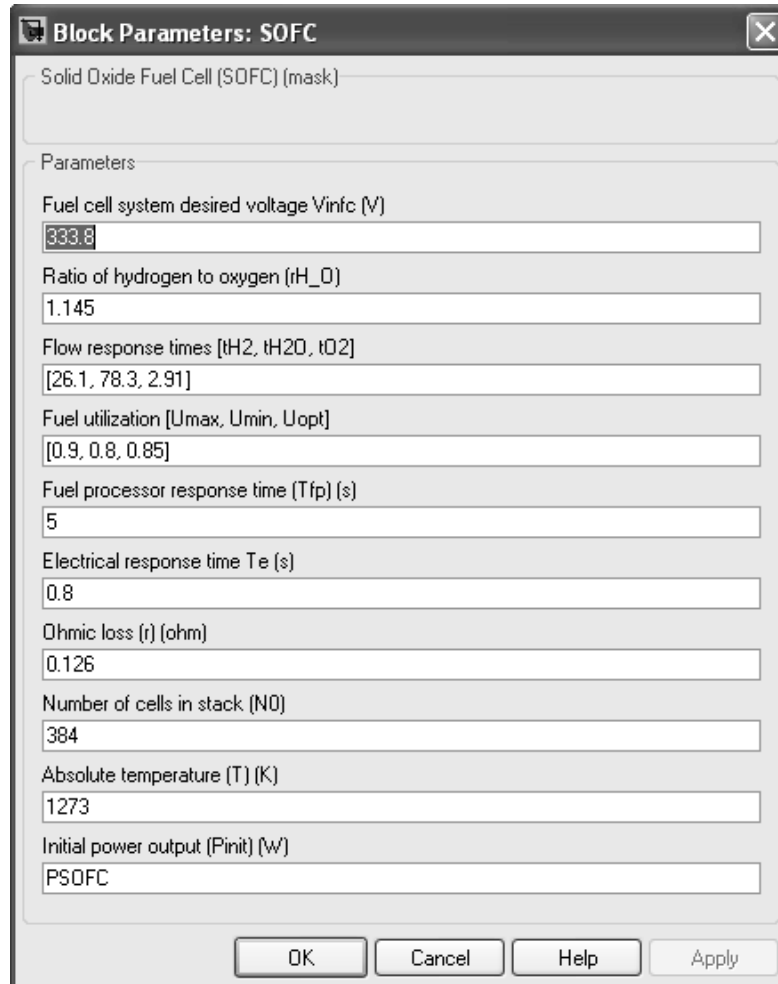


Figure 3-6: SSMT model, including the SSMT mechanical part, the PMSG and the machine side converter

The main idea that is important to retain is the modularity of the simulation platform that was developed under the Matlab/Simulink environment. As it can be observed from the figures presented above, the Matlab/Simulink environment allows the development of very user friendly models.

Concerning the SOFC model, it was also developed according to the same concepts previously described for the implementation of the SSMT model. In order to illustrate the Matlab/Simulink “mask” functionality for the SOFC model, Figure 3-7 shows the dialog box that is opened when the SOFC block is double clicked. As can be observed in Figure 3-7, this dialog box allows the input of all the SOFC parameters, according to the model described in [4-5]. By looking under the mask of the SOFC block, it is possible to see additional blocks which contain the detailed model of the

SOFC, the model of the grid-tied inverter and the secondary load frequency control (Figure 3-8). Continuing to explore the main blocks (masks), it is possible, for example, to observe the implementation of the SOFC electrochemical model (Figure 3-9).



The image shows a software dialog box titled "Block Parameters: SOFC". It contains a list of parameters for a Solid Oxide Fuel Cell (SOFC) model, each with a corresponding input field. The parameters and their values are as follows:

Parameter	Value
Fuel cell system desired voltage V_{infc} (V)	333.8
Ratio of hydrogen to oxygen (r_{H_2O})	1.145
Flow response times [t_{H_2} , t_{H_2O} , t_{O_2}]	[26.1, 78.3, 2.91]
Fuel utilization [U_{max} , U_{min} , U_{opt}]	[0.9, 0.8, 0.85]
Fuel processor response time (T_{fp}) (s)	5
Electrical response time T_e (s)	0.8
Ohmic loss (r) (ohm)	0.126
Number of cells in stack (N_0)	384
Absolute temperature (T) (K)	1273
Initial power output (P_{init}) (W)	PSOFC

At the bottom of the dialog box, there are four buttons: "OK", "Cancel", "Help", and "Apply".

Figure 3-7: Dialog box of the SOFC model

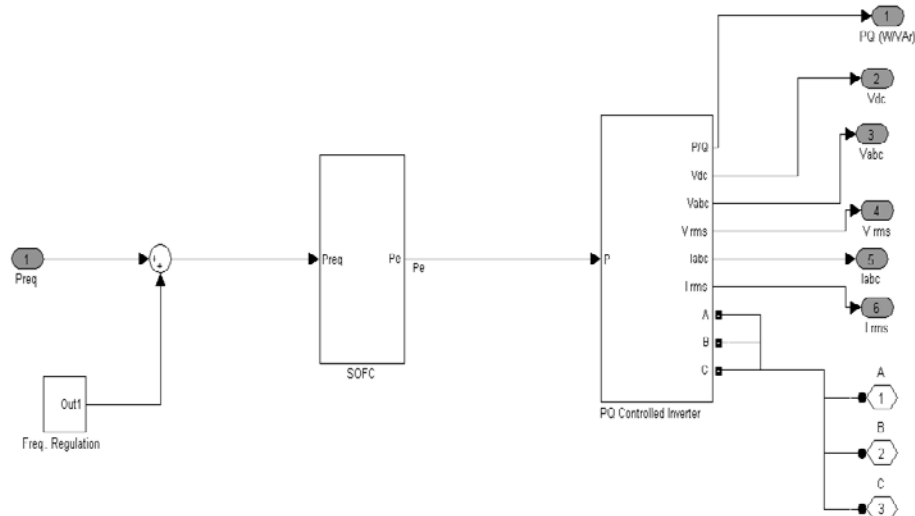


Figure 3-8: A detail of the SOFC mask

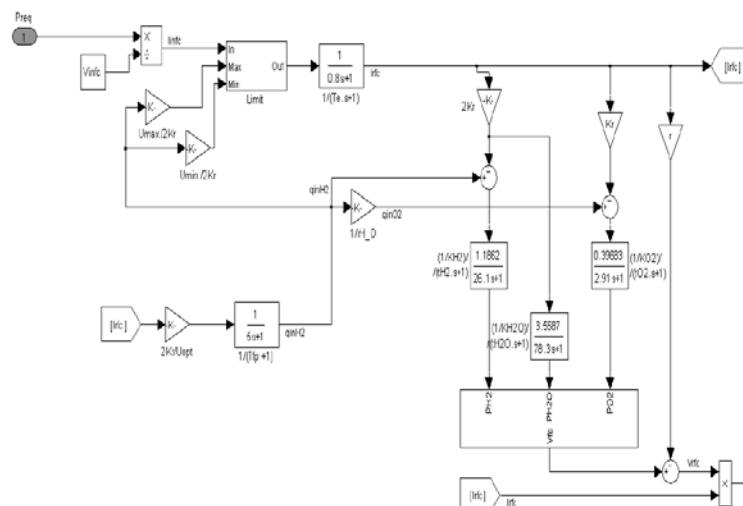


Figure 3-9: SOFC electrochemical model in the Matlab/Simulink environment

3.1.2 Adaptations and Enhancements

The development of the previously described MG simulation platform allows the evaluation of the feasibility of MG islanding operation through the analysis of the LV network dynamic behaviour considering only three-phase balanced operation, despite the fact that this is not the most common situation in LV distribution networks. In fact, the connection of single-phase loads and microgeneration units, together with the fact that many EV power electronic interfaces will be also single-phase units, the existing simulation platform was adapted and enhanced, taking into consideration the following issues:

- Development and implementation of models for representing the behaviour of single-phase power electronic interfaces, both for EV and microgeneration units;
- Development and implementation of the control model that enables EV contributing for improving MG operating conditions through active (dis)charging control depending of MG operational issues.
- Enhancement of models for micro-wind generators, including the development of a micro-wind generator models based on a PMSG.

Identification and development of additional control mechanisms to be placed at the power electronic converter level in order to improve MG operating conditions during islanding in case of excessive voltage imbalance.

3.1.2.1 Unbalanced Systems

Due to the nature of a low voltage MG, the coexistence of single-phase connected loads and microgeneration, together with single-phase connected EV power electronic interfaces can significantly jeopardize power quality due to voltage imbalance problems. The evaluation of the unbalancing is performed through the *Voltage Unbalance Factor (VUF)*, as used in the European power quality standard EN50160 "Voltage characteristics of electricity supplied by public distribution systems", being defined as:

$$\%VUF = (V_2 / V_1) \cdot 100\% \quad (3-4)$$

where V_1 and V_2 are respectively the positive and negative sequence voltage values.

Accurate power measurements are essential for robust operation of MG. The following approach was adopted in order to evaluate active power for an unbalanced four-wire three-phase system. For a three-phase power system, instantaneous voltages and instantaneous currents can be expressed as instantaneous space vectors, described by

$$\bar{v} = \begin{bmatrix} v_a \\ v_b \\ v_c \end{bmatrix}, \quad \bar{i} = \begin{bmatrix} i_a \\ i_b \\ i_c \end{bmatrix} \quad (3-5)$$

The instantaneous active power of a three-phase circuit, p and the reactive (non-active) power, q , is calculated as:

$$P = \bar{v}^T \cdot \bar{i} \quad (3-6)$$

$$q = \|q_{space}\| = \|\bar{v} \times \bar{i}\| \quad (3-7)$$

For a single-phase connection, the measurement was made based on the proposal of Burger and Engler [6]. With this approach no zero crossing detection is required. The power is computed by using the complex apparent power split up in its real and imaginary part, as described next:

$$\underline{s} = p + jq = \frac{1}{2} \underline{v} \cdot \underline{i}^* = \frac{1}{2} (v_r + jv_i)(i_r - ji_i) \quad (3-8)$$

where v_r and i_r are fictitious orthogonal components of the voltage and current, similar to the space vectors in three phase systems.

3.1.2.2 Power electronic interfaces

The characteristics of the energy produced in several MS require the use of power conditioning units in order to interface them with the LV grid. It is also important to note that MG are inverted dominated grids: it will not be common to find fully controllable synchronous generators in a MG, which are normally responsible for voltage and frequency control in conventional power systems. Therefore, implementing and adopting adequate inverter control strategies is a key issue to ensure stable MG operation in the presence of arbitrary varying conditions (load or generation variations).

The inverter control strategies for power export to an AC system can be generally divided in two types [4-5]:

- PQ inverter control: the inverter is used to supply a given active and reactive power set-point. In this case, the inverter operates in a grid-connected mode (grid tied inverter), being the power injected into an energized network. The inverter is not able to form the grid itself by imposing a voltage waveform with suitable amplitude and frequency.
- Voltage Source Inverter control: the inverter is controlled to supply the load with pre-defined values for voltage and frequency. Depending on the load, the Voltage Source Inverter (VSI) real and reactive power output is defined. In this case, the inverter is responsible to establish the voltage wave form with suitable amplitude and frequency. The inverters themselves produce an AC voltage; therefore it is possible to control voltage and frequency in the AC system by means of inverter control.

Due to the fast response of power electronic converters, they can be modelled from the network point of view by a controllable AC voltage source. The magnitude and phase of this voltage source is to be controlled according to the referred control strategies. It is also important to highlight that, when analysing the dynamic behaviour of the MG, inverters are modelled based only on their control functions, so that, fast switching transients, harmonics and inverter losses are neglected. This a general procedure adopted by several authors when dealing with power electronic interfaces in dynamic stability studies [4-5].

In addition to these general considerations, modelling single-phase and three-phase inverters requires different approaches, which are also described next.

PQ inverter control

The PQ inverter is operated under a grid-connected mode and should inject a given active and reactive power set-point into the network (the set-points are determined through specific algorithms or control functionalities). In addition to active and reactive power flow control, this inverter is also responsible for the control of the DC-link voltage of the cascading DC/AC/DC system [7]. Therefore, the internal voltage of the inverter is controlled in order to maintain the DC-link voltage at a specified reference and the reactive power output at the desired set-point. Neglecting losses, the power balance in the capacitor of the DC-link (P_C) is the difference between the power received from the MS (P_{MS}) and the inverter output power (P_{inv}), as shown in Figure 3-10:

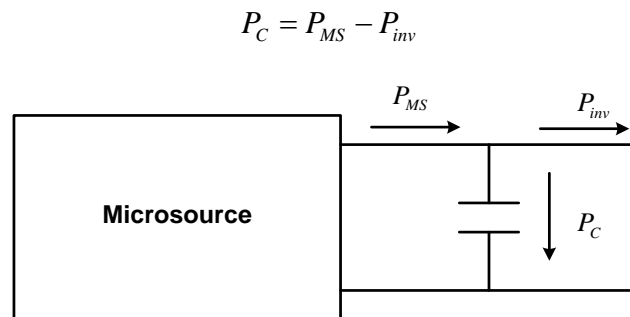


Figure 3-10: DC-link capacitor power balance

The power delivered by the capacitor can also be written as:

$$P_C = V_{DC} \times I_{DC} \quad (3-9)$$

where V_{DC} is the DC-link voltage and I_{DC} is the capacitor current. The DC-link voltage can be computed as:

$$V_{DC} = \frac{1}{C} \int I_{DC} dt \quad (3-10)$$

where C is the value of the capacitance in the DC-link. Combining the previous equations taking the Laplace transform, the DC-link dynamics can be modelled as in Figure 3-11.

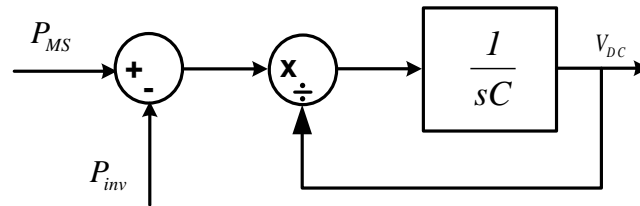


Figure 3-11: DC-link dynamic model

After modelling the dynamics of the DC link, it is now important to make specific references to the modelling approached for single-phase and three-phase PQ inverters.

Single-Phase PQ inverter

The PQ inverter control is implemented as a current-controlled voltage source, as shown in Figure 3-13. Current components in phase (i_{act}) and quadrature (i_{react}) with the inverter terminal voltage are computed based on a method presented in [6] and [8] for mean power calculation in single-phase inverters. Power variations in the MS induce a DC-link voltage error, which is corrected via the PI-1 regulator by adjusting the magnitude of the active current output delivered to the grid. The reactive power output is controlled via the PI-2 regulator by adjusting the magnitude of the inverter reactive current output. As it can be observed in Figure 3-12, the single-phase PQ inverter control system is formed by two cascaded loops. The inner most control loop regulates the inverter internal voltage (v^*) to meet a desired reference current (i_{ref}). The outer most control loop consists on active and reactive power regulators.

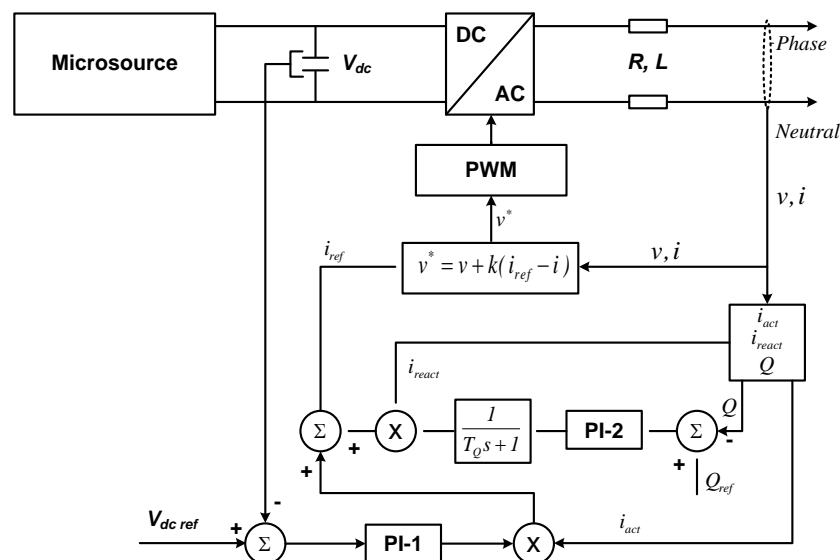


Figure 3-12: Single-phase PQ inverter control

Three-Phase PQ inverter

The control logic for the DC/AC PQ inverter control is also associated to the control of the DC voltage in the DC-link capacitor. Under such approach, the DC voltage error is used in order to generate the i_d current reference. The error that is generated between the reference value of reactive power and the actual injected power or between the reference voltage and the measured terminal voltage are used in order to generate the i_q current reference. The d-q reference currents are then transformed to the α - β stationary reference frame. Afterwards, the inner current control loop based on a proportional controller is used in order to generate the converter output voltages [7]. The described modelling approach is depicted in Figure 3-13.

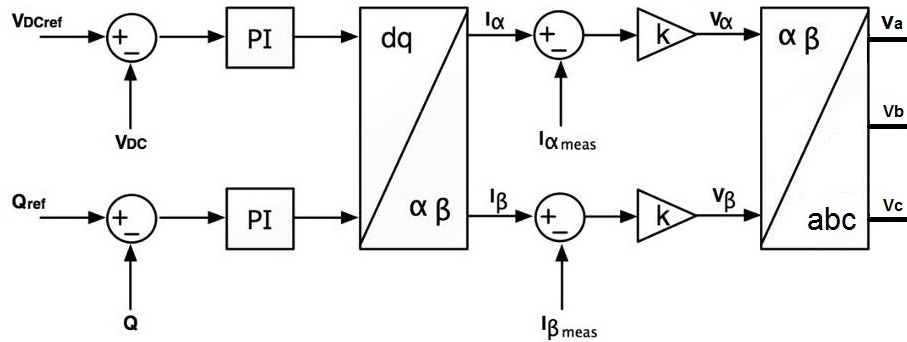


Figure 3-13: Three-phase PQ inverter control

Voltage source inverter control

The VSI is used in order to interface a storage device (such a flywheel or a battery) with the AC grid. By making use of the energy stored in such devices, the VSI is able to emulate the behaviour of a synchronous machine, thus controlling voltage and frequency on the AC system [4-6]. In conventional power systems, synchronous generators share any load increase by decreasing the frequency according to their governor droop characteristic. This principle is also implemented in inverters by decreasing the reference frequency when there is an increase in the load. Also, reactive power is shared by introducing a droop characteristic in the voltage magnitude. Therefore, the VSI acts as a voltage source, with the magnitude and frequency of the output voltage controlled through droops, as described in the following equations:

$$\begin{aligned}\omega &= \omega_0 - k_p \times P \\ V &= V_0 - k_Q \times Q\end{aligned}\tag{3-11}$$

where P and Q are the inverter active and reactive power outputs, k_p and k_Q are the droop slopes (positive quantities) and ω_0 and V_0 are the idle values of the angular frequency and voltage (values of the inverter angular frequency and terminal voltage at no load conditions).

When a VSI is interconnected with a stiff AC system, characterized by an angular frequency ω_{grid} and terminal voltage V_{grid} , the voltage and frequency references are externally imposed [4]. In this case, the desired output powers P_l and Q_l can be obtained in the VSI output by adjusting the idle values of the angular frequency ω_{0l} and voltage V_{0l} as follows (illustration in Figure 3-14):

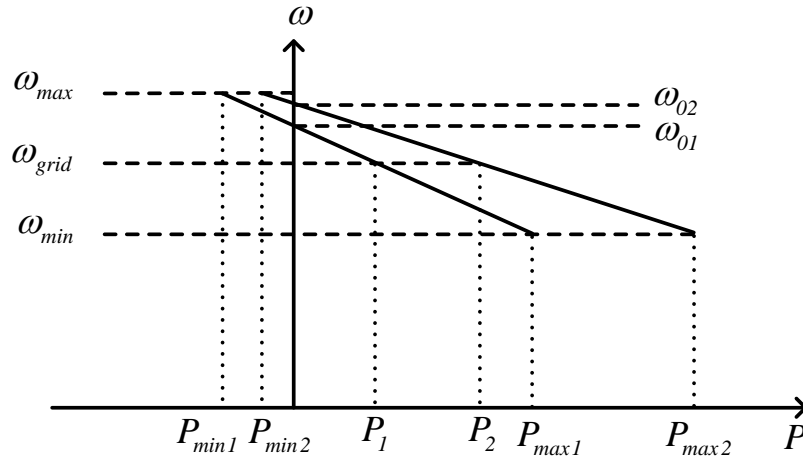


Figure 3-14: Frequency versus active power droop

$$\begin{aligned}\omega_{0l} &= \omega_{grid} + k_p \times P_l \\ V_{0l} &= V_{grid} + k_Q \times Q_l\end{aligned}\tag{3-12}$$

A three-phase balanced model of a VSI implementing the described droop concepts was derived from a single-phase version presented in [6], [8]. The general block diagram of the control scheme is presented in Figure 3-15. The VSI terminal voltage and current are measured in order to compute active and reactive powers. This measuring stage introduces a delay for decoupling purposes. The active power determines the frequency of the output voltage by the active power/frequency droop k_p . Similarly, the reactive power determines the magnitude of the output voltage by the reactive power/voltage droop k_Q . A phase feed-forward control was included for stability purposes, corresponding to the k_{ff} gain in Figure 3-15. The output voltages are the reference signals that control the VSI switching.

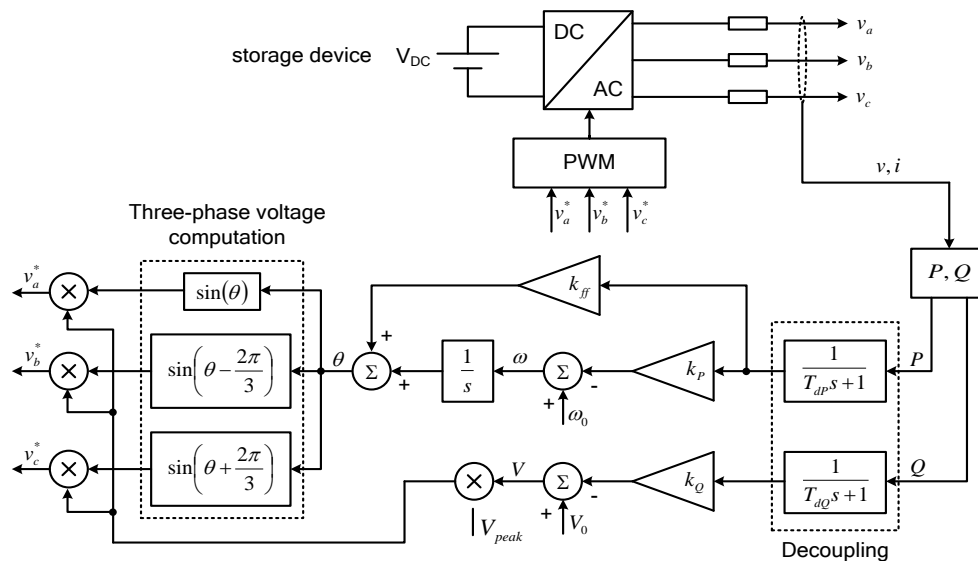


Figure 3-15: Three-phase balanced VSI control model

VSI with voltage balancing control mechanisms

The VSI model previously described presents at its terminals a set of three-phase balanced voltages in case it feeds a three-phase balanced system. However, the presence of unbalanced operating conditions in the low voltage MG will result in an unbalanced set of voltages at the VSI input voltage due to unbalanced voltage drops in the inverter coupling inductance. In order to mitigate the corresponding power quality problem resulting from voltage imbalance, the VSI model previously described was complemented with additional control functionalities aiming to reduce negative and zero sequence voltages at its connection node. In order to be possible to derive such control approach, it is necessary to assume that the VSI will be based on a four-legged inverter, since it is the only power converter structure that allows an independent control of all the single-phase voltages.

The VSI unit with the voltage balancing mechanism is to be interfaced with a storage device (such as battery or flywheel) and the MG, and has the ability to produce three independent output voltages, regardless of loading. The operating principle of the balancing unit is based on cancelling all unwanted negative and zero sequence voltage components, according to the control structure described in [9]. In order to allow the operation under interconnected or isolated operation mode, it is necessary to provide a variable-frequency operation mechanism, which can be provided through the use of droop-control concepts (active power versus frequency droop and reactive power versus voltage droop), as described in [4]. The use of droop control concepts allows the definition of the voltage reference for the voltage balancing unit.

As shown in Figure 3-16, the main control system of the VSI inverter with a voltage balancing control mechanism consists on a voltage-current regulation block and an external droop control block. The droop control block provides a voltage reference signal at its output. This reference signal depends on the actual active and reactive

power output of the inverter, as it was previously mentioned in relation to the three-phase balanced VSI control system. The control structure is implemented in the stationary $\alpha\text{--}\beta\text{--}0$ reference frame. The use of the stationary reference frame is computationally more efficient, since it avoids frame transformations for the positive and negative voltage components [9]. However, it requires the use of a specific controller, which is the resonant controller, in opposition to simple PI controllers that can be used when a synchronous reference frame control structure is adopted. The basic idea of a resonant controller is: for a DC control signal, the PI controllers provide an infinite gain at a zero frequency (DC signal); in a stationary frame controller, in order to be possible to make the controller to follow accurately the reference signal, it is necessary to have an infinite gain (resonance) at a specific operating frequency. The transfer function of the resonant controller is written as:

$$G(s) = K_p + \frac{K_i s}{s^2 + \omega^2} \quad (3-13)$$

where ω is the resonance frequency of the controller, K_p is the proportional gain and K_i is the integral gain of the controller. The characteristic of this controller is the fact it achieves a very high gain (tends to infinite) around the resonance frequency, which makes it capable of eliminating the steady state error between the controlled and the reference signal. However, the practical implementation of such controller is not feasible due to the resulting gains around the resonance frequency. Therefore, a more practical implementation form can be written according to the following transfer function, which approximates the ideal integrator by [10]:

$$G(s) = K_p + \frac{K_i \omega_{cut} s}{s^2 + 2\omega_{cut} s + \omega^2} \quad (3-14)$$

where ω_{cut} is the low-frequency cutoff (being $\omega_{cut} \ll \omega$). According to Figure 3-16, the use of resonant controller is used in each of the $\alpha\text{--}\beta\text{--}0$ coordinates. The inner current control block (current control in Figure 3-16) is simply a proportional controller that allows the derivation of the inverter individual phase voltages from the inverter current references.

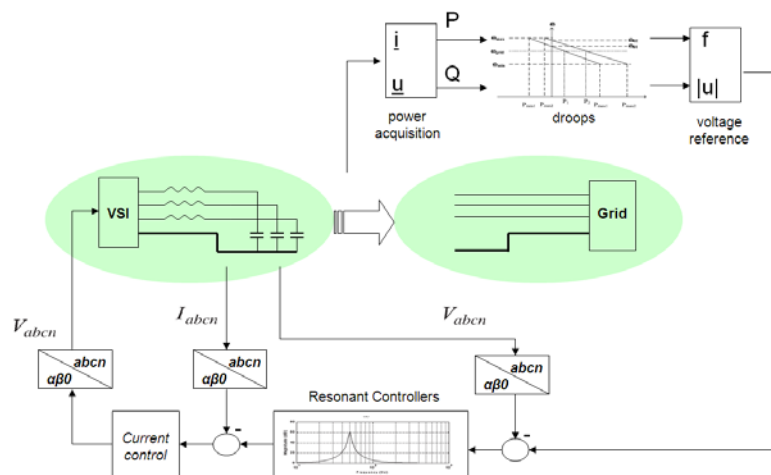


Figure 3-16: General block diagram of the three-phase VSI with voltage balancing mechanism

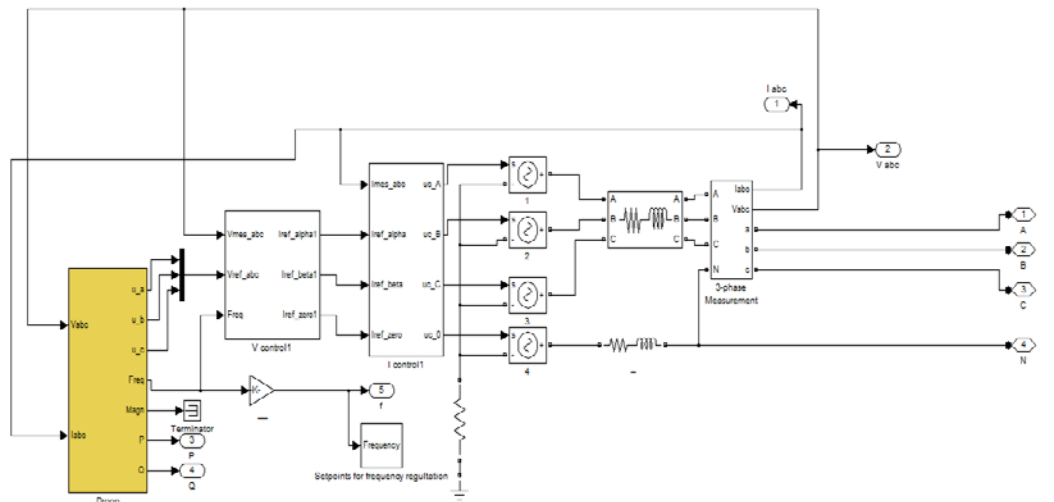


Figure 3-17: General block diagram of the three-phase VSI with voltage balancing mechanism in Matlab/Simulink

Regarding the VSI model with voltage balancing mechanism implementation in the Matlab/Simulink simulation platform, Figure 3-17 and Figure 3-18 shows its major control blocks. It is important to mention that the voltage control block is composed by resonant controllers with different sets of control parameters: a set of control parameters is used for the MG interconnected operation mode, while a different set of parameters is required for MG islanding operating conditions. This is due to stability problems at these types of controllers when working on emergency mode or in grid-connected mode. In grid-connected mode, the proportional gain K_p of the controller has to be close to zero, otherwise the whole system will suffer from stability problems. On the other hand, on island mode of operation, the MG would only be stable for higher values of proportional gain (K_p), cut-off frequency (ω_c) and integral gain (K_i). Again, due to stability problems, if K_p is chosen rather low, the dynamic simulations also collapse.

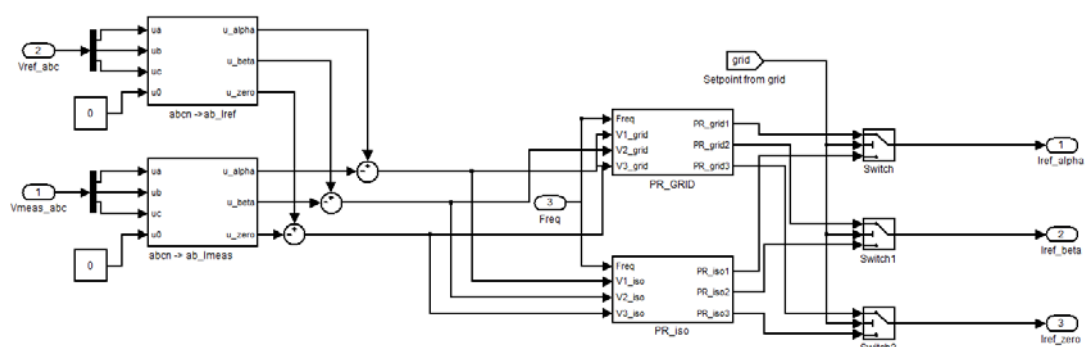


Figure 3-18: Voltage control block implementation in Matlab/Simulink

Referring to the Current Control Block (Figure 3-19), the error signal generated between the reference current and the grid measured current is controlled by

proportional controllers only, because any steady state error in this loop would not affect the outer voltage loop accuracy substantially [9]. The output signal of the current block suffers an inverse Clarke transformation to obtain the output signal in the natural reference frame. This signal will be responsible for controlling the balancing unit, in this case, the ideal voltage sources.

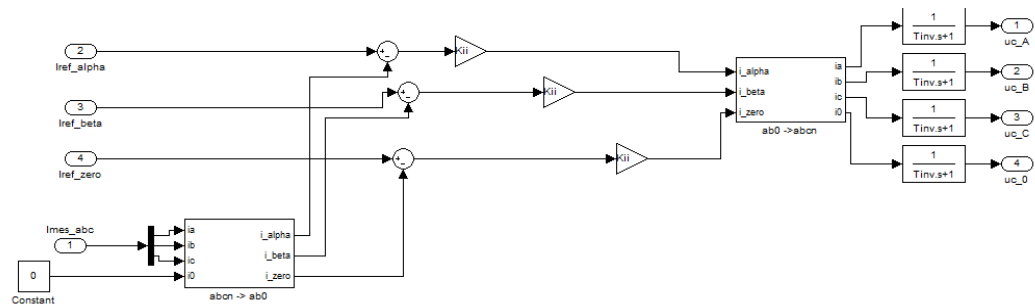


Figure 3-19: Current control block in the Matlab/Simulink simulation platform

3.1.2.3 Modelling and control of EV connected to the LV grid

The EV modelling approach followed in this research assumes that the EV grid connection is single-phase (between a phase and the neutral conductor), as it is depicted in Figure 3-20. The DC-DC converter, linking the battery to the capacitor, takes the role of controlling the (dis)charging current on the battery side. On the other side, the AC-DC converter assures the link between the grid and the DC-link capacitor. The capacitor voltage is controlled to be constant by an adequate adjustment of the power flow with the AC grid. The variations seen in the DC-link capacitor voltage are due the power demand/injection on the battery side. Therefore, the general control approach that is followed in the operation of the DC/AC EV power electronic interface is the same presented in section 3.1.2.2 for single-phase PQ controlled inverters. Therefore, in addition to the power electronic interface model for the EV, the main issue concerning EV modeling is related to the control loops that are required in order to make EV power electronic interface to respond to specific grid operating conditions, and therefore contribute to improve its operational conditions by delivering system services for voltage and power/frequency control (for example).

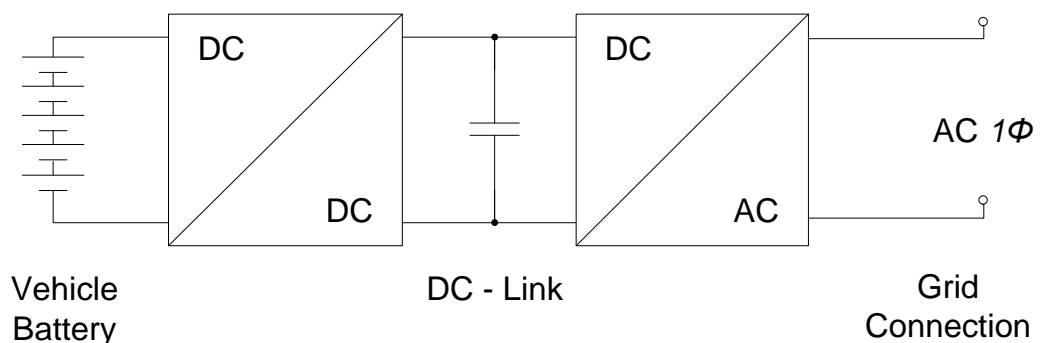


Figure 3-20: Schematic representation of an EV battery power electric interface with the AC grid

Concerning the development of the EV interface model, the following assumptions were made:

- The grid connection is single phase;
- There is no need to have a distinguishable model for each vehicle, assuming that the main difference between them is the rated power, which will be a parameter of the control model;
- Concerning the time frame for dynamic simulation of a MG, there is no need to model the battery in detail (it can be represented by the power consumption/ injection at the DC-link level);
- Losses in the converters can be neglected (the power set point represents the power demand seen on the grid side and therefore accounts for all losses);
- There is an upper limit for the power drawn from the grid and an upper limit for the power injected in it (those limits are assumed to be equal, but could be adapted asymmetrically, by means of the model parameters).

As it was previously mentioned, modeling EV integration in low voltage MG is focused on deriving specific control loops to be used for the definition of the EV power converter set point depending on grid specific conditions, namely frequency or voltage. Independently of the control loops, the models that were developed are oriented for the definition of set points based on information that is available locally at the EV connection point. The derivation of such local controllers allows EV to react in a very fast way to grid operating conditions, without need to rely in fast communications with any control structure of the grid.

EV control based on MG frequency

One possibility of adapting the power set point of the EV power electronic interface is reducing the power drawn from the grid with respect to the system frequency. The frequency is a value that can be measured in any point of the grid and therefore this does not require a communication link. During islanded operation conditions, the frequency is an instantaneous indication for the power balance in the MG. It is therefore used to adapt the active power (dis)charging of the EV batteries, as described in Deliverable D1.2 [2]. For this purpose, the following control approach was developed (see Figure 3-21):

- EV charge up their batteries, at frequencies above f_{dz} , by absorbing power at a certain reference value P_{ab} (equal or lower to the nominal charging rate). A dead-zone area is introduced in order to avoid EV reaction to small frequency deviation below the nominal grid frequency f_{nom} that result from small consumption or generation changes.
- The power consumption is linearly reduced to zero, with a droop k_{p1} , when the frequency drops below f_{dz} . The zero-crossing frequency, f_0 , is a parameter of free choice.

- If the system frequency drops below f_0 , the EV start to inject power into the grid, with a droop k_{p2} , becoming a Vehicle-two-Grid (V2G) device. At f_{neg} , another parameter of free choice, the V2G device injects a certain amount of available power P_{inj} (equal or lower than the maximum available power).

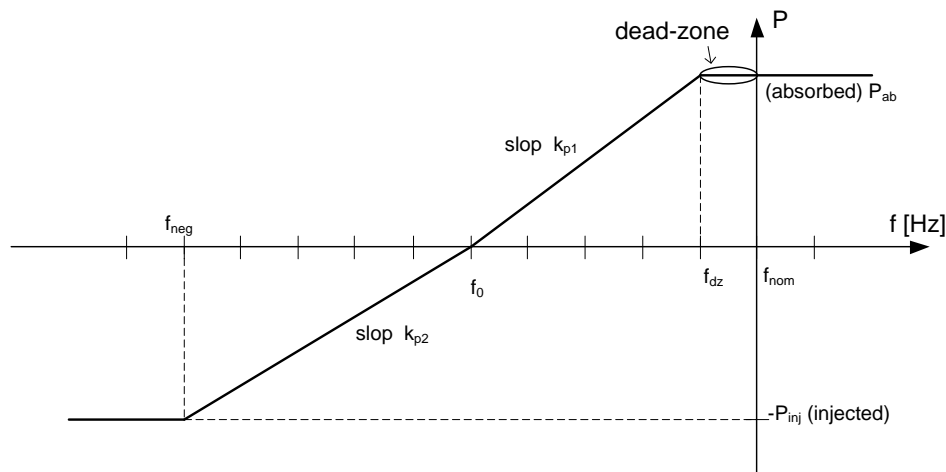


Figure 3-21: Frequency droop control strategy for EV in a MG

This proportional control to be implemented at EV power electronic interfaces is inspired by the existing droop characteristics of the VSI and is therefore called “frequency droop control”. Nevertheless, it is important to notice that this control mechanism is implemented in an opposite way to the droop control implemented in the VSI / balancing unit, where power measurements are used for a frequency like control. In this case, a local measurement of grid frequency is taken by the EV connection node and is used in order to define a set point for the power exchange with the LV grid.

The selection of the most adequate values for the EV control parameters (f_{dz} , f_0 , f_{neg} , k_{p1} , k_{p2} , P_{ab} and P_{inj}) depends on the willingness of EV owners to participate in such services, as well as on the effectiveness of local secondary frequency control and on the MG strategies for primary frequency control (load shedding schemes, availability of energy storage devices and their state of charge). These parameters may differ from grid to grid and can be changed by the MGCC, using the communication link that is supposed to exist. This will require a communication protocol between the MGCC and EV interfaces that needs to be further researched.

EV control based on voltage

The MG is a LV network with lines having high R/X coefficients. If voltage sags occur, it has been shown that they cannot be corrected efficiently by injecting reactive power. In the present case it is more efficient to reduce the load or inject active power. Therefore a similar control approach as the one used for frequency regulation can be implemented to deal with voltage drops that may result from normal or abnormal operation of the MG. Figure 3-22 shows the proposed control

approach, which is similar to the control strategy defined for MG frequency control purposes.

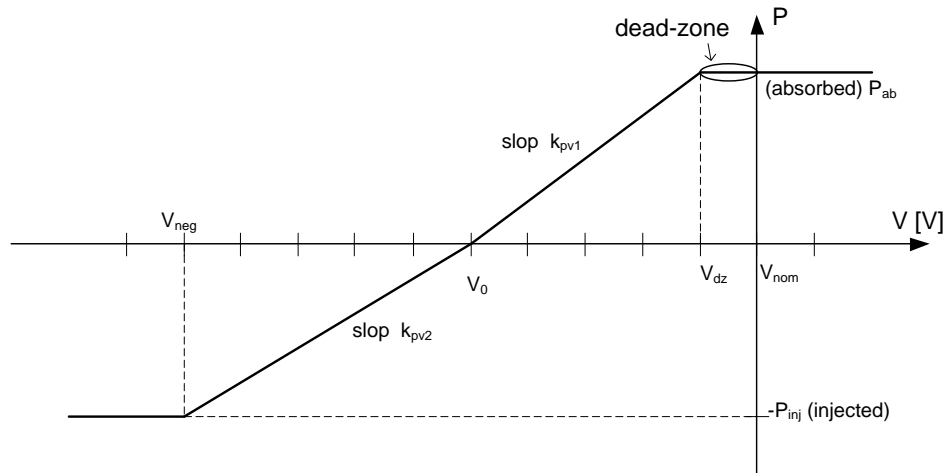


Figure 3-22: Voltage droop control strategy for EV in a MG

A combination of these two control strategies can be done by defining the power set point to be followed by each EV. The adoption of a mean value approach is not optimal, as both parameters (frequency and voltage) would have to be simultaneously at the lower defined limit (f_{neg} and V_{neg}) for the EV to inject its maximum available power. In islanding mode, load balancing should be considered as the key concern. Therefore the power set point to be adopted by each V2G device is defined in the following equation. In this way, local generation scarcity is taken into account with priority regarding local voltage drops.

$$P_{set} = \begin{cases} P_{set_f} & \text{if } P_{set_f} < P_{set_V} \\ P_{set_V} & \text{otherwise} \end{cases}$$

3.1.2.4. Micro-wind generator

Being the most common design in small and micro wind turbines, the horizontal axis design is the one to be considered in this work. It generally consists of a rotor where the turbine is solidly fixed, an electrical generator, a mainframe and a tail. The turbine usually consists of two or three blades. The electrical generator is specifically designed for the wind turbine. Permanent magnet generators are popular since they do not require the need of brushes as in direct current machines and in some conventional synchronous generators with separate excitation systems. In most small and micro wind turbine designs, the rotor is connected directly to the shaft of the permanent magnet generator, thus creating variable frequency and voltage AC power, according to the wind speed. The output power is then rectified to DC to either charge batteries or feed a grid-synchronous inverter. In the designs with a direct coupling between the turbine and the generator, high reliability and

lower cost is achieved since the design eliminates the additional maintenance of gears and the relatively low reliability indexes of these devices.

The electrical generator is assumed to be a three-phase two-pole PMSG with a non-salient rotor. The machine electrical equations can be written in the rotor d - q reference frame as follows [11]:

$$\begin{aligned}v_d &= R_s i_d - p\omega L_q i_q + L_d \frac{di_d}{dt} \\v_q &= R_s i_q + p\omega L_d i_d + L_q \frac{di_q}{dt} + p\omega \Phi_m \\T_e &= \frac{3}{2} p \left[\Phi_m i_q + (L_d - L_q) i_d i_q \right]\end{aligned}$$

where:

L_d, L_q	d and q axis inductances (H)
R_s	stator windings resistance (Ω)
i_d, i_q	d and q axis currents (A)
v_d, v_q	d and q axis voltages (V)
ω	angular velocity of the rotor (rad.s ⁻¹)
Φ_m	flux induced by the permanent magnets in the stator windings (Wb)
p	number of pole pairs
T_e	electromagnetic torque (N.m)

The mechanical equation needs to take into account the combined inertia and load viscous friction of the PMSG and wind turbine that are mounted in the same shaft:

$$T_e - T_m = J \frac{d\omega}{dt} + F\omega \quad (3-15)$$

where:

T_m	load mechanical torque (N.m)
J	combined inertia of the load, PMSG, shaft, turbine and compressor (kg.m ²)
F	combined viscous friction factor of the load, PMSG, shaft, turbine and compressor (N.m.s.rad ⁻¹)

The variable frequency AC power produced in the PMSG must be rectified and inverted in order to be injected into the AC grid. The machine side converter is responsible for controlling the PMSG operation in terms of rotation speed and power factor [11]. A block diagram of the machine side converter and its control structure is shown in Figure 3-23. The wind turbine speed is controlled through its operational characteristics in order to extract maximum power from the wind. The turbine speed error is used to compute the i_q reference current, which is supplied to a PI controller in order to regulate v_q and thus the turbine angular velocity. The i_{dref} current can be calculated by another regulator in order to insure a unit power factor for the PMSG.

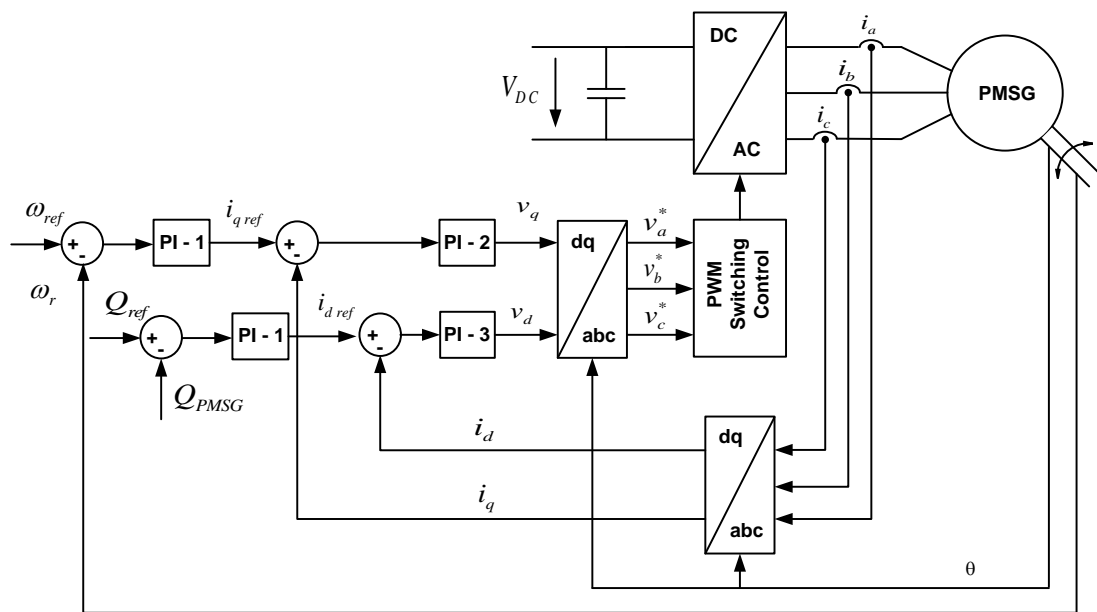


Figure 3-23: Micro-wind turbine machine side converter

3.1.2.5 Low Voltage grid unbalanced modelling

In this section it is presented a brief overview of the models that were adopted in the Matlab/Simulink simulation platform for representing grid elements (utility source, LV lines/cables and loads) using the SimPowerSystems tool-box.

Utility Grid

The model of the utility grid used on the simulation platform aims to represent the voltage level at the secondary of a MV/LV distribution transformer. Therefore, it corresponds to a three-phase-four wire model of ideal voltage sources with infinite power rating, as depicted in Figure 3-24:

$$V_a(t) = V_0 \cdot \sin(\omega \cdot t + \phi)$$

$$V_b(t) = V_0 \cdot \sin\left(\omega \cdot t + \phi - \frac{2\pi}{3}\right)$$

$$V_c(t) = V_0 \cdot \sin\left(\omega \cdot t + \phi + \frac{2\pi}{3}\right)$$

In order to be possible to make the transitions between grid connected and islanded operating modes of the MG, a three-phase breaker was installed, controlled externally through a step signal.

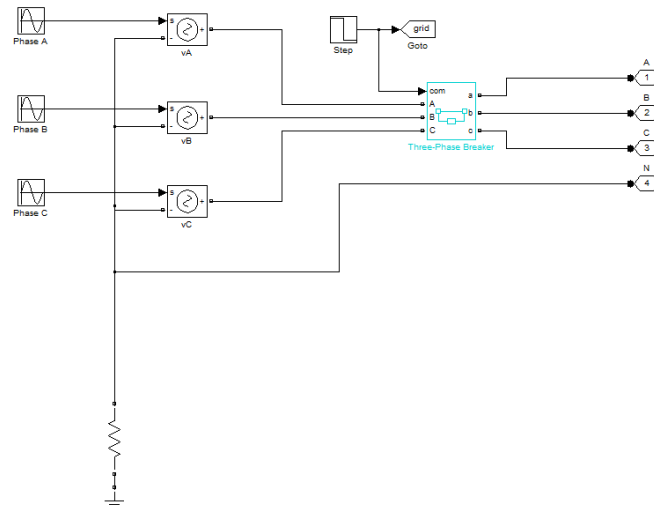


Figure 3-24: Utility grid model

Low Voltage Lines/Cables

The model used for representing LV lines and cables corresponds to a simple parallel RL parallel model (Figure 3-25). The RL parallel model is preferred to other models (e.g. PI model) as those would cause significantly lower simulation speed.

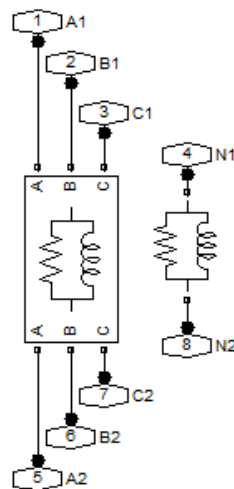


Figure 3-25: Four-wire line model

Loads

Load models, for both single- and three-phase loads, consist in series connected RL branches with constant impedances, as depicted in Figure 3-26.

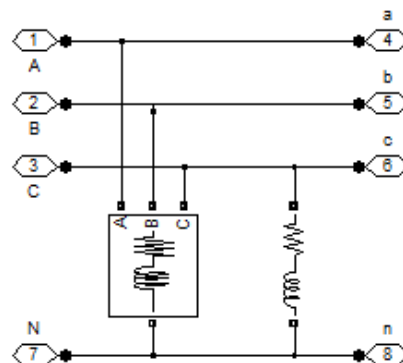


Figure 3-26: Three and single-phase loads

By integrating the models described in the previous sections, together with the network element models, Figure 3-27 presents a general overview of the simulation platform, which presents important aspects related to modularity and simplicity of use and simplicity for different MG modelling.

3.1.3 Preliminary Results

In order to test the performance of the modelling approach presented in this report, together with the control approaches for voltage balancing units and EV (dis)charging, the simulation platform previously described was used in order to

simulate the dynamic behaviour of a MG, which is represented in Figure 3-27. It consists on:

- A energy storage unit coupled to a VSI with voltage balancing mechanism;
- Two SSMT;
- 10 EV interfaces (single phase);
- 2 PV panels;
- 1 micro-wind generator
- several single phase and three-phase loads.

Prior to islanding, the MG is importing 20.7 kW from the upstream grid (6.9 kW in Phase A, 6.7 kW in phase B and 7.1 kW in Phase C). The main control approach that were tested in this phase is the use of frequency droop control in EV, as well as the effectiveness of the VSI with voltage balancing in the mitigation of voltage imbalance issues in the islanded MG. In a first stage, the dynamic simulation platform was used in order to test MG islanding when EV acts as passive loads, without any response to grid operational conditions. MG islanding was simulated at $t=2$ s. In Figure 3-28 it is possible to observe MG frequency during and in the moments subsequent to MG islanding. In Figure 3-29 it is possible to clearly observe that EV power (negative values mean power consumption from EV) appears as constant loads to the MG system during the period under analysis. Therefore, frequency restoration to the nominal value is possible by active by acting at controllable MS level (in this case, the SSMT). Figure 3-30 shows the power output per phase at the VSI. It can be easily concluded that the mean output power at the VSI (sum of the power in each phases) tends to zero as the frequency is progressively restored to the nominal value. In Figure 3-31 it is possible to observe the voltage imbalance at VSI terminals. Due to the voltage balancing mechanisms implemented at this unit, it is able to provide a balanced voltage at its output terminals, even at unbalanced loading conditions. In Figure 3-32, it is possible to observe the voltage imbalance at the bottom part of the MG. It is possible to conclude that, even during unbalanced operating conditions, voltage imbalance is kept in lows values.

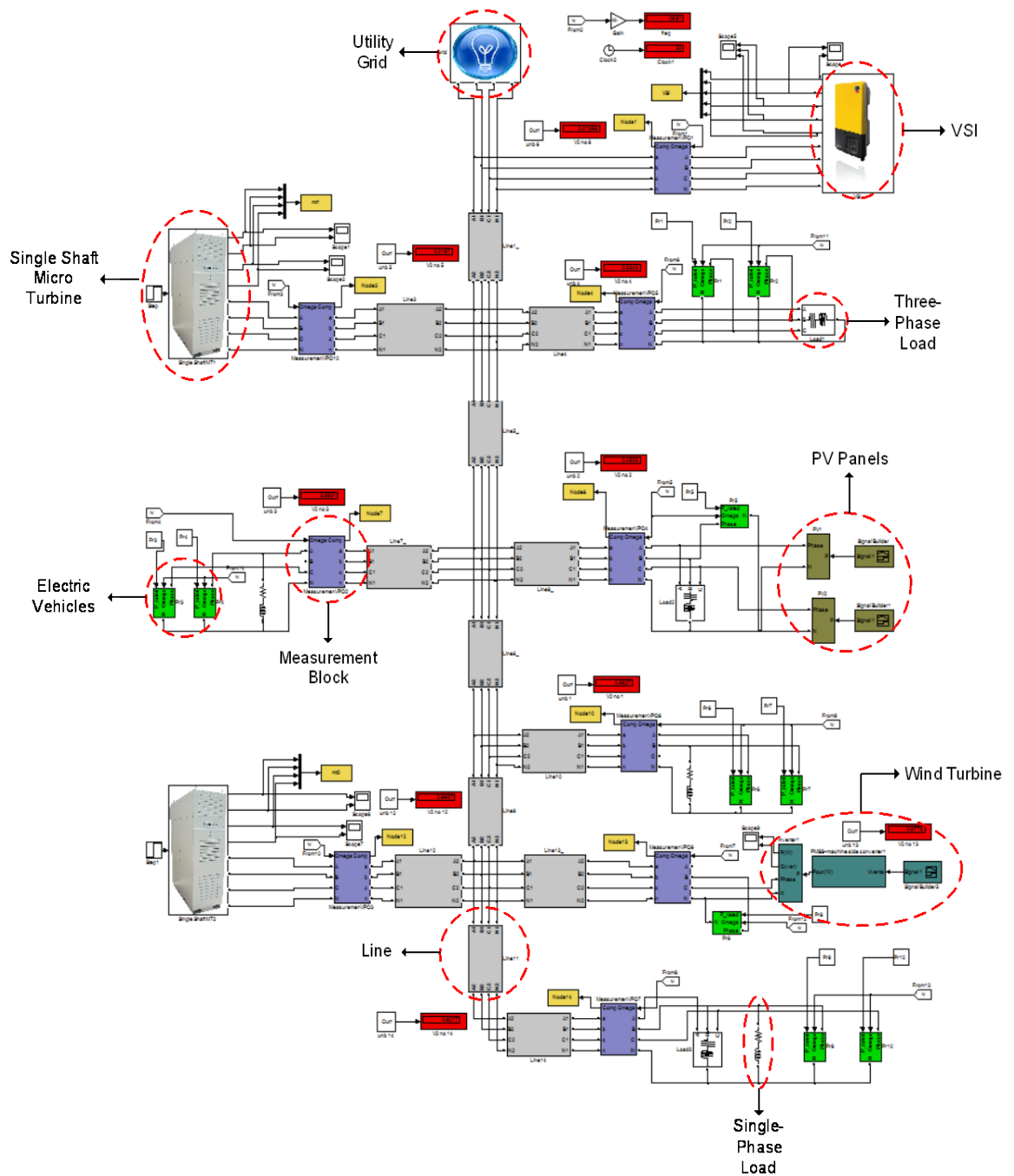


Figure 3-27: General overview of the adapted MG simulation platform

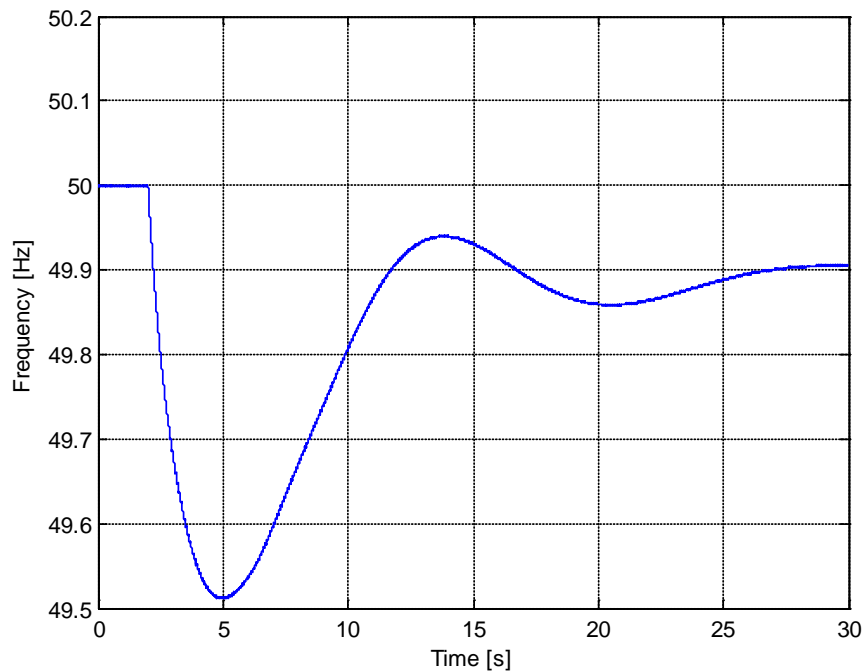


Figure 3-28: MG frequency during and in the moments subsequent to islanding (EV with no control capabilities)

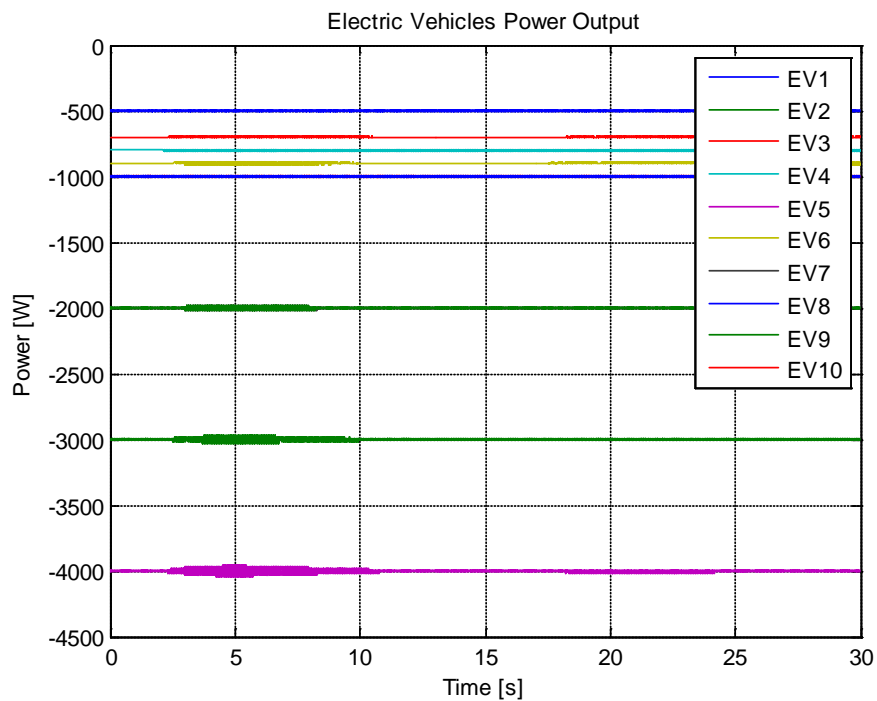


Figure 3-29: EV active power (EV with no control capabilities)

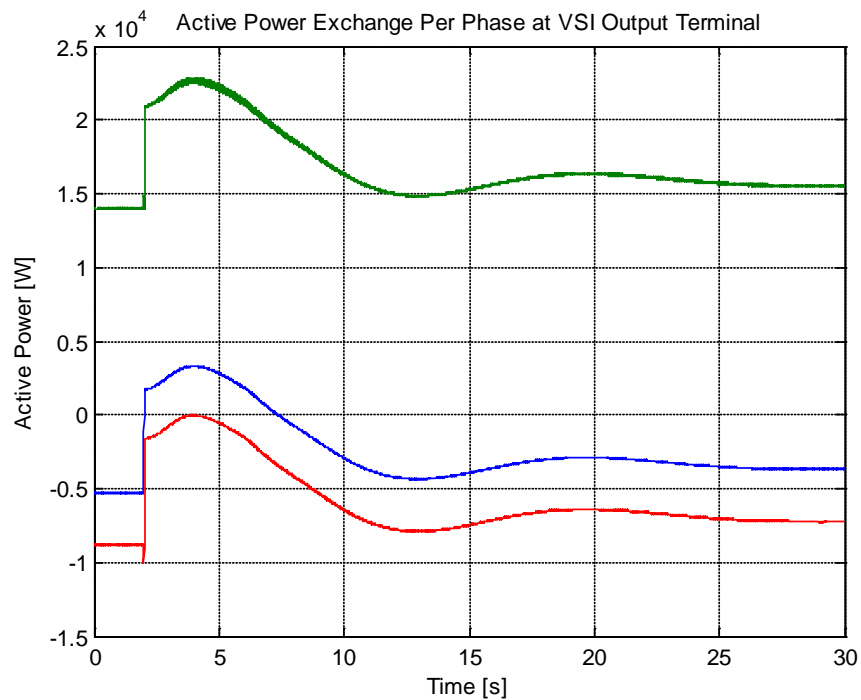


Figure 3-30: Active power per phase at VSI output terminal (EV with no control capabilities)

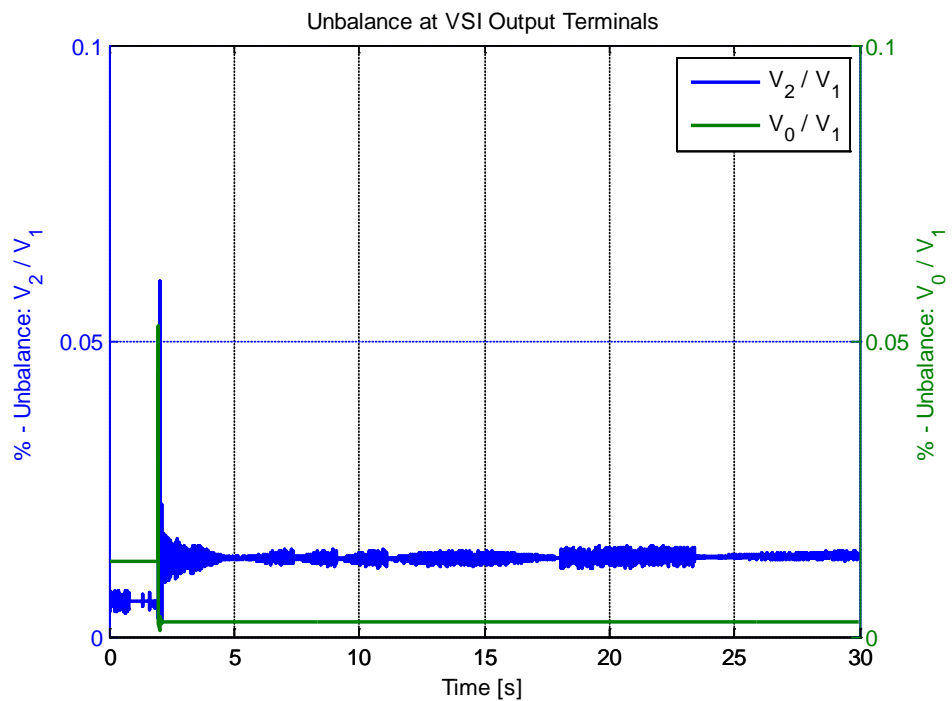


Figure 3-31: Voltage imbalance at VSI terminals

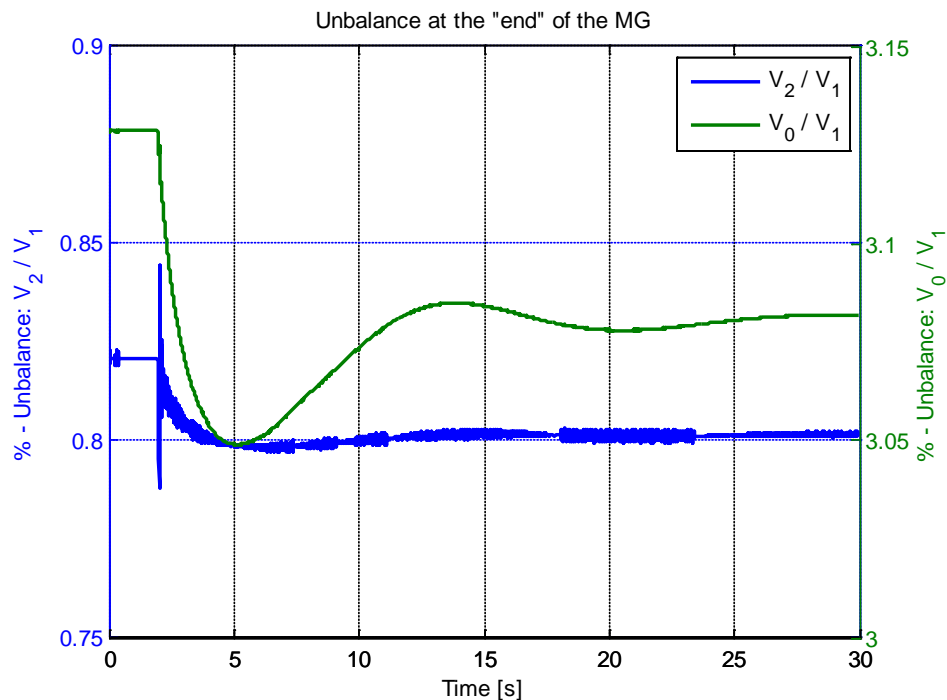


Figure 3-32: Voltage imbalance at the bottom node of the MG

After these initial tests, the MG simulation platform was now used in order to illustrate the potential benefits EV may have for MG operational conditions during and in the moments subsequent to islanding. Taking into consideration the same MG operating scenario that was previously described, the active power set point in EV was assumed to be locally controlled through a power/frequency droop, as it was previously described. As it can be observed in Figure 3-33, MG frequency deviation is now substantially reduced, when compared to the values presented in Figure 3-28. This is due to the active response of EV interfaces that are able to quickly adapt their power flow with the MG according to the locally parameterized droop control. As it can be observed in Figure 3-34, EV have different responses to MG frequency, depending on the droop parameters implemented in each one. Therefore, some EV just reduce the power being absorbed from the grid, while other start injecting power into the grid (V2G operation). In Figure 3-35, it is possible to observe that VSI coupled to storage devices has now a smaller contribution to the initial balanced between load and generation in the MG following islanding, since EV provide also an important contribution for the primary frequency control. In Figure 3-36 it is possible to observe the voltage imbalance at VSI terminals. Due to the voltage balancing mechanisms implemented at this unit, it is able to provide a balanced voltage at its output terminals, even at unbalanced loading conditions. In Figure 3-37, it is possible to observe the voltage imbalance at the bottom part of the MG. It is possible to conclude that, even during unbalanced operating conditions, voltage imbalance is kept in lows values.

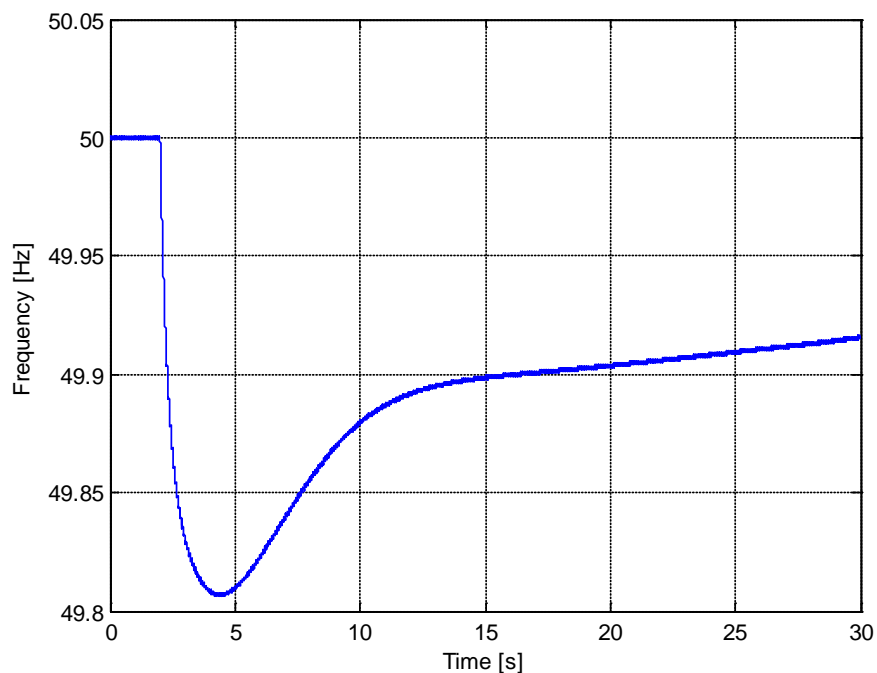


Figure 3-33: MG frequency during and in the moments subsequent to islanding (EV with droop control)

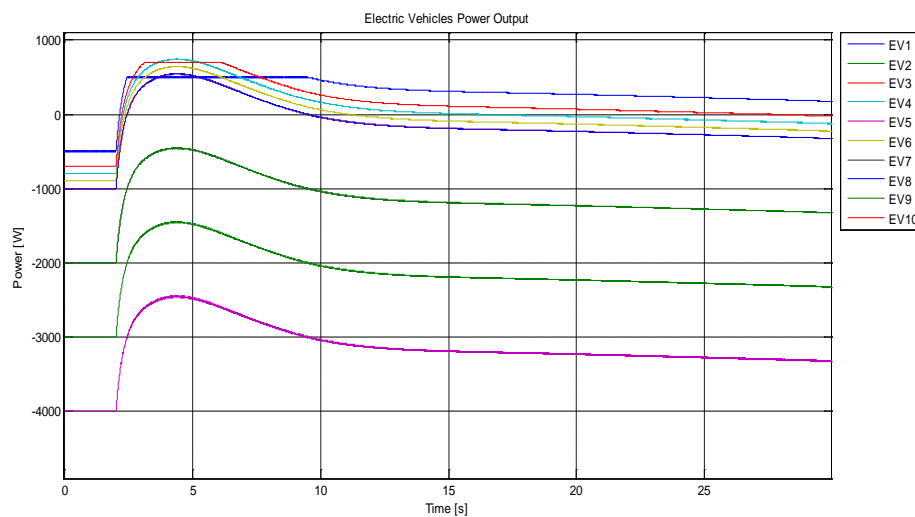


Figure 3-34: EV active power (EV with droop control)

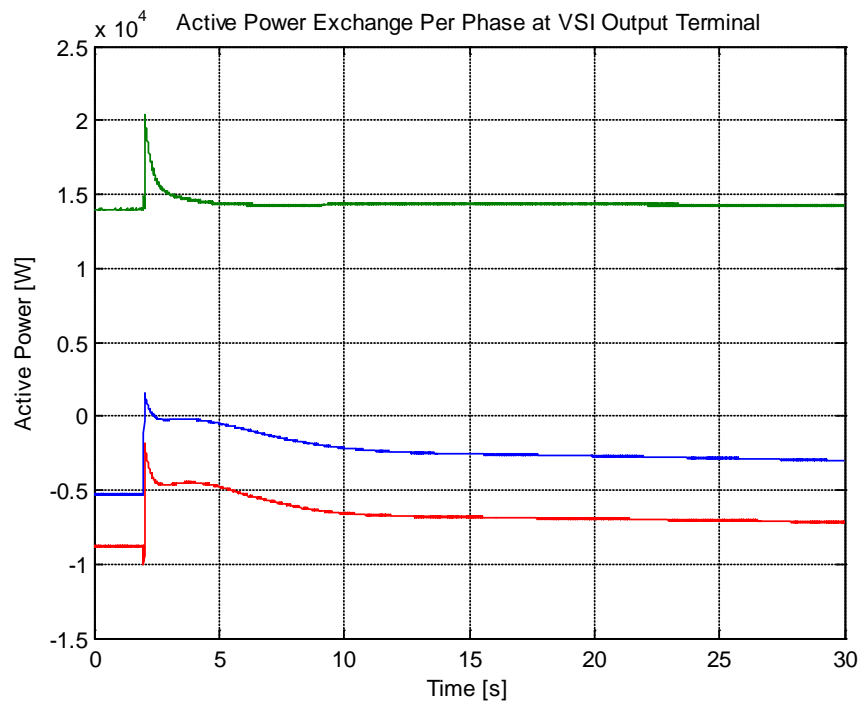


Figure 3-35: Active power per phase at VSI output terminal (EV with no control capabilities)

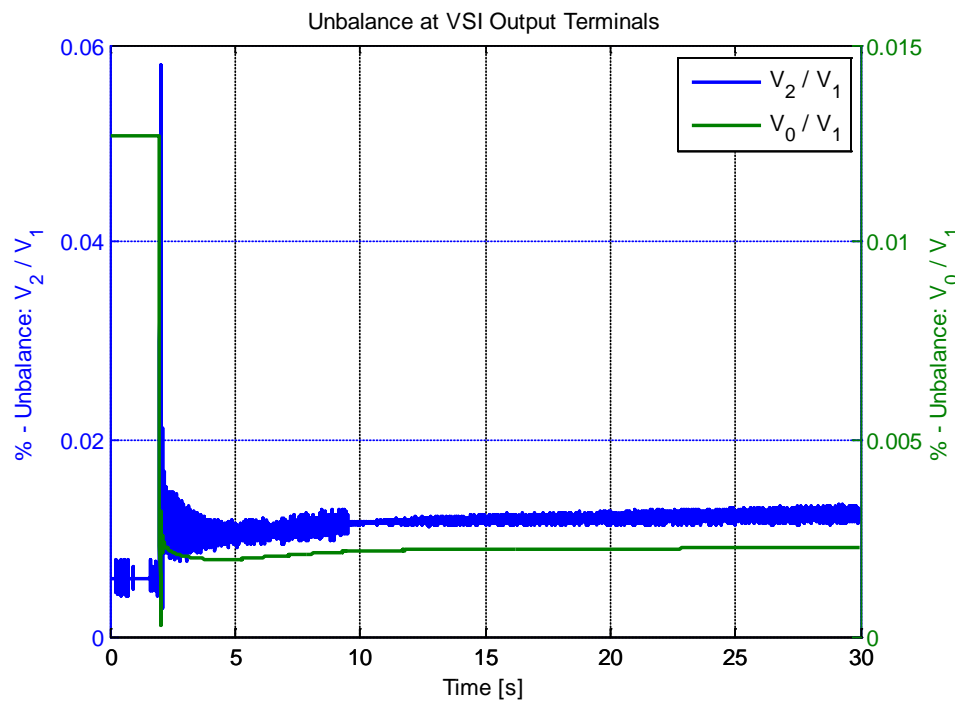


Figure 3-36: Voltage imbalance at VSI terminals

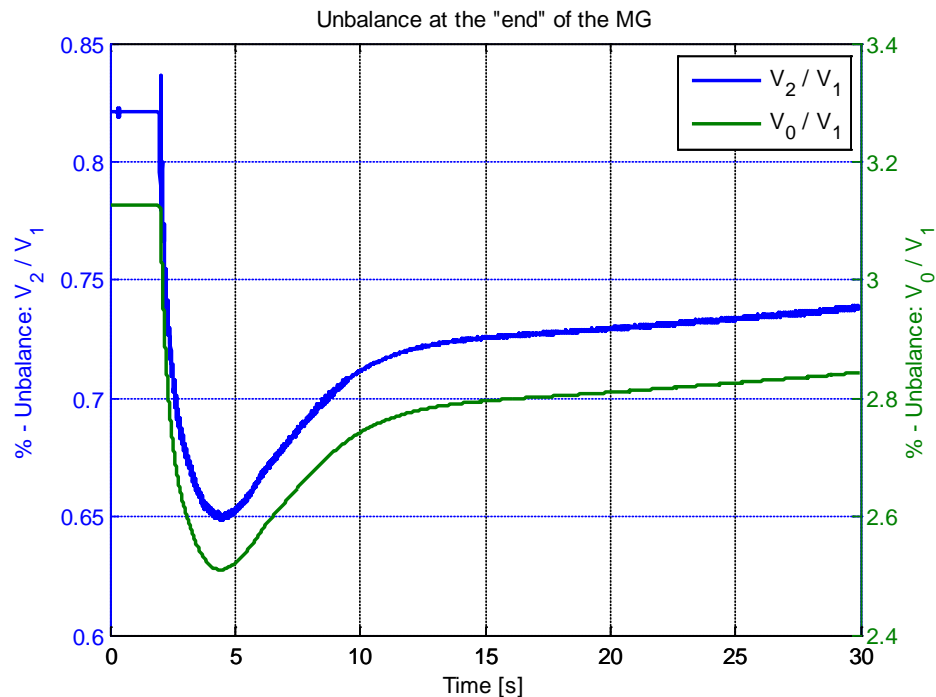


Figure 3-37: Voltage imbalance at the bottom node of the MG

The results presented in this section clearly put in evidence the adaptations and enhancements that were made upon the existing MG simulation platform, which include model development for MS and especially for EV power electronic interfaces. Additionally, the simulation platform was tested in order to illustrate its potential for being used regarding the dynamic analysis of the MG concept with EV under unbalanced operating conditions. Additional studies are required in order to understand EV contributions for voltage control under the active power-voltage droop concept that was previously described. In cases where voltage imbalance might become a critical issue in MG operation, additional functionalities need to be identified in order to determine the most adequate set points for EV and MS power set points regarding the need of mitigating the voltage imbalance problem. Such advanced control procedure will make use of the simulation platform described in this document in order to identify the most adequate control structures and in order to test its effectiveness.

3.2 The Simulation Platform Developed in NTUA

Power system analysis software is used as a general practice at the design and operational stage to make sure that a power system shall operate as specified and to pinpoint potential problems. The micro-grid has been a novel system in many respects, requiring specific modelling and analysis software. Its concept is to integrate dispersed generation mainly based on renewable energy and storage devices in the LV distribution network [12], [13]. Key features that make the micro-grid different from a conventional power system are the ability of the resulting active network to operate a part from connected with the upstream network in island mode

as well, the necessity that the generators are connected to the network via electronic converters and finally the singularities of the LV network itself. Therefore, a simulation tool was developed in the context of the Microgrids project [13], to perform steady state analysis and to simulate the dynamic behaviour of the system during typical operational events such as: the load change, the variation in the production of the integrated sources, the loss of local generation portion and the transition to the island state. With the integration of electric vehicles in the LV distribution a considerable number of residents' vehicles is anticipated to be connected in the system. These vehicles may also employ control capabilities so that in the event of isolation from the upstream network they may discharge their stored energy and in addition they support the local voltage with the reactive power produced or absorbed by their inverters. The purpose of this investigation is to re-evaluate the capability of the micro-grid simulation tool to model and simulate a micro-grid accounting for the presence and controlled behaviour of the electric vehicles.

3.2.1 Characteristics of the Simulation Tool

The LV micro-grid may involve numerous micro-sources dispersed along an extended network, as it is the case in the low voltage distribution. Moreover many of the sources may present long time constants in the production process. So, a simulation tool was developed following the methodology of the transient stability algorithms. The focus is on the slower transients, from a few cycles up to several seconds or minutes, of the typical operational events of the system. Faster transients are ignored and the modelling of the sources and their interfacing converters action and control is adapted accordingly. The classical power system stability approach is based on the synchronous machines and their rotational inertia while the micro-grid may incorporate only voltage source converters to form the system. The development of the simulation tool deals with the adjustment of the stability approach for application in the conditions prevalent in the micro-grid [14]-[16]. In doing so the LV network unbalance is taken into account as well. A power flow solution module was also developed to initialize the states of the dynamic solution. It can be used for the steady state analysis of the system and it is described first below. MatLab and Simulink were used to realize the simulation tool.

a) Steady state analysis

The steady state analysis tool is a three phase power flow implemented in MatLab. It can be used for the study of the micro-grid system only in the connected operation with the upstream network. Since it provides also the initial values of the state variables it follows that the subsequent dynamic analysis starts always with the micro-grid in the connected mode. The Newton – Rapshon method is used with full Jacobian matrix. The system is represented with phase quantities in the admittance matrix. In this way any network topology, radial or meshed, with whatever R/X ratio of lines can be handled.

Sources may be represented in the following three ways:

- PV type like synchronous machine with AVR and limits in the reactive power output. Known quantities are the total 3ph power and the voltage magnitude

of the positive sequence at the terminals. It is turned into a PQ type when the limits are reached.

- PQ type sources as for example the sources that use inverters for the network connection, since the power flow deals with the connected operation only. In this category fall the sources that have capability to regulate their output as well. Total 3ph P and Q are known.
- Unregulated sources like induction machines connected directly to the network. Known quantity in this case is for example only mechanical torque.

The total 3ph powers (P and / or Q) are considered known in the internal node of the source i.e. at the output of the inverter before its filter and at the internal emf of the synchronous machines in the voltage behind reactance representation.

Three possibilities are given for the load representation:

- Constant power loads three phase or single phase. P and Q are known per phase.
- Constant impedance loads three phase or single phase.
- Loads like three phase induction motors where only mechanical torque is known.

Constant current loads are not included. Single-phase induction motors can be considered only as constant PQ loads.

Sources and loads are considered connected between the phase and neutral conductor.

b) Transient analysis

The stability algorithm is modified so that it can be applied in the case of the LV micro-grid. In the conventional algorithm instantaneous values of voltages and currents from the numerical integration of machine dynamic models are used to solve the algebraic equations of the network using phasor representation. The argument of the phasors is defined in relation to the system reference frame, which rotates with the synchronous speed and corresponds to the slack bus or the machine with the larger inertia in the system. The instantaneous quantities of each machine are converted to phasors and back using the rotor angle derived from its swing equation. In the implemented algorithm the phasors have arguments that change with the frequency integral and all quantities in the numerical integration of machine and inverter models are represented in the stationary frame. In this way the application of the algorithm becomes possible in the case of an isolated system with exclusively inverter-interfaced sources. Moreover machine and inverter transient equations are written so that the network unbalance is accounted for. Simulink is used to implement the modelling of prime source, control actions and the numerical integration. The post processing of results is carried out with MatLab.

3.2.2 Description of the Battery and Inverter Model

The switching operation of inverters is not modelled of course and the fast control loops are ignored. Modelling is restricted to a representation of inverters as controllable AC voltage sources at the fundamental frequency that have magnitude and angle controlled by the power exchange with the network, thus accounting only for the outer slower control loops. As far as the prime sources connected to the inverters are concerned, the power production process is modelled so long as it falls in the time frame of interest. Inverter control may refer to a source with regulation capabilities in the power output or to an unregulated one such as a renewable energy source. Droop control of active power with frequency, $P - f$, is employed for the inverter of the first source type, while the inverter of the latter is controlled to transfer the available power. For reactive power regulation, droop control with voltage magnitude, $Q - V$, is used or in the opposite case inverter output is controlled at constant power factor or at a constant reactive power. Ignoring the inverter switching losses the active power at the inverter output equals the power at the DC side. In this way the prime source model with its power available from each integration step is interfaced with the inverter model through the equation of the capacitor, which maintains the voltage at the DC side.

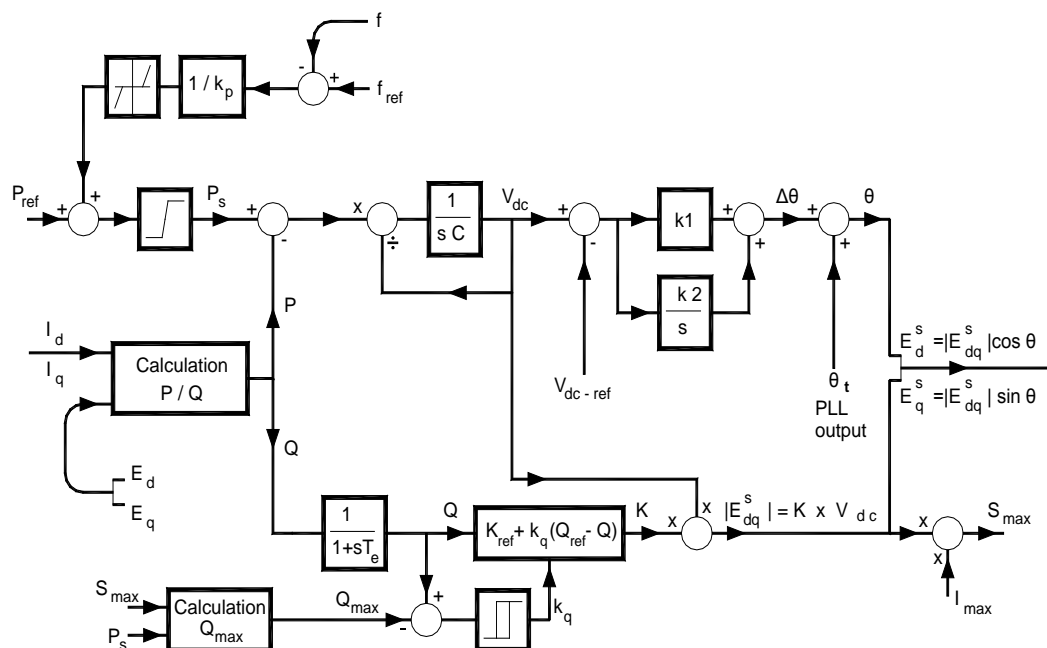


Figure 3-38: EV battery & inverter model

Figure 3-38 pictures the model of the electric vehicle battery and inverter. Power demanded from the battery is defined with an $f - P$ droop control measuring the system frequency. A dead zone is imposed so that the power remains unaffected for small changes. The total power, after considering the reference, is limited to the allowed maximum charge/discharge rate. From the current returned from the network solution and the inverter output voltage, the output power is calculated which is compared with the battery output to define the DC capacitor voltage. The

control of the capacitor voltage determines the angle advance or lag of the inverter internal voltage with respect to the terminal voltage. A PLL provides the terminal voltage angle to be added to the angle difference to form the inverter internal voltage angle with respect to the stationary reference frame.

Reactive power output is measured to determine the voltage magnitude of the inverter internal voltage. Actually the reactive power determines with droop control, $Q - K$, the factor K by which the DC side voltage is multiplied to give the inverter voltage magnitude. The maximum inverter current and the active power that is currently exchanged limit reactive power. It is kept within the limits by controlling the droop constant k_q .

The resulting inverter voltage is applied to the network equations to acquire the current for the computation of the dynamic model in the next time step. The described inverter model may represent either a single phase or a three phase inverter. In the case of the single phase inverter that is more likely to be used for EV battery interfacing, the d , q coordinates of voltage and current in Figure 3-38 are the real and imaginary part of the corresponding phase quantities. In the case of a three phase inverter they are the real and imaginary part of the positive sequence voltage and current. Transformation to and from the phase domain precedes and follows the network solution then.

3.2.3 Simulated Micro-Grid with EVs

The micro-grid analysis tool is tested on a micro-grid where electric vehicles are participating. The micro-grid is realized in a residential LV feeder along which various sources are connected. The resulting system is pictured in Figure 3-39. The electric vehicles with nominal charging rate 3kW are considered at the load nodes, which correspond to residential buildings. The number of vehicles is in proportion to the load demand of each specific node. The total load demand of the feeder taking into account the coincidence factor, without the EVs, is 115 kVA and its distribution can be found in per phase in Table 3-1. A p.f. of 0.85 is considered for every node. The line data are shown in Table 3-2. It includes the line identifier, which is also marked in the drawing of Figure 3-39, the conductor type, cross section and the positive and zero sequence impedances. Length of each line is shown in Figure 3-39. The neutral conductor is considered practically isolated from earth. Therefore given that simulation of fault cases is not in the scope of the investigation, zero sequence current flows through the neutral conductor alone and the impedances of Table 3-2 are computed accordingly.

Table 3-1

LOAD NODE	<i>Per phase S (kVA) 0.85 p.f.</i>		
	<i>A</i>	<i>B</i>	<i>C</i>
D (O1)	5	-	-
G (O2)	19.95	18.24	18.81
M (O3)	9.2	7.36	6.44
S (O4)	-	-	5
U (O5)	10	8	7

Table 3-2

<i>ID</i>	<i>Line type</i>	<i>Z₁₁ (Ω/km)</i>	<i>Z₀₀ (Ω/km)</i>
1	Twisted single core AL 4x120 mm ²	0.284+j0.084	1.136+j0.406
2	Twisted single core AL 3x70mm ² +	0.497+j0.086	2.387+j0.437
8	Cu 4x16mm ² Concentric neutral	1.380+j0.094	5.52+j0.113
9	Cu 4x25mm ² Concentric neutral	0.871+j0.089	3.484+j0.107
10	50mm ² + Cu 35mm ² Concentric neutral	0.822+j0.070	2.394+j0.105
7, 11	Cu 2x16mm ² Concentric neutral	2.76+j0.056	

All simulated cases start with the micro-grid connected to the upstream network and disconnection and isolated operation follows, breaking the connection at the MV/LV transformer secondary node. For the purpose of frequency and voltage regulation during isolated operation two battery units are connected at nodes L and T with inverters of 60 kVA capacity at 0.85 p.f., each. The inverters are controlled with $P - f$, $Q - V$, droops. As it was already stated for the inverter modelling so far, the powers at the inverter output is regulated instead of the terminal, controlling the inverter internal voltage. These two units produce zero active and reactive power when the micro-grid operates in connected mode. So for the initial system condition with the nominal demand of Table 1 it is specified that $P_{ref} = 0$ for $f_{ref} = 50\text{Hz}$ and $Q_{ref} = 0$. The droop constants of both are such that the maximum (nominal) active power is produced when the frequency drops by 1Hz, or in other words the $P - f$ droop constant is $k_p = 2\%$. The $Q - V$ droop constant of the two battery inverters is $k_q = 1.25\%$.

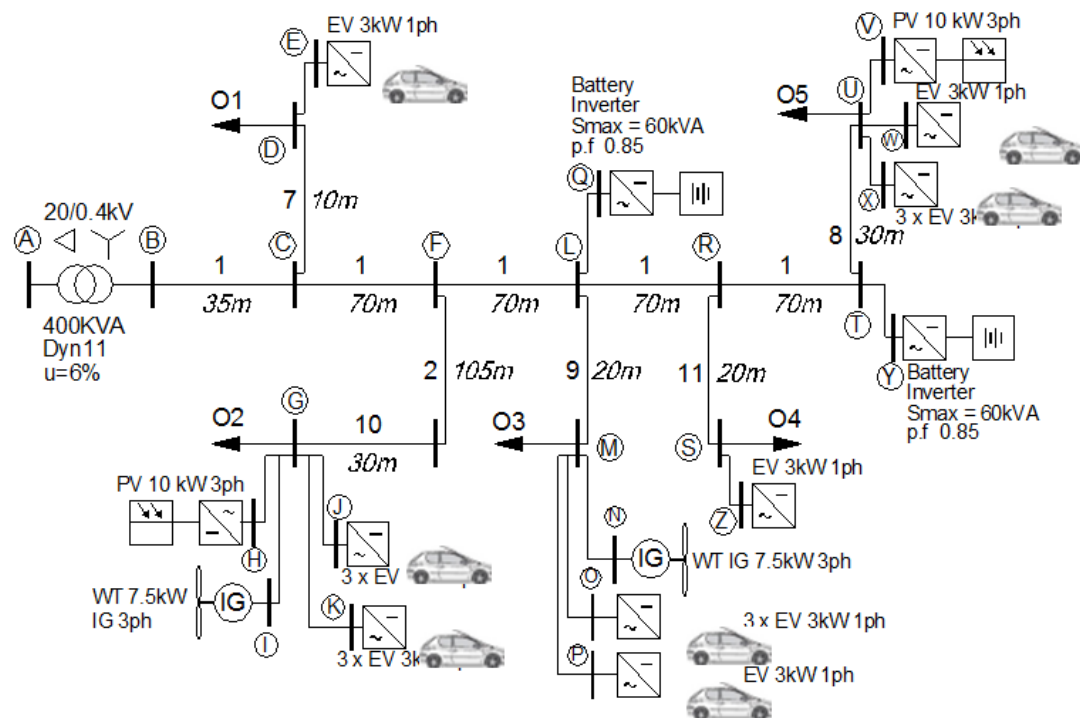


Figure 3-39: Diagram of the simulated micro-grid system

Sources of unregulated output are also connected along the LV feeder. In specific, two photovoltaic units of 10kW each are connected via three phase inverters at the load nodes G and U. The inverters are controlled so that they transfer the available power at unity power factor. Additionally, two wind turbines of 7.5kW each with induction generators are connected directly to the network at the load nodes G and M. These sources are considered connected to the network and producing at the nominal output right from the start of each simulated case when the micro-grid system is in the connected mode. As far as the EVs are concerned they are considered connected via single-phase inverters, which are able to exchange the nominal maximum power of 3kW at 0.85 p.f., meaning that the maximum current corresponds to a single phase socket outlet of 16A. The EV inverters are droop controlled as well in the manner described in the previous paragraph and illustrated in Figure 3-39. The droop constants are chosen to be the same with the centrally installed battery inverters i.e. $k_p = 2\%$ and $k_q = 1.25\%$. When in the connected mode at the start of the simulation, the inverters are considered to charge the EV batteries with 3kW at unity power factor.

3.2.4 Results

The load flow results for the loading conditions of Table 3-1 and the generation described in the previous paragraph are presented in Tables 3-3 and 3-4. The short circuit capacity at the 20kV node A is considered 250MVA and the slack node SL is connected to this node. From this state we proceed to examine various cases regarding the dynamic behavior of the system. We are interested in testing the



effectiveness of the simulation tool to record the typical operational events following the transition to the isolated mode such as the fluctuations of load and generation and the loss of generation. In particular we seek to simulate the contribution of the EV inverters that are equipped with droop controllers in the support of frequency and voltage assuming the corresponding system load.

Table 3-3

NODE ID	<i>A (p.u./deg)</i>	<i>B (p.u./deg)</i>	<i>C (p.u./deg)</i>
SL	1.00027/0.00	1.00027/-119.9999	1.00027/119.9999
A	1.00002 / -0.026	0.99996 / -120.024	1.00002 / 119.977
B	0.98868 / 28.940	0.98979 / -90.867	0.99113 / 149.074
C	0.97835/ 29.034	0.98369 / -90.775	0.98351 / 149.265
D	0.97076 / 29.187	-	-
F	0.96397 / 29.244	0.96985 / -90.432	0.96685 / 149.492
G	0.93730 / 29.943	0.94722 / -89.672	0.94142 / 150.348
L	0.95745 / 29.363	0.96200 / -90.221	0.95767 / 149.533
M	0.95202 / 29.499	0.95989 / -90.227	0.95684 / 149.674
R	0.95587 / 29.400	0.95816 / -90.057	0.95039 / 149.502
S	-	-	0.94283 / 149.655
T	0.95260 / 29.594	0.95267 / -90.041	0.94908 / 149.452
U	0.94651 / 29.821	0.94726 / -89.846	0.94247 / 149.587
Q	0.95904 / 29.559	0.95904 / -90.441	0.95904 / 149.559
Y	0.95145 / 29.668	0.95145 / -90.332	0.95145 / 149.668
E	0.97027 / 27.362	-	-
K	0.93675 / 27.985	0.94669 / -91.589	0.94088 / 148.407
J	0.93675 / 27.985	0.94669 / -91.589	0.94088 / 148.407
O	0.95150 / 27.601	0.95938 / -92.093	0.95632 / 147.795
P	0.95150 / 27.601	-	-
Z	-	-	0.94229 / 147.720
X	0.94598 / 27.901	0.94673 / -91.763	0.94193 / 147.651

W	-	-	0.94193 / 147.651
V	0.94446 / 32.422	0.94446 / -87.578	0.94446 / 152.422
H	0.94102 / 32.793	0.94102 / -87.206	0.94102 / 152.793
N	0.95202 / 29.499	0.95989 / -90.226	0.95684 / 149.674
I	0.93730 / 29.943	0.94722 / -89.672	0.94142 / 150.348

Table 3-4

1st Node	2nd Node	1st node Sending		2nd node Sending		Line Currents
		kW	kvar	kW	kvar	p.u./deg
SL	A	38.69 35.28 32.73	21.43 26.34 20.93	-38.69 - 35.28 - 32.73	-21.41 - 26.31 - 20.91	0.442/-28.984 0.440/-156.745 0.388/87.400
B	C	39.61 32.44 34.65	24.53 22.25 19.42	-39.15 - 32.20 - 34.32	-24.34 - 22.17 - 19.39	0.471/-2.834 0.397/-125.317 0.401/119.801
C	D	7.07 0.00 0.00	2.58 0.00 0.00	-7.01 0.00 0.00	-2.57 0.00 0.00	0.077/9.011 0.000 0.000
D	E	3.00 0.00 0.00	0.10 0.00 0.00	-3.00 0.00 0.00	0.00 0.00 0.00	0.031/27.362 0.000 0.000
C	F	32.09 32.20 34.32	21.17 22.17 19.39	-31.54 - 31.62 - 33.66	-21.56 - 22.04 - 19.19	0.396/-5.117 0.397/-125.317 0.401/119.801
F	G	15.42 14.75 15.11	10.72 10.78 10.45	-14.86 - 14.26 - 14.56	-10.61 - 10.71 - 10.39	0.195/-5.568 0.188/-126.585 0.190/114.834
G	H	-3.66 -3.20 -3.15	-0.20 0.56 0.10	3.66 3.20 3.15	0.38 -0.42 0.04	0.039/26.818 0.034/-79.756 0.033/152.152



G	I	-2.37 -2.45 -2.38	1.38 1.34 1.31	2.37 2.45 2.38	-1.38 -1.34 -1.31	0.029/60.069 0.029/-60.959 0.029/179.185
G	J	3.00 3.00 3.00	0.10 0.10 0.10	-3.00 -3.00 -3.00	0.00 0.00 0.00	0.032/27.985 0.032/-91.589 0.032/148.408
G	K	3.00 3.00 3.00	0.10 0.10 0.10	-3.00 -3.00 -3.00	0.00 0.00 0.00	0.032/27.985 0.032/-91.589 0.032/148.408
F	L	16.12 16.87 18.55	10.84 11.27 8.75	-15.99 - 16.69 - 18.37	-10.80 - 11.24 - 8.68	0.202/-4.681 0.209/-124.175 0.212/124.247
L	Q	-1.57 1.77 -0.21	-0.76 1.43 -0.65	1.57 -1.77 0.21	0.76 -1.42 0.65	0.018/ 3.516 0.024/-129.074 0.007/77.307
L	M	10.78 6.32 5.67	5.94 5.05 4.53	-10.71 -6.31 -5.65	-5.94 -5.04 -4.54	0.129/ 0.502 0.084/-128.827 0.076/110.926
M	O	3.00 3.00 3.00	0.10 0.10 0.10	-3.00 -3.00 -3.00	0.00 0.00 0.00	0.032/27.601 0.031/-92.094 0.031/147.795
M	P	3.00 0.00 0.00	0.10 0.00 0.00	-3.00 0.00 0.00	0.00 0.00 0.00	0.032/27.601 0.000 0.000
M	N	-2.38	1.39 1.34	2.38 2.45	-1.39	0.029/59.718



		-2.45 -2.38	1.33	2.38	-1.34 -1.33	0.029/-61.491 0.028/178.765
L	R	6.77 8.59 12.91	5.62 4.76 4.80	-6.75 -8.55 -12.82	-5.61 -4.77 -4.76	0.092/-10.320 0.102/-119.209 0.144/129.123
R	S	0.00 0.00 6.84	0.00 0.00 2.44	0.00 0.00 -6.78	0.00 0.00 -2.44	0.000 0.000 0.076/129.863
S	Z	0.00 0.00 3.00	0.00 0.00 0.10	0.00 0.00 -3.00	0.00 0.00 0.00	0.000 0.000 0.032/147.721
R	T	6.75 8.55 5.98	5.61 4.77 2.32	-6.71 -8.50 -5.97	-5.61 -4.74 -2.31	0.092/-10.320 0.102/-119.209 0.067/128.286
T	U	7.30 6.20 7.68	5.06 4.15 3.43	-7.23 -6.15 -7.62	-5.06 -4.15 -3.42	0.093/-5.153 0.078/-123.848 0.089/125.381
U	V	-3.38 -2.95 -3.67	0.24 0.28 -0.07	3.38 2.95 3.67	-0.08 -0.16 0.25	0.036/33.859 0.031/-84.431 0.039/148.570
U	X	3.00 3.00 3.00	0.10 0.10 0.10	-3.00 -3.00 -3.00	0.00 0.00 0.00	0.032/27.901 0.032/-91.763 0.032/147.651
U	W	0.00 0.00 3.00	0.00 0.00 0.10	0.00 0.00 -3.00	0.00 0.00 0.00	0.000 0.000 0.032/147.651

T	Y	-0.59 2.30 -1.71	0.55 0.59 -1.12	-0.59 -2.30 1.71	-0.55 -0.58 1.13	0.008/72.623 0.025/-104.468 0.022/116.231
---	---	------------------------	--------------------	------------------------	------------------------	---

Total System losses are 5.560kW

The program converged after 4 iterations for a mismatch of 0.0001p.u.

In the first simulated case the micro-grid is disconnected at 0.5 sec and the load at nodes G, M, U increases by 25% one second later. Results for this case at selected network points are presented in Figure 3-40 up to 3-46. It is noted that all plotted graphs are with load convention. Upon disconnection of the LV feeder from the upstream grid the sources capable to form an isolated system supporting voltage and frequency, namely the two battery units at nodes T and L and the dispersed EVs, start regulating their output accordingly. With the chosen droop constants all grid forming sources produce power in proportion to their nominal rating. So, all EVs initially reduce their active power consumption by 2kW. The dead zone component shown in Figure 3-38 restricts active power by $\pm 500\text{W}$. When the load increases at 1.5 sec, EV charging power drops further to only 500W. This can be observed in Figure 3-40 along with the currents, for the four EVs at node U, which are connected to phases A,B,C and C.

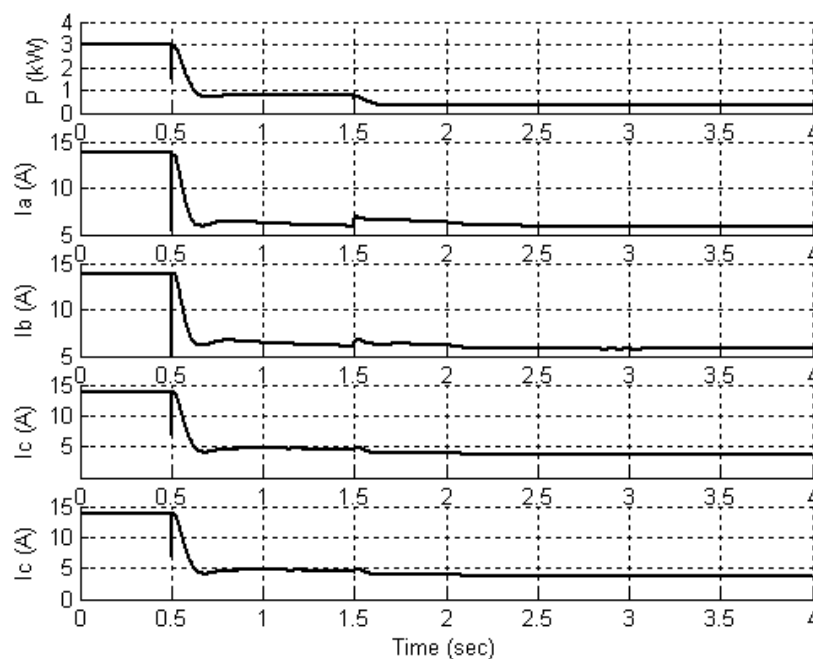
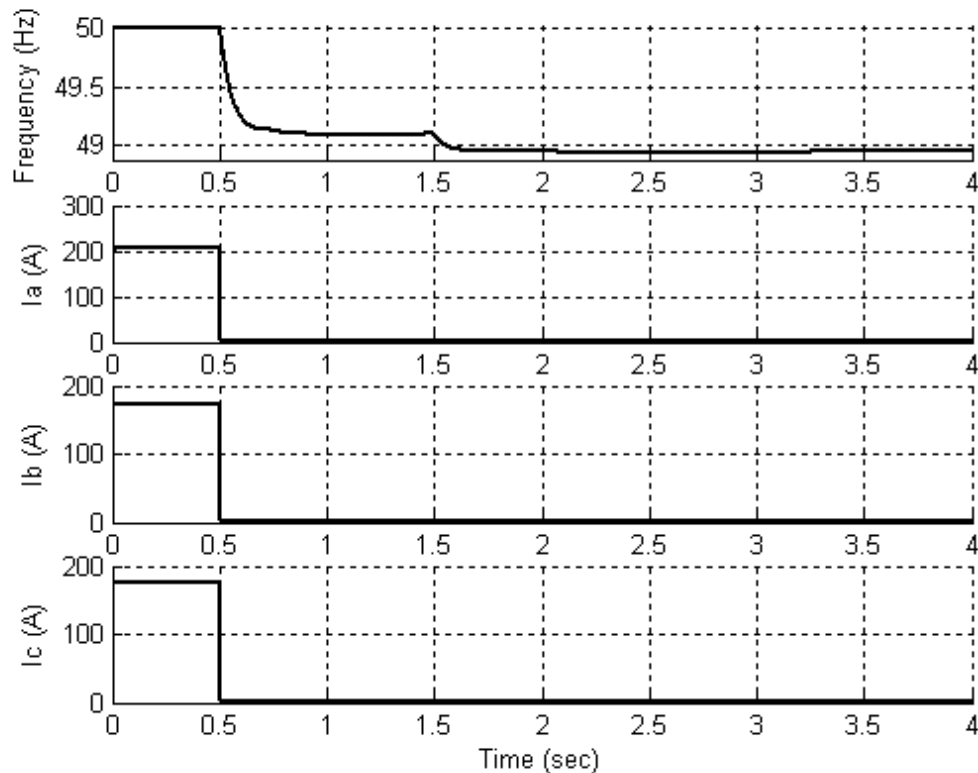


Figure 3-40: Active power and RMS currents of each one of the four EV inverters at node U

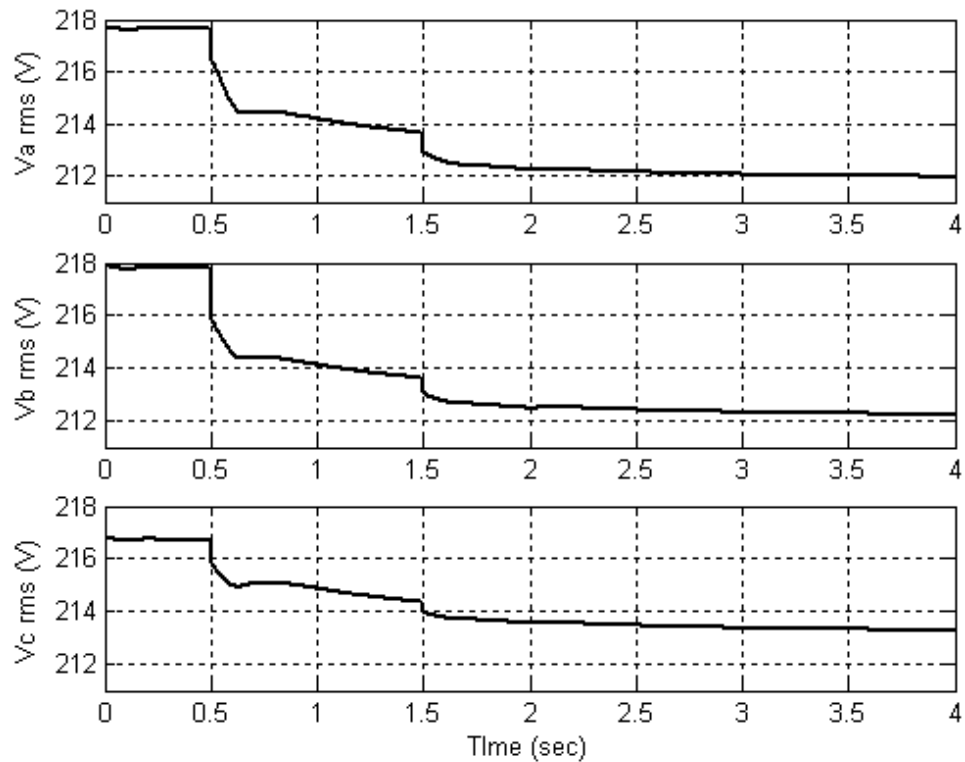


▪ **Figure 3-41: System frequency / RMS LV feeder currents from transformer secondary**

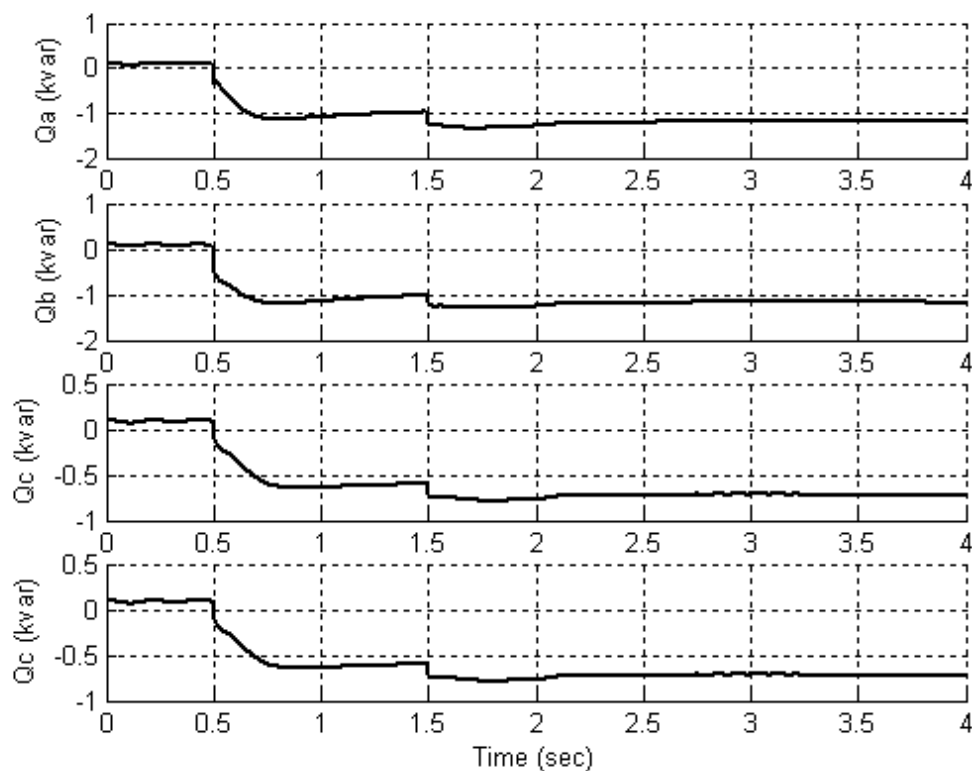
Figure 3-41 depicts system frequency and the current at the transformer secondary i.e. through the network branch BC. Frequency drops close to 49.2Hz following disconnection and then below 49Hz after the load increase. The EV inverters support voltage as well, as long as the available margin imposed by the maximum inverter current allows it, as it was described in Figure 3-38. This is demonstrated for node U in Figure 3-42 and 3-43. Figure 3-42 shows voltage at node U, while the reactive power output of the four EV inverters at the same node are shown in Figure 3-43. We can observe that the voltage of phase C is lower than the other two phases during connected operation, due to the heavier load of this phase. However phase C voltage is better supported after micro-grid isolation because two EV inverters are connected to that phase. At the end of the simulation, after the load increase, the EV inverters connected to phases A, B, produce approximately 1kvar each and the EV inverters connected to phase C produce 0.7kvar each.

To form an overall picture and to better validate the results, power flows through the supply cable to node U (branch TU), through the branch feeder RT, as well as active and reactive power output of the battery inverter at node T are plotted in the following three Figure 3-44~46. The battery inverter total active and reactive power exchanged with the network, are controlled to zero while in the connected mode. With the transition to islanded operation the inverter assumes, according to its droop control, approximately 30kW and 12kvar in total and when the load increases, 35kW

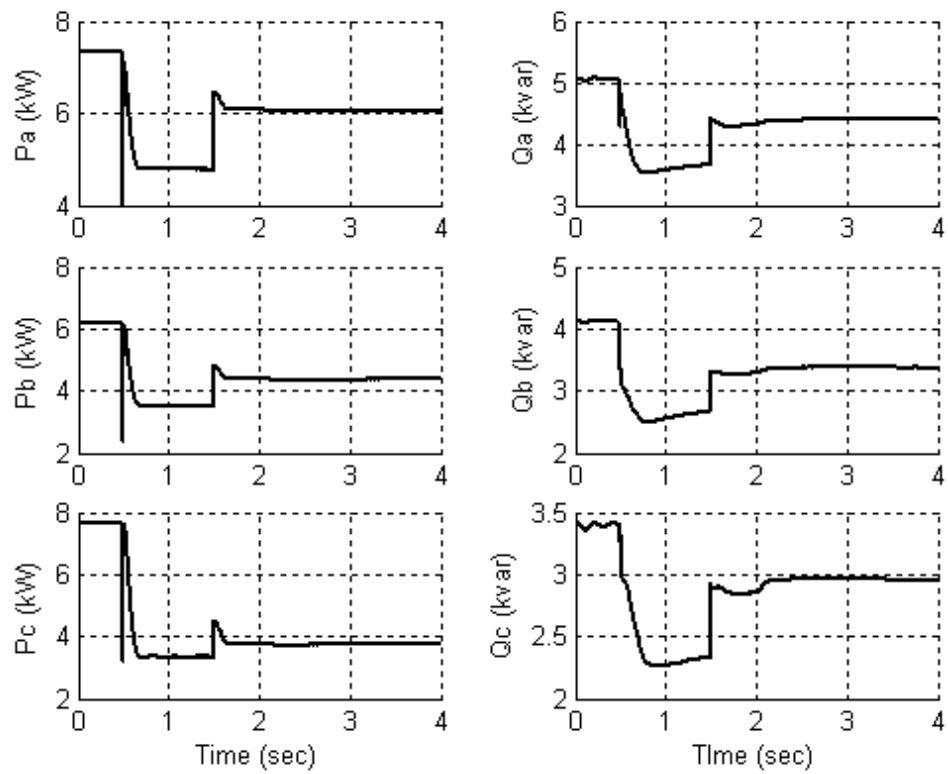
and 15kvar. Some of the inverter P, Q is consumed by the load at node U and some, especially most of the active power, cover the rest of the system load, as it can be seen from Figure 3-46 where power flow through feeder branch RT is reversed in the island mode.



▪ **Figure 3-42: RMS phase voltage at the load node U**



▪ **Figure 3-43: Reactive power of the four EV inverters at node U**



▪ **Figure 3-44: Active and reactive power of the grid supply cable to node U**

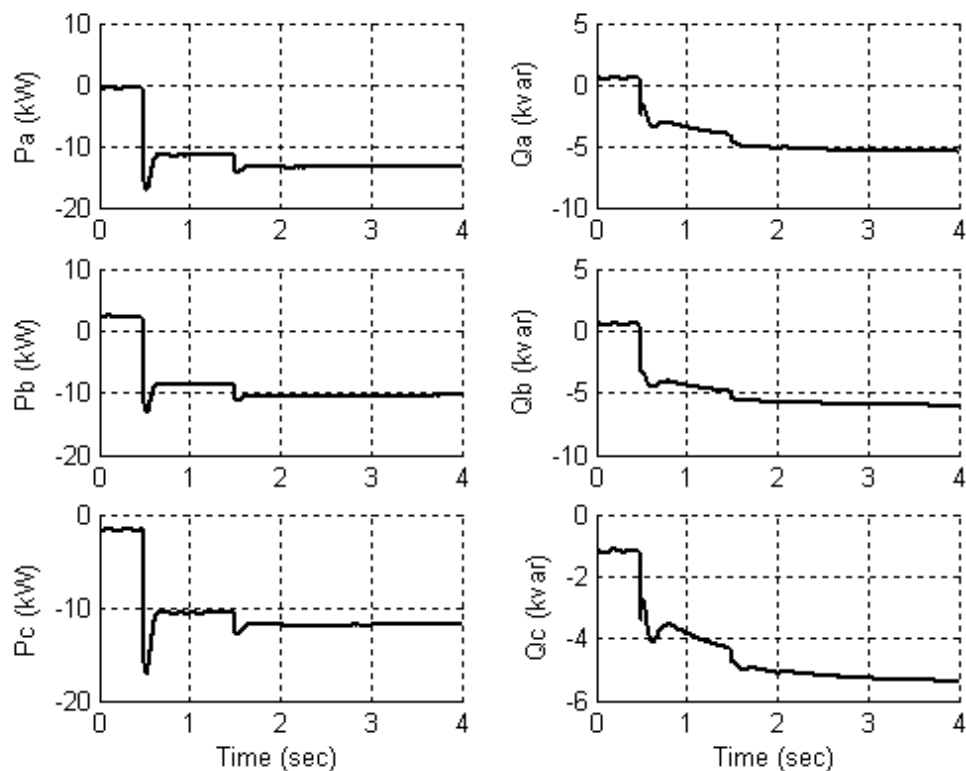
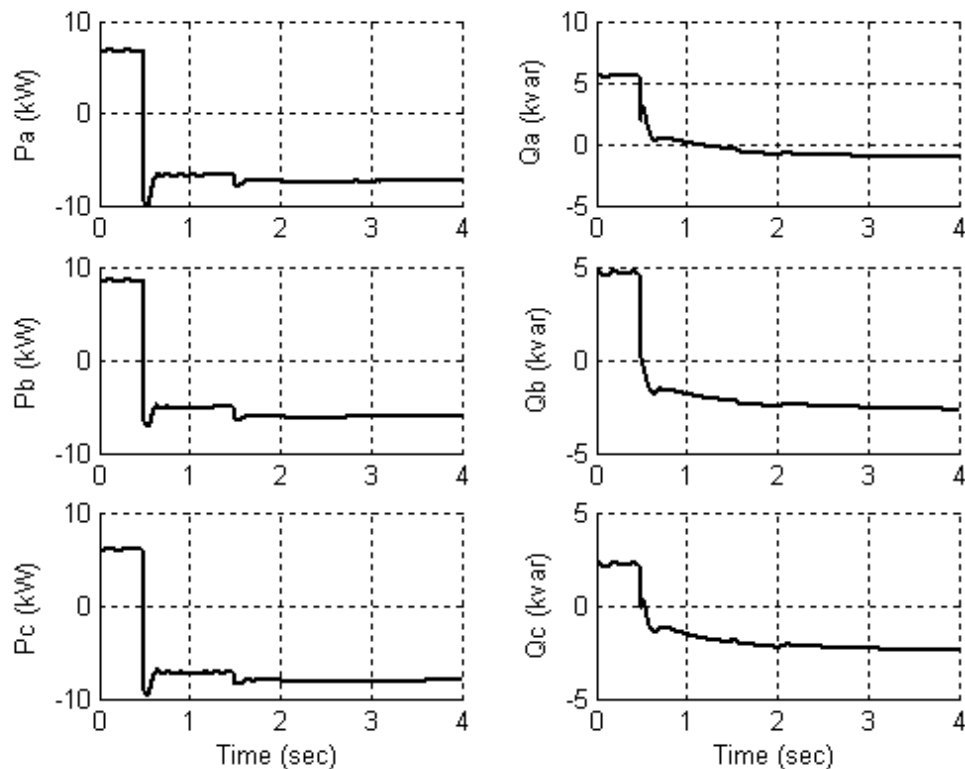


Figure 3-45: Active and reactive power of the battery inverter at node T



▪ **Figure 3-46: Active and reactive power of the feeder from node R to node T**

In the second simulated case disconnection occurs at 0.2 sec. At 1sec the battery inverter at node T is disconnected and one second later the output of the two photovoltaic units is reduced to zero. Results are presented in Figure 3-47~54.

Charging rate of the EVs drops again to 1kW after micro-grid isolation and with the loss of the battery inverter at node T it reduces to zero and the EVs start discharging at approximately 300W each. At 2sec, EV discharging increases and it reaches 1kW. This can be seen for the EV located at node S in Figure 3-47 and for the four EV inverters at node M in Figure 3-50. The EV inverters start contributing to the reactive demand of the system right from the moment the micro-grid is disconnected thus supporting the voltage of the micro-grid. Figure 3-47,51, 52 demonstrate this EV inverter action. The reactive production of the EV and battery inverters is defined from their droop control as well as from their position in the network. The active and reactive power output of the two battery inverters at nodes L, T are depicted in Figure 3-48, 49. When the inverter at node T is disconnected at 1sec the battery unit at node L compensates almost for all the active power deficit. From the moment the PV units reduce their output (see Figure 3-54 for the PV inverter at node G), the remaining battery unit and the EV batteries share the additional load. System frequency finally drops close to 48.5Hz as depicted in Figure 3-53. This figure shows the powers, current and p.u. slip of the WT IG at node M as well.

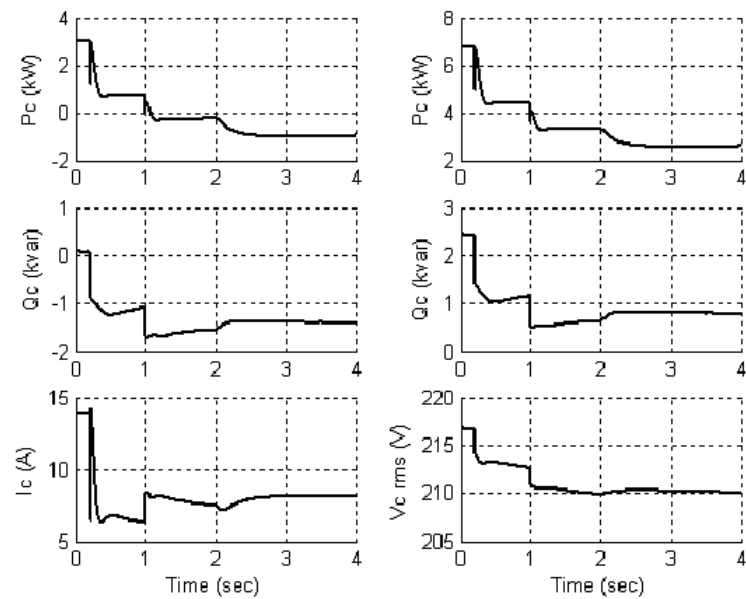
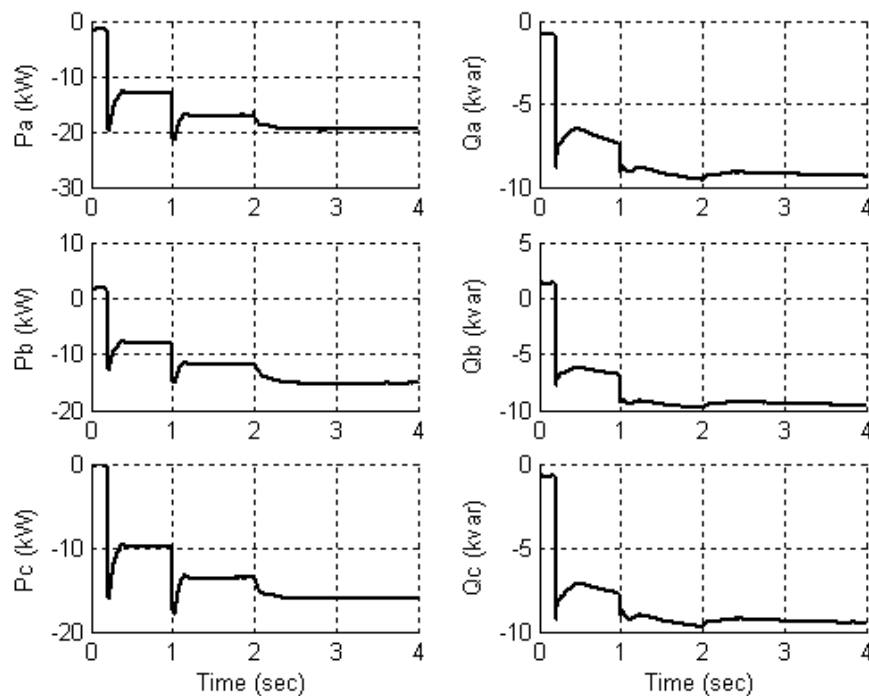
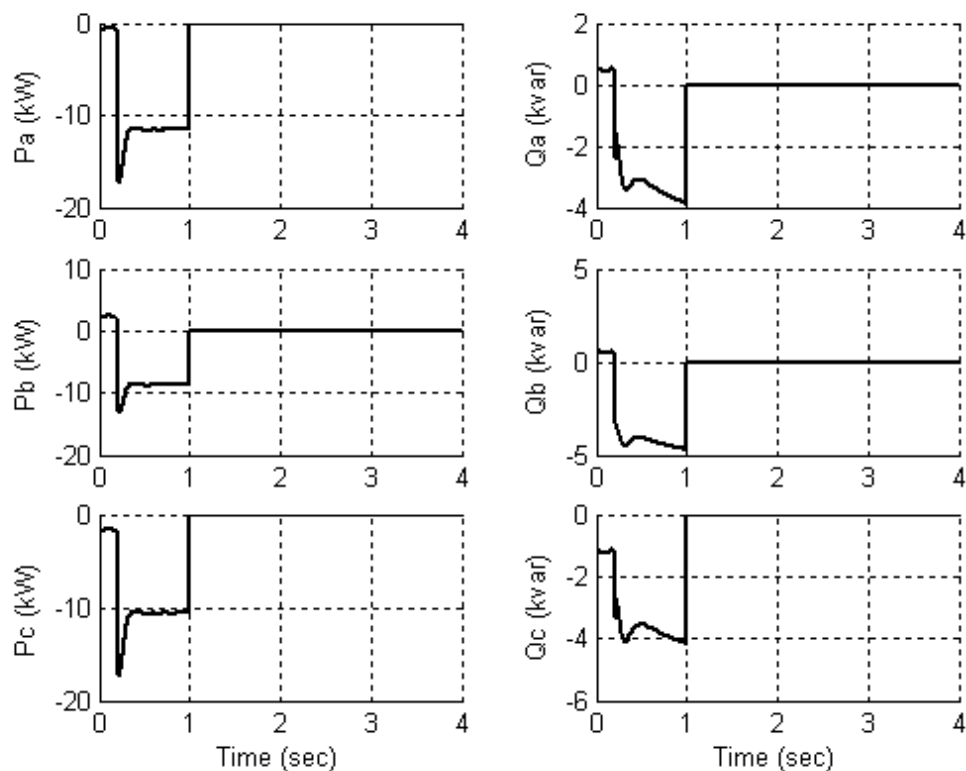


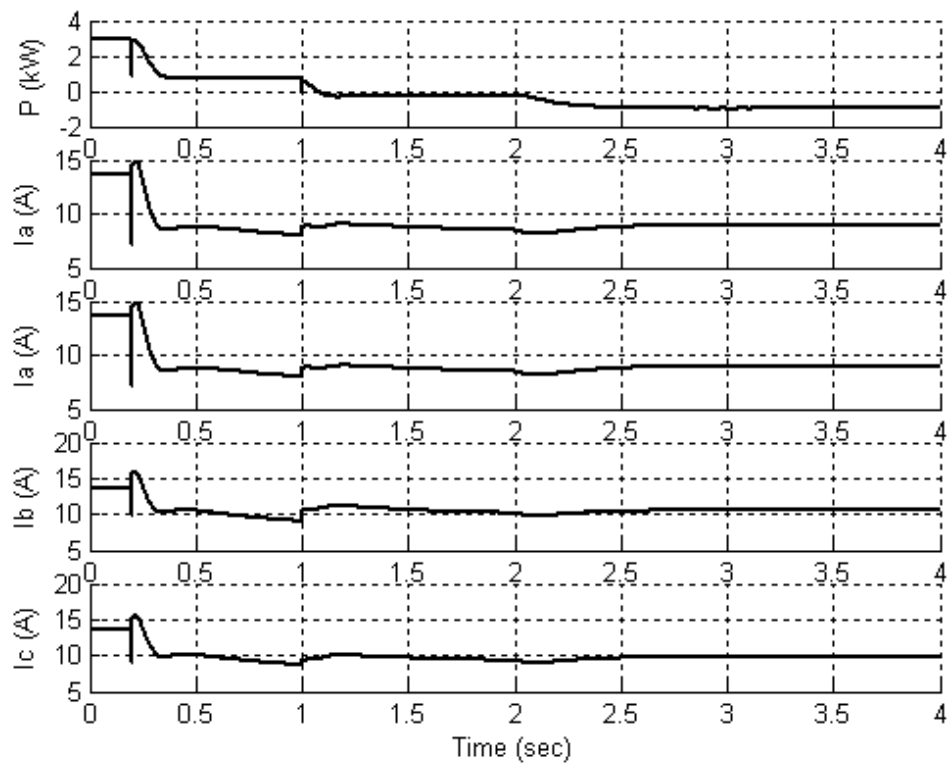
Figure 3-47: On the left column: active, reactive power and rms current of the EV inverter at node S. On the right column: active and reactive power through the supply cable to node S (network branch RS) and voltage of node S.



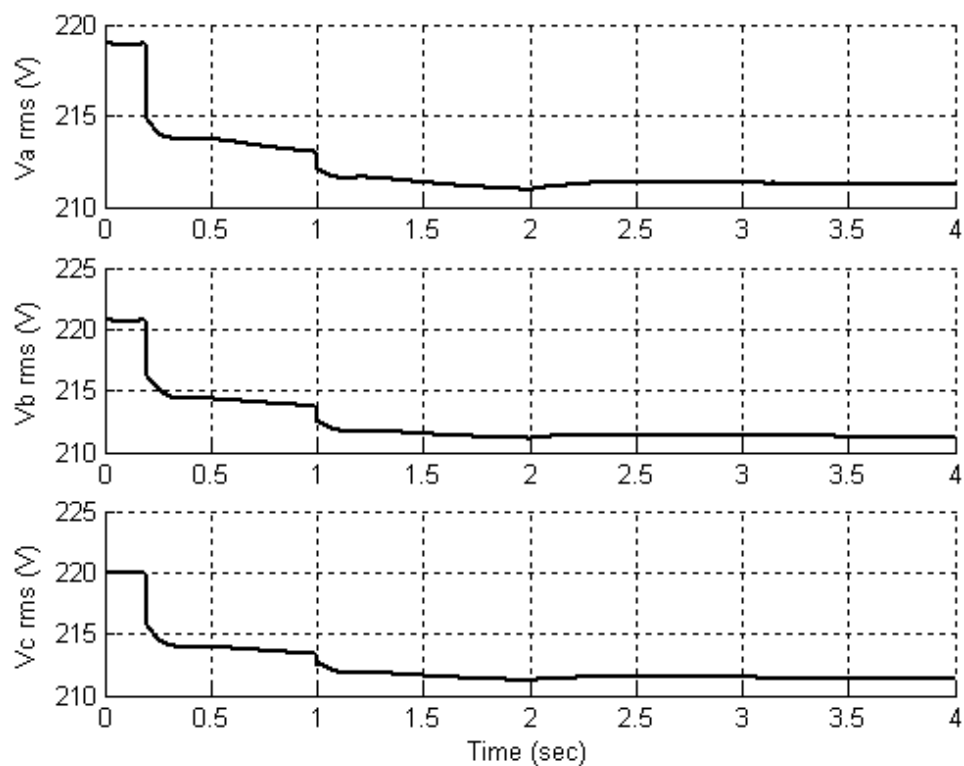
▪ **Figure 3-48: Active and reactive power of the battery inverter at node L**



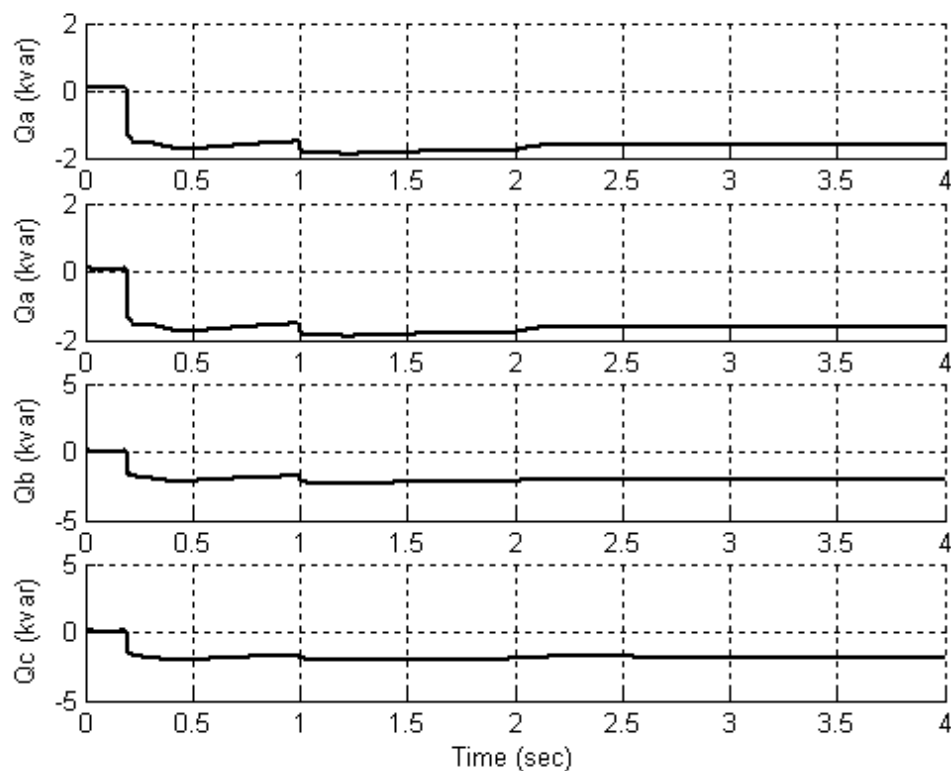
■ **Figure 3-49: Active and reactive power of the battery inverter at node T**



- **Figure 3-50: Active power and RMS currents of each one of the four EV inverters connected to phases A, A, B and C at node M**



▪ **Figure 3-51: RMS voltage at node M**



▪ **Figure 3-52: Reactive power of the four EV inverters at node M**

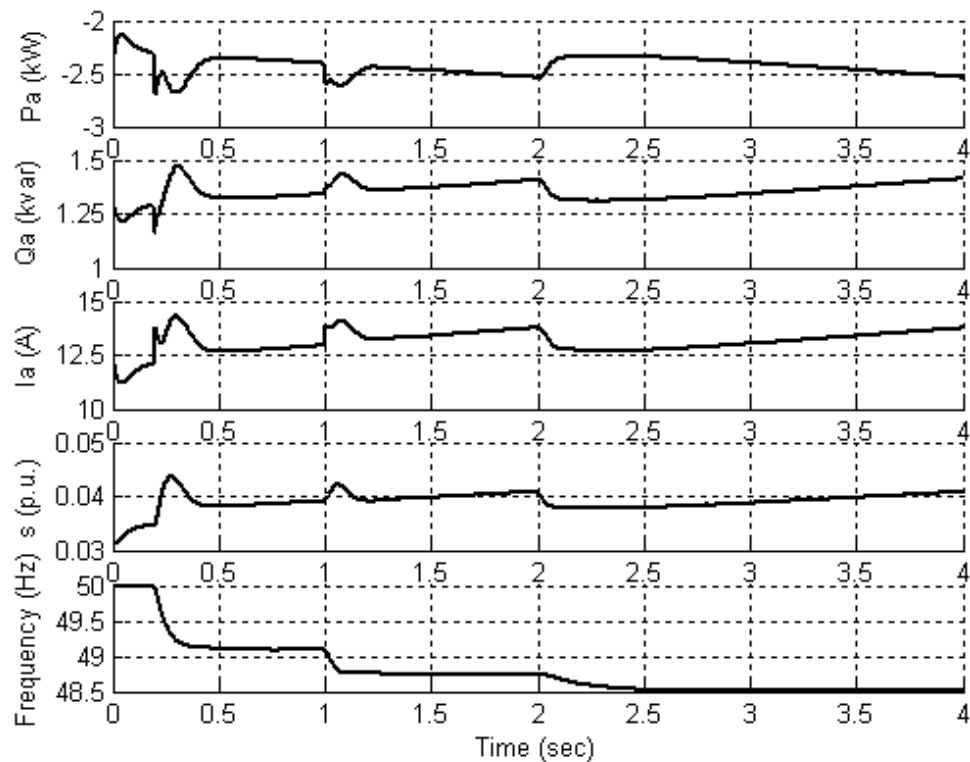


Figure 3-53: Active, reactive power, current, per phase, p.u. slip of the WT IG at node M, frequency.

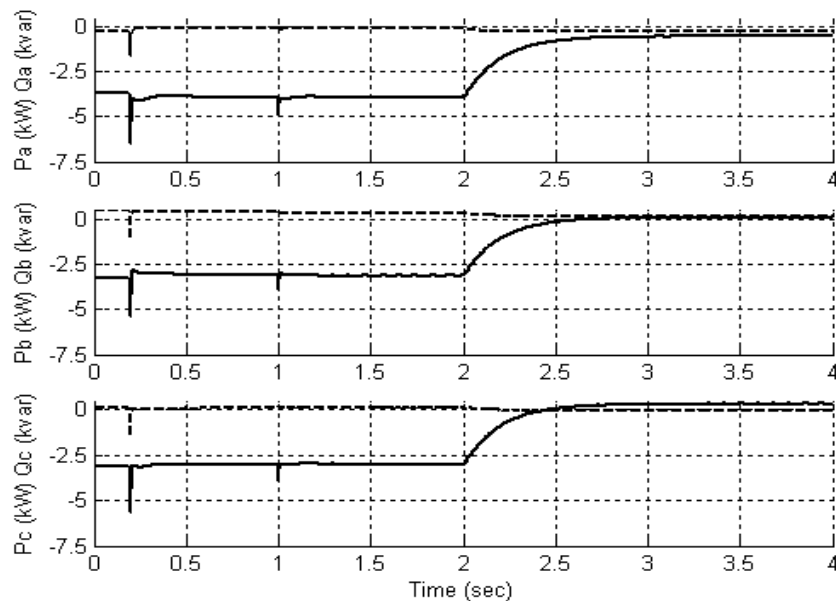


Figure 3-54: Active, reactive (dashed line) power output of the PV unit at node G.

3.2.5 Conclusions

The simulation tool developed for the steady state and transient examination of micro-grids was applied for the investigation of a LV micro-grid with electric vehicles. The EV inverters are so controlled that they are able to regulate their active and reactive power exchange and thus to support the isolated operation of the system. The existing micro-grid analysis tool is an adaptation of the stability algorithm to inertia-less island systems with sources coupled with the network via inverters. LV network unbalance is also accounted for. Modelling of the EV battery inverter was adjusted to the specific demands of the stability analysis tool. A LV micro-grid with EVs and other sources with or without (renewable sources) regulation capabilities was presented whereupon the steady state power flow and transient analysis were performed. The steady state part of the examination dealt with the connected mode of the system while the dynamic behaviour was simulated in grid-connected and in isolated mode of operation. The simulation of typical events such as the isolation of the system, load change and variations in the production of the sources rendered reasonable results in all cases and proved the reliable performance of the micro-grid analysis tool in the dynamic investigation of a micro-grid with EVs. The results using the suggested modelling are subject to the restrictions and limitations of the stability type transient analysis. Therefore the tested simulation tool is suitable for slow transients only. The modelling of the inverter control of all sources has to be in accordance with the targeted time frame including only the slow outer control loops that define the power exchange with the system and excluding any faster control action. Consequently the simulation tool is able to successfully record the dynamic events of micro-grids with EVs that pertain to the load following behaviour of the system.

3.3 References

- [1] J. A. Peças Lopes, F. J. Soares, and P. M. R. Almeida.; , "Integration of Electric Vehicles in the Electric Power System," Proceedings of the IEEE , vol.99, no.1, pp.168-183, Jan. 2011.
- [2] MERGE Project deliverable D2.1: "Extend concepts of MG by identifying several EV smart control Approaches to be embedded in the smartgrid concept to manage EV individually or in clusters", June 2010
- [3] European Research and Development project MICROGRIDS, [Online.] Available: <http://www.microgrids.eu>
- [4] J. A. Peças Lopes, C. L. Moreira, and A. G. Madureira, "Defining control strategies for microgrids islanded operation," IEEE Transactions on Power Systems, vol. 21, no. 2, pp. 916-924, May 2006.
- [5] MICROGRIDS project deliverable DD1, " Emergency Strategies and Algorithms." [Online.] Available: http://www.microgrids.eu/micro2000/delivarables/Deliverable_DD1.pdf

- [6] A. Engler and B. Burger, "Fast signal conditioning in single phase systems." in *Proceedings 9th European Conference on Power Electronics and Applications*, Graz, Germany, 27-29 August 2001.
- [7] F. Blaabjerg, R. Teodorescu, M. Liserre, and A. V. Timbus, "Overview of control and grid synchronization for distributed power generation systems." *IEEE Transactions on Industrial Electronics*, vol. 53, no. 4, pp. 1398-1409, October 2006.
- [8] A. Engler, "Control of battery inverters in modular and expandable island grids." PhD Dissertation submitted to the University of Kassel, 2001 (in German).
- [9] Y. Li, D. M. Vilathgamuwa, and P. C. Loh, "Microgrid power quality enhancement using a three-phase four-wire grid-interfacing compensator." *IEEE Transactions on Industry Applications*, vol. 41, no. 6, pp 1707-1719, November/December 2005.
- [10] Daniel Nahum Zmood, Donald Grahame Holmes, and Gerwich H. Bode, "Frequency-domain analysis of three-phase linear current regulators", *IEEE Transactions on Industry Applications*, vol. 37, no. 2, pp. 601-610, March/April 2001.
- [11] C. L. Moreira, "Identification and Development of MicroGrids Emergency Control Procedures." PhD dissertation submitted to the Faculty of Engineering of University of Porto, Porto, 2009.
- [12] N. Hatziargyriou, H Asano, R. Iravani, C. Marnay, "Microgrids" *IEEE Power & Energy magazine*, Vol. 5, No 4, pp 78 – 94, 2007.
- [13] "MICROGRIDS – Large Scale Integration of Micro-Generation to Low Voltage Grids", EU Contract ENK5-CT-2002-00610, Technical Annex, May 2002
- [14] N. L. Sultanis, S. A. Papathanasiou, N. D. Hatziargyriou, "A stability algorithm for the dynamic analysis of inverter dominated unbalanced LV Microgrids", *IEEE Trans. on Power Systems*, Vol. 22, No. 1, pp 294-304, Feb. 2007
- [15] N. L. Sultanis, N. D. Hatziargyriou, "Dynamic simulation of inverter dominated L.V. micro-grids" *IEEE PES General Meeting*, Montreal, 18 – 22 June, 2006
- [16] K. Karoui, V. Chuvychin, A. Sauhats, O. Samuelsson, M.H.J. Bollen, N. D. Hatziargyriou, N. L. Sultanis, "Analysis and Modeling challenges induced by a growing penetration of inverter interfaced DER" *IEEE PES General Meeting*, Montreal, 18 – 22 June, 2006Results

4 EUROSTAG AND MATLAB SIMULATION PLATFORM

This section approaches a simulation platform developed to evaluate Multi-Micro grids under normal and emergency operation conditions. The platform was implemented using the EUROSTAG (version 4.3) [1] and MATLAB (version 2009b) [2] environments. The EUROSTAG environment was utilized to emulate the static and dynamic behavior of distribution system elements, including several sorts of distributed generators (DGs) such as combined heat and power (CHP) generation units, hydro generation units, wind generation units, micro turbine (MT) generation units, fuel cell (FC) generation units, etc. On the other hand, the MATLAB environment was applied to the development of specific scripts which invoke EUROSTAG functionalities aiming at simulating the Multi-Micro grid frequency control schemes.

The original edition of the simulation platform was enhanced to emulate the Multi-Micro grid quasi-steady state behavior as well as to incorporate the EV grid integration. EV static and dynamic models were represented in the EUROSTAG environment. Furthermore, the Multi-Micro grid frequency control schemes as well as the MATLAB scripts were adapted to account for the EV operation and control. The enhanced simulation platform will allow the evaluation of EV charging procedures on the distribution system operation. Individual EVs are represented in connection with low voltage (LV) nodes, while clusters of EVs on parking areas as well as fast battery charging stations are in turn modeled in connection with medium voltage (MV) nodes.

This chapter of the document is organized as follows. In Section 4.1, the simulation platform is introduced with emphasis on the Multi-Micro grid control and management approach, the Multi-Micro grid frequency control schemes, as well as the EUROSTAG-MATLAB implemented interactions. In Section 4.2, the adaptations and enhancements that have been developed on the original edition of the platform are described. At last, in Section 4.3, simulation results using a test network with large scale integration of distributed energy resources are presented.

4.1 Description of the Simulation Platform

4.1.1 Multi-Micro Grid Control and Management Approach

A micro grid is a low voltage (LV) network with micro generators (such as micro turbines, photovoltaic generators, etc.), storage devices (such as flywheels, capacitor banks, etc.) and controllable loads. A micro grid normally operates interconnected to the main distribution network. Otherwise, the micro grid may be islanded operated in case of contingencies in the upstream system or if maintenance actions are occurring. Hence, a micro grid central controller (MGCC), to be housed in MV/LV substations, is the entity responsible for the control and management of a micro grid.

A multi-micro grid is an extension of the micro grid concept. It consists of a MV network with micro grids, controllable loads and DG units connected to the feeders. In this sort of system, micro grids, DG units, and MV controllable loads are considered as active cells, for control and management purposes. The technical

operation of such a system requires the transposition of the micro grid concept to the MV level, where all these active cells should be controlled by a central autonomous management controller (CAMC) to be installed at the HV/MV substation. The CAMC is envisioned to interface with and accommodate functionalities normally assigned to distribution management systems (DMSs), as well as to operate under the responsibility of a distribution system operator (DSO). The described architecture for multi-micro grid control and management is illustrated in Figure 4-1.

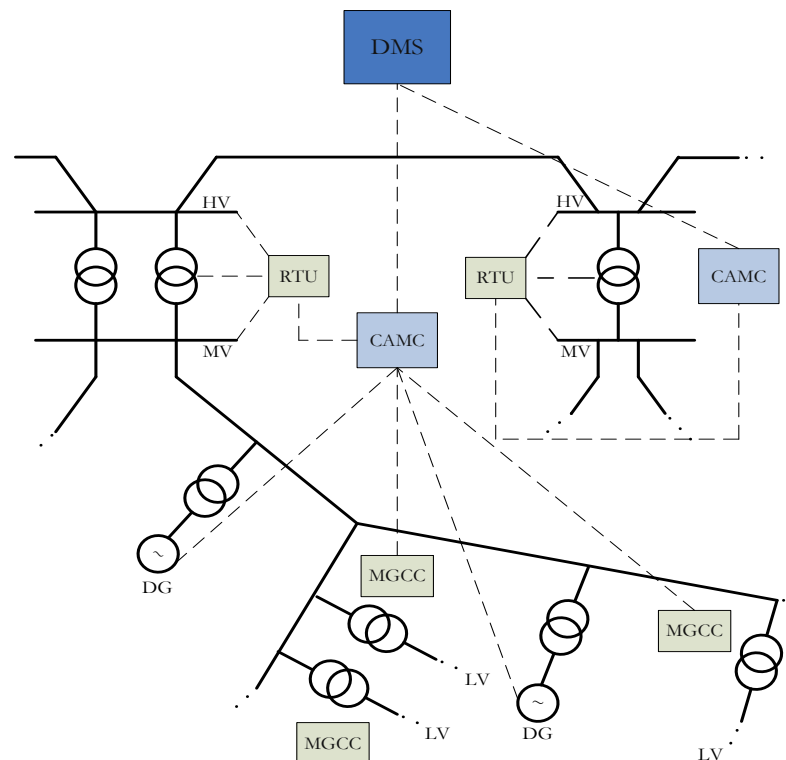


Figure 4-1 Control and management architecture of a Multi-Micro grid.

Several functionalities are envisioned to be provided by the Multi-Micro grid architecture. Such functionalities include frequency control coordination, voltage control coordination, control scheduling (from a market point of view), emergency functions, state estimation, etc (see [3] for a full description). The availability of such functionalities will depend on the characteristics of the local DG units.

The simulation platform was particularly developed to tackle issues related to frequency control coordination for islanding and islanded operation purposes. The Multi-Micro grid frequency control scheme is presented in the following subsection.

4.1.2 Multi-Micro grid frequency control

In order to achieve a robust islanding and islanded operation, frequency control coordination functionalities are assigned to the CAMC. The frequency control rules resemble those implemented on regular bulk power system automatic generation control (AGC). The frequency control procedure can be summarized as follows. For

a given time interval T_s (sample time), in case significant changes in the system frequency are verified, the total imbalance into the Multi-Micro grid is estimated and new power setpoints are sent to the MGCCs, DG units, and controllable loads. Using the received setpoints, the MGCCs are in turn responsible to compute and send new setpoints to their associated micro sources and controllable loads. The described procedure is illustrated in Figure 4-2.

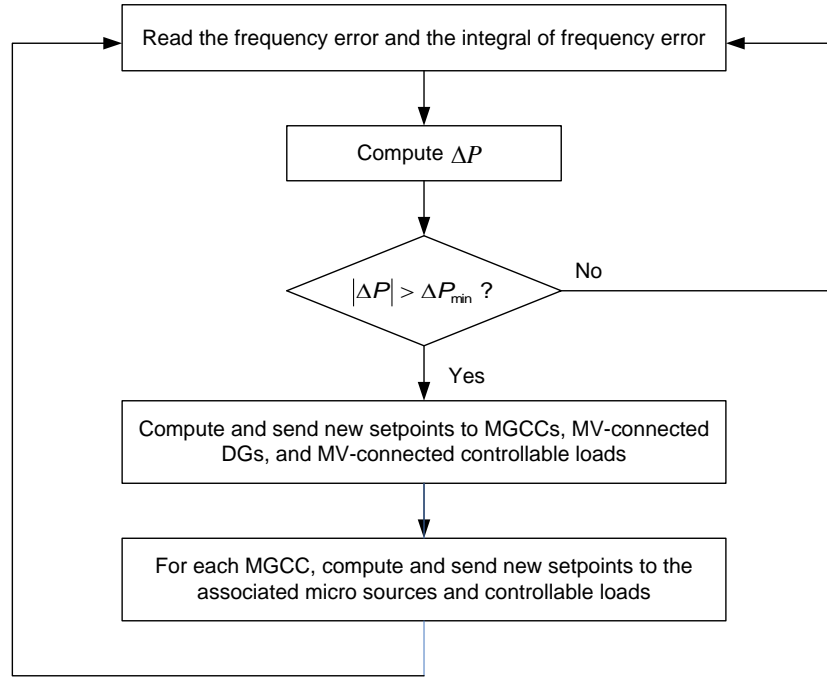


Figure 4-2 Multi-Micro grid frequency coordination procedure.

The frequency deviation and the integral of the frequency deviation are utilized to compute the additional power ΔP to be requested from the entities within the Multi-Micro grid and under the CAMC control. The additional power is computed as follows

$$\Delta P \leftarrow K_P [f_{rated} - f(t)] + K_I \int_0^t [f_{rated} - f(u)] du \quad (4-1)$$

in which K_P is the predefined proportional gain, K_I denotes the predefined integral gain, f_{rated} stands for the nominal frequency value, and $f(t)$ is the actual frequency value at instant t .

Whether $|\Delta P|$ is larger than a threshold, the CAMC control system proceeds in computing and sending power requests to its associated available sources. We point out that there are several ways of designing the distribution of setpoints among the entities under control. In the developed approach, the setpoints are allocated by solving the following optimization problem.

$$\min_{\mathbf{x}} \mathbf{c}^T \mathbf{x} \quad (4-2)$$

subject to

$$\begin{aligned} \sum_i x_i &= \Delta P \\ \mathbf{x} &\leq \mathbf{b} \end{aligned} \quad (4-3)$$

where \mathbf{c} is a vector of generation costs, MGCC costs, and MV load curtailment prices, $\mathbf{x}=\{x_i\}$ is a vector of generation, MGCC or load setpoint variations, and \mathbf{b} is a vector which contains the smallest and largest power variations allowed.

The MGCCs apply a similar formulation to compute power requests for their associated micro sources and controllable loads. After receiving the setpoint ΔP_k , the MGCC_k allocates the power requests according with the following formulation.

$$\min_{\mathbf{y}} \mathbf{d}^T \mathbf{y} \quad (4-4)$$

subject to

$$\begin{aligned} \sum_i y_i &= \Delta P_k \\ \mathbf{y} &\leq \mathbf{e} \end{aligned} \quad (4-5)$$

where \mathbf{d} is a vector of micro generation costs and LV load curtailment prices, $\mathbf{y}=\{y_i\}$ is a vector of micro generation and load setpoint variations, and \mathbf{e} is a vector which contains the smallest and largest power variations allowed. Some of the micro sources are not considered in these procedures due to limitations in primary resource availability (e.g. photovoltaic and wind generators).

Finally, we emphasize some limits are enforced to ΔP . As a matter of fact, ΔP cannot be larger than the available reserve or lower than the total generation available for curtailment. In the developed approach, the CAMC can also respond to other disturbances, such as loss of load while in islanded mode, managing generation sources to reduce their power output (including generation curtailment, if necessary).

4.1.3 Platform implementation

The EUROSTAG software allows fast simulation of power systems static and dynamic behaviors. In addition, this software provides a suitable environment for the implementation of tailored-made models through embedded elementary blocks. Despite of these advantages, EUROSTAG has limitations regarding the implementation of control algorithms, namely in establishing logic/decision rules. Moreover, the software does not provide support for performing matrix operations and optimization procedures. Such limitations made impossible to simulate the Multi-Micro grid frequency control coordination only using the EUROSTAG development environment.

Hence, MATLAB scripts were developed aiming at performing computations related with the secondary load-frequency control coordination (see Figure 4-3). These MATLAB scripts are designed to invoke EUROSTAG functionalities for a distribution

network which is completely represented in the EUROSTAG environment (including the static and dynamic models for components and generation sources).

The simulation procedure can be described as follows.

- (i) MATLAB scripts read the network data and invoke the EUROSTAG load flow module to compute the system steady state.
- (ii) A MATLAB script calls the EUROSTAG modules to simulate the dynamic behavior of the Multi-Micro grid during the next T_s seconds.
- (iii) The frequency deviation and the integral of the frequency deviation are automatically computed by EUROSTAG and saved in a file F .
- (iv) A MATLAB script reads the information in file F to compute the additional power ΔP using .
- (v) Whether $|\Delta P|$ is larger than a given threshold, setpoint variations for the sources associated with the CAMC are computed using (4-2)-(4-3).
- (vi) The setpoints variations for the sources associated with the MGCCs are computed using (4-4)-(4-5).
- (vii) The new setpoints are computed (current setpoint + setpoint variation) and saved in the EUROSTAG event simulation file.
- (viii) If the end time was not reached, go to (ii). Otherwise finalize the simulation.

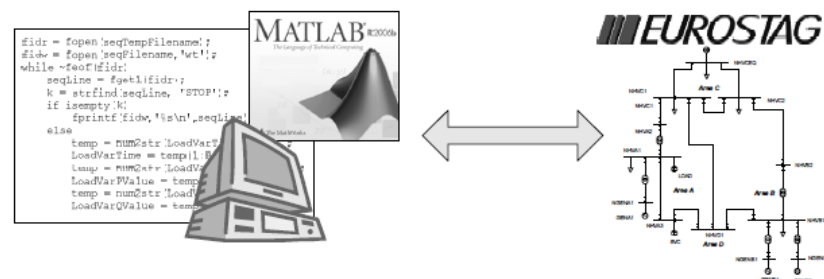


Figure 4-3 EUROSTAG-MATLAB platform interaction.

The platform includes data files for a test distribution network with multiple micro grids and several kinds of larger DG systems. A diagram of this test network is shown in Figure 4-4. This MV test network includes several DG units and microgrids as well as several clusters of EVs seen as connected directly at the MV level or assumed to be connected at the LV microgrids.

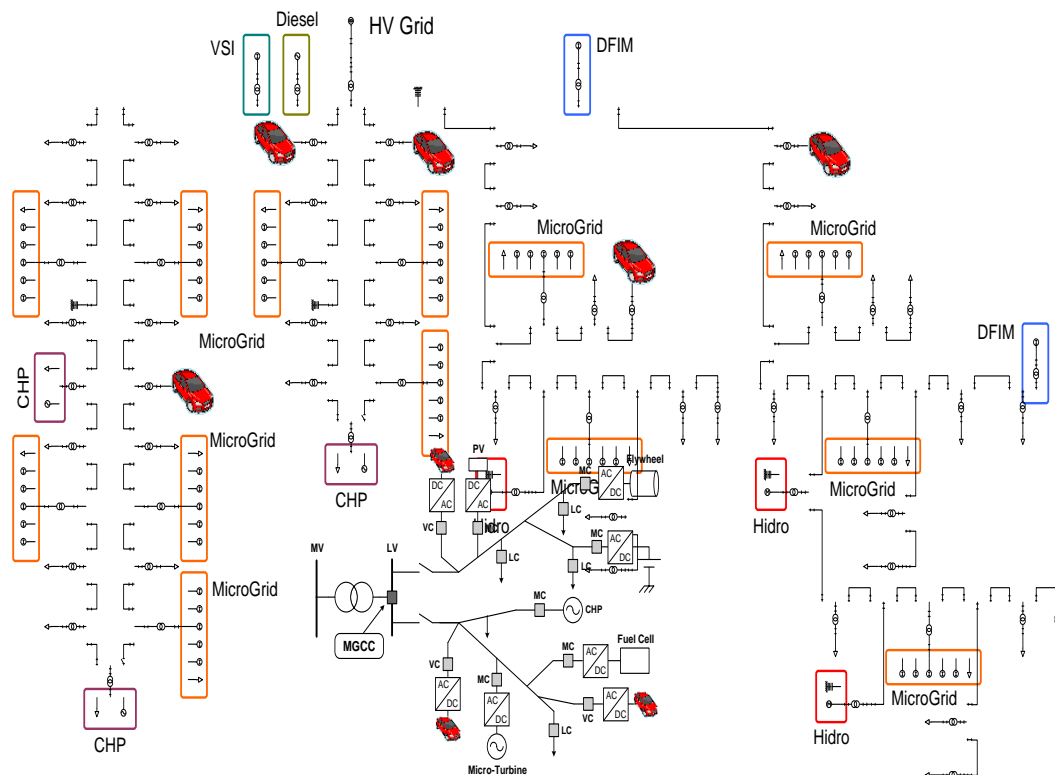


Figure 4-4 Test network.

Two rural areas and two urban areas are represented in this test network. The urban zones are characterized by a loop network structure while the rural areas are radial structured without alternative supply. DG oriented-generation systems are considered such as: a small diesel group, several CHP and hydro units, two doubly-fed induction machines (DFIM) corresponding to wind-generator systems, and a storage element interfaced with the MV grid via a voltage source inverter (VSI). In addition, 13 micro grids are represented, each one with a controllable load, a small wind generator, a FC generation unit, a MT generation unit, a photovoltaic (PV) generation unit, and a storage element connected to the grid via a VSI (representing storage elements).

Some of the dynamic models were obtained directly from EUROSTAG's library. Nevertheless, the DFIM, storage elements with VSI, MTs and FCs had to be implemented from scratch in the platform. The DFIM model was coded based on [4]-[5], but including additional modules for pitch and de-load control to enable primary frequency regulation [6]. The FC and MT models are based on [7] with few adaptations. As most of the user EUROSTAG models, the VSI was implemented as a power injector programmed to emulate the behavior of a synchronous machine (e.g., injecting active power when system frequency temporarily drops [8]). The VSI model is then equipped with a standard proportional controller and also responds to setpoints received from the control system.

Despite the EUROSTAG's standard data developed to represent the system components and generation sources, a set of additional data is required to emulate the Multi-Micro grid frequency control coordination. Table 4-1, Table 4-2 and Table 4-3 provide an example of this additional data information for a Multi-micro grid with one hydro unit, one CHP unit and two micro grids. Table 4-4 presents a description of the data fields.

Table 4-1 Example of CAMC level additional data required to simulate the Multi-Micro grid frequency control coordination

ID	LMin	LMax	Cost	Delay	MGCC	Adjust	Factor	MinVar	Address1	Address2	Speed
MGCC01	0.00	1.00	20	0.50	1	1	1	0.01	DIESEL	AGCHELP	0
MGCC02	0.00	1.00	20	0.50	1	1	1	0.01	DIESEL	AGCHELP	0
HYDRO	0.00	1.00	10	0.50	0	1	100	0.01	HYDROASM	PREQ	1
CHP	0.10	1.00	25	0.50	0	1	100	0.01	STEAM	PREQ	1

Table 4-2 Example of MGCC level additional data required to simulate the Multi-Micro grid frequency control coordination

ID	Macroblock	Setpoint	LMin	LMax	Cost	Delay	Adjust	Factor	MinVar	Speed
PV1	INTERPV	PREQ	0.00	1.00	10	0.30	0	-1	0.01	1
MT1A	INTERMT	PREQ	0.10	1.00	10	0.30	1	-1	0.01	1
VSI1	INTERVSI	PREQ	0.00	1.00	12	0.30	0	-1	0.01	1
FC1	INTERFC	PREQ	0.10	1.00	11	0.30	1	-1	0.01	1
MT1B	INTERMT	PREQ	0.10	1.00	10	0.30	1	-1	0.01	1
MT1A	INTERMT	PREQ	0.10	1.00	10	0.30	1	-1	0.01	1

Table 4-3 Example of controllable load additional data required to simulate the Multi-Micro grid frequency control coordination

Node	LMin	LMax	Cost	Delay	MGCC	Adjust	Factor	MinVar	MinTime	Speed
NLV3	0;00	0.15	13	0.50	MGCC01	0	100	0.01	20	1
NLV8	0;00	0.15	13	0.50	MGCC02	0	100	0.01	20	1

Table 4-4 Data fields for the additional data required to simulate the Multi-Micro grid frequency control coordination

Field	Description
ID	Name of the EV module/cluster
LMin	Minimum load power allowed (use negative values if injector behaviour is allowed) [p.u.]
LMax	Maximum load power allowed [p.u.]
Cost	Relative curtailing or injecting cost (comparing with other sources) [relative value]
Delay	Combined communications and reaction delay [s]
Adjust	Is this EV adjustable? {0,1}
Factor	Correction factor for Eurostag data (MW->kW, signal conventions, etc.)
MinVar	Minimum power variations allowed (threshold) [p.u.]
Speed	Relative speed to other sources (not currently used) [relative value]

The fields *Macroblock*, *Setpoint*, *Address1* and *Address2* are used to specify where and how to modify the EUROSTAG event data files in order to obtain the required micro source simulation response.

The additional data is read from a data file (.txt) by a MATLAB script. New components and generation sources can be added to the network through the EUROSTAG environment and by updating the referred data file.

4.2 Adaptations and Enhancements

The existing EUROSTAG-MATLAB platform, described in the previous section, needed some adaptations and enhancements in order to be applied in this context. These adaptations and enhancements were implemented at different levels, as the EUROSTAG-MATLAB platform has several layers that needed to be worked out separately. This subsection describes the EV control approach as well as the implemented EUROSTAG EV model. In addition, the adaptations and enhancements on the EUROSTAG-MATLAB are presented, focusing on the developments related with the simulation of the Multi-Micro grid quasi-steady state behaviour as well as frequency control coordination.

4.2.1 EV Control Approach

The EV control approach is closely based on the one already adopted on previous works (see [9]). EVs can be controlled externally, through setpoints, or internally (autonomously), following a frequency droop and observing some preset limits.

Figure 4-5 shows the EV control approach where an EV is modelled as an active load (positive P_{charge} indicates a load). Three different setpoints are simultaneously represented, all for the same values of P_{max} (maximum power input) and P_{min} (minimum power input).

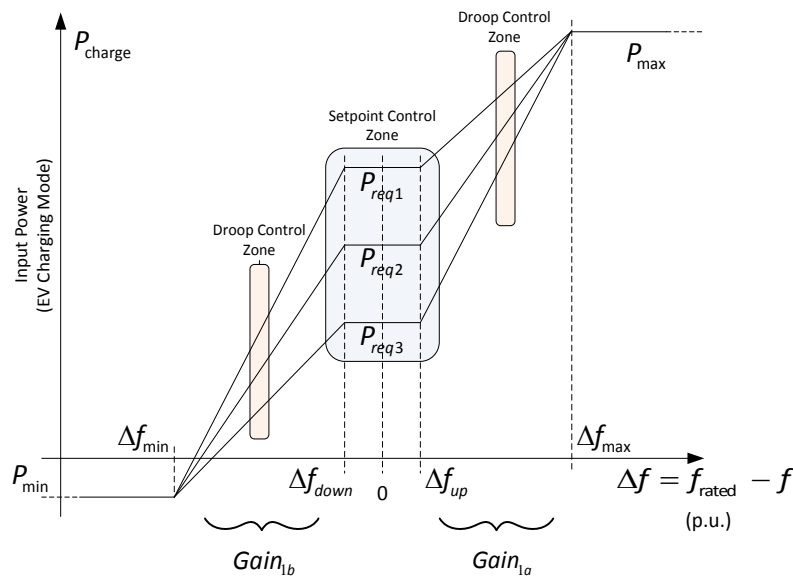


Figure 4-5 Adopted EV control approach.

Two important issues should be noted in this model:

- P_{min} must be less or equal than P_{max} , and may or may not assume negative values. Hence, the user can preset which EVs will (or will not) be able to inject power in the grid.

- It was considered that droop values are not constant, but updated dynamically according to the power setpoint values (and they also depend on other EV settings and limits).

The droop values (proportional gains) are thus determined using one of the following expressions, depending if the frequency is above or below the rated value:

$$Gain_{1a} = \frac{P_{max} - P_{req1}}{\Delta f_{max} - \Delta f_{up}} \quad Gain_{1b} = \frac{P_{req1} - P_{min}}{\Delta f_{down} - \Delta f_{min}}$$

Setpoints are handled externally, and in this simulation platform this is done through the MATLAB part of the system, as previously described.

4.2.2 EUROSTAG EV Model

The EUROSTAG EV model was built using the power injector available in the EUROSTAG's library. According to EUROSTAG's convention, a positive output indicates the component is behaving as a load, while a negative output indicates the component is injecting power into the grid. All tailored-made models using power injectors, including the EV model, follow this reverse convention. For quasi-steady state purposes, the EUROSTAG injector behaves as a constant active power which consumes/produces a portion of the load/generation of the network connection node. On the other hand, for dynamic simulation purposes, the injector follows the control approach introduced in the previous section.

Figure 4-6 shows the implementation of the EV control model in EUROSTAG, while Table 4-5 presents the parameters we have applied to the EV model.

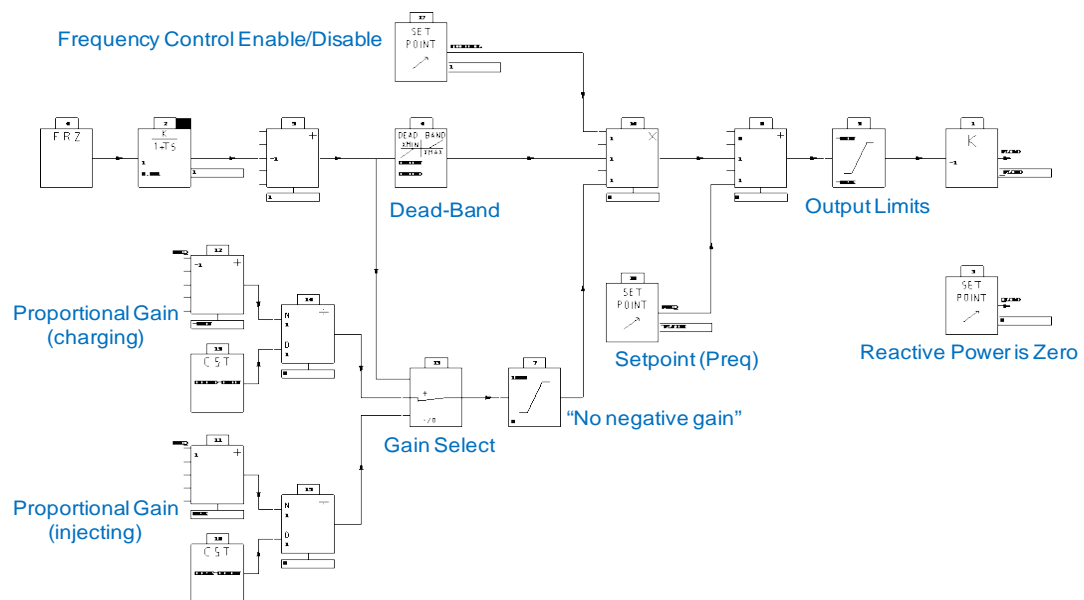


Figure 4-6 Developed EUROSTAG EV model.

Table 4-5 EV model parameters

Parameter	Values (p.u.)	Description
DFMAX	+0.040	Frequency deviation corresponding to maximum load
DFMIN	-0.040	Frequency deviation corresponding to minimum load
DFMIND	+0.002	Upper dead-band frequency threshold
DFMINU	-0.002	Lower dead-band frequency threshold
PMAX	+1.000	Maximum load power
PMIN	+0.800	Minimum load power (use negative values if injector behaviour is allowed)

On the top-left part of this model, one begins by determining the system's frequency deviation. (The initial first-order low-pass filter is included just to overcome a minor EUROSTAG limitation in the frequency measurement.) This frequency deviation value is utilized to select the appropriate gain, which is in turn computed using (4-8). These expressions appear, in the figure, in an adapted form in order to account for the change in the convention for the sign of P_{req} (the P_{req} input is multiplied by -1).

The autonomous frequency control is only utilized if the frequency deviation surpasses a specified dead-band limiter. This avoids frequent changes in the EV operation point. The autonomous frequency control can also be optionally turned off (FCONTROL setpoint). Such option was implemented to model the EVs which are not supposed to respond to frequency deviations. Hence, in this case (FCONTROL setpoint equal 0), these EVs behave as active constant powers specified by their respective P_{req} . Furthermore, a safeguard is applied in order to prevent negative gains are used. These could show up if P_{req} is inadvertently set higher than P_{max} or lower than P_{min} .

Finally, it should be noted that the output power limiter settings are reversed, again to maintain coherency with EUROSTAG's power injector convention. Regarding reactive power, it was chosen to be kept at zero as, for now, it is not considered to be of relevance for the implemented control scheme.

4.2.3 Adaptations and Enhancements on the EUROSTAG-MATLAB Interaction

The EUROSTAG-MATLAB interaction was developed in two different ways. Both are based on the already existing and described simulation platform. The first one deals with dynamic simulation, in order to study the contribution of the EVs to the transient phenomena that occur in the networks they are integrated (Part A). The

second one deals with successive load-flow calculations to simulate the quasi-steady state behaviour of the network (Part B). The quasi-steady state simulation refers to a much larger time frame and will enable the study of how the system should react to changes in the EV usage patterns and EV charging strategies. Parts A and B are described in the following.

Part A

Due to the generalization effort that was made during the implementation of the MATLAB part of the simulation platform, a correct model implementation leads to the need of few changes in the simulation algorithm programmed in MATLAB. Therefore, almost no adaptations were required, at this point, to integrate the EV model in the existing simulation platform.

The EV model also performs the internal computations in per unit, thus the same model can be used to represent a single EV or a cluster of EVs with the same behaviour.

It is, however, necessary to describe each of these EV or cluster of EVs. Besides the already mentioned dynamic model parameters, it is required to specify how these elements should be controlled. Using a procedure similar to the one already applied to the other generator units and controllable loads, these parameters are inputted to the simulation platform using a formatted text file which is read by MATLAB.

The information which pertains to EVs can be of two types, depending on the location of the EV unit (or cluster of units):

- The EV may belong to a micro grid (controlled by a MGCC);
- The cluster of EVs, EVs connected in parking areas, or fast battery charging stations may be controlled directly by the CAMC.

Table 4-6 shows an example of data set for an EV outside a micro-grid. Table 4-6 Example of MV level additional data required to include the EV in the Multi-Micro grid frequency control coordination

ID	LimMin	LimMax	Cost	Delay	MGCC	Adjust	Factor	MinVar	Address1	Address2	Speed
EV1	0.8	1	30	0.5	0	1	-1	0.01	INTEREV	PREQ	1

Another example of data set is presented in Table 4-7, now for an EV which belongs to a micro grid. In this case, the responsible MGCC was named MGCC01.

Table 4-7 Example of MGCC level additional data required to include the EV in the Multi-Micro grid frequency control coordination

ID	Macroblock	Setpoint	LimMin	LimMax	Cost	Delay	Adjust	Factor	MinVar	Speed
EV3	INTEREV	PREQ	0.8	1	10	0.3	0	-1	0.01	1

EV integration is transparent and not much different from the integration of any other micro source. The only difference lies on the power limits, which are not necessarily non-negative, due to the power injection capabilities that some EVs may have.

Part B

In order to simulate the step by step response of the system in quasi-steady state when following the load diagram in critical periods and when adopting different charging strategies, it was necessary to develop a set of MATLAB functions to repeatedly call EUROSTAG load flow computation module.

These functions will allow the testing of the adoption of different charging strategies: dumb, tariff based, smart charging. These may involve the need to deal with network restrictions through hierarchical control solutions. In this case, the distribution management system plays a key role in adjusting, from time to time, the power consumption or the power injections from EV batteries.

The simulation process implemented for the quasi-steady state simulation of Multi-Microgrids is described in the “pseudo-code” shown in Figure 4-7.

```
*BEGIN*
for i = 0 to 0.3 step 0.1 [e.g.: for EV integration from approx. 0% to 30% in 10% steps]
    for j = (each of hour of the day)
        Modify EUROSTAG network description [ECH file]
        [modification includes system bus load variation according to j]
        [EV integration levels according to i are also integrated]
        [EV load changes due to the adoption of different charging strategies is also integrated]
        Compute Load Flow in EUROSTAG
        Save Results and Reference Data [EUROSTAG LF and ECH files]
    end
end
Look for Overloaded Branches in LF Results [scan EUROSTAG LF files]
Save Data File [a MATLAB .MAT file containing a structure with branch data]
*END*
```

Figure 4-7 Pseudo-code applied to simulate the quasi-steady state behaviors of Multi-Micro grids.

The number of EVs connected in each network node is preset for each hour of the day. The consumed/produced active power per hour of each EV must be also provided to the software. Given an EV integration scenario, a EUROSTAG file that describes the network state (ECH file) is then created for each of the 24 load levels of a typical load diagram and each of the 24 EVs consumption/production per node. Then, load-flow computations are run using EUROSTAG and the results of which are processed and saved for further analysis. Such analysis can be directed at some of the more critical issues of the distribution system operation. For instance, in case of a tariff based strategy, most of the EVs can be assumed to charge on the

tariff change time. In case of a smart charging strategy, the EV consumption/production can be reduced/increased to avoid, for instance, network overloadings in some scenarios.

The analysis results can be applied to determine which actions should be taken in order to limit the eventual negative effects of the potential massive amounts of future EV integration. This will use the resources of the hierarchical control structure already in place, sending the appropriate commands to EV clusters or single EVs in the right locations.

4.3 Results

The results obtained from the two described parts (A and B) are presented in the following subsections.

4.3.1 Multi-Micro grid frequency control coordination (Part A)

The results presented here are based on the test network shown in Section 4.1.3 as well as the setup described in [10]. The main difference is the consideration of a 10% load evolution totally based on the massive arrival of EV to the grid, considering that all of them have frequency responsive battery charging interfaces.

As the system was already working very close to the feasible islanding limits, it was decided to consider an increase in the wind-generated power of about 1 MW. This allowed the test of the transition to islanded operation with a minimum amount of changes to the rest of the network.

In this specific scenario, all the EVs have the autonomous proportional frequency control in an active state. Since it is considered to be the option most agreed upon, the EVs were disabled to inject power into the grid, behaving therefore as frequency dependent controllable loads.

The EVs can also receive setpoints for their power consumption (or power injection). However, this capability is restricted to the EVs under control of a management unit which is higher in the hierarchy (the CAMC or a MGCC). In this particular case, all EVs have the potential to receive this setpoints, but this capability is disabled for a large number of them in order to better select those that participate in the secondary frequency regulation and to better observe their effect.

Figure 4-8 shows the frequency response due to the chosen system disturbances:

- Emergency transition to islanded operation (worst-case scenario – a loss of about 4 MW of imported power) ①;
- Load-following operation (ramp load increase of approximately 1.5 MW during 10 seconds) ②.

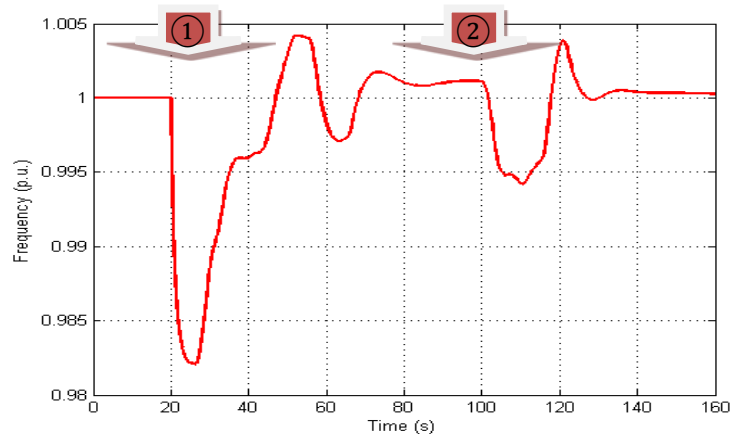


Figure 4-8 Frequency response during islanding and islanded operation (load following).

The figure above shows that the frequency stabilization was achieved at the frequency rated value after the described disturbances. This result highlights the islanding process and the islanded operation can be successfully accomplished for this test network using the presented Multi-Micro grid control schemes. Due to system frequency deviations, the frequency control coordination was triggered and the conveyance of setpoints initiated. As examples, the control setpoints and generation responses for the CHP and Hydro units are illustrated in Figure 4-9 and Figure 4-10.

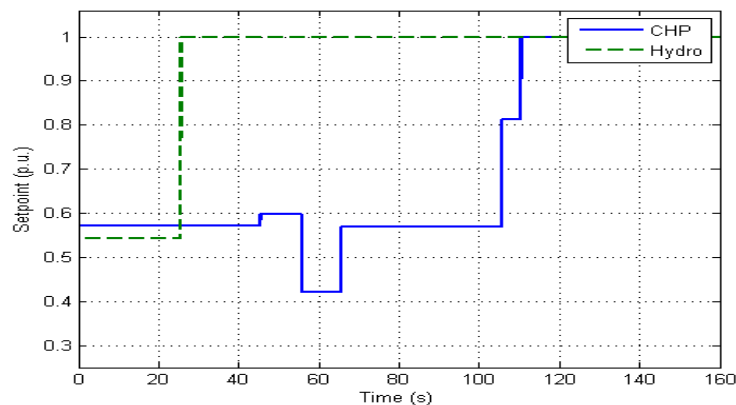


Figure 4-9 Control setpoints for the CHP and Hydro units during islanding and islanded operation (load following).

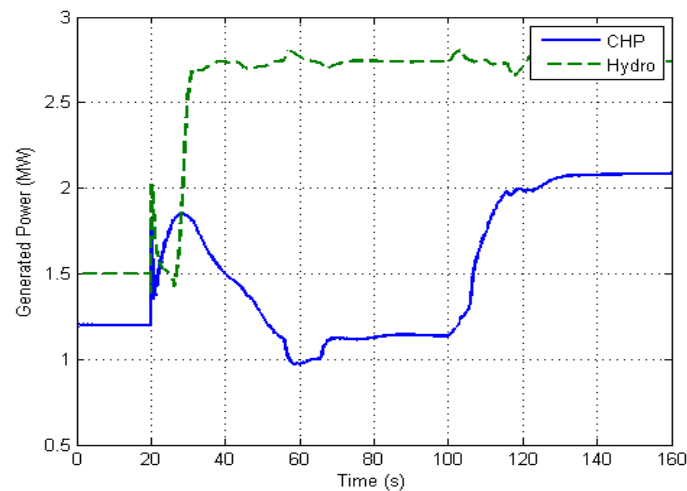


Figure 4-10 Generated power response for the CHP and Hydro units during islanding and islanded operation (load following).

The Hydro unit was commanded to change its control setpoint before the CHP unit. Such result was expected since the system setup includes a Hydro unit cost inferior to the CHP cost. The Hydro unit changed its control setpoint about five seconds after the islanded operation is characterized. This change is clearly associated with frequency coordination during the islanding process. On the other hand, the CHP control setpoint change considerably at $t = 105\text{s}$ is related with the load following procedure.

Similarly, micro grids act (at the CAMC control level) as a generic MV source. Therefore, they can be also analysed as a standard MV connected generator (see [11]). As an example, the control setpoints and generation response behaviour of the micro grid 01 are illustrated in Figure 4-11 and Figure 4-12.

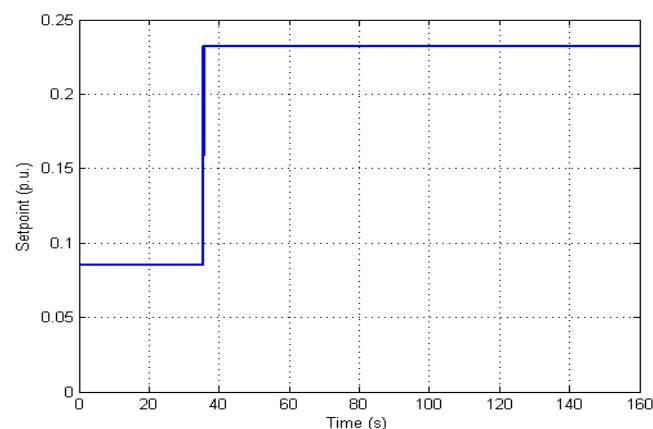


Figure 4-11 Control setpoint for the micro grid 01 during islanding and islanded operation (load following).

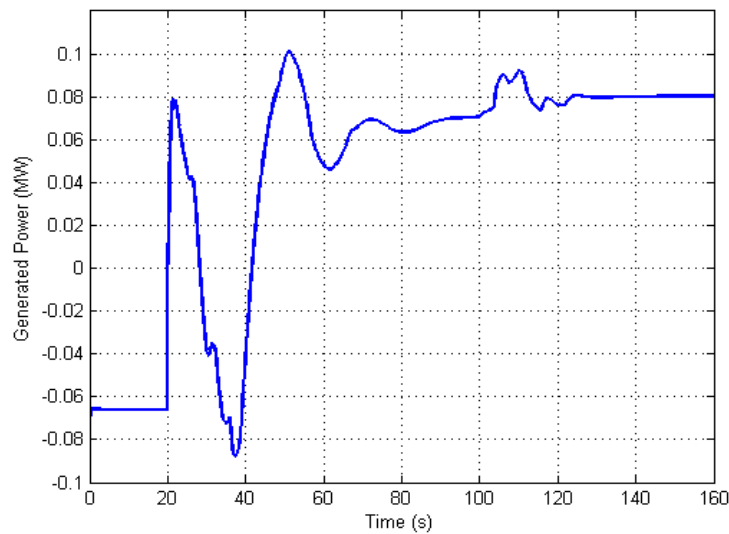


Figure 4-12 Generated power response for the micro grid 01 during islanding and islanded operation (load following).

The generation sources within the micro grid respond to the MGCC setpoint commands. As an example, the micro turbine control setpoint and the corresponding response are illustrated in Figure 4-13 and Figure 4-14. This micro turbine is under the control of the MGCC associated to the micro grid 01.

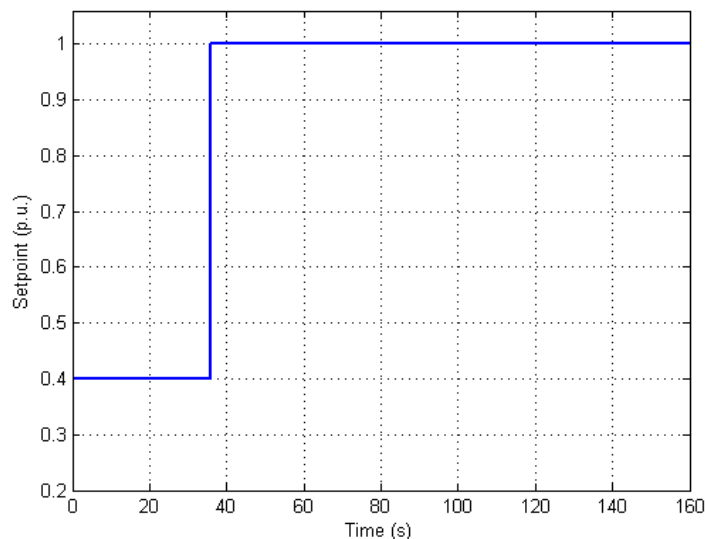


Figure 4-13 Control setpoint for a micro turbine during islanding and islanded operation (load following).

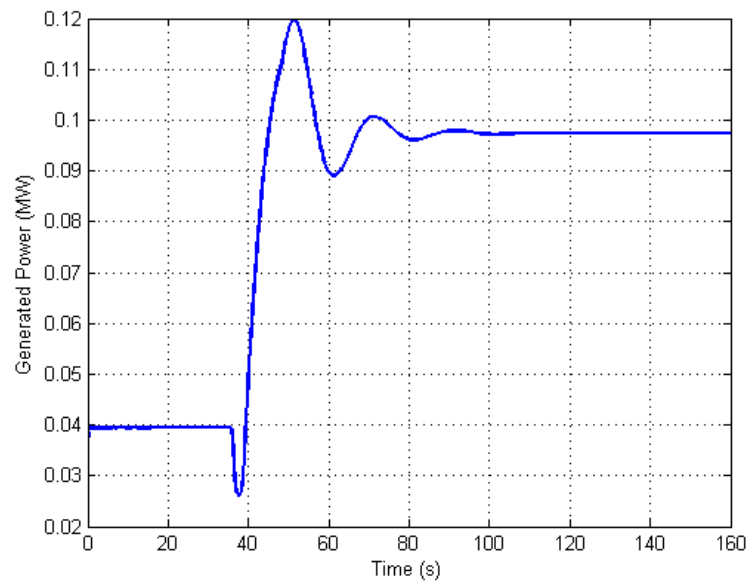


Figure 4-14 Generated power response of a micro turbine during islanding and islanded operation (load following).

Finally, Figure 4-15 shows the effect of the EV droop frequency control on the system islanding and islanded operation. The EV3 belongs to the micro grid 01. Conversely, the two other EVs are connected at the MV level.

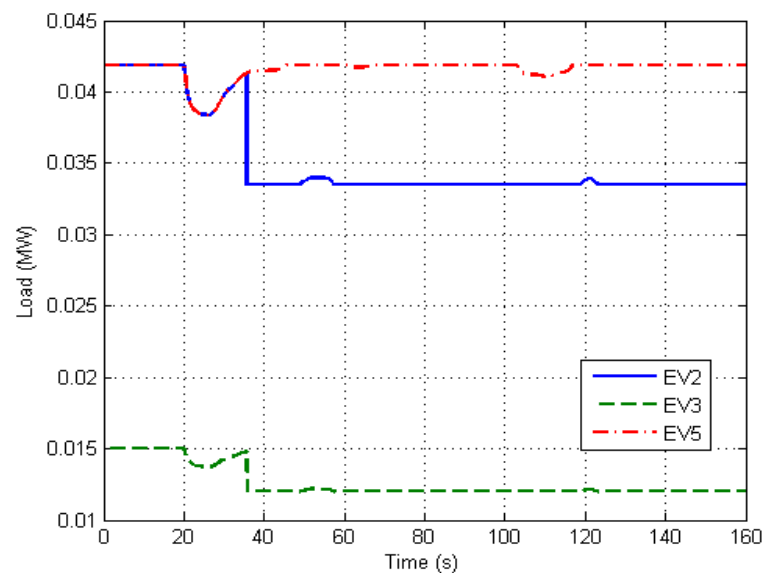


Figure 4-15 Load response for EVs during islanding and islanded operation (load following).

The EVs at the MV level can represent, for instance, a larger battery charging station or a cluster of EVs in a shopping centre parking garage. It is also noticeable

the influence of the higher level, hierarchic, frequency control on the power input of EV3 and EV5 when both of these EVs receive a setpoint change command at around $t = 35s$, just after their initial droop based response. Thus, the combined effects of these two independent types of control systems (contribution to primary frequency control and contribution to secondary frequency control) are shown, in this picture, superimposed on each other.

4.3.2 Quasi-steady state simulation (Part B)

As the title of this section implies, this is almost a steady state simulation. These results will show how consecutive load flow calculations can help in determining the branches most susceptible to overload due to the increase in EV grid presence. In order to find out the most critical times of the day, the load increase due to EV connection and charging will be superimposed on a daily time load evolution (load diagram).

As an example, different levels of EV integration were applied to the test system introduced in the previous section. For illustration purposes, the EVs were all assumed to consume 3 kW. We have also considered a change in EV penetration from 0% to 30% related with the network peak load using step increments of 10%, as shown in Table 4-8.

These levels of integration were rounded to obtain the number of cars connected at each node. The resultant data input is shown in

Table 4-9.

The load variation during a typical day can be derived from the normalization of a given load curve (see results from MERGE Project for the different countries studied [28]). Similarly, a normalized version of the EV dumb charging profile, as described in [28], is also used to create the EV charging conditions per node class, as shown in Table 4-10 ~Table 4-15 for a given country. The data presented next corresponds to the Portuguese case. As an example, the normalized EV dumb charging profile can be obtained from [28], as illustrated in Figure 4-16 and Figure 4-17.

Table 4-8 EV Penetration Levels

Time Period (Scenario)	Base	Level 1	Level 2	Level 3
% EV Level	0	10%	20%	30%

Table 4-9 Number of EVs connected to some network nodes for each of the scenarios under evaluation

Class	Node	Nominal Load	nEV (10%)	nEV (20%)	nEV (30%)
A	NLV1, NLV1A, NLV2, NLV2A	838 kW	28	56	84
	NLV6, NLV6A, NLV7, NLV7A NLV13A, NLV14A, NLV16A		(84 kW total)	(168 kW total)	(252 kW total)
B	NLV4, NLV4A, NLV5, NLV5A	419 kW	14	28	42
	NLV9, NLV9A, NLV11A		(42 kW total)	(84 kW total)	(126 kW total)
	NLV18A				
C	NLVR1, NLVR1A	216 kW	7	14	22
	NLVR5, NLVR5A		(21 kW total)	(42 kW total)	(66 kW total)
	NLVR17A				
D	NLV3, NLV3A, NLVR6	150 kW	5	10	15
	NLVR6A, NLV8, NLV8A				
	NLV10, NLV10A, NLVR11				
	NLVR11A, NLV12A, NLV17A				
	NLVR19A				
E	NLVR2, NLVR2A, NLVR3	135 kW	5	9	14
	NLVR3A, NLVR7, NLVR7A				
	NLVR9, NLVR9A, NLVR21A				
	NLVR24A				
F	NLVR4, NLVR4A, NLVR8	86 kW	3	6	9
	NLVR8A, NLVR10, NLVR10A				
	NLVR22A, NLVR25A				

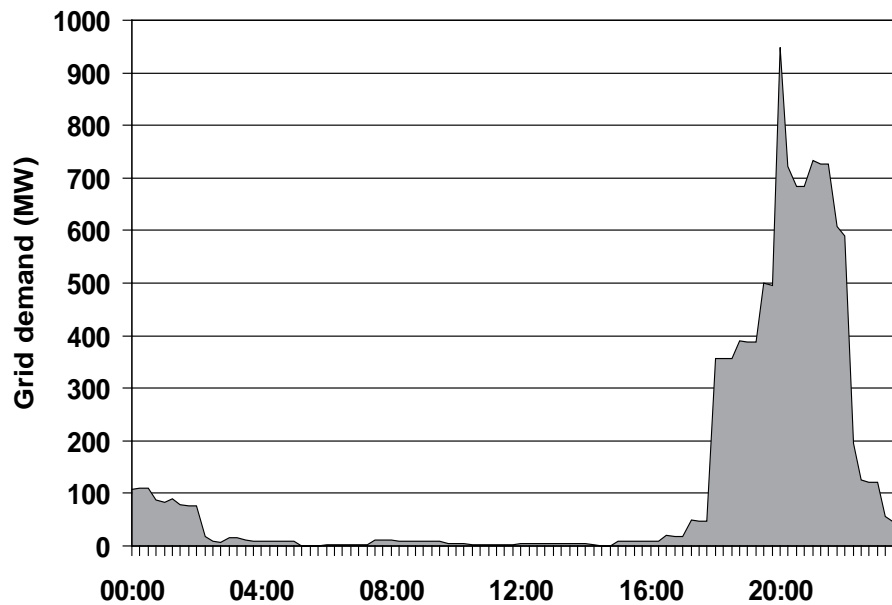


Figure 4-16 EV charging load for dumb charging scenario, Portugal (source [28]).

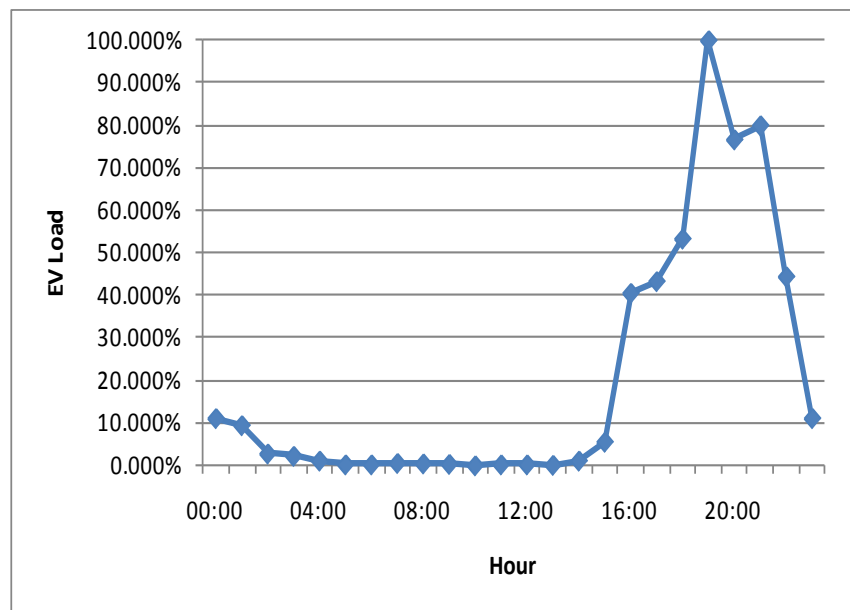


Figure 4-17 EV charging load for dumb charging scenario (100% corresponds to the total number of EVs under consideration).

Table 4-10 Number of EVs per node class from 1h to 12h of a typical day (10% EV integration)

Class/Hour	1	2	3	4	5	6	7	8	9	10	11	12
A	3	2	0	0	0	0	0	0	0	0	0	0
B	1	1	0	0	0	0	0	0	0	0	0	0
C	0	0	0	0	0	0	0	0	0	0	0	0
D	0	0	0	0	0	0	0	0	0	0	0	0
E	0	0	0	0	0	0	0	0	0	0	0	0
F	0	0	0	0	0	0	0	0	0	0	0	0

Table 4-11 Number of EVs per node class from 13h to 24h of a typical day (10% EV integration)

Class/Hour	13	14	15	16	17	18	19	20	21	22	23	24
A	0	0	0	1	11	12	14	28	21	22	12	3
B	0	0	0	0	5	6	7	14	10	11	6	1
C	0	0	0	0	2	3	3	7	5	5	3	0
D	0	0	0	0	2	2	2	5	3	4	2	0
E	0	0	0	0	2	2	2	5	3	4	2	0
F	0	0	0	0	1	1	1	3	2	2	1	0

Table 4-12 Number of EVs per node class from 1h to 12h of a typical day (20% EV integration)

Class/Hour	1	2	3	4	5	6	7	8	9	12	11	12
A	6	5	1	1	0	0	0	0	0	0	0	0
B	3	2	0	0	0	0	0	0	0	0	0	0
C	1	1	0	0	0	0	0	0	0	0	0	0
D	1	0	0	0	0	0	0	0	0	0	0	0
E	1	0	0	0	0	0	0	0	0	0	0	0
F	0	0	0	0	0	0	0	0	0	0	0	0

Table 4-13 Number of EVs per node class from 13h to 24h of a typical day (20% EV integration)

Class/Hour	13	14	15	16	17	18	19	20	21	22	23	24
A	0	0	0	3	22	24	29	56	42	44	24	6
B	0	0	0	1	11	12	14	28	21	22	12	3
C	0	0	0	0	5	6	7	14	10	11	6	1
D	0	0	0	0	4	4	5	10	7	8	4	1
E	0	0	0	0	4	4	5	10	7	8	4	1
F	0	0	0	0	2	2	3	6	4	4	2	0

Table 4-14 Number of EVs per node class from 1h to 12h of a typical day (30% EV integration)

Class/Hour	1	2	3	4	5	6	7	8	9	10	11	12
A	9	7	2	1	0	0	0	0	0	0	0	0
B	4	3	1	0	0	0	0	0	0	0	0	0
C	2	1	0	0	0	0	0	0	0	0	0	0
D	1	1	0	0	0	0	0	0	0	0	0	0
E	1	1	0	0	0	0	0	0	0	0	0	0
F	0	0	0	0	0	0	0	0	0	0	0	0

All this data originate the four base case scenarios that were simulated using the EUROSTAG load flow module. Non-converging cases, if any, are stored for further analysis. The entire relevant branch data is written to a EUROSTAG Tabular Output file. The four base case scenarios can be straightforwardly modified to test different charging strategies such as: tariff-based, smart charging and V2G.

The tabular files are scanned to find overloaded branches (see Table 4-16). In the example, these branches are those marked with an "X". The overhead lines rated apparent power was determined based on a worst-case operating condition (summer temperatures). Ground cables were considered to be rated for normal operation. Therefore, overhead lines (50 mm²) have a rated power of 3 MVA, while ground cables (120 mm²) are rated for 7.4 MVA.

Table 4-15 Number of EVs per node class from 13h to 24h of a typical day (30% EV integration)

Class/Hour	13	14	15	16	17	18	19	20	21	22	23	24
A	0	0	0	4	34	36	44	84	64	67	37	9
B	0	0	0	2	17	18	22	42	32	33	18	4
C	0	0	0	1	8	9	11	21	16	16	9	2
D	0	0	0	0	6	6	7	15	11	12	6	1
E	0	0	0	0	6	6	7	15	11	12	6	1
F	0	0	0	0	3	3	4	9	6	7	3	0

Table 4-16 Example formatted output data

Sending node name	Receiving node name	Active power on line	Reactive power on line	Rated apparent power	Current on line	Rated current
		p.u.	p.u.	MVA	p.u.	p.u.
NMV	NMVL1	0.007528	-0.002023	7.400000	0.007794	0.074000
NMV	NMVL1A	0.011692	-0.000372	7.400000	0.011697	0.074000
NMV	NMVL6	0.011242	0.004284	7.400000	0.012030	0.074000
NMV	NMVL6A	0.025331	0.009397	7.400000	0.027017	0.074000
NMV	NMVR1	-0.006453	0.009201	3.000000	0.011238	0.030000
NMVL1	NMVL2	0.001911	-0.003953	7.400000	0.004391	0.074000
NMVL3	NMVL2	0.000899	0.004805	7.400000	0.004888	0.074000
NMVL6	NMVL7	0.005627	0.002354	7.400000	0.006101	0.074000
NMVR12	NMVR13	0.000576	0.000289	3.000000	0.000642	0.030000
NMVR16	NMVR9	0.015000	-0.004277	3.000000	0.015429	0.030000
NMVR14	NMVR11	-0.001482	-0.000745	3.000000	0.001651	0.030000
NMVR14	NMVR15	0.000576	0.000289	3.000000	0.000642	0.030000
NMVR8	NMVR3	0.010456	-0.006873	3.000000	0.012453	0.030000
NMVR8	NMVR9	-0.011902	0.006137	3.000000	0.013328	0.030000
NMVR13A	NMVR12A	0.019424	-0.000744	3.000000	0.018444	0.030000
NMVR1A	NMV	0.028452	-0.015168	3.000000	0.032054	0.030000
NMVR2A	NMVR1A	0.030218	-0.014266	3.000000	0.033008	0.030000
NMVR3A	NMVR2A	0.031453	-0.013639	3.000000	0.033636	0.030000
NMVR3A	NMVR4A	0.001487	0.001069	3.000000	0.001797	0.030000
NMVR8A	NMVR3A	0.033291	-0.012387	3.000000	0.034594	0.030000
NMVR8A	NMVR9A	-0.034738	0.011653	3.000000	0.035685	0.030000
NMVL7	NMVL8	0.002817	0.001448	7.400000	0.003169	0.074000
NMVL8	NMVL9	0.002813	0.001169	7.400000	0.003047	0.074000
NMVL4	NMVL3	0.000900	0.005085	7.400000	0.005163	0.074000

As an illustration, Table 4-17 shows the number of branches found to be in overload during the 24 hours of the day for each of the four EV integration base scenarios for the Portuguese case study. It can be seen that less overloaded branches are assigned to greater amounts of EV integration and also when system load is greater. This happens because this system has a large amount of generation capacity, and a load increase will contribute to alleviate the difficulties already experienced in making all this power production flow upstream, towards the HV network. Therefore, for the test network under evaluation, the EV integration facilitates a higher penetration of distributed energy resources.

Table 4-17 Number of overloaded branches for each scenario during a summer day

	1	2	3	4	5	6	7	8	9	10	11	12	13	14	15	16	17	18	19	20	21	22	23	24
0%	4	5	5	5	5	5	5	5	5	5	5	4	4	4	4	4	4	4	4	3	2	3	3	4
10%	4	5	5	5	5	5	5	5	5	5	5	4	4	4	4	4	3	3	2	2	2	2	2	3
20%	4	5	5	5	5	5	5	5	5	5	5	4	4	4	4	4	2	2	2	1	1	1	2	3
30%	3	5	5	5	5	5	5	5	5	5	5	4	4	4	4	4	2	2	2	0	1	1	2	3

Finally, as already mentioned, the overloaded branch results can be used to determine/evaluate the most suitable EV charging strategies (dumb, tariff-based, smart charging, V2G) to prevent these overloads without the need for infrastructure investment.

4.4 References

- [1] Tractebel Engineering, EDF. EUROSTAG. Home Page: www.eurostag.be.
- [2] Mathworks. MATLAB. Home Page: <http://www.mathworks.com/>.
- [3] A. G. Madureira, J. C. Pereira, N. J. Gil, J. A. Peças Lopes, G. N. Korres, and N. D. Hatziaargyriou. "Advanced control and management functionalities for multi-microgrids". *European Transactions on Electrical Power*, 2010 (in press).
- [4] N. Jenkins, L. Holdsworth, and X. Wu, "Dynamic and Stead-State Modelling of the Doubly-Fed Induction Machine (DFIM) for Wind Turbine Applications," MCEE UMIST 14th, January 2002.
- [5] A. Vladislav, "Analysis of Dynamic Behaviour of Electric Power Systems with Large Amount of Wind Power," PhD Thesis, Technical University of Denmark, 2003.
- [6] R. G. de Almeida and J. A. Peças Lopes, "Participation of Doubly Fed Induction Wind Generators in System Frequency Regulation", *IEEE Transactions on Power Systems*, vol. 22, no. 3, pp. 944-950, August 2007.
- [7] Y. Zhu and K. Tomsovic, "Development of models for analyzing the load-following performance of microturbines and fuel cells", *Electric Power Systems Research*, 2002.
- [8] J. A. Peças Lopes, C. L. Moreira, and A. G. Madureira, "Defining Control Strategies for MicroGrids Islanded Operation", *IEEE Transactions on Power Systems*, vol. 21, no. 2, pp. 916-924, May 2006.
- [9] J. A. Peças Lopes, P. M. Rocha Almeida, F. J. Soares. "Using vehicle-to-grid to maximize the integration of intermittent renewable energy resources in islanded electric grids", *International Conference on Clean Electrical Power*, 2009, pp.290-295, 9-11, June 2009.
- [10] N. Gil, J. A. Peças Lopes, "Exploiting Automated Demand Response, Generation and Storage Capabilities for Hierarchical Frequency Control in Islanded Multi-Microgrids", *Proceedings of PSCC2008 - 16th Power Systems Computation Conference*, Glasgow, Scotland, July 2008.



- [11] N. Gil, J. A. Peças Lopes, "Hierarchical Frequency Control Scheme for Islanded Multi-Microgrids Operation", *Proceedings of IEEE Lausanne Power Tech 2007*, Lausanne, Switzerland, July, 2007.
- [12] P. M. Subcommittee. IEEE reliability test system. *IEEE Transactions on Power Apparatus and Systems*, 98(6):2047-2054, November 1979.
- [13] MERGE Project. "Identification of Traffic Patterns and Human Behaviors", Deliverable 1.1 – Task 1.5. (in Press).



5 PSS/E SIMULATION PLATFORM

A simulation platform that works over PSS/E software was adapted to incorporate aggregated models of EV for steady state and dynamic studies of large interconnected transmission systems having conventional generation and a large penetration of renewable power sources (namely wind power). The aggregated EV response to frequency changes or other control signals was embedded in dynamic load models that represent clusters of aggregated EV. Specific scripts were developed to simulate the step by step response of the system in quasi-steady state and in dynamic behavior when following the load diagram in critical periods and adopting different charging strategies (dumb, tariff based approaches, smart charging strategies). For these studies, the Models of intermittent renewable generation (in particular wind power) were also developed.

5.1 Steady-State Simulation

The foreseen rollout of EV will considerably affect the way distribution grids will be managed and operated. The extra amount of power they will demand from the grid will oblige system operators to understand the impacts resulting from EV connection into distribution networks. Several approaches to this problem have been pursued. In papers [1], [2] and [3] are presented two strategies for assessing EV integration impacts. Papers [1] and [2] follow a deterministic strategy to locate EV along the network buses and, consequently, determine EV loads during an entire day. Conversely, paper [3] introduced a probabilistic method for determining EV load. Both options proved to be interesting approaches, though they were only able to reveal the effects of a possible scenario for a given period.

Also transmission grids will be affected by the presence of new loads associated with EV battery charging. However, it is expected that in normal operation grid restrictions will not turn into a limiting factor to the increase of the EV integration. It is, though, expectable that, regarding steady state security assessment, some impacts may arise.

Therefore, it is important to develop tools that allow exploring different scenarios in a coordinated way, which may result in both average scenarios and extreme case scenarios to be used for network steady state evaluation. Such tools can be used to help system operators in planning their operation for the next hours or to enhance existing system operators planning techniques, allowing them to obtain additional knowledge on the impacts of a new type of load, so far unknown or negligible to the power systems, the EV battery charging.

Given the fact that EV are mobile loads that may appear in almost any bus of a given electricity network, voltage profiles, lines loading, peak power and energy losses variations need to be properly evaluated for the simulation of the operating conditions or for the planning exercise.

In this sense, a stochastic model to simulate EV movement in a geographic region and a Monte Carlo method to create different scenarios were developed in this task, using PSS/E and Python programming language, in order to accurately estimate the EV impacts along one typical week in Low and Medium Voltage (LV/MV) networks.



In subsection 5.1.1 will be presented all the EV charging approaches that were considered within the MERGE Project and that were thoroughly described in Deliverable 1.1, Section II, Task 1.2 [5].

Subsection 5.1.2 presents the modelling approach under PSS/E environment that used in the tool developed.

The EV fleet characterization details are given in subsection 5.1.3, while the EV movement simulator tool is presented in subsection 5.1.4.

The following three subsections discuss the implementation details of the three EV charging approaches that were considered in this simulation tool.

Subsection 5.1.8 presents the case studies used to evaluate the simulation tool performance, while in 5.1.9 are presented some preliminary results.

5.1.1 EV Charging Approaches

As mentioned in the Deliverable 1.2 of the MERGE project, [6], within this project five different charging strategies were defined, according to the expected business models in this area:

- Dumb Charging
- Multiple Tariff Charging
- Smart Charging:
 - Controlled by the EV Supplier/Aggregator (EVS/A)
 - Controlled by the Distribution System Operator (DSO)
- Vehicle-to-Grid (V2G)

However, smart charging controlled by the EV supplier/aggregator and vehicle-to-grid will not be implemented in the developed simulation tool, as it will explained along with the detailed description of each charging strategy.

Dumb Charging

This is a no control mode where EV can be freely operated having no restrictions or incentives to modulate their charging. Therefore, EV are regarded as normal loads, like any other appliance. In this mode, commonly referred to as “dumb charging”, it is then assumed that EV owners are completely free to connect and charge their vehicles whenever they want. The charging starts automatically when EV plug-in and lasts until its battery is fully charged or charge is interrupted by the EV owner.

In addition, electricity price for these users is assumed to be constant along the day, what means that no economic incentives are provided in order to encourage them to put their vehicles charging during the valley hours, when the grid operating conditions are more favourable to an increment in the energy consumption.

For scenarios of large EV deployment, this approach will provoke technical problems in the generation system and on the grid (potential large voltage drops and branch overloads). The only way to tackle the foreseen problems provoked by EV is then to reinforce the existing generation system and grid infrastructures and plan new networks in such way that they can fully handle EV grid integration. Yet this is a somewhat expensive solution that will require high investments in network infrastructures that the entities responsible for the grid management, most likely, would like to avoid.

Multiple Tariff Policy

As in the previous approach, the dual tariff policy assumes that EV owners are completely free to charge their vehicles whenever they want. However, electricity price is assumed not to be constant along the day, existing some periods where its cost is lower. This method is based on that existing already in many countries where during valley hours, normally during the night, electricity price is lower. However, as this is not an active management strategy, the success of this method depends on the EV owner willingness to take advantage of this policy, and thus only part of the EV load eventually would shift towards valley hours.

It should be taken into account that the economic signals provided to EV owners with the fixed-tariff policy might have a perverse effect in scenarios characterized by a high integration level of EV. It might happen that a big number of EV connect simultaneously in the beginning of the cheaper electricity periods, making the grid reach its technical limits.

Smart Charging

The smart charging strategy envisions an active management system, where there are two hierarchical control structures, one headed by an EVS/A and other by the DSO.

Smart Charging Controlled by the EV Supplier/Aggregator

When operating the grid in normal conditions, EV will be managed and controlled exclusively by the EVS/A, whose main functionality will be grouping EV, according to their owners' willingness, to exploit business opportunities in the electricity markets.

The EVS/A will monitor all the EV connected to the grid and its state, providing power or requesting from them the services that it needs to cope with what was previously defined in the market negotiations. This is accomplished by sending set-points to vehicle controllers related with rates of charge or requests for provision of ancillary services. To accomplish successfully such a complex task, it is required that every fixed period (likely to be defined around 15 minutes), the State of Charge (SOC) of each EV battery is communicated to the EVS/A, to assure that, at the end of the charging period, batteries will be charged according to EV owners requests.

This charging strategy will not be included in the current implementation as it implies modelling the complete market structure (including day-ahead market). Such feature is out of the scope of this task and so smart charging controlled by the EV supplier/aggregator will not be addressed in this work.

Smart Charging Controlled by the Distribution System Operator

Due to high uncertainties related to when and where EV owners will charge their vehicles, the existence of a grid monitoring structure will be required, controlled by the DSO, with the capability of acting over EV charging in abnormal operating conditions, i.e. when the grid is being operated near its technical limits, or in emergency operating modes, e.g. islanded operation. In these situations, EV might receive simultaneously two different set-points, one from the EVS/A and other from the monitoring and management structure headed by the DSO. To avoid violation of grid operational restrictions, the DSO signals will override the EVS/A ones.

This type of EV charging management provides the most efficient usage of the resources available at each moment, enabling congestion prevention and voltage control, while avoiding the need to invest largely in network reinforcements.

Vehicle-to-Grid

This approach is an extension of the previous one where, besides the charging, the EVS/A controls also the power that EV might inject into the grid. In the V2G mode of operation, both EV load controllability and storage capability are exploited. From the grid perspective, this is the most interesting way of using EV capabilities given that besides helping managing branches' congestion levels and voltage related problems in some problematic spots of the grid, EV have also the capability of providing peak power in order to make the energy demand more uniform along the day and to perform primary frequency control. Nevertheless, there are also some drawbacks related with the batteries degradation. Batteries have a finite number of charge/discharge cycles and its usage in a V2G mode might represent an aggressive operation regime due to frequent shifts from injecting to absorbing modes. Thus the economic incentive to be provided to EV owners must be even higher than in the "smart" charging approach, so that they cover the battery damages owed to its extensive use.

Being the most aggressive mode for charging EV, due to possible implications with EV batteries lifecycle, this option is not likely to be a reality neither in the short run nor in the medium term. Only in the very long term, when battery technology has reached a high maturation stage, this strategy may be adopted. Therefore, it has not been considered in the current implementation of this software tool.

5.1.2 Advanced PSS/E Modelling Approach

The previous sub-section described all the approaches to manage EV charging that were discussed in Deliverable 1.1. [5]. As mentioned, from these five approaches, only the first three were implemented in the steady-state simulation tool exploiting PSS/E and Python.

This tool was developed to perform two different types of studies:

1. Evaluate the impacts of a given number of EV in a distribution network. For this type of study, a Monte Carlo Simulation Method was implemented to make the tool capable of simulating several different scenarios (for the same EV integration percentage), in order to provide a reliable characterization of the grid operating conditions, regarding voltage profiles, branch loadings, grid peak power, energy losses and the networks components that are more likely to be operated near, or even above, their technical limits; An overview of the Monte Carlo Simulation Method is given in Figure 5-18 and the details of its implementation will be discussed in detail in the following subsections of this document;
2. Compute the maximum number of EV that can be integrated in a given network, by using iteratively the procedure described in 1., increasing in a stepwise manner the integration of EV. The algorithm, whose flowchart is presented in Figure 5-3, is stopped when one of the following conditions is verified:
 - a. Violation of the voltage limits specified;
 - b. Branch overloading;
 - c. Violation of the limit specified for the number of EV forced to charge in a fast charging station. This might happen when these EV charging power is reduced by the DSO in order to mitigate network problems (this condition is applied only if the scenario being studied considers the existence of smart charging adherents).

The user of the simulation tool has the possibility of analyzing different networks from all over Europe, according to the functional diagram depicted in Figure 5-18.

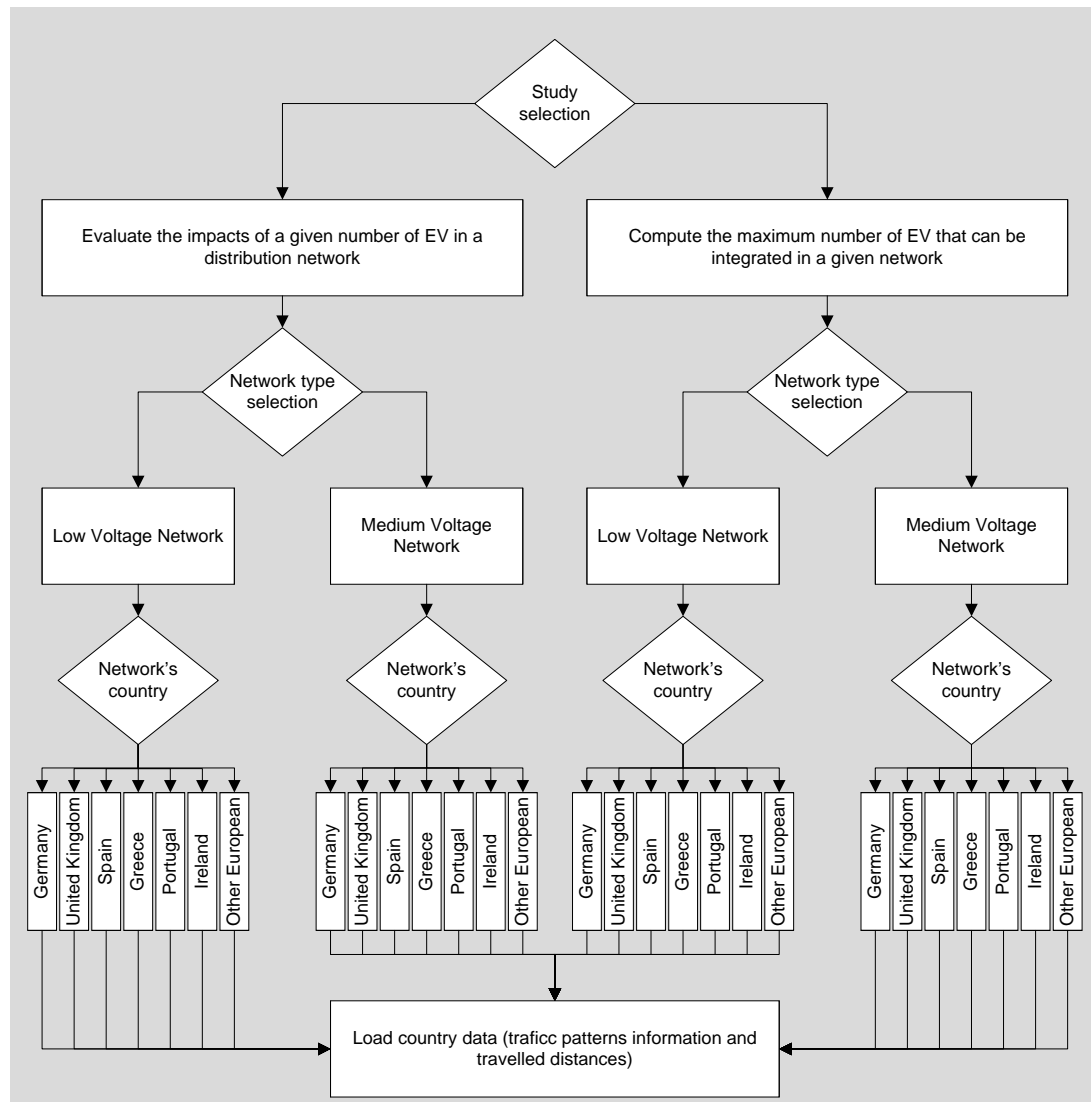


Figure 5-18 Studies that can be performed with the tool developed

After defining the type of study to be performed, the algorithm described in 1. runs, for each Monte Carlo simulation, the following 10 main procedures:

- I. Read input data – The input data is obtained from two separate files: an Excel file ("SCENARIO_CHARACTERIZER.xls") and a PSS/E file ("network.sav"). The Excel file contains data related with variables defined by the user (for each case study), data obtained from Deliverables 1.1 [5] and 2.1 [6] and data from the assumptions taken into account during the algorithm development. The PSS/E file contains data exclusively related with the network. More information about the input data will be provided in subsection 5.1.3.
- II. Run power flows for the initial scenario, without EV, and record relevant results – A power flow for each time step is run considering only the network

base load (no EV considered). The network indexes (voltages, lines ratings, losses and peak load) are recorded to compare them later with the different EV integration scenarios evaluated.

- III. Characterize the EV fleet – During this procedure, all the EV characteristics relevant for the simulation are generated and recorded in an array with the following attributes for each EV: battery capacity (kWh), charging power (kW), initial battery State of Charge (SoC) (%), consumption per km (kWh/km), driver behaviour, charging method selected by the EV owner, network bus where the EV stays parked during the night, the departure time for the first journey of the day and the arrival time from the last journey of the day. More details about this step will be provided in subsection 5.1.4.
- IV. Simulate EV movement and charging – Since the data regarding the first and the last journeys of the day was available from the Merge survey results (Deliverable 1.1, task 1.5), it was assumed that EV only make two journeys per day. If more data about the daily journeys would be available, a different approach might have been followed, where EV were able to make more than two travels per day, such as the one followed in [4]. Nevertheless, to make the EV energy consumption adopted closer to reality, in this approach it was assumed that the average of the real daily travelled distance is similar to the sum of the travelled distances in the two daily journeys of the simulation. The full EV simulation routine will be thoroughly described in subsection 5.1.5. The EV movement simulator encloses the following 5 steps:
 - a. Define the EV state – At each time step, the EV that, according to their departure time and arrival time, are in movement, are flagged as not being connected to any network bus. For the remaining EV, one of the following three states is drawn for each EV: “parked in a residential area”, “parked in a commercial area” and “parked in an industrial area”.
 - b. Compute the travelled distance – A travelled distance is drawn for all the EV that are “in movement”. The travelled distance is drawn using a Gaussian probability density function based on the average daily travelled distance in the country of the network under analysis.
 - c. Compute the EV bus location – EV that were in parked states, in the previous time step, are kept in the same bus in the current time step. EV that were in movement after the first journey of the day change their location and, therefore, a new bus for them is drawn. If an EV was in movement for the last journey of the day, it will return to its residential bus (drawn during the EV characterization procedure). The probability of an EV be located at a specific bus, after the first journey of the day, is proportional to the load installed in that node. Therefore, buses with higher loads will have a higher probability of having EV parked.
 - d. Register the power absorbed from the network by each EV – Having computed the EV locations for parked EV, taking the EV owners’

behaviour, it is possible to define the EV that will charge during this current time step and allocate the corresponding load to a network bus.

- e. Compute the EV battery SoC variations – Knowing the EV that were in movement, parked without being charging and those who were charging, it is possible to calculate the EV SoC variation during the current time step.
- V. Compute the network load discriminated per bus (initial load + EV load) – The total load in each bus is obtained by simply summing the network initial load to the EV load (in each bus).
- VI. Run a power flow to evaluate network operating conditions – A power flow is run for the current time step. The network indexes (voltages, lines ratings, losses and peak load) are recorded.
- VII. In case of network problems, adjust the load of the EV that adhered to the smart charging and that are contributing for the network problem identified – The network indexes recorded in VI. are evaluated. If a network problem occurs and if there are smart charging adherents in the scenario being analyzed, a load reduction signal is sent to the smart charging EV.
- VIII. Compute new network total load – The total load in each bus is computed again, taking into account the load reduction of the smart charging EV.
- IX. Run a power flow to evaluate new network operating conditions – A new power flow is run with the current network load. The network indexes (voltages, lines ratings, losses and peak load) are recorded again.
- X. In case of network problems, adjust again the load of the EV that adhered to the smart charging and that are contributing for the network problem identified – The new network indexes recorded in IX. are evaluated. If a network problem occurs, a new load reduction signal is sent to the smart charging EV. Steps VIII. to X. are repeated while the network problem persists or while there are smart charging EV load to be reduced.

The first two procedures are run only once, in the beginning of the simulation. The following are repeated at each time step of 30 minutes, for a one week period (336 time steps).

In Figure 5-2 it is presented a simplified flowchart of the algorithm referred in 1.

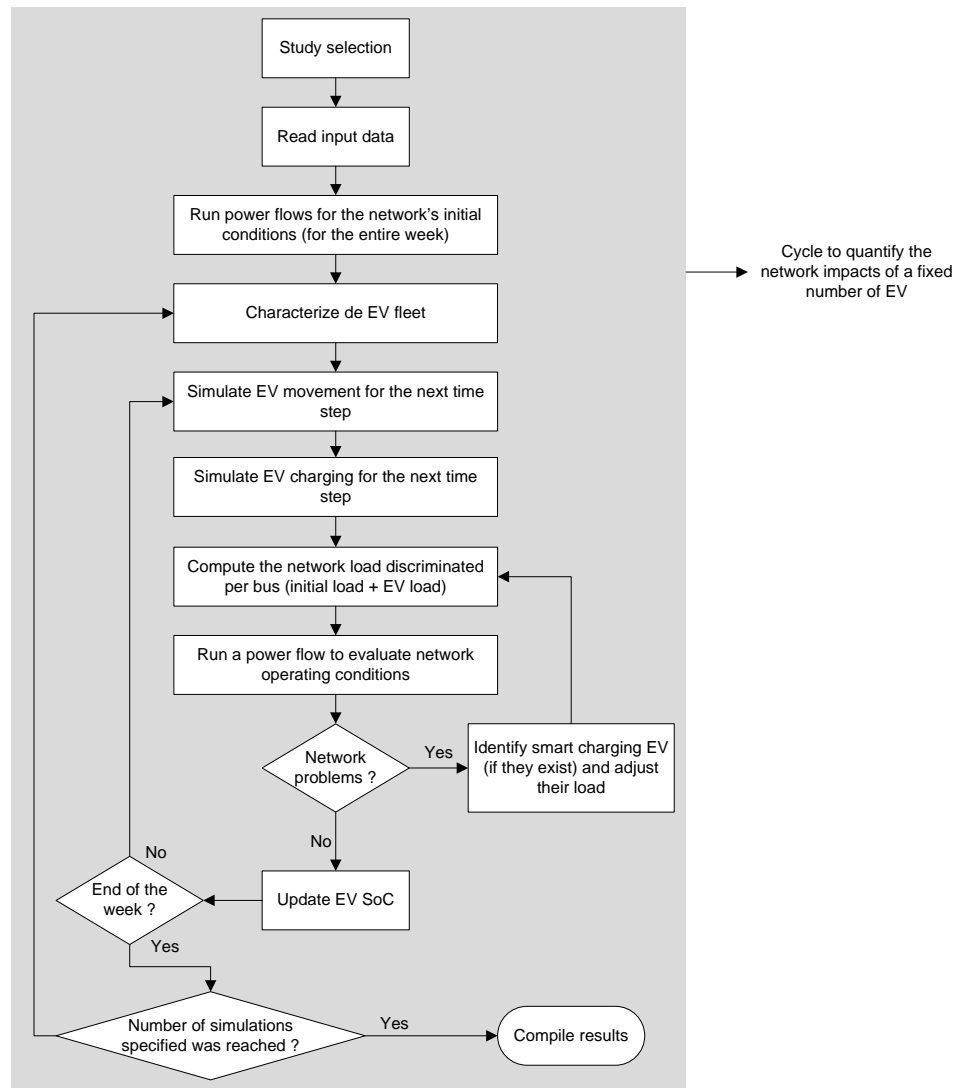


Figure 5-2 Flowchart of the Monte Carlo algorithm to assess the impacts of a fixed number of EV in a distribution network

The study to compute the maximum number of EV that can be integrated in a given network, described in 2., is performed by using iteratively the procedure described in 1. In each iteration, the EV integration percentage is increased in a stepwise manner and the algorithm is stopped when one of the conditions referred in 2. is verified. Figure 5-3 shows a simplified flowchart of the algorithm.

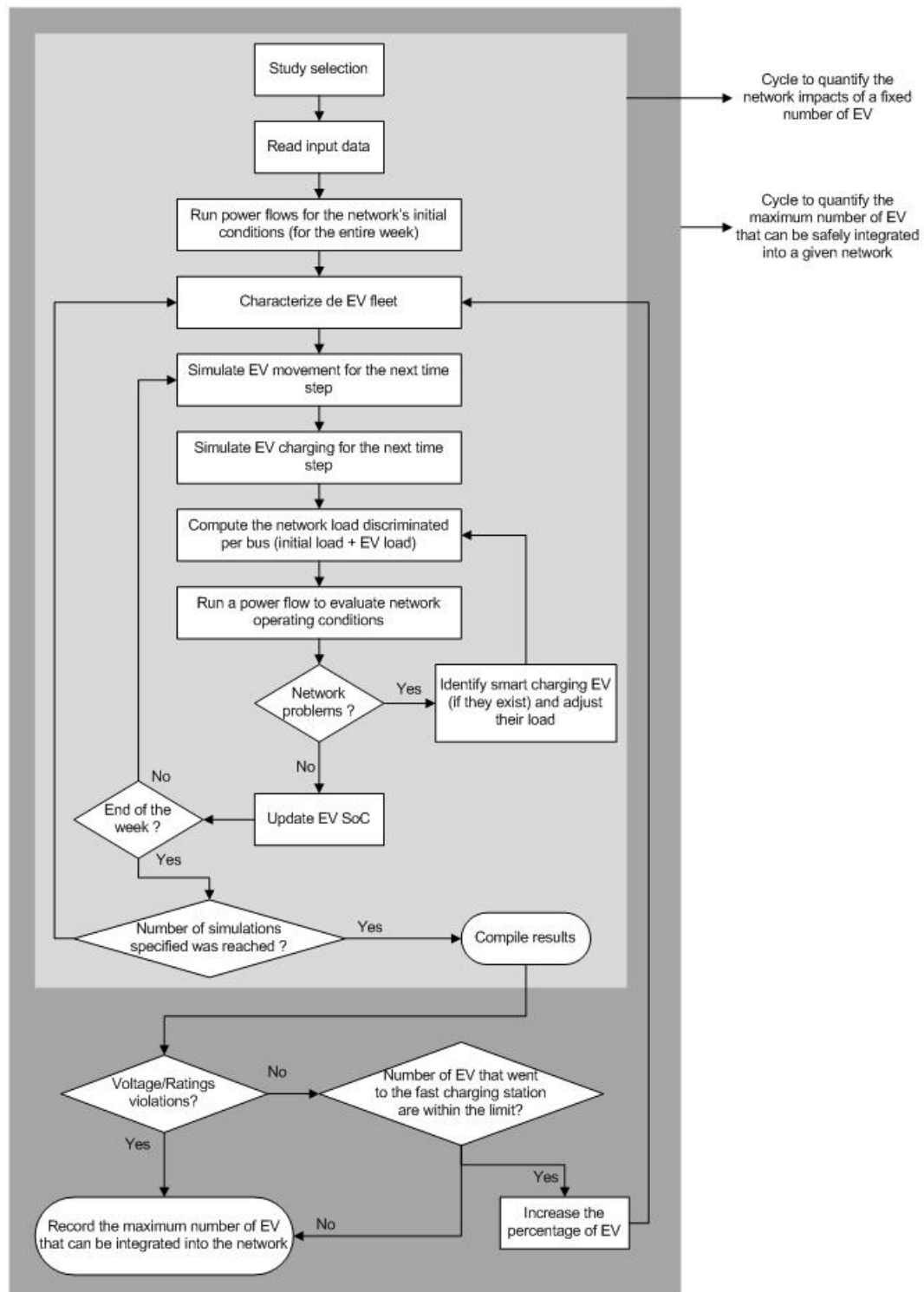


Figure 5-3 Flowchart of the iterative algorithm to compute the maximum number of EV that can be integrated in a distribution network

All the calculations of the EV load were made in Python programming language. After allocating EV load to the network nodes, the psspy library of Python was used to make the link with the PSS/E software which, after updating the network load, was used to run the power flows. Finally, using the same Python library, the power flow results from PSS/E were gathered and recorded in Python environment.

5.1.3 Input Data

The input data for the simulation tool is gathered from two different files: an Excel file ("SCENARIO_CHARACTERIZER.xls") and a PSS/E file ("network.sav").

"SCENARIO_CHARACTERIZER.xls"

This Excel file contains data related with variables defined by the user (for each case study), data obtained from Deliverables 1.1 [5] and 2.1 [6] and data from the assumptions taken into account during the algorithm development.

In Figure 5-4 are presented the variables that are defined by the user to characterize the case study to be analyzed.

Variables to be defined by the user for each case study:				
Study selection:	Fixed_EV_share	Load diagram (kW):	Nr. of feeders:	2
Country of the network being analysed:	Portugal	Hour	Power (kW)	
Type of network:	Medium Voltage	1		Feeders initial buses
Nr. of simulations per EV integration percentage:	10	2		Feeder Initial bus nr.
Increment of the EV integration percentage:	0	3		1 62
Number of vehicles in the grid:	7035	4		2 299
Starting percentage of EV (%):	30.0	5		
Percentage of multiple tariff policy adherents (referred to the nr. of EV) (%):	0.0	6		
Starting hour of the lower electricity cost period (h):	22	7		
Finishing hour of the lower electricity cost period (h):	6	8		
Percentage of smart charging adherents (referred to the nr. of EV) (%):	100.0	9		
Initial SOC - normal distribution average (%):	90.0	10		
Initial SOC - normal distribution standard deviation (%):	25.0	11		
Initial SOC - maximum value allowed (%):	100.0	12		
Initial SOC - minimum value allowed (%):	50.0	13		
Minimum battery capacity that triggers the charging of EV that "charge only when it needs" (%):	50.0	14		
Minimum battery capacity that triggers fast charging need (%):	5.0	15		
Fast charging station bus:	231	16		
Power factor for network base load (cos φ):	0.96	17		
(Fill only if the load diagram is not available) Yearly energy consumption in the network (MWh):	32547	18		
Percentage of EV that are allowed to charge in a fast charging station (%):	10.0	19		
Power reduction for smart charging adherents that are causing network problems (%):	25	20		

Figure 5-4 Variables defined by the user to characterize the case study

In the "Study Selection" field, the user can define the type of study to be performed:

- Fixed_EV_share – to perform an impact study of a fixed number of EV;
- Max_EV_share – to evaluate the maximum number of EV that can be safely integrated in a given network.

In the "Country of the network being analyzed" field, as the name indicates, the user must choose the country of the network to be studied.. The options of this field are countries that will be studied in WP3. The choice made in this field influences the daily travelled distances and the traffic patterns that will be used to define the EV movement. The travelled distances for the countries that can be chosen in this field are presented in Table 5-20. The following charts show the probability of EV departures for the first journey of the day and the arrivals after the last journey of the

day, for all the countries considered. The data presented was gathered from the survey reported in Deliverable 1.1, task 1.5 [5].

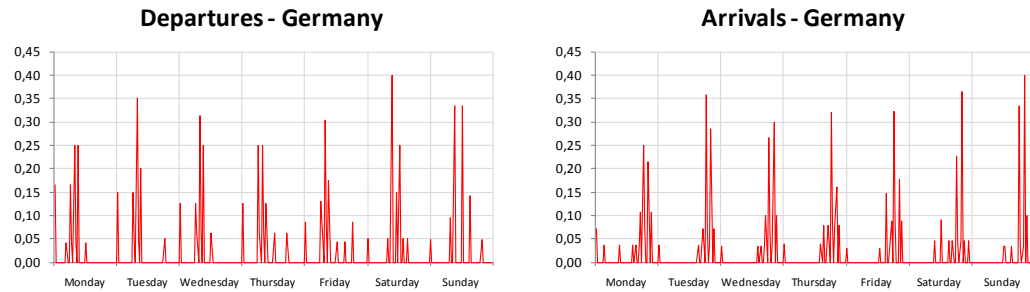


Figure 5-5 Departures and arrivals probabilities for Germany

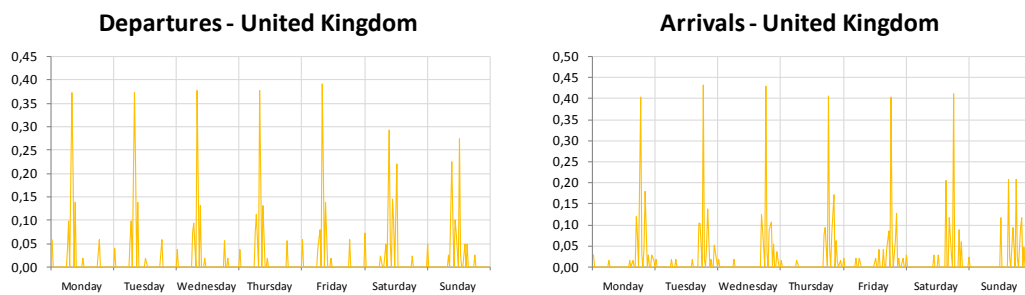


Figure 5-6 Departures and arrivals probabilities for United Kingdom

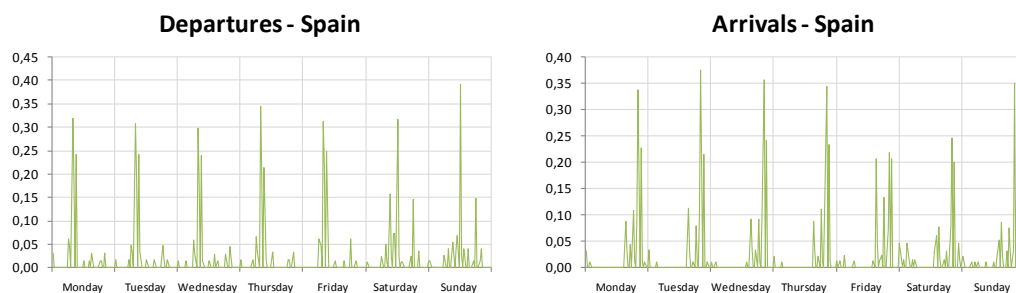


Figure 5-7 Departures and arrivals probabilities for Spain

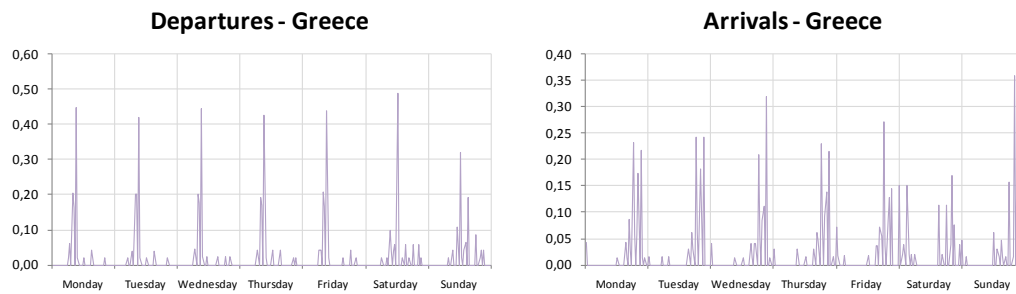


Figure 5-8 Departures and arrivals probabilities for Greece

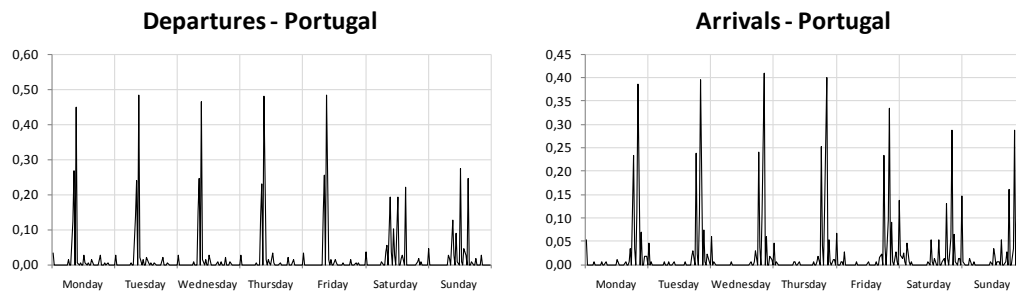


Figure 5-9 Departures and arrivals probabilities for Portugal

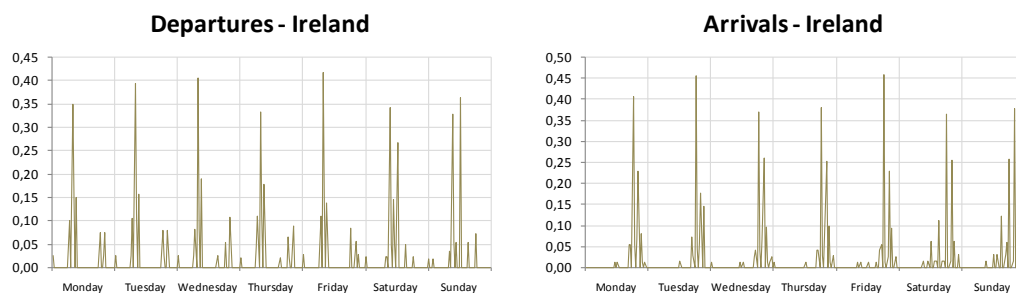


Figure 5-10 Departures and arrivals probabilities for Ireland

As the MERGE Project has the objective of assess EV impacts in networks from all over Europe, it was left open the possibility of analyzing networks from other countries by creating an average set of data for departures and arrivals. This average set was obtained by calculating the average of the six countries analyzed. The user has the possibility of choosing this average set by selecting “Europe” in the “Country of the network being analyzed” field. The average set of data obtained are presented in Figure 5-.

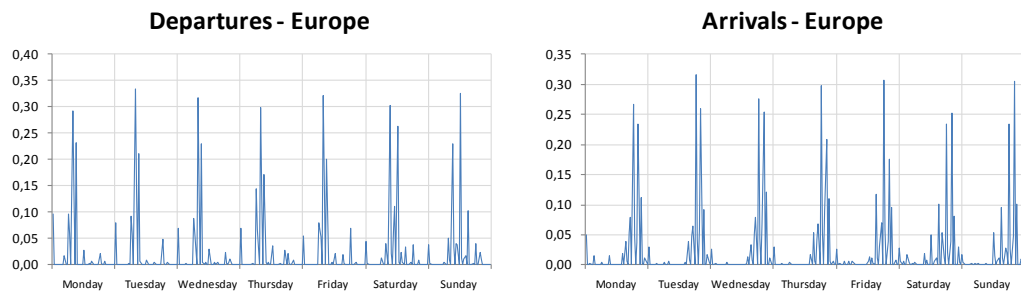


Figure 5-11 Departures and arrivals probabilities for networks from European countries different from the six involved in the MERGE Project

In the “Type of network” field, the user can choose the voltage level being analyzed: Low Voltage (LV) or Medium Voltage (MV).

The “Nr. of simulations per EV integration percentage” field represents the number of Monte Carlo simulations that are run for the EV integration percentage defined by the user. If the study being performed is the calculation of the maximum number of EV that can be integrated in a given network (Max_EV_share selected in the “Study selection field”), this field represents the number of simulations run per each iteration. This means that every time that the EV percentage is incremented, the algorithm runs the number of simulations defined in this field. A different approach could have been considered to guarantee the Monte Carlo convergence, like, for instance, assure that the variations in the last five iterations of the aggregated network load variances, of each one of the 336 time instants, were all lower than a specified number [4]. If at least one of the 336 variances does not meet this convergence criterion, the process keep running more iterations until all the variances variations are lower than the predefined value. However, given the algorithm complexity and the considerable amount of time required to run such a higher number of iterations. The variances variation could be calculated using equation (5-1):

$$\Delta \text{Variance} = |\text{Variance}_h^t - \text{Variance}_{h-5}^t| < x \quad (5-1)$$

where:

- Variance_h^t – represents the variance of the network load at time instant t , $t \in [1, 336]$, in the h^{th} iteration;
- x – is a predefined number.

In alternative, the option of using a variable where the user can define the “Nr. of simulations per EV integration percentage” was taken in order to provide flexibility regarding the trade-off between the results accuracy and the simulation time.

For the same study referred in the previous paragraph (Max_EV_share), the increment of the EV integration percentage that occurs at each iteration is defined in the “Increment of the EV integration percentage” field. The user can choose between the following increment rates: 0.1, 0.2, 0.5, 1, 2 and 5%.

As the name indicates, the “Number of vehicles in the grid” field is used to enter the number of conventional vehicles that currently exist in the network geographical area.

The “Starting percentage of EV” field is the percentage of conventional vehicles that are assumed to be electric. In the Fixed_EV_share study, this number is kept constant along the simulations, while in the Max_EV_share this number is used as a starting point for the simulation. After each iteration, this number is incremented by the quantity defined in the “Increment of the EV integration percentage” field.

In the “Percentage of multiple tariff policy adherents” field are define the percentage of EV owners that adhered to this charging scheme. Thus, this percentage is always referred to the number of EV and not to the number of conventional vehicles in the network.

The “Starting hour of the lower electricity cost period” and the “Finishing hour of the lower electricity cost period” fields are used to define the period when electricity is cheaper. It was assumed, in this algorithm, that the multiple tariff charging adherents only charge their vehicles during this period.

In the “Percentage of smart charging adherents” field are define the percentage of EV owners that adhered to this charging scheme. As for the multiple tariff adherents, this percentage is always referred to the number of EV and not to the number of conventional vehicles in the network.

For the EV battery SoC in the beginning of the simulation, a Gaussian probability density function was used with mean and standard deviation values define by the user in the fields “Initial SOC – normal distribution average” and “Initial SOC - normal distribution standard deviation”. The values that are drawn with this function for each EV were limited to an interval also defined by the user in fields “Initial SoC – maximum value allowed” and “Initial SoC – minimum value allowed”. These fields were included to avoid having initial battery SoC values above 100% or below 0%.

As referred previously, when the characterization of EV is made, in the beginning of each simulation, an EV owner behaviour is defined. The possible EV owners’ behaviours considered were: “charge at the end of the day”, “charge whenever possible” and “charge only when the EV needs”. For the latter, it was needed to define when the EV needs to recharge in terms of battery SoC value. To make the algorithm flexible to this value, it was introduced in the Excel input data file a field where this value can be chosen by the user. The name of this field is “Minimum battery SoC that triggers the charging of EV that *charge only when the EV needs*”.

As it will be detailed in subsection 5.1.5, it was considered the existence of a fast charging station in the geographic area of the network to make the study more realistic. In addition, the existence of fast charging station allows to solve the problem of the EV that attain very low battery SoC when a long trip occurs and they don’t have enough energy in the battery to conclude it. The fast charging station is assumed to be located in the network bus defined by the user in the field “Fast charging station bus”. Additionally, the user has the possibility to define the battery

SoC that triggers the charging of an EV in the fast charging station. This value can be introduced in the field “Minimum battery SOC that triggers fast charging need”.

In the absence of information regarding the consumption of reactive power by the network loads, the user can define a global value for it in the field “Power factor for network base load ($\cos \phi$)”. This power factor will then be applied to all network conventional loads. As it was assumed that EV do not absorb any reactive power, a unity power factor was considered for EV loads.

In case of the user having selected the Max_EV_share type of study and having considered the existence of smart charging adherents, it is needed to define the number of EV that are allowed to charge in the fast charging station in all the iterations being performed. This must be defined due to a perverse effect that the fast charging station introduces in the simulation. As an example of this effect, let's assume that all EV in a given simulation are smart charging adherents. When a network problem occurs, the DSO is able to reduce the load of the EV that are contributing to the problem (or even disconnect them) in order to solve it. Then, the EV whose charging was reduced might not have enough energy in the battery to perform their daily journeys, being obliged to charge in the fast charging station. After each iteration, as the DSO is able to solve all network problems by reducing smart charging adherents' load, the number of EV is increased and the same procedure is repeated. Under these conditions, we might have a huge number of EV charging in the fast charging station due to the restrictions imposed by the DSO. To overcome this problem, it was introduced in the Excel file a field where the user can define the maximum number of EV that are allowed to charge in the fast charging station due to DSO actions. This field name is “Percentage of EV that are allowed to charge in a fast charging station”.

Following the problem referred in the previous paragraph, when a network problem occurs, the DSO will try to overcome it by progressively reducing the load of the smart charging adherents that are contributing for the problem, instead of suddenly disconnect them. The load of these EV is progressively reduced in an iterative process. Thus, the network conditions are evaluated after each load reduction and, if the problem persists, a new reduction is ordered by the DSO. This procedure goes on until the problem is solved or the smart charging adherents load is reduced to zero. The power reduction step, in percentage, can be defined by the user in the “Power reduction for smart charging adherents that are causing network problems” field.

It was included in the Excel a field to introduce the typical weekly load diagram of the network under study. The name of the field is “Load diagram (kW)” and the user can introduce there the load diagram for the entire typical, in time steps of half hour (total of 336 load values). In the absence of a typical load diagram for the network under study, the user can opt by using a predefined load diagram that is already included in the Excel file. For that, the user only has to provide in the field “Yearly energy consumption in the network (MWh)” the total energy consumed in the network. The Excel file generates automatically a load diagram adjusted to the network yearly consumption. The diagram general profile is presented in Figure 5-.

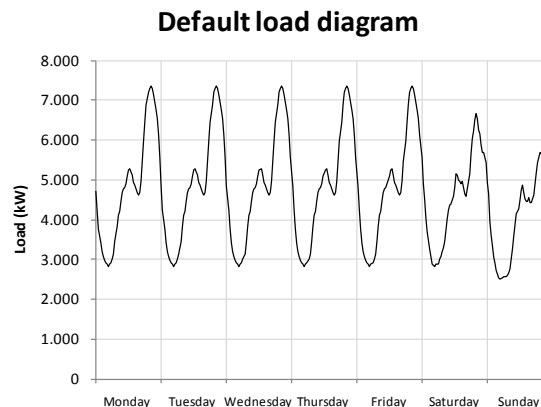


Figure 5-12 Default load diagram used in the simulation tool

As explained above, when a problem occurs in the network and there are smart charging adherents in the scenario being studied, the DSO sends a load reduction signal to the smart charging adherents that are contributing to the problem. During the implementation of this procedure in the algorithm, it was needed to identify, from all the smart charging adherents, those who were contributing for the problem identified in the network. The strategy used to solve this issue was to identify the network feeder where the problem occurred and order a load reduction to the smart charging EV located on it. Therefore, in the presence of a network problem, there is a function in the algorithm that processes the problematic feeder topology and creates a list of the EV whose load can be reduced. This is a rather slow procedure. Thus, to make it faster, the user must include in the Excel file the number of feeders in the network and the number of the initial bus of each feeder. This information can be given in the fields “Nr. of feeders” and “Feeders initial buses”, respectively.

In Figure 5- is presented the data that was obtained from Deliverable 2.1. [6]. This data is included in the Excel file and cannot be changed being, therefore, kept constant in all the case studied addressed. The way how these variables are used within the algorithm will be thoroughly described in subsection 5.1.4. The variables from Deliverable 2.1 that will be used in the algorithm are the following:

- Battery nominal power - normal distribution average (level 1 charging) (kW): 3.0 – this value is used as the mean of the Gaussian probability density function designed to characterize EV nominal charging power;
- Battery nominal power - maximum value allowed (level 1 charging) (kW): 9.0 – this value is used as a higher limit to the values obtained with the Gaussian probability density function designed to characterize EV nominal charging power;
- Battery nominal power - minimum value allowed (level 1 charging) (kW): 2.0 – this value is used as a lower limit to the values obtained with the Gaussian probability density function designed to characterize EV nominal charging power;

- Battery capacity - normal distribution average (kWh): 29.0 – this value is used as the mean of the Gaussian probability density function designed to characterize EV battery capacities;
- Battery capacity - max value allowed (kWh): 72.0 – this value is used as a higher limit to the values obtained with the Gaussian probability density function designed to characterize EV battery capacities;
- Battery capacity - min value allowed (kWh): 10.0 – this value is used as a lower limit to the values obtained with the Gaussian probability density function designed to characterize EV battery capacities;
- kWh consumption per km - normal distribution average (kWh/km) : 0.16 – this value is used as the mean of the Gaussian probability density function designed to characterize the EV energy consumption when moving;
- kWh consumption per km - maximum value allowed (kWh/km) : 0.25 – this value is used as a higher limit to the values obtained with the Gaussian probability density function designed to characterize the EV energy consumption when moving;
- kWh consumption per km - minimum value allowed (kWh/km) : 0.10 – this value is used as a lower limit to the values obtained with the Gaussian probability density function designed to characterize the EV energy consumption when moving.

Data obtained from deliverable 2.1:	
Battery nominal power - normal distribution average (level 1 charging) (kW):	3.0
Battery nominal power - maximum value allowed (level 1 charging) (kW):	9.0
Battery nominal power - minimum value allowed (level 1 charging) (kW):	2.0
Battery capacity - normal distribution average (kWh):	29.0
Battery capacity - max value allowed (kWh):	72.0
Battery capacity - min value allowed (kWh):	10.0
kWh consumption per km - normal distribution average (kWh/km):	0.16
kWh consumption per km - maximum value allowed (kWh/km):	0.25
kWh consumption per km - minimum value allowed (kWh/km):	0.10

Figure 5-13 Data obtained from Deliverable 2.1 [6]

In Figure 5- is presented the data that was obtained from Deliverable 1.1, task 1.5. [5]. This data is included in the Excel file and cannot be changed being, therefore, kept constant in all the case studied addressed. The way how these variables are used within the algorithm will be thoroughly described in subsections 5.1.4 and 5.1.5. The variables from Deliverable 1.1, task 1.5 that will be used in the algorithm are the following:

- Travelled distance normal distribution average (km): 30.0 – this value is used as the mean of the Gaussian probability density function designed to characterize the EV travelled distance in each journey; this value varies from country to country, thus, this field's value is automatically updated every time that the "Country of the network being analysed" is changed by the user;
- Travelled distance - maximum value allowed (km): 200.0 – this value is used as a higher limit to the values obtained with the Gaussian probability density function designed to characterize the EV travelled distance in each journey;

this value also varies from country to country, being automatically updated every time that the "Country of the network being analysed" is changed by the user;

- Travelled distance - minimum value allowed (km): 10.0 – this value is used as a lower limit to the values obtained with the Gaussian probability density function designed to characterize the EV travelled distance in each journey; as the previous two variables, this value also varies from country to country, being automatically updated every time that the "Country of the network being analysed" is changed;
- Percentage of EV that "*charge at the end of the day*" (%): 57.0 – this value is used as the probability of an EV driver behaviour be of the type that "charge at the end of the day";
- Percentage of EV that "*charge whenever possible*" (%): 23.0 – this value is used as the probability of an EV driver behaviour be of the type that "charge whenever possible";
- Percentage of EV that "*charge only when it needs*" (%): 20.0 – this value is used as the probability of an EV driver behaviour be of the type that "charge only when it needs".

Data obtained from deliverable 1.1 task 1.5:
 Travelled distance normal distribution average (km): 30.0
 Travelled distance - maximum value allowed (km): 200.0
 Travelled distance - minimum value allowed (km): 10.0
 Percentage of EV that "charge at the end of the day" (%): 57.0
 Percentage of EV that "charge whenever possible" (%): 23.0
 Percentage of EV that "charge only when it needs" (%): 20.0

Figure 5-14 Data obtained from Deliverable 1.1, task 1.5 [5]

In Figure 5-, it is presented the data that was obtained from Deliverable 1.1, task 1.1. [5]. This data is included in the Excel file and cannot be changed being, therefore, kept constant in all the case studied addressed. The way how these variables are used within the algorithm will be thoroughly described in subsections 5.1.5. The variables from Deliverable 1.1, task 1.1 that will be used in the algorithm are the following:

- Fast charging power (level 3 charging) (kW): 40.0 – this value is used as the standard charging power for all the EV that, during the simulation, need to go to the fast charging station;
- Level 2 charging power (kW): 12.0 – this value is used as the standard charging power for all the EV that, during the simulation, are parked in a commercial area.

Data obtained from deliverable 1.1 task 1.1:
 Fast charging power (level 3 charging) (kW): 40.0
 Level 2 charging power (kW): 12.0

Figure 5-15 Data obtained from Deliverable 1.1, Task 1.1 [5]

In Figure 5- it is presented the data from the assumptions taken into account during the algorithm development. The way how these variables are used within the

algorithm will be described in the following subsections. The assumptions made are described in the following points:

- Battery nominal power - normal distribution standard deviation (level 1 charging) (kW): 1.5 – this value is used as the standard deviation of the Gaussian probability density function designed to characterize the EV charging power; this value was assumed to be half of the mean value of the Gaussian probability density function;
- Battery capacity - normal distribution standard deviation (kWh): 14.5 – this value is used as the standard deviation of the Gaussian probability density function designed to characterize the EV batteries capacity; this value was assumed to be half of the mean value of the Gaussian probability density function;
- kWh consumption per km - normal distribution standard deviation (kWh/km): 0.08 – this value is used as the standard deviation of the Gaussian probability density function designed to characterize the EV energy consumption when moving; this value was assumed to be half of the mean value of the Gaussian probability density function;
- Travelled distance for fast charging station - normal distribution average (km): 7.5 – this value is used as the mean of the Gaussian probability density function designed to characterize the EV travelled distance in the detours made to the fast charging station; this value was assumed to be ¼ of the mean of the Gaussian function used to characterized the travelled distances in common journeys; this value varies from country to country, thus, this field's value is automatically updated every time that the "Country of the network being analysed" is changed by the user;
- Travelled distance for fast charging station - normal distribution standard deviation (km): 3.75 – this value is used as the mean of the Gaussian probability density function designed to characterize the EV travelled distance in the detours made to the fast charging station; this value was assumed to be half of the mean value of the Gaussian probability density function; this value varies from country to country, thus, this field's value is automatically updated every time that the "Country of the network being analysed" is changed by the user;
- Travelled distance for fast charging station - maximum value allowed (km): 50.0 – this value is used as a higher limit to the values obtained with the Gaussian probability density function designed to characterize the EV travelled distance in the detours made to the fast charging station; this value was assumed to be ¼ of the one applied in the Gaussian function used to characterized the travelled distances in common journeys; this value also varies from country to country, being automatically updated every time that the "Country of the network being analysed" is changed by the user;
- Travelled distance for fast charging station - minimum value allowed (km): 2.5 – this value is used as a lower limit to the values obtained with the

Gaussian probability density function designed to characterize the EV travelled distance in the detours made to the fast charging station; this value was assumed to be $\frac{1}{4}$ of the one applied in the Gaussian function used to characterized the travelled distances in common journeys; as the previous three variables, this value also varies from country to country, being automatically updated every time that the “Country of the network being analysed” is changed;

- Fast charging duration (min): 30 – this variable is used to define the amount of time that EV are charging at 40 kW in the fast charging station; this way, each EV that goes to the fast charging station can absorb a maximum of 20 kWh;
- Maximum voltage allowed (p.u.): 1.05 – this value is used in the Max_EV_share type of study and works as a restriction to the maximum number of EV that can be connected in the network under study; this restriction is used for all the time steps except the one with the lowest load; for the time step with the lowest load, a tolerance margin regarding the maximum voltage allowed is given, as explained in the next point; however, it should be referred that currently, this variable is irrelevant given that the V2G mode of operation will not be simulated; high voltage problems can only occur under these conditions, since EV might inject active power into the network and, given the typical high R/X ratio of distribution networks, make the voltages values raise;
- Maximum voltage allowed in the lowest load hour (p.u.): 1.07 – as during the lowest load time step it is likely that voltages get higher, namely if V2G is considered, a tolerance margin regarding the maximum voltage allowed is given in order to provide a higher flexibility to the integration of EV in the network; nevertheless, as mentioned in the previous point, this variable is irrelevant given that the V2G mode of operation will not be simulated;
- Minimum voltage allowed (p.u.): 0.90 – this value is used in the Max_EV_share type of study and works as a restriction to the maximum number of EV that can be connected in the network under study; this restriction is used for all the time steps except the one with the highest load; for the time step with the highest load, a tolerance margin regarding the minimum voltage allowed is given, as explained in the next point;
- Minimum voltage allowed in the peak hour (p.u.): 0.88 – as during the highest load time step it is likely that voltages get lower, a tolerance margin regarding the minimum voltage allowed is given in order to provide a higher flexibility to the integration of EV in the network;
- Maximum line rating allowed (%): 100.0 – this value is used in the Max_EV_share type of study and works as a restriction to the maximum number of EV that can be connected in the network under study; this restriction is used for all the time steps except the one with the highest load; for the time step with the highest load, a tolerance margin regarding the maximum line rating allowed is given, as explained in the next point;

- Maximum line rating allowed in the peak hour (%): 105.0 – as during the highest load time step it is likely that line ratings increase, a tolerance margin regarding the maximum line rating allowed is given in order to provide a higher flexibility to the integration of EV in the network;
- Charging efficiency for all charging levels (%): 0.90 – this value is used in the algorithm to emulate the losses that occur during the charging process in the inverter and in the battery cells.

Data assumed that should be kept constant:	
Battery nominal power - normal distribution standard deviation (level 1 charging) (kW):	1.5
Battery capacity - normal distribution standard deviation (kWh):	14.5
kWh consumption per km - normal distribution standard deviation (kWh/km):	0.08
Travelled distance for fast charging station - normal distribution average (km):	7.5
Travelled distance for fast charging station - normal distribution standard deviation (km):	3.8
Travelled distance for fast charging station - maximum value allowed (km):	50.0
Travelled distance for fast charging station - minimum value allowed (km):	2.5
Fast charging duration (min):	30
Maximum voltage allowed (p.u.):	1.05
Maximum voltage allowed in the lowest load hour (p.u.):	1.07
Minimum voltage allowed (p.u.):	0.90
Minimum voltage allowed in the peak hour (p.u.):	0.88
Maximum line rating allowed (%):	100.0
Maximum line rating allowed in the peak hour (%):	105.0
Charging efficiency for all charging levels (%):	0.90

Figure 5-16 Assumptions made during the algorithm development

“network.sav”

This PSS/E file contains data exclusively related with the network. The minimum data required to be introduced in this file is the data commonly used to run power flows, which is related with the network buses, loads, plants and branches/transformers.

5.1.4 EV Fleet Characterization

The first step of the Monte Carlo sampling process is to make the initial characterization of all the EV. Figure 5- presents an overview of this procedure.

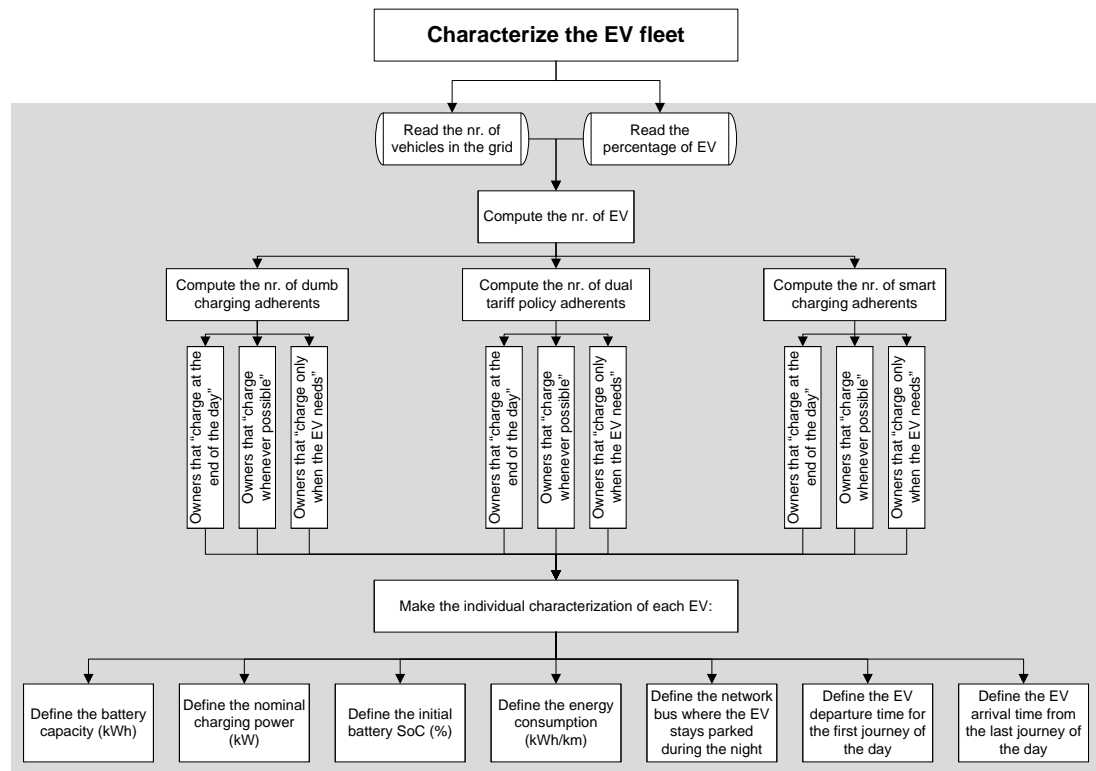


Figure 5-17 Flowchart of the EV characterization procedure

During this procedure, all the EV characteristics relevant for the simulation are generated by a Monte Carlo sampling procedure and recorded in an array with the following attributes for each EV: battery capacity (kWh), charging power (kW), initial battery State of Charge (SoC) (%), consumption per km (kWh/km), driver behaviour, charging method selected by the EV owner, network bus where the EV stays parked during the night, the departure time for the first journey of the day and the arrival time from the last journey of the day.

The EV battery capacity, charging power, initial battery SoC and consumption per km are defined according to a Gaussian probability density function, whose average, standard deviation, maximum and minimum values allowed are presented in Table 5-18.

Table 5-18 Gaussian distributions for EV characterization

	Average	Standard deviation	Maximum value allowed	Minimum value allowed
Battery capacity (kWh)	29.0	14.5	72.0	10.0
Charging rated power (kW)	3.0	1.5	9.0	2.0
Energy consumption (kWh/km)	0.16	0.08	0.25	0.10
Initial battery SoC (%)	90.0	25.0	100.0	50.0

While the initial battery SoC values were assumed for the purpose of this work, the values for battery capacity, charging rated power and energy consumption were obtained from the Deliverable 2.1. [6].

One of the EV characterization tasks was to choose a charging method for each EV. As referred above, only three different charging modes were assumed to be possible in this simulation tool: dumb charging, dual tariff policy and smart charging controlled by the DSO. The number of EV owners that adhere to each one of the charging modes is defined by the user in the Excel file. Then, taking into account the values introduced by the user, a draw is made to define which EV adhere to which charging mode. During this process, it is guaranteed that an EV only adheres to one charging mode.

As mentioned previously, a given driver behaviour was also assigned initially to each EV. The different behaviours considered in this study were defined according with the findings of the first survey made within the framework of the MERGE Project, whose results were presented in the Deliverable 1.1, task 1.5. [5]. The results revealed that there are four major types of behaviours regarding EV charging, as presented in Table 5-19.

For the purpose of the development of this simulation tool, regarding the behaviours modelling and simulation, it was assumed that there were no relevant differences between the drivers that “charge at the end of the day” and those who “charge whenever is convenient and they have time”. Therefore, the EV to which one of these drivers’ behaviours was assigned, were assumed to behave equally along the simulations.

Table 5-19 Drivers' behaviours considered

	Percentage of the responses
EV charge at the end of the day	33%
EV charge only when it needs	23%
EV charge whenever possible	20%
EV charge whenever is convenient and the driver has time	24%

Regarding the draw for the network bus where the EV stays parked during the night, the probability of an EV be located at a specific bus was assumed to be proportional to the load installed in that node:

$$P(\text{Bus } b) = \frac{\text{Load}_{\text{Bus } b}}{\sum \text{Load}} \quad (5-2)$$

where:

- $P(\text{Bus } b)$ – probability of an EV be located in bus b ;
- $\text{Load}_{\text{Bus } b}$ – load installed in bus b ;
- $\sum \text{Load}$ – total network load.

Therefore, buses with higher loads will have a higher probability of having EV parked.

The departure time for the first journey of the day and the arrival time from the last journey of the day were drawn, for each EV, according to the weekly probability distribution functions presented in Figure 5- to Figure 5-. The probability distributions used in the algorithm are automatically obtained from the Excel file in accordance with the “Country of the network being analyzed” chosen by the user. For each EV, a departure and an arrival time are defined for the weekdays, Saturdays and Sundays. These values define the time steps when EV are moving. As referred previously, it was assumed that each EV only make two journeys per day, being one made in the time step when the EV departs for the first journey of the day and the other when the EV travels for the last journey of the day, after which it will park.

5.1.5 EV Movement Simulator

The EV movement simulator was designed to emulate EV movement along one week, according to the data gathered from previous MERGE deliverables.

The procedures of the EV movement simulator at each time step will be described in the following subsections.

Time step = 0

The EV states (in movement, parked in a residential area, parked in a commercial area or parked in an industrial area) for the first time instant were defined according to the values obtained in the EV characterization procedure for the departure and arrival time. If the EV was parked, it was assumed to be located on its residential bus.

0 > Time step < 337

The EV are supposed to move in the time steps when make the first and the last journey of the day, which were drawn in the EV characterization procedure. If the EV is moving in the current time step, a travelled distance will be assigned to it, as explained later in this subsection. If the EV is parked, it is needed to check in which state was the EV in the previous time step.

If the EV was in movement and finished a journey, a bus location is attributed to it according to the following rules:

- LV network studies:
 - If the EV was making the first journey of the day, it is assumed that it will travel for outside the network, so no network bus will be attributed to it; this EV is not allowed to charge;
 - If the EV was making the last journey of the day, it is assumed that it will travel for its residential bus (defined during the EV characterization phase); this EV is allowed to charge;
- MV network studies:
 - If the EV was making the first journey of the day, it is assumed that it will travel to another bus within the network and a new state will be attributed to it (parked in a commercial or industrial area), as well as a new network bus, in accordance with equation (5-2); this EV is allowed to charge;
 - If the EV was making the last journey of the day, it is assumed that it will travel for its residential bus (defined during the EV characterization phase); this EV is allowed to charge;

In the LV network studies, the EV are not present in the network in the time period between the first and the last journey of the day. To make a worst case scenario analysis, it was assumed that the EV will not be able to charge during this period.

Therefore, EV will only be able to charge in their residential bus or, in case of being necessary, in the fast charging station. It is important to stress that the fast charging station is assumed to be directly connected to a MV grid. Thus, the load of the EV that charge in the fast charging station is not allocated to any bus of the LV grid.

On the other hand, in MV network studies, the EV are assumed to be always within the network geographical area and, when charging, connected to one of the LV grids that are downstream the MV network. However, as in this type of simulation the MV networks are only modelled until the MV/LV substation, the load of the EV that are connected to a given LV grid is grouped and represented as a single load in the substation bus. As EV are assumed to be always within the network geographical area, it was assumed that they are always able to charge, provided that they are parked in a network bus. In MV networks studies, as in the LV ones, EV will be able to charge, in case of being necessary, in the fast charging station. In this case, the fast charging station is assumed to be directly connected to one node of the MV grid (which is defined by the user in the Excel file). Therefore, the load of the EV that charge in the fast charging station will be allocated to the fast charging station bus. This value is recorded to be used in the procedure to calculate the total network load (network initial load + EV load).

The charging power of the EV that are charging depends always on their current state, as described next:

- Parked in a residential area – EV charges at their nominal charging power (value define in the EV characterization procedure) – Level 1 charging;
- Parked in a commercial area – EV charges at 12 kW – Level 2 charging;
- Parked in an industrial area – EV charges at their nominal charging power (value define in the EV characterization procedure) – Level 1 charging.

The charging in commercial areas was assumed to be of Level 2, since it is predictable that this type of charging facilities appear first in the most populated areas, such as malls, supermarkets and other big commercial surfaces.

For the EV that are in movement, a procedure was developed to account their energy consumption and the respective reduction in the battery SoC. First a Gaussian probability density function (see Table 5-20) was used to draw the travelled distances for all the EV in movement. After, if an EV was in movement in time instant t and it is predictable that its battery SoC goes below a predefined threshold (defined by the user in the Excel file) in time instant $t+1$, it is considered that the EV makes a short detour to a fast charging station for recharging purposes. The travelled distance during the detour is obtained using also a Gaussian probability density function, whose parameters are presented in Table 5-3.

Table 5-20 Gaussian distributions for travelled distances in common journeys and in the travels to the fast charging station

	Country	Average	Standard deviation	Maximum value allowed	Minimum value allowed
Travelled distance in common journeys (km)	Europe average	40	20	200	10
	Germany	20	10	200	10
	United Kingdom	40	20	200	10
	Spain	70	35	200	10
	Greece	40	20	200	10
	Portugal	30	15	200	10
	Ireland	50	25	200	10
Travelled distance to fast charging station (km)	Europe average	10	5	50	2.5
	Germany	5	2.5	50	2.5
	United Kingdom	10	5	50	2.5
	Spain	17.5	8.75	50	2.5
	Greece	10	5	50	2.5
	Portugal	7.5	3.75	50	2.5
	Ireland	12.5	6.75	50	2.5

The fast charging was assumed to be made during a period of time defined by the user in the Excel file, with a constant power of 40 kW – Level 3 charging.

The average of the Gaussian distribution used to characterize the travelled distance in common journeys was obtained from Deliverable 1.1, task 1.5. [5]. The standard deviation of this distribution was assumed to be 50% of the average.

The values of the Gaussian function used for the travelled distance to the fast charging station were obtained by assuming that they were 25% of those used in the travelled distance in common journeys distribution function.

At each time instant, the EV battery SoC is updated according to the energy spent travelling (for EV in movement), equation (5-3), or according to the energy absorbed in the fast charging station, equation (5-4).

$$EV_{SoC}^{t+1}(\%) = EV_{SoC}^t - \frac{EV_{kWh/km\ consumption} \times EV_{travelled\ distance}}{EV_{battery\ capacity}} \times 100 \quad (5-3)$$

$$EV_{SoC}^{t+1}(\%) = EV_{SoC}^t + \frac{EV_{charging\ efficiency} \times EV_{Level\ 1\ charging\ power} \times \frac{1}{2}}{EV_{battery\ capacity}} \times 100 \quad (5-4)$$

where:

- EV_{SoC}^{t+1} – represents the battery SoC in time step $t + 1$;
- EV_{SoC}^t – represents the battery SoC in time step t ; $EV_{kWh/km\ consumption}$ – is the EV energy consumption in kWh/km ;
- $EV_{travelled\ distance}$ – is the distance that the EV travels in time step t ;
- $EV_{battery\ capacity}$ – is the capacity of the EV battery in kWh ;
- $EV_{charging\ efficiency}$ – is the efficiency of the EV charging process; $EV_{charging\ efficiency} \in [0,1]$
- $EV_{Level\ 1\ charging\ power}$ – is the nominal charging power attributed to the EV in kW ; $EV_{Level\ 1\ charging\ power} < 10\ kW$.

Figure 5- presents a flowchart of the procedure adopted to simulate EV movement during one week.

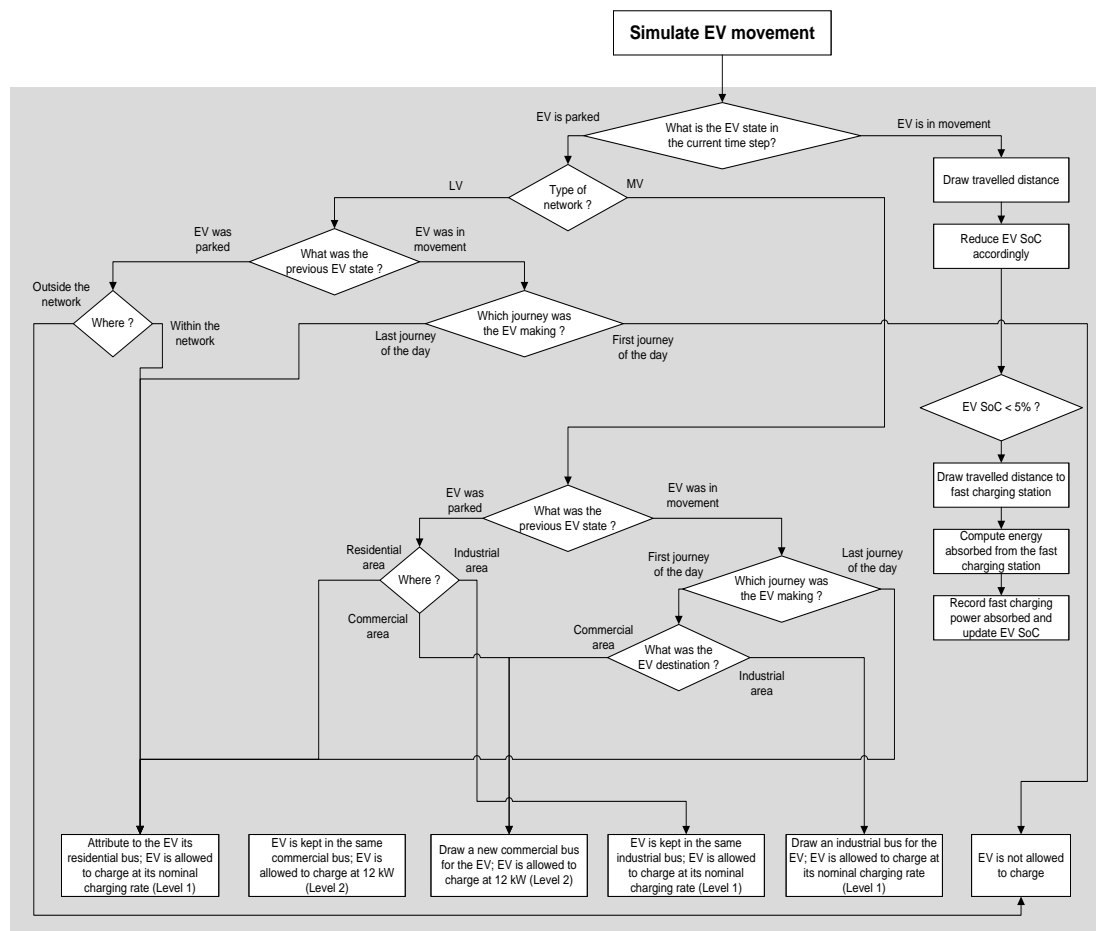


Figure 5-18 Flowchart of the procedure to define the EV state at each time step and the related allowed charging power

Having defined the EV states, locations and the allowed charging rates, it is needed to define, for each time step, if the EV that are parked will charge or not. This is a rather difficult task since it needs to be taken into account the EV owners' behaviour and the charging mode attributed to each EV. The details of how this procedure was implemented in the algorithm are thoroughly explained next in the subsections 5.1.6, 5.1.7 and 5.1.8.

5.1.6 Dump Charging Implementation

As referred in the previous subsection, the problem of defining, in each time step, if the EV that are parked will charge or not is a rather difficult task, given that it needs to take into account, first, the charging mode attributed to each EV and, after, the EV owners' behaviour.

When an EV, during the EV characterization phase, is flagged as a dumb charging adherent, it is assumed that it will charge as soon as it connects to a grid point where it is allowed to charge. In the LV network studies, the EV are allowed to charge every time they are parked, whereas in the MV network studies they are only

allowed to charge when they are within the network boundaries, i.e., they cannot charge during the time period between the first and the last journey of the day.

However, this is not the only condition that influences the decision of putting the EV charging, or not, in a given time step. One must also consider the drivers' behaviour. As referred in subsection 5.1.3, the different behaviours considered in this simulation tool were defined according to the results of a survey made within the framework of the MERGE Project. The survey results are presented in Deliverable 1.1, task 1.5 [5]. For the time steps when EV are allowed to charge, the drivers' behaviour will influence the EV charging as follows:

- EV owners that "*charge at the end of the day*" – this type of EV owners will only charge the EV in the time period that goes from the last journey of the current day until the first journey of the next day, regardless of the type of network being analyzed (LV or MV network) and regardless of the battery SoC when they arrive home;
- EV owners that "*charge whenever possible*" – this type of EV owners will charge every time they have the opportunity to do it; in LV network studies, they are only allowed to charge the EV in the time period that goes from the last journey of the current day until the first journey of the next day, as it happens for the owners that "charge at the end of the day"; in MV network studies, they are always allowed to charge, provided that the EV is parked and its battery SoC is lower than 100%;
- EV owners that "*charge only when the EV needs*" – regardless of the type of network being analyzed, this type of EV owners will only charge their EV when its battery SoC goes below a predefined value; this value is defined by the user in the field "Minimum battery capacity that triggers the charging of EV that *charge only when it needs*" of the input data Excel file.

5.1.7 Dual Tariff Policy Implementation

The dual tariff policy adherents are assumed to charge only during the period when electricity price is lower. This period is defined by the user in the fields "Starting hour of the lower electricity cost period" and "Finishing hour of the lower electricity cost period" of the Excel file.

However, as for the dumb charging adherents, this is not the only condition that influences the decision of putting the EV charging or not in a given time step. Again, the drivers' behaviour must also be considered. Thus, for the time steps within the cheaper electricity period, the drivers' behaviour will influence the EV charging as follows:

- EV owners that "*charge at the end of the day*" – this type of EV owners will only charge the EV in the time steps that obey to these two different conditions: the time step is within the time period that goes from the last journey of the current day until the first journey of the next day and within the lower electricity cost period;

- EV owners that "*charge whenever possible*" – this type of EV owners will charge every time they have the opportunity to do it, provided that the time step being considered is within the lower electricity price period; in LV network studies, additionally, they are only allowed to charge the EV in the time period that goes from the last journey of the current day until the first journey of the next day (while parked in a residential area), as it happens for the owners that "*charge at the end of the day*"; in MV network studies, they are always allowed to charge, provided that the EV is parked and its battery SoC is lower than 100%;
- EV owners that "*charge only when the EV needs*" – regardless of the type of network being analyzed, this type of EV owners will only charge their EV when the time step under consideration is within the lower electricity cost period and when its battery SoC goes below a predefined value; this value is defined by the user in the field "Minimum battery capacity that triggers the charging of EV that *charge only when it needs*" of the input data Excel file.

5.1.8 Implementation of the Smart Charging Controlled by DSO

In the beginning of each simulation, all the smart charging adherents are modelled similarly to the dumb charging adherents. The difference between them is that the smart charging EV are supposed to be available to reduce their load if a network problem occurs, as described in the next points:

- Identification of the problem and identification of the EV that are charging under a smart charging concept – As explained previously, when a problem occurs in the network and there are smart charging adherents in the scenario being studied, the DSO sends a load reduction signal to the smart charging adherents that are contributing for the problem. During the implementation of this procedure, in the algorithm, it was needed to identify, from all the smart charging adherents, those who were contributing for the problem identified in the network. The strategy used to solve this issue requires an identification of the network feeder where the problem occurred and order a load reduction to the smart charging EV located on it. Therefore, in the presence of excessive voltage drops or overload problems, there is a function in the algorithm that processes the problematic feeder topology and creates a list of the EV whose load can be reduced.
- Send a load reduction request to the smart charging EV identified before and re-evaluate the network's operating conditions – The DSO will try to overcome the identified problem by progressively reducing the load of the smart charging adherents, instead of suddenly disconnecting them. The load of these EV is progressively reduced in an iterative process. Thus, the network conditions are evaluated after each load reduction and, if the problem persists, a new load reduction is supposed to be ordered by the DSO. This procedure goes on until the problem is solved or until the smart charging adherents' load is reduced to zero.

Figure 5- presents an overview of the algorithm developed to emulate the behaviour of the dumb charging, dual tariff policy and smart charging adherents.

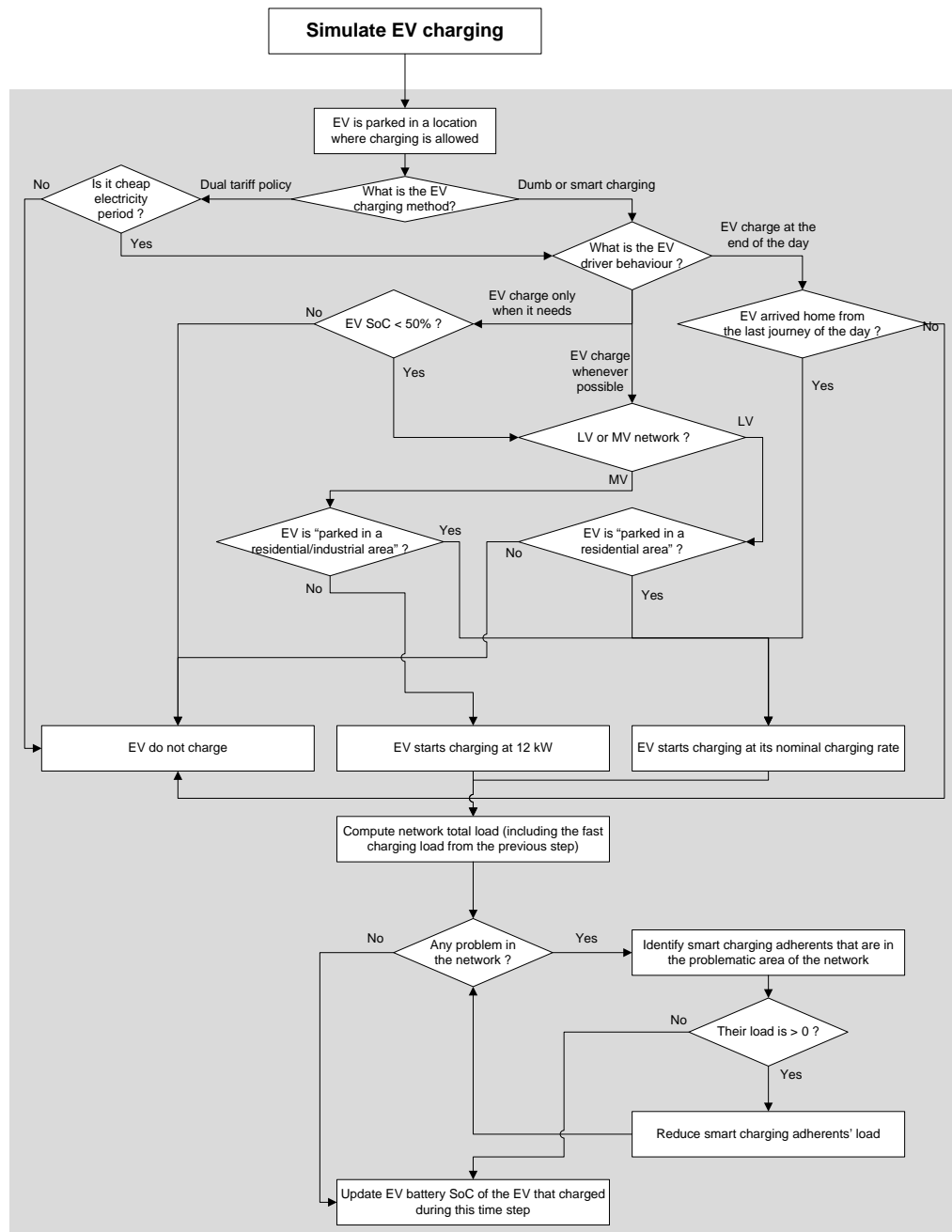


Figure 5-19 Implementation of the three charging modes considered in the algorithm

5.1.9 Test Cases

In order to test the developed simulation platform and demonstrate its usefulness in performing steady state impact analysis, operation/control planning and planning, two test cases were considered: a LV network and a MV network.

Although being specifically developed for distribution networks, this simulation tool might also be used as an ancillary tool to perform steady state studies in transmission networks. The Monte Carlo procedure developed can be used to analyze the EV impacts in the MV grids downstream a given transmission network. By running a high number of scenarios, it will be possible to obtain reliable EV load profiles that can then be allocated to the respective node of the transmission network. The full analysis of the transmission network can then be performed by adding, node by node, the respective EV load profile to the conventional load profile.

For each of the networks, three EV charging scenarios were considered:

- All EV in dumb charging mode;
- All EV in multiple tariff mode;
- All EV in smart charging mode.

By considering these three extreme scenarios, it is possible to evaluate separately the effectiveness of the implemented algorithm for every charging strategy. Combinations of charging strategies would also be feasible, but for the purpose of validation, would not be as meaningful.

It was considered that 30% of the total fleet of vehicles are electric and their initial SoC averaged 90%, with a standard deviation of 25% and minimum and maximum possible values for the initial distribution of 50% and 100%, respectively. For vehicles whose owners charge “only when it is needed”, the value of SoC that triggers the charging process is 50%. During a travel period, if the EV SoC drops below 5%, this EV uses a fast charging station, as described in the previous subsections.

For the EV charging scenario that considers the multiple tariff policy, the period of lower energy price is between 23h and 6h, every day of the week.

For the smart charging scenario, when there is a technical constraint violation, the reduction of EV load influencing the operation of the network is of 25% per iteration. At each of these iterations, 25% of the problematic charging adherents' load is reduced and a power flow study is conducted to evaluate if the existing problem was solved.

Next, the characteristics of each of the studied networks will be presented.

Low Voltage Network

Figure 5- presents the single line diagram of the LV test network. It is a representation of a residential area, which has a peak load value of 25.1 kW, distributed over 69 of the 75 buses of the network, and an annual energy

consumption of 111 MWh. The power factor assumed for the conventional load is 0.96.

The total number of vehicles in this network is 30. Being a LV network it has no fast charging station directly connected to it. However, EV are still allowed to charge in a virtual fast charging station. This situation may occur if between travels, to commute to either commercial or industrial areas, EV need charging. Even though using a fast charging station does not directly affect grid technical constraints, it influences the amount of energy each vehicle requires and consequently the power each EV absorb from this LV grid.

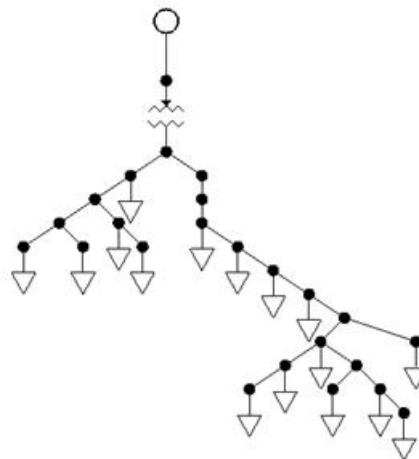


Figure 5-20 Single line diagram of the LV test network

Medium Voltage Network

Figure 5- depicts the single line diagram of the used MV test network. It is composed by residential, industrial and commercial areas, as it covers a larger geographical area and thus allows tracking each EV while commuting to and from work and to and from leisure activities. The peak of conventional load is 6 MW, distributed over 115 of the 309 network buses, and the yearly energy consumption assumes the value of 32 GWh. The power factor assumed for the conventional load is 0.96.

There is a total of 7035 EV on this grid and there is only one fast charging station located in a very robust area, not prone to technical limits violations.

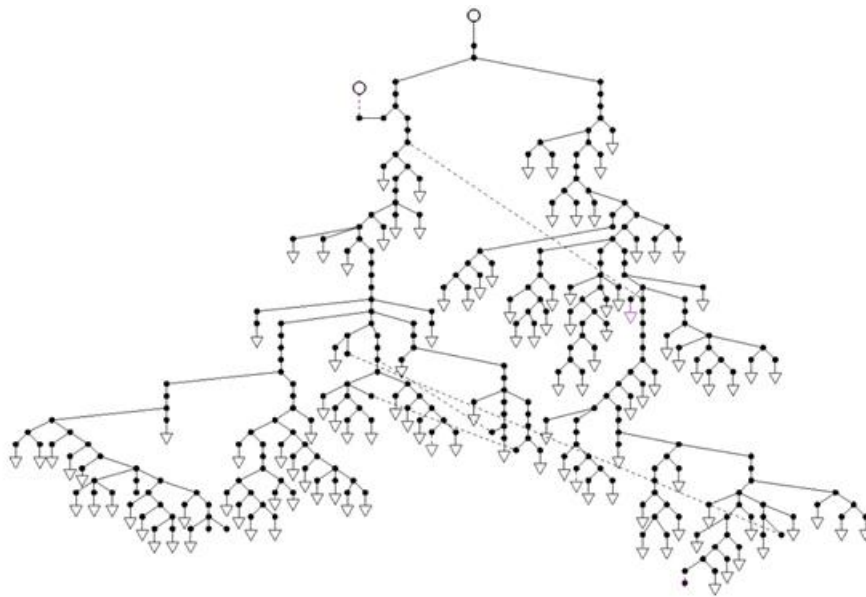


Figure 5-21 Single line diagram of the MV test network

5.1.10 Results

In the next subsections will be presented some of the results obtained from the simulations performed. Much more data could have been presented, like the EV travelled distances, the EV battery SoC variation, the number of EV that went to the fast charging station, the power absorbed by EV in the networks and in the fast charging station, etc. However, as the purpose of this subsection of results is only to prove the tool's efficacy in performing the evaluation of the impacts that arise from the integration of EV in distribution networks, only results concerning the power demand changes, the voltage profiles, the branches loading, the energy losses and the problematic elements in the network will be presented.

Low Voltage Network

Power Demand

Figure 5- shows the power demand for the week period studied with an EV integration percentage of 30%, as well as for the grid in its initial conditions, where no EV were considered. The network consumption, during the peak hour, increases 130% with the dumb charging, from 25 to 58 kW, 119% with the dual tariff policy, to 55 kW, and 30% with the smart charging, to 33 kW.

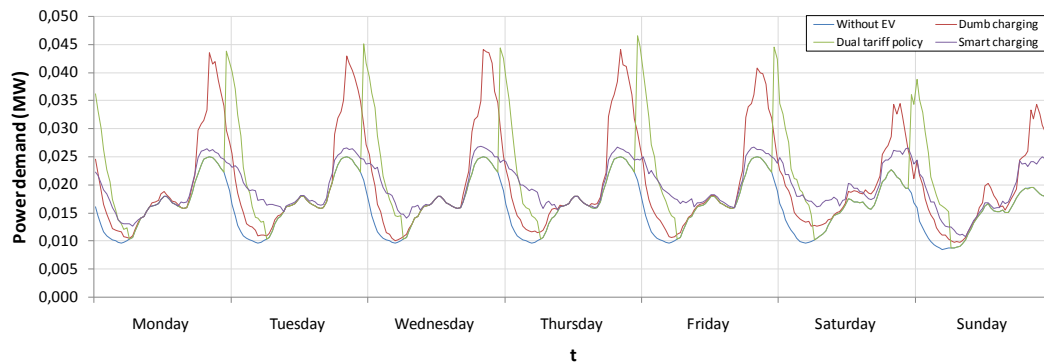


Figure 5-22 LV network power demand

From the results obtained, it is possible to conclude that both uncontrolled charging modes lead to a significant raise in the network peak load. This increase will originate large voltage drops and the overloading of some network branches, as it will be shown in the following subsections. The smart charging mode, by its turn, reduces the EV power consumption every time that a problem occurs, leading a higher number of EV to charge during the night periods.

Voltage Profiles

In order to assess the worst voltage conditions that these levels of EV integration might lead to, the highest peak load scenarios obtained along the simulations were recorded, and the corresponding voltage values were plotted in Figure 5-.

The extra power demanded by EV, when the dumb charging and the dual tariff policy are implemented, provokes a significant voltage drop along the grid, namely during the periods when the demand is higher, that, as Figure 5- shows, violate by far the lower limit of 0.90 p.u.. However, the implementation of the smart charging allows adjusting the charging of EV when a voltage violation occurs, allowing, this way, keeping the voltage values always within the predefined limits.

The network voltage profile in the scenario without EV is also presented in Figure 5-, for comparison purposes, as well as the reference voltage level stipulated by EN 50160 [7].

The integration of 30% of EV under uncontrolled charging modes, in this network, lead voltages to considerably low values, which in 63% of the buses are below the 0.90 p.u. threshold (considering the dumb charging). When the dual tariff is implemented, the percentage of buses with low voltage problems is reduced to 29%.

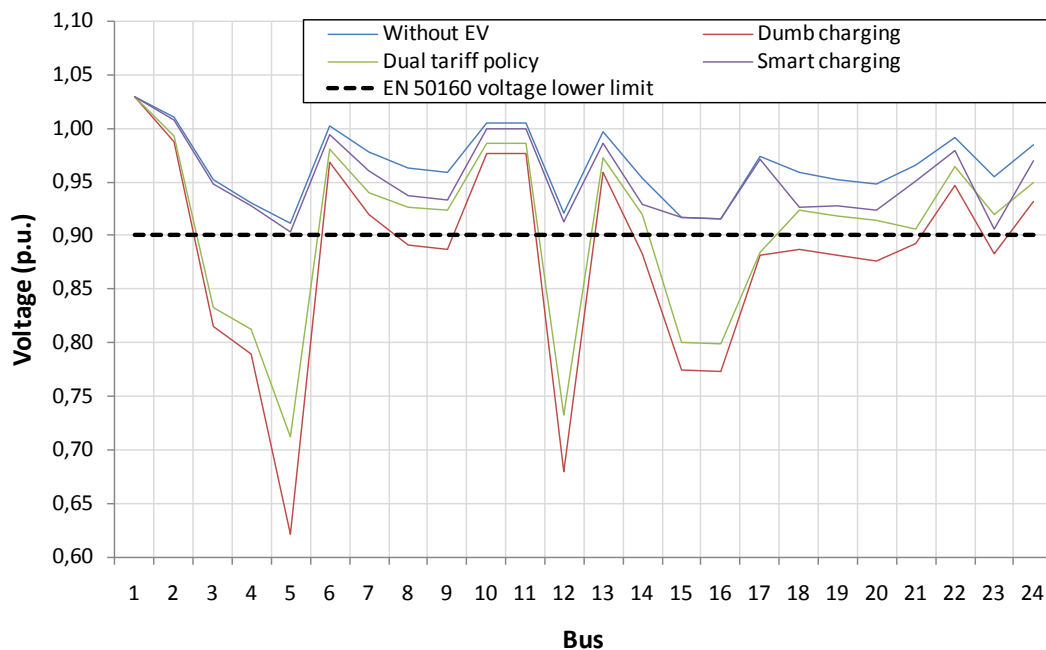


Figure 5-23 LV network voltage profiles for the highest peak load

Branches Loading

Figure 5- provides an overall idea of the impact provoked by EV in the network branches loading, for the peak load demand. The upper left image is referred to the peak load of the base scenario without EV, the upper right image is referred to the scenario with 30% of EV and with the dumb charging implemented, the lower left image is referred to the scenario with 30% of EV and with the dual tariff policy implemented and, finally, the lower right image is referred to the scenario with 30% of EV with the smart charging implemented.

The colour grading between dark blue and dark red stands for increasing line loading values, ranging from 0 to 100%.

As expected, the line loadings are higher in the uncontrolled charging modes, being the most problematic branches those located in the beginning of the most loaded feeders.

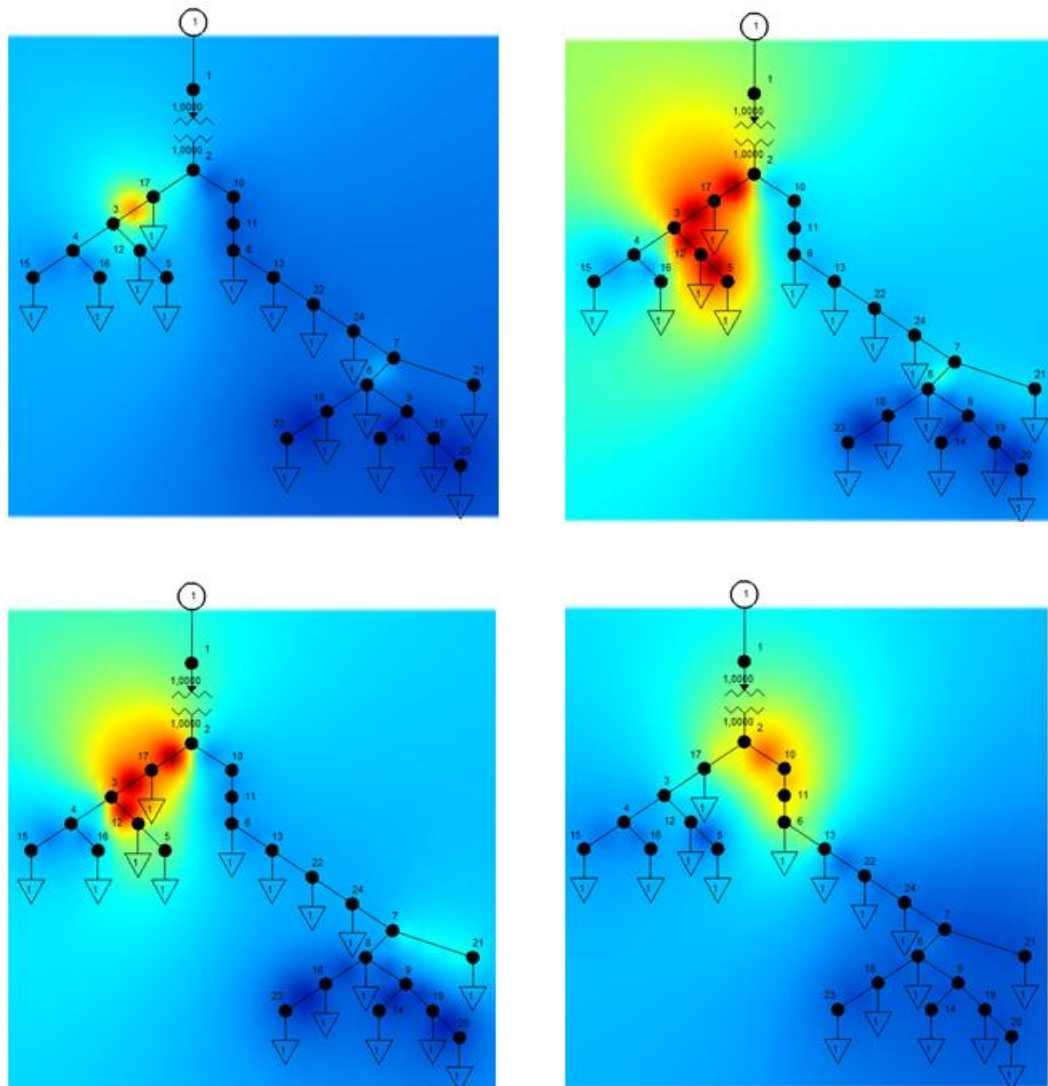


Figure 5-24 LV network branches loading for the peak load

Energy Losses

In Figure 5-, it is depicted the average value of the weekly energy losses, obtained along all the simulations performed.

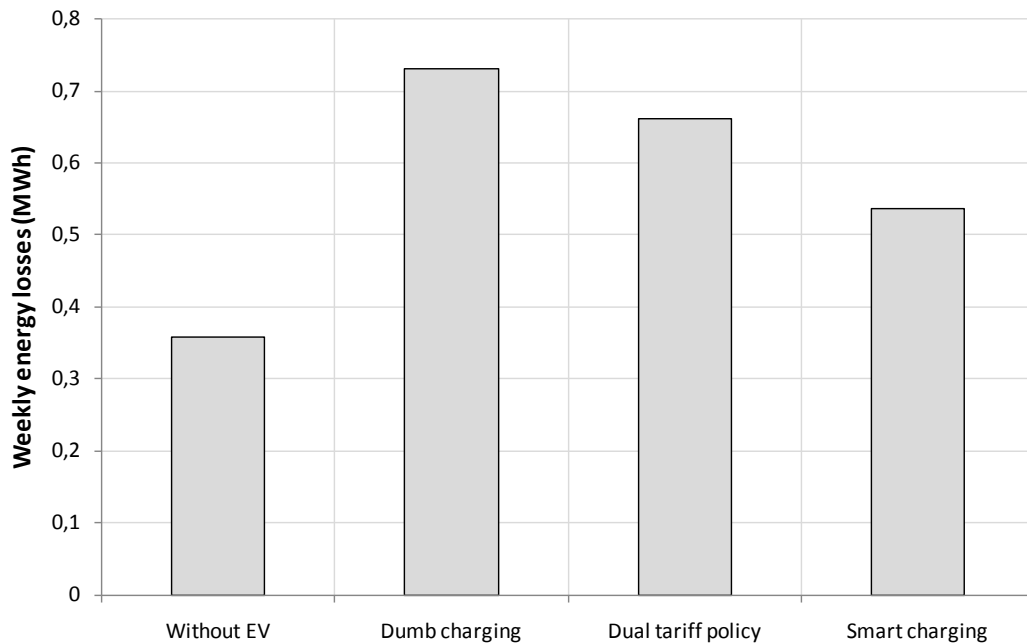


Figure 5-25 LV network average weekly losses

Problematic Network Components

As mentioned previously, all the voltage and branches loading limit violations were recorded along the simulation, in order to keep track of the most problematic areas of the network. Given that the EV integration only increases consumption, only voltages decrease will occur and so, as it is obvious, no voltages above the higher limit were recorded. Conversely to high voltage problems, voltages below the lower limit and lines loading above 100% occurred very often, as denoted in Figure 5- and Figure 5-.

The probabilities presented in Figure 5- and Figure 5- were obtained using equations (5-5) and (5-6), respectively:

$$P_{Voltage\ violation}^{Bus\ k} = \frac{Voltage\ violations^{Bus\ k}}{Nr.iterations \times 336} \times 100 \quad (5-5)$$

$$P_{Rating\ violation}^{Line\ l} = \frac{Rating\ violations^{Line\ l}}{Nr.iterations \times 336} \times 100 \quad (5-6)$$

When the dumb charging and the dual tariff policy are implemented, the probability of having voltages below the imposed limit and branches overloading is rather significant in some network buses and lines. The highest probabilities appear in buses 5, 12, 15 and 16, reaching values around 17%, and in line 6, reaching values around 10%.

The probability of having problems in the network due to EV is reduced to zero when the smart charging strategy is implemented.

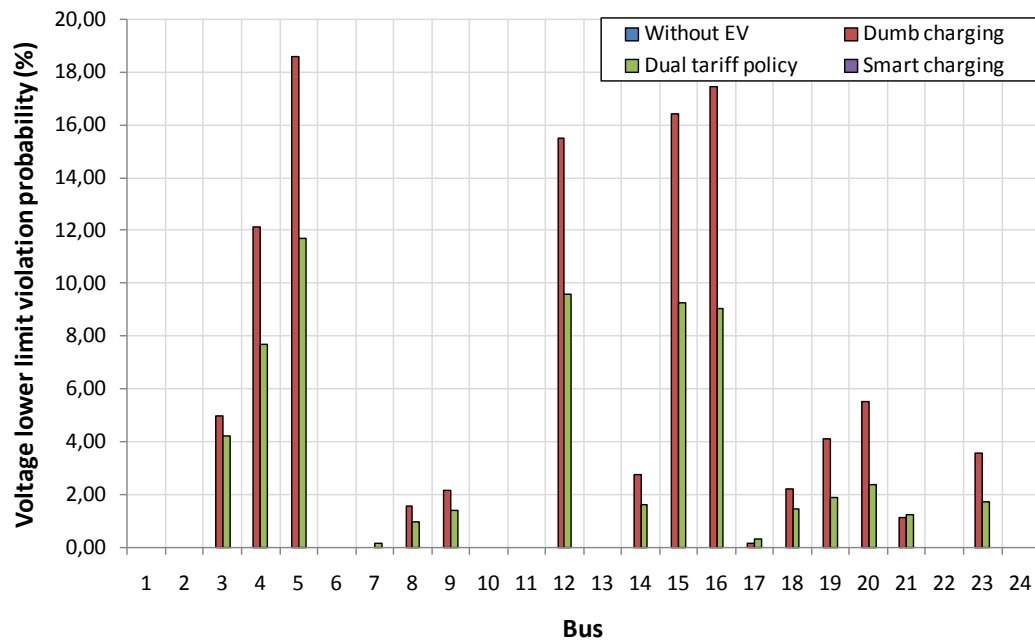


Figure 5-26 Voltage lower limit violation probability for the scenario with 30% of EV in the LV network

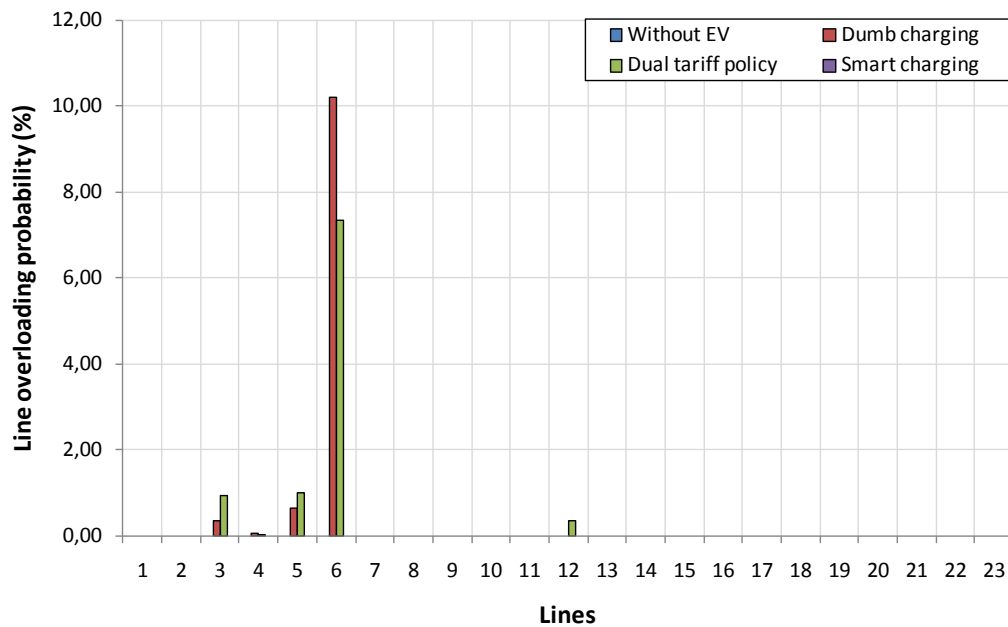


Figure 5-27 Branches overloading probability for the scenario with 30% of EV in the LV network

Medium Voltage Network

Power Demand

Figure 5- shows the power demand for the week period studied with an EV integration percentage of 30%, as well as for the grid in its initial conditions, where no EV were considered. The network consumption, during the peak hour, increases 79% with the dumb charging, from 7.3 to 13.1 MW, 93% with the dual tariff policy, to 14.2 MW, and 36% with the smart charging, to 10.0 MW.

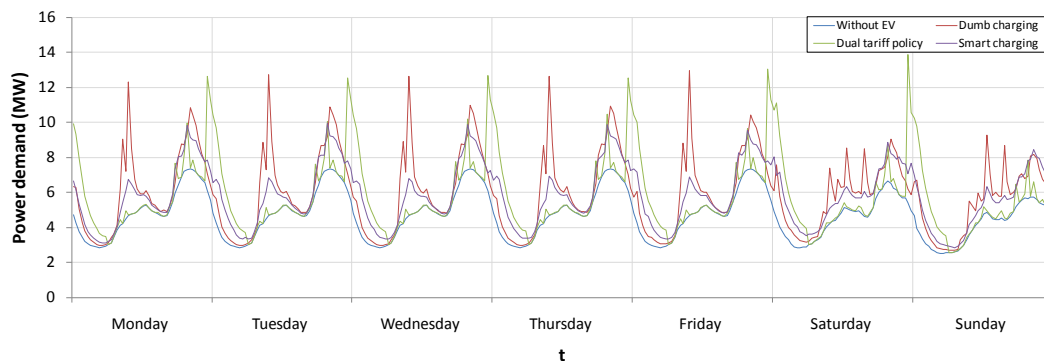


Figure 5-28 MV network power demand

Voltage Profiles

As done for the LV network, in order to assess the worst voltage conditions that these levels of EV integration might lead to, the highest peak load scenarios obtained along the simulations were recorded, and the corresponding voltage values were plotted in Figure 5-.

The extra power demanded by EV, when the dumb charging and the dual tariff policy are implemented, provokes a significant voltage drop along the grid, namely during the periods when the demand is higher, that, as Figure 5- shows, violate by far the lower limit of 0.90 p.u.. However, the implementation of the smart charging allows adjusting the charging of EV when a voltage violation occurs, allowing, this way, keeping the voltage values always within the predefined limits.

The network voltage profile in the scenario without EV is also presented in Figure 5-, for comparison purposes, as well as the reference voltage level stipulated by EN 50160 [7].

The integration of 30% of EV under uncontrolled charging modes, in this network, lead voltages to considerably low values, which in 50% of the buses are below the 0.90 p.u. threshold (considering the dumb charging). When the dual tariff is implemented, the percentage of buses with low voltage problems increases to 60%.

The reason why dual tariff policy strategy leads, in this specific situation, to worst network operating conditions is due to the fact that this charging mode leads all the adherent EV owners to postpone their EV charging to the periods when electricity cost is lower. When this period arrives, the high number of EV that almost

simultaneously are connected to the grid, provoke a very large voltage drop due to the sudden increase in the power demand.

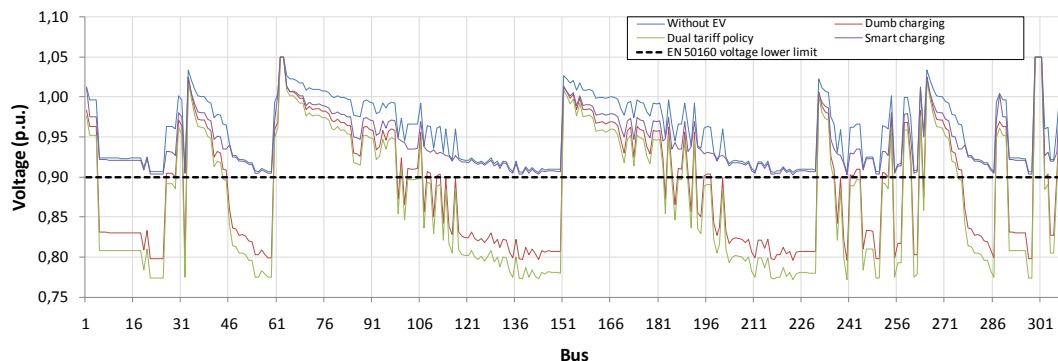


Figure 5-29 MV network voltage profiles for the highest peak load

Branches loading

Figure 5-, Figure 5-19, Figure 5- and Figure 5- provide an overall idea of the impact provoked by EV in the network branches loading, for the peak load demand.

The colour grading between dark blue and dark red stands for increasing line loading values, ranging from 0 to 100%.

As expected, the line loadings are higher in the uncontrolled charging modes, being the most problematic branches those located in the beginning of the most loaded feeders.

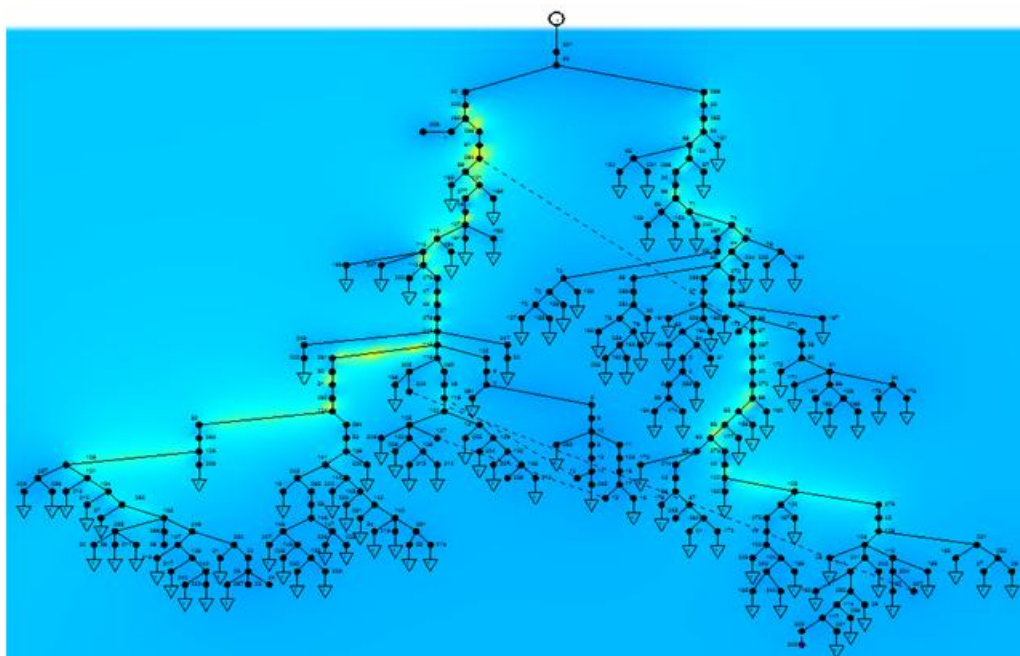


Figure 5-30 MV network branches loading for the peak load in the scenario without EV

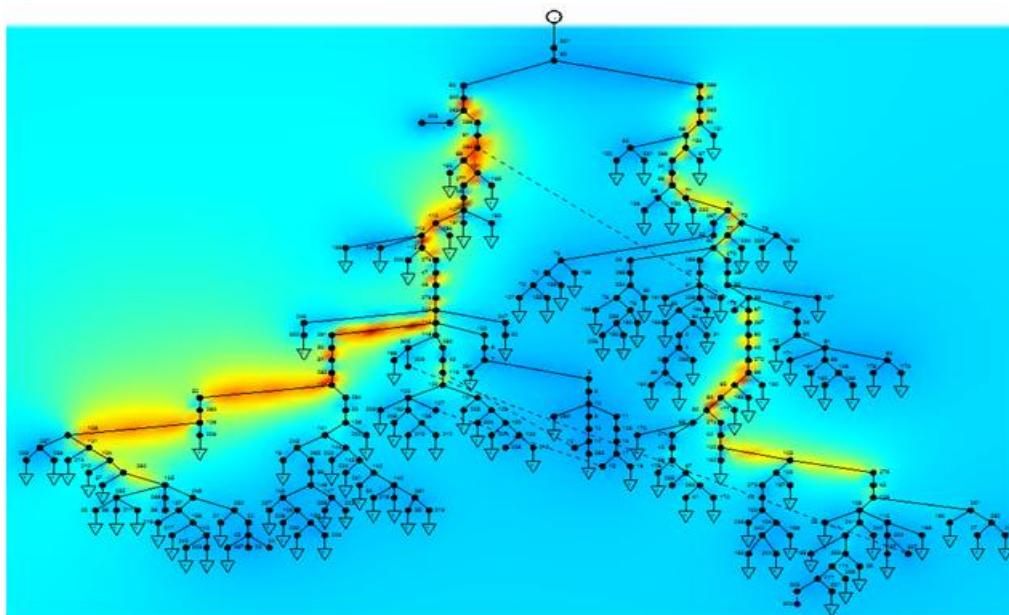


Figure 5-19 MV network branches loading for the peak load in the scenario with 30% of EV and with the dumb charging implemented

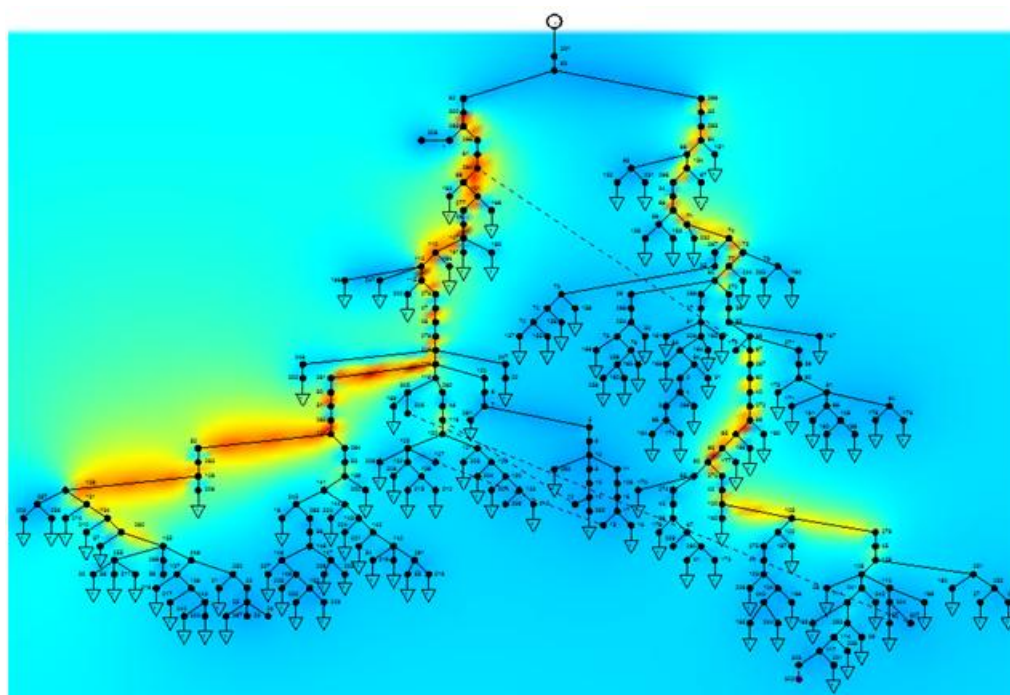


Figure 5-32 MV network branches loading for the peak load in the scenario with 30% of EV and with the dual tariff policy implemented

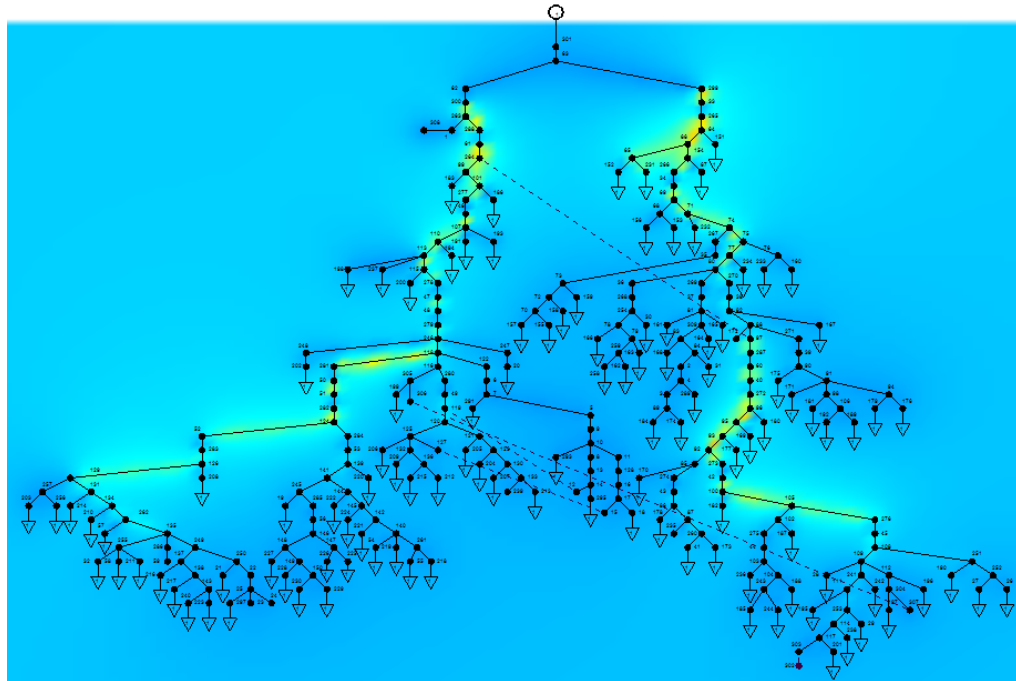


Figure 5-33 MV network branches loading for the peak load in the scenario with 30% of EV and with the smart charging implemented

Energy Losses

In Figure 5-, it is depicted the average value of the weekly energy losses, obtained along all the simulations performed.

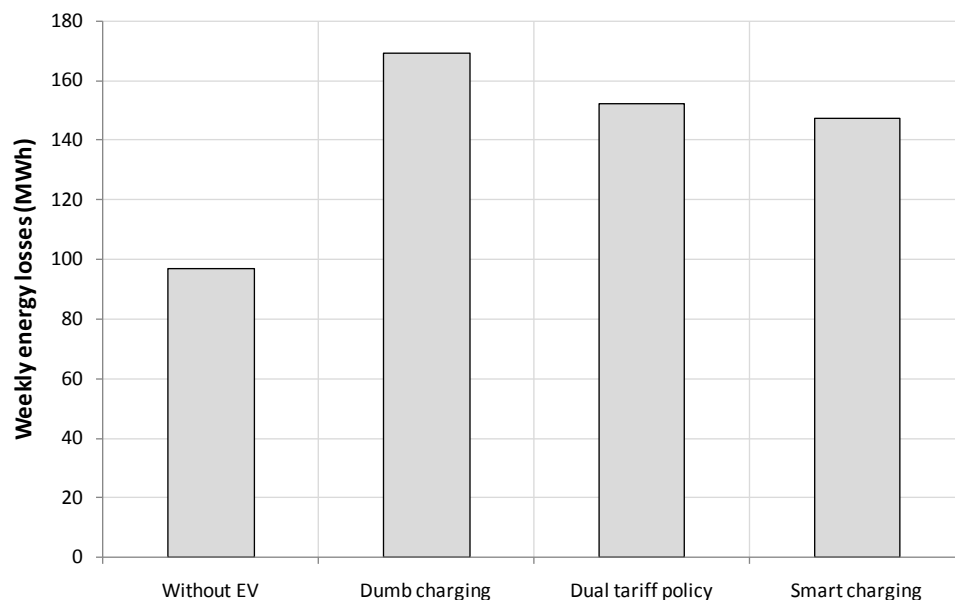


Figure 5-34 MV network average weekly losses

Problematic Network Components

As mentioned previously, all the voltage and branches loading limit violations were recorded along the simulation, in order to keep track of the most problematic areas of the network. Given that the EV integration only increases consumption, only voltages decrease will occur and so, as it is obvious, no voltages above the higher limit were recorded. Conversely to high voltage problems, voltages below the lower limit occurred very often, as denoted in Figure 5-.

The problems with branches loading above 100% were not so often, yet, as denoted in Figure 5-, some problems were registered in two of the network branches.

The probabilities presented in Figure 5- and Figure 5- were obtained using equations (5-5) and (5-6), respectively.

When the dumb charging and the dual tariff policy are implemented, the probability of having voltages below the imposed limit is rather significant in some network buses. As shown in Figure 5-, there are several network buses reaching values above 16%.

The probability of having problems in the network due to EV is reduced to zero when the smart charging strategy is implemented.

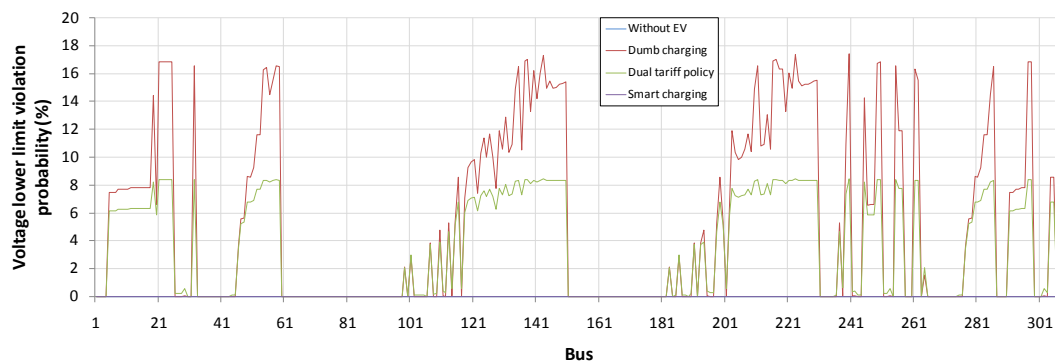


Figure 5-35 Voltage lower limit violation probability for the scenario with 30% of EV in the MV network

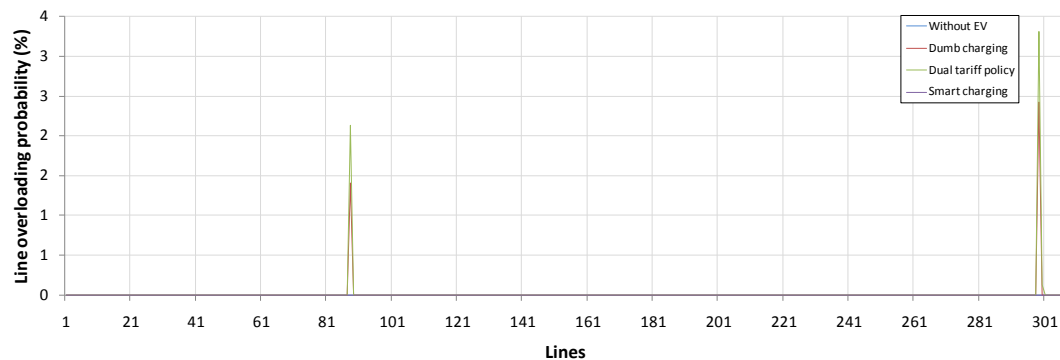


Figure 5-36 Branches overloading probability for the scenario with 30% of EV in the MV network

5.1.11 Conclusions

The simulation platform developed in this work is a very efficient tool to perform a realistic evaluation of the impacts that result from a massive integration of EV in distribution networks. Besides the evaluation of the steady state operating conditions of the grid, it also allows identifying the most critical operation scenarios, the identification of the maximum number of EV that can be connected in a given distribution network and the network components that are subjected to more demanding conditions that might need to be upgraded.

As referred above, although being specifically developed for distribution networks, this simulation tool might also be used as an ancillary tool to perform steady state studies in transmission networks. The Monte Carlo procedure developed can be used to analyze the EV impacts in the MV grids downstream a given transmission network and generate EV load profiles that can then be allocated to the respective node of the transmission network. The full analysis of the transmission network can then be performed by adding, node by node, the respective EV load profile to the conventional load profile.

Furthermore, this tool may be further enhanced to include micro-generation and other dispersed generation units in the formulation of the Monte Carlo simulation procedure. This way, it would be possible to evaluate not only the network impacts owed to EV, but also the changes that micro-generation and other dispersed generation units will provoke in the same networks, provided that the typical generation profiles of these facilities are available.

5.2 Dynamic Simulation

As it was previously mentioned, PSS/E is a power system simulation software that is widely used, not only by universities, but also by the industry. Since this simulation tool has such a large utilization, it was considered as mandatory to develop models capable to describe properly the dynamic behaviour of EV for this simulation environment. Several utilities have their power systems data in PSS/E format and in

this way, impact analysis resulting from the large scale presence of EV will be easy to be performed.

In the Deliverable D1.2, [8], the functionalities envisioned for EV were detailed. With particular interest for PSS/E simulation environment, primary reserve provision by EV and Automatic Generation Control (AGC) with EV were described.

The next section of this document will first explain the active role of EV, while reserve providers. Then, the possible modelling strategies of EV under PSS/E will be presented, followed by the description of the implementation details of primary and secondary control with EV. Finally, a test case and its results when applying the developed models will be described.

5.2.1 Primary and Secondary Frequency Control with EV

Primary Control

As mentioned in the deliverable D1.2, the MERGE concept, envisages the participation of EV in primary frequency control. Such capability becomes particularly useful in situations where the electricity grids are weak, i.e. grids where the deviations between generation and load are felt at the level of EV:

- Electricity grids of small island
- Unintentional or scheduled islanding of Microgrids
- Unintentional or scheduled islanding of Multi-Microgrids

In order to provide this service, the framework described in D1.2, which extended the concepts of Microgrids and Multi-Microgrids must also be considered. First, it was assumed that EV owners will communicate their willingness to participate in primary reserve delivery to the EVS/A via the MGAU. Then, once this communication is established, the EV will be flagged as primary reserve provider and the control will be locally activated. When leaving the service provision, the EV again sends a signal to the EVS/A and, if within a new regulatory framework this service can be paid, the EV will get remunerated according to the period of time when the service was provided.

Regarding the control for EV participating in primary frequency control, a proper electronic interface control should be adopted, different from a simple diode bridge usually adopted for these purposes. Being the system frequency an instantaneous indication of the power balance in a network, it must therefore be used to adapt the active power charging/discharging of the EV batteries. A frequency control droop loop can then be adopted to adjust the active power set-point of an EV inverter interface (Figure 5-37), which is an integrant part of the VC. In this way, a smart EV grid interface, capable of responding locally to frequency changes, is adopted, instead of a passive battery charging solution.

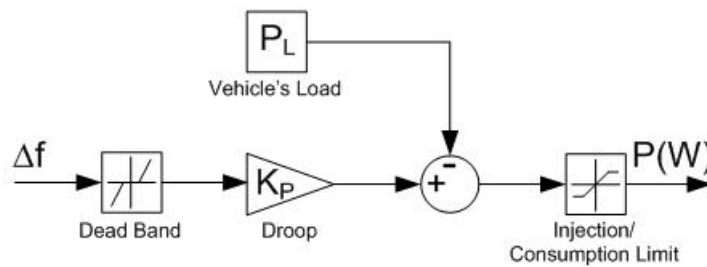


Figure 5-37 Control loop for EV active power set-point

To this conventional control method, a dead band, where EV do not respond to frequency deviations, should be added to guarantee longevity of the batteries and thus a beneficial synergy between parties, the grid operator/EVS/A and the EV owners. This dead band, as well as the slopes of the droops, should be defined according to the composition of the system, as well as the EV owners' willingness to help with system frequency regulation. After several tests for these case studies, a ± 0.1 Hz dead zone was used and a MW/Hz droop was defined.

As EV batteries, under a V2G concept, can either absorb or inject active power, a saturation block with upper and lower limits must be added. A block providing the steady-state set-point of active power must also be included, working as an offset to the droop. This block represents EV normal consumption status.

Figure 5-38 shows schematically the droop configuration that can be implemented for the EV grid interface control strategy. For frequency deviations larger than the defined dead band, the EV battery will respond according to one of the given slopes. If frequency suffers a negative deviation then the battery charging will, first, reduce its power consumption and, if frequency decreases further, it will inject power into the grid. On the contrary, if there is a positive deviation then the battery will increase the power absorbed from the grid.

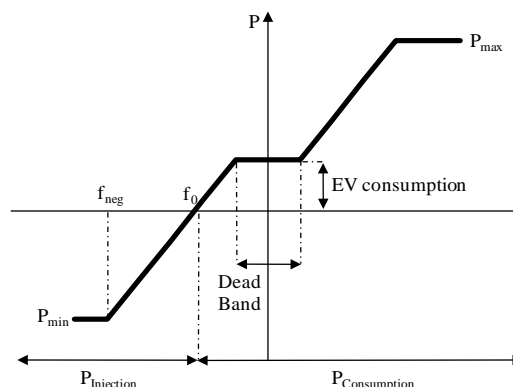


Figure 5-38 Droop control for VC

According to the UCTE Operation handbook, [9], the deployment time for primary reserve is up to 15 s for deploying up to 50% of the total reserve level and not more

than 30 s to fully deploy primary reserve. This reserve should be able to be delivered for at least 15 minutes, which is the necessary period to fully deliver the secondary control reserves. With the increased penetration of intermittent sources of energy, EV contribution for primary reserve deployment may be fundamental for the correct operation of the system.

Secondary Control

The management of EV charging for secondary frequency control purposes is also envisaged within the MERGE concept, in large interconnected systems or isolated systems such grids of island, Microgrids or Multi-Microgrids operating in islanding mode.

In secondary frequency control, the Automatic Generation Control (AGC) operation is the centrepiece in the control hierarchy. In a scenario characterized by large scale EV deployment, the TSO, who is responsible for the AGC, will acquire in the electricity markets the secondary reserves that it needs from GENCO and/or EVS/A.

If a sudden loss of generation or load increase takes place in a control area, the AGC exploits the available secondary reserves, set up by the market, by sending set-points to the participants in the secondary frequency regulation service. If EV EVS/A are participating in this service, the AGC will send set points to adjust loads from these EVS/A that afterwards will send set-points to the EV willing to provide this service. The set-points EV will receive from the EVS/A will lead to a load charging adaptation for the period of time the AGC requires this service.

In order to provide secondary reserves, EV must be an active element within the power system. Typically, participants of the reserves market would be the transmission company, providing buying bids, and generation companies, selling bids. If EV would enter this market individually their visibility would be small and due to their stochastic behaviour rather unreliable.

Nonetheless, if an aggregating entity exists, as defined in the MERGE project, with the purpose of grouping EV to enter in the market negotiations, then reserve quantities would be more significant and the confidence on its availability much more accurate.

To perform AGC operation with EV, some modifications, presented in Figure 5-39, need to be introduced in conventional AGC systems in order to make the regulation of EV power consumption/output possible in response to deviations of system frequency, f_i , in relation to its reference, f_{REF} , and of the tie-lines active power flow, P_{if_i} , in relation to the interchanges scheduling, $P_{if_{REF}}$. As in the conventional AGC, B is the frequency bias that measures the importance of correcting the frequency error, when compared with the correction of the interchange power error; k_i is the gain of the integral controller; $P_{e_m}^{ini}$ is the current dispatch for machine m , fP_m its participation factor and P_{ref_m} its new active power set-point value. $P_{a_k}^{ini}$ is the current load of EV EVS/A k (entity whose importance will be further developed in this section) and fP_{A_k} and $P_{ref_{A_k}}$ the EVS/A k participation factor and new active power set-point.

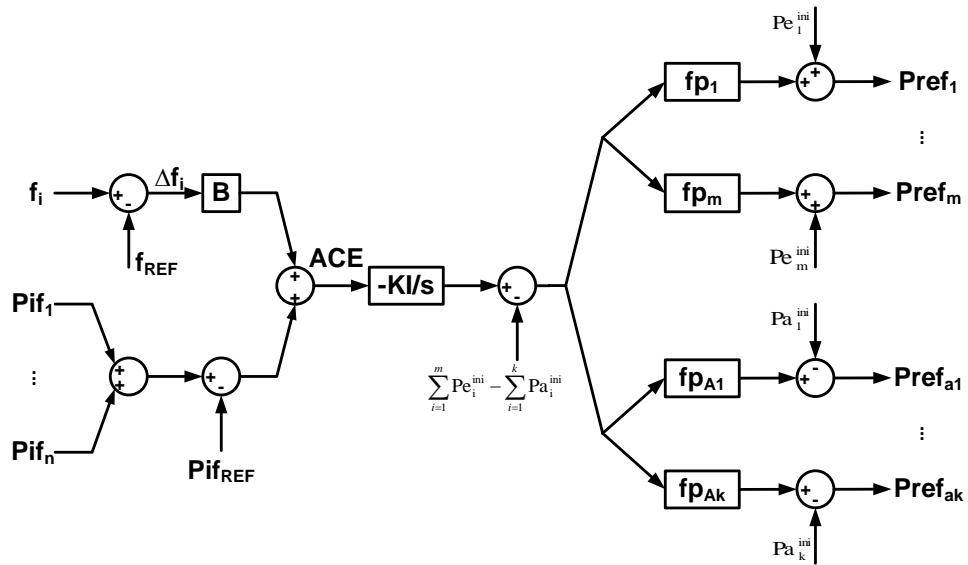


Figure 5-209 AGC operation in the presence of EV EVS/A

These control functionalities to be provided by EV are intended to keep the nominal system frequency and to keep the established power flow interchange with other areas within predefined limits.

According to the UCTE Operation Handbook, [9], the control action of the AGC must start the control action after a disturbance, 30 s at latest. The controller cycle time must be within 1 to 5 s. Measurement cycle times, integration times and controller cycle time must be co-ordinated within the control loop. Moreover, there are three different schemes for the organisation of secondary control: centralised, pluralistic and hierarchical. The last two are decentralised implementations, which are not performed in this work.

5.2.2 EV modelling for Dynamics Simulation

For the purpose of dynamic simulation, EV charging can be modelled, as any load, as constant power load, constant current load, constant admittance load or a combination of those. The following equation presents the mathematical formulation of such a modelling, [10]:

$$P = P_0[p_1\bar{V}^2 + p_2\bar{V} + p_3] \quad (5-7)$$

$$Q = Q_0[q_1\bar{V}^2 + q_2\bar{V} + q_3] \quad (5-8)$$

Where:

P is the active power

Q is the reactive power

p_1 to p_3 and q_1 to q_3 are coefficients that define the proportion of each component

In addition to this dependency on voltage, loads may suffer the influence of frequency and so equations 5-7 and 5-8 may be written as:

$$P = P_0[p_1\bar{V}^2 + p_2\bar{V} + p_3](1 + k_{pf}\Delta f) \quad (5-9)$$

$$Q = Q_0[q_1\bar{V}^2 + q_2\bar{V} + q_3](1 + k_{qf}\Delta f) \quad (5-10)$$

Where:

Δf is the frequency deviation

k_{pf} and k_{qf} are coefficients that reflect the dependency of the load value to Δf

Typically, in dynamic simulation a simplification is done and all loads are considered to be of constant admittance type. This occurs due to the fact that is virtually impossible to achieve perfect knowledge on the loads distributed through the network that is being studied. Some particular cases, such as networks representative of industrial areas, may consider certain portions of the load to have specific behaviours, and consequently specific models are adopted to study their influence. This happens in the case where large induction motors or air conditioning devices have a large presence, which requires additional load modelling.

In the particular case of this study, EV represent are assumed to be a know proportion of the total load and so EV load was distinguished from the conventional load. Being interfaced with the electricity grid by power electronics, EV charging is controlled, following well known patterns. The constant current constant voltage charging process of a lithium-ion battery cell, [4], is depicted in Figure 5-40. It is observable that current is constant during most of the time, while voltage slowly varies over time, except for very low values of State Of Charge (SOC). When SOC reaches a high value, then voltage is kept constant and current decreases tending to zero.

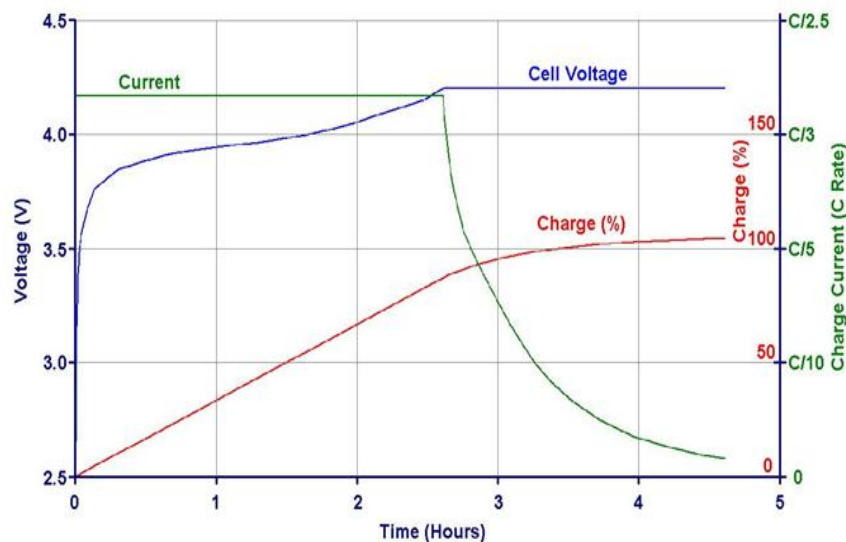


Figure 5-40 Constant Current Constant Voltage Charging [4]

AGC operation regards time periods of 15 minutes. For these small periods of time one can assume a constant power load for the EV battery charging process, also because variations of voltage at EV terminals are quite small during the large majority of this period of time and can therefore be neglected.

When advanced management strategies are considered, to the adopted model, extra control loops have to be added to EV loads, enabling them to respond to:

- Frequency, when working in primary frequency control.
- Upstream active power set-points, when participating in AGC operation.

The following sub-sections will describe the modelling approach used and provide the details of each implemented control schemes.

5.2.3 Advanced PSS/E Modelling Approach

The previous sub-section described the general procedure for load modelling. In this topic, the methodology used to implement the required control procedures – EV droop control and AGC operation – is presented.

In PSS/E environment, there are two approaches to the implementation of the desired control actions:

- Conventional implementation, PSS/E focused – internal to the simulation procedures used by the software.
- Python script focused, interacting with PSS/E – external to the simulation procedures used by the software.

To implement the first option, it is necessary to develop a model using FORTRAN, including specific Fortran-PSS/E routines and global variables, compile it and declare its usage in the dynamic simulation data input file for PSS/E. Following the typical implementation scheme the developed model gets embedded in the simulation. This alternative is robust and does not delay the simulation time. The simulation is stopped only when an event, such as load variation or bus fault, occurs. Event file is coded using Python. Figure 5-41 is a flowchart of the simulation process using the conventional model implementation. On the left, the activities external to PSS/E operation are presented, whereas PSS/E simulation is depicted, on the right (this part was adapted from PSS/E Operation Manual, [12]).

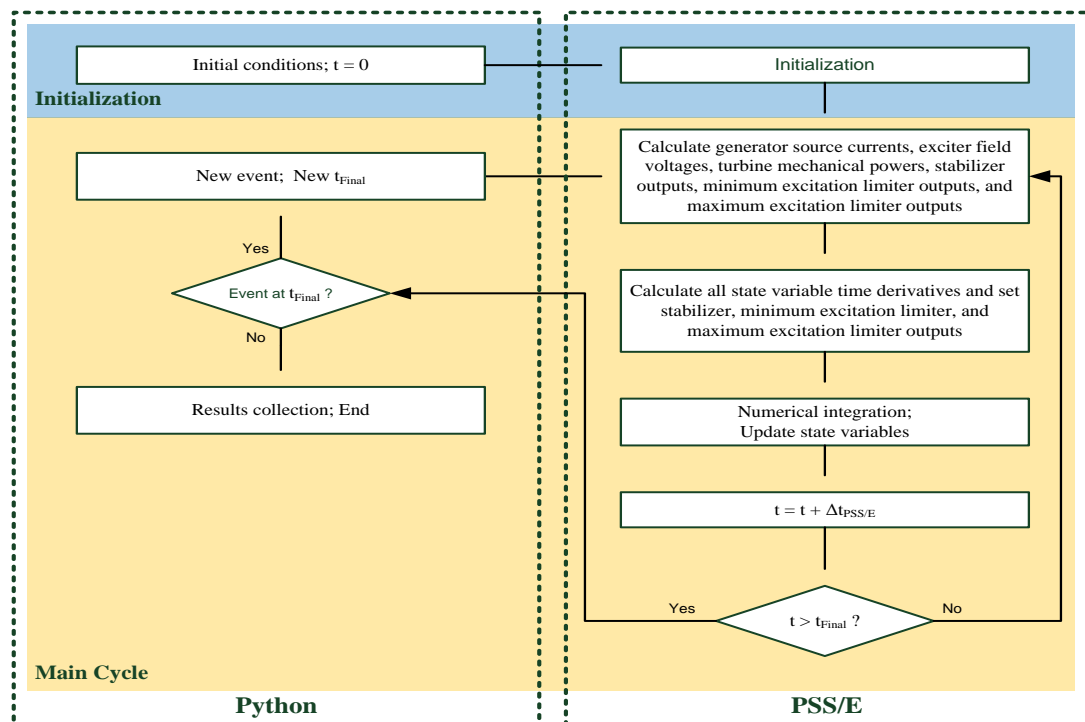


Figure 5-41 Simulation scheme with conventional modelling, PSS/E focused

To implement the second option, the dynamic data input file remains unchanged, keeping all the data related to generation. Advanced modelling is now executed using a Python script. Instead of being used only to generate events, the Python file is also used to collect the system state evolution and manage control variables. In opposition to what happened with the FORTRAN modelling the data collection period, in this case, is user defined and can be as short as the integration period defined internally by PSS/E. To create fast controllers using this implementation, the script must stop the simulation with time steps close to that used by PSS/E (using a larger time step means that a larger delay is being introduced to the response time of the controllers). Then, the state evolution is evaluated and used to update the control variables that are passed into PSS/E. Similarly to Figure 5-41, Figure 5-42 depicts a flowchart of the simulation scheme with Python script modelling, interacting with PSS/E. The highlighted text boxes are the new functionalities necessary within this approach.

This method is as robust as the previous but more flexible regarding the control options that may be taken. However, external state evaluations and control actions may lead to an increase in simulation time that with nowadays processing capability is not a real drawback.

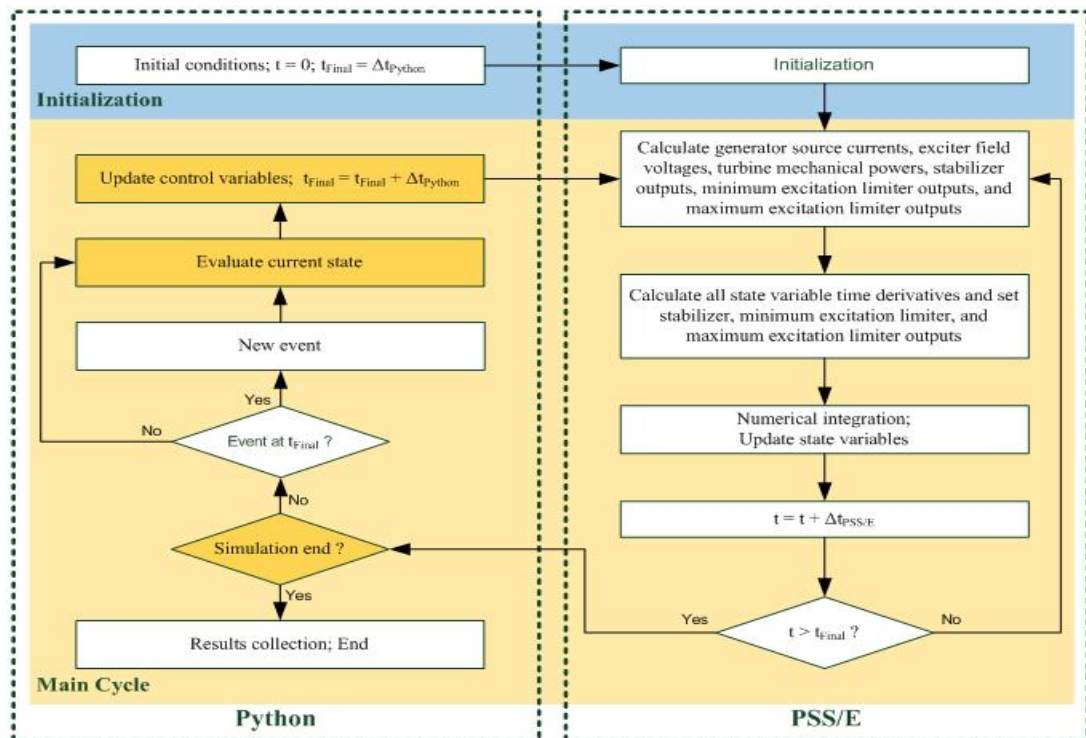


Figure 5-42 Simulation scheme with Python script modelling, interacting with PSS/E

For the EV frequency control droop implementation, the conventional modelling technique would likely be the easiest implementation method, due to the fact that the power electronic interface that is being emulated works in a decentralized way. It reads a local state variable and controls, locally, EV power consumption.

Nevertheless, when AGC operation is sought, a centralized control unit is needed. This unit requires the knowledge of state variables spread over the grid – interconnection power flows and the frequency of the centre of inertia of the system. The implementation of such a control unit under the conventional approach is possible, by programming a subroutine of the simulation process of PSS/E called CONET. As previously explained, it would have to be compiled along with the rest of the models, but the outputs would have to be treated in a different way when compared with typical local models. In this case, the script included in the CONET sub-routine would not deal only with global state variables that allow direct observation in the PSS/E post-simulation environment. Consequently, a post-processing work would be necessary within the Python script to collect all the data to replicate the state variables necessary to illustrate the reaction of the controller. If this activity is used to implement the controller in the Python environment, then there is no need to repeat it, as results get created along with the evolution of the script.

Therefore, Python script modelling, interacting with PSS/E, was chosen to model the AGC and, as it involved part of the variables needed to implement the EV droop control, this functionality was also implemented using the same strategy.

5.2.4 EV Droop Control Implementation

Implementing the EV droop control, applying the already discussed concepts, is a straightforward problem.

As presented in sub-section 5.2.1, the EV droop frequency control has only one input state variable, the bus frequency deviation. To this deviation the controller multiplies a constant, the proportional gain, and outputs a new EV load value. A pseudo-code for this simple script is shown below.

```
for every  $\Delta t_{python}$  from 0 to simulation end
    read  $\Delta f$  from PSS/E
    for every EV
        read  $P_{now}^{EV}$  from PSS/E
         $P_{next}^{EV} = P_{now}^{EV} + \Delta f \cdot K_P$ 
```

Where:

P_{now}^{EV} is the current active power value for the selected EV

P_{next}^{EV} is the new active power value for the selected EV

Δf is the frequency deviation

K_P is the EV controller proportional gain

To this basic implementation a dead band that limits the values of frequency for which the controller reacts can be created as described next.

```
for every  $\Delta t_{python}$  from 0 to simulation end
    if  $\Delta f > dead\_band$  then
         $P_{next}^{EV} = P_{now}^{EV} + \Delta f \cdot K_P$ 
```

Where:

$dead_band$ is a frequency range for which the controller does not react

5.2.5 AGC with EV Implementation

Using the previously described implementation methodology, a script using Python was created to define all the required functionalities of an AGC unit.

In the sub-section 5.2.1, the AGC main conceptual architecture was presented as a block diagram. Its core block is the integration function that was programmed using the numerical integration Trapezoidal Rule.

To calculate numerically the integral of a given function, $f(t)$, over the period $[0; T]$, using this rule, an integration time step Δt is defined and each of the intervals for integration is approximated by the area of a trapezoid, as illustrated in Figure 5-43 (the function $f(t)$ is depicted in blue and the trapezoidal approximation is shown in red).

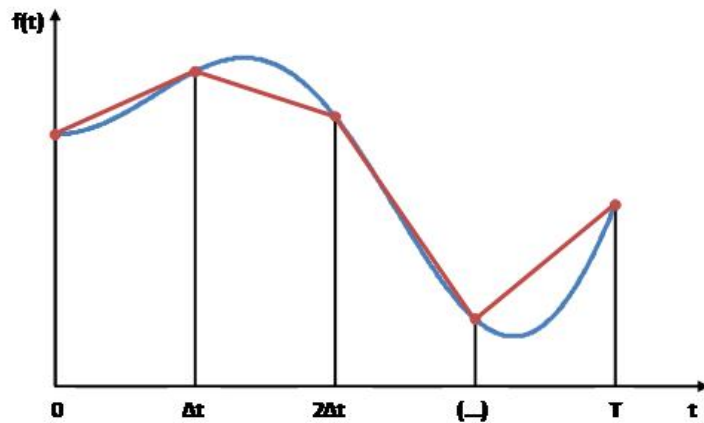


Figure 5-43 Integration of function $f(x)$ using the Trapezoidal Rule

The mathematical formulation for the Trapezoidal integration of the function $f(t)$ is the following:

$$\int_0^T f(t) dt \approx \sum_{k=1}^N \frac{f(t_{k-1}) + f(t_k)}{2} \Delta t \quad (5-11)$$

Where:

$$t_k = k\Delta t$$

$$N = \frac{T}{\Delta t}$$

k is the current interval of integration

N is the number of periods for integration

Returning to the case of the AGC, the Trapezoidal Rule was used to integrate the value of the ACE, which is a measure of the interconnection power flows deviations in relation to a specified value plus frequency deviations. To add these two values a constant is multiplied by a constant that reads the variation in frequency as active power. As a central controller, the frequency value must be that of the centre of inertia of the system, which is composed by the individual synchronous machines of a given control area, multiplied by their individual inertia over the inertia of that area:

$$\Delta f_{centre\ of\ inertia} = \frac{\sum_{k=1}^N \Delta f_k \cdot H_k}{\sum_{k=1}^N H_k} \quad (5-12)$$

Where:

$\Delta f_{centre\ of\ inertia}$ is the frequency deviation of the centre of inertia of a given control area

k is the iterator for the synchronous machines of a given control area

N is the number of synchronous machines of a given control area

Δf_k is the frequency deviation of machine k

H_k is the inertia of machine k

The box below shows in pseudo-code the implementation of the routine that determines and integrates the ACE, which has to be conducted at every integration step for each of the controlled areas.

```
for every  $\Delta t_{python}$  from 0 to simulation end
    get  $\Delta f$  from PSS/E
    get  $\Delta P$  from PSS/E
     $ACE = \Delta f \cdot B + \Delta P$ 
     $\int ACE_{now} = \int ACE_{previous} + K_I \left[ \frac{ACE_{now} + ACE_{previous}}{2} \Delta t_{python} \right]$ 
```

Where:

Δt_{python} is the Python script integration step

Δf is the frequency deviation

ΔP is the interconnection power flow deviation

ACE is the Area Control Error

$\int ACE_{now}$ is the value of the integral of ACE at the current integration step

$\int ACE_{previous}$ is the value of the integral of ACE at the previous integration step

K_I is the integral gain of the AGC controller

The value of the integral of the ACE then has to be distributed through the machines participating in AGC operation, using the machines' participation factors. When a certain generation unit is not providing secondary reserve, its participation factor is 0. The sum of all participation factors must be equal to 1, in order to fully deploy the

needed reserve value. Each participation factor is multiplied by the integral of the ACE and the result summed to the scheduled value of the corresponding generator active power. This process is described next:

for every generation unit

if $PF_{gen} > 0$ then

$$P_{new}^{gen} = P_{Scheduled}^{gen} + PF_{gen} \cdot \int ACE_{now}$$

send P_{new} to PSS/E

Where:

PF_{gen} is the participation factor of the selected generation unit

P_{new}^{gen} is the new active power set-point for the selected generation unit

$P_{Scheduled}^{gen}$ is the scheduled active power value for the selected generation unit

When EV are incorporated in AGC operation, then the participations factors get readjusted to include EV and keep their sum equal to 1. As EV are modelled as loads, their participation factor multiplied by the integral of the ACE is subtracted to their scheduled load value. This is schematically presented by the following pseudo-code:

for every EV

if $PF_{EV} > 0$ then

$$P_{new}^{EV} = P_{Scheduled}^{EV} - PF_{EV} \cdot \int ACE_{now}$$

send P_{new} to PSS/E

command PSS/E to factorize the admittance matrix

Where:

PF_{EV} is the participation factor of the selected EV

P_{new}^{EV} is the new load set-point for the selected EV

$P_{Scheduled}^{gen}$ is the scheduled load value for the selected generation unit

With this code block, the main functionalities of the AGC were presented. Next, the implementation of the additional restrictions is shown, for:

- Generators ramp rate limitation
- Participation factor recalculation in case of generator/load minimum/maximum active power injection/consumption limit reached
- Measurement cycle times, integration times and controller cycle time

To implement the generator ramp rate limiter, the new active power set-point must be compared with the set-point from the previous period and its difference compared to the generator limit (expressed in MW/min). If the difference is bigger than the limit then the new power set-point is adjusted to maximum allowable limit. The pseudo-code is as follows:

for every generation unit

if $(P_{new}^{gen} - P_{previous}^{gen}) > 0$ then

if $(P_{new}^{gen} - P_{previous}^{gen}) \cdot \frac{60}{\Delta t_{python}} > ramp_rate_up^{gen}$ then

$$P_{new}^{gen} = P_{previous}^{gen} + ramp_rate_up^{gen}$$

else

if $(P_{previous}^{gen} - P_{new}^{gen}) \cdot \frac{60}{\Delta t_{python}} > ramp_rate_down^{gen}$ then

$$P_{new}^{gen} = P_{previous}^{gen} - ramp_rate_down^{gen}$$

Where:

$P_{previous}^{gen}$ is the active power of the selected generation unit on previous time interval

$ramp_rate_up^{gen}$ is the ramp rate to increase active power for the selected generation unit

$ramp_rate_down^{gen}$ is the ramp rate to decrease active power for the selected generation unit

To create the participation factor recalculation method in case of generator/load minimum/maximum active power injection/consumption limit reached, when an AGC unit reaches a limit the participation factor of this unit is distributed evenly by the non-saturated units, as described below.

for every generation unit

read P_{now}^{gen} from PSS/E

if $\int ACE_{now} > 0$ then

if $P_{now}^{gen} = P_{max}^{gen}$ then

for every AGC participation unit/EV except saturated unit

$$PF_{gen/EV} = PF_{gen/EV} + \frac{PF_{gen}^{saturated}}{n_{not\ saturated}}$$

$$PF_{gen}^{saturated} = 0$$

else

if $\int ACE_{now} < 0$ then

if $P_{now}^{gen} = P_{min}^{gen}$ then

for every AGC participation unit/EV except saturated unit

$$PF_{gen/EV} = PF_{gen/EV} + \frac{PF_{gen}^{saturated}}{n_{not\ saturated}}$$

$$PF_{gen}^{saturated} = 0$$

for every EV

read P_{now}^{EV} from PSS/E

if $\int ACE_{now} < 0$ then

if $P_{now}^{EV} = P_{max}^{EV}$ then

for every AGC participation unit/EV except saturated unit

$$PF_{gen/EV} = PF_{gen/EV} + \frac{PF_{EV}^{saturated}}{n_{not\ saturated}}$$

$$PF_{EV}^{saturated} = 0$$

else

if $\int ACE_{now} > 0$ then

if $P_{now}^{EV} = P_{min}^{EV}$ then

for every AGC participation unit/EV except saturated unit

$$PF_{gen/EV} = PF_{gen/EV} + \frac{PF_{EV}^{saturated}}{n_{not\ saturated}}$$

$$PF_{EV}^{saturated} = 0$$

Where:

P_{now}^{gen} and P_{now}^{EV} are the current active power value for the selected generation unit/EV

P_{max}^{gen} , P_{min}^{gen} , P_{max}^{EV} and P_{min}^{EV} are the upper/lower limits of the participating generation units/EV

$PF_{gen}^{saturated} = 0$ and $PF_{EV}^{saturated} = 0$ are the participation factors of the generation unit/EV that has reached the limit

$n_{not\ saturated}$ is the number of generation units/EV that have not reached the limit

Finally, to include measurement cycle times, integration times and controller cycle time, additional delays have to be added to the code. Instead of reading the state variables, integrating and sending control actions to participating machines at the same moment a small delay is introduced to each of these actions. Each of the introduced delays is a function of Δt_{python} .

5.2.6 Case Studies

In this section, two case studies are presented. The first is used to test the EV droop control, whereas the second is used to validate the AGC implementation.

Primary Frequency Control

In order to test the developed algorithm, a small test network was modelled. Figure 5-44 presents the single line diagram of this islanded system.

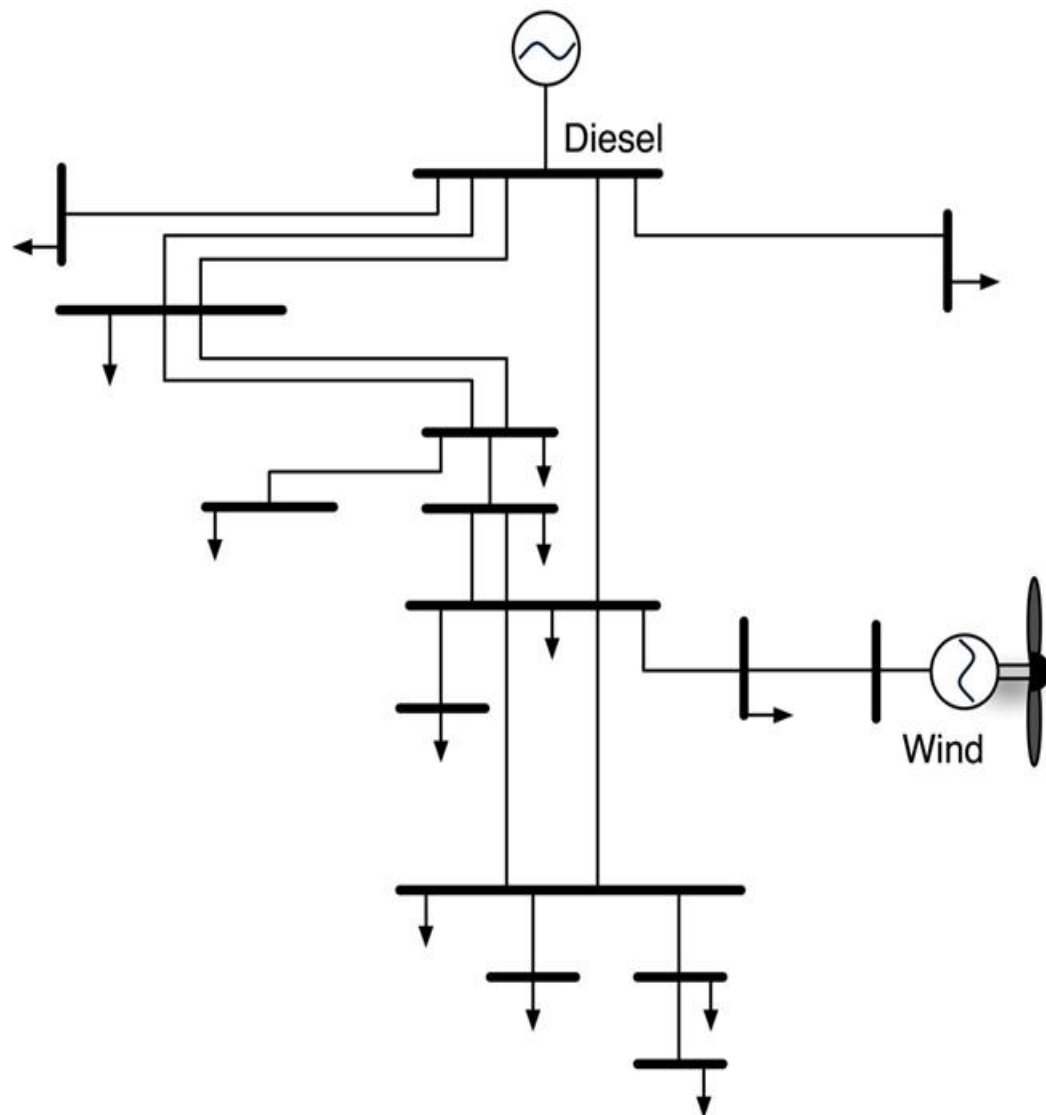


Figure 5-44 Isolated system single-line diagram

The period chosen to perform this study refers to a valley hour (5 a.m.), where wind power represents a considerable share in the electricity being generated. Such period was selected once it represents a worst case scenario for frequency deviation issues. Due to the system's high dependency on the wind power production, if a sudden decrease in wind speed occurs, system frequency might drop to risky levels. The wind profile considered to assess the dynamic behaviour of the islanded system is presented in Figure 5-45. As one can observe, in just 1 s, the wind speed suffers a change of 37%, falling from 9.5 to 6 m/s.

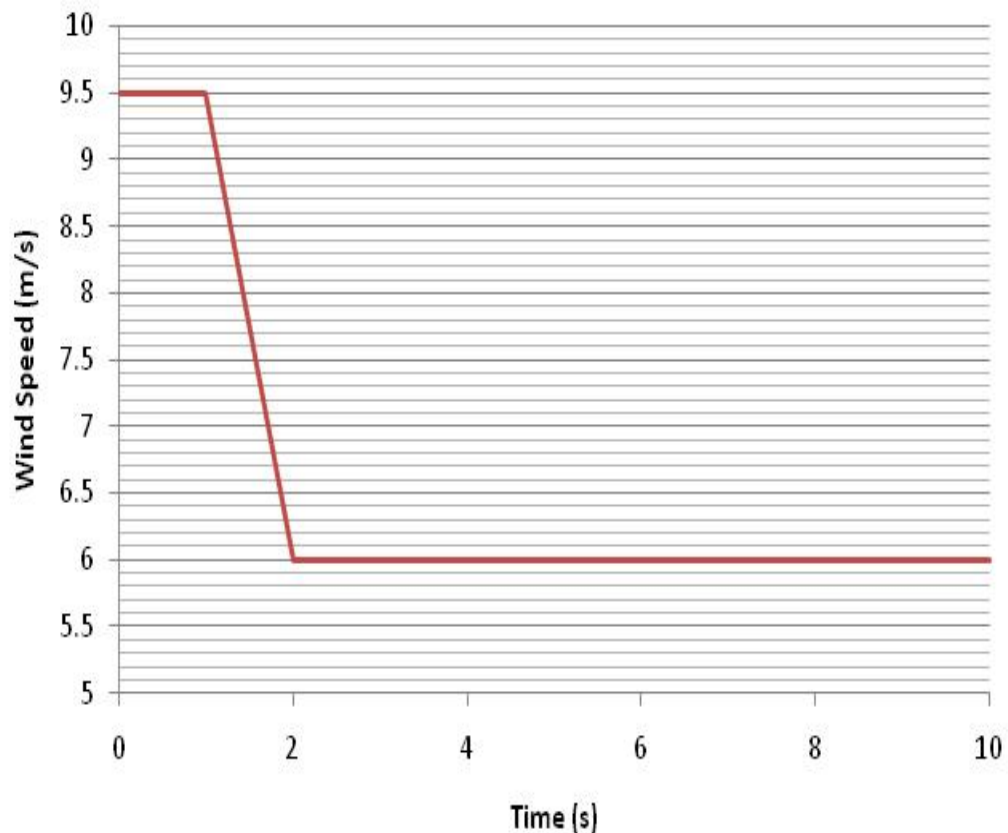


Figure 5-45 Wind speed profile

It was assumed a total number of 2150 vehicles on the island and, from these, 323 (15%) were assumed to be electric.

The EVs fleet considered includes plug-in hybrid vehicles and two types of full electric vehicles, each one of them with a different rated power charging: 1.5 kW for the hybrid, 3 kW for the medium sized EV and 6 kW for the large sized EV, [13]. The medium sized EV (EV1) and the large sized EV (EV2) intend to represent cars with different driving ranges developed by automotive manufacturers to face different customers' needs. The share of hybrid EVs was considered to be 40%, whereas the remaining 60% was equally split by EV1 and EV2. This distribution was chosen since it is almost certain that plug-in hybrid vehicles will start to be sold far before full electric vehicles.

The total load resulting from the EVs battery charging, at 5 a.m. and when the aforementioned smart charging strategy is considered, is of 402 kW (19% of the total), being the remaining conventional load of 1770 kW. It was assumed for the purpose of this study that the total instantaneous power that is available from EVs' batteries, connected to the grid at 5 a.m., either for injection or consumption is approximately 851 kW. This means that all the vehicles are in an intermediate state of charge.

Concerning generation capacity, the island contains 4 diesel generators (two with 1500 kW capacity and the other with 1800 kW), 100 kW of dispersed solar PV plants (which will not be taken into account in the studies performed since they are related to night period scenarios) and 2 wind turbines (with 660 kW each).

The following table shows the electric system's characterization, in terms of load and generation, for the test scenario (at 5 a.m.):

P_{Total load} (kW)	2172
P_{load} (kW)	1770
P_{EV load} (kW)	402
P_{EV available} (kW)	851
P_{wind} (kW)	900
P_{sync1} (kW)	636
P_{sync2} (kW)	636

Secondary Frequency Control

With the AGC algorithm created, a case study is needed to verify its correct implementation. Therefore, a test network that is available in the PSS/E example files was adopted, the savnw case. This is a 3 area transmission network with 21 buses and 6 generation units (2 per area). There are two voltage levels at the transmission level, 230 kV and 500 kV, and frequency is set to 60 Hz. The single line diagram is presented in the figure below.

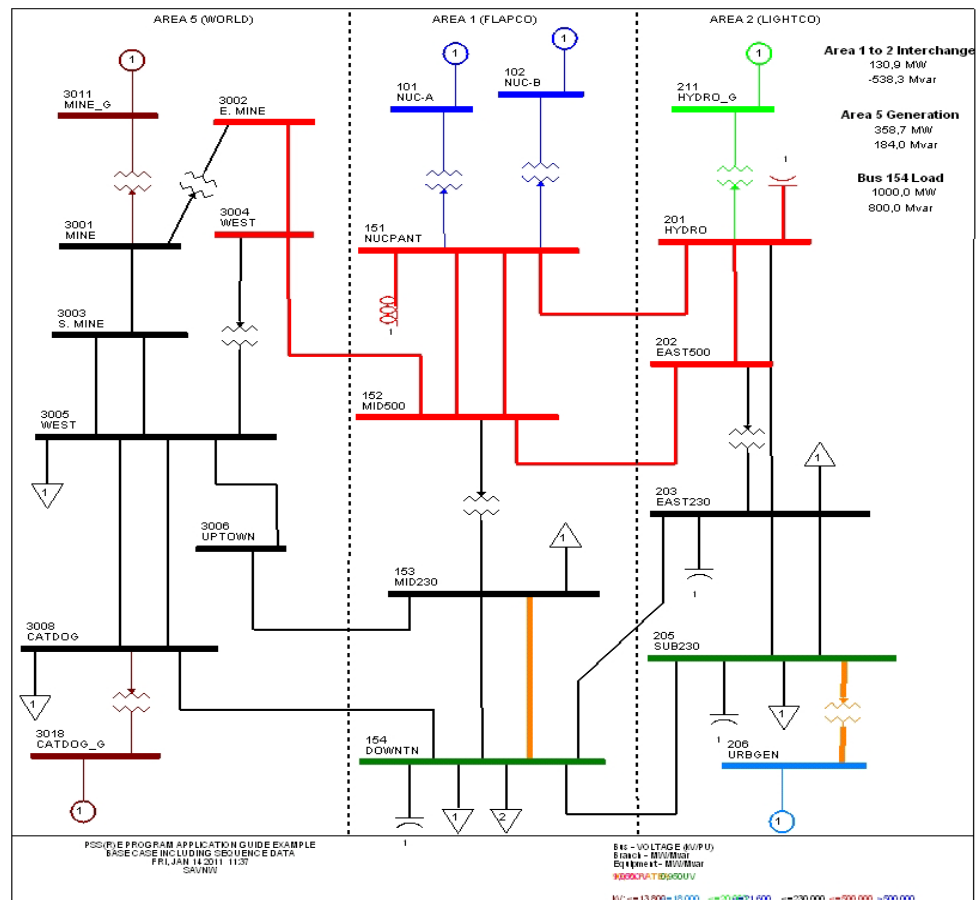


Figure 5-46 Single Line Diagram of the savnw Example Grid

This system has a total load of 3200 MW divided by each of the areas as follows:

Area		Load (MW)
Number	Name	
1	FLAPCO	1200
2	LIGHTCO	1500
5	WORLD	500

Regarding the existence of EV, it was considered that 20% of the load at each bus was due to the EV presence. Again, this part of the load was modelled as constant power, whereas the remaining 80% of conventional load were considered as constant admittance.

In terms of the generation system, the following table details the generators by primary resource, type, rated power, minimum/maximum active/reactive power, exciter type and governor. Only two generator types are considered: GENROU (round rotor generator) and GENSAL (salient pole generator). Three exciter types

are used: IEEE1 (IEEE Type 1 Excitation System), SCR (Bus Fed or Solid Fed Static Exciter) and SEXS (Simplified Excitation System). Two governor types, one per primary resource, are adopted: TGOV1 (Steam Turbine-Governor) and HYGOV (Hydro Turbine-Governor). The units of 5 are not equipped with a governor so that they will not react to frequency deviations. All the described models are explained in detail in the PSS/E model library manual, [14].

Bus	Area	Primary Resource	Rated power (MVA)	Pmin (MW)	Pmax (MW)	Qmin (MW)	Qmax (MW)	Generator	Exciter	Governor
101	1	Diesel/Fuel	900	0	810	-100	600	GENROU	IEEE1	TGOV1
102	1	Diesel/Fuel	900	0	810	-100	600	GENROU	IEEE1	TGOV1
206	2	Diesel/Fuel	1000	0	900	0	600	GENROU	IEEE1	TGOV1
211	2	Hydro	725	0	616	-100	400	GENSAL	SCR	HYGOV
3011	5	Diesel/Fuel	1000	0	900	-100	600	GENROU	SEXS	None
3018	5	Diesel/Fuel	130	0	117	0	80	GENROU	SEXS	None

The following steps to test the AGC implementation were to enable the developed model for areas 1 and 2 and to define a disturbance to force AGC operation. The load in bus 154 of area 1 was increased by 100 MW. Figure 5-47 presents the total load of the system during the simulation period. As the AGC action should be fully deployed in 15 minutes, the period chosen for simulation was 1100 s, providing 100 s of pre-disturbance period and 100 s after the maximum deployment period for the AGC.

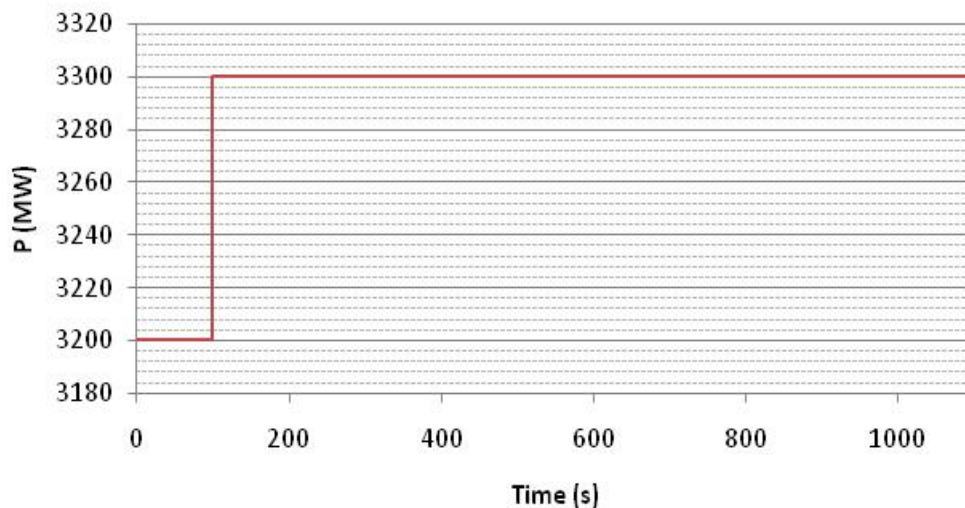


Figure 5-47 Defined System Disturbance for AGC Operation Testing Purposes

Having defined a disturbance, the case is ready for simulation. In the first simulation the AGC included EV in its operation (AGC with EV). Then, in order to compare responses, the conventional AGC architecture was adopted (AGC without EV).

Finally, the system was operated without AGC. A table with the participation factors is presented next for each scenario. EV participation factor is shown for global EV participation, due to the fact that it was evenly distributed between all EV.

Scenario	Area 1			Area 2		
	Machine		EV	Machine		EV
	101	102		206	211	
AGC with EV	0.05	0.05	0.9	0	0.1	0.9
AGC without EV	0.5	0.5	0	0	1	0
Without AGC	0	0	0	0	0	0

5.2.7 Results

In this sub-section, the results of the usage of the implemented algorithms on the described case studies, for:

- Primary frequency control;
- And, secondary frequency control.

Primary Frequency Control

Dynamic simulations were performed for the chosen scenarios, taking into account the wind power disturbance described in Figure 5-45.

Figure 5-48 shows that during the valley hours, when there are only two diesel units online, the system frequency drops to 49.40 Hz following the considered disturbance. In this case only the diesel units are responsible for frequency control. Nevertheless, if EVs participate in frequency control, not only will the frequency drop to a smaller value, 49.65 Hz, but also the pre-existing overshoot will cease to occur.

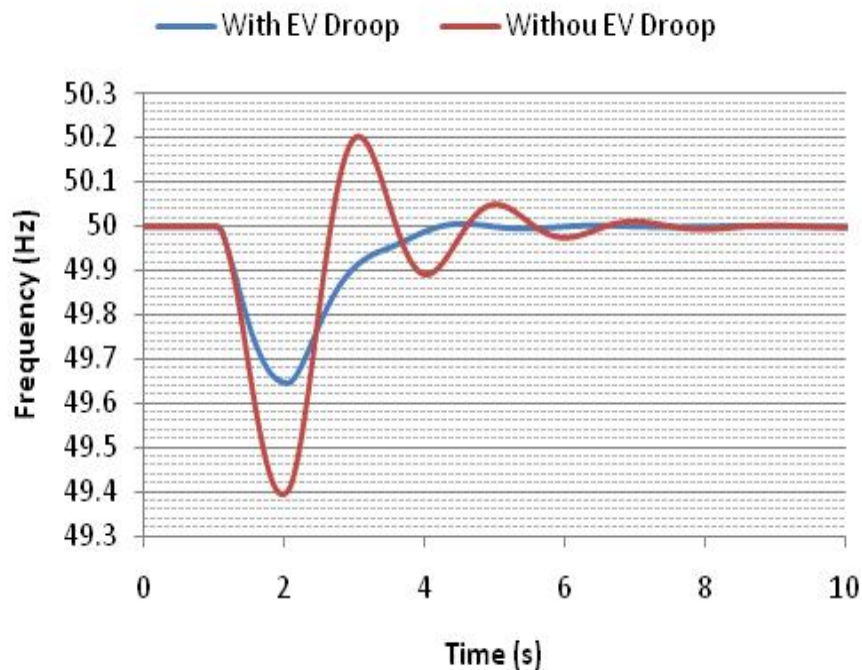


Figure 5-48 System frequency

Figure 5-49 to Figure 5-51 depict the active power behaviour of the several generation units that compose the local generation portfolio at the time of the shortfall on wind generation. When the diesel units are the only load followers frequency oscillations take place due to the integral control loop that tries to swiftly push frequency to its steady state value.

When EVs participate in frequency control then this under damping situation disappears as the inverters of EVs have very small delays, participating actively in the frequency control either by injecting or absorbing active power. So, EVs interfaced with smart grid interfaces bring stability to the system just by reducing their level of consumption from 401 kW to 141 kW. Another visible phenomenon is that when frequency starts to drop in both cases the system evolves equally. This is due to the dead band in the EVs droop control that avoids premature wear of the batteries but also prevents EVs reaction to smaller frequency deviations.

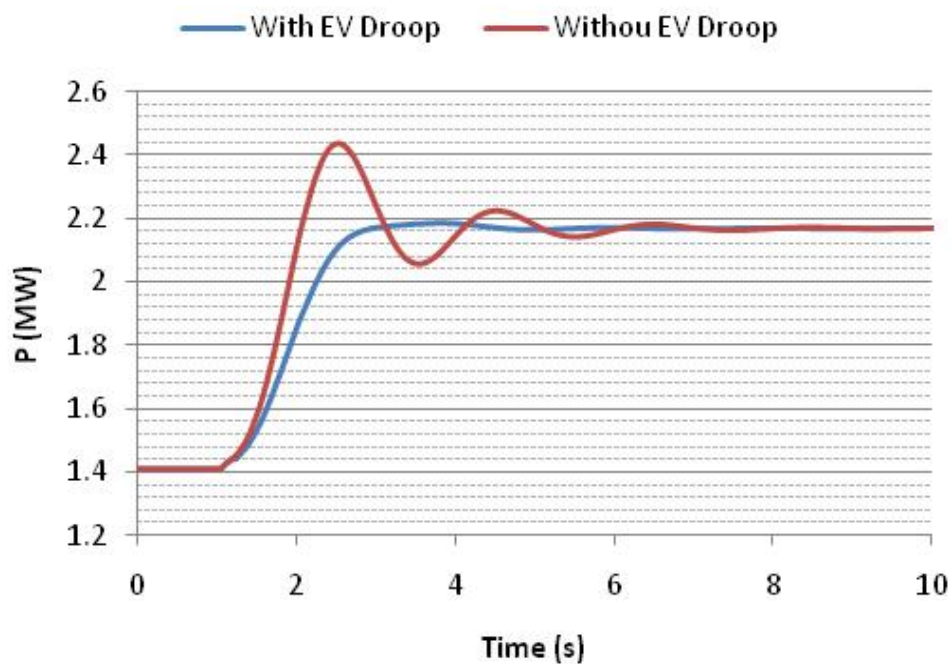


Figure 5-49 Diesel units active power

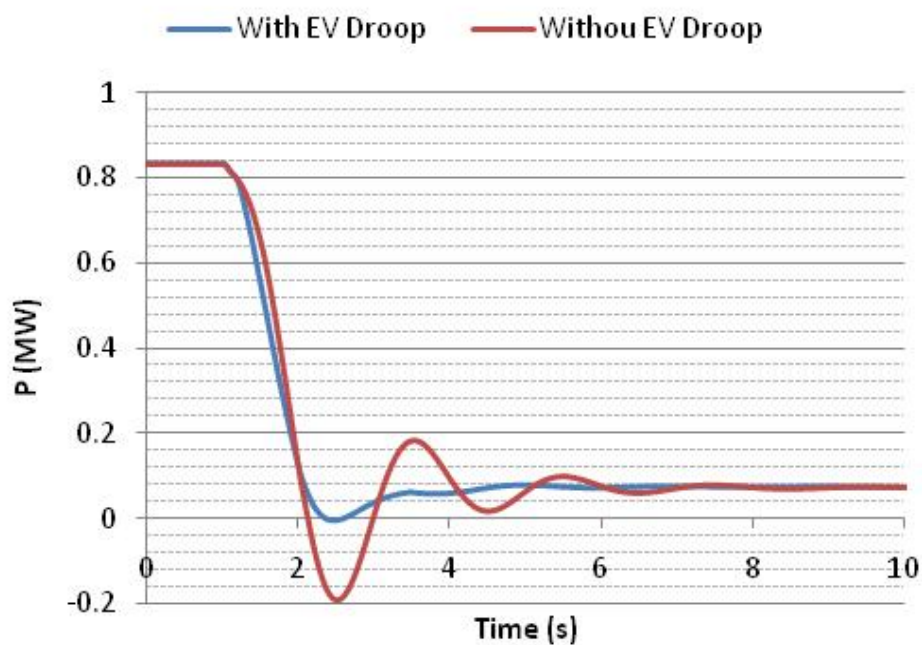


Figure 5-50 Wind generators active power

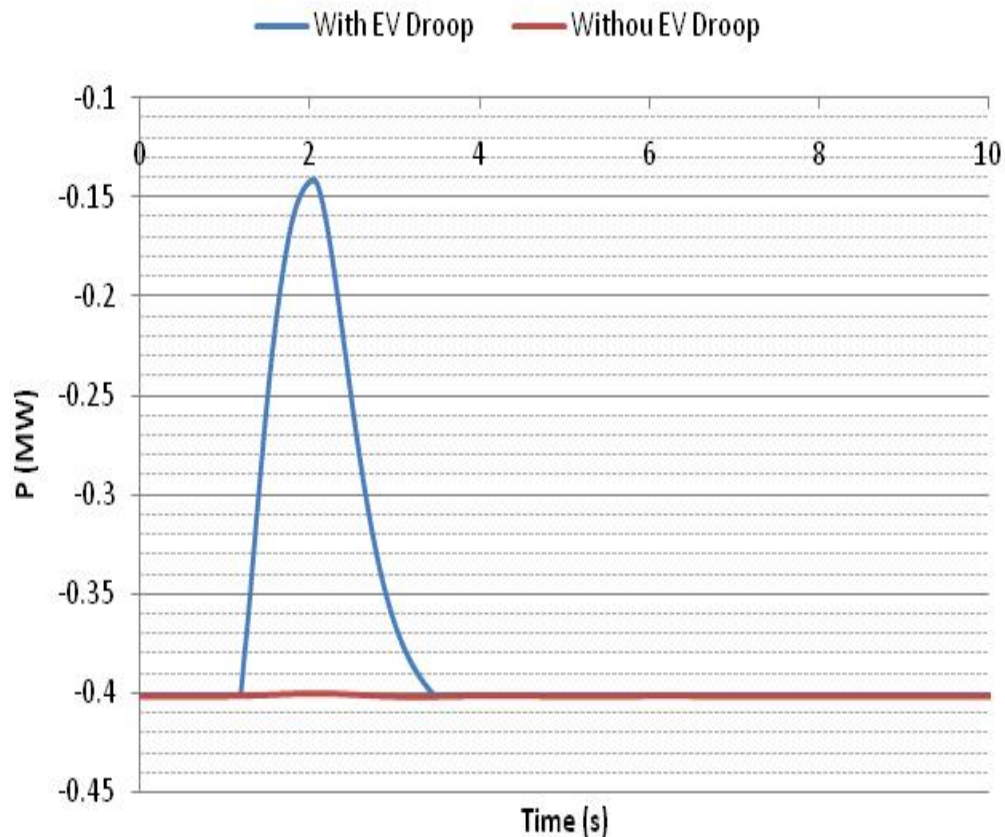


Figure 5-51 EVs active power

Secondary Frequency Control

In this sub-section sufficient results for the conducted studies will be presented, in order to validate the developed algorithm of the AGC.

Regarding control area 1, after the load increase, frequency dropped to 59.81 Hz, as depicted in Figure 5-52. Exclusively with the primary frequency control of the synchronous machines, frequency in post-disturbance stabilizes at 59.87 Hz. The conventional AGC, as well as the AGC with EV, manages to set frequency very close to its nominal value within the time period of 15 minutes (900 s). However, the AGC without EV is takes approximately 500 s more to enter the 0.01 Hz deviation band.

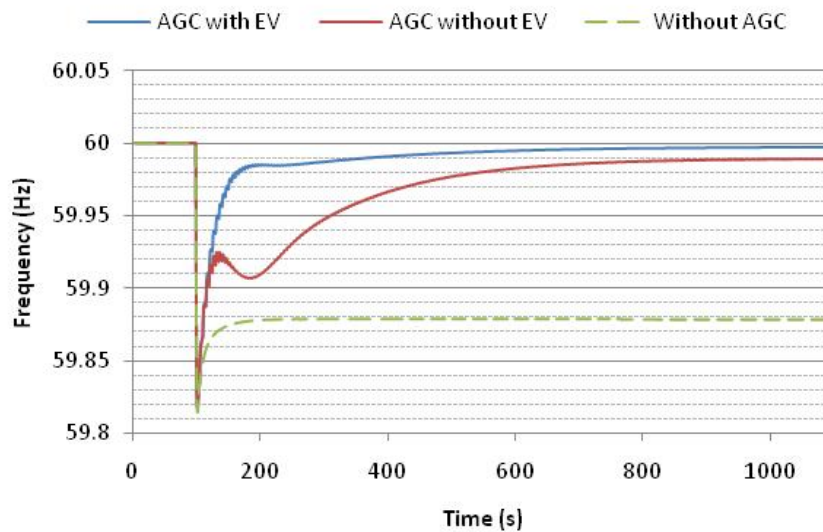


Figure 5-52 Frequency of Area 1

Concerning the interconnection power flow, Figure 5-53 shows that in the initial conditions area 1 was exporting to area 2 more or less 100 MW. As the load increase occurred in area 1, then if AGC is not present, this value is reduced to 10 MW. Using AGC the interconnection power flow is restored within 200 s after the disturbance. When EV are present the controller reaction is smoother.

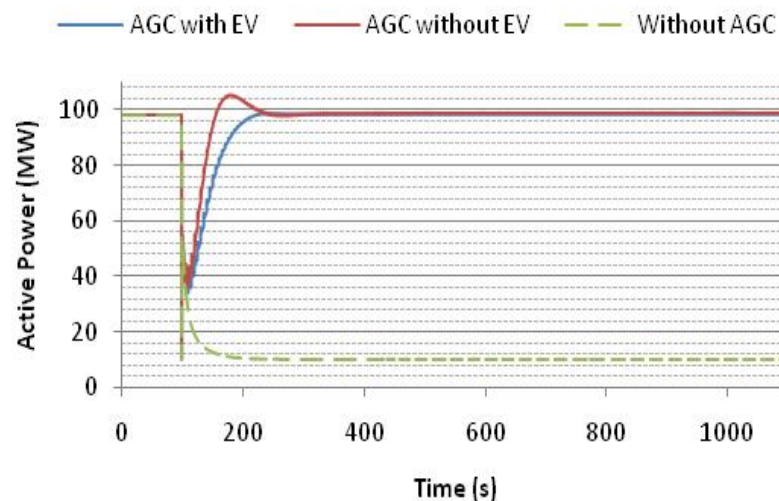


Figure 5-53 Interconnection Active Power Flow of Area 1

Looking at frequency in area 2, Figure 5-54 shows that there are no noticeable differences between the value of this area and that of area 1.

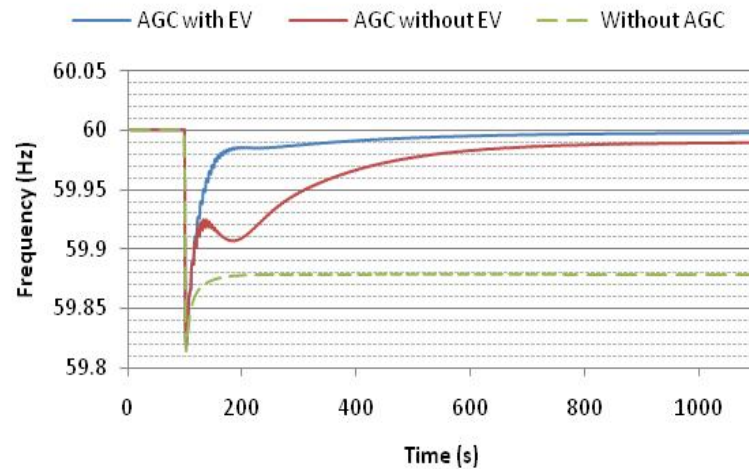


Figure 5-54 Frequency of Area 2

Figure 5-55 presents the interconnection power flow from area 2 to area 1. Area 2 in the pre-disturbance period was importing roughly 93 MW of active power. This value differs from that found in area 1 export due to the losses in the tie-lines. Apart from this fact the reaction is very close to that observed previously and if no AGC would exist, then the import value would tend to decrease and stabilize at a value below 10 MW.

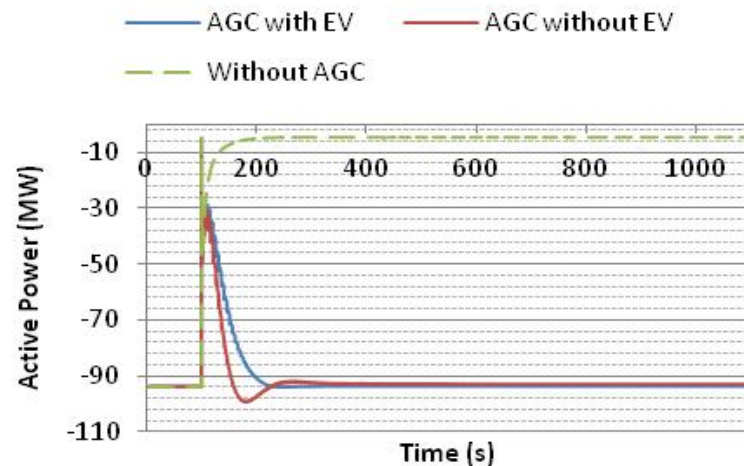


Figure 5-55 Interconnection Active Power Flow of Area 2

Figure 5-56 provides the global contribution of EV load for the AGC operation. It is noticeable that when EV participate in AGC the largest part of their load reduction occurs before 100 s of post-disturbance analysis. If EV do not participate in AGC or if AGC is not working, then EV load remains unchanged, not reacting to systems state variables.

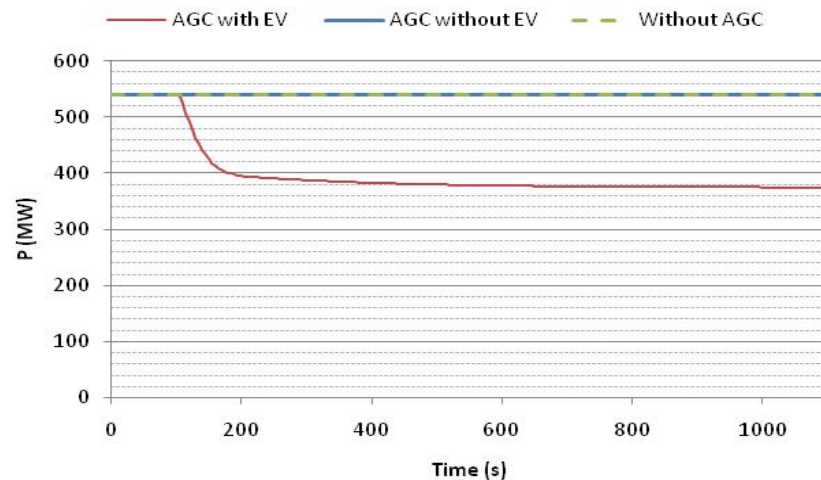


Figure 5-56 Total EV Load

The individual behaviour of EV per bus (in the case of AGC with EV) is illustrated in Figure 5-57. The initial reaction of EV is ensured by those located in area 1. Only after some time, the EV from area 2 proceeded with minor load changes. This happens because the initial integral of the ACE in area 1 demands an increase in generation or reduction on load, whereas on area 2 the demand is on the opposite direction and EV cannot increase their load consumption.

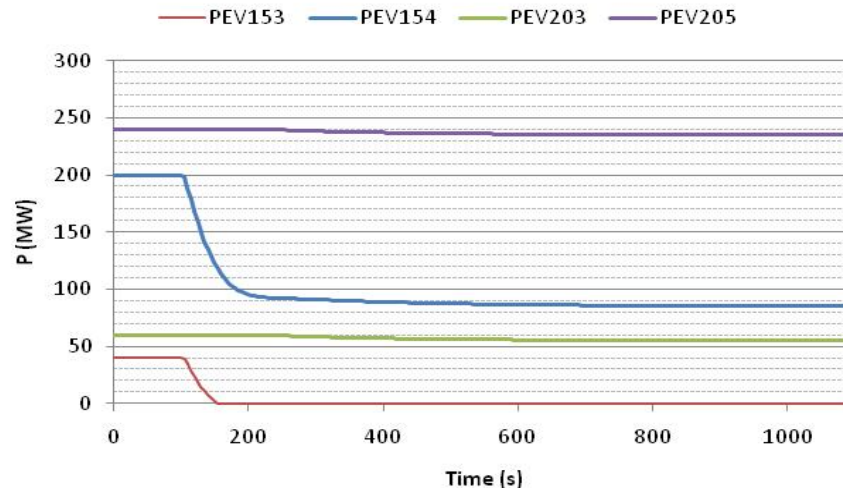


Figure 5-57 Individual EV Load in the Scenario AGC with EV

Concerning the machines of area 1, as their participation factors were equal, their contribution tends to be very similar in all studied cases. If their initial operating point would be the same then their reaction to the disturbance would be exactly the same. Figure 5-58 and Figure 5-59 present this effect and also show that when EV are used in AGC operation the machines almost return to their original operation state. Such situation is a direct consequence of the value of the participation factors

attributed to the machines and to EV. As global EV participation factor is 9 times greater than that attributed to machines 101 and 102 together, EV load is forced to correct the greatest part of the error.

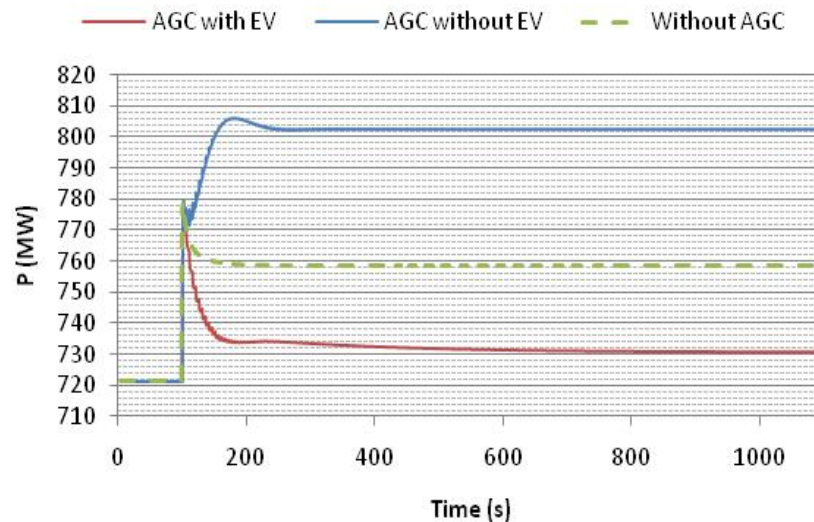


Figure 5-58 Active Power Generated by Machine 101 of Area 1

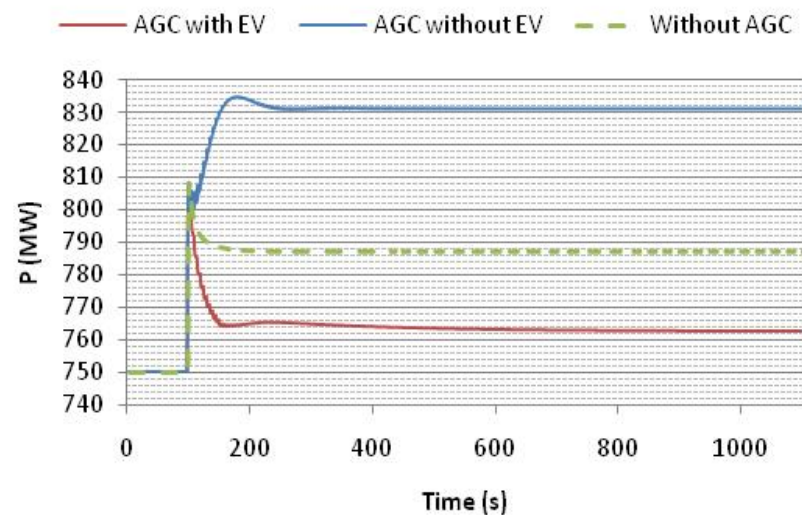


Figure 5-59 Active Power Generated by Machine 102 of Area 1

Regarding the machines of area 2, Figure 5-60 and Figure 5-61 show their reaction. As EV of area 2 did not react much to the disturbance, the final post-disturbance value is very similar in both AGC with and without EV. As the participation factor of machine 206 is set to 0, the participation of this machine tends to 0 and its final

value tends to the original active power generation. Although the effect of EV in this area is not so visible, the AGC with EV is much smoother and the requests to the machines are not so harsh.

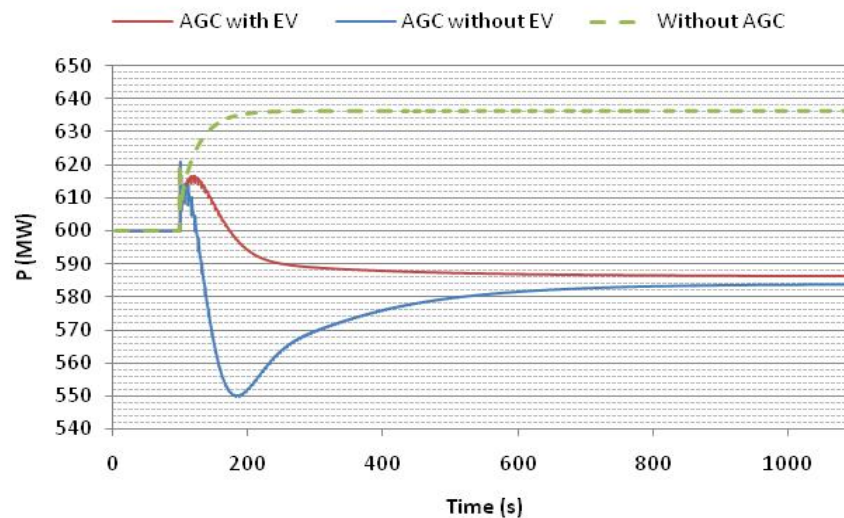


Figure 5-60 Active Power Generated by Machine 211 of Area 2

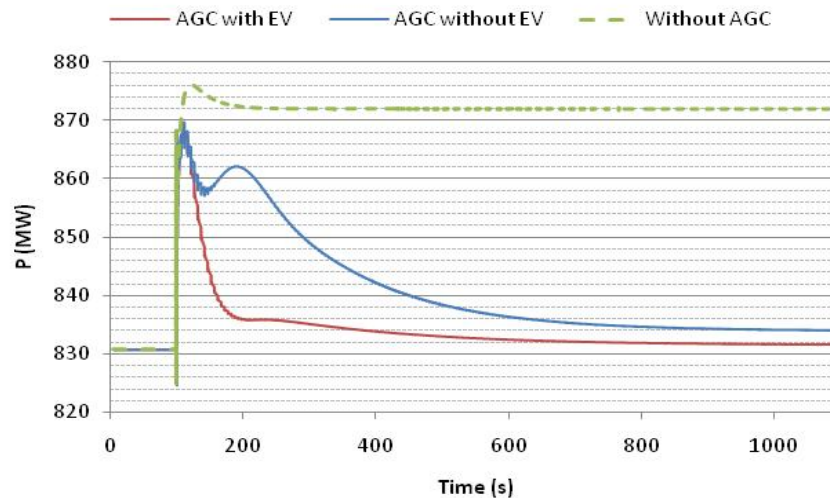


Figure 5-61 Active Power Generated by Machine 206 of Area 2

Finally, the results presented are consistent with what was expected and evidence a careful implementation of the envisioned algorithm. In this case study different conditions were explored, such as equally and unequally divided participation factors, distinct machine types, with and without the presence of EV and with and without the existence of AGC. These situations indicate that the algorithm is resilient and prepared to analyze bigger dimension networks with greater complexity.

5.3 References

- [1] . A. P. Lopes, F. J. Soares, P. M. R. Almeida, "Identifying management procedures to deal with connection of Electric Vehicles in the grid," PowerTech, 2009 IEEE Bucharest, vol., no., pp.1-8, June 28 2009-July 2 2009.
- [2] J. A. Peças Lopes, F. J. Soares, P. M. Rocha Almeida, "Integration of Electric Vehicles in the Electric Power System", Proceedings of the IEEE, vol. 99, no. 1, pp. 168–183, Jan. 2011.
- [3] K. Clement-Nyns, E. Haesen, J. Driesen, "The Impact of Charging Plug-In Hybrid Electric Vehicles on a Residential Distribution Grid," Power Systems, IEEE Transactions on, vol.25, no.1, pp.371-380, Feb. 2010.
- [4] F. J. Soares, J. A. Peças Lopes, P. M. Rocha Almeida, "A Monte Carlo Method to Evaluate Electric Vehicles Impacts in Distribution Networks", 2010 IEEE Conference on Innovative Technologies for an Efficient and Reliable Electricity Supply, Boston, USA, September, 2010.
- [5] N. Downing, M. Ferdowsi, "Specifications for EV-Grid Interfacing, Communication and Smart Metering Technologies, Including Traffic Patterns and Human Behaviour Descriptions", Deliverable D1.1, EU MERGE Project, April, 2010.
- [6] "Extend Concepts of MG by Identifying Several EV Smart Control Approaches to be Embedded in the Smartgrid Concept to Manage EV Individually or in Clusters", EU MERGE Project, Deliverable D1.2, June, 2010.
- [7] EN 50160:2007, "Voltage characteristics of electricity supplied by public distribution systems", European Committee for Electrotechnical Standardization – CENELEC.
- [14] "Extend Concepts Of Mg By Identifying Several Ev Smart Control Approaches To Be Embedded In The Smartgrid Concept To Manage EV Individually Or In Clusters" Deliverable D1.2, MERGE Project, June 2010
- [15] UCTE, "Operation Handbook", March 2009, [online] available: <https://www.entsoe.eu/resources/publications/former-associations/ucte/operation-handbook/> [accessed 15 January 2011]
- [16] Kundur, P., "Power Systems Stability and Control", Electric Power Research Institute, McGraw Hill, 1994
- [17] AGM Battery Technology (2004) "Product Datasheet", Lithium-ion Cell ICR34490HC [online] available: <http://www.agmbatteries.com/documents/ICR34490HC.pdf> [accessed 15 January 2011]
- [18] Siemens PTI, "Volume II: Program Application Guide", PSS®E 32.0.5, October 2010



- [19] W. Kempton, T. Kubo, "Electric-drive vehicles for peak power in Japan", Energy Policy, vol. 28, pp. 9-18, January 2000
- [20] Siemens PTI, "PSS®E Model Library", PSS®E 32.0.5, October 2010



6 PROBABILISTIC AND FUZZY POWER FLOW PLATFORM

Computation of power flows in the electric power system is one of the major tasks facing power system planners and operators. All types of computations involve evaluations of currents and voltages at specified locations under predetermined power system conditions. The power system conditions prevailing at a given time in the future cannot be specified precisely, it is quite obvious that performing power system studies for a specified set of conditions can, at best, give us only a feel for the situation which will be actually realized in the future. Apart from the deterministic simulations used to address steady impacts resulting from the presence of EV on the network for extreme conditions (WP3), an evaluation of the ranges of power flows, voltages levels and losses in the transmission network is needed when large variations of EV penetration and the use of different charging strategies takes place, leading to significant uncertainty in node injections. In order to tackle this issue, in a situation characterized by lack of relevant statistical information regarding EV behaviour, probabilistic and fuzzy modelling techniques are applied. For this purpose, INESC Porto adapted and enhanced its fuzzy power flow tool to cope with EV nodal loads in a way that the important dependencies among EV load uncertainties in the nodes was taken into consideration. Besides propagating the uncertainties from the data to the results, providing fuzzy descriptions of the branch flow, node voltages and losses, the tool is able to identify the risk of congestion in branches and the degree of repression in the node injections and in the system. ICCS/NTUA similarly adapted its probabilistic load flow tools to provide probabilistic density functions of flows, voltages and losses.

6.1 Probabilistic Power Flow Platform

All the basic variables entering power system studies can actually be represented as random variables. Available generation is often represented as a discrete random variable, as is the configuration of the transmission system, whereas the load is modelled as a continuous random variable. Therefore, the computed quantities such as power flows and voltages are also random variables. Performing probabilistic power system studies gives us, at least, a better feel for future system conditions and will provide more confidence in making judgments concerning investment and operating decisions [1], [2].

In this work a Probabilistic Load Flow tool is constructed in order to provide Probabilistic Density Functions (PDF) of branch power flows, node voltages and active power line losses with large variations of Electric Vehicles (EV) and Renewable Energy Resources (RES) integration. As a case study, the large distribution power system of Greece with high integration of RES and EV using PLF techniques is examined. When different charging strategies of EV (for example: dump charging, dual tariff policy) take place then lead to significant uncertainty in node injections. Two methods are investigated for the calculation of PDF of RES production, Gram–Charlier and Cornish–Fisher. All the PLF results are compared with Monte Carlo (MC) method. Promised results are gained.

6.1.1 Description of the Probabilistic Power Flow

Deterministic Load Flow (DLF) Equations

The Load Flow (LF) study performs the steady state simulation of the power system. The input data usually include real and reactive loads at load buses, as well as real power generation and voltage magnitude at generating buses. The computed quantities are voltage magnitudes and angles at the load buses, angles and reactive power requirements at the generating buses, and active and reactive power flows in the transmission lines.

There are many methods of calculating the load flows in power systems, differing in computing speed, accuracy, and computer storage requirements. Some of them are: Newton-Raphson, Gauss-Seidel, Fast Decoupled, DC etc., [2], [3]. The LF equations can be written in a general form, namely:

$$\mathbf{Y} = \mathbf{g}(\mathbf{X}) \quad (6-1)$$

where \mathbf{Y} represents the measured quantities, \mathbf{X} is the state vector representing quantities to be computed, and \mathbf{h} is a set of nonlinear functions.

The exact non-linear form of LF equations with reference to Figure 6-1, are:

$$P_i = U_i \sum_{k=1}^n U_k (G_{ik} \cos \theta_{ik} + B_{ik} \sin \theta_{ik}) \quad (6-2)$$

$$Q_i = U_i \sum_{k=1}^n U_k (G_{ik} \sin \theta_{ik} - B_{ik} \cos \theta_{ik}) \quad (6-3)$$

$$P_{ik} = -t_{ik} G_{ik} U_i^2 + U_i U_k (G_{ik} \cos \theta_{ik} + B_{ik} \sin \theta_{ik}) \quad (6-4)$$

$$Q_{ik} = t_{ik} B_{ik} U_i^2 - B'_{ik} U_i^2 + U_i U_k (G_{ik} \sin \theta_{ik} - B_{ik} \cos \theta_{ik}) \quad (6-5)$$

$$Q_{i(sh)} = U_i^2 B_{i(sh)} \quad (6-6)$$

where P_i and Q_i are the net active and reactive power injection at bus i ; P_{ik} and Q_{ik} are the active and reactive power flows in line $i-k$ at the bus i side; U_i and U_k are the voltage magnitude at bus i and k ; θ_{ik} is the angle difference between the voltages at bus i and k ; G_{ik} and B_{ik} are the real and imaginary part of the corresponding admittance matrix; t_{ik} is the transformer tap ratio and $B'_{ik} = 0.5B_{ik}$.

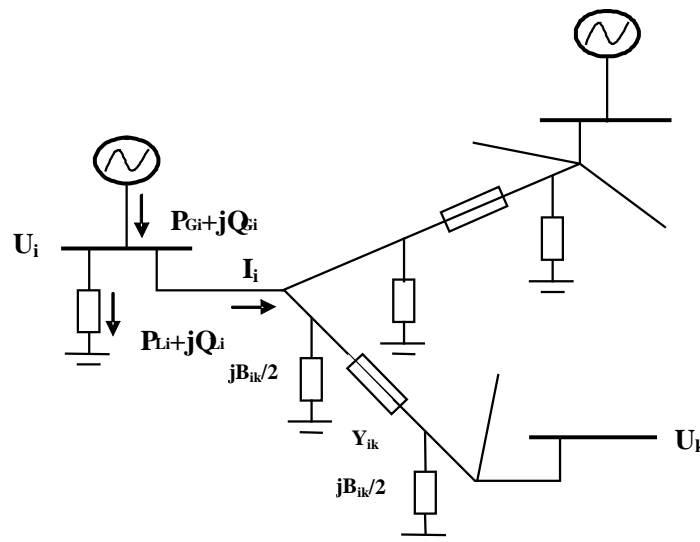


Figure 6-1 Network for the derivation of LF equations [1]

The Probabilistic Load Flow Problem

The DLF is used to analyze and assess the planning and operating of power systems on a daily routine. DLF uses specific values of power generations and load demands of a selected network configuration to calculate system states and power flows. Therefore, DLF ignores uncertainties in the power systems, e.g. the outage rate of generators, the change of network configurations and the variation of load demands.

Furthermore, modern power systems with integration of Dispersed Generation (DG) units, such as Wind Turbines (WTs), Photovoltaic Systems (PV), and Electric Vehicles (EV) introduce additional power fluctuations into the system due to their uncontrollable prime sources. Therefore, the deterministic approach is not sufficient for the analysis of modern power systems and the results from DLF may give an unrealistic assessment of the system performance.

In order to take the uncertainties into consideration, different mathematical approaches for uncertainty analysis can be used. The probabilistic approach has a solid mathematical background and has been applied to power systems in different areas.

The PLF was first proposed in 1974, and has been further developed and applied into power system normal operation, short-term/long-term planning as well as other areas [4]. The PLF requires inputs with PDF or Cumulative Density Function (CDF) to obtain system states and power flows in terms of PDF or CDF, so that the system uncertainties can be included and reflected in the outcome [5], [6].

Many PLF methods have been proposed to study load flow uncertainty problem, [1], [7], [8]. These methods can be classified into two categories: numerical approach and analytical approach.

Objectives

With the introduction of electric vehicles (EVs) into the transport system, the energy sector (mainly the electric power system) will suffer a dramatic change due to this important and expected issue. In this work a Probabilistic Load Flow tool (written in Matlab program) is constructed in order to provide Probabilistic Density Functions (PDF) of branch power flows, node voltages and active power line losses with large variations of Electric Vehicles (EV) and Renewable Energy Resources (RES) integration. As a case study, the large distribution power system of Greece with high integration of RES and EV using PLF techniques is examined. When different charging strategies of EV take place then lead to significant uncertainty in node injections. Promised results will be gained.

Approach

Probabilistic Load Flow methods can be classified into two categories: numerical approach and analytical approach.

Numerical Approach

The numerical approach adopts a Monte Carlo (MC) method for the PLF analysis. The two main features of MC simulation are random number generation and random sampling [6], [9], [10]. Software such as Matlab provides algorithms for pseudorandom number generation. Although sampling techniques can be rather sophisticated, the PLF using MC is in principle doing DLF for a large number of times with inputs of different combinations of nodal power values.

Analytical Approach

Stochastic Load Flow (SLF)

One approach, often referred to as SLF, uses a state estimator type algorithm, with the a posteriori (past or present measurement data) uncertainly problem redefined to represent long term a priori (future planning) uncertainties. In essence, it assumes that the long term nodal generation/load vector \mathbf{Y} varies about an expected operating point. Equation (3.5.1-1) is then written in the form:

$$\mathbf{Y} = g(\mathbf{X}) + \mathbf{n} \quad (6-7)$$

where \mathbf{n} is a random noise vector whose covariance defines the variations of the power injections about their base case mean values. The object of the SLF analysis is to obtain the covariance matrix and the 'best' estimates of the state vector and line flows. The stochastic algorithm is easily built from existing state estimator algorithms, but the drawbacks of the SLF is that it handles only Gaussian nodal PDF data for practical system sizes, [11], [12], [13].

Probabilistic Load Flow (PLF)

Another approach, commonly referred to as Probabilistic Load Flow (PLF) algorithm, uses linear or quadratic approximations of equations (6-1). With these approximations, equations (1) is solved for \mathbf{X} in a direct fashion and the probability density function (PDF) of \mathbf{X} (or its moments) is obtained from the given probabilistic

description of **Y**. The price we pay for the ability to obtain the PDF of **X** is the simplification of the LF equations (and, hence, presumably less accurate solution vectors). In addition, it has been necessary to assume, for realistic system sizes, that the nodal power injections are independent in order to be able to apply convolution techniques (Fast Fourier Transform – FFT, etc.), [14], [15], [16], [17]. However, the difficulties of solving PLF equations by the convolution of PDFs of input power variables are mainly twofold:

- LF equations (6-2)-(6-6) are non-linear
- Input power variables at different buses are usually not completely independent of or linear-correlated. Therefore, a number of assumptions are usually made to be able to perform the PLF easily using an analytical approach. These assumptions are:
 - Linearization of LF equations,
 - Total independent or linear-correlated power variables,
 - Normal distribution and discrete distribution are usually assumed for the load and generation, respectively,
 - Network configuration and parameter are constant.

Mathematical Formulation for the PLF

For PLF analysis, the various quantities in the below mathematical formulation are related with power system load flow problem. The various quantities in below equations are defined in terms of load flow quantities as:

Y: Load flow data

X: Bus state variables V and θ

J: Jacobian of load flow equation

Z: Output quantities of load flow computed from **X** e.g. line flows

K: Jacobian of output quantities **Z** with respect to load flow variables **X**

Specifically the load flow problem can be described mathematically by two sets of non-linear equations, [6-1], [6-4], [18].

$$\mathbf{Y} = \mathbf{g}(\mathbf{X}) \quad (6-8)$$

$$\mathbf{Z} = h(\mathbf{X}) \quad (6-9)$$

where \mathbf{Y} represents the injected active powers at all busbars (PQ and PV) and the injected reactive powers at load busbars (PQ). The state vector \mathbf{X} represents the voltage angle and magnitude. Finally, the random vector \mathbf{Z} represents all the parameters that can be obtained from the state vector, such as active and reactive flows, losses, etc.

Let \mathbf{Y}_0 , be the expected value of the input random variable \mathbf{Y} and \mathbf{X} such that it satisfies the following equation:

$$\mathbf{Y}_0 = g(\mathbf{X}_0) \quad (6-10)$$

In the same way, vector \mathbf{Z}_0 is an approximation for the expected value of \mathbf{Z} and must satisfy the following equation:

$$\mathbf{Z}_0 = h(\mathbf{X}_0) \quad (6-11)$$

Linearising equations (6-8) and (6-9) by Taylor's series expansion around the points $(\mathbf{Y}_0, \mathbf{X}_0)$ and $(\mathbf{Z}_0, \mathbf{X}_0)$, called the region of the expected value gives:

$$\mathbf{Y} \approx \mathbf{Y}_0 + \mathbf{J}(\mathbf{X} - \mathbf{X}_0) \quad (6-12)$$

$$\mathbf{Z} \approx \mathbf{Z}_0 + \mathbf{K}(\mathbf{X} - \mathbf{X}_0) \quad (6-13)$$

When the load flow equations are linearized around the expected value region, the information around this region will be mapped more accurately than in any other region. The same concept can be applied to any other point of linearization and the information obtained around this point would be the most accurate, [19], [20]. Therefore, the combination of different points of linearization achieves a very good approach of the PLF. The main advantage of the analytical methods is to avoid the computer simulation, but more assumptions and complex mathematical algorithms are required for these methods.

In the DLF solved by using Newton-Raphson method, the Jacobian matrix \mathbf{J} is also computed for each iteration until errors of the results are less than specified values. However, in the PLF here, the Jacobian matrix is only computed once for the computation of each LF. Therefore, errors caused by the linearization of LF equations should be noted and taken care of. Equation (6-12) shows that the system states are expressed by a linear combination of input power variables. With the assumption of independence, a convolution technique can then be applied to derive the PDFs of system states \mathbf{X} , which is:

$$f(\mathbf{X}_i) = f(\mathbf{Y}_1 - \mathbf{Y}_{10}) * f(\mathbf{Y}_2 - \mathbf{Y}_{20}) * \dots * f(\mathbf{Y}_n - \mathbf{Y}_{n0}) \quad (6-14)$$

Comparison between Methods of PLF

One practical way of comparing the linear model and the exact one is through a Monte Carlo Simulation (MCS) which consists of running and processing probabilistically several cases of individual load flows where the inputs are generated by pseudo-random numbers. Therefore, Monte Carlo solutions for both the linearised and exact models are computed for comparison.

The PLF can be solved numerically, i.e. using a Monte Carlo (MC) method, or analytically, e.g. using a convolution method, or a combination of them. The main concern about the MC method is the need of large number of simulations, which is very time-consuming; whereas the main concerns about the analytical approach are the complicated mathematical computation and the accuracy due to different approximations.

Methods for the Calculation of the PDFs

Two of the most common analytical methods are used to approach the PDF of random variables in this work. Both of them use the concept of cumulants and the normal distribution. The advantage of the methods is that they avoid the complex convolution calculations.

Gram-Charlier Expansion

This method combines the concept of Cumulants and Gram-Charlier expansion theory to compute the PDF and CDF of power system variables in a systematic way and with one run. This method significantly reduces the storage since low order Gram-Charlier expansion is able to achieve enough accuracy to approximate PDF and CDF of power system variables. Therefore, it is able to handle large practical systems. Study results have shown that this method can calculate the probability distribution accurately with much less computation effort. The procedure for the calculation of PDFs and CDF using Gram – Charlier method is described in [21]. According to Gram – Charlier expansion, the density functions can be written as:

$$f(x) = \phi(x) + \frac{c_1}{1!}\phi'(x) + \frac{c_2}{2!}\phi''(x) + \frac{c_3}{3!}\phi'''(x) + \dots \quad (6-15)$$

where $\phi(x)$ represents the PDF of normal distribution with $m=0$ and $\sigma=1$; c_i are constant coefficients.

Cornish-Fisher Expansion

The Cornish – Fisher expansion provides an approximation of a quantile α of a distribution function $F(x)$ in terms of the quantile of a normal $N(0,1)$ distribution Φ and the cumulants of $F(x)$. Using the first cumulants, the expansion is:

$$\begin{aligned} x = z &+ \frac{1}{6}(z^2 - 1)\kappa_3 + \frac{1}{24}(z^3 - 3z)\kappa_4 - \frac{1}{36}(2z^3 - 5z)\kappa_3^2 + \frac{1}{120}(z^4 - 6z^2 + 3)\kappa_5 \\ &- \frac{1}{24}(z^4 - 5z^2 + 2)\kappa_3\kappa_4 + \frac{1}{324}(12z^4 - 53z^2 + 17)\kappa_3^3 - \frac{1}{384}(3z^5 - 24z^3 + 29z)\kappa_4^2 \\ &+ \frac{1}{288}(14z^5 - 103z^3 + 107z)\kappa_3^2\kappa_4 - \frac{1}{7776}(252z^5 - 1688z^3 + 1511z)\kappa_3^4 + \dots \end{aligned} \quad (6-16)$$

where $x=x(\alpha)=F^{-1}(\alpha)$ and $z=z(\alpha)=\Phi^{-1}(\alpha)$ and κ_r is the cumulant of order r of the distribution function F . Although the convergence properties of Cornish – Fisher series are difficult to demonstrate, and are somehow related to Gram – Charlier series, their behavior for non-Gaussians PDF is better than the latter. The procedure

for the calculation of PDFs and CDFs using Cornish – Fisher method is described in [22], [23].

DESCRIPTION OF THE PLF MODEL

In this unit, the PLF tool will be described, along with the details of input and output data. Some initial information is:

- **Written in:** Matlab program.
- **Input Data**
 - Grid data (Buses data, Lines Data),
 - Wind [25] and PV power data,
 - Conventional generation data,
 - Power load demand data,
 - EV data.
- **The program uses the AC load flow equations, which means that all the variables of the system are available.**
- **Output Data PDF of:** voltages, angles, active and reactive power flows in lines, active power losses. The output data contains a set of results represented by PDFs of variables for a given pre-determined network and system configuration, allowing the Transmission System Operator (TSO) to analyze the power grid operation conditions for the different feasible generation and load scenarios. With these results, it becomes possible to easily identify possible voltage violations in buses and possible congestions in the network branches, helping the TSO to evaluate and analyze for example the risk of congestion.

Data Preparation

In order to perform a probabilistic power flow analysis by the Newton-Raphson method in the MATLAB environment, the following variables must be defined [2]:

- power system base MVA,
- power mismatch accuracy,
- acceleration factor, and
- maximum number of iterations.

In addition, the following data files are required.

Bus Line Data File: Busdata Matrix

The format for the bus entry is chosen to facilitate the required data for each bus in a single row. The information required must be included in a matrix called Busdata_Matrix. Column 1 is the bus number. Column 2 contains the bus code (1: slack bus, 0: PQ buses, 2:PV buses). Columns 3 and 4 are voltage magnitude in per unit and phase angle in degrees. Columns 5 and 6 are load MW and MVar. Columns 7 through 10 are MW, MVar, minimum MVar and maximum MVar of generation, in that order. The last column is the injected MVar of shunt capacitors.

Bus Line Data File: Linedata Matrix

Lines are identified by the node-pair method. The information required must be included in a matrix called Linedata_Matrix. Columns 1 and 2 are the line bus numbers. Columns 3 through 5 contain the line resistance, reactance, and one-half of the total line charging susceptance in per unit on the specified MVA base. The last column is for the transformer tap setting; for line, 1 must be entered in this column. The lines may be entered in any sequence or order with the only restriction being that if the entry is a transformer, the left bus number is assumed to be the tap side of the transformer.

Probabilistic Bus Data

The introduction of probabilistic data for the following units: Photovoltaics (PV), Wind Turbines (WT), Hydro Units, Thermal Units, and Electric Vehicles (EV), etc. PDFs of them by Cram-Charlier and Cornish-Fisher methods.

Load Flow Bus

This program requires the line and transformer parameters and transformer tap settings specified in the input file named Linedata_Matrix. It converts impedances to admittances and obtains the bus admittance matrix. The program is designed to handle parallel lines.

Load Flow Newton

This program obtains the power flow solution by the Newton-Raphson method and requires the matrices named Busdata_Matrix and Linedata_Matrix. It is designed for the direct use of load and generation in MW and MVar, bus voltages in per unit, and angle in degrees. Loads and generation are converted to per unit quantities on the base MVA selected. A provision is made to maintain the generator reactive power of the voltage-controlled buses within the specified limits.

Bus Out

This program produces the bus output result in a tabulated form. The bus output result includes the voltage magnitude and angle, real and reactive power of generators and loads, and the shunt capacitor/reactor MVar. Total generation and total load are also included as outlined in the sample case.

Line Flow

This program prepares the line output data. It is designed to display the active and reactive power flow entering the line terminals and line losses as well as the net power at each bus. Also, included are the total real and reactive losses in the system. The output of this portion is also shown in the sample case. This program prepares the line output data.

PLF Linearisation Convolution

PLF Methods as described in above paragraph.

PLF Linearisation Convolution Gram-Charlier

The above PLF Methods with the Gram-Charlier expansion method.

PLF Linearisation Convolution Cornish-Fisher

The above PLF Methods with the Cornish-Fisher expansion method.

PLF MC

It gives the solution of PLF using the Monte Carlo technique.

Data Correlations

The generation of the random variables should have to take into account spatial dependence between them for an accurate representation. It was considered that correlations can take place between generation, load, injected power or even in a mixed way, considering correlations between different types of variables (e.g. correlation between active injected power in node "i" and the active load in node "j"). Note that if between two variables there are not correlation coefficients then the variables are considered to have $\rho=1$. In addition, each variable may also include an independent and a dependent part.

Computational Procedure for the PLF

The following Figure 6-2 shows a simplified flow chart for the basic solution of the PLF.

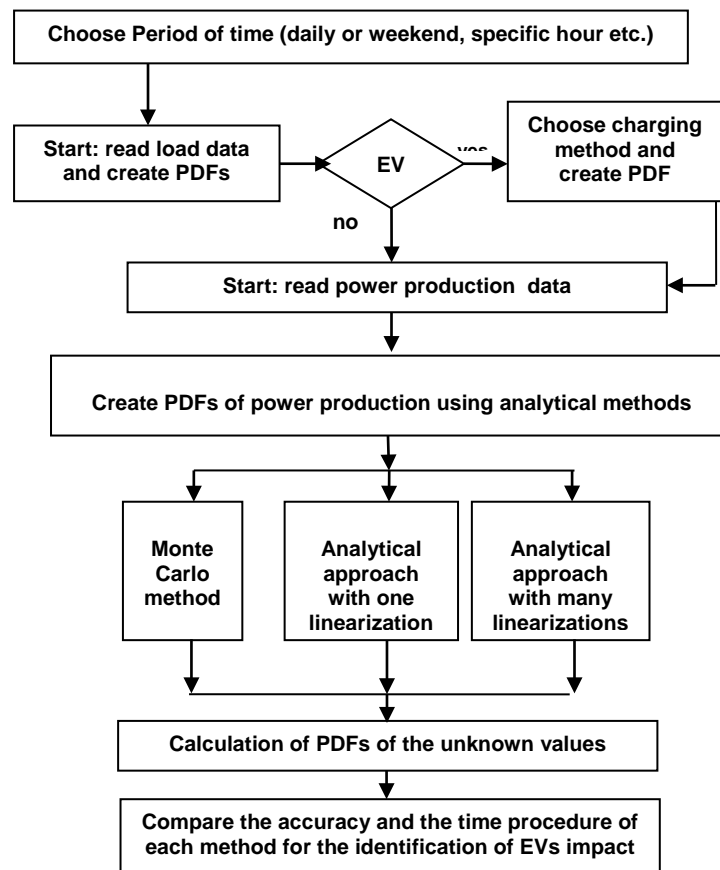


Figure 6-2 Simplified flow chart for basic solution of the PLF

6.1.2 Adaptations and Enhancements

The EV is a new kind of load. The uncertainty related to when and where EVs will charge will become a critical issue that needs to be considered to guarantee an efficient and robust operation of the electricity networks. Many management procedures of the EVs charging are identified for the purpose of the present study, [24]. Two of the most important are: dumb charging and dual tariff policy. In the dumb charging approach it is assumed that EVs' owners are completely free to connect and charge their vehicles whenever they want. The dual tariff policy intends to simulate a situation where electricity is cheaper during some specific hours of the day.

In most published PLF methods, one or more known sets of generation and loads are assumed, i.e., the input variables are assumed deterministically known. The method developed in takes into account load uncertainties and generating unit unavailability modelled as probability density functions. A new formulation of probabilistic load flow tool suitable for modern power systems with RES generation and electric vehicles (EV) demand and the dependency between EVs and loads is represented. The developed stochastic model of EV demand and the RES models are incorporated into probabilistic load flow studies. In addition, two methods are investigated for the calculation of PDF of RES production, Gram–Charlier and

Cornish–Fisher. All the PLF results are compared with Monte Carlo (MC) method. In addition, probabilistic load flows for the mainland Greek power system considering all the types of power units and large penetration of electrical vehicles is examined.

In conclusion, this work contributes clearly with: 1) the new formulation of the PLF problem incorporating RES and EV stochastic profiles, 2) development of general EV demand model for load flow studies.

6.1.3 Results

In order to show the capabilities of the PLF tool, a test with the power system shown in **Figure 6-3** was performed. It is about the large distribution power system of Greece with high integration of Renewable Energy Resources (RES) and Electrical Vehicles (EV). The probabilistic load flow techniques provide Probabilistic Density Functions (PDF) of branch power flows, node voltages and active power line losses. The only requirements needed for the implementation are to include the end user preferences and needs and real cases and data.

In order to show the capabilities of the followed method, an example has been run and some outputs are given.

The chosen system

The chosen system for study is the one of mainland Greece. It is a simplified version of 89 buses from the real system. It includes a slack bus, twenty four PV buses and sixty four PQ buses. In the PV buses, the system has power generation from wind, photovoltaics, hydroelectric power plants, conventional stations and EV that can perform as well as load. For the calculation of PDF of above power production units the two analytical methods are used from the given data of the system, [26], [27], Appendix. Also, the PDF of load is assumed as a normal distribution.



Figure 6-3 Simplified Electrical Power System of Mainland Greece, projected to 2010.

System Data and Definition

Hours to be Study

12:00, 16:00, 18:00, 20:00, 22:00, 02:00

Years to Be Study

2010, 2020, 2030

Load Scenarios

Winter peak load, Winter valley load, Summer peak load, Summer valley load.

PDFs (using Gram-Charlier and Cornish-Fisher methods), [26], [27]

Load (normal, $\cos\phi=0.95$), Dependency.

WT (short-term period)

PV (short-term period)

Hydro (Discrete, Constant, Continuous)

Thermal Units (Discrete, Continuous)

The following results (Figure 6-4,

All connections of Bus 50 (From – To)	Before EV	After EV
50-31	576.7947	539.1925
50-37	382.0973	322.6424
57-50	872.7974	823.4485
51-50	88.2946	90.4865
Demand in bus 50	2,2	52,2

, Figure 6-6, Figure 6-, Table 6-1,

Table 6-2) should be considered only as indicative, since they depend on many parameters. Later, all the results of the system's operation will be given in details.

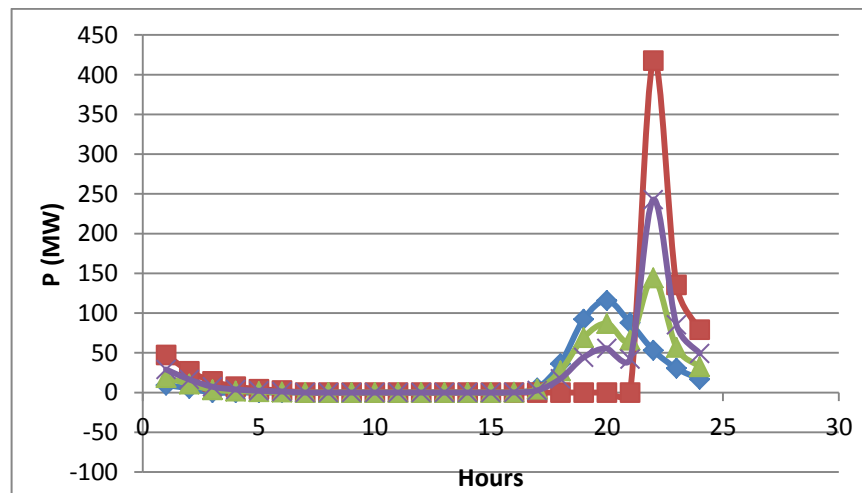


Figure 6-4 Year-2020. EV demand for a typical day. The blue line indicates the dump charging strategy, the red one indicates the dual charging strategy.

Using the dump charging strategy, the maximum EV demand of 70.000 vehicles (projected to 2020) is 120 MW at 8 p.m. It is assumed that 50 MW of them are established in bus 50 (Athens region) and other 50 MW in bus 49 (other Athens region). The results are summarized in Table 6-1, 2. Using the MC simulation for 3000 iteration and the Gram – Charlier method Figure 6-5, 6 are obtained. Due to the low EV demand and because of very “strong” electric power system the values of standard deviation of PDFs are very small. Clearly, the MC is failed to depict the PDFs accurately for low number of iterations.

Table 6-1

Mean value of voltages with very small standard deviation (Year:2020)

Buses	Voltage_Before (pu)	Voltage_After (pu)	Total number of connections
44	0,9948	0,9945	6
41	1,0299	1,0299	3
49 (-1% variation)	1,0204	1,0111	2
55	0,9955	0,9943	5
56	0,9955	0,9944	2

Table 6-2

**Mean value of active power (MW) with very small standard deviation
(Year: 2020)**

All connections of Bus 50 (From – To)	Before EV	After EV
50-31	576.7947	539.1925
50-37	382.0973	322.6424
57-50	872.7974	823.4485
51-50	88.2946	90.4865
Demand in bus 50	2,2	52,2

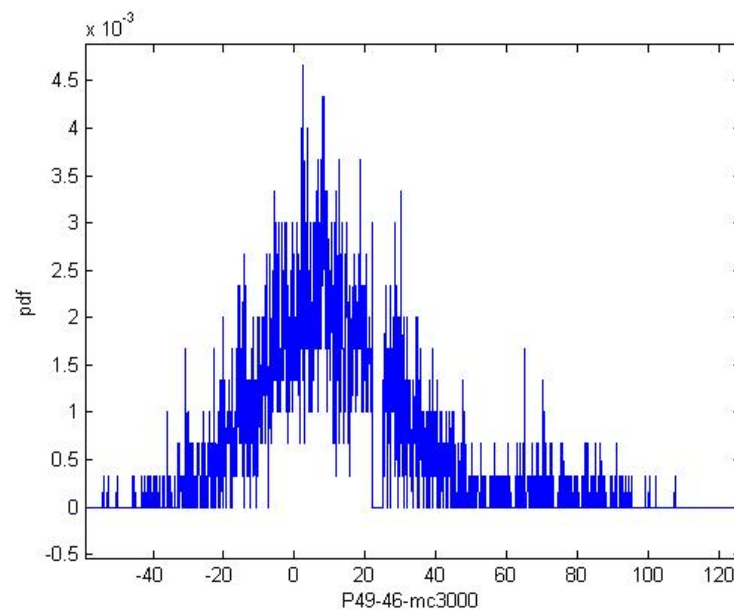


Figure 6-5 PDF of the active power of line connection 49 to 46 after the EV penetration. MC simulation for 3000 iterations. (Year: 2020)

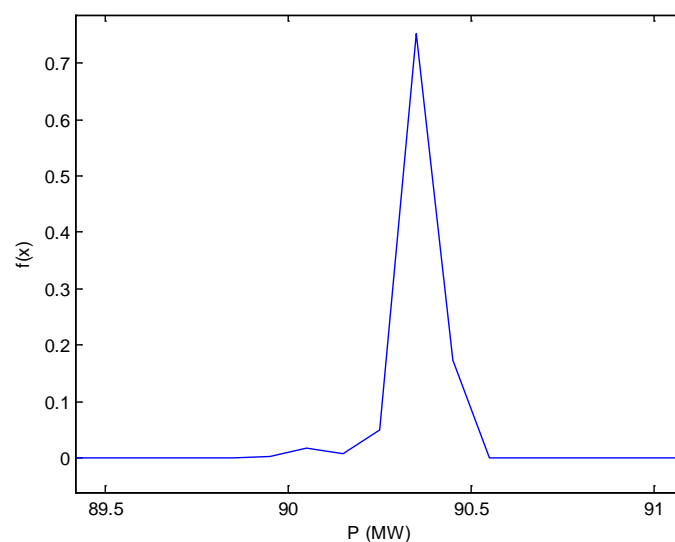


Figure 6-6 PDF of the active power of line connection 51 to 50 after the EV penetration. MC simulation and Gram-Charlier method for 3000 iterations. (Year: 2020)

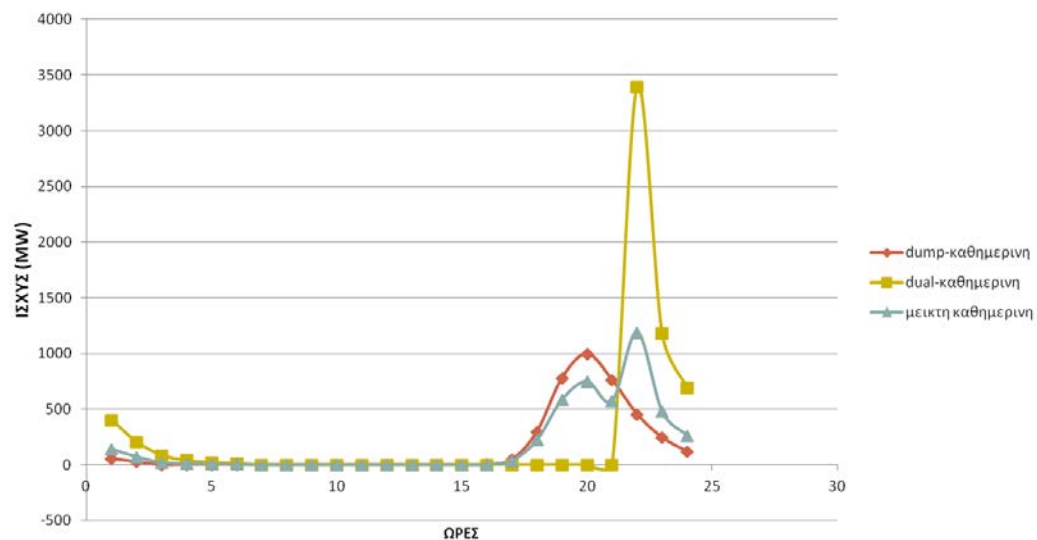


Figure 6-7 Year-2030. EV demand for a typical day of the winter. The red line indicates the dump charging strategy

Using the dump charging strategy, the maximum EV demand of 700.000 vehicles (year: 2030) is 1000 MW at 8 p.m. In more details:

- Athens Area: 30 buses,
- Total Load Demand (TLD): 5659,52 MW,
- Total EV Demand of 2020: 120MW (2,12% of TLD),
- Total EV Demand of 2030: 1000MW (17,67% of TLD),
- Bus 49: 500MW (or 350000 vehicles), Bus 56: 500MW (or 350000 vehicles).

Applying the linearization method and the Gram-Charlier expansion the Table 6-3 and the Figure 6-8 are obtained. It is observed high accuracy with only one run.

Table 6-3

Mean value of voltages with very small standard deviation (Year:2030)

Buses	Voltage_Before (pu)	Voltage_After (pu)	Total number of connections
49 (-5,09% variation)	1,0204	0,9684	2
56 (-2,38% variation)	0,9955	0,9718	2

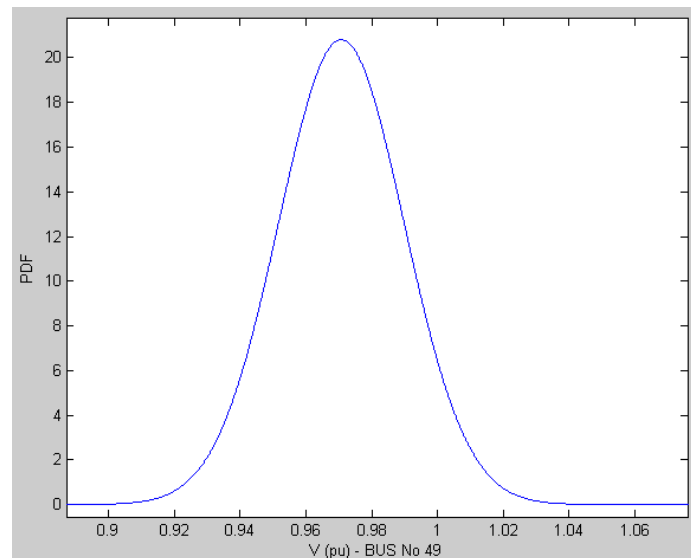


Figure 6-8 PDF of the voltage (bus 49) after the EV penetration. (Year: 2030)

6.1.4 Discussion

Although Monte Carlo Simulation method is able to provide accurate results, the computation is really time consuming, therefore is not suitable to handle practical systems especially for few number of iterations. The conventional convolution technique is another method to obtain the PDF. By applying linearization methods, the state vector and line power flow are presented as variables, a convolution technique can be applied to obtain the PDF's of the desired variables, accurately.

In conclusion, computation results have proved that the linearization method with combined cumulants and Gram-Charlier expansion method enables system planners to estimate 10% and 90% confidence levels accurately enough to determine the security level and the maximum power rating of the line with confidence.

6.1.5 Conclusion

- The PLF identifies the risk of congestion in branches and the degree of domination in node injections and in the system's overall performance.
- In this task the probabilistic load flows for the mainland Greek power system considering all the types of power units and large penetration of electrical vehicles is examined.
- The previous results should be considered only as indicative, since they depend on many parameters.
- In summary, this method enables system planners to obtain the possible ranges of power flow and the probability of occurrence quickly enough to meet planning requirements in the deregulated power markets. With this information, the probability of any bus and line being overloaded can be easily computed.

6.1.6 Recommendations

- The dependency between EVs and loads must be taken into consideration.
- The study of other PLF methods for comparison.
- Identification of traffic patterns and human behaviors have to be taken into account as well as the strategies proposed for EV charging and the amplitude of additional EV loads to be added to baseline load diagram.
- Many scenarios with various EV charging strategies (dump, dual tariff, smart charging, etc.) must be considered.

6.2 Fuzzy Power Flow Platform

Fuzzy numbers are used to represent non-deterministic and non-probabilistic uncertainties. Furthermore, they try to reproduce, in terms of mathematical values, some aspects of common language that would be very difficult to describe by probabilistic functions. Thus, the application of fuzzy theory to the power flow concept allowed the input of power injection ranges in the nodes, instead of single deterministic values. Uncertainties related with renewable energy sources and EV can be represented through a fuzzy modelling.

Regarding the demand of the EV batteries, there are many issues that may change the behaviour of the power injections in the nodes. Therefore, the Fuzzy Power Flow is used in order to perform a network analysis for steady state conditions. This analysis can be improved, if some charging characteristics were taking into account as a form of dependences (correlations).

INESC Porto Fuzzy Power Flow tool was enhanced so that EV could be included. Thus, in order to reduce the pessimism or overstatement on the fuzzy uncertainty estimation, now it is possible to consider some characteristics of dependences between buses to correct estimate the fuzzy numbers. This procedure can be added to represent similar behaviours in the nodes based on previous operator/planner experience. On the other hand, a new methodology to solve the Fuzzy Power Flow problem was developed. This new approach aims to adapt the concept to long-term period conditions, enhancing some characteristics regarding uncertainties, and mainly improving the classic approach through the elimination of artificial uncertainties previously incorporated.

This document describes some changes performed in the classic application of Fuzzy Power Flow, in order to include the concept of dependences between buses. The Symmetric Fuzzy Power Flow concept is introduced and a methodology to implement it is also presented. Afterwards, the results from the previous and the new versions of Fuzzy Power Flow are compared and discussed. For that purpose, these methodologies are applied to a small didactic test system.

6.2.1 Description of the Fuzzy Power Flow

Deterministic, Probabilistic, and Fuzzy Power Flow approaches

Deterministic power flow calculation methods do not allow identifying different types and levels of uncertainties during a performed study. The need in capturing

uncertainties lead to the development of probabilistic power flow models, which in general is able to represent several levels of uncertainties. Usually, these models represent the bus load as probabilistic functions, taking into account previous information regarding the most probable power consumed. These methods provide system operators with major probabilistic information such as, the probability of reaching voltages and lines limits. However, the information required for these methods is not always available, namely in new situations like the massive deployment of EV.

On the other hand, Fuzzy Power Flow does not require any information regarding probabilistic functions. Furthermore, it may be described as a procedure that uses unstructured information coming from the Transmission System Operator regarding possible load variation, in order to find the maximum range of power flows and bus voltages. Hence, this approach is important to identify congestion situations and excessive voltage drop (both characterized by a possibility value), conveying important information to the TSO [39].

Finally, since for studies related with EV we do not have information from the past, methods based on the fuzzy description of loads have the advantage of not requiring the knowledge of probability density functions [38].

Classic Approach

Uncertainties of power system variables are mainly related with qualitative aspects that have non-random sources. These aspects come from empirical knowledge and personal experience of the engineers that worked in the grid operation field during many years. Thus, information such as “load is between 10 MW and 20 MW” cannot be described by a probabilistic approach, since it is impossible to ensure that the events in the past will happen in the future, due to the high influence of external factors, like man influence. Therefore, the representation through fuzzy numbers, operating according to the fuzzy sets theory [29][30], becomes a consistent solution, in order to describe some vague information that is not related with event repetition, but emerge from the qualitative predictions regarding the incomplete human knowledge about the future and other imprecise aspects of the language.

The application of fuzzy sets to power system was first proposed in [31] and further developments of Fuzzy Power Flow theory were presented in [32]. Fuzzy Power Flow aims determining the intervals of voltage magnitudes and phases at the nodes as well as currents and losses in the lines, considering a given range of power injections at the buses, which may represent uncertainties related with EV charging or any type of generation, such as wind or solar PV. The first approach proposed regarding Fuzzy Power Flow was the DC formulation, which is based on the methodology of the traditional DC power flow. However, the active power injections are modelled as trapezoidal numbers and, afterwards, multiplied by the coefficients of the (crisp) sensitivity matrix according to the fuzzy arithmetic rules. The branch flows are therefore calculated after

$$\tilde{P}_{i-k} = A \cdot \tilde{P} \quad (6-17)$$

Where A represents the corresponding coefficient of the sensitivity matrix, \tilde{P} is the power injections vector, and \tilde{P}_{i-k} denotes the branch power flow vector.

AC Fuzzy Power Flow [32] and [33] extends the DC formulation to the uncertainties of the reactive powers, voltage magnitudes and losses. The traditional algorithm is based on a linearization of the AC power flow equations near the central point of operation, which comprises the crisp values of the power injections in the nodes. The central values are used to run a crisp power flow adopting, for instance, the Newton-Raphson algorithm, so that the voltage magnitudes and phases central values can be obtained. Afterwards, their deviations are determined through the multiplication of the active and reactive power deviations by the inverted Jacobian matrix evaluated at the last iteration, as shown in the following equations (fuzzy arithmetic applies):

$$\begin{bmatrix} \Delta\tilde{\theta} \\ \Delta\tilde{V} \end{bmatrix} = [J]^{-1} \begin{bmatrix} \Delta\tilde{P} \\ \Delta\tilde{Q} \end{bmatrix} \quad (6-18)$$

$$[\tilde{\theta}] = [\theta^{ct}] + [\Delta\tilde{\theta}] \quad (6-19)$$

$$[\tilde{V}] = [V^{ct}] + [\Delta\tilde{V}] \quad (6-20)$$

Although power flows in the lines are non-linear functions of the voltage magnitudes and phases, as shown in (6-21), their exact expressions can be approximated through a linear function by taking the first terms of their Taylor series expansion near the crisp points, as presented in (6-22).

$$P_{ik} = -g_{ik} \cdot V_i^2 + V_i V_k (g_{ik} \cos \theta_{ik} + b_{ik} \sin \theta_{ik}) \quad (6-21)$$

$$\Delta P_{ik} \approx \frac{\partial P_{ik}}{\partial V_i} \Delta V_i + \frac{\partial P_{ik}}{\partial V_k} \Delta V_k + \frac{\partial P_{ik}}{\partial \theta_i} \Delta \theta_i + \frac{\partial P_{ik}}{\partial \theta_k} \Delta \theta_k \quad (6-22)$$

The voltage magnitude and phase deviations can be written as a function of the power injection deviations, considering the elements of the inverted Jacobian matrix, as shown in (6-23). Thus, one is assuming a linear relationship between the power flow deviations and the injected powers (active and reactive) deviation. Equation (6-24) introduces this representation, considering fuzzy values in the nodal power injections.

$$\Delta P_{ik} \approx \begin{bmatrix} \frac{\partial P_{ik}}{\partial V_i} & \frac{\partial P_{ik}}{\partial V_k} & \frac{\partial P_{ik}}{\partial \theta_i} & \frac{\partial P_{ik}}{\partial \theta_k} \end{bmatrix} \begin{bmatrix} [J^{-1}]_i^\theta \\ [J^{-1}]_i^V \\ [J^{-1}]_k^\theta \\ [J^{-1}]_k^V \end{bmatrix} \begin{bmatrix} \Delta P \\ \Delta Q \end{bmatrix} \quad (6-23)$$

$$\Delta \tilde{P}_{ik} \approx \sum_j SP_{ik,j} \Delta \tilde{P}_j + \sum_j SQ_{ik,j} \Delta \tilde{Q}_j \quad (6-24)$$

Where $SP_{ik,j}$ and $SQ_{ik,j}$ are sensitivity coefficients.

The main adaptations

Although dependences are important to reduce a possible pessimism regarding uncertainties of the power injections in the nodes, it is expected that we still find a

wide range of load and generation intervals, since we are dealing with long-term scenarios. Thus, in this situation, some careful actions should be taken, in order to avoid the excess of uncertainty and its consequent propagation during the Fuzzy Power Flow calculations. Hence, it is important to stress that the traditional approach previously presented was developed under the assumption that the fuzzy sets in the nodes were relatively narrowed. This assumption is necessary not only to ensure the linearization feasibility, but also to allow the use of the slack bus, which has a considerable role in the overvaluation of the uncertainties. In fact, in the Fuzzy Power Flow classic approach, this node compensates the deviations in the injections of the other buses, increasing their own interval through the use of artificial uncertainties inclusions. In order to understand this phenomenon, one can consider a system with 3 node and 3 lines, as the one presented in Figure 6-9. Just by simplification reasons, DC Model is assumed and the slack bus chosen is 1.

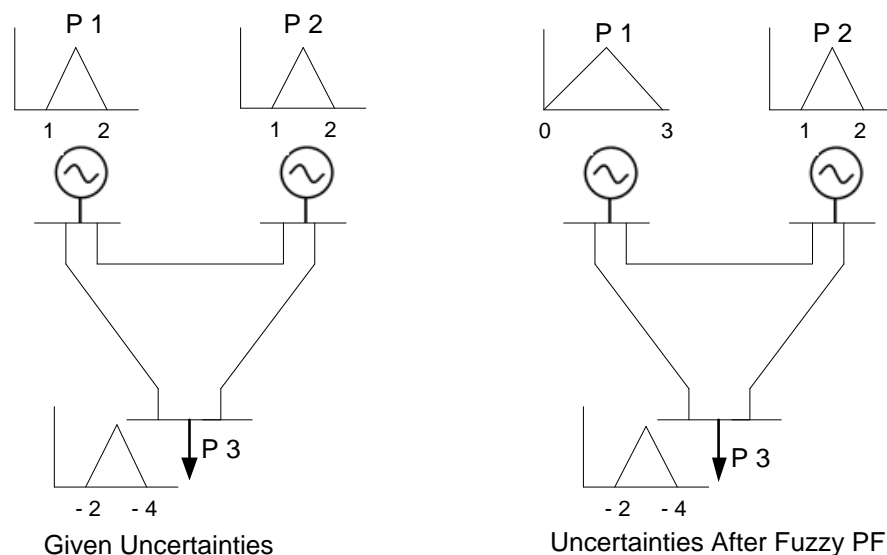


Figure 6-9 Effect of the slack bus in the standard formulation

If the maximum demand happens in bus 3 (4 MW) and node 2 is generating at the minimum level (1 MW), the bus 1 should generate 3 MW. On the other hand, if bus 3 is consuming at a low level (2 MW) and the maximum generation occurs in node 2 (2 MW), there is no need of generation in bus 1 (0 MW). Therefore, as shown in Figure 6-9, the interval of the slack bus increased from [1,2] to [0,3]. Although the presence of the slack bus is just a mathematical concept to solve the Power Flow equations, in the Fuzzy Power Flow classic approach, it affects the final results since it compensates the uncertainties of the other buses including the new set of uncertainties. Thus, in order to avoid this compensation, which jeopardizes the accuracy of the results, new approaches without slack bus were developed.

6.2.2 Adaptations and Enhancements

As stated already, the Fuzzy Power Flow can represent the system behaviour when uncertainties in the nodal power injections exist. These uncertainties can represent

unpredictable and chronological characteristics regarding energy sources. On the other hand, they may also represent some vagueness aspects of the load, which may not correspond strictly to the forecasting results. Furthermore, these uncertainties will increase with the presence of EV in the grids. In fact, the uncertainties added by them can be very wide, if some aspects are taking into account, like human and society behaviour, traffic, type of vehicles, etc. Some of these aspects were already tackled in the last MERGE studies, for example the traffic patterns and human behaviour [34] as well as EV characteristics [35]. However, in the previous work, they were modelled using a probabilistic approach, describing the frequency of finding a certain charging rate (considering the different EV types) or giving information about the percentage of people that prefer to charge vehicles at home. Although these aspects were treated as probabilities in these deliverables, for the studies presented in this item, the uncertainties will be modelled all together under the form of fuzzy sets representing active and reactive power in the buses.

Charging Strategies under Fuzzy Concept Model

The load variation studied on MERGE project intends to represent a typical day, or more specifically typical week days that can be derived from the normalization of the entire year load curve with 8760 h (see results from MERGE Project for different countries [28]). In the same way, a normalized version of the EV charging profiles, as described in [28], is also exploited to create the EV charging conditions for different countries. The data presented in these reference studies are used here to characterize some bordering charging strategies, where both good (smart charge) and bad (dumb charge) situations are represented as fuzzy numbers. Firstly, a fuzzy load diagram can be represented through the visualization of the load profile, where it is possible to see the uncertainty variation during the 24 hours of the day. Figure 6-8 and 6-9 show some possible fuzzy representation of the charging strategies taking into account both smart and dumb charging.

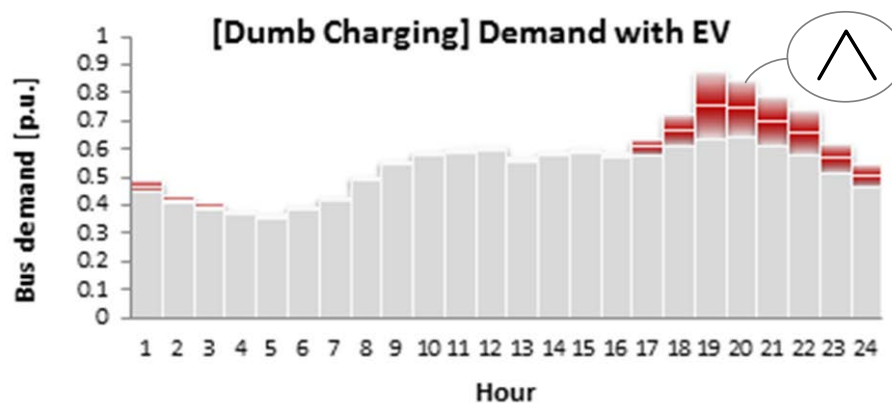


Figure 6-10 Uncertainty in industrial node in Dumb Charging mode

Considering the dumb charging scenario where it is assumed that all EV are plugged in, and start charging immediately when they return from their last journey of the day, the uncertainty varies from small values to high values on different hours.

As the Figure 6-10 shows, the dumb charging provides the baseline for the effect of introducing significant penetrations of EV, if no action is taken to optimize the effects of the increase in grid demand.

On the other hand, the smart charging strategy, where it is assumed EV can be controlled usually in load valley hours, and instructed to start/stop charging, or even limiting charge rates, so that the total demand for EV charging at a particular time is controlled. In this case, the uncertainty also varies from small values to high values on different hours during load valley avoiding peak load.

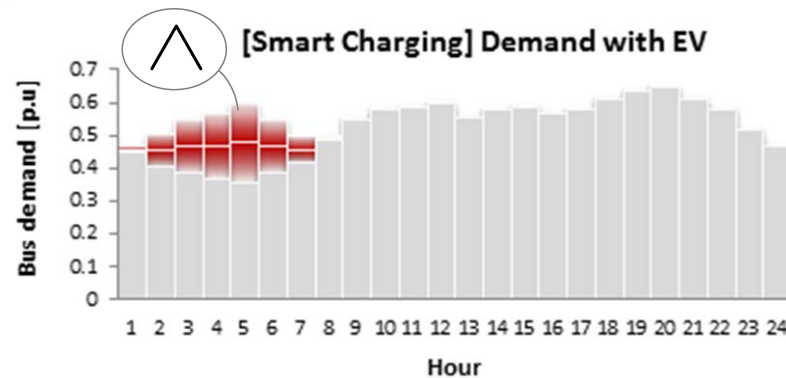


Figure 6-11 Uncertainty in industrial node in Smart Charging mode

As it is possible to see in Figure 6-11, the smart charging represents the ideal situation where the overall load on the grids is leveled, so that valleys of demand are filled and existing peaks are not increased. The smart charge fuzzy representation represents a theoretical condition explored in the MERGE project.

Considering the scenarios used for the construction of the electricity demand [28], using the profiles of times of return from last journeys of the day and assuming a 10% penetration of EV in the total vehicle fleet, it is possible to draw a fuzzy number for each hour of a full day and to see the effects of the charging strategies. Figure 6-12 and Figure 6-13 show some possible fuzzy strategies representation, considering demand with and without EV.

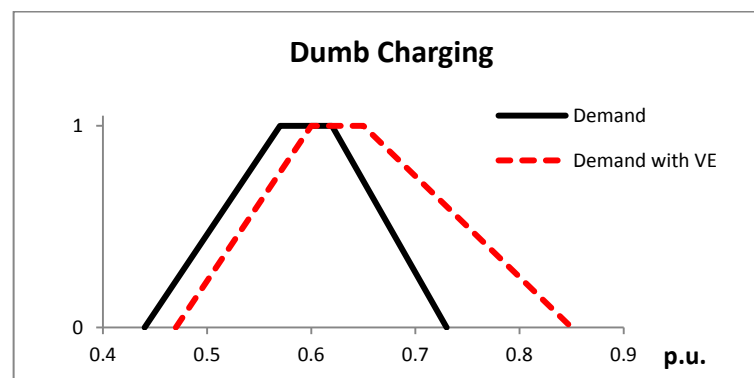


Figure 6-12 Fuzzy number for dumb charging on specific hour

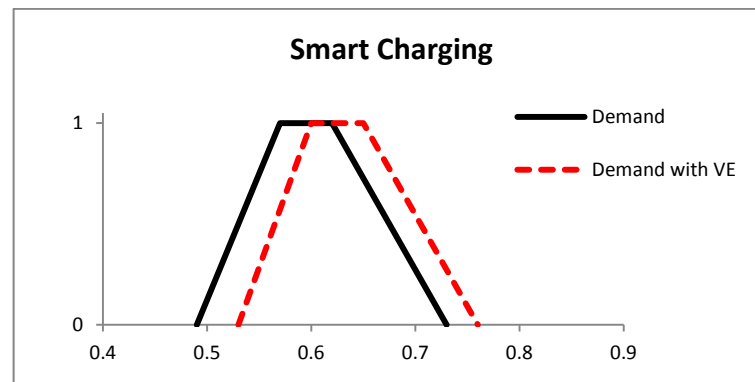


Figure 6-13 Fuzzy number for smart charging on specific hour

It is interesting to observe that, in the dumb fuzzy number representation, the highest value of the load changes, increasing the peak load, otherwise in the smart fuzzy representation, the lowest value of the load also changes. However, the peak load of the diagram does not change, essentially because there is no EV influence in the peak load.

In order to clarify all presented concepts, it is assumed a specific node, where the base load uncertainties, the vehicles number, type and charging power along the day will be described as a range of values that are injected in this node. Considering an industrial node in the transmission grid, one can find different types vehicles connected: L7e, M1, N1, N2 and PHEV. These are both industrial and personal vehicles that are expected to be connected in the industrial zones. Figure 6-14 illustrates this example:

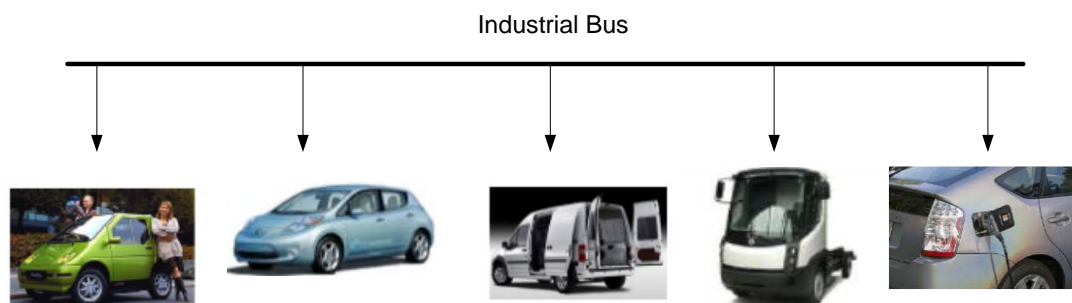


Figure 6-14 Industrial node

The charging rates for each type of vehicles can be found in reference [35]. Regarding the charging behaviour and the time that these vehicles are connected into the grid, it is possible to estimate a percentage of power that is most expected in that node, taking into account the type of vehicles and the utilization factors.

For example, for people/family vehicles, such as L7e, M1 and PHEV, one admits a factor of 0.1, assuming that they are also charged in other places. For industrial vehicles one considers an expected charging of 0.3%. The number of vehicles connected as well as the maximum and most expected power injections are presented in the Table 6-4.

Table 6-4 Characterization of the industrial node

Type	Number of vehicles	Charging Rate (kW)	Max Power (kW)	Expected Charging (%)	Most expected power (kW)
L7e	40	3	120	0.1	12
M1	25	6	150	0.1	15
N1	90	4	360	0.3	108
N2	100	10	1000	0.3	300
PHEV	20	3	60	0.1	6
Total	275	26	1690		441

Considering the values in the table above and neglecting the base demand (related with non-EV source), it is possible to model the power consumption at this hour in the industrial node through a fuzzy number, which is described in the Figure 6-15.

Table 6-5 Active power injection values

Industrial node	Number of vehicles
Min	0
Most Expected	441
Max	1690

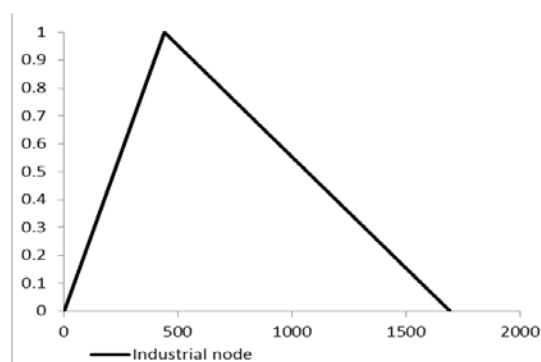


Figure 6-15 Fuzzy active power of the industrial node

The previous example presented a way of modelling non-probabilistic uncertainties by fuzzy sets. Once again, the example is including boundaries values in order to

highlight the methodology. In fact, more aspects could be included. For instance, more than one value could be considered in the charging rate since each type of vehicle can have different rates, as shown in [35]. Nevertheless it was clear that, taking into account the information regarding EV and the system operator knowledge about the most expected power in each node, the modelling through fuzzy sets can be a good approach to represent uncertainties. It is important to highlight that there are others aspects related to the load uncertainties, which are not represented on this work. Obviously, the treatment of the load uncertainty can be easily included in the Fuzzy Power Flow analysis.

Data Dependences Procedure (Correlations)

The typical approach to the fuzzy power flow problem includes an independence assumption between all the sources of uncertainty (energy sources, such as wind power and PV, due to its intermittent characteristics, EV, etc). This may lead to pessimistic results, in the sense that artificial uncertainty is included due to the independence assumption. Hence, the information regarding node dependences can be used to keep the uncertainty level at its correct level, in order to ensure the credibility and usability of the solutions presented in Fuzzy Power Flow. In fact, it is possible to find levels of dependences between some buses of the transmission grid. For instance, when the wind is not blowing in a given region, one can expect that the wind farms in that zone are not generating. On the other hand, considering standards of quotidian life, if the EV are connected to a typical residential bus during the night, one can assume a similar behaviour in the other residential nodes. This idea is schematized in the Figure 6-16.

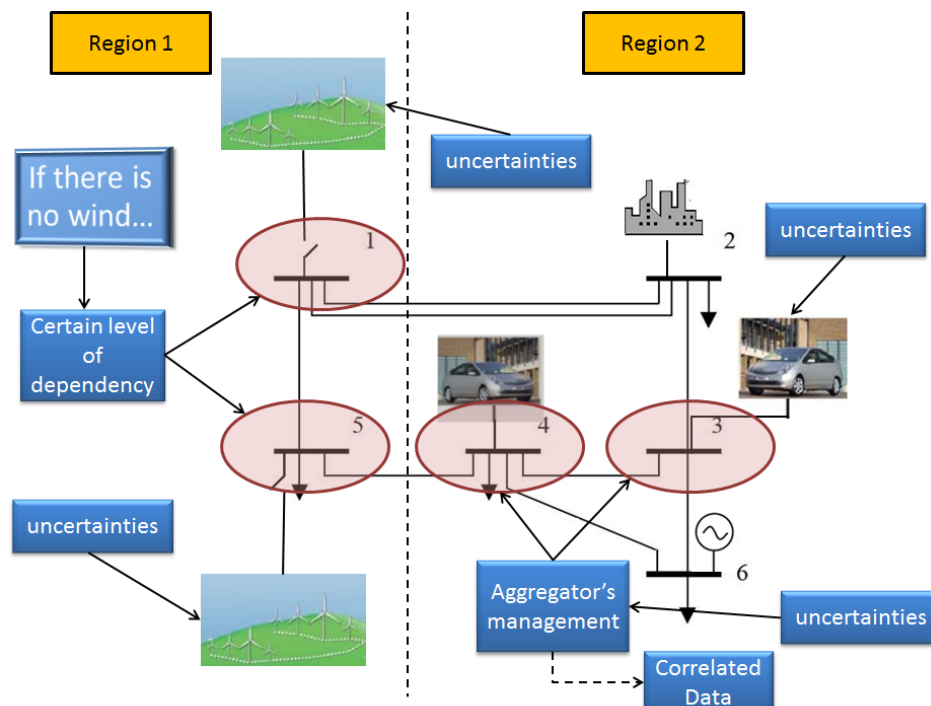


Figure 6-16 Dependences on the nodes

A model to address dependence data for Fuzzy Power Flow applications was proposed in [36]. The basic concept of this model, which can be expressed by the equation (6-25), is to represent the load and generation in a given bus as a sum of two terms: \tilde{P}_{ic} is the part of the total bus load (\tilde{P}_i) that is defined as being correlated with a base power, \tilde{P}_{base} . The dependence is given by a real number m_i . The second term, \tilde{P}_{if} , corresponds to the free part of \tilde{P}_i , meaning that it has no correlation with any other power. This model is general, in the sense that a particular power can be completely uncorrelated ($m_i = 0$) or can be defined in a mixed way. Thus, base \tilde{P}_{base} can be any user defined power or, alternatively, the active power load in another bus j , \tilde{P}_j ($j \neq i$).

$$\tilde{P}_i = \tilde{P}_{ic} + \tilde{P}_{if} = m_i \cdot \tilde{P}_{base} + \tilde{P}_{if} \quad (6-25)$$

Note that the information that allows us to implement this method and model the dependences between the nodes is not aimed to be obtained through statistical analysis. On the contrary, it is based on the experience of the system operator, which is familiarized with the system behaviour. Thus, considering two nodes related with residential zones with similar demand, one can assume the first as a reference and give a value of $m_i = 1$ to the second, with a certain degree of freedom specified by \tilde{P}_{if} . If the second node has mixed characteristic, for example with residential and commercial zones, the level of dependence can be lower (around 0.5) since some difference exist in the life styles of the two zones. Hence, it is expected a higher free factor (\tilde{P}_{if}) in this situation.

Symmetric Fuzzy Power Flow

The problem of the slack node influence in classic FPF was already tackled in [37] and new approaches of Fuzzy Power Flow were proposed in [38] and [39]. The use of these approaches seems to be more efficient when one is dealing with long-term uncertainties, since they avoid problems regarding the excess of uncertainties related with the slack buses. Therefore, in this chapter, these methodologies will be presented and a comparison with the traditional approach will be performed.

The concept of the Symmetric Fuzzy Power Flow (see [38] for DC model and [39] for AC case) is not related with the symmetry of fuzzy sets used and their distance between the central point and both extremes of the interval, but rather on the requirement of equal specifications for all the nodes, something that doesn't happen in the classic FPF, due to the asymmetric situation of the slack bus. This approach works by maximizing and minimizing each variable (voltages, phases, currents, losses) subject to all the possible variations of the others, so that the extremes of the intervals for each α level can be found. Thus, power injections in the nodes (active and reactive), that are inputs of the classic approach, here are represented as constraints of the problem. Hence, taking into account a voltage in a given bus, one can calculate its upper limit by the maximum value that this voltage can assume, considering that power injections in all buses are within their fuzzy range. These optimizations are performed for different α cuts, from the top ($\alpha = 1$) to the base of the fuzzy number ($\alpha=0$). The Symmetric AC Fuzzy Power Flow [39] formulation for a variable \tilde{Z} in a level α is given by the equations (6-26) to (6-32).

$$\max/\min \tilde{Z}(\alpha) \quad (6-26)$$

subject to

$$P_i = V_i \sum_{k=1}^n V_k (G_{ik} \cos \theta_{ik} + B_{ik} \sin \theta_{ik}) \quad \text{all buses } i; \quad (6-27)$$

$$Q_i = V_i \sum_{k=1}^n V_k (G_{ik} \sin \theta_{ik} - B_{ik} \cos \theta_{ik}) \quad \text{all buses } i; \quad (6-28)$$

$$P_i \in \tilde{P}_i(\alpha) \quad \text{all buses } i; \quad (6-29)$$

$$Q_i \in \tilde{Q}_i(\alpha) \quad \text{all buses } i; \quad (6-30)$$

$$V_i = V_i^{SP} \quad \text{PV and Slack buses;} \quad (6-31)$$

$$\theta_{REF} = 0 \quad (6-32)$$

where G_{ik} and B_{ik} are the components of the admittance matrix elements (real and imaginary part, respectively). $\tilde{P}_i(\alpha)$ and $\tilde{Q}_i(\alpha)$ are the α -level intervals of the active and reactive injected powers.

Optimization Procedure

In the Symmetric Power Flow formulation previously presented, besides the limits of the active and reactive power, the Power Flow equations are also constraints of the problem, which inserts a non-linear formulation. On the other hand, variables are optimized one-by-one and, for each variable, the algorithm should be run twice (minimum and maximum). These facts can lead to a huge computational effort in large systems applications. However, voltage magnitudes and phases rely on power injections found in the inverted Jacobian matrix of the Newton-Raphson algorithm. Thus, according to the signal of the correspondent element of the matrix, it is possible to know if the power injections should increase or decrease, in order to minimize/maximize the variables. Figure 6-17 illustrates this process for the maximization of given variable (MV), considering the active power injected in bus i .

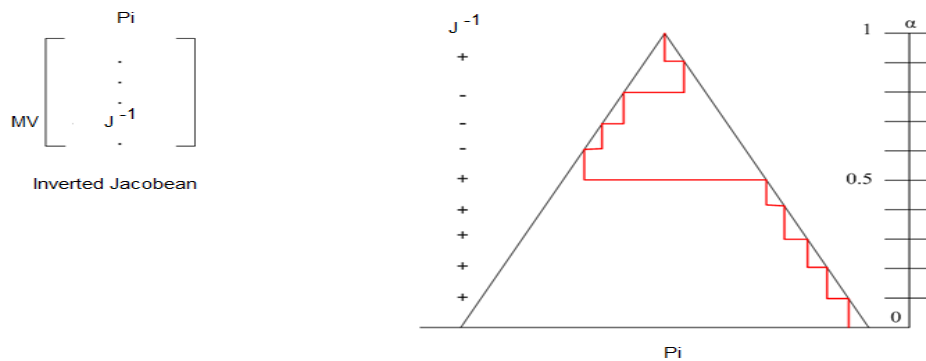


Figure 6-17 Illustration of the optimization process

As shown in the Figure 6-17, for the maximization problem, if the element of the inverted Jacobian is positive, the injected power assumes its maximum value and if

it is negative the power decrease to minimum. For the minimization problem, the reverse situation occurs.

This methodology is applied to all PV and PQ buses. The slack node used to perform the Newton-Raphson algorithm should be able to compensate the variations that occur in the other buses without exceed its fuzzy limits. Thus, from the optimization problem point of view, the power injections in the slack bus are state variables that should be checked so that the solution can be accepted. The variables type is described in Table 6-6.

Table 6-6 Variables type of the optimization problem

	Slack	PV	PQ
Active Generation (Mw)	State Variable	Control Variable	Control Variable
Reactive Generation (Mvar)	State Variable	State Variable	Control Variable
Active Load (Mw)	Control Variable	Control Variable	Control Variable
Reactive Load (Mvar)	Control Variable	Control Variable	Control Variable
Voltage (p.u.)	State Variable	State Variable	State Variable
Phase (p.u.)	Constant	State Variable	State Variable

Corrections Procedure

Although the correspondent elements of inverted Jacobian matrix can indicate the nodal power values that maximize or minimize a given variable, it is necessary to check if the new active and reactive injections of the slack bus are within limits, after running a Newton-Raphson Power Flow. If the limits are violated, some corrections to the PV and PQ injections should be done. Reference [36] presents a method that performs those corrections through successive eliminations of the variations done in nodal powers, according to a bus order. This order is established based on the sensitivity coefficients (S_i) of the inverted Jacobian row related with the optimization variable. Thus, if the absolute value of a given coefficient is low, it means that the node variation associated is not important for the optimization. The selection of the nodes to be corrected is done according to the following rules:

- If the non-feasibility is due to the violation of the minimum limit, then the next bus chosen is the one that, having not yet been corrected, has a larger non positive sensitivity coefficient, S_i ;
- if the non-feasibility is due to the violation of the maximum limit, then the next bus chosen is the one that, having not yet been corrected, has a larger non negative sensibility coefficient, S_i ;

The nodal variations are eliminated successively until the generation of the slack bus is on its limits. In order to check this condition, the approximation presented in (6-33) is assumed. For the reactive power case, it is necessary to check not only the limits of the slack node, but also the reactive injections on the PV buses, which must be kept inside their interval. Thus, the balance expression should change, as shown in (6-34).

$$\Delta P_{slack} \approx \sum_{i=1}^n \Delta P_i \quad (6-33)$$

PV PQ

$$\Delta Q_{slack} + \sum_{i=1}^n \Delta Q_i \approx \sum_{i=1}^n \Delta Q_i \quad (6-34)$$

PV PQ

Dependences procedure in the Symmetric Fuzzy Power Flow

As mentioned above, symmetric approach formulates the Fuzzy Power Flow as an optimization problem, in which the injected powers in the nodes are considered as control variables. Therefore, when the dependences between the nodes are included, there is a component of the power that is chosen by the base bus (reference node of a certain zone). Hence, the control margin of the dependent nodes corresponds only to the free part of the power, according to (6-25). This means that if a node is totally correlated ($\tilde{P}_{if} = 0$) the power on that node becomes a state variable, since it is defined exclusively by the reference bus of the zone.

In case of being a control variable, it is important to understand how the injected power is defined in the dependent nodes, during the optimization process. Thus, the selected power of the correlated buses depends on their parameters of the inverted Jacobian matrix as well as the ones that are related with the base node. The element of the reference bus determines the power injected in this node for each α cut. The multiplication of this value by the correlation factor ($m_i \cdot \tilde{P}_{base}$) give us an estimation of the point of the operation. Afterwards, the element of the inverted Jacobian matrix regarding the correlated node determines if the power for that α level corresponds to the maximum or minimum of the free part (\tilde{P}_{if}) value.

In order to illustrate the effect of correlations in the Symmetric Fuzzy Power Flow optimization process, let us consider the power in a correlated bus (P_i). For each α cut, let P_n be the power that is dependent on the base node ($P_n = m_i \cdot P_{base}$) and \tilde{P}_{if} the free part. Considering the elements of the inverted Jacobian matrix, Figure 6-18 can describe how P_i depends on P_n and \tilde{P}_{if} .

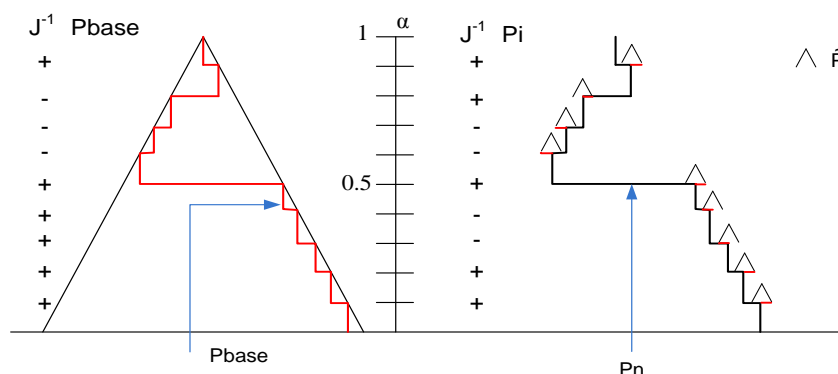


Figure 6-18 Illustration of the optimization process including correlations

6.2.3 Results

As stated previously, a didactic test system will be used to show the proposed enhancements made in the Fuzzy Power Flow Platform. For that purpose, consider the six node network presented in Figure 6-19. The configuration of the network consists of the two generating units connected on buses 1 and 6, respectively. It also consists of four bus loads, through the buses 2, 5, 4, and 6, respectively, with some electrical characteristics presented in Table 6-7.

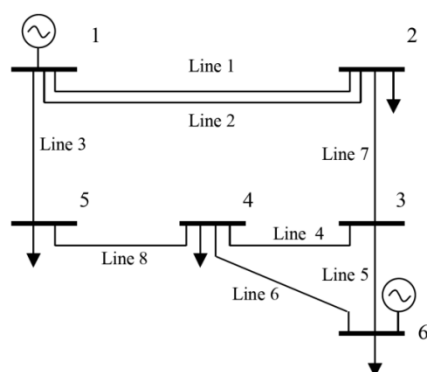


Figure 6-19 Network Proposed

Table 6-7 Line Information

	R	X	B
1	0.723	1.05	0.01
2	0.6	0.9	0.009
3	0.282	0.64	0.003
4	0.097	0.407	0.0575
5	0.08	0.37	0.05
6	0.123	0.518	0.0915
7	0	0.3	0
8	0	0.133	0

The operation point to the peak load of the 24 hours of the load diagram is presented in Table 6-8. Through the use of these deterministic conditions, there are no voltages and/or overloads problems in the network.

Table 6-8 Variables type of the optimization problem

N	Type	Vsp	P Load (Mw)	Q Load (Mvar)	P Generation (Mw)	Q Generation (Mvar)
1	Slack	1	0	0	-	-
2	PQ		2.75	1.1	0	-
3	PQ		0	0	0	-
4	PQ		1.65	0.825	0	-
5	PQ		2.75	1.1	0	-
6	PV	1	1.375	0.275	6.875	-

In Figure 6-20, when it is assumed a possible undervoltage limit of 10% to all system buses, it is possible to say that the system is in accordance with the proposed undervoltage limitation, when it a deterministic calculation is used. Figure 6-18 shows that, voltage magnitudes at buses 2, 4, and 5 are below 0.95 p.u. Although this situation can be viewed as a good performance of the network, from the deterministic view it is important to note that there are no uncertainty considerations in power injections and load.

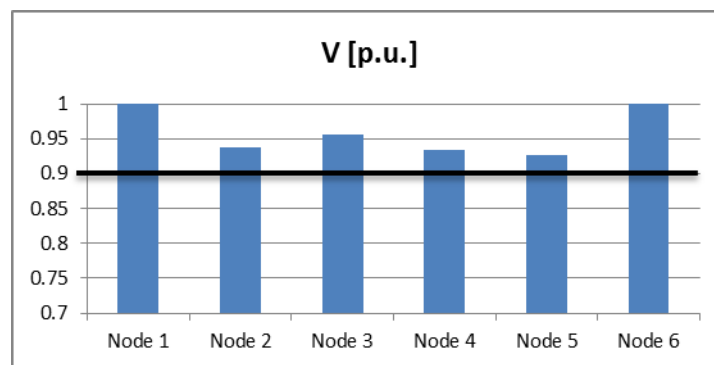


Figure 6-20 Voltage for different nodes without EV

From the line power flow point of view, it is assumed that 0.55 p.u. can be considered as a generalized limit to the lines 5 and 6. From this perspective, the same interpretation can be used. Note that there are no deterministic power flows higher than 0.3 p.u. Once again, this situation can be interpreted as a good performance of the system, since there are no overloads in the system.

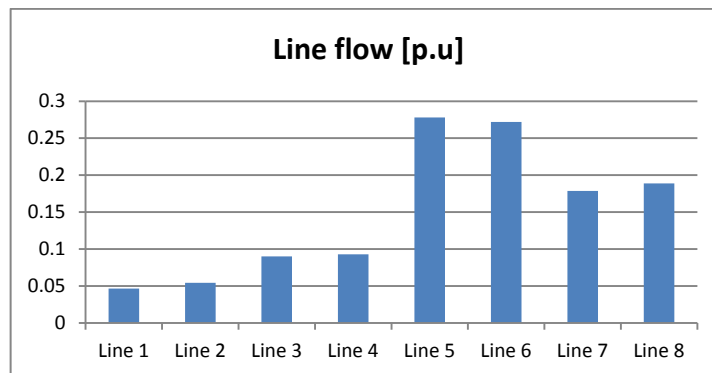


Figure 6-21 Line Flow for different lines without EV

The effect of the EV

A second situation where the load profile increases due to the EV presence can be assumed. In this case, observe that an amount of EV are added to the buses 2, 4, 5, and 6, increasing the existing loads as shown in Figure 6-22.

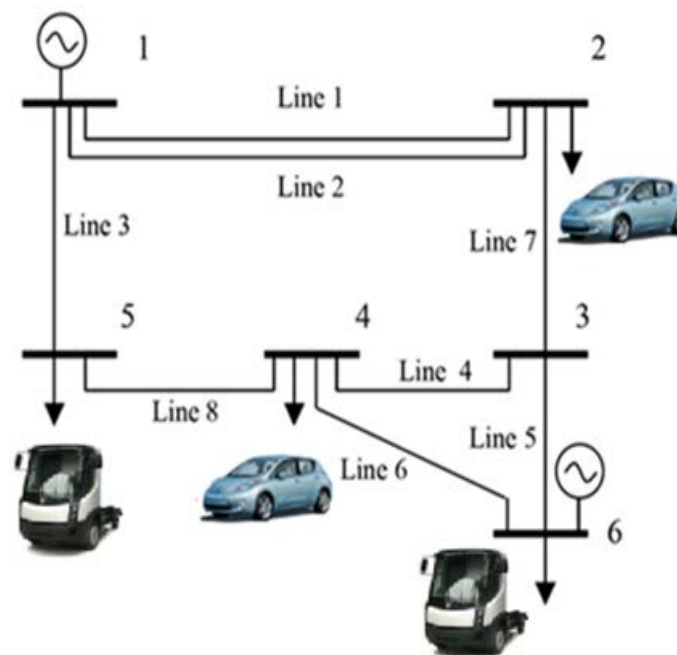


Figure 6- 22 Network Proposed

After a deterministic calculation, the new operation point is shown in Table 6-9. In this case, it is important to highlight that the power injection increases from 6.875 MW to 13.750 MW. This situation changes completely the network performance.

Table 6-9 Variables type of this case

N	Type	Vsp	P Load (Mw)	Q Load (Mvar)	P Generation (Mw)	Q Generation (Mvar)
1	Slack	1	0	0	-	-
2	PQ		5.5	2.2	0	-
3	PQ		0	0	0	-
4	PQ		3.3	1.65	0	-
5	PQ		5.5	2.2	0	-
6	PV	1	2.75	0.55	13.75	-

Observe that, the undervoltage limit of 10% was critically violated in comparison with no EV conditions previously discussed. Figure 6-23 shows a comparison by both situations, where there are undervoltage violations on buses 2, 3, 4, and 5, respectively.

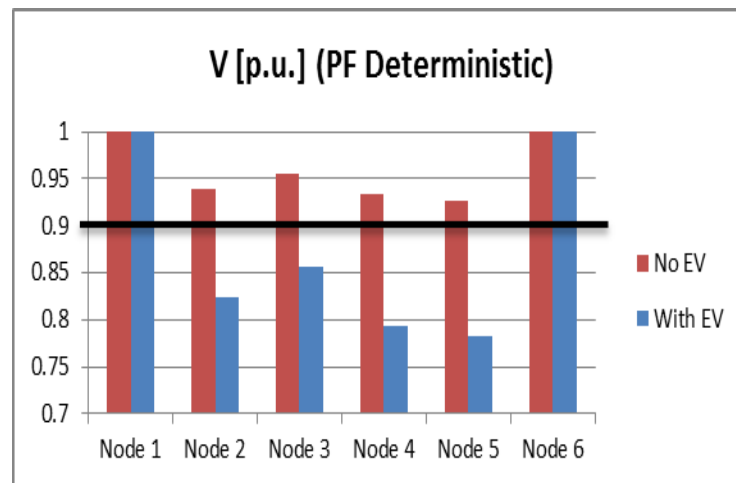


Figure 6-23 Comparing voltage for different nodes

Therefore, the performance of the system can be considered inadequate, essentially when power injections and load uncertainties are unconsidered. Figure 6-24 shows the same comparison to the line power flows, where it is possible to note that the power flow in line 5 and line 6 are near from the limit of 0.55 p.u.. However, from the deterministic perspective, there are no limit violations.

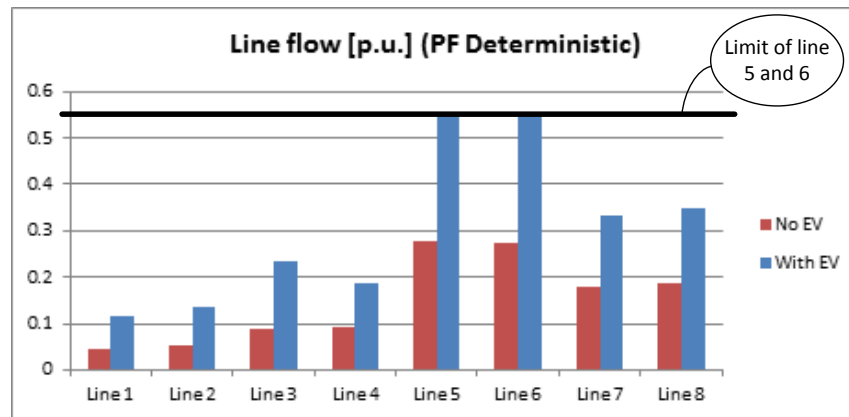


Figure 6-24 Comparing line flow for different lines

The effect of the uncertainty of EV

Considering the uncertainties caused by EV in the demand side and the variation of the renewable sources in the generation side, the information regarding each node are described in the Table 6-10. Therefore, a third situation is introduced. In terms of power flow input data (operation point), there are some evident differences between the deterministic and fuzzy approaches. Some knowledge of the system operator is included in order to represent the possible power injections and load uncertainties.

Table 6-10 Variables type with uncertainties

N	Type	Vsp	P Load (Mw)			Q Load (Mvar)			P Generation (Mw)			Q Generation (Mvar)		
1	Slack	1	0	0	0	0	0	0	4.7	4.95	5.2	3.4	3.8	4.2
2	PQ		5	5.5	6	2	2.2	2.4	0	0	0	0	0	0
3	PQ		0	0	0	0	0	0	0	0	0	0	0	0
4	PQ		3	3.3	3.6	1.5	1.65	1.8	0	0	0	0	0	0
5	PQ		5	5.5	6	2	2.2	2.4	0	0	0	0	0	0
6	PV	1	2.5	2.75	3	0.5	0.55	0.6	12.5	13.75	15	4.2	5.35	6.5

As stated already, the enhancements done in Fuzzy Power Flow tool were related with two main aspects: dependences between buses and a symmetric approach. In order to understand the effects in voltages and phases uncertainties regarding each one of these enhancements, a comparison with the previous version of the tool could be performed. However, the effects should be better clarified through the use of a large network. It will be emphasized during the study phase of the project.

The third situation can be described through the consideration of power injection and load uncertainties. Figure 6-25 shows the third situation. Table 6-10 shows the

input data needs to characterize a fuzzy analysis previously presented. In this case, it is possible to see the main results through the use of fuzzy numbers representations. Another important aspect is to compare the deterministic and fuzzy results. For instance, from the deterministic point of view, the power flow of line 3 is about 0.23 p.u., whereas from the fuzzy perspective it vary from 0.12 to 0.39 p.u., due to the uncertainty consideration.

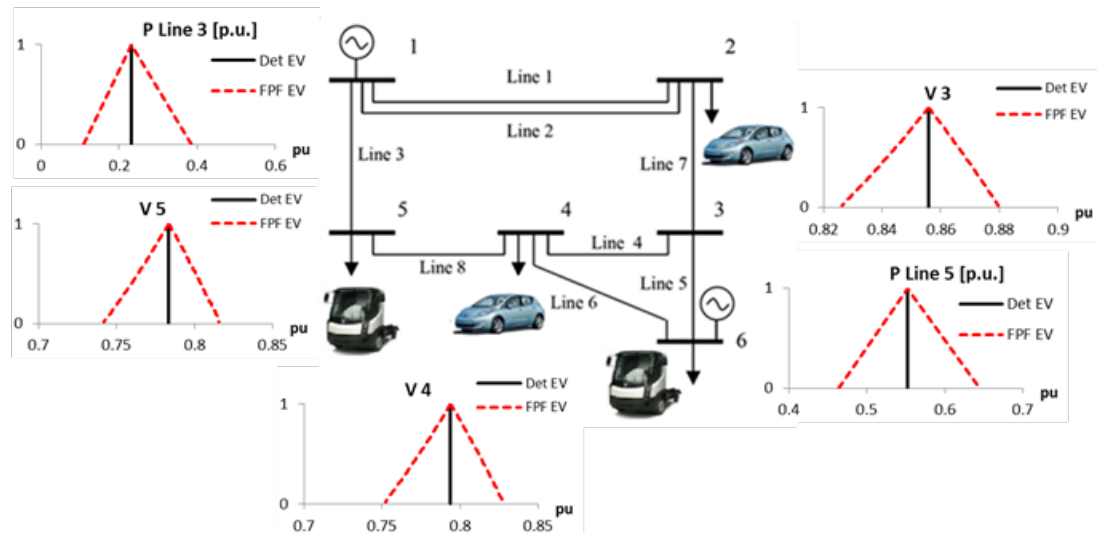


Figure 6-25 The effect of the uncertainty of the EV

It may be highlighted in Figure 6-26 that buses 2, 3, 4, and 5 have different levels of uncertainties, where the highest undervoltage situations appears on buses 4 and 5. Observe that, even that a 10% limit violation are being considered, the fuzzy analysis includes a new observation when the uncertainties are considered. In Figure 6-26 it is possible to know how adequate and/or inadequate could be the voltage violation in each bus.

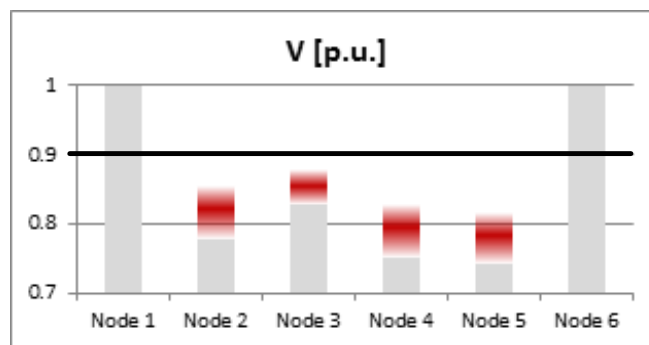


Figure 6-26 Effect of the uncertainty in the voltage

In the same way Figure 6-27 shows that, it is possible to identify the severity of the power flow through the transmission lines. Note that, the power flow in line 3 is performing huge variations when uncertainty is considered. The same evaluation

can be performed on lines 5 and 6, where through the fuzzy interpretation there is a possibility of the violation conditions.

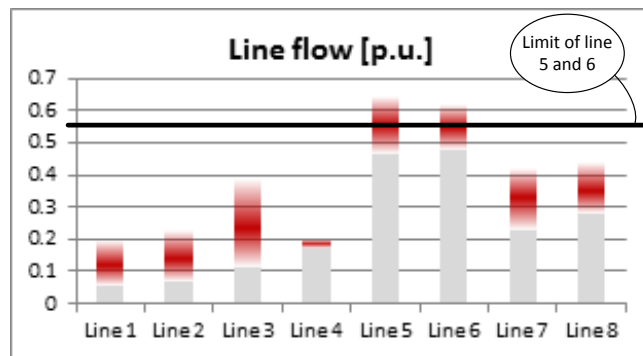


Figure 6-27 Effect of the uncertainty in the line flow

However, it is also plausible to consider that the system operator could overestimate the fuzzy considerations or only disregards some dependence between buses. In this case, it is important to introduce the fuzzy dependences effect. For this purpose, a fourth situation will be discussed.

The effect of dependences procedure

In order to assess the effect caused by the usage of dependences procedure in the nodes, it was assumed that the buses 2 and 6 have similar behaviours in terms of EV load. The node 2 was taken as a reference for those correlations and the level of the dependence used in node 6 was 0.5. The remaining part was kept free. The test results are presented in Figure 6-28, in which it is possible to observe the effect of EV dependences. As shown possibilities functions, the uncertainties are reduced.

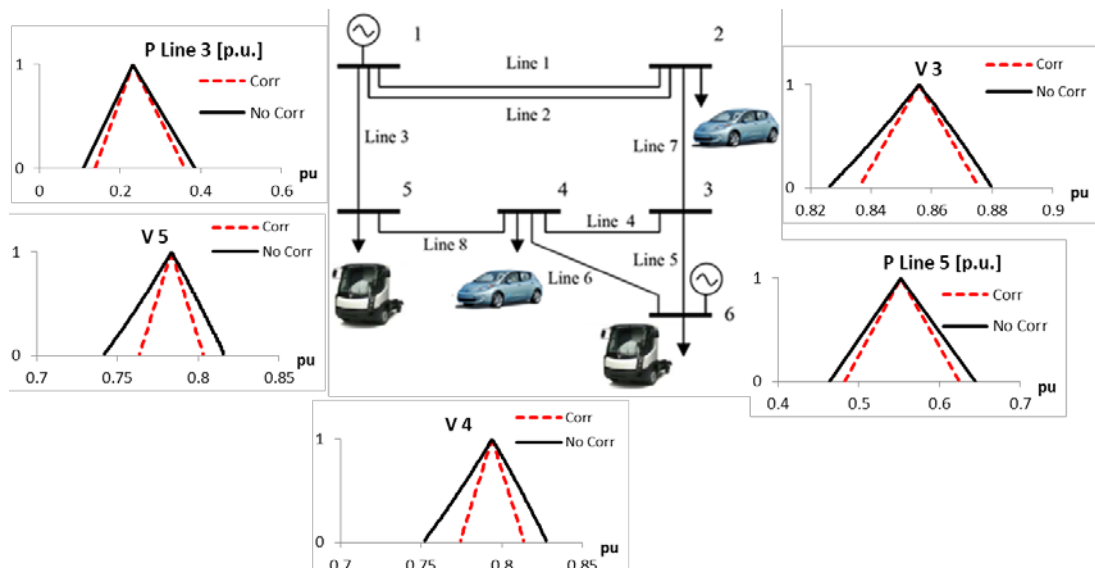


Figure 6-28 The effect of the dependence procedure

Figure 6-29 shows the reduction of the fuzzy result previously presented in the Figure 6-26. In this case, it is possible to see a better characterization of the undervoltage violation experienced in the third situation. The buses 2, 3, 4, and 5 are clearly below the violation criterion of 10%.

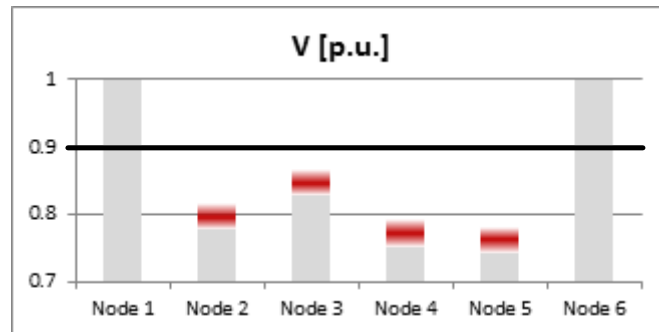


Figure 6-29 Effect of the uncertainty in the voltage

On the other hand, Figure 6-30 shows that the previous fuzzy interpretation can be confirmed, where the possible power flow violation experienced in lines 5 and 6 remaining being considered, since the power flow remain within the fuzzy interval.

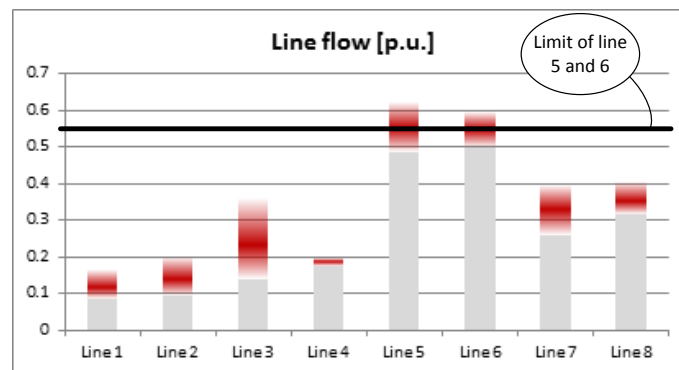


Figure 6-30 Effect of the uncertainty in the line flow

It is important to stress that the fuzzy analysis presented in this report consists of a didactic illustration of the use of the fuzzy sets. The broad potential of this methodology cannot be explored through the use of a didactic example. However, it will be fully explored in the study phase of the MERGE project.

6.2.4 Conclusions

As stated previously, Fuzzy Power Flow may represent an important way to assess power system conditions in the presence of uncertainties. Different from probabilistic evaluations, they try to reproduce, in terms of mathematical values, some aspects of ordinary behaviour that would be very difficult to describe by probabilistic functions. Besides the document have introduced the symmetric Fuzzy Power Flow approach, which works by maximizing and minimizing each system variable (voltages, phases,

currents, losses) subject to all the possible variations of the others, it has also introduced a new procedure of dependences.

Considering that the uncertainties will increase with the presence of EV in the electrical grids, the inclusion of a mechanism that eliminates the independence assumption (commonly assumed by the classic fuzzy power flow) between all the sources of uncertainties, such as EV uncertainty integration was incorporated in the Fuzzy Power Flow platform. This independence assumption may lead to pessimistic results, in the sense that artificial uncertainty is included due to the lack of information about some ordinary actions that may occur between buses. Hence, the information regarding node dependences can be used to keep the uncertainty level at its correct level, in order to ensure the credibility and usability of the solutions presented in Fuzzy Power Flow.

6.3 References

- [1] G. J. Andres, Probability Concepts in Electric Power Systems, New York: Wiley, 1990.
- [2] H. Saadat, Power System Analysis, Second Edition, McGraw-Hill, 2002.
- [3] B. Stott, Review of load flow calculation methods, Proc. IEEE, pp. 916-929, 1974.
- [4] B. Borkowska, "Probabilistic load flow," IEEE Trans. Power Apparatus and Systems, vol. PAS-93, no.3, pp 752-755, May-Jun, 1974.
- [5] R. L. Sullivan, Power System Planning, McGraw-Hill, New York, 1977.
- [6] A. Papoulis and S. Pillai, Probability, Random Variables, and Stochastic Processes, 4th ed. New York: McGraw-Hill, 2002.
- [7] P. Chen, Z. Chen, B. Bak-Jensen, Probabilistic Load Flow: A Review, Nanjing China, 6-9 April, 2008.
- [8] M. Th. Schilling, A. M. Leita da Silva, R. Billinton and M. A. El-Kady, "Bibliography on power system probabilistic analysis (1962-1988)," IEEE Trans. On Power Systems, vol. 5, no. 1, pp. 1-11, Feb. 1990.
- [9] W. G. Cochran, Sampling Techniques, 2nd ed., New York: Wiley, 1977.
- [10] R. N. Allan, C. H. Grigg and M. R. G. Al-Shakarchi, "Numerical techniques in probabilistic load flow problems," International Journal for Numerical Methods in Engineering, vol. 10, pp 853-860, Mar. 1976.
- [11] K. Kinsner, A. Serwin, M. Sobierajski, Wroclaw, Practical Aspects of Stochastic Load Flow Calculations, Archiv for Elektrotechnik 60, 283-288, 1978.
- [12] M. Sobierajski, A method of Stochastic Load Flow Calculation, Arch. F. Elektrotech. 60, pp 37-40, 1978.

- [13] J. F. Dopazo, O. A. Klitin, and A. M. Sasson, "Stochastic load flows," IEEE Trans. on Power Apparatus and Systems, Vol. PAS-94, pp. 299-309, 1975.
- [14] R. N. Allan, B. Borkowska and C. H. Grigg, "Probabilistic analysis of power flows," Proceedings of the Institution of Electrical Engineers (London), vol. 121, no. 12, pp. 1551-1556, Dec. 1974.
- [15] A. M. Leite da Silva, S. M. P. Ribeiro, V. L. Arienti, R. N. Allan and M. B. Do Coutto Filho, "Probabilistic load flow techniques applied to power system expansion planning," IEEE Trans. Power Systems, vol.5, no.4, pp.1047-1053, Nov. 1990.
- [16] R. N. Allan, A. M. Leite da Silva and R. C. Burchett, "Evaluation methods and accuracy in probabilistic load flow solutions," IEEE Trans. Power Apparatus and Systems, vol. PAS-100, no. 5, May 1981.
- [17] R. N. Allan, A. M. Leite da Silva and R. C. Burchett, "Discrete convolution in power system reliability," IEEE Trans. Reliability, vol. R-30, no. 5, Dec. 1981.
- [18] T. S. Karakatsanis and N. D. Hatzargyriou, "Probabilistic constrained load flow based on sensitivity analysis ," IEEE Trans. Power Systems, vol.9, no.4, pp.1853-1860, Nov. 1994.
- [19] R. N. Allan, A. M. Leite da Silva, "Probabilistic load flow using multilinearisations", IEEE Proc., Part C: Generation, Transmission and Distribution, vol.128, no.5, pp 280-287, Sep.1981.
- [20] Leite da Silva A.M., Arianti V.L. "Probabilistic load flow by a multilinear simulation algorithm" IEE Proc., Vol. 137 Pt. C, pp. 276-282I, July 1990.
- [21] Pei Zhang and Stephen T.Lee, "Probabilistic Load Flow Computation Using the Method of Combined Cumulants and Gram-Charlier Expansion", IEEE Trans. Power Systems, vol. 19, no 1, February 2004.
- [22] Jaschke S.R. "The Cornish-Fisher-Expansion in the Context of Delta-Gamma-Normal Approximations", <http://www.jaschke-net.de/papers/COFi.pdf>. Discussion Paper 54, Sonderforschungsbereich 373, Humboldt-Universitat zu Berlin.
- [23] Usaola J. "Probabilistic load flow with wind production uncertainty using cumulants and Cornish-Fisher expansion." Proceedings of the 2008 Power System Computation Conference. Glasgow (UK), July 2008
- [24] J.A. Pecas Lopes, "Identifying Management Procedures to Deal with Connection of Electric Vehicles in the Grid", IEEE Bucharest Power Tech Conference, June 28th – July 2nd, Bucharest, Romania, 2009.
- [25] N.D. Hatzargyriou T.S. Karakatsanis M. Papadopoulos, "Probabilistic Load Flow in Distribution Systems Containing Dispersed Wind Power Generation", IEEE Trans. Power. Sys., vol. PWR8-8, pp. 159-165, February 1993.
- [26] Public Power Corporation S.A., www.dei.gr



- [27] Hellenic Transmission System Operator S.A., www.desmie.gr
- [28] MERGE Project. "Identification of Traffic Patterns and Human Behaviors", Deliverable 1.1 – Task 1.5. (in Press).
- [29] Zadeh, L.A., 1965, "Fuzzy sets", Information and Control, 8, 338-353
- [30] Zadeh, L.A., 1978, "Fuzzy sets as a basis for a theory of possibility", Fuzzy Sets and Systems, 1, 3-28
- [31] Miranda V., Matos, M., "Distribution System Planning with fuzzy models and techniques", CIRED 89, Bristol, England.
- [32] Miranda V., Matos, M., Saraiva, J.T., "Fuzzy Load Flow – New Algorithms Incorporating Uncertain Generation and Load Representation", 10th PSCC, Graz, August 1990; in Proceedings of 10th PSCC, Butterworths, London, 1990.
- [33] Saraiva, J.T., Miranda V., Matos, M., "Generation and Load Uncertainties Incorporated in Load Flow Studies", Proceedings of MELECON 91, Ljubljana.
- [34] Merge Team, "Identification of the Traffic Patterns and Human Behaviors", WP1, Task 1.5, D1.1.
- [35] Merge Team, "Modeling Electric storage devices for EV", WP2, Task 2.1, D2.1.
- [36] Saraiva, J.T., Fonseca, N., Matos, M., "Fuzzy Power Flow – an AC model addressing correlated data", Proceedings of PMAPS'04, Ames, Iowa, pp.519-524.
- [37] Dimitrovski, A, Tomsovic, K, "Slack Bus Treatment in Load Flow Solutions with uncertain Nodal Powers", PMAPS, Iowa State University, Ames, Iowa, September 2004.
- [38] Matos, M, Gouveia, E., "The Fuzzy Power Flow Revisited", Proceedings of the IEEE PowerTech 2005, Saint Petersburg.
- [39] Matos, M, Gouveia, E., "Symmetric AC fuzzy power flow model", European Journal of Operational Research, 2009, 197, 1012-1018.



6.4 Appendix

```

clear
basemva = 100; accuracy = 0.001; maxiter = 20;

% IEEE 90-BUS TEST SYSTEM (Greek Electric Power)
% Bus Bus Voltage Angle ---Load--- Generator----- Injected
% No code Mag Degree MW Mvar MW Mvar Qmin Qmax Mvar
busdata=[1 0 1 0.0 92.509 57.331 0 0.0 0 0 0%10231-orestiad
2 0 1 0.0 60.861 37.717 0 0.0 0 0 0%10631-alexandr
3 2 1 0.0 68.385 42.381 420 150 -144 250 0%10831-komotini
4 0 1 0.0 139.092 86.202 0.0 0.0 0 0 0%10931-iasmos
5 0 1 0.0 0 0 0.0 0.0 0 0 0%12011-filippo
6 0 1 0.0 371.486 225.826 0.0 0.0 0 0 0%12131-filippo
7 0 1 0.0 0 0 0.0 0.0 0 0 0%12138-D1.filipp
8 0 1 0.0 203.827 126.32 0.0 0.0 0 0 0%13331-babdos
9 0 1 0.0 1117.275 675.264 0.0 0.0 0 0 0%14031-K_Qes/N1
10 0 1 0.0 0 0 0.0 0.0 0 0 19%14038-K_Qes/N
11 0 1 0.0 0.0 0.0 0.0 0.0 0 0 0%15011-K_thes
12 2 1 0 0 0 350 63.955 -147 87 0%19131-QHSAUROS
13 1 1 0 0 0.0 577.417 55.353 0 0 0%19911-boulgari
14 2 1 0 31.67 19.627 900 160 -279 374 0%21011-amuntaio
15 2 1 0 0 0 1440 450 -476 630 0%22011-ag.dimitr
16 2 1 0 0 0 1180 300 -360 584 0%23011-kardia.k
17 2 1 0 0 0 360 150 -112 131 0%24031-kardial
18 0 1 0 0 0 0 0 0 0 0%24038-d1.kardi
19 2 1 0 572.02 322.82 550 210.853 -199 363 0%25031-ptolemai
20 0 1 0 110.518 68.492 0 0 0 0 0%26631-katerini
21 2 1 0 268.265 166.258 386 220.459 -137 192 0%26931-beroaia
22 0 1 0 0.0 0.0 0.0 0 0 0 0%30011-larisa.k
23 0 1 0 608.904 368.961 0 0 0 0 0%30231-larisa.k
24 0 1 0 0.0 0.0 0 0 0 0 4.3%30236-d3.laris
25 0 1 0 0.0 0.0 0 0 0 0 0%30238-d1.laris
26 2 1 0 331.232 205.96 111 19.658 -36 63 0%32131-lamia
27 0 1 0 158.75 87.205 0 0 0 0 0%33131-sovel
28 0 1 0 0 0.0 0 0 0 0 0%34011-k.trikal

78 77 0.0084 0.0049 0 1
80 79 0.0018 0.0065 0 1
80 81 0. 0.0001 0. 1
80 83 0.0152 0.0611 0.04617 1
80 85 0.05289 0.13023 0.023525 1
81 78 0.0071 0.0262 0 1
82 76 0.0071 0.0262 0 1
82 80 0.0314 0.1266 0.09563 1
83 86 0.03328 0.14418 0.023685 1
83 89 0.0014 0.0214 0 1
84 73 0.0230 0.0761 0.10084 1
85 83 0.0239 0.08902 0.134505 1
86 83 0.04937 0.13229 0.019785 1
86 87 0.0473 0.11516 0.016895 1
87 83 0.0194 0.0784 0.038085 1
89 88 0.0223 0.0108 0 1];

```




%	Bus bus		R	X	Line code	
%	nl	nr	p.u.	p.u.	1/2 B	= 1 for lines
%					p.u.	> 1 or < 1 tr. tap at bus nl
linedata=[
	1	4	0.05438	0.23559	0.0387	1
	2	1	0.03685	0.12015	0.064215	1
	2	3	0.02374	0.09582	0.01809	1
	3	2	0.025	0.10092	0.019055	1
	3	4	0.00244	0.01004	0.03059	1
	4	6	0.0227	0.088263	0.06062	1
	5	11	0.00172	0.02336	0.42834	1
	6	12	0.004883	0.0198	0.060225	1
	6	7	0.0014	0.0214	0	1
	7	5	0.0223	0.0108	0	1
	8	6	0.0566	0.16366	0.074375	1
	8	9	0.0190	0.05965	0.039825	1
	9	6	0.04763	0.19227	0.0363	1
	9	10	0.0003	0.0022	0	1
	10	11	0.0027	0.0014	0	1
	11	13	0.009	0.0111	0.61006	1
	11	14	0.0014	0.0130	0.74827	1
	11	15	0.0011	0.0109	0.62775	1
	14	16	0.0001	0.0012	0.36997	1
	14	22	0.001315	0.0127	0.72902	1
	16	22	0.001345	0.01301	0.74673	1
	16	28	0.0012	0.0112	0.64385	1
	17	18	0.0014	0.0057	0	1
	17	19	0.002	0.0081	0.00613	1
	17	21	0.0069	0.0248	0.025855	1
	18	16	0.0086	0.0048	0	1
	19	21	0.02254	0.09088	0.017155	1

62	0	1	0.0	21.70	12.7	0.0	0.0	0	0	0%55131-argur/LH
63	2	1	0.0	2.4	1.2	330	51.578	-109	177	0%56031-ahsagi
64	2	1	0.0	7.6	1.6	760	465	-258	523	0%59011-laur_gis
65	2	1	0.0	94.2	19.0	254	141.664	-98	171	0%59531-laurio t
66	0	1	0.0	0.0	0.0	0.0	0.0	0	0	0%59538-d1.laur
67	0	1	0.0	22.8	10.9	0.0	0.0	0	0	0%60031-korinthos
68	0	1	0.0	30.0	30.0	0.0	0.0	0	0	0%60231-argos2
69	0	1	0.0	0.0	0.0	0.0	0.0	0	0	0%60431-kranidi
70	2	1	0.0	5.8	2.0	820	230.981	-255	416	19%61031-meg.ites
71	0	1	0.0	0.0	0.0	0.0	0.0	0	0	0%61631-molaoi
72	0	1	0	11.2	7.5	0	0	0	0	0%62731-kalamat1
73	0	1	0	0	0.0	0.0	0	0	0	0%64231-patra2
74	2	1	0	6.2	1.6	60	20.645	-20	20	0%65131-purgos
75	0	1	0	8.2	2.5	0	0	0	0	0%70011-distomo
76	0	1	0	3.5	1.8	0	0	0	0	0%70038-d1.distomo
77	2	1	0	9.0	5.8	300	0	0	0	0%71011-ancelwos
78	0	1	0	3.2	0.9	0	0	0	0	0%71037-d2.ancel
79	0	1	0	9.5	3.4	0	0	0	0	0%71038-d1.ancel
80	2	1	0	2.2	0.7	170	76.103	-69	82	0%71131-ancelwos
81	2	1	0	17.5	11.2	260	150.752	-120	108	0%71132-ancelwos
82	0	1	0	0.0	0.0	0.0	0	0	0	0%75031-distomo
83	2	1	0	3.2	1.6	226	77.798	-100	127	0%80031-karacqou
84	2	1	0	8.7	6.7	180	60.7	-72	89	4.3%81032-lamprakh
85	0	1	0	0	0.0	0	0	0	0	0%82831-aktio
86	0	1	0	3.5	2.3	160	28.486	-66	72	0%85131-giannen1
87	0	1	0	0	0.0	0	0	0	0	0%85431-mourtos
88	0	1	0	0	0.0	0	0	0	0	0%88011-karacqou
89	0	1	0	2.4	0.9	0	0	0	0	0%88038-d1.aracq



29	0	1	0	0	0	0	0	0	0	0	0%34038-d1.trika
30	0	1	0	190.515	118.071	0	0	0	0	0	0%34431-k.trikal
31	0	1	0.0	0.0	0.0	0.0	0.0	0	0	0	0%40011-k.larumn
32	0	1	0.0	372.46	208.23	0.0	0.0	0	0	0	0%40231-larumna
33	0	1	0.0	0	0	0.0	0.0	0	0	0	0%40238-d1.larumn
34	0	1	0.0	209.167	123.221	0.0	0.0	0	0	0	0%41131-schmatar
35	0	1	0.0	79.188	49.074	0.0	0.0	0	0	0	0%42231-yacna
36	2	1	0.0	79.741	46.385	300	121.571	-90	147	0	0%43031-aliberi
37	0	1	0.0	0	0	0.0	0.0	0	0	0	0%50011-acarnes
38	2	1	0.0	0.0	0.0	0.0	0.0	0	0	0	0%50037-
39	0	1	0.0	0.0	0.0	0.0	0.0	0	0	0	0%50038-d1.acarn
40	2	1	0.0	101.952	63.184	0.0	0.0	-6	24	0	19%50131-acarnes1
41	0	1	0.0	0.0	0.0	0.0	0.0	0	0	0	0%50132-acarnes2
42	0	1	0	11.2	7.5	0	0	0	0	0	0%50831-n.calci
43	2	1	0	0	0.0	0.0	0	-6	24	0	0%50832-n.calci2
44	0	1	0	6.2	1.6	0	0	0	0	0	0%51011-koumoun
45	0	1	0	8.2	2.5	0	0	0	0	0	0%51131-koumoun1
46	0	1	0	3.5	1.8	0	0	0	0	0	0%51132-koumoun2
47	0	1	0	9.0	5.8	0.0	0	0	0	0	0%51133-koumoun3
48	0	1	0	3.2	0.9	0	0	0	0	0	0%51136-d3.koumoun
49	0	1	0	9.5	3.4	0	0	0	0	0	0%51137-d2.koumou
50	0	1	0	2.2	0.7	0	0	0	0	0	0%52011-ag.stefan
51	0	1	0	17.5	11.2	0	0	0	0	0	0%52038-d1.ag stef
52	2	1	0	0.0	0.0	0.0	0	0	0	0	0%52131-ag stef
53	0	1	0	3.2	1.6	0	0	0	0	0	0%52136-d4.koumou
54	0	1	0	8.7	6.7	0	0	0	0	0	4.3%52138-d6.koumou
55	0	1	0	0	0.0	0	0	0	0	0	0%53031-rouf1
56	0	1	0	3.5	2.3	0	0	0	0	0	0%53032-rouf2
57	0	1	0	0	0.0	0	0	0	0	0	0%54011-pallini
58	0	1	0	0	0.0	0	0	0	0	0	0%54038-t2.pallini
59	0	1	0	2.4	0.9	0	0	0	0	0	0%54131-pallini
60	0	1	0	10.6	1.9	0	0	0	0	0	0%55011-
61	0	1	0.0	0.0	0.0	0.0	0.0	0	0	0	0%55038-

7 CONCLUSIONS

Electric power systems still follow planning rules and procedures defined for the traditional operational paradigm. It is necessary to identify and prepare solutions for the operational problems caused by the large penetration of EVs. There are a number of software models and tools available to carry out steady state and dynamic studies of the eclectic power system, but without or with very limited capability to consider the impact from EVs. Several exiting simulation platforms, which include IPSA+, MATLAB SIMULINK, EUROSTAG and MATLAB, PSS/E, and probabilistic and fuzzy power flow tools, were adapted and enhanced to deal with the integration of EV into the power system.

IPSA+ software was adapted/enhanced to accommodate EVs by using its UDM (User Defined Model) tool and the scripted extension library for Python. Individual EV battery models based on UDM were developed considering two types of interfacing structures, fast charging and shower charging, and different voltage levels, which are capable of incorporating specific control procedures; Reserve and frequency response models were adapted and enhanced to evaluate the performance of a network with different levels of EV penetration for providing the ancillary service; A spatial-temporal analysis tool was developed and integrated into the exiting IPSA+ tool to address the correlation of the mobility with population movement in an urban area.

The simulation platforms based on the MATLAB Simulink software developed in the EU Microgrids projects were adapted to incorporate EV models for smart charging and V2G operation in both normal and islanded modes. This development focuses on assessing impacts of EVs in Microgrids. These simulation platforms are now capable of assessing the steady state and dynamic behaviour of Microgrids in three-phase balanced mode and unbalanced modes. The dynamic stability of inverter dominated Microgrids was investigated.

The simulation platform that works over Eurostag and MATLAB software was adapted to incorporated EV models for smart charging and V2G operating in both normal and islanded modes in MV distribution networks. MATLAB was used as a user interface and logic controller. Specific scripts (describing external procedures that invoke the basic simulation tools) were developed to simulate the step by step response of the system in quasi-steady state and in dynamic behaviour when following the load diagram in critical periods and adopting different charging strategies (dumb, tariff based approaches, smart charging strategies). The capability to perform load following in these networks with large EV presence was addressed with these tools.

A simulation platform that works over PSS/E software was adapted to incorporate aggregated models of EV. This model provides a platform to assess the impacts of EVs in steady state operation and dynamic behavior for large interconnected transmission systems having conventional generation and large penetration of renewable power sources (namely wind power). The aggregated EV response to frequency changes or other control signals was embedded in dynamic load models that represent clusters of aggregated EV. Specific scripts were developed to simulate the step by step response of the system in quasi-steady state and in

dynamic behavior when following the load diagram in critical periods and adopting different charging strategies (dumb, tariff based approaches, smart charging strategies). The Models of intermittent renewable generation (in particular wind power) were developed.

Apart from the deterministic simulations used to address steady impacts resulting from the presence of EV on the network for extreme conditions, fuzzy and probabilistic tools were developed to evaluate the ranges of power flows, voltages levels and losses in the transmission network when large variations of EV penetration and the use of different charging strategies takes place leading to significant uncertainty in node injections. The fuzzy power flow tool was adapted and enhanced to cope with EV nodal loads in a way that the important dependencies among EV load uncertainties in the nodes is taken into consideration. Besides propagating the uncertainties from the data to the results, providing fuzzy descriptions of the branch flow, node voltages and losses, the tool is able to identify the risk of congestion in branches and the degree of repression in the node injections and in the system. The probabilistic load flow tools were also adapted and enhanced to provide probabilistic density functions of flows, voltages and losses.

All the Sub-Tasks detailed in the Description of Work were completed successfully. With these adapted and enhanced platforms, the comprehensive analysis of the EV impact on the electric power system and the provision of decision-making capability are possible.



MOBILE ENERGY RESOURCES IN GRIDS OF ELECTRICITY

ACRONYM: MERGE

GRANT AGREEMENT: 241399

**WP 2
TASK 2.4
DELIVERABLE D2.2**

MARKET ISSUES

15 FEBRUARY 2011



REVISION HISTORY

VER.	DATE	NOTES (including revision author)
01	11/12/2010	First draft. F. Báñez, A. Ramos, J. M. Latorre (Comillas), G. E. Asimakopoulou (NTNU)
02	13/01/2011	Revised by M. Rosa, L. Carvalho, L. Bremermann (INESC Porto).
03	01/02/2011	Second draft. F. Báñez, A. Ramos, J. M. Latorre (Comillas).
04	07/02/2011	Revised by J.A. Peças (INESC Porto).
05	15/02/2011	Final version approved
06		
07		
08		
09		
10		



AUTHORS

Fernando Báñez	Fernando.Banez@upcomillas.es
Andrés Ramos	Andres.Ramos@upcomillas.es
Jesús M. Latorre	Jesus.Latorre@upcomillas.es
Georgia Asimakopoulou	gasimako@power.ece.ntua.gr
Aris Dimeas	adimeas@power.ece.ntua.gr
Nikos Hatzigiorgiou	nh@power.ece.ntua.gr

CONTRIBUTORS

APPROVAL

DATE

Project Coordinator	PPC	N. Hatzigiorgiou	15/02/2011
Technical Coordinator	INESC Porto	J. A. Peças Lopes	07/02/2011
Work Package Leader	INESC Porto	J. A. Peças Lopes	07/02/2011

Access:

☒

Project Consortium

☒

European Commission

☐

Public

Status:

☐

Draft Version

☐

Submission for Approval (deliverable)

☒

Final Version (deliverable, approved)





SUMMARY

A massive introduction of electric vehicles (EV) in the society could have an important impact into the electric power systems, creating new challenges for the electricity sector in its structure and operation.

The conventional system expansion models and market ones will not be able to deal correctly with this integration of the electric vehicles in addition with other expected developments that will take place in Europe during the same period (integration of more renewable energy sources (RES), active demand, distributed generation, etc).

The objective of this report is to specify and explain the tools that are going to be used in order to evaluate the technical and economic impact of the electric vehicles into the medium-term system operation, for instance, system reliability, marginal costs, generation mix, CO₂ emissions.

The report has been divided in two parts, one for each tool developed. Each part explains the basics and the possible applications of their respective tool.

In order to see the effects of the presence of the electric vehicles in the system, three scenarios are examined:

- In Scenario 1 the market is simulated without EVs.
- In Scenario 2 two different levels of EV penetration are considered, while EVs act as simple loads: their owners simply define the timing and the amount of energy for charging; thus, the total load (households and EVs) grows.
- In Scenario 3 EVs can absorb or inject energy to the grid, depending on the price levels. By this way, load flexibility is achieved to a certain level.



TABLE OF CONTENTS

1	INTRODUCTION	6
2	APPROACH	6
3	MATHEMATICAL PROGRAMMING AND SIMULATION METHODOLOGIES	7
3.1	Introduction	7
3.2	Characteristics and structure of the model	7
4	DESCRIPTION OF THE ROM MODEL.....	8
4.1	Formulation of the day-ahead Market Operation	8
4.2	Real Time Simulation.....	11
5	DEVELOPMENTS FOR THE CONSIDERATION OF THE EVs	14
5.1	Adaptations in the formulation of the day-ahead Market Operation	14
6	ROM MODEL RESULTS.....	17
7	GAME THEORY METHODOLOGY	21
7.1	Static games	21
7.2	Dynamic games	22
8	DESCRIPTION OF THE GAME THEORY MODEL	22
8.1	The players	23
8.2	The rules of the game.....	23
8.3	The payoff function of each player.....	26
9	DETAILED ALGORITHM OF THE MODEL.....	33
9.1	Consumer function.....	33
9.2	Distributed generation function	33
9.3	EVs function.....	34
9.4	Aggregator function	35
10	SIMULATION RESULTS.....	35
10.1	Input data.....	35
10.2	Results.....	37
11	PRELIMINAR CONCLUSIONS	8
12	REFERENCES.....	42

DELIVERABLE D2.2 – MARKET ISSUES

1 INTRODUCTION

Integration of EVs into the electrical grid will prove challenging not only for the operation of the grid, but also for the operation of the market, since EVs are seen both as a load and as a source of energy previously stored in their batteries. In order to assess the impact (technical and economical) to the market operation of different penetration levels of EVs, and the interaction of EVs with RES (analyzing the benefits and problems of this coexistence), a simulation tool is deemed necessary. Two different tools with different approaches have been developed to reach these objectives.

Such a simulation should take into account the fact that, autonomous individuals that are part of the electricity grid (e.g. consumers, EVs, distributed generation) act according to their notion of maximizing their personal profit. However, its individuals' decision inadvertently affects the optimal "state" of market equilibrium. The decisions of each individual are affected by the decisions of the other individuals because they are all part of the same market.

In order to compute the short-term system operation and evaluate the economic and technical impacts of the integration of EVs and other RES, mathematical programming and simulation is a powerful tool in order to evaluate the system operation.

In addition, in the attempt to re-produce and predict the actions of the "players" in such a complex environment, game theory has been proved to be a valuable ally.

In the following sections, a short introduction to the two tools developed is presented and then, the details of their application for the case of the EVs integration will be specified.

2 APPROACH

The first tool that is presented is the ROM Model (Reliability and Operation Model for Renewable Energy Sources). It uses the mathematical programming for optimizing (minimizing costs) the system in conjunction with a simulation process to evaluate the system in real time.

The ROM Model is able to compute reliability indices (e.g. LOLP, LOLE), marginal costs and operation results (e.g. different technologies output, emissions, primary energy surplus) resulting from the medium term system operation. Thus, by comparing results obtained with different penetration levels of EVs and RES, the impact of these technologies can be estimated.

The second tool uses the game theory as a way to solve the problem, studying the interaction of multiple players in competitive situation, trying to reach the equilibrium state at which all the players achieve the optimal gain.

PART I. ROM Model

3 MATHEMATICAL PROGRAMMING AND SIMULATION METHODOLOGIES

This section introduces the ROM Model, giving a brief overview over the structure and the characteristics of it.

3.1 Introduction

The ROM Model has been developed at the Instituto de Investigación Tecnológica (IIT), ICAI, Universidad Pontificia Comillas.

The first objective of the model is to determine technical and economic impact of the EVs and RES into the medium-term system operation, including reliability assessment.

3.2 Characteristics and structure of the model

In order to compute the short-term system operation and evaluate the EVs and other RES integration, the ROM tool follows a combined modelling approach whereby a daily optimization model [9] is followed by a sequential hourly simulation [12], with a resolution of one hour. This replicates the sequence of the markets and the decisions, reproducing the hierarchy and the chronology of the decision levels and allows representing that uncertainty is revealed over time (forecasting techniques become more accurate when the interest hour approaches). A chronological approach is used to sequentially evaluate the system operation for every day of a year. Decisions above this scope as the weekly scheduling of pumped storage hydro plants are done internally in the model by heuristic criteria. The management of hydro resources and seasonal pumped storage that exceeds the year time frame must be computed by another higher-level model and be taken as an input into the ROM. Monte Carlo simulation of many yearly scenarios is used to deal with the stochasticity of the demand and the intermittent generation.

As it will be shown in the next section, detailed operation constraints (minimum load, ramping rates...) are included into the daily unit commitment model. The hourly simulation is run afterwards to account for intermittent generation production errors and unit failures, and therefore revises the previous schedule. The differences among optimization and simulation decisions can be due to wind generation forecast errors and generation outages, and represent the value of the perfect Intermittent Generation IG forecast.

4 DESCRIPTION OF THE ROM MODEL

This section has the description of the two fundamental parts (optimization and simulation) of the model.

4.1 Formulation of the day-ahead Market Operation

In this section, the optimization model that is responsible for determining the initial daily program for the generators production is going to be described. This model calculates the daily economic dispatch, considering the demand and wind power generation forecasted one day in advance. Subsequently, these estimates may be altered by changes in the values of the random variables (electricity demand, intermittent generation, availability of the generators, etc.) that are taken into account by a simulation model that will be described in the next section.

The tables below show the main elements of the model: indexes, parameters and variables.

Table 21. Sets

Name	Meaning
p	Periods (hours)
g	Generators
t	Thermal units ($\{t\} \subset \{g\}$)
h	Hydro plants (reservoirs) ($\{h\} \subset \{g\}$)
b	Pumped storage hydro plants (reservoirs) ($\{b\} \subset \{h\}$)
i	Concentrated solar power (CSP) plants ($\{i\} \subset \{g\}$)

Table 22. Parameters

Name	Meaning	Unit
D_p	Demand for period p	MW
WG_p	Wind and other RES generation for period p	MW
UR_p, DR_p	Upward and downward reserve in period p	MW
\overline{GP}_p^g	Maximum output of generator g in period p	MW
RU^t, RD^t	Ramp-up and ramp-down of thermal unit t	MW/h
\overline{GC}_p^h	Maximum consumption of pumped storage hydro plant $h \in b$ in period p	MW

I_p^h	Inflows in reservoir h for period p	MWh
In_p^i	Irradiation in CSP plant i for period p	MWh
IRC^i, IRD^i	Charging and discharging ramp of storage of CSP plant i	MWh/h
URC, DRC	Upward and downward reserve deficiency cost	€/MWh
$NSEC$	Non-supplied energy cost	€/MWh
FC^t	Fixed cost of thermal unit t	€/h
VC^g	Variable cost of thermal unit g including fuel cost and O&M	€/MWh
SC^t	Start-up cost of thermal unit t	€

Table 23. Variables

Name	Meaning	Unit
$opcost$	Total system operation cost	€
nse_p	Non-supplied energy in period p	MW
sp_p	Energy spillage in period p	MW
$urdef_p, drdef_p$	Upward and downward reserve deficiency in period p	MW
st_p^t, sh_p^t	Start-up and shut-down of thermal unit t in period p	[0,1]
c_p^t	Commitment of thermal unit t in period p	[0,1]
ih_p^h	Indicator of pumping or generation of hydro plant h in period p	[0, 1]
gp_p^g	Output of generator g in period p	MW
gc_p^h	Consumption of pumped storage hydro plant $h \in b$ in period p	MW
r_p^h, s_p^h	Reservoir level and spillage of hydro reservoir h in period p	MWh
gur_p^g, gdr_p^g	Upward and downward power reserve of generator $g \notin b$ in period p	MW
pur_p^h, pdr_p^h	Upward and downward power reserve of pumped storage hydro plant $h \in b$ in period p	MW
ie_p^i, is_p^i	Energy stored and spilled in CSP plant i in period p	MWh
ic_p^i, id_p^i	Power output and power consumption of CSP plant i in period p	MW

4.1.1 Objective function

The operations costs minimization of the electric system is expressed as follows:

$$opcost = \sum_p \left[\sum_t \left(FC^t c_p^t + SC_t st_p^t + VC^g gp_p^g \right) + NSEC nse_p + URC urdef_p + DRC drdef_p \right] \quad (1)$$

Model constraints are described in the following sections. Note that the duration of all periods is one hour and therefore the formulation becomes simplified.

4.1.2 Demand and reserve constraints

- The equation that controls the balance of generation and demand by the generation units for each period is (2). The set of generators g includes thermal units, hydro plants and CSP plants as well. The wind generation considers its forecasted production:

$$D_p - WG_p - nse_p + sp_p = \sum_g gp_p^g \quad \forall p \quad (3)$$

- The total upward and downward reserve for each period p :

$$\begin{aligned} \sum_{g \in b} gur_p^g + \sum_{h \in b} pur_p^h + urdef_p &\geq UR_p \\ \sum_{g \in b} gdr_p^g + \sum_{h \in b} pdr_p^h + drdef_p &\geq DR_p \end{aligned} \quad \forall p \quad (4)$$

4.1.3 Thermal unit constraints

- The commitment, start-up and shut-down of thermal units is controlled by these variables, with the following logical relation. Only commitment variable needs to be defined as binary.

$$c_p^t - c_{p-1}^t = st_p^t - sh_p^t \quad \forall p, t \quad (5)$$

- The output plus the power reserve of each thermal unit is bounded by the maximum output of the unit, given by the parameter \overline{GP}_p^g .

$$gp_p^g + gur_p^g \leq \overline{GP}_p^g \quad \forall p, g \in t \quad (6)$$

- The generators could have a minimum time that, once the generator has been switched on (respectively switched off), it must be kept running (respectively stopped). The up and down ramps limit the variation of the thermal unit output including the up and down power reserves in consecutive hours:

$$\begin{aligned} (gp_p^g + gur_p^g) - (gp_{p-1}^g - gdr_{p-1}^g) &\leq RU^g \\ (gp_{p-1}^g + gur_{p-1}^g) - (gp_p^g - gdr_p^g) &\leq RD^g \end{aligned} \quad \forall p, g \in t \quad (7)$$

4.1.4 Hydro plant constraints

- The model considers an equation that ensures that if a unit is pumping, it cannot be generating at the same time.

$$\begin{aligned} gp_p^h &\leq ih_p^h \overline{GP}_p^h \\ gc_p^h &\leq (1 - ih_p^h) \overline{GC}_p^h \end{aligned} \quad \forall p, h \quad (8)$$

- The maximum output (pumping) of the hydro units is bounded by technical limitations of the unit.

$$gp_p^g + gur_p^g \leq \overline{GP}_p^g \quad \forall p, g \in h \quad (9)$$

- The account of the hydro reservoir is controlled by the following hourly constraint:

$$r_p^h - r_{p-1}^h = -gp_p^h + gc_p^h - s_p^h + I_p^h \quad \forall p, h \quad (10)$$

4.1.5 CSP plant constraints

- The equation that controls the energy balance in the CSP plant:

$$In_p^i - gp_p^i - ic_p^i + id_p^i = 0 \quad \forall p, i \quad (11)$$

- The balance of the CSP plant storage is given by the following equation:

$$ie_p^i - ie_{p-1}^i = ic_p^i - id_p^i - is_p^i \quad \forall p, i \quad (12)$$

- The constraints in the charge and discharge of the CSP plants:

$$\begin{aligned} ie_p^i - ie_{p-1}^i &\leq IRC^i \\ ie_{p-1}^i - ie_p^i &\leq IRD^i \end{aligned} \quad \forall p, i \quad (13)$$

4.2 Real Time Simulation

The correction of the deviations identified previous to the hour 14 (this is the hour when the daily programming is sent to the System Operator [10]) of the day before the operation has been modelled in the optimization module. After the 14 h, the adjustments that have to be done in the commitment of the units, the program of the

units and the level of the different loads of the system are computed by a simulation module. This module is divided in two steps:

- In the first step, the simulation module performs **corrections to the commitment specified by the daily optimization module**, applying them in the 24 h of the day before the operation (D-1). The Midnight is assumed to be the last time where the commitment decision of a group would allow this group to reach the ramping hours in the morning (7-12 am). These deviations could be produced by an error in the forecast of the intermittent generation or the failure of the generation units. The corresponding corrective actions are the commitment of new generation units or the shutting down of others, whose objective is to reduce the deviation into safe margins that can later be handled by the use of reserve (for instance reducing error to less than 1 GW).
- The second step deals with the **monitoring of each hour of the interest day and it takes the adequate decisions in order to correct the error** in the forecasting of the wind production, the demand or failure of the thermal units. Once the hour 24 of the day D-1 has gone by, these corrective actions cannot be the commitment or shutting down of any unit (except the fast peaking units). The actions that can be selected to achieve this objective are the use of the reserves, the commitment of the fast start-up peaking units and finally load shedding.

Table 24. Daily Operation chronological resume

Time	Action
Hour 14 of day D-1	Estimation of intermittent generation for each hour of day D (errors for 10 to 34 h in advance)
	Daily dispatch of day D using the optimization module
Hour 24 of day D-1	Estimation of the intermittent generation for each hour of day D (errors for 1 to 24 h in advance)
	Commitment (disconnection) correction of units related to the error estimation for peak (low consumption) periods
Each hour of day D	Knowledge of actual intermittent generation
	Selection of adequate decisions for forecast deviations correction according to priorities (as can be seen in Figure 21)
Last hour of day D	Data regarding the commitment of the different units, production and the reservoir level is stored to be used in the unit commitment of the next day

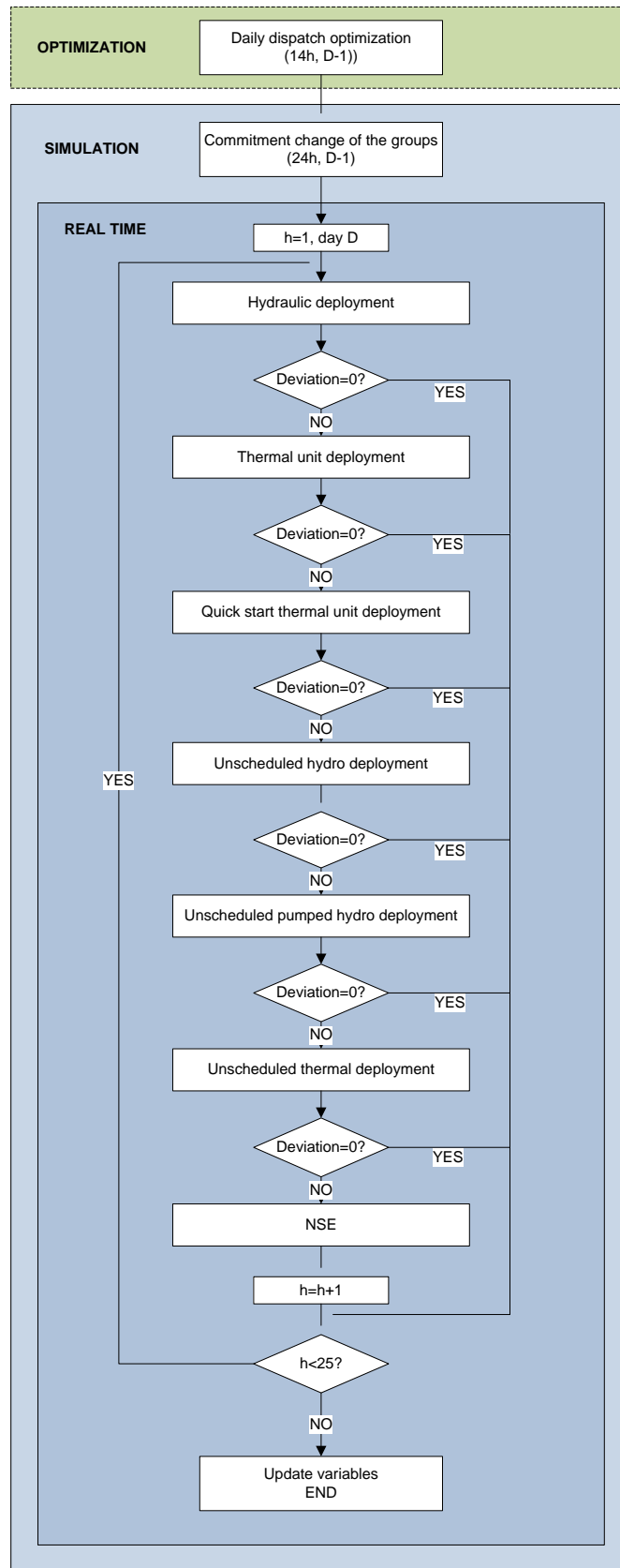


Figure 21. Simulation scheme

5 DEVELOPMENTS FOR THE CONSIDERATION OF THE EVs

This section describes the adaptations that have been done to the ROM Model in order to accomplish with the objectives of the MERGE project.

First of all, the new sets, parameters and variables that have been necessary to include the EV in the model are shown. Afterwards, the new constraints that are included in the model are described.

In order to model the EV behaviour two sets have been added: the type of EV (technical characteristics and traffic patterns) that can exist in the system (which are defined in tasks 1.5 [11] and 2.1 [6]) and the state in which these EVs can be.

The EV state can be: parked and connected to the grid (sc), parked and disconnected from the grid (su) and moving (sm).

These states make possible three different situations in the use of the batteries of the EVs, depending if the vehicle is connected, disconnected or moving:

- The connected ones can be charging/ discharging their batteries or be in a neutral state (neither charging nor discharging). It has to be considered that the charging and discharging process have different efficiencies.
- It is assumed that the disconnected vehicles, as has been mentioned previously, are parked and their batteries do not have losses.
- The moving EVs have a pattern of distance and time of the movement (in fact, the energy consumed) given by a parameter. The transformation of energy to mechanic movement has a different efficiency than the charging and discharging processes.

It has to be stressed that the model decides the best way to charge/discharge the batteries of the EVs in order to satisfy the needs of the users (use the EVs according to their usage pattern) and to improve the operation of the system. So when doing smart charging the system decides when and how much to either charge or discharge the EV or just not doing anything with the EV.

5.1 Adaptations in the formulation of the day-ahead Market Operation

This section will describe the new sets, parameters, variables and equations introduced in the model described in section 4 in order to include the characteristics and behaviour of the EV.

Table 25. New sets

Name	Meaning
e	Types of EV
s, s'	State of the EV (sc , su and sm)

Table 26. New parameters

Name	Meaning	Unit
$\overline{EC}_p^e, \overline{ED}_p^e$	Maximum power charged and discharged by EV e in the period p	MWh
$\underline{EE}^e, \overline{EE}^e$	Minimum and maximum energy charged by EV e	MWh
ERC^e, ERD^e	Battery charge and discharge ramp of EV e within a period	MWh/h
$EP_p^{e,s}$	Percentage of EVs of type e and in the state s for each period p	p.u.
$EPT_p^{e,s,s'}$	Percentage of EVs of type e and in the state s' that move to the state s for each period p	p.u.
$ET_p^{e,s}$	Use of the battery energy in transport of each type of EV e in each state s for each period p	MWh
$EEfGtB^e$	Grid to battery efficiency for each type of EV e	p.u.
$EEfBtG^e$	Battery to grid efficiency for each type of EV e	p.u.
$EEfBtW^e$	Battery to wheel efficiency for each type of EV e	p.u.

Table 27. New variables

Name	Meaning	Unit
$ee_p^{e,s}$	State of charge (SOC) of the battery of EV e at the end of period p in each state in state s	MWh
$ep_p^{e,s}, ec_p^{e,s}$	Generation and consumption of EV e in state s in period p	MW
eur_p^e, edr_p^e	Upward and downward power reserve available for EV e in period p	MW
$eurc_p^e, eurd_p^e, edrc_p^e, edrd_p^e$	Upward and downward power reserve of charging and discharging available for EV e in period p	MW
ch_p^e	EV e discharging or charging in period p	{0,1}

5.1.1 Objective function

The objective function of the optimization model is the same one than the model described in section 4. EVs affect the objective function indirectly, by demand and reserve constraints.

5.1.2 Demand and reserve constraints

- The equation that controls the balance of generation and demand for each period has to include the production and consumption of the EV:

$$D_p - WG_p - nse_p + sp_p = \sum_g gp_p^g + \sum_{e,s} (ep_p^{e,s} - ec_p^{e,s}) \quad \forall p$$

(14)

- Furthermore, the total upward and downward reserve for each period p also takes into consideration the contribution of the EV to the reserves:

$$\begin{aligned} \sum_{g \notin b} gur_p^g + \sum_{g \in b} pur_p^g + \sum_e eur_p^e + urdef_p &\geq UR_p \\ \sum_{g \notin b} gdr_p^g + \sum_{g \in b} pdr_p^g + \sum_e edr_p^e + drdef_p &\geq DR_p \end{aligned} \quad \forall p \quad (15)$$

5.1.3 EVs constraints

- The battery energy inventory keeps track of the SOC at any period p each EV e and each state s as a function of the energy charged into the battery, the energy discharged from the battery and the SOC at the end of the previous hour.

$$ee_p^{e,s} - ee_{p-1}^{e,s} = ec_p^{e,s} EEfGtB^e - \frac{ep_p^{e,s}}{EEfBtG^e} - \frac{ET_p^{e,s}}{EEfBtW^e} + \sum_{s' \neq s} ee_{p-1}^{e,s'} EPT_{p-1}^{e,s,s'} \quad \forall p, e, s \quad (16)$$

- The logical constraints of the charge, discharge and the movement of the EVs e in the period p is as follows:

$$\begin{aligned} ec_p^{e,s} &= 0 \quad \forall s \notin sc \\ ep_p^{e,s} &= 0 \quad \forall s \notin sc \quad \forall p, e, s \\ ET_p^{e,s} &= 0 \quad \forall s \notin sm \end{aligned} \quad (17)$$

- The maximum power that the EV e can charge and discharge in each state s for each period p is limited by the maximum charge and discharge of a individual battery times the number of EVs in that state, and taking into account the logical condition that an EV cannot charge and discharge at the same period:

$$\begin{aligned} ec_p^{e,s} &\leq (1 - ch_p^e) \overline{EC}^e EP_p^{e,s} \\ ep_p^{e,s} &\leq ch_p^e \overline{ED}^e EP_p^{e,s} \end{aligned} \quad \forall p, e, s \quad (18)$$

- The maximum power the EVs e can consume and generate in each state s and for each period p is constrained by the amount of energy stored in the battery:

$$\begin{aligned} ec_p^{e,s} &\leq EP_p^{e,s} \left(\overline{EE}^e - ee_p^{e,s} \right) \\ ep_p^{e,s} &\leq EP_p^{e,s} \left(ee_p^{e,s} - \underline{EE}^e \right) \end{aligned} \quad \forall p, e, s \quad (19)$$

- The charging and discharging ramps of the batteries the EV e (affect the battery, not the energy stored in it) have to perform in each state s and for each period p :

$$\begin{aligned} ec_p^{e,s} - ec_{p-1}^{e,s} &\leq RC^e \\ ep_p^{e,s} - ep_{p-1}^{e,s} &\leq RD^e \end{aligned} \quad \forall p, e, s \quad (20)$$

- The provision of battery energy for the mobilization of power reserves. If EVs e are providing (up and down) power reserves in period p some energy has to be kept in the battery in case this energy will be actually required by the system:

$$\begin{aligned} ee_p^{e,s} &\geq \underline{EE}^e + \sum_{p' \leq p} \left(\frac{eurd_{p'}^e}{EEfBtG^e} + eurc_{p'}^e EEfGtB^e \right) \\ ee_p^{e,s} &\leq \overline{EE}^e - \sum_{p' \leq p} \left(\frac{edr_{p'}^e}{EEfBtW^e} + edrc_{p'}^e EEfGtB^e \right) \end{aligned} \quad \forall p, e, s \quad (21)$$

- The upward and downward power reserve of an EV e in period p is the amount of upward and downward power reserve of charging and discharging available for EV e in period p :

$$\begin{aligned} eur_p^e &= eurc_p^e + eurd_p^e \\ edr_p^e &= edrc_p^e + edrd_p^e \end{aligned} \quad \forall p, e \quad (22)$$

- The maximum amount of power that can be provided to the upward and downward power reserves for an EV e in period p :

$$\begin{aligned} eur_p^e &\leq EP_p^{e,s} \left(\overline{EC}_p^e + \overline{ED}_p^e \right) \\ edr_p^e &\leq EP_p^{e,s} \left(\overline{EC}_p^e + \overline{ED}_p^e \right) \end{aligned} \quad \forall p, e, s \in sc \quad (23)$$

6 ROM MODEL RESULTS

In this section, a preliminary analysis has been carried out to give a quick show of the type of results that could be obtained by the ROM.

In order to examine the influence in the system and the market of the EVs, three scenarios were considered:

Scenario 1: there is no existence of EVs.

Scenario 2: EVs are added acting only as a load.

Scenario 3: as in Scenario 2, considering the extra capability of the EVs to offer energy to the grid.

For the cases where EVs are present, the penetration level considered is as much as EVs as the 25% of the peak demand.

The technical characteristics of the type of EV considered are shown in Table 28, and their use pattern is similar to Figure 29.

Table 28. Technical characteristics of the EV considered

Capacity of the batteries	24 kWh
Battery to wheel efficiency	0.15 kWh/km
Charge and discharge efficiency	89.44 %
Charge and discharge rate	3.43 kWh/h
Range	160 km

The generation results for the different cases simulated are shown in Table 29 and Table 30.

Table 29. Energy sources distribution without EV

% of peak demand	0%	
Source	GWh	%
Nuclear	16466	35,8%
Coal	18832	40,9%
Oil	1545	3,4%
Hydro	6030	13,1%
Wind	3128	6,8%
OtherRES	0	0,0%
BEV	0	0,0%

Table 30. Energy sources distribution with EV

% of peak demand	25%			
Source	Smart		No V2G	
	GWh	%	GWh	%
Nuclear	16466	35,8%	16466	35,8%
Coal	19985	43,5%	19467	42,3%
Oil	1273	2,8%	1567	3,4%
Hydro	6056	13,2%	6045	13,1%
Wind	3128	6,8%	3128	6,8%
OtherRES	0	0,0%	0	0,0%
BEV	890	1,9%	0	0,0%

The marginal price of the system and the Non-Served Energy (NSE) for the different cases of study are shown in Table 31 and Table 32.

Table 31. Marginal price and NSE without EV

% peak demand	NSE		Cost
	GWh	%	€/MWh
0%	2,7	0,0%	62

Table 32. Marginal price and NSE with EV

% peak demand	No V2G			Smart		
	NSE		Cost	NSE		Cost
	GWh	%	€/MWh	GWh	%	€/MWh
25%	2,7	0,0%	64	0,6	0,0%	56

A comparison of the prices between the different case studies, is presented in the Figure 22.

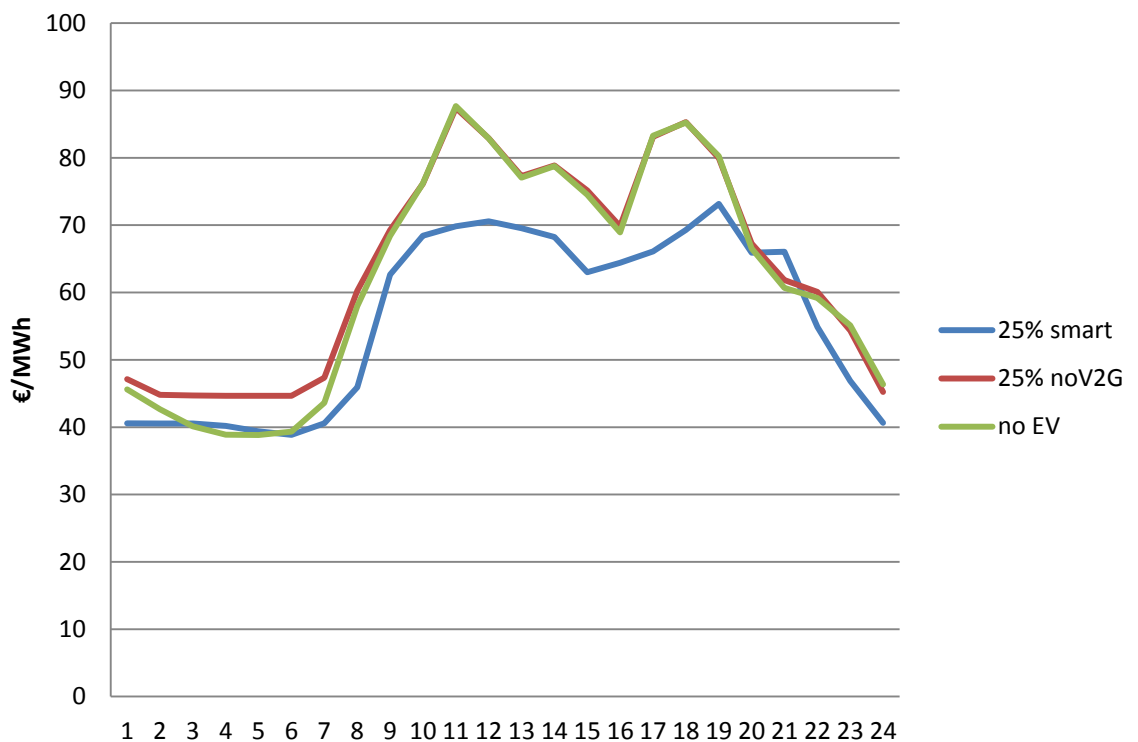


Figure 22. Marginal price for the study cases.

The previews results given in Table 31 and Table 32 show that the introduction of EVs, that are able to introduce energy into the system, improve its reliability (NSE is reduced almost a 78%) and reduce the costs of energy (almost a 10%). Figure 22 shows a graphical view of the evolution of the cost during a day, so that it can be appreciated the major reduction of cost is during the peak hours.

PART II. Game theory model

7 GAME THEORY METHODOLOGY

Game theory is a branch of applied mathematics that studies the interaction of multiple players in competitive situations. Its goal is the determination of the equilibrium state at which the optimal gain for each individual is achieved. More specifically, the theory of non-cooperative games studies the behaviour of agents in any situation where each agent's optimal choice may depend on his forecast of the choices of his opponents [1].

Various categories of games exist depending on the assumptions regarding the timing of the game; the knowledge associated with the payoff functions; and last but not least the knowledge regarding the sequence of the previously made choices. More specifically, the games can be categorized as follows:

- Static/dynamic games: the players choose actions either simultaneously or consecutively.
- Complete/incomplete information: each player's payoff function is common knowledge among all the players/at least one player is uncertain about another player's payoff function.
- Perfect/imperfect information (defined only for dynamic games): at each move in the game the player with the move knows or does not know the full history of the game thus far [2].

7.1 Static games

One of the most fundamental definitions in game theory is that of the Nash equilibrium which applies to *static games*. In the n-player normal-form game $G=\{S_1, \dots, S_n; u_1, \dots, u_n\}$ (where S_1, \dots, S_n are the players' strategy spaces and u_1, \dots, u_n are their payoff functions), the strategies (s_1^*, \dots, s_n^*) are a *Nash equilibrium* if, for each player i , s_i^* is player i 's best response to the strategies specified for the $n-1$ other players, $(s_1^*, \dots, s_{i-1}^*, s_{i+1}^*, \dots, s_n^*)$:

$$u_i(s_1^*, \dots, s_{i-1}^*, s_i^*, s_{i+1}^*, \dots, s_n^*) \geq u_i(s_1^*, \dots, s_{i-1}^*, s_i, s_{i+1}^*, \dots, s_n^*)$$

for every feasible strategy s_i in S_i ; that is, s_i^* solves

$$\max_{s_i \in S_i} u_i(s_1^*, \dots, s_{i-1}^*, s_i, s_{i+1}^*, \dots, s_n^*)$$

Such a game-theoretic problem is solved by what is called *iterated elimination of strictly dominated strategies*. Firstly, it is necessary to define what a strictly dominated strategy is:

In the normal-form game $G=\{S_1, \dots, S_n; u_1, \dots, u_n\}$, let s_i' and s_i'' be feasible strategies for player i (i.e., s_i' and s_i'' are members of S_i). Strategy s_i' is strictly dominated by

strategy s_i'' if for each feasible combination of the other player's strategies, i's payoff from playing s_i' is strictly less than i's payoff from playing s_i'' :

$$u_i(s_1, \dots, s_{i-1}, s_i', s_{i+1}, \dots, s_n) < u_i(s_1, \dots, s_{i-1}, s_i'', s_{i+1}, \dots, s_n)$$

for each $(s_1, \dots, s_{i-1}, s_{i+1}, \dots, s_n)$ that can be constructed from the other players' strategy spaces $S_1, \dots, S_{i-1}, S_{i+1}, \dots, S_n$.

Rational players do not play strictly dominated strategies. Assuming that it is a common knowledge that all the players are rational, it is to be expected that in any case the strategies of the players will be such that the Nash equilibrium will be reached.

7.2 Dynamic games

For the case of *dynamic games* of complete and perfect information the state of equilibrium is no longer the Nash equilibrium; the *backwards-induction outcome* directly refers to the fact that the play is now sequential. In such a game the timing is as follows:

- 2) Player 1 chooses an action a_1 from the feasible set A_1 .
- 3) Player 2 observes a_1 and then chooses an action a_2 from the feasible set A_2 .
- 4) Payoffs are $u_1(a_1, a_2)$ and $u_2(a_1, a_2)$.

We solve the previously described game using *backwards induction*. At the second stage of the game, player 2 will solve the following problem, given the action a_1 previously chosen by player 1:

$$\max_{a_2 \in A_2} u_2(a_1, a_2)$$

It is assumed that for each a_1 in A_1 , player 2's optimization problem has a unique solution, denoted by $R_2(a_1)$. This is player 2's best response to player 1's action. Since player 1 can solve player 2's problem as well as player 2 can, player 1 should anticipate player 2's reaction to each action a_1 that player 1 might take, so player 1's problem at the first stage amounts to:

$$\max_{a_1 \in A_1} u_1(a_1, R_2(a_1))$$

It is assumed that this optimization problem for player 1 also has a unique solution, denoted by a_1^* . $(a_1^*, R_2(a_1^*))$ is the backwards-induction outcome of the game.

8 DESCRIPTION OF THE GAME THEORY MODEL

As will become clear later on, when the rules of the game will be defined, the most appropriate class of games for the task at hand is the dynamic game of complete and perfect information, while the solution of such a game is determined as the backwards-induction outcome.

In order to define the game, it is necessary to define the following:

- 1) The players
- 2) The rules of the game
- 3) The payoff functions of each player

8.1 The players

For the case of the integration of EVs and their affect in the operation of the retail market, the following players are defined:

- Household consumers
- Distributed generation units (DG)
- EVs
- Aggregator

8.2 The rules of the game

In our dynamic game of complete and perfect information the timing is as follows:

- 4) The aggregator chooses price levels for buying and selling electric energy for the next hour.
- 5) According to these prices, household consumers select their load level, DG units select their production levels, while EVs choose whether to absorb or give electricity to the grid depending on the state of charge of the batteries.
- 6) At the final step, the payoff of each player is calculated.

Figure 23 depicts the game previously described in its extensive form representation. This procedure is repeated consecutively for each hour of one day at which point the payoff of each participant is settled according to the choices made by each and every one of them.

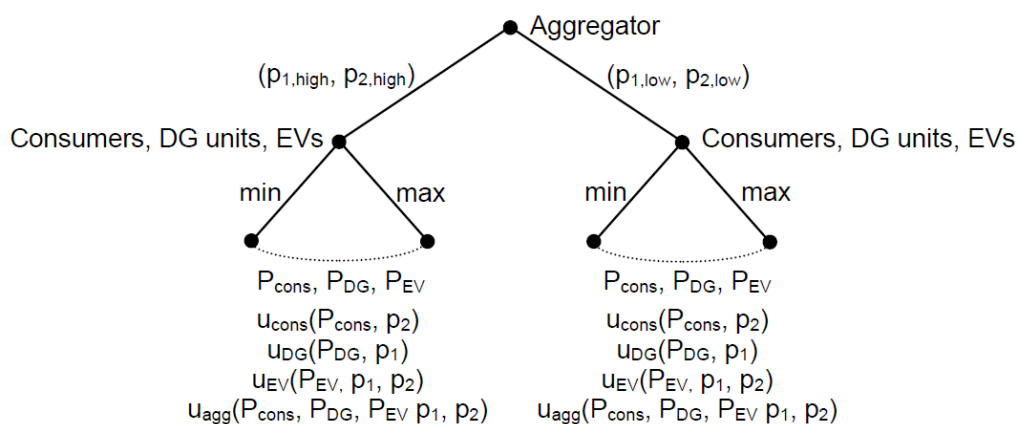


Figure 23: Extensive form representation of the game

As game theory suggests, each player's predicted strategy must be the best response to the predicted strategies of the other players (that is, each participant chooses the strategy that maximizes his or her payoff). Such a prediction is called strategically stable or self-enforcing, because no single player wants to deviate from his or her predicted strategy. In order to determine each player's optimal strategy, backwards-induction is applied as follows:

- 7) $t = 24$
- 8) For all possible strategies of the aggregator s_i^t , $i = 1, \dots, N$, the optimal response of each player is computed ($P_{con,i}^t(s_i^t)$, $P_{DG,i}^t(s_i^t)$, $P_{EV,i}^t(s_i^t)$).
- 9) For each combination of strategies the payoff of each player is calculated.
- 10) Selection of the optimal combination for the t^{th} hour is done by maximizing the payoff of the aggregator.
- 11) $t = t-1$
- 12) If $t \geq 1$ return to step 2.
- 13) End.

Figure 24 gives an overview of the above described procedure.

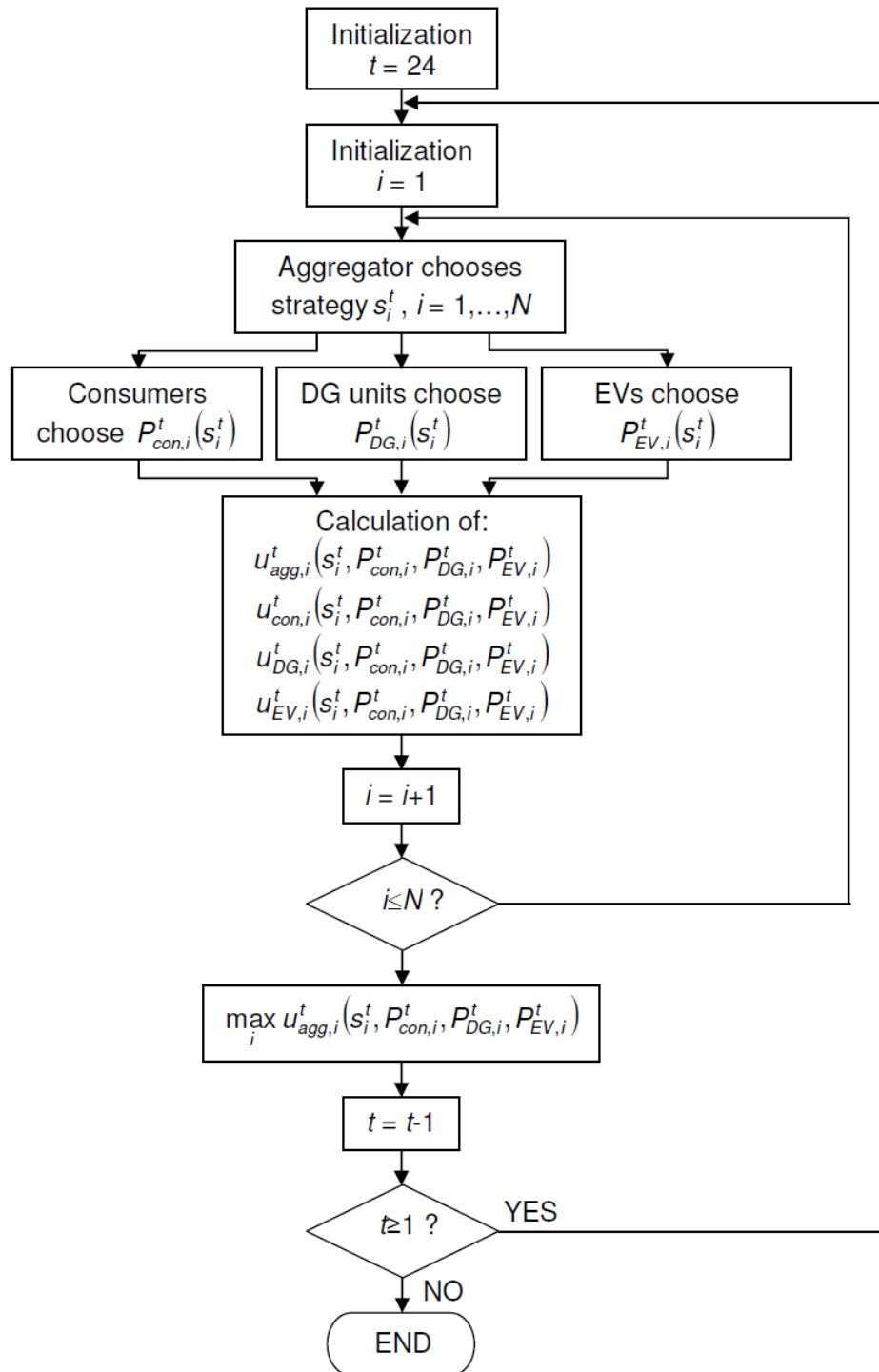


Figure 24: Flow chart of the procedure for determining the optimal strategies of each participant, using the backwards induction method

8.3 The payoff function of each player

8.3.1 Household consumers

Household consumers select their consumption level (which is their strategy space) according to the price announced by the aggregator. In order to describe/model that kind of behaviour, the demand curve is the most appropriate. Such a curve depicts the relationship between the amount of electricity and the price the consumers are willing to pay for it. Ideally such a curve is as the one presented in Figure 25.

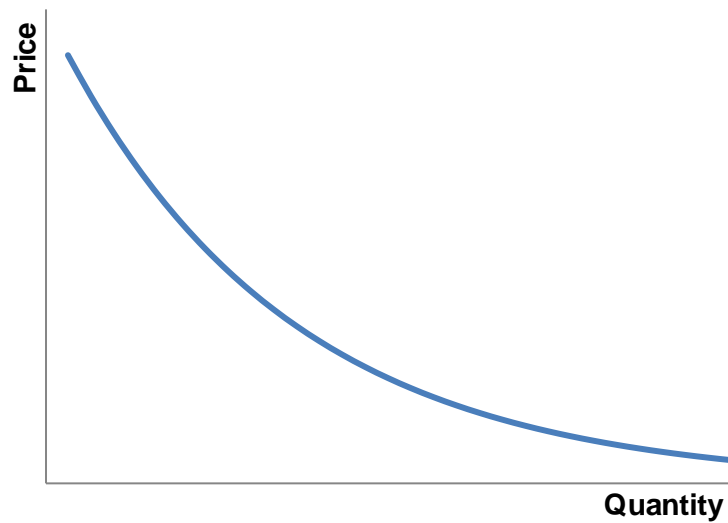


Figure 25: Demand curve describing the consumer behavior.

For the sake of simplification, the demand curve is approximated by a linear function of the form $\text{Quantity} = a - b \cdot \text{Price}$. In fact the inverse demand curve is being used: $\text{Price} = a - b \cdot \text{Quantity}$ that describes the linear part of the graph in Figure 26. Two priority levels were considered for the load: high and low priority. The first category includes the refrigerator and lighting, which are inflexible, while the rest of the loads are characterized as low-priority, and can be influenced by the price levels. The linear part of the graph is parameterized as follows:

$$p(P_{con}) = p_m \left(1 - \frac{1}{\varepsilon_m} \right) + \frac{p_m}{P_m \cdot \varepsilon_m} \cdot P_{con}$$

where ε_m : is the price elasticity of demand and $(p_m, P_m) \in p(P_{con})$ (see Table 33).

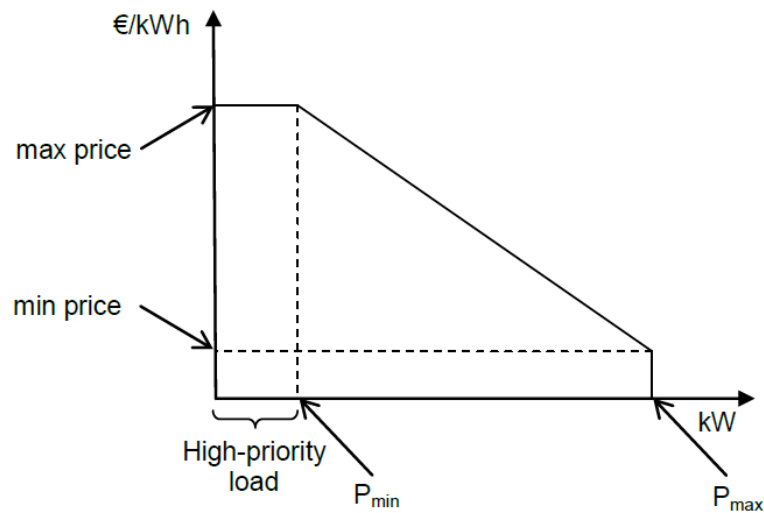


Figure 26: Simplified demand curve describing the consumer behavior

Table 33: Parameters of the inverse demand curve of the household consumers

ϵ_m	p_m (€/kWh) ¹	P_m (kW) ¹	a	b
-1.2	0.1676	0.428	0.307	-0.326

Parameters P_{min} and P_{max} vary throughout the day: P_{min} is equal to the sum of the refrigeration and lighting load (the last one is considered to be a high priority load only after the sunset and before the sunrise), while P_{max} is the maximum load to be served at each hour of the day, as shown in Figure 27. This figure shows accumulated load curves for a typical European household for a typical week day of the year (in Watts), which were put to use in order to derive P_{min} and P_{max} as described previously [3].

Parameters (p_m , P_m) derive as follows: according to the load curve of Figure 27 it is concluded that the annual consumption of the typical European household is approximately 2.700kWh. Therefore, the specific household belongs to Band DC (which includes consumers with annual consumption between 2.500kWh and 5.000kWh), according to the categorization established by Eurostat [4]. For this consumption Band the European average for the half-yearly prices during the 1st semester of 2010 is 0.1676 €/kWh, while the whole Band is considered to be represented by the mean value (3.750kWh per annum, which is translated to 0.428kW average load per hour).

¹ Source of data: Eurostat

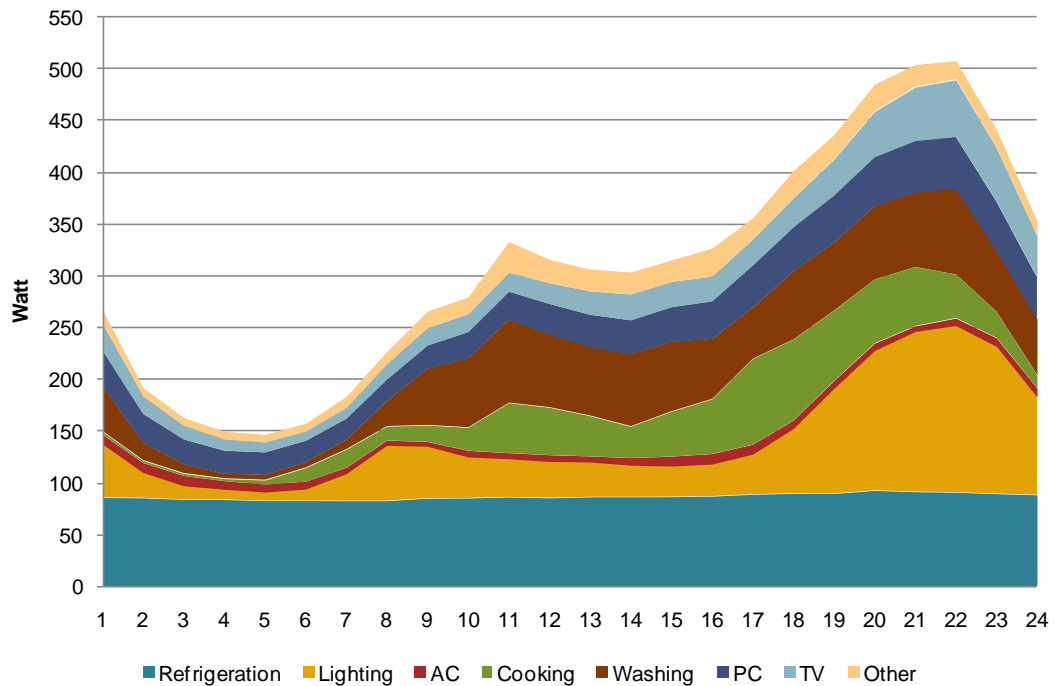


Figure 27: Accumulated load curves for a typical European household for a typical week day of the year

For a given price (p_1) announced by the aggregator the optimal response of the consumer (P_{con}) derives directly from the inverse demand curve (see Figure 28). In that case, the payoff for the consumer (more precisely, the utility the consumer acquires from using the specific amount of energy purchased at price p_1 , the consumer surplus) is the area marked with blue in Figure 28.

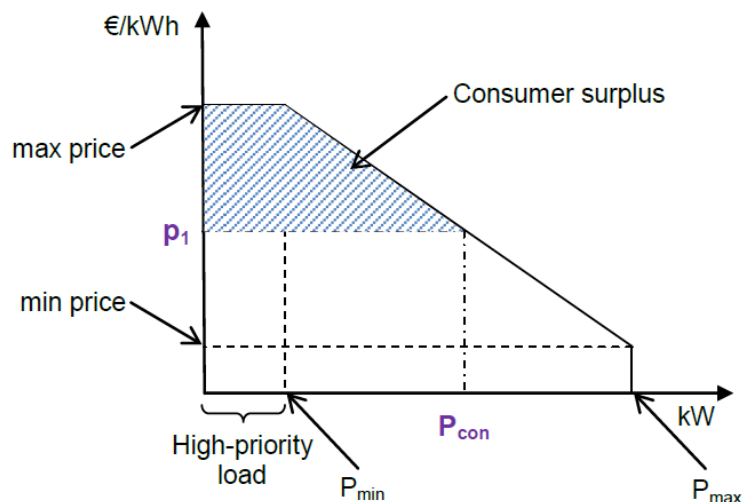


Figure 28: Inverse demand curve and payoff of the consumer

8.3.2 Distributed generation units (DG)

Microturbines select their production level (strategy space) according to the price announced by the aggregator. For our modelling, microturbines that use natural gas as fuel have been considered as distributed generation units. For the optimization of the production of the microturbine, only the variable costs have been taken into account.

Thus, the cost function describing the microturbine is:

$$p = A \cdot P_{DG}^2 + B \cdot P_{DG} + C$$

For a given price (p_2) announced by the aggregator, DG units solve the following problem, in order to determine the optimal production level:

$$\max \left\{ p_2 \cdot P_{DG} - (A \cdot P_{DG}^2 + B \cdot P_{DG} + C) \right\} \Rightarrow P_{DG} = \frac{p_2 - B}{2 \cdot A}$$

Naturally the optimal power production of the DG unit is not independent from the production during the previous hour. The ramp rate as well as the technical minimum of the unit poses two restrictions, which are by no means negligible and are properly taken into account.

8.3.3 EVs

EVs can act either as a load or as production. They are, therefore modelled in a different way depending on the operation mode. In any case, a set of parameters needs to be defined:

- 14) The capacity of the batteries (in kWh)
- 15) The average charging time (in h)
- 16) The efficiency (in kWh/km)
- 17) The range (in km)
- 18) The charge rate (in kWh/h)
- 19) The charge and discharge efficiency (in %)
- 20) The availability of the vehicle (1 when the vehicle is connected to the grid, 0 otherwise).

Parameters 1-6 depend on the vehicle, while parameter 7 depends solely on the behaviour of the driver. Figure 29 presents the kilometers driven (per hour of the day) as a percentage of the total kilometers on a weekly basis [5]. Such a diagram allows us to define the hours of the day when the vehicle will be on the move (mainly 8:00-9:00 in the morning and 17:00-18:00 in the afternoon).

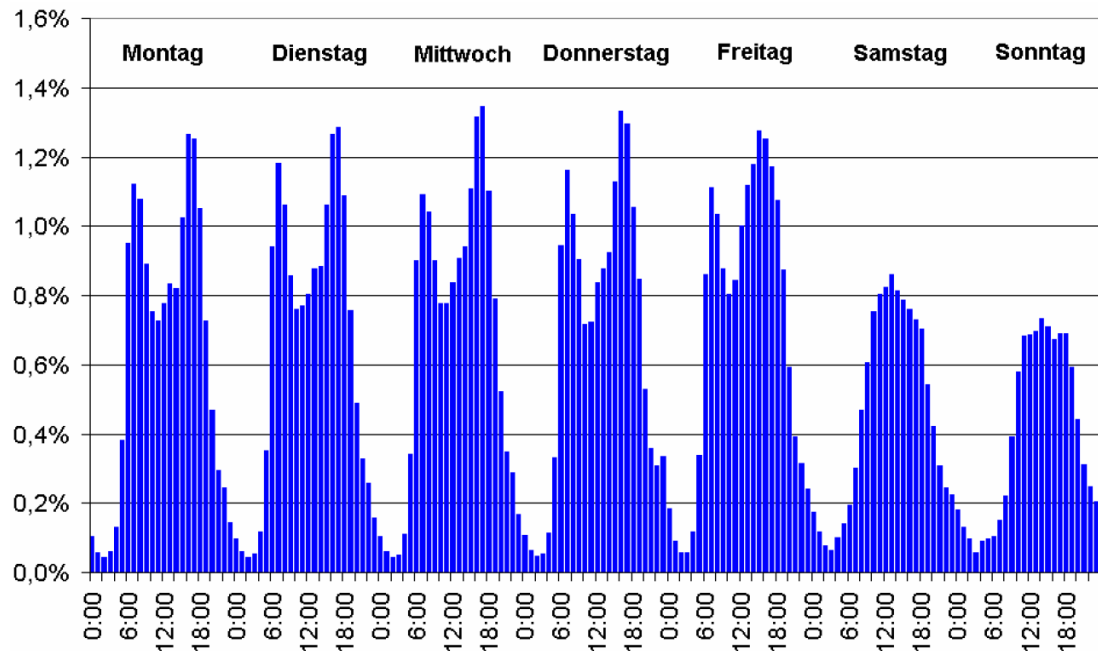


Figure 29: Kilometers driven (per hour of the day) as a percentage of the total kilometers on a weekly basis

Taking into account the fact that the owner of an EV aims at maximizing his personal comfort level, it is only logical to assume that while the vehicle can inject energy to the grid, the state-of-charge (SOC) of the batteries should be such that at any time the owner can perform his tasks without having to relinquish any of the activities that depend on his vehicle. This minimum SOC can be named mobility comfort level and is calculated by considering an average range of the journeys performed in a day. According to [6] for an EV with 160km range, 68.4% of all weekday journeys are 60km (return) or less. Thus, the minimum SOC will be $60\text{km}/160\text{km} = 37.5\%$.

For simulating the behaviour of the EVs, maximum and minimum values for the SOC per hour are defined. While the EV is available, the SOC lies between 100% and the mobility comfort level as defined earlier. While the EV is on the move, discharging of the batteries takes place and the SOC lies between $100\% - \text{km}/\text{range}$ and $(\text{mobility comfort level}) - \text{km}/\text{range}$. In the worst case scenario, in which after the completion of the journey the SOC is lower than the minimum allowed, the EV will not be considered available directly after the journey, since the batteries will need to be recharged until the minimum allowed SOC is reached (mobility comfort level). The distance travelled affects the SOC of the batteries. As a result the EV might not be available for discharging, even though it is grid-connected. Thus, the availability of the vehicle for the hours directly after the journey is modified in a proper manner, to take into account the charging of the vehicle. Figure 30 depicts the results of previously described procedure applied for an EV with the following characteristics: range = 160km, efficiency = 0.15kWh/km, charge rate = 3.43 kWh/h, charge efficiency = discharge efficiency = 89.44%, battery capacity = 24 kWh, which performs two journeys of 30km each during one day.

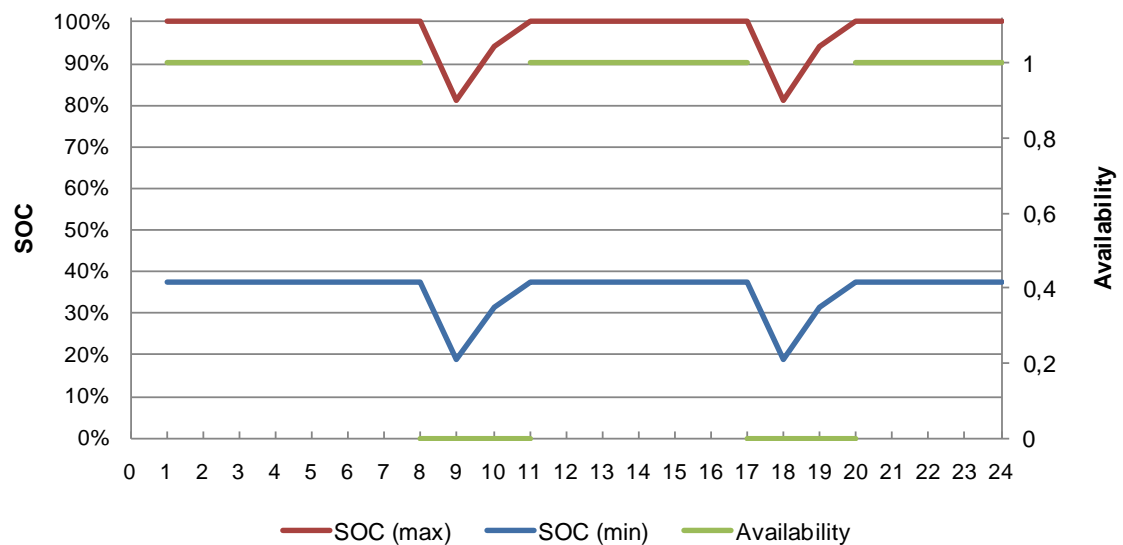


Figure 30: Minimum and maximum allowable SOC and availability of the EV

Having already defined the values that envelope the SOC of the batteries, during the hours of availability, EVs act so as to maximize their payoff. Two cases are considered:

- 21) Discharging: the payoff for the EVs is merely the product of the energy supplied times the price offered by the aggregator for buying that amount of energy.
- 22) Charging: the payoff for the EVs is calculated in a similar manner as for the consumers.

Every hour that the EV is available, the choice whether to charge or to discharge depends on a simple comparison between the two payoffs achieved by the two different states.

8.3.4 Aggregator

As already mentioned, the aggregator chooses the prices at which he sells (p_1) and buys (p_2) electricity (strategy space). These prices are directly affected by the price at which the aggregator purchases the electricity from the wholesale market. However, he can follow two strategies: either low prices, or high prices. Depending on his forecast regarding the loads he has to serve, he chooses a different strategy: for the hours when the load is very high (low), p_1 as well as p_2 are high (low) in order to achieve lower (higher) demand levels and higher (lower) production levels (Figure 31).

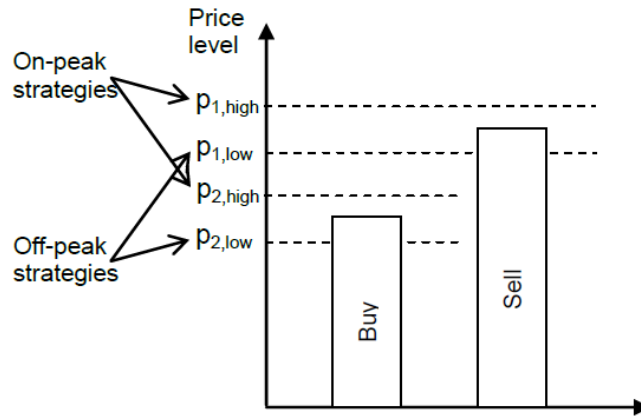


Figure 31: Off-peak and on-peak strategies followed by the aggregator

In order for the simulation to be as close to reality as possible, for $p_{2,low}$ real wholesale market data have been used (see paragraph 10.1.4, Figure 32) made available by the Hellenic TSO [7]. The other three price levels are derived as follows:

$$p_{1,low} = 1.2 \cdot p_{2,low}$$

$$p_{2,high} = f(p_{2,low})^2$$

$$p_{1,high} = 1.2 \cdot p_{2,high}$$

The payoff function of the aggregator depends on whether the EVs charge, discharge or do nothing:

- EVs charge

$$u_{agg} = p_1 \cdot (P_{con} + P_{EV}) - p_2 \cdot P_{DG} - p_{wholesale} \cdot (P_{con} + P_{EV} - P_{DG}) - p_{fine} \cdot (P_{con,total} - P_{con})$$

If $P_{con} + P_{EV} - P_{DG} > 0$, $p_{wholesale}$ is the price at which the aggregator buys electricity from the wholesale market.

If $P_{con} + P_{EV} - P_{DG} < 0$, $p_{wholesale}$ is the price at which the aggregator sells electricity to the wholesale market.

- EVs discharge

$$u_{agg} = p_1 \cdot P_{con} - p_2 \cdot (P_{DG} + P_{EV}) - p_{wholesale} \cdot (P_{con} + P_{EV} - P_{DG}) - p_{fine} \cdot (P_{con,total} - P_{con})$$

- EVs do nothing

$$u_{agg} = p_1 \cdot P_{con} - p_2 \cdot P_{DG} - p_{wholesale} \cdot (P_{con} - P_{DG}) - p_{fine} \cdot (P_{con,total} - P_{con})$$

where

² In order to perform the simulation, values for $p_{2,high}$ were artificially generated by using a random term so that they vary between 110% and 130% of $p_{2,low}$.

p_1 : selling price to the consumers

P_{con} : consumers' optimal consumption levels

p_2 : buying price from production units

P_{DG} : production units' optimal production levels

P_{EV} : EVs optimal response (either charging or discharging)

$p_{wholesale}$: wholesale prices for selling/buying the excess/deficit of energy

p_{fine} : fine imposed on the aggregator for the part of the load that is not served.

$P_{con,total}$: total load level ideally served (Figure 27)

For $p_{wholesale}$ let it be noted that two price levels were considered (one for buying and one for selling electricity), which cannot be influenced by the aggregator.

The fine imposed on the aggregator for the part of the load that is not served (p_{fine}) is constant throughout the day and motivates the aggregator to offer lower p_1 in order for a greater part of the load to be served using the available energy stored in the batteries of the EVs (if any).

9 DETAILED ALGORITHM OF THE MODEL

The general procedure followed has already been described in Figure 24. In this paragraph we elaborate the procedures that each player follows in order to calculate his optimal response from an algorithmic point of view.

9.1 Consumer function

Input: p_1 , $P_{con,max}$, $p(P_{con,max})$, $P_{con,min}$, $p(P_{con,min})$

Output: $P_{con}(t)$, $u_{con}(t)$

- If $p_1 > p(P_{con,min})$, then only the high-priority load is served ($P_{con} = P_{con,min}$) and the payoff for the consumer equals zero ($u_{con} = 0$).
- If $p_1 \leq p(P_{con,min})$, then the consumer selects his consumption level as depicted in Figure 28 (P_{con} such that $p(P_{con}) = p_1$) and his payoff equals the consumer surplus (u_{con} = area marked with blue in the same figure).

9.2 Distributed generation function

Input: p_2 , $P_{DG}(t+1)^3$, A, B, C, ramp rate, $P_{DG,min}$, $P_{DG,nominal}$

³ Since the problem is solved using the backwards-induction method, the previous state of the DG is $P_{DG}(t+1)$, and the current state is $P_{DG}(t)$. As a result, when the optimal is to have $P_{DG}(t) = 0$ while $P_{DG}(t+1) \neq 0$, it is only natural that the DG unit turns on, in which case the payoff function should include the start-up cost.

Output: $P_{DG}(t)$, $u_{DG}(t)$

Given p_2 , the optimal production level is calculated as: $P_{DG} = \frac{p_2 - B}{2 \cdot A}$ and the payoff

received for the specific production level as: $\left(p_2 - (A \cdot P_{DG}^2 + B \cdot P_{DG} + C) \right) \cdot P_{DG}$

- If $P_{DG} > P_{DG,nominal}$ then the production is fixed on the maximum the unit allows ($P_{DG} = P_{DG,nominal}$) and the payoff is recalculated.
- If $P_{DG} < P_{DG,min}$ two possibilities are examined:
 - If it is allowed by the ramp rate, then $P_{DG} = 0$ and the payoff has to take into account the start-up cost of the unit⁴.
 - If the ramp rate of the unit does not allow P_{DG} to be equal to 0, then $P_{DG} = P_{DG,min}$ and the payoff is recalculated.
- For all the other cases, the optimal production level should not be higher or lower than the ramp rate allows.

9.3 EVs function

Input: p_1 , p_2 , $SOC(t+1)$, SOC_{max} , SOC_{min} , availability, $P_{DG,max}$, $p(P_{DG,max})$, $P_{DG,min}$, $p(P_{DG,min})$

Output: $SOC(t)$, $u_{EV}(t)$, charge flag(t)⁵

- If the EV is not available for t-1 and if $SOC(t) < SOC_{min}$, it is in charging mode. Otherwise the EV chooses between charge and discharge mode by comparing the payoff offered by each one of them (see below).
- If the EV is not available for t, then by default it is in discharging mode due to travel ($SOC(t) = SOC(t+1) - km \cdot efficiency / capacity$, charge flag = 0) and $u_{EV} = 0$.
- For all the other cases the EV chooses between charge and discharge mode by comparing the payoff offered by each one of them.
 - The discharge profit is equal to the product (discharge rate $\cdot a \cdot p_2$), where a is the discharge efficiency.
 - The charge profit is calculated using exactly the same method as the consumers, but with different values for $P_{con,max}$, $p(P_{con,max})$, $P_{con,min}$, $p(P_{con,min})$, which are now $P_{EV,max}$, $p(P_{EV,max})$, $P_{EV,min}$, $p(P_{EV,min})$. In Table 34 the parameters of the inverse demand curve used for the EVs charging mode are presented, where EVs are considered load best described by Band DD, according to the categorization established by Eurostat.

Table 34: Parameters of the inverse demand curve of the EVs for the charging mode

ε_m	p_m	$P_m (kW)^5$	a	b
-----------------	-------	--------------	---	---

⁴ The start-up cost of the unit is considered constant and equal to $0.8 \cdot C$.

⁵ The charge flag equals 1 when the EV is in charging mode, 0 when the EV batteries discharge due to travelling and -1 when the EV is in discharging mode.

	(€/kWh) ⁶			
-1.2	0.1604	1.712	0.294	-0.078

9.4 Aggregator function

Input: p_1 , p_2 , $p_{\text{wholesale}}$, p_{fine} , $P_{\text{con}}(t)$, $P_{\text{DG}}(t)$, $P_{\text{EV}}(t)$, $\text{charge_flag}(t)$

Output: $u_{\text{agg}}(t)$

- If the EV is in charging mode ($\text{charge_flag}(t)=1$), then:

$$u_{\text{agg}}(t) = p_1 \cdot (P_{\text{con}}(t) + P_{\text{EV}}(t) - p_2 \cdot P_{\text{DG}}(t) - p_{\text{wholesale}} \cdot (P_{\text{con}}(t) + P_{\text{EV}}(t) - P_{\text{DG}}(t)) - p_{\text{fine}} \cdot (P_{\text{con},\text{total}} - P_{\text{con}}(t)))$$

- If the EV is in discharging mode ($\text{charge_flag}(t)=-1$), then:

$$u_{\text{agg}}(t) = p_1 \cdot P_{\text{con}}(t) - p_2 \cdot (P_{\text{DG}}(t) + P_{\text{EV}}(t)) - p_{\text{wholesale}} \cdot (P_{\text{con}}(t) + P_{\text{EV}}(t) - P_{\text{DG}}(t)) - p_{\text{fine}} \cdot (P_{\text{con},\text{total}} - P_{\text{con}}(t)).$$

- If the EV is unavailable due to travelling ($\text{charge_flag}(t)=0$), then:

$$u_{\text{agg}}(t) = p_1 \cdot P_{\text{con}}(t) - p_2 \cdot P_{\text{DG}}(t) - p_{\text{fine}} \cdot (P_{\text{con},\text{total}} - P_{\text{con}}(t)).$$

Note: $P_{\text{EV}}(t) = \text{SOC}(t+1) - \text{SOC}(t) \cdot \text{capacity}$

10 SIMULATION RESULTS

The above described procedure is applied in order to examine the impact of the EVs on the operation of the retail market. Two cases are examined: with and without the presence of EVs. Furthermore, in the first case, various penetration levels of EVs are examined.

10.1 Input data

10.1.1 Household consumers

As already mentioned in paragraph 8.3.1, household consumers are described by the demand curve given in Figure 26. The parameters of that curve vary from hour to hour (Table 33). By combining these parameters with the load curves describing the consumption of a typical European household (Figure 27) we obtain, for each hour of the day, a vector consisting of four values ($P_{\text{con},\text{max}}$, $p(P_{\text{con},\text{max}})$, $P_{\text{con},\text{min}}$, $p(P_{\text{con},\text{min}})$) that fully describes the specific demand curve.

10.1.2 Distributed generation

The values of the parameters A, B and C of the DG cost function are presented in Table 35 [8]. The remaining characteristics of the microturbine are given in Table 36.

⁶ Source of data: Eurostat

Table 35: Constants A, B and C of the DG cost function

A (¢€/kWh)	B (¢€/kWh)	C (¢€/h)	Minimum capacity (kW)	Maximum capacity (kW)
0.01	4.37	0.01	6	30

Table 36: Technical and economical characteristics of the microturbine

Ramp-rate	10%/min
Start-up cost	80%·C

10.1.3 Electric vehicles

Table 37 presents the technical characteristics of the EV considered for the simulation, which is a Nissan Leaf, while Table 38 presents the mobility characteristics of the driver considered for the simulation.

Table 37: Technical characteristics of the EV

Capacity of the batteries	24 kWh
Average charging time	7-8 h
Efficiency	0.15 kWh/km
Range	160 km
Charge rate	3-3.43 kWh/h
Charge and discharge efficiency	89.44%

Table 38: Mobility characteristics of the driver

Availability hours	9:00-17:00, 18:00-8:00
Average daily distance travelled	60km

10.1.4 Aggregator

The results of the application of the procedure for obtaining the price levels that will comprise the strategies of the aggregator as described in paragraph 8.3.4, on real wholesale market data are given in Figure 32.

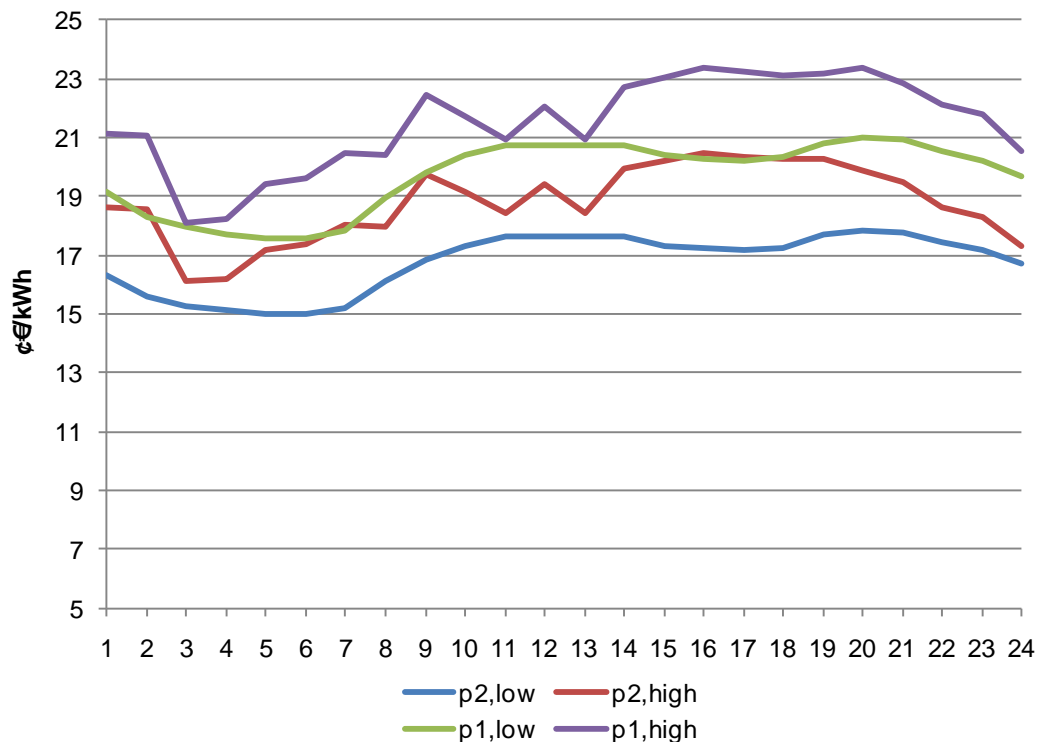


Figure 32: Strategies followed by the aggregator ($p_{1,low} - p_{2,low}$, $p_{1,high} - p_{2,high}$)

10.2 Results

In order to examine the influence of the existence of the EVs on the retail price levels, three scenarios were considered:

Scenario 1: the only players considered are the consumers, the DG units and the aggregator.

Scenario 2: EVs are added as a fourth player acting only as a load.

Scenario 3: as in Scenario 2, considering the extra capability of the EVs to offer energy to the grid.

For the cases where EVs are present, two penetration levels are considered:

- Low penetration: 10% of the total vehicle fleet are EVs,
- High penetration: 25% of the total vehicle fleet are EVs.

Figure 33 and Figure 34 present the optimal selection for the aggregator for buying and selling prices for the three scenarios considered for two penetration levels of EVs. The comparison of Scenarios yields some useful conclusions:

- During hours of high load (10:00-24:00) the aggregator selects the high priced strategies (Scenario 1, Figure 33), which leads to a substantial reduction in the actual load served (Scenario 1, Figure 35).
- The additional load due to the EVs (Scenario 2), leads – as previously – to higher prices (during hours 1:00, 8:00 and 9:00) (Scenario 2, Figure 33 and

Figure 34). High prices during 8:00pm lead to a further reduction in the load served (Scenario 2, Figure 35).

- Considering EVs not only as a load but as a potential source of energy (Scenario 3) leads to even greater variations in the price levels when compared to Scenarios 1 and 2. While for hours 10:00 and 23:00 high load levels would have been responsible for high prices (as in Scenario 1), this is not the case for Scenario 3 (Figure 33). At the specific hours, EVs inject energy to the grid (Figure 38), which allows for a greater part of the household load to be served (Figure 35, Scenario 3).
- Higher levels of EV penetration affect the prices even more. In addition to the aforementioned changes in the prices for hours 10:00 and 23:00, lower prices are now achieved for hour 22:00. However, during hours of low household load, during hours of low household load, EVs optimal response – which is to charge – (Figure 37 and Figure 38, hours 5:00, 6:00 and 7:00) leads to an increase in the total load to be served, thus, resulting in higher price levels (Figure 34, Scenario 3)

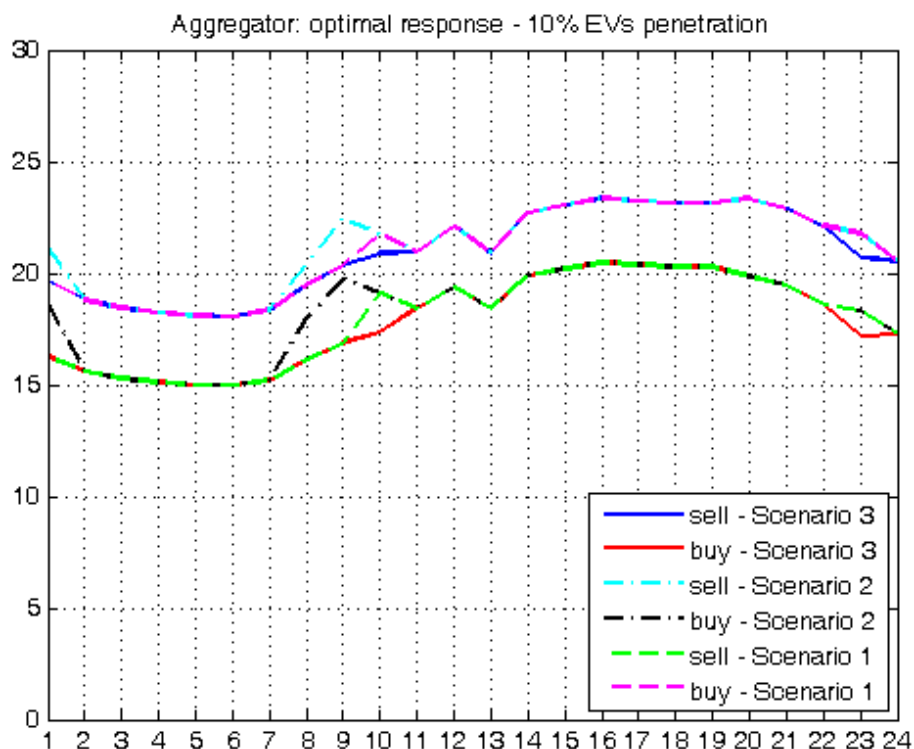


Figure 33: Aggregator optimal selection for buying and selling prices for the three scenarios – EV penetration: 10%

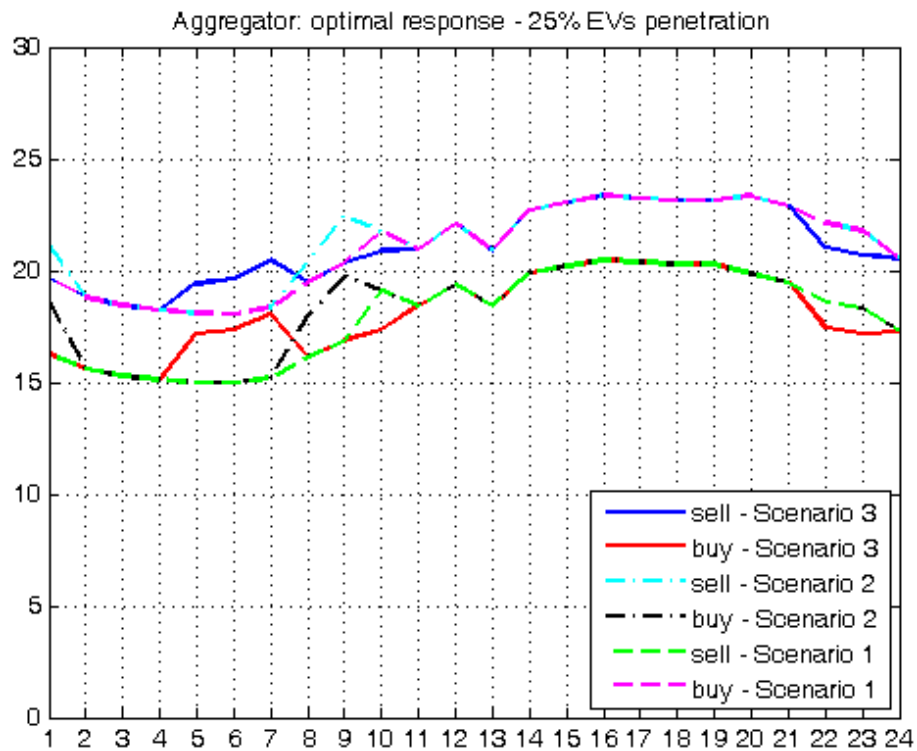


Figure 34: Aggregator optimal selection for buying and selling prices for the three scenarios – EV penetration level: 25%

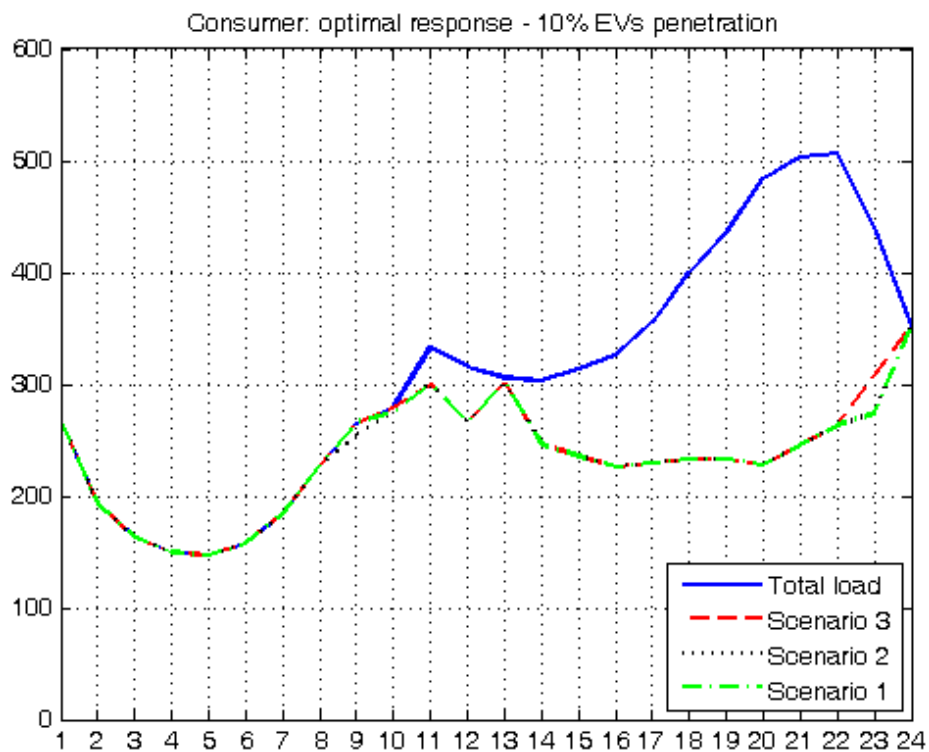


Figure 35: Consumer's optimal response for the three Scenarios- 10% penetration level

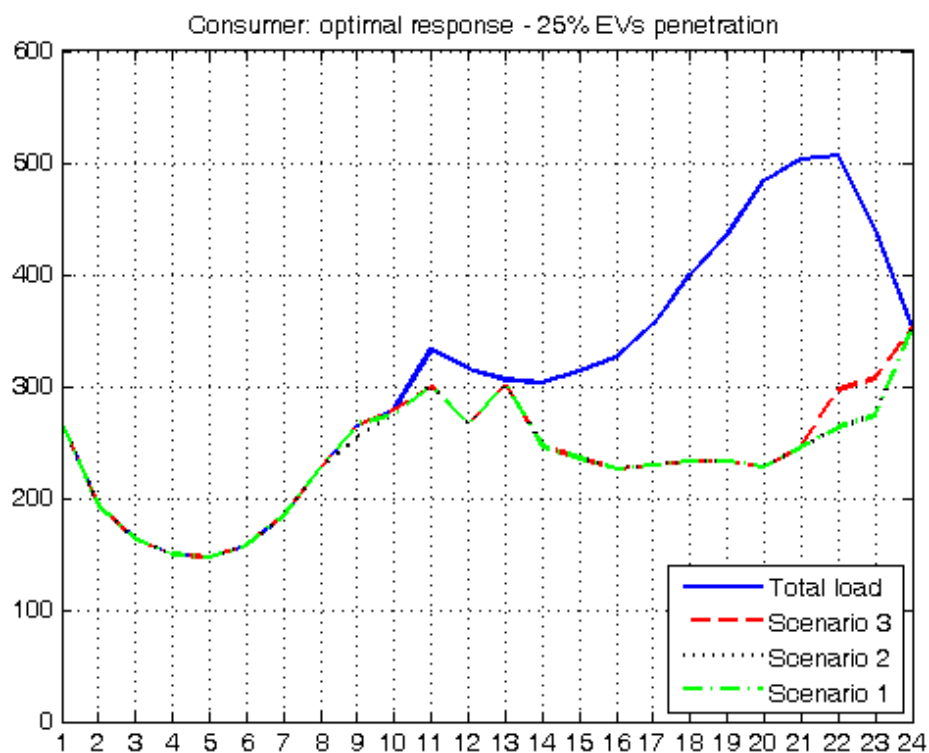


Figure 36

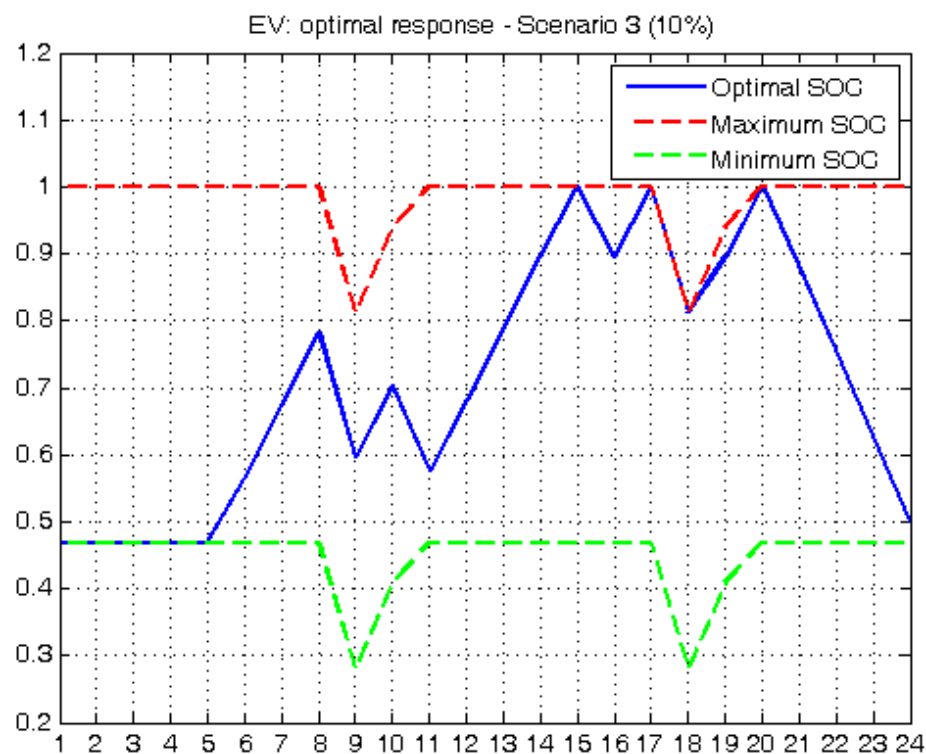


Figure 37: State of charge of the EV batteries for Scenario 3 – EV penetration level: 10%

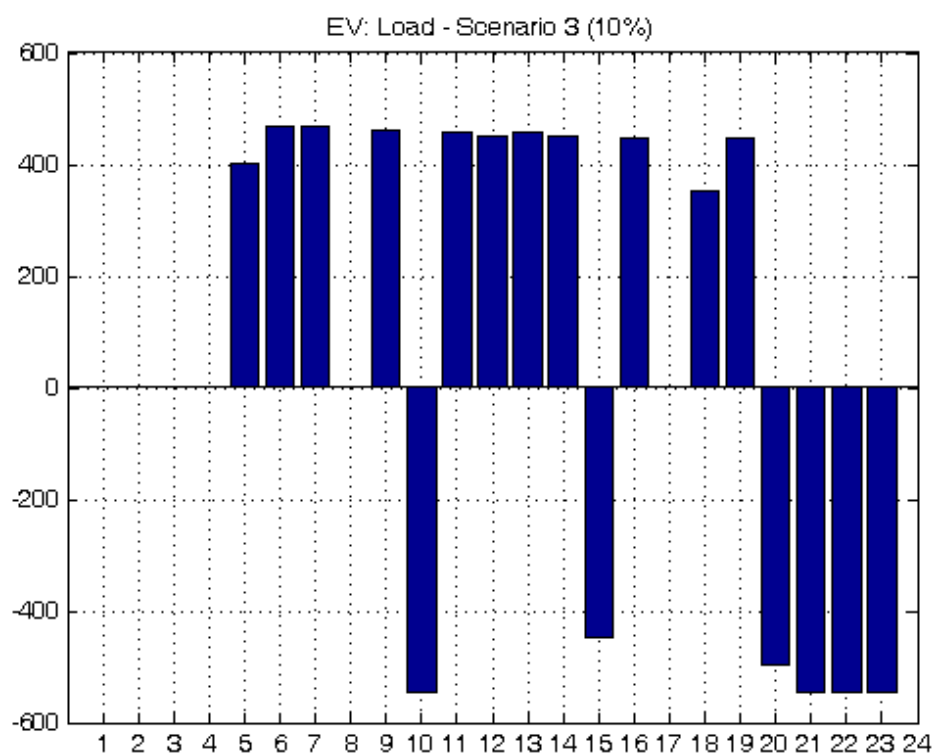


Figure 38: EVs' optimal response – Scenario 3, 10% penetration level

11 PRELIMINAR CONCLUSIONS

Simulation of the operation of the electricity market in the presence of various levels of EV penetration is performed by using two different approaches: optimization in conjunction with simulation and game theory with the results showed previously.

Using both optimization and simulation, the comparison of the results obtained in the study cases presented lead to the conclusion that when there is a high penetration of EVs with the ability to give power to the grid, the prices of the system decrease. When the EVs do not have the ability to give power to the grid, the price increases lightly (not so lightly in the valley hours).

Moreover, the use of smart EVs not only reduces the prices, it also improves the reliability of the system, reducing the NSE.

Using the game theory approach, the comparison of the results of these three scenarios with their variations (penetration level), leads to the following conclusions:

- During hours that the load is expected to be high the aggregator chooses high price levels in order to attenuate the increase in load.
- The addition of EVs that act only as load, results – as previously – to high prices.
- For the third scenario, the previous observations hold for the hours when EVs absorb energy from the grid. The opposite effect is observed during the hours that EVs inject energy to the grid: the prices are pushed downwards, and a greater part of the load is served. Furthermore, higher EVs' penetration level affects the prices in a similar way during a greater part of the day.

12 REFERENCES

- [1] Fudenberg, D., Tirole, J., "Game Theory," The MIT Press, Cambridge, Massachusetts, London, England, 1991.
- [2] Gibbons, R., Game Theory for Applied Economists, Princeton University Press, Princeton, New Jersey, 1992.
- [3] REMODECE, Residential Monitoring to Decrease Energy Use and Carbon Emissions in Europe, Analysis of Monitoring Campaign in Europe, November 2008.
- [4] Eurostat: <http://epp.eurostat.ec.europa.eu/portal/page/portal/eurostat/home/>
- [5] Forschungsstelle für Energiewirtschaft e.V., Elektrostraßenfahrzeuge, Elektrizitätswirtschaftliche Einbindung von Elektrostraßenfahrzeugen, Endbericht © Ffe, Dezember 2007
- [6] RD.10-10003.1, Analysis of European electric vehicle battery parameters-MERGE Task 2.1
- [7] Hellenic Transmission System Operator S.A., www.desmie.gr



- [8] Hatziargyriou, N. D., Anastasiadis, A. G., Vasiljevska J., Tsikalakis, A. G., "Quantification of Economic, Environmental and Operational Benefits of Microgrids," IEEE PowerTech 2009, Bucharest, Romania, paper no 512.
- [9] A. J. Wood y B. F. Wollenberg, "Power Generation, Operation, and Control", 2^o ed. Wiley-Interscience, 1996.
- [10] "Reglas de Funcionamiento del Mercado de Producción de Energía Eléctrica". BOE 20/04/2001.
- [11] "Identification of Traffic Patterns and Human Behaviours", MERGE Task 1.5, deliverable D1.1.
- [12] A. M Law, W. D Kelton, y W. D Kelton, "Simulation modeling and analysis", vol. 2, McGraw-Hill New York, 1991.





MOBILE ENERGY RESOURCES IN GRIDS OF ELECTRICITY

ACRONYM: MERGE

GRANT AGREEMENT: 241399

**WP 2
TASK 2.5
DELIVERABLE D2.2**

RESERVE ADEQUACY

15 FEBRUARY 2011



REVISION HISTORY

VER.	DATE	NOTES (including revision author)
01	05/02/2011	First draft completed
02	07/02/2011	Approved by João A. Peças Lopes
03	15/02/2011	Final version approved
04		
05		
06		
07		
08		
09		
10		



AUTHORS

INESC Porto	Mauro Rosa	marosa@inescporto.pt
	Leonardo Bremermann	leb@inescporto.pt
	Leonel Carvalho	leonel.m.carvalho@inescporto.pt
	Manuel Matos	mmatos@inescporto.pt
	Mariana Liquito	mariana.s.liquito@inescporto.pt

CONTRIBUTORS

INESC Porto	J. A. Peças Lopes	jpl@fe.up.pt
INESC Porto	Manuel Matos	mmatos@inescporto.pt

APPROVAL

DATE

Project Coordinator		PPC	N. Hatzigiargyriou	15/02/2011
Technical Coordinator		INESC Porto	J. A. Peças Lopes	07/02/2011
Work Leader	Package	INESC Porto	J. A. Peças Lopes	07/02/2011

Access:	<input checked="" type="checkbox"/>	Project Consortium
	<input checked="" type="checkbox"/>	European Commission
	<input type="checkbox"/>	Public
Status:	<input type="checkbox"/>	Draft Version
	<input type="checkbox"/>	Submission for Approval (deliverable)
	<input checked="" type="checkbox"/>	Final Version (deliverable, approved)



SUMMARY

RESERVE model is prepared to perform reliability assessment of generating systems based on probabilistic methods. The generating capacity reserve evaluation problem can be traditionally split in two conceptually different research areas: static reserve and operating reserve. The tool can perform both evaluations at the same simulation. The objective of this task is to develop enhancements in the RESERVE model in order to include EV models in the security of supply and operating reserve assessment. A first approach is proposed to create an EV model that should be incorporated in RESERVE model algorithm.

The mobility process is a phenomena strongly linked to urban planning. Understand mobility behaviour is very important to understand EV owner behaviour. This report proposes an EV model based on the mobility process. In order to facilitate the understanding of the proposed methodology, the Distribution Network perspective will be used to clarify the methodology, where EV is represented by a new hourly random variable, which essentially impact in the operational reserve.

Analogously of generating units, EV load has a random characteristic. The amount of EV load added, hourly, on the load can vary with the number of vehicles in charging mode. The approach is to estimate the amount of vehicles per hour in each charging point and in each charging station along of the day through a Poisson process.

With the purpose of illustrating the proposed methodology, a simple example was created. This example is based on survey information and occurs for a specific area of Portugal. Afterwards, a preliminary discussion is presented using the IEEE-RTS 96 power system which was modified in order to include hydro and wind variations of their primary energy resources, increasing the portion of renewable resources. It will be shown that, given the current generating resources within the system, the Dumb Charging mode has revealed to be aggressive to the security of supply point of view. On the contrary, the Smart Charging mode it is possible to guarantee a long term security of supply similar to the scenario where there is no EV. The results indicate a smooth integration of EV on the generation system, if a EV controllable mode such as Smart Charging philosophy will be considered.

TABLE OF CONTENTS

1	INTRODUCTION	7
2	OBJECTIVES	7
3	DESCRIPTION OF THE RESERVE MODEL.....	7
3.1	Static Reserve	8
3.2	Operational Reserve.....	9
3.3	Generation System Components.....	9
3.4	Failure and Repair Cycle	11
3.5	Maintenance Representation.....	14
3.6	Interconnection Representation	14
3.7	Uncertainties Representation	15
3.8	Scheduling of Generating Units	16
3.9	Simulation Process	16
3.10	RESERVE Outputs	19
4	DESCRIPTION OF THE ADAPTATIONS AND ENHANCEMENTS.....	20
4.1	Static reserve evaluation in the presence of large scale integration of EV in the electric systems	21
4.2	Operational reserve evaluation in the presence of large scale integration of EV in the electric systems	21
4.3	Population Mobility process	22
4.4	Electric Vehicles Mobility Representation	25
4.5	Generating Systems Evaluation Considering EV Integration	32
4.6	EV charging impact on Generating Systems	35
4.7	Enhancement in the evaluation of the wind power forecasting uncertainty method	40
5	DESCRIPTION OF THE PRELIMINARY EVALUATION.....	41
6	DISCUSSION - RESULTS OF THE PRELIMINARY EVALUATION	43
7	CONCLUSIONS	45
8	REFERENCES	46

TABLE OF FIGURES

Figure 1: Operating reserve model.....	9
Figure 2: Two-State model.	10
Figure 3: Multi-State model.	11
Figure 5: RESERVE model structure	17
Figure 6: EV representation on the operational reserve evaluation.	22
Figure 7: Arrival distribution along of the day per transport mode.....	24
Figure 8: Arrival distribution along of the day per activity.....	25
Figure 9: Charging points.	27
Figure 11: Generation failure/repair process.....	32
Figure 12: Load profile.	32
Figure 13: Random behaviour of the EV load.	33
Figure 14: System generation and equivalent system load.....	34
Figure 15: Arrivals distribution at 2 am.....	36
Figure 16: Arrivals distribution at 1 pm.....	36
Figure 17: Arrivals distribution at 7 pm.....	37
Figure 18: Average number of arrivals vs average EV consumption.	39
Figure 19: Peak load scenario.....	39
Figure 20: Maximum energy scenario.	40
Figure 22: Daily load profile of the smart and dumb charging scenarios in percentage of the peak load.....	42
Figure 23: Operational reserve monthly LOLE.....	43
Figure 24: Operational reserve needs discrete cumulative probability distribution.	45

RESERVE ADEQUACY EVALUATION CONSIDERING EV

1 INTRODUCTION

The massive integration of Electric Vehicles (EV) into the electric network poses new challenges. On the one hand, EV will represent a new load to the system mainly, but not only, at valley hours; on the other hand, EV will also be able to provide support in situations where the system requires additional power by decreasing their consumption. Determining the effects of this alternating and stochastic behaviour on the schedule of the operating reserve needs is of a particular interest of the System Operator, especially when in presence of other sources of uncertainty, like wind power production or the short and long term load variation.

In order to assess the impact of EV in the long-term operating reserve, an enhanced version of the RESERVE model is presented. The core of the original tool was developed in a joint project of INESC Porto REN and REE. This new model accounts for an hourly EV charging and also for the possible support of EV to the system at specific hours. Thus, it is possible to deal with EV behaviour to estimate conventional reliability indices, like the LOLE (Loss of Load Expectation) or nonconventional indices, like the average renewable energy spilled, through the use of RESERVE model.

The following sections consist of an introduction to the RESERVE model, on the description of its adaptations and enhancements namely, the description of EV model developed and finally a case study is analysed and discussed.

2 OBJECTIVES

In order to assess the impact of EV on the long-term operational reserve, an enhancement of a previous tool developed in a joint project of INESC Porto, REN and REE for the assessment of the security of supply in terms of the static and operating reserve adequacy is to be made. RESERVE model is based on the sequential Monte Carlo method (MC), the simulation is organized chronologically in order to preserve the relation between load variations, wind power variation, hydro conditions and other variables, such as, maintenance management, pumped storage operation, CHP generation, and small hydro generation and, more recently, EV behaviour. As a result, it constitutes an adequate basis to assess the impacts on the long-term adequacy of the system from the EV integration in the electric systems. For that purpose, models of the additional features associated with the massive EV are developed and integrated in the tool's algorithm, enabling representing different scenarios of EV integration and mobility patterns.

3 DESCRIPTION OF THE RESERVE MODEL

RESERVE model is prepared to perform reliability assessment of generating systems based on probabilistic methods. The generating capacity reserve evaluation problem can be traditionally split in two conceptually different research areas: static reserve and operating reserve. RESERVE model can perform both evaluations at the same simulation. The basic consideration for both analyses is to

concentrate all generating units and load in a single bus. This tool also considers special issues like the integration of intermittent power sources (as wind generation) and interconnection impacts.

Figure 39 summarizes the RESERVE model simulation process, where the inputs are the components' representation, models and parameters that will be described in the next sections.

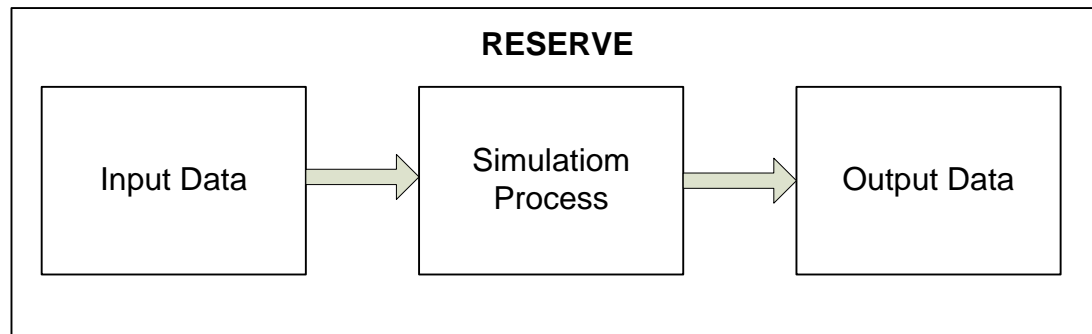


Figure 39: RESERVE model.

The main idea is to make possible studying the behaviour of reliability indices, such as: LOLE (Loss of Load Expectation), EENS (Expected Energy Not Supplied), and LOLF (Loss of Load Frequency) which are conventional reliability indices, and also well-being indices (outputs) when a major portion of energy is renewable.

Static reserve and operating reserve will be described in the next section, as well as the components' representation used by RESERVE model.

3.1 Static Reserve

The interest of the long-term reserve requirement evaluation, is verify if a given configuration of generation will be able to meet the forecasted load demand for a specific year in the future. To estimate static reserve indices, each state contained in the sequence is evaluated according to the following power balance equation [1]:

$$R_{STA} = G - L < 0 \quad (1)$$

where, G represents the system available generating capacity at hour t , L is the total system load at hour t and R_{STA} is the static reserve.

The random variable G depends on the equipment's availability and on the capacity fluctuations due to, for instance, hydrologic and wind resources. The random variable L depends on the hourly load observation and both can be affected by short and on the long-term uncertainties.

3.2 Operational Reserve

Due the inherent uncertainty of the load demand forecast, forced outages of the generating units and the intermittent generation sources, operating reserve is assessed to cover these uncertainties. To account for these short-term decisions, new variables for the power balance equation have to be defined to represent the uncertainties.

The power balance equation is represented in equation (2) which is set to assess the risk indices associated to the operational reserve [2].

$$R_{OPE} = R_S + R_T < \Delta L + \Delta P_w + \Delta G \quad (2)$$

where, ΔL represents the short-term load deviation at hour t , ΔP_w represents the possible wind power capacity variation at hour t and ΔG represents the generating capacity variation due to forced outages at hour t .

The structure of the operating reserve evaluation is presented in Figure 40. The RESERVE model considers that the primary (R_p) and the secondary (R_s) reserves are pre-defined and set as a fixed amount of power. The amount of spinning reserve can always be redefined if its performance is below a pre-established acceptable value. The tertiary reserve (R_t , non-spinning reserve) is composed by generators which can be synchronized within 1 hour. When the power balance equation is true, it means that there is no generation source enough to meet the uncertainties considered. Otherwise, the system is considered reliable.

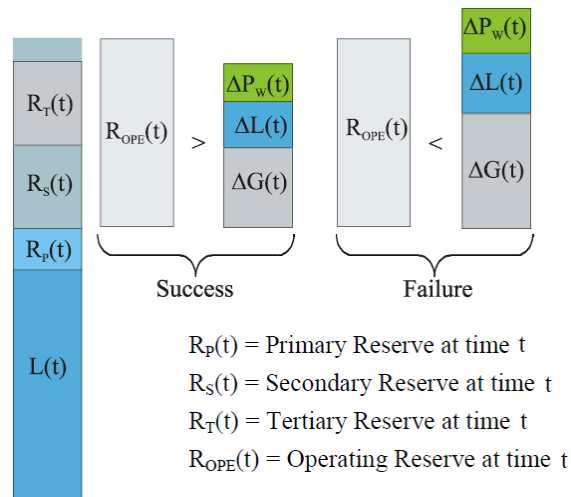


Figure 40: Operating reserve model.

3.3 Generation System Components

In this section, a detailed description of the models and/or representations of the power system's components contained in RESERVE model are presented.

3.3.1 Load Representation

Since load curves vary seasonally along of the year, reliability characteristics of a system may also change throughout the days of the year. These curves are built from many years of observations and the most detailed load profile extents all 365 days of the year and consist of 8760 hourly demand points.

In chronological representations, the standard chronological load model is used containing all hours of the year. The chronological MC simulation will sequentially follow these load steps during the simulation process

3.3.2 Two-State Model

Markovian process representation is used when a component can be resides in two different states, as depicted in Figure 41. In the up-state the component is at its full capacity and in down-state the component is unavailable. Traditionally, it is assumed that the transitions between states follow an Exponential distribution [1]; however, it is possible to use any other distributions, such as the Normal probability distribution or the Weibull probability distribution.

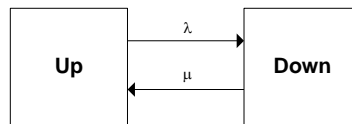


Figure 41: Two-State model.

Assuming exponentially distributed transitions between states, it is possible to calculate the state residence time by using the inverse transform method equations:

$$T^{UP} = -\frac{1}{\lambda} \ln U_1 \quad (3)$$

$$T^{DOWN} = -\frac{1}{\mu} \ln U_2 \quad (4)$$

where, U_1 and U_2 are numbers belonging to the $[0,1]$ interval sampled from the Uniform probability distribution; $\lambda = \frac{1}{MTTF}$ and $\mu = \frac{1}{MTTR}$ are, respectively, the failure rate and repair rate of the component.

3.3.3 Multi-State Model

This type of representation is used when there are many components with the same stochastic and deterministic parameters [2]. On the opposite of the Two-State

representation, this one has an aggregation of N components results in a model with $N + 1$ different states.

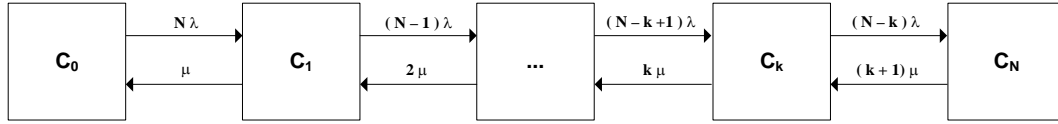


Figure 42: Multi-State model.

Figure 42 depicts the Multi-State representation constituted by $N + 1$ states. The parameter N represents the number of generating units of the wind farm. If C is the unit capacity, the amount of power associated with the k^{th} state is given by C_k .

$$C_k = (N - k) \times C, \quad k \in N_0, k < N \quad (5)$$

The cumulative probability P_k (from 0 to k) associated with this state can be easily calculated. In order to reduce the number of these states during the chronological MC simulation, a simple truncation process sets the desired order of accuracy. Therefore, instead of $N + 1$ states, a much smaller number up to the capacity C_N will limit this representation. If the current state is either the first one or the last one, the state residence time is computed using equation (3) and equation (4), respectively; If the current state is neither the first one nor the last one, the state residence time is computed by:

$$T^{C_k} = \min \left\{ -\frac{1}{(N - k)\lambda} \ln U_1, -\frac{1}{(k + 1)\mu} \ln U_2 \right\}, \quad k \in N_0, k < N \quad (6)$$

where, T^{C_k} is the state residence time in the state C_k ; N is the number of components; U_1 and U_2 are numbers belonging to the $[0,1]$ interval sampled from the Uniform probability distribution; $\lambda = \frac{1}{MTTF}$ and $\mu = \frac{1}{MTTR}$ are, respectively, the failure rate and repair rate of the component.

3.4 Failure and Repair Cycle

To determine the component status of a given state, capacity time-dependent and failure and repair cycle need to be taken into account. It determines the component's availability and the corresponding parameters. The components' availability consists on determining the theoretical maximum capacity that a component holds when in a given state.

Capacity time-dependent is concerned with the representation of components' capacity time dependence, since it usually exhibits an hourly, monthly or even yearly variation. The availability of water resources, for instance, is incorporated in the RESERVE model through annual series which represent the resource characteristic of the year. Therefore, to properly model the behaviour of a given component, its theoretical maximum capacity has to be affected by its time-varying characteristic.

3.4.1 Thermal Units Representation

Large thermal units generators are all of those which have a significant size and convert the thermal energy, contained in fossil fuels or in the atomic nuclear, to electricity by a thermodynamic cycle.

The failure/repair cycle of this type of generators is represented by a Two-State model, whose transitions follow an Exponential probability distribution.

When in the up-state, a conventional generator is able to produce its maximum capacity, and when in down-state the generator's capacity is zero.

3.4.2 Hydro Units Representation

Hydro generators are those which have a significant size and convert the potential energy of the water to electricity.

Like conventional generators, the failure/repair cycle of this type of generators is represented by a Two-State model, like depicted in Figure 41, whose transitions follow an Exponential distribution.

The power available in each month for each hydro unit can be associated to the volume stored in different ways. An example may be highlighted at the corresponding basin (considering the affectation of water inflows) by using the following equation:

$$P(V) = A + B(V - C)^x \quad (\text{MW}) \quad (7)$$

where $P(V)$ is the power available in each month according to the stored volume V (hm^3). Constants A (MW), B (MW/hm^3), C (hm^3) and the parameter x are characteristic of each large hydro unit.

The value of available hydro power, in equation (7), derives from monthly volume stored series (in hm^3). When a new year in the simulation begins, a new hydro regime is selected, based on random sampling, and each basin is assigned its corresponding series. Additionally, it is considered an additional production capacity due to the eventual pumping capabilities.

3.4.2.1 Hydro Generating Units Representation Considering Pumping

The incorporation of the pumping operation process in RESERVE is made by two models:

- pure pumped-storage, which consists only on shifting water between upstream and downstream reservoirs;

- combined pumped-storage, which considers not only the possibility of generating electricity by moving water from the reservoirs but also the generation of electricity through natural stream-flow.

The approach used for modelling combined pumped-storage considers that the volumes pumped are added to the existing volume in the reservoir, causing an increase on the water availability which will then be converted into additional power during the normal process of estimating the monthly available power. This approach also includes the assumption that operation of hydro power plants is fairly regular throughout the month.

After the pumping process, the corresponding additional volume stored, V_B , is given by:

$$V_B = \frac{P_{bomb} \cdot h_{bomb}}{k_B} \quad \text{hm}^3 \quad (8)$$

where, P_{bomb} is the pumping power (MW), h_{bomb} is the number of hours in a typical day where pumping process takes place, k_B is a coefficient (MWh/hm³), relating the pumped volume with the energy consumed on that process.

In the cases where it is not possible to obtain a reliable estimate of k_B , or if the pumping regime corresponds to a typical pumping nominal flow, C_{bomb} (m³/s), the following alternative expression can be used:

$$V_B = C_{bomb} \cdot h_{bomb} \quad \text{hm}^3 \quad (9)$$

In the case of pure pumped-storage it is considered that total volume of the reservoir is always available. Thus, the available power equals the capacity of the water use by the hydro unit affected by a factor translating the availability of the installed power. This factor, f_{disp} , reflects the effect of possible failures and the enforcement of maintenance programs.

$$P_{BP} = f_{disp} P_{BPinst} \quad \text{MW} \quad (10)$$

where, P_{BP} is the available production capacity and P_{BPinst} is the maximum production capacity.

3.4.3 Wind Farm Representation

Wind generators are those which convert wind energy to electricity. Taking advantage of the fact that wind generators within wind farms traditionally are equal, a Multi-State representation is used to represent the failure and repair cycle of the aggregation of wind generators. This cycle follows an Exponential distribution.

The maximum available capacity of the aggregation of wind generators is affected by hourly wind series. These series relate the total power output of a wind farm with the hour of the year. At the beginning of the year each wind farm is assigned its corresponding wind series which are selected, based on random sampling, taking into account their probability. Despite having a probabilistic nature, they are used as deterministic parameters.

3.4.4 Small Generating Units Representation

Given the diversity of the units of Mini-Hydro, CHP, CSP and PV units, the RESERVE model considers that these units, which have similar values for the stochastic parameters and/or capacity can be modelled as a single group. The different stochastic and deterministic parameters of the units belonging to the aggregation are averaged to determine the parameters of the corresponding Multi-State representation.

Similar to the large hydro and wind farm cases, it is possible to consider the impact of the hour on the capacity of the aggregation. It is considered that the relation between total available power and hour or month is linear, and the amount of power available is affected by historical series through a determined value (in percentage). The power available is obtained directly by multiplying the capacity of the aggregation state with the corresponding hourly percentage. The historical series are selected considering their associated probability. Despite having a probabilistic nature, they are used as deterministic parameters. When a new year in the simulation begins, a new series for each type of aggregation is selected, based on random sampling.

3.4.5 Other Units Representation

If the power system under evaluation contains other type units, like biomass units, biofuel units, geothermal units, etc, they are modelled using the model described in the section 3.4.4.

3.5 Maintenance Representation

Each month will be considered an amount of power that will be out for maintenance. This value is subtracted from the total installed capacity of the system.

3.6 Interconnection Representation

Physical interconnections between countries were represented as large power generating units. The units' reliability parameters are similar to the ones of the transmission system connecting the two countries' power systems (i.e. the power transmission lines constituting the interconnections). The following pre-defined stochastic parameters can be used as a reference to each interconnection:

- Failure rate: $\lambda = 1 \text{ occ./year}$;
- Mean Time to Repair: $MTTR = 5 \text{ h}$.

For simulation purposes, these units were represented by a two-state Markov model analogous to the one used to represent large thermal generation units. It is assumed that units representing interconnections can be fully mobilized within one hour.

The available power of units representing interconnections is limited by the Net Transfer Capacity (NTC) during winter and summer and also by the availability of the neighbouring system which may not be able to provide all that capacity. To meet this condition, the available power of the equivalent unit generator is determined based on simulations of the neighbouring system, which did not consider the presence of interconnections. From the probability density function of the monthly average power available obtained from those simulations and taking also into account the NTC, hourly series of the average power available that can be transferred to the neighbouring system are built. Afterwards a new simulation takes place, this time considering the presence of interconnections modelled as large power generating units.

3.7 Uncertainties Representation

On the short-term analysis, the summation of the forced outages generation capacity value, the uncertainties inherent to load and wind forecast should be meeting by the operating reserve.

The objective of this section is to describe the representation of the uncertainties related to the intermittent portion of the wind generation and the variability of the load on the RESERVE model.

3.7.1 Wind Power Forecast Uncertainty Representation

RESERVE model represents the uncertainty of wind power forecasts assuming that the persistence method will be used to make unit commitment in the period under analysis. According to this method, the total wind power forecast uncertainty ΔP_w of a given hour t is computed according to equation (11):

$$\Delta P_w(t) = P_w(t) - P_w(t-1) \quad (11)$$

where, t is current hour; $t-1$ is the preceding hour; P_w is the total wind power production (MW).

Therefore, in order to simulate the wind power forecast error, RESERVE model just calculate the wind power value between the present hour and the next hour. This is a cumulative option since better forecast methods lead to smaller forecast errors than persistence.

3.7.2 Load Forecast Uncertainty Representation

Many authors suggest the Normal distribution as an accurate representation of the uncertainties associated with short-term and long-term forecasts [1].

To compute the hourly uncertainty associated with short-term forecast an impulse of the binomial distribution is randomly sampled. The mean of this distribution is zero

and its standard deviation is σ_{ST} . The value of σ_{ST} is set at the beginning of the simulation process of the RESERVE.

To compute the annual uncertainty associated with long-term forecast an impulse of the binomial distribution is randomly sampled at the beginning of each year. Similar to the short-term uncertainty, this distribution has zero mean and a standard deviation σ_{LT} . The value of σ_{LT} is set at the beginning of the simulation process of the RESERVE. The value of ΔL is computed by adding the short-term uncertainty sampled at the current hour and the long-term uncertainty sampled at the beginning of the year.

3.8 Scheduling of Generating Units

In order to simulate the scheduling of the available generators, a merit order strategy is used. In this strategy the generators with a higher rank are preferably dispatched at its full capacity. This strategy follows the subsequent procedure:

- i. Find the next available generator with the highest merit order that has not been dispatched yet;
- ii. Dispatch the generator at its full capacity;
- iii. Check if the load was totally covered;
- iv. If (iii) is true, end procedure; if (iii) is false, go to (i).

The merit order is established based on lists provided by the utilities, in which a mobilization order for each type of generation technology is specified. This can be done for a multiplicity of scenarios, similarly hydro inflows scenarios (wet years, dry years, for instance)

The following example will illustrate the unit commitment order.

Table 39: Unit Commitment Order.

Generation classes	Order
Wind units	10
Hydro units	20
Thermal units	30

3.9 Simulation Process

RESERVE model is based on a chronological representation and it allows assessing the performance of the generating system in terms of static reserve and operational reserve. The core of this model is based on four stages, as depicted in Figure 43, which are consecutively executed until convergence is reached. Static reserve

indices are estimated using the mean values of appropriate test functions [3], according to:

$$\tilde{E}[F] = \frac{1}{NY} \sum_{n=1}^{NY} F(y_n) \quad (12)$$

where: $\tilde{E}[F]$ is the estimate of the static reserve indices; NY is the number of simulated years; y_n is the sequence of system states in the year n ; and $F(y_n)$ is the function to calculate yearly reliability indices over the sequence y_n . As an example, the $F(y_n)$ test function of the LOLE index is equal to the sum of the duration of all those states within the sequence y_n in which there is load curtailment.

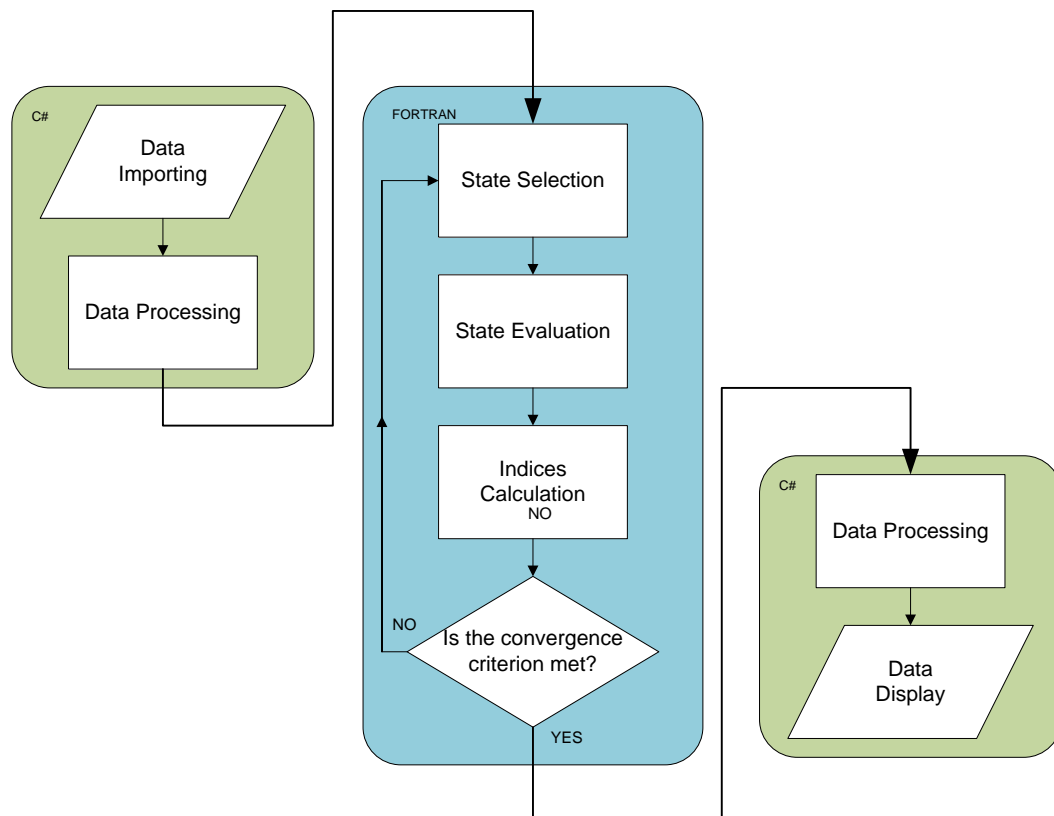


Figure 43: RESERVE model structure

In the first stage, a system state and the time in which it will remain in is sampled. Sampling a new state depends on each component's failure/repair cycle stochastic model and its corresponding capacity time-dependent model, to the load model, and most important, to the previous system state. In the chronological type of sampling,

a new system state differs from the previous one in the state of one and only one of its components.

In the second stage, the system state sampled is evaluated. In this stage the available generating units are scheduled according to the merit order defined at the beginning of the simulation process. This stage allows determining the outcome of equations (1) and (2).

The third stage involves updating the reliability indices by confronting the results of the state evaluation process to a series of test-functions. Each of those test-functions represents mathematically the meaning of a given reliability index. By using these test functions it is possible to calculate unbiased estimates of the reliability indices.

The last stage of the RESERVE model is to check whether the convergence criterion has been met. If the convergence criterion has not been met, the simulation process continues to the state selection stage; otherwise the simulation is stopped. One of the most used criteria to stop the simulation is when the coefficient of variation of a given reliability index is below a pre-specified threshold; other criterion is when the number of years sampled are above a threshold value.

The coefficient of variation β also termed as the uncertainty of the Monte Carlo simulation process, is given by:

$$\beta = \frac{\sqrt{\tilde{V}(\tilde{E}(F))}}{\tilde{E}(F)} \quad (13)$$

where: $\tilde{E}(F)$ is the estimate of a given reliability index and $\tilde{V}(\tilde{E}(F))$ is the variance of the estimator $\tilde{E}(F)$, given by:

$$\tilde{V}(\tilde{E}(F)) = \frac{V(E(F))}{NS} \quad (14)$$

where: NS is the number of years simulated.

The RESERVE model can provide, at the end of the simulation process, estimates of the reliability indices and their underlying probability distribution. Moreover, it allows obtaining other type of indices such as the average renewable energy spilled.

3.10 RESERVE Outputs

The RESERVE model can provide several different types of results. If the aim of the study is to analyse the static and operational reserves, estimates that can be on a monthly or on an annual basis will provide the following reliability indices:

- Loss of Load Probability – LOLP;
- Loss of Load Expectation – LOLE (hour/year);
- Expected Power Not Supplied – EPNS (MW);
- Expected Energy Not Supplied – EENS (MWh/year);
- Loss of Load Frequency – LOLF (occurrence/year);
- Loss of Load Duration – LODD (hour/occurrence);
- Loss of Load Cost – LOLC (currency/year).

Moreover, the RESERVE model also makes available probability distributions of the conventional indices.

The RESERVE model also provides estimates of the indices of the well-being concept. This concept allows including deterministic criteria in the probabilistic evaluation. It can provide a measure for the degree of success or failure of the states sampled by categorizing them as *healthy*, *marginal* and *at risk*. The states deemed *healthy* contain sufficient resources (generation and/or transmission) to meet the load and the pre-defined deterministic criteria; if there are sufficient resources to meet the load but at the same time they are insufficient to meet the pre-defined deterministic criteria, then the state is deemed *marginal*; if there is not enough resources to meet the system load, the state is deemed *at risk*. Estimates on a monthly or annual basis for the following well-being indices can be obtained by the RESERVE model:

- Probability of the Healthy State – $P \{H\}$;
- Probability of the Marginal State – $P \{M\}$;
- Expected Frequency of the Healthy State – $F \{H\}$ (occurrence/year);
- Expected Frequency of the Marginal State – $F \{M\}$ (occurrence/year);
- Expected Duration of the Healthy State – $D \{H\}$ (hour/day/week);
- Expected Duration of the Marginal State – $D \{M\}$ (hour/day/week).

Similarly to conventional indices, RESERVE model also makes available probability distributions of the well-being indices. As RESERVE model follows a chronological representation of the system states, other type of results can also be obtained, depending on the type of study selected. As such, an important result that can be obtained is the operational reserve requirements. This result consists on identifying the expected reserve needs based on the load short and long-term uncertainty, wind power deviations and the up/down cycle of the generating units. Furthermore, a probability density function of the reserve needs is also made available.

RESERVE model also makes available detailed reports on the performance of individual generation units and/or of classes/aggregations of generating units. These reports consist on information about the installed and available capacity, the power and supplied energy, as well the production cost. Furthermore, all these reports can

include information about the unavailability of each unit or class as well as the probabilities density functions associated.

Another set of results that can be obtained is related to the renewable energy spilled. These results consist on a set of indices based on energy and power observations during the simulation process. Despite the fact that the renewable spill evaluation does not consider any optimization process, it is possible to perform a good evaluation of the renewable energy spilled based on the schedule of the generating units. The result of this study is a set of indices, build upon energy and power observations, such as:

- probability of the renewable spill events;
- frequency of the renewable spill events;
- average duration of the renewable spill events;
- average renewable energy and power spilled.

These indices can give an idea regarding the amount of renewable energy spilled considering that there is a quantity of power that must always be produced by a set of large thermal units. These thermal units are preferably scheduled to ensure the dynamic stability of the system.

Finally, results related to the exported power can also be attained. These results consist on information about power available on the interconnections, or, in other words, the power available that can be used by the interconnected system.

4 DESCRIPTION OF THE ADAPTATIONS AND ENHANCEMENTS

The large deployment of EV into the electric system can be represented by two different models: EV as a new load into the system, mainly, but not only, at valley hours and also they could be able to provide support in situations where the system needs additional power by decreasing their consumption automatically.

The objective of this task is to develop enhancements in a tool in order to include EV models in the security of supply and operating reserve assessment. An important feature of the tool is the operational reserve assessment which estimates, in each simulated state, the unforeseen change in load (as described in section 3.7.2) using a discrete normal distribution of the forecast error and in wind power (as described in section 3.7.1) assuming the forecast by a persistence method. These methods were improved by the implementation of a continuous Normal distribution and the Weibull distribution, respectively.

In order to assess the reserve requirements and to evaluate the need for peaking generation units in the future, the impact on long term reserve adequacy expected from the EV integration in the electric systems must be considered.

4.1 Static reserve evaluation in the presence of large scale integration of EV in the electric systems

In analogy with the static evaluation presented in 3.1, the reliability assessment has been changed through some adaptations in the equations (1) and (2). The static reserve evaluation is defined as follows:

$$R_{STA} = G - (L + P_{EV}) < 0 \quad (15)$$

where, P_{EV} is the amount of EV load connected in the electric system, and will be incorporated as a random part of the load.

4.2 Operational reserve evaluation in the presence of large scale integration of EV in the electric systems

The EV load introduced in Figure 44 below, related to the operational reserve, and represents the possible EV load requirement, which is unpredictable and dependent directly on the EV users' behaviour. Therefore, in analogy with generating availability fluctuation represented by failure and repair cycle of generating units, the proposed methodology consider that part of the total load will be represented by a new random variable that comes from the EV usage. Hence, the operational reserve evaluation is defined as follows:

$$R_{OPE} = R_S + R_T < \Delta L + \Delta P_W + \Delta G + \Delta P_{EV} \quad (16)$$

where, ΔP_{EV} is the fluctuation of the EV amount connected in the electric system.

In this work, load controllability is performed, namely in order to move EV load from one period to another. Smart Charging can be understood as a complex procedure involving local control, responding to local variables, and response to an upper level management, that corresponds to a controlled charging approach as used in this work. In this report the designation *Smart Charging* was adopted for the controllable EV charging mode. This Smart Charging is incorporated on the simulation process through a concurrent procedure that is threaded together with the failure and repair processes. The equations (15) and (16) show the adaptations proposed to cope with EV integration in the operational reserve assessment.

As already stated in 3.2, the Figure 44 represents the operating reserve structure. The EV load will add a random feature in the observed load. This random behaviour should be meeting by the operational reserve.

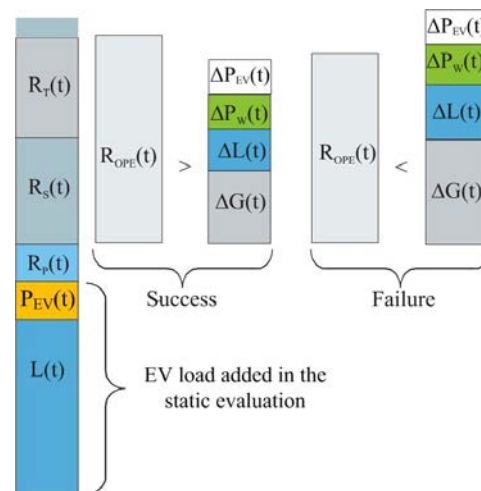


Figure 44: EV representation on the operational reserve evaluation.

The way how the EV owners will charge their vehicles is linked to several daily factors and can be characterized by their mobility behaviour. In fact, there are several research areas linked to the population mobility behaviour, mainly to study the population movement phenomena. Therefore, based on the reference [3] and the survey carried out in the MERGE WP 1, the mobility behaviour of the citizens can be exploited.

4.3 Population Mobility process

The mobility process is a phenomena strongly linked to urban planning. It integrates land use and transportation planning to improve the economic and social environments of communities. It also is a life quality indicator which leads the government institutions and companies to invest in surveys that should obtain enough data to develop urban planning, or strategy planning (transport sector, for instance).

The survey [3] was developed by Portuguese Statistic Institute and it had the purpose to create a database to characterize the mobility of the citizens throughout a set of variables such as: the trips' number, duration and departure hour, the type of transport used, changes between different transports, classification by activities, distinction between the mobility of week-days and weekends. It was used to support some model decisions in order to improve Reserve Model.

One of the most relevant results of this study revealed a reduced spectrum of the regional variation on mobility practices. Albeit each studied region had different practices of social and economic structuration. This relative region homogeneity has a set of common characteristics, namely with the trips intensity per day, such as: the strong dependence of cars, and work, school and public activities. These are the main reasons of the journeys. The duration of the travels and their synchronization along of the day also are ordinary characteristics of the regions under analysis in the survey. Obviously, the study is referring Portuguese regions, which can be different to other countries.

From [3] an average of 2.5 trips per person per day happens on the studied regions, which is shown in Table 40 among other interesting results.

A major concern may be highlights the importance of the mobile population; in general, it represents always more than 2/3 of the global population. Other major aspect is the rate between the mobile population and the mobile population motorized, where the latter represents the dependence of a combustion vehicle. Finally, the reduced rate of the external trips represent that their destination are the origin places.

Table 40: Mobility observations.

Week-day	Cávado/Ave	Grande Porto	Vale do Sousa / Baixo Tâmega	Entre Douro and Vouga	Total
Nº of trips / per person / per day:					
Departure in the region	2.6	2.5	2.2	2.1	2.5
Departure in the residence region	2.4	2.1	2.0	2.9	2.1
Nº of trips / per family / per day:					
Departure in the residence region	8.0	5.9	6.5	6.1	6.6
Mobile population / residence population (%)	78.2	75.7	71.1	67.0	74.9
Mobile population with car / mobile population (%)	76.0	80.9	79.6	81.0	79.2
Nº of trips / per mobile pop. / per day	3.4	3.3	3.3	3.2	3.3
Nº of external trips / nº travels with departure in the region (%)	3.9	4.7	6.9	6.1	
Nº of external trips / per person / per day	0.10	0.12	0.15	0.13	

A set of interesting results is cited in the mentioned survey, for instance, the number of trips per mobile population per day is about 3.3. However, this report will concentrate on the results that analyse the dependence of the vehicles. Table 40 shows the number of trips per type of transport, and is clearly observed that cars have a huge importance in how people move around.

Table 41: Number of trips by transport and reason.

Week-day	Cávado/Ave	Grande Porto	Vale do Sousa / Baixo Tâmega	Entre Douro and Vouga	Total
Trips by type of transport					
Nº of trips / person / day:					
by foot	0.79	0.61	0.56	0.46	0.64
by car	1.29	1.31	1.17	1.31	1.28
by public transport	0.32	0.44	0.32	0.14	0.35
other	0.14	0.09	0.22	0.20	0.14
Trips by reason					
Nº of trips / person / day:					
work	0.70	0.58	0.63	0.58	0.63
school	0.21	0.16	0.17	0.15	0.18
shopping	0.12	0.15	0.09	0.06	0.12
leisure	0.23	0.31	0.21	0.21	0.26
return to home	1.19	1.08	1.07	0.99	1.11
other	0.18	0.22	0.16	0.16	0.19

Notice from Table 40 that 52% of the trips are made by car and in certain regions as “Entre Douro and Vouga” it achieves 61%. The public transportation appears in third place and is more relevant in Porto metropolitan region. The work and school are the main reasons to the departures, which it means that is very important to relate the mobility practices with the active and student population in this region.

The Figure 45 illustrates the arrival hour of the trips in a week-day; from this, three periods of intensity were highlighted from 7h-9h, 12h-14h, and 18h-19h.

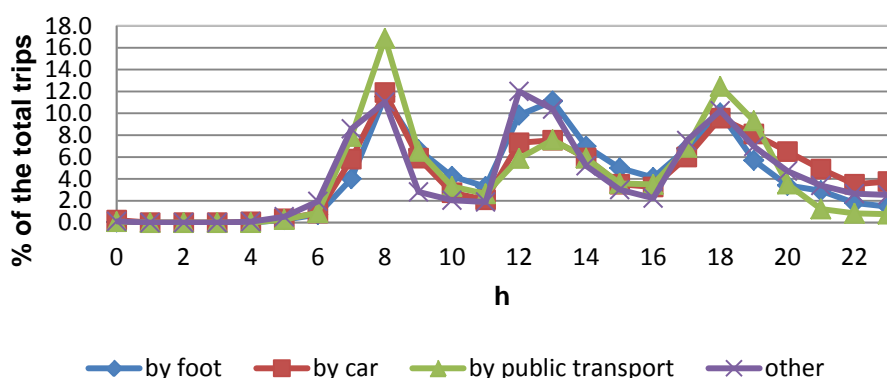


Figure 45: Arrival distribution along of the day per transport mode.

Figure 46 presents the mobility distribution per activity related with the departure hour in a week-day. Notice that the trips alternate along the day however the school and work are the main reasons for their starting.

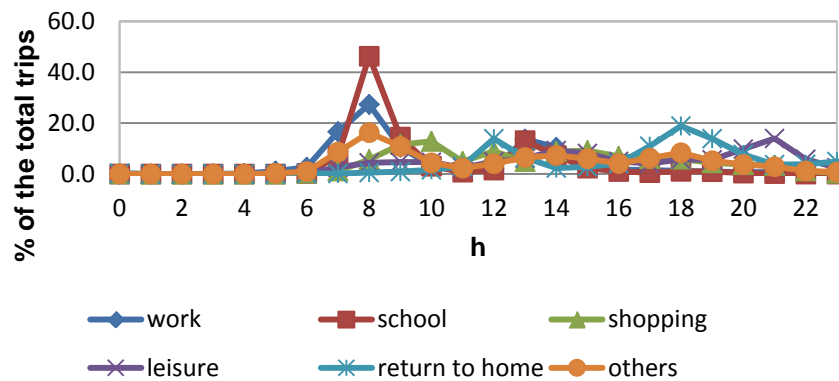


Figure 46: Arrival distribution along of the day per activity.

The analysis done reveals interesting information for the task's purpose. In a general way, the analysis presents, as already mentioned, that there is no relevant variation of mobility behaviour among the regions observed. There is an elevated number of departures and arrivals in the same area. This means that long journeys in a week-day are not relevant for the mobility representation.

4.4 Electric Vehicles Mobility Representation

In order to facilitate the understanding of the proposed methodology, the Distribution Network perspective will be used, where EV represent an additional load that changes from hour to hour according to the mobility patterns. All the considerations applied for the distribution systems will be extended to the evaluation of generating systems. That effect has a strong dependence of the charging mode used by the EV owners [5]. As already stated in 3, the basic consideration for static and operational reserve evaluation is to concentrate all generating units and load in a single bus. It leads to the creation of an EV power model that may be able to represent the mobility process and to capture the random behaviour of EV. Next, it should be integrate, considering an hourly resolution, to the observed system load. In other words, part of the system load will be represented by a new random variable, which varies hourly along the year.

In analogy of the generating units, EV load has a random characteristic. The amount of EV load added, hourly, on the load can vary with the number of vehicles in charging mode. A first approach of the mobility is to estimate the amount of vehicles per hour in each Charging Point (CP) and in each Charging Station (CS) along of the day. A CP is a distribution transformer allocated in a determined area. Thus, the distribution transformer is used to feed typical loads and EV batteries. It may be viewed as an analogy of a gas station which has the tank size as limiting factor of how many vehicles can be fuelled, a CS has a distribution transformer as limiting factor of how many EV can be charged.

The EV behaviour is a stochastic process, and its events occur continuously and independently of one another. Therefore, a stochastic counting process may be used to model its behaviour. Examples of that can be cited such as: the number of goals in (90 minutes of) a soccer match, the arrival of "customers" in a queue, the number of telephone calls arriving at a switchboard, and the number of vehicles that

arrive in a such gas station. Next sections will present the mathematic procedure used to model, in the RESERVE program, the EV counting process in different areas.

4.4.1 Proposed Methodology

The number of EV is a discrete random variable that is often modelled by a Poisson distribution [6]. Thus, $\{X(t): t \geq 0\}$ is a collection of random variables, where $X(t)$ is the number of vehicles arrivals (events) that have occurred up to time t . The number of events between time a and b is given by $X(b) - X(a)$ and has a Poisson distribution [6]. In other words the Poisson process is a continuous-time counting process that possesses the following properties:

- the number of occurrences counted in disjoint intervals are independent from each other;
- the probability distribution of the number of occurrences counted in any time interval only depends on the length of the interval;
- no counted occurrences are simultaneous.

Considering the previous properties and supposing that each EV arrival happens one at a time, the problem can be approached by a Poisson process.

It is assumed that a physical zone is divided in the following areas:

- industrial area;
- school area;
- commercial area (for instance, downtown of the cities);
- public area (leisure, public parks, botanical gardens, etc);
- residential area;
- others (hospitals, stadium, etc).

These areas are the reasons why a journey begins or finishes, such as classified in [4]. The objective of the methodology is catching, along of the day, the number of EV in each area to compute the equivalent EV load.

Figure 47 illustrates the following areas: residential, industrial, public leisure, and commercial areas. It shows in each area a typical load profile that represents the ordinary behaviour of consumers, and also it illustrate a possible EV load profile on the different types of charging points. The summation of these profiles may represent the EV impact in each physical area on different regions.

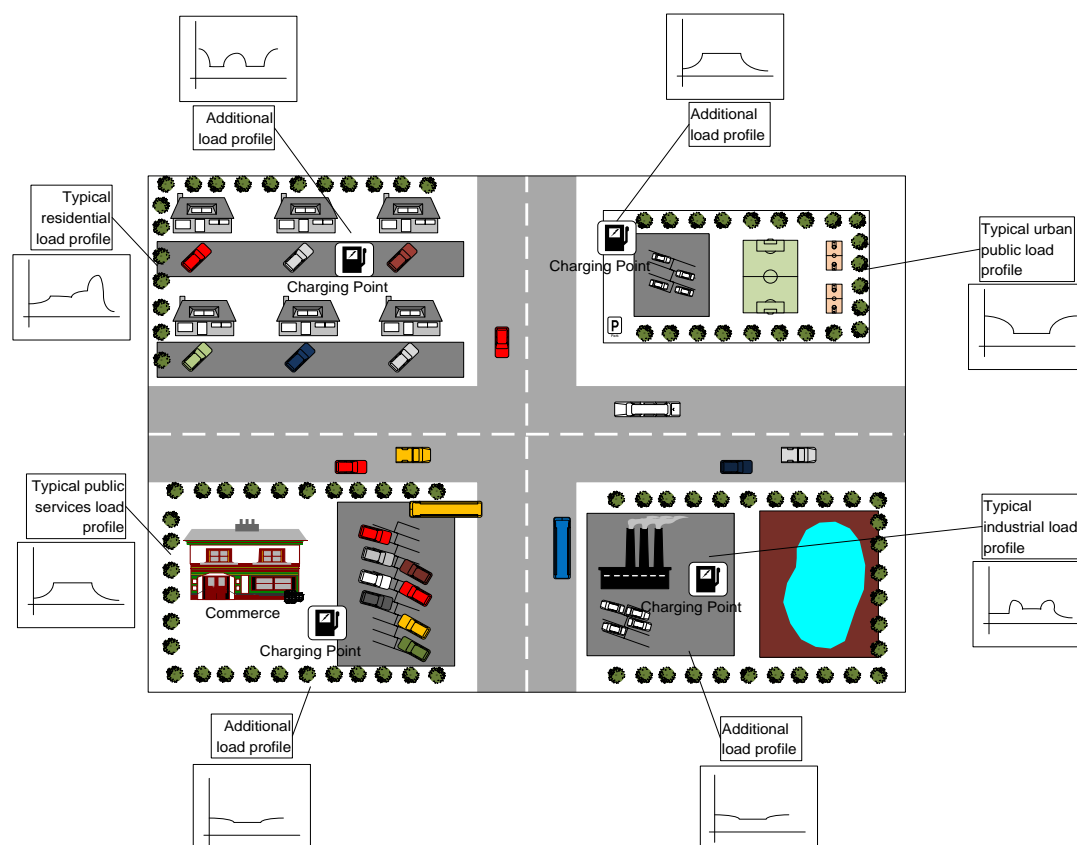


Figure 47: Charging points.

Besides of these areas, CS should be represented. As previously stated, the amount of EV connected depends of the distribution transformer capacity, which also depends on the limit of simultaneous connections in each CP and CS.

4.4.2 Charging Points

From Figure 47, each area has its own typical load profile which is characterized by Figure 48. In [7] was presented a study concerning with the additional investments in distribution networks with high integration of electric vehicles and, from this study, nominal capacities of the distribution transformers will be considered. The nominal capacity of the distribution transformer will limit the number of vehicles connected in a same CP. The Table 42 presents the conventional distribution transformers chosen from [7].

Table 42: Distribution transformers capacities.

Capacity (kVA)	400
	630
	800
	1000

Regarding the CP and CS, the constraints which should be taking into account, are as following:

- the nominal capacity of the distribution transformers in each area and in the CS;
- the EV capacities considered in such scenario.

4.4.3 Typical load profiles of CP

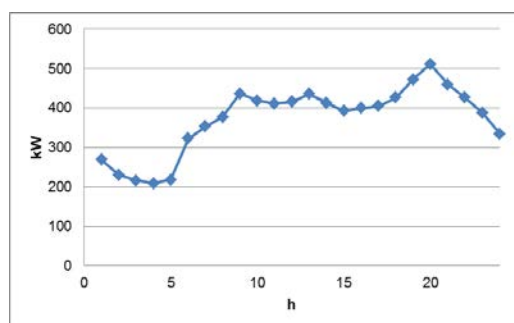
From [8] typical load profiles were obtained for different situations. These load profiles are hourly divided per areas and typical days, such as: week-day, Saturday, Sunday/holiday. Based on these profiles, the impact of the large integration of EV in the distribution transformer can be evaluated.

Figure 48 shows some typical load profiles of a week-day. In a) is presented a typical load profile of a residential area. Notice that there are three peaks during the day which are from 8-10 am, 11 am - 1 pm and 7-9 pm. From Figure 46, the home return represents the arrivals to the residential area. The peak of arrival distribution curve occurs jointly with the peak load hour (7-9 pm).

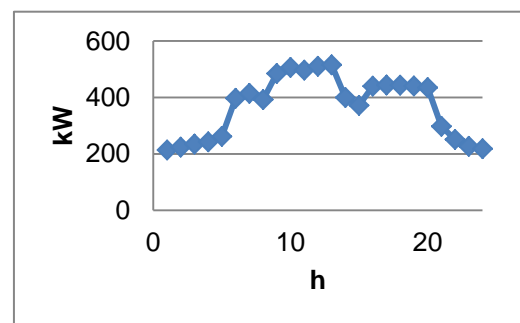
The commercial zone is represented by curve b). Notice from Figure 46, that the peak of arrivals to shopping happens between 8-10 am and 12-5 pm. At the same intervals occurs the peak of consumption in a commercial area.

Curve c) represents the typical load in an industrial area. From Figure 46, the peak of arrival by work reason happens between 7-9 am, just at the same time of the peak consumption in this area.

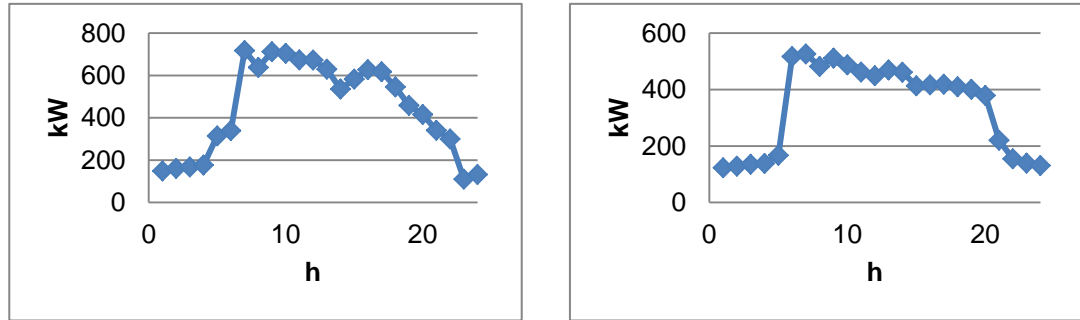
Finally, curve d) represents a public typical load profile. This includes public activities such as: public offices, public schools, etc. The peak load happens between 6-9 am, but it remains almost constant during the day. The slope is very slight. The peak of arrivals by the work and school reasons also coincides with this range.



a) Residential load profile



b) Commercial load profile



c) Industrial load profile

d) Public load profile

Figure 48: Typical load profiles.

From these analyses it is possible to see the importance that the charging mode will have in the electric systems. If a dumb mode (strategy) is used, the peak loads are summed, which consists in the worst scenario for the reliability perspective. Otherwise, using a smart charging mode, as referred before, the EV load becomes a controlled load which can be moved to another hour without compromising the reliability of the electric systems too much, and promoting an enlarge use of renewable sources, namely wind power. Obviously, other variables are involved, such as: the incentives from the government, electric companies, autonomy of the EV, etc. However, the EV large integration will change the typical load curve and it must be consider in the reserve adequacy evaluation.

4.4.4 The Counting Process Algorithm

In order to estimate the EV load, it is necessary to count, hourly, the number of EV in each area and, therefore, the Poisson process [6] will be used to incorporate it on RESERVE model. This process is characterized by a mean rate λ , which is the number of events in time interval $(t, t + \tau]$ and follows a Poisson distribution with associated parameters $\lambda \tau$. This relation is given by:

$$P[(X(t + \tau) - X(t)) = k] = \frac{e^{-\lambda \tau} (\lambda \tau)^k}{k!} \quad k = 0, 1, 2, 3, \dots, \quad (17)$$

where $X(t + \tau) - X(t)$ is the EV number in time interval $(t, t + \tau]$.

The mean rate λ is the main parameter to obtain the EV number in time interval. Thus, this rate is obtained from the mobility process already presented. One of the main advantages of this proposed methodology is that the counting process incorporated on RESERVE model depends only the parameter λ . Figure 45 shows the mobility distribution curve of departure trips along a week-day. It is very useful information to obtain the EV arrival mean rate per unit of time.

In order to enhance the method, another important data is related with the mobility distribution by activity. It will refine the mean rate λ per each considered area, as represented in Figure 46.

λ is the mean rate of the amount of EV that arrives in a Charging Point, and is given by:

$$\lambda = \sum_{k=0}^{\infty} kp_k \quad (18)$$

where p_k is the probability of k arrivals in a given time interval.

In order to generate a Poisson random variable (to quantify hourly the EV number) an algorithm based on Inverse Transform Method is used [3]. This algorithm is given by the following steps:

- i. set $n = 1$ and $a = 1$;
- ii. generate $U_n \sim U(0,1)$ and set $a = aU_n$;
- iii. if $a \geq e^{-\lambda}$, then set $n = n + 1$ and go to step 2;
- iv. otherwise, return $X = n - 1$ as a random variable from $Poi(\lambda)$.

Therefore, it is possible to quantify the number of EV in each Charging Point considered.

4.4.5 Converting Number of EV on EV Load

In this sense, this algorithm returns the EV number for each area in analysis. The EV load of each area is given by the EV number in this area (estimated by the Poisson process), multiplied for the capacity of the EV battery. From WP 2 the EV were divided in four classes as following:

- L7e – four wheels vehicle, with a maximum unladen mass of 400kg or 550kg for a goods carrying vehicle (not include the mass of the batteries in an electrically powered vehicle) and a maximum net power, whatever the type of engine or motor. of 15kW;
- M1 – passenger vehicle, four wheels and to up 8 seats in addition to the driver's seat;
- N1 – goods-carrying vehicle, four wheels. with a maximum laden mass of 3500kg;
- N2 – good-carrying vehicle, four wheels, with a maximum laden mass between 3500kg and 12000kg.

The electric parameters are summarized in Table 43. The equation (19) gives the equivalent EV load in a determined time t .

$$P_{EVload} = \sum_j^M [P_{EVj}(t) \cdot N_j(t) \cdot C_{ji}(t)] \quad j = 1, 2, \dots, M \quad (19)$$

where N is the number of EV in a given time t obtained from the inverse transformed Poisson distribution, P_{EVload} is the quantity of EV load in (MW) which is





affected by C that is a usage factor of EV in order to determine the EV load consumption in a given time t , j is the EV class, and M is the number of EV classes.

As mentioned in the beginning of the section, the objective is estimating the EV load to aggregate in the typical load observed. In order to evaluate the reserve adequacy indices, the total load equivalent is given by:

$$L_{eq} = \sum_i^N [P_{Li}(t) + P_{EVload,i}(t)] \quad i = 1, 2, \dots, N \quad (20)$$

where P_{Li} is the typical load of area i in a given time t , P_{EVload} is the total EV load of the area i in a given time t . N is the number of areas available and i is the specific area such as: 1 is the residential area, 2 is the industrial area and so on.

Table 43: Parameters of the EV classes.

Vehicle Class					
EV type		L7e	M1	N1	N2
Description		Quadricycle. with a maximum unladen mass of 400 kg or 550 kg	Passanger vehicle up to 8 seats in addition to the driver's seat	Goods-carrying vehicle. with a maximum laden mass of 3.500 kg	Goods-carrying vehicle. with a maximum laden mass between 3.500 kg and 12.000 kg
Vehicle fleet in 2008		-	87.1%	-	-
Battery capacity for simulations	Type and technology	BEV / PbA (possible replacement by Li-ion)	BEV / Li-ion	BEV / Li-ion	BEV / Li-ion and Zebra (However. this battery type will be replaced by Li-ion)
	Max	15 kWh	72 kWh	40 kWh	120 kWh
	Mean	8.7 kWh	29 kWh	23 kWh	85 kWh
	Min	3 kWh	10 kWh	9.6 kWh	51 kWh
Standard battery charge rates	Fast charge rate	from 3 kW (that is expected to be standard charging rate) to 7.5 kW	from 3 kWh to 240 kW	from 10 kW to 45 kW	from 35 kW to 60 kW
	Max	3 kW	8.8 kW	3.3 kW	-
	Mode	3 kW	3 kW	3 kW	10 kW
	Min	1 kW	2 kW	1.3 kW	-

4.5 Generating Systems Evaluation Considering EV Integration

The RESERVE model is based on a chronological representation as mentioned in 3.9. In analogy of the generation stochastic process, the number of EV that arrives to charging their batteries, and the time that the EV remains charging it, are a set of random variables that characterize the EV behaviour as a stochastic process. At the end, the evaluation is given by the test functions represented by equations (15) and (16).

The Figure 49 shows the generation failure/repair process already mentioned in 3.4.

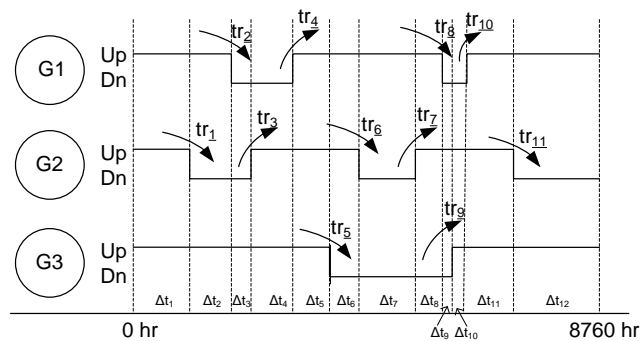


Figure 49: Generation failure/repair process.

RESERVE model build such up and down sequences through the use of a Markovian process, where the transition monitoring procedure to quantify system performances indices is carried out. On the same way, another process named counting process will be incorporated on the RESERVE simulation procedure to deal with EV integration.

Figure 50 shows the equivalent load profile in time. From 3.3.1, load curves vary with the season of the year and the day of the week. In the RESERVE model the load is modelled using a chronological representation containing as many steps as hours in the year. As previously discussed, usually, the system load is characterized by an observation that may be affected by a level of uncertainty. As the simulation advances through time the RESERVE follows sequentially these loads steps and the amount of load will also be affected according with the sampled EV load counted.

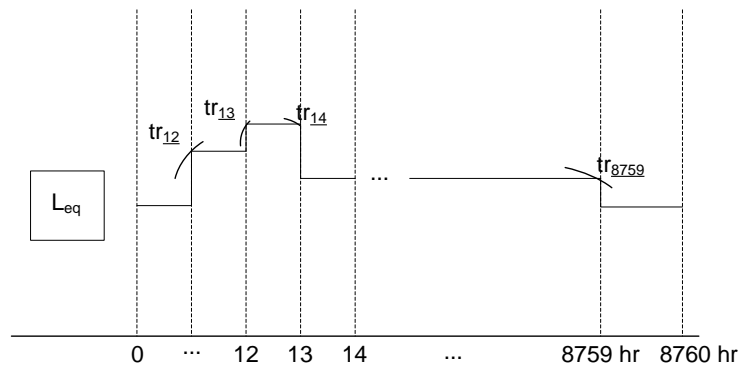


Figure 50: Load profile.

The data of the load profiles are obtained through years of observation. The EV load has an important characteristic which is the additional random portion of load in each hour on the observed load profile. It means that the EV load represented in Figure 44 will vary in a random way along of the simulation process considering an hourly resolution. Each hour of the typical load amount will be affected with an addition or reduction amount provide by EV load. This amount of load is given by (19) and is strongly dependent of the number of EV. The stochastic behaviour of EV load is represented in Figure 51.

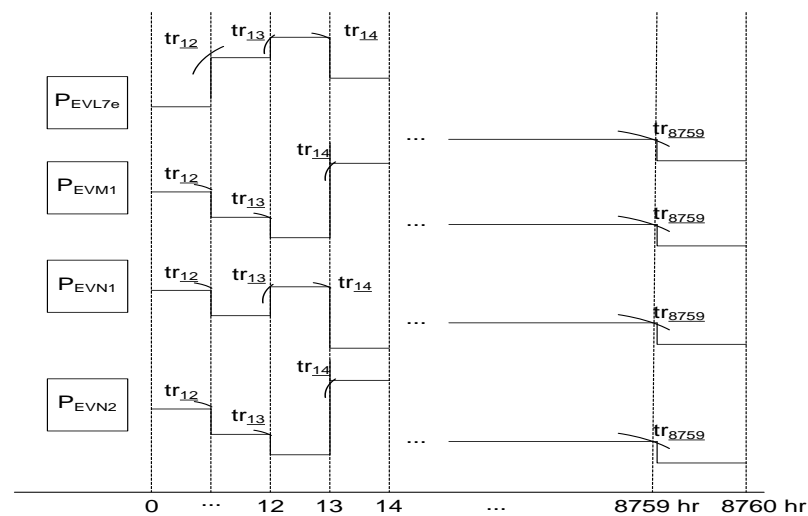


Figure 51: Random behaviour of the EV load.

The reserve adequacy evaluation is made in the same way as described in 3.1 and 3.2. The power balance equation used to obtain the reliability indices remain the same. However, part of the load now will follow a random behaviour based on EV counting process on each hour. Figure 52 shows the sum between the total typical load and the EV load resulting in the equivalent load. When $G < L_{eq}$ is true (hachured parts), typical risk indices are calculated.

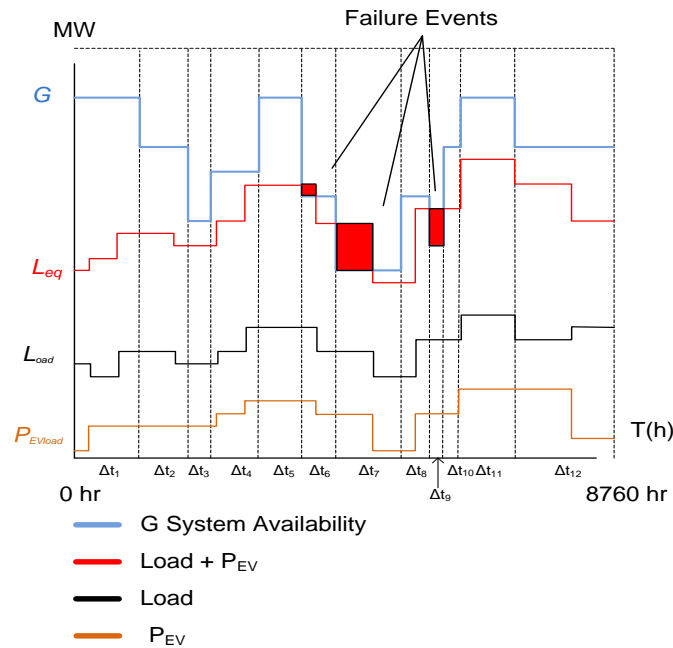


Figure 52: System generation and equivalent system load.

4.5.1 Proposed Generating System Evaluation Algorithm considering EV

Taking into account the new EV random variable over the observed system load, the RESERVE model algorithm that is based on Monte Carlo method will change as well, and it can be summarized on the following steps:

- i. Generate a yearly synthetic sequence of system states y_n by sequentially applying the failure and repair stochastic models of generating units; usually, in the first sample, it is assumed that all generation components are initially in the success or up state, even though other approaches may be used. The duration of each generation component residing in its present state is sampled from its probability distribution. The duration of each generation component will follow the equations (3) and (4).
- ii. Start the EV counting process chronologically converting the number of EV on EV load chronologically; the initial number of EV connected in the electric system will be estimate through equation (17).
- iii. If the load uncertainty mode is on, identify the observed part of system load considering its associated uncertainty on MW and define the level of observed system load at each hour. Conversely, if the load uncertainty mode is off, consider only the part system load observation chronologically;
- iv. In analogy of the load, for this first approach the duration of EV connected in the electric system to fill the batteries is assumed to be variable (e.g. 5 hours considering the power) and the number of EV is given by the inverse of the Poisson distribution in each hour;
- v. Chronologically evaluate each system state x_k in the sequence y_n and accumulate the values;

- vi. In order to obtain yearly reliability indices, calculate the test function $F(y_n)$, equation (12), over the accumulated values;
- vii. Estimate the expected mean values of the yearly indices as the average over the yearly results for each simulated sequence y_n ;
- viii. The stop criterion is also based on the relative uncertainty of the estimates. Therefore, calculate β (coefficient of variation) using the equation (13);
- ix. Verify if the degree of accuracy or confidence interval is acceptable. If it is true, stop the simulation; otherwise, go back to step (i).

4.6 EV charging impact on Generating Systems

With the purpose of illustrating the proposed methodology, a simple example was created. Suppose that a given residential area is fed by a distribution transformer which has 800 kVA of nominal capacity with a power factor of 0.95. Figure 48 a) presents the daily load profile of a given week day of this area.

Considering that the residential peak load is of 480 kVA and also supposing that householders can consume at most 10.35 kVA, the number of houses supplied by the distribution transformer is approximately 46. It is also considered that each householder possesses an EV which will be plugged into the network upon each arrival during an average time of 6 hours. It is assumed also that the average charging rate of each EV is 3 kW in one hour.

At this point, it should also be stressed that these assumptions were made in order to create a simple illustrative example. If a detailed and thorough analysis ought to be made the following issues should have to be taking into account:

- Not all householders possess an EV;
- Different householders can own different types of EVs with different characteristics. As a result, detailed information regarding the capacity of their batteries and their corresponding charging rates ought to be incorporated in the analysis;
- The charging behaviour differs from each EV owner. It is influenced by the EV state of charging upon the arrival, the projection of when the EV will begin the next travel and the electricity tariffs. As a result, the EV charging time can be seen as a random variable with a behaviour following a given probability distribution.

From [4] the average number of arrivals of each vehicle is approximately 1.5, per vehicle per day. Therefore, the total number of arrivals at the residential area is approximately 148 which, and is distributed as following [4]:

Table 44: Distribution along a week day of the arrivals at a residential area.

Hour	1	2	3	4	5	6	7	8	9	10
%	0.325	0.044	0.039	0.000	0.000	0.000	0.041	0.118	0.354	0.680
	11	12	13	14	15	16	17	18	19	20
%	1.268	2.244	7.079	4.658	1.538	2.040	3.107	7.462	12.195	10.353
	21	22	23	24						
%	6.355	2.978	2.383	3.740						

From this daily distribution, the λ parameter of the hourly Poisson distributions is obtained. Three examples of the Poisson distributions of the arrivals at a residential area at a given hour are presented in Figure 53, Figure 54 and Figure 55.

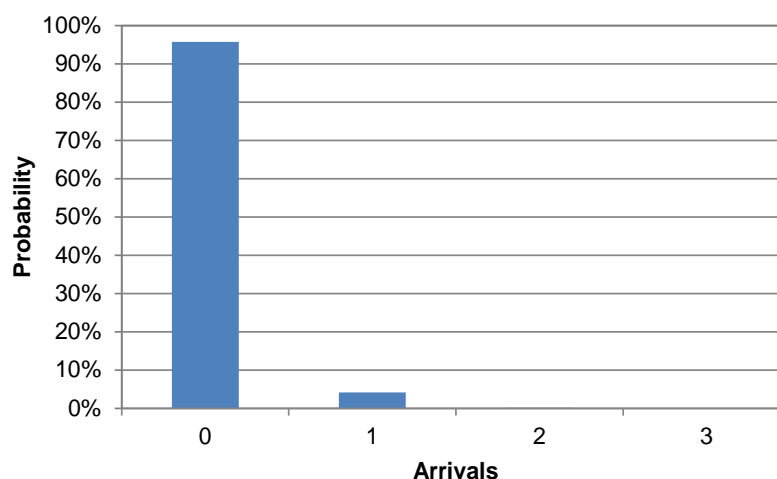


Figure 53: Arrivals distribution at 2 am.

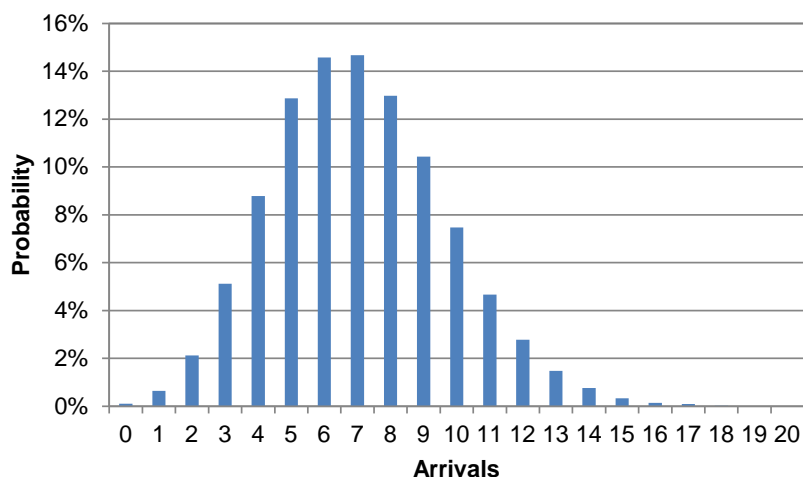


Figure 54: Arrivals distribution at 1 pm.

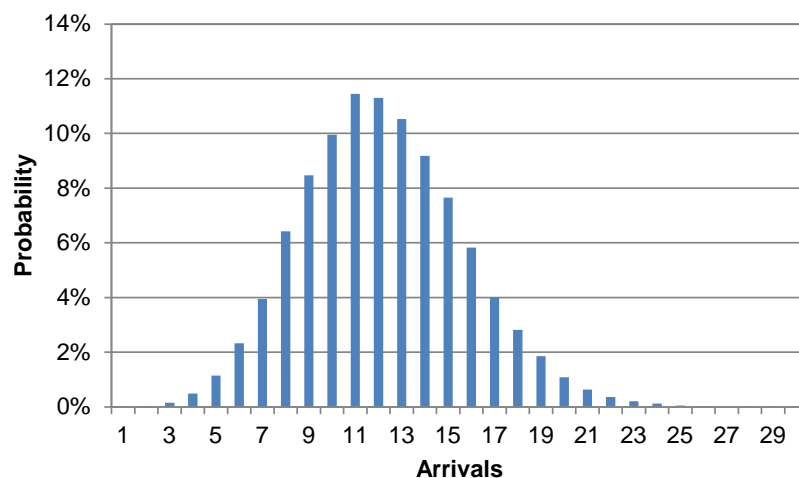


Figure 55: Arrivals distribution at 7 pm.

To obtain the EV load profile, 36500 samples of arrivals for each hour were obtained, which is equivalent to say that 36500 scenarios of arrivals of 24 hours were sampled. The 24 hourly distributions obtained from the 36500 samples are characterized in the following table.

Table 45: Hourly probability distributions of the arrivals.

			Interval of Confidence (99%)	
Hour	Average	Coefficient of Variation (%)	Left limit	Right limit
1	0.32455	0.92349	0.31683	0.33227
2	0.04395	2.51824	0.04109	0.04680
3	0.04038	2.60335	0.03768	0.04309
4	0	100	0	0
5	0	100	0	0
6	0	100	0	0
7	0.04107	2.58326	0.03834	0.04380
8	0.11918	1.51754	0.11452	0.12384
9	0.35449	0.88405	0.34642	0.36257
10	0.67899	0.63354	0.66791	0.69007
11	1.26512	0.46409	1.25000	1.28025
12	2.24589	0.34959	2.22567	2.26612
13	7.05756	0.19736	7.02168	7.09344
14	4.66386	0.24299	4.63467	4.69306
15	1.52948	0.42496	1.51274	1.54622
16	2.03548	0.36594	2.01629	2.05467
17	3.12077	0.29382	3.09715	3.14439
18	7.47970	0.19211	7.44268	7.51671
19	12.18027	0.15053	12.13304	12.22750
20	10.35063	0.16246	10.30731	10.39395
21	6.35586	0.20865	6.32170	6.39002
22	2.98016	0.30342	2.95687	3.00346
23	2.39416	0.33883	2.37327	2.41506
24	3.73910	0.26905	3.71318	3.76501

Upon arrival each EV begins charging resulting on an increase of the load profile of 3 kW during the subsequent 6 hours. This assumption allows estimating the average EV consumption for each hour of the day and obtaining probability distributions. The following table summarizes the result of the EV hourly load. The results presented on Table 45 show that no EV arrives at hours 4 am, 5 am and 6 am. However, the EV load at these hours is different from zero, as shown on, Table 46 since there are some EVs still charging.

Table 46: EV hourly load probability distributions.

Hour	Average (kW)	Coefficient of Variation (%)	Interval of Confidence (99%)	
			Left Limit (kW)	Right Limit (kW)
1	78.43085	0.10274	78.22328	78.63842
2	47.51227	0.13225	47.35041	47.67414
3	28.56633	0.16961	28.44152	28.69114
4	19.62608	0.20506	19.52241	19.72976
5	12.44359	0.25557	12.36167	12.52551
6	1.22663	0.82252	1.20064	1.25262
7	0.37619	1.48234	0.36183	0.39056
8	0.60189	1.16801	0.58378	0.62000
9	1.54422	0.73246	1.51508	1.57336
10	3.58118	0.47743	3.53713	3.62522
11	7.37655	0.33335	7.31320	7.43989
12	14.11422	0.24020	14.02689	14.20155
13	35.16370	0.15237	35.02568	35.30172
14	48.79775	0.12993	48.63443	48.96108
15	52.32271	0.12595	52.15296	52.49247
16	56.39219	0.12126	56.21603	56.56835
17	61.95912	0.11556	61.77469	62.14356
18	77.66055	0.10315	77.45419	77.86690
19	93.02868	0.09429	92.80272	93.25465
20	110.08899	0.08653	109.84361	110.33437
21	124.56814	0.08132	124.30719	124.82909
22	127.40219	0.08045	127.13815	127.66623
23	125.22238	0.08102	124.96102	125.48374
24	114.00058	0.08518	113.75043	114.25072

Figure 56: shows that the average EV peak load occurs at a different moment than the hour where there is the highest average number of arrivals.

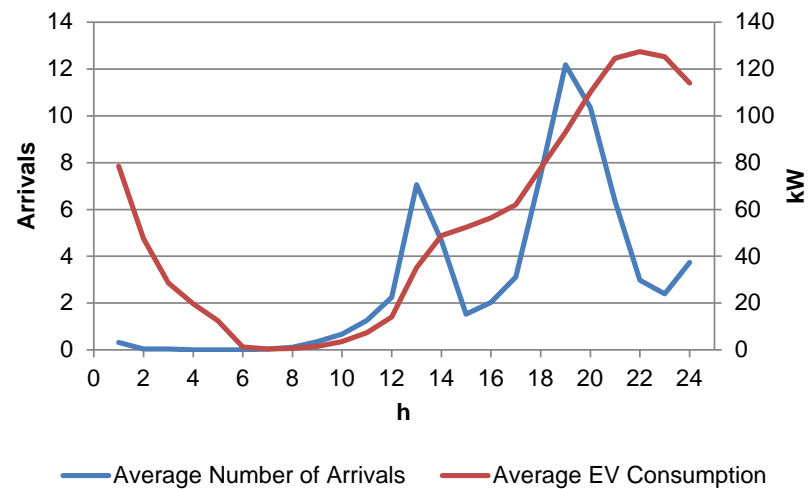


Figure 56: Average number of arrivals vs average EV consumption.

This methodology also allows determining which of EV load daily scenarios sampled pose more difficulties to the system operation. In this sense, one is interested in determining the scenario which has the highest peak of EV consumption as well as the scenario where the peak of EV consumption is the lowest. Furthermore, the scenarios where EVs charging result in the highest and lowest energy consumption at the end of the day are also of interest.

Figure 57 shows the scenario where the load of the residential area plus the load of the EV results in the maximum peak. For this scenario the capacity of the transformer is exceeded during two hours.

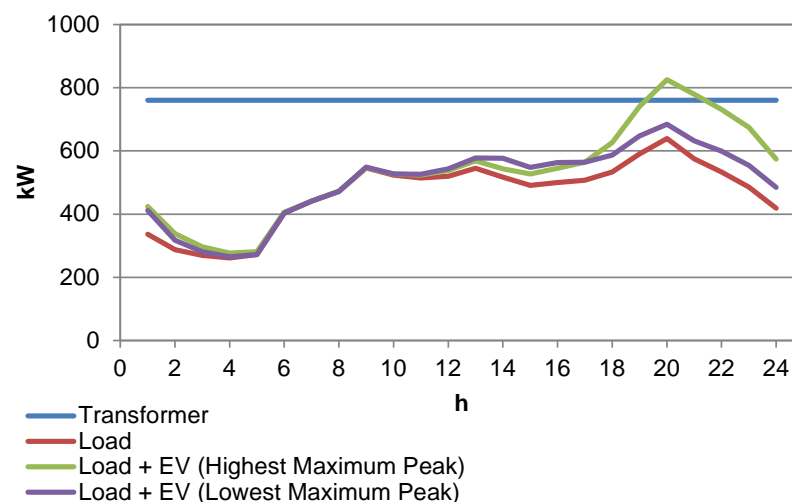


Figure 57: Peak load scenario.

Figure 58 exhibits the scenario where at the end of the day the load of the residential area plus the load of the EV results in the maximum energy consumption. For this scenario the capacity of the transformer is exceeded during one hour. It is also worth mentioning that the scenario of the maximum peak load is not the same scenario that leads to the highest energy consumption.

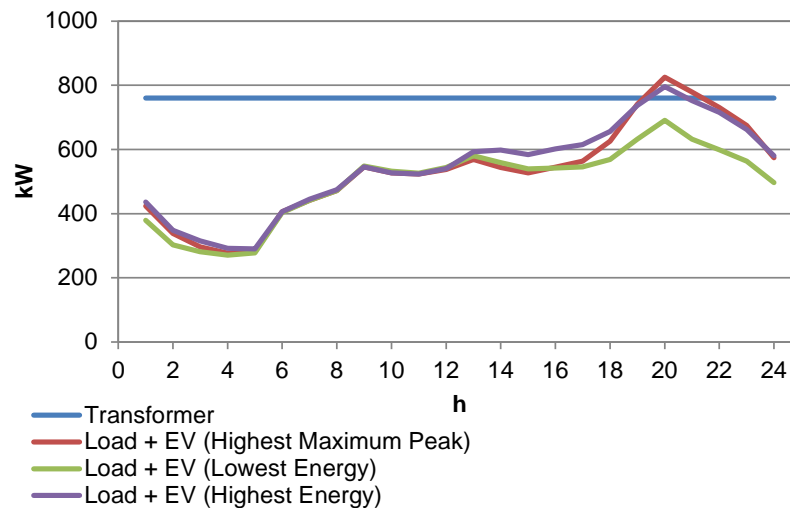


Figure 58: Maximum energy scenario.

The same analysis can be extended for other days of the year. To this purpose, one has to take into account the hourly of load for all the months of the year and also the different pattern of arrivals of weekdays, of Saturdays and of Sundays/holydays. This complete model was integrated in the RESERVE model.

4.7 Enhancement in the evaluation of the wind power forecasting uncertainty method

The uncertainty of wind power forecast is estimated as presented in section 3.7.1. There was implemented the persistence method which it consists in the difference of wind power between the current hour and the hour before.

Although persistence method has been one of the simplest forecast methods it is not advisable for weather conditions which change significantly in the short-term range. Unlike that, persistence method is very useful to predict long-term weather conditions, because this method assumes that the conditions at the time of the forecast will not change. So, it usually works well in regions there are no significant changes in the weather conditions or in the long-term, for example, it is often used to predict monthly and seasonal weather conditions. Therefore another forecast method was implemented in the algorithm tool. The Weibull distribution relies in a continuous probability distribution used to estimate errors [3]. The density function is given by:

$$f(x, k, \lambda) = \begin{cases} \frac{k}{\lambda} \left(\frac{x}{\lambda} \right)^{k-1} e^{-(x/\lambda)^k}, & x \geq 0 \\ 0, & x < 0 \end{cases} \quad (21)$$

where $k > 0$ is the shape parameter and $\lambda > 0$ is the scale parameter of the distribution.

The Weibull distribution is used in reliability and life data analysis due to its versatility. Based on parameters values, it can be used to model a variety of life behaviours which goes in line with the adaptation of the tool for the introduction of EV. The Weibull probability density function is given by:

$$f(T) = \frac{\beta}{\eta} \left(\frac{T - \gamma}{\eta} \right)^{\beta-1} e^{-\left(\frac{T - \gamma}{\eta} \right)^\beta} \quad (22)$$

where $f(T) \geq 0$, $T \geq 0$ or γ , $\beta \geq 0$, $\eta \geq 0$, and $-\infty \leq \gamma \leq \infty$, and η is the scale parameter, β is the shaper parameter (or slope), and γ is the location parameter.

5 DESCRIPTION OF THE PRELIMINARY EVALUATION

In order to determine the effects of EV on the system reliability a preliminary evaluation was conducted. To that purpose, a modified configuration of the original IEEE RTS 96 [9] was developed. The purpose is to include hydro and wind variations of their primary energy resources.

The original IEEE RTS 96 power system has a peak load of 8550 MW powered by a total generation capacity of 10215 MW. The unit with the lowest generation capacity is of 12 MW whereas the largest unit is of 400 MW. The share of hydro capacity in the total is 8.8%. Furthermore, the hydro units' model does not consider the chronology of the hydrological resources.

The IEEE RTS 96 HW variation, besides considering five monthly time series for each of the three 300 MW clusters of hydro units of the system, it also contains three wind farms having two of them a total of 534 MW of capacity and the other a total of 458 MW. The wind hourly variation of the wind farms is also included in the RESEVE by means of three time series for each wind farm.

As there are no studies regarding the integration of EV on this test system EV were modelled as a simple load. To build an hourly load profile of the EV the following procedure was performed:

- The EV 24-hour load profile obtained on task 1.5 for the Portuguese case was copied 365 times to obtain an annual profile;
- This annual profile was set in percentage of the peak Portuguese peak load of that year;

- The EV annual load profile of the IEEE RTS 96 HW results from multiplying the EV hourly percentages by the IEEE RTS 96 HW peak load.

This procedure was repeated to obtain the EV load profile for a smart charging scenario and for a dumb charging scenario. Figure 59 shows the smart and dumb charging scenarios daily profile which was afterwards replicated 365 times to obtain the annual EV load profile.

It is also worth to point out that the uncertainty associated to EV in these simulations was modelled via a binomial distribution since its hourly profile was added to the hourly load profile of the IEEE RTS 96 HW power system.

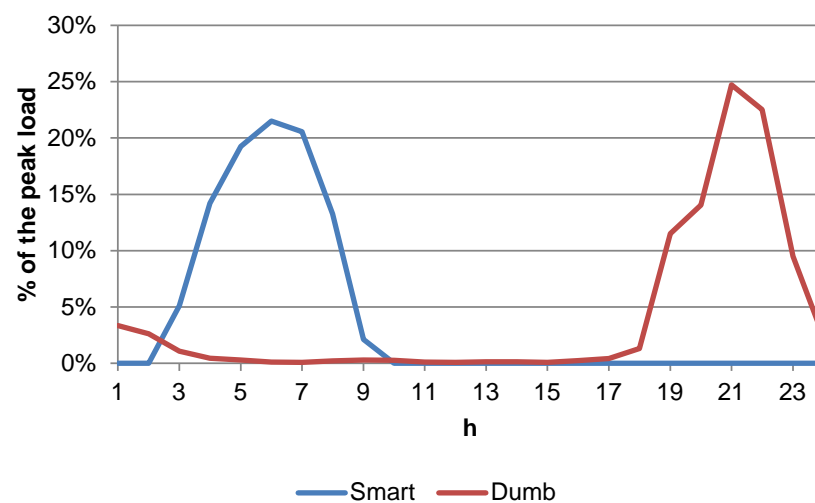


Figure 59: Daily load profile of the smart and dumb charging scenarios in percentage of the peak load.

In the smart charging scenario the peak load remained unaltered; conversely, in the dumb charging scenario, the peak load increased from 8550 MW to 9894.4 MW.

To assess the adequacy of the operational reserve, the primary reserve was set to 85 MW and the secondary to 315 MW. The standard deviation of the probability distribution of the short term uncertainty was set to 2% of the hourly load; the standard deviation of the probability distribution of the long term uncertainty was set to 1% of the annual peak load. Both these probability distributions have zero mean. It is also assumed that the units capable of providing unsynchronized reserve are the 20MW and 400MW thermal units plus the 50 MW hydro units.

All the experiments follow the standard version of RESERVE.

6 DISCUSSION - RESULTS OF THE PRELIMINARY EVALUATION

In terms of adequacy of the system, the results that can provide the highest amount of information are the estimates of the reliability indices both for the static reserve and the operational reserve.

Table 47: Static reserve indices.

Scenario	LOLE (h/yr)	LOLF (oc/yr)	EENS (MWh/yr)
No EV	0.4417	0.2781	81.62
Smart charging	0.584	0.3736	109.6
Dumb charging	31.48	22.66	9666

Table 48: Operational reserve indices.

Scenario	LOLE (h/yr)	LOLF (oc/yr)	EENS (MWh/yr)
No EV	3.469	6.007	325.8
Smart charging	4.144	7.095	404.7
Dumb charging	44.18	34.99	13370

From Table 47 it is possible to conclude that, given the current generating resources within the system, only with a smart charging mode it is possible to guarantee a long term security of supply similar to the scenario where there is no EV. The same is valid for the operational reserve adequacy as shown in Table 48. It is worth also to mention that if a dumb charging mode is followed, the performance of the system becomes greatly degraded.

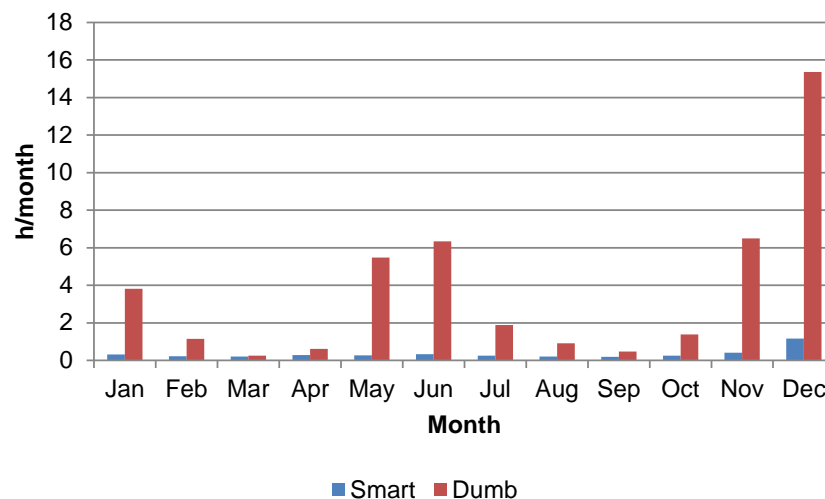


Figure 60: Operational reserve monthly LOLE.

Figure 60 contrasts the monthly LOLE index of the operational reserve of the smart charging scenario with the same index for the dumb charging scenario. This figure shows that the smart charging scenario has a constant LOLE index profile during the year, increasing slightly at the end of the year. This means that the number of hours during the month where there is not enough operational reserve to meet the uncertainty of the load, plus the uncertainty of the wind and of the failure of generating units remain constant during the entire year. The increase of the LOLE index in December results from two effects: first, this month is the most demanding in terms of load, and as a result, the ΔL associated with load forecasts is higher and cannot easily be covered with the available generating resources; second, this month is the one where there is less water available to be used by the fast starting hydro units, and consequently, the portion of the operational reserve resulting from the unsynchronized capacity becomes reduced originating more events where there is not enough operational reserve to meet the uncertainties.

Furthermore, from this figure it can be seen that, for the dumb charging scenario, the months where the lack of operating reserve is more perceptible are the winter months (November, December and January) and the months of May and June. In the case of the winter months, the same previous description is also applicable, apart from the fact that, in these months, the ΔL associated with load forecasts is more evident due to the increase of the load peak resulting from the EV dumb charging. For the purposes of this test system example the value of the load for both Smart and Dumb charging modes may be considered the same. However, it happens in different hours of the year. Consequently, the expected value of the operational reserve needs remains almost the same, mainly due to the previous knowledge about this deterministic load. This result confirms the needs for a flexible model as described in 4. Where it is possible to distinguish two portions of load: observed (with or without uncertainty) and random (EV load) ones.

Table 49: Operational reserve needs

	Expected value (MW)
No EV	50.72
Smart charging	53.59
Dumb charging	53.89

Table 49 presents an estimate of the expected value of the probability distribution which results from adding ΔL , ΔP_w , and ΔG thought the simulation. This probability distribution associates the different levels of uncertainty resulting from adding those three variables with a probability of occurrence. Therefore, this probability distribution is extremely helpful to analyse the operational reserve requirements of the system.

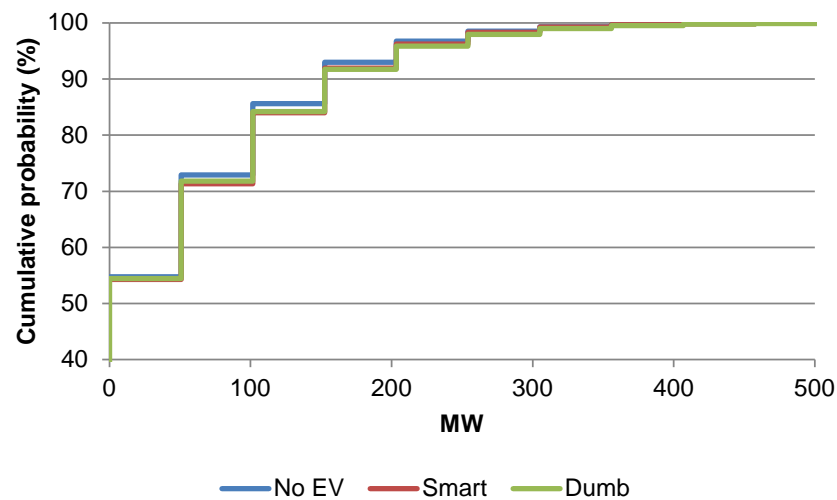


Figure 61: Operational reserve needs discrete cumulative probability distribution.

From the numbers presented on Table 49 it is possible to see that EVs, independently of the charging mode, does not significantly affect the average value of the probability distribution of the operational reserve requirements. The same is valid for the probability distributions itself since, as depicted in Figure 61, the charging modes have similar shapes to the scenario where there are no EVs. This observation results from the fact that the uncertainty of EVs load is integrated in the uncertainty of the total system load.

Under the assumptions of this preliminary analysis, and taking into account that the system peak load is 8550 MW for the smart charging scenario and 9894.4 MW for the dumb charging scenario, it can be honestly said that to guarantee that the uncertainties are accommodated without any risk of not being duly covered, one has to schedule 500 MW of operational reserve.

7 CONCLUSIONS

This task has as objective presents the methodology to include the massive integration of EV in the electric system in order to assess the impact of them in the reserve adequacy evaluation. The approach presented is based on the mobility patterns of the citizens. The EV will be another appliance that needs electricity to charge their batteries and this could be done in home, work, while the people have shopping or even in Charging Stations like the current combustion vehicles.

The preliminary results highlighted some considerations:

- the importance of the charging mode on the impact of the massive integration of EV in the electric systems;
- the lack of reserve in certain months of the year considering the dumb charging mode;

- the increase of renewable resources, namely wind generation, when the smart charging mode is used;

Besides of that, the methodology shows how the EV will impact on the current load profile. The reserve assessment has to take into account the random behaviour of the EV load. This is the main assumption that justifies the use of probability methods, as Poisson distribution, to represent the EV in order to create scenarios for the simulation process. These scenarios aim assess the impact of EV in the future reserve adequacy indices to prepare the power system's structure.

Finally, the approach presented seems suitable to make the necessary studies in order to present reliable results for the security of supply assessment.

8 REFERENCES

- [1] R. Billinton, RN. Allan, "Reliability Evaluation of Power Systems – 2nd Edition", New York: *Plenum Press*, 1996.
- [2] M. Matos, J. A. Peças Lopes, M. da Rosa, "Probabilistic evaluation of reserve requirements of generating systems with renewable power sources: the Portuguese and Spanish cases", *International Journal of Electrical Power and Energy Systems* 31 (2009), pages: 562-569.
- [3] RY. Rubinstein, DP. Kroese, "Simulation and Monte Carlo Method - 2nd Edition". New York: *John Wiley & Sons*, 2008.
- [4] Instituto Nacional de Estatística, INE, "Inquérito à Mobilidade da População Residente 2000", Direção Geral de Transportes Terrestres.
- [5] J. A. Peças Lopes, F. J. Soares, P. M. Rocha Almeida, "Identifying Managements Procedures to Deal with Connection of Electric Vehicles in the Grid", *PowerTech 2009*, Bucharest, Romania, June/July 2009.
- [6] D. D. Pestana, S. F. Velosa, "Introdução à Probabilidade e à Estatística", vol.1, 3^a Edição, Fundação Calouste Gulbenkian, 2008.
- [7] R. Cossent, P. Frías, T. Gómez, C. Mateo, "Functional Specification for Estimating Additional Investments in Distribution Networks with High Penetration of Electric Vehicles", *MERGE Project, Work Pack 2, Task 2.6, Deliverable 2.4*, 2011.
- [8] Manuel Matos, A. Gomes Martins, J. Nuno Fidalgo, Humberto Jorge, "Characterization of Consumers and Networks - 1st phase Report", Technical Report, Project CCR, December 2002 (in Portuguese).
- [9] IEEE APM Subcommittee. 'IEEE Reliability Test System'. *IEEE Trans. on PAS*, 1979; 99(6): 2047-2054.